

**PROCEEDINGS**  
*of the*  
**CALTECH - JPL**  
**LUNAR AND PLANETARY CONFERENCE**

September 13 - 18, 1965

GPO PRICE \$ \_\_\_\_\_

CFSTI PRICE(S) \$ \_\_\_\_\_

Hard copy (HC) 7.00

Microfilm (MF) 1.75

#653 July 65

FACILITY FORM 8	N66 31446	N66 31481
	(ACCESSION NUMBER)	(THRU)
	357	1
	(PAGES)	(CODE)
	CR-74142	30
	(NASA CR OR TMX OR AD NUMBER)	(CATEGORY)

CALIFORNIA INSTITUTE OF TECHNOLOGY  
and  
JET PROPULSION LABORATORY  
With the Cooperation of the  
NATIONAL AERONAUTICS AND SPACE ADMINISTRATION





***PROCEEDINGS***  
***of the***  
***CALTECH – JPL***  
***LUNAR AND PLANETARY CONFERENCE***

***September 13 – 18, 1965***

***Edited by***  
***Harrison Brown***  
***Gordon J. Stanley***  
***Duane O. Muhleman***  
***Guido Münch***

***June 15, 1966***

***CALIFORNIA INSTITUTE OF TECHNOLOGY***  
***and***  
***JET PROPULSION LABORATORY***  
***Pasadena, California***  
***With the Cooperation of the***  
***NATIONAL AERONAUTICS AND SPACE ADMINISTRATION***

JPL Technical Memorandum No. 33-266

Copyright © 1966  
California Institute of Technology

Prepared Under Contract No. NSR 05-002-050  
National Aeronautics & Space Administration

## CONTENTS

### PART I. THE MOON

H. C. Urey, Observations on the <i>Ranger VIII</i> and <i>IX</i> Pictures . . . . .	1
G. P. Kuiper, Interpretation of the <i>Ranger</i> Records . . . . .	24
E. M. Shoemaker, Progress in the Analysis of the Fine Structure and Geology of the Lunar Surface From the <i>Ranger VIII</i> and <i>IX</i> Photographs . . . . .	30
B. C. Murray, Current Problems in the Interpretation of Lunar Physical Observations . . . . .	32
V. S. Troitsky, Investigation of the Surfaces of the Moon and Planets by the Thermal Radiation . . . . .	34
V. S. Troitsky, Some Remarks on New Measurements of Lunar Temperature at the Antisolar Point . . . . .	59
B. J. Levin, The Structure of the Moon . . . . .	61
G. J. F. MacDonald, On the Constitution and Origin of the Moon . . . . .	77
D. L. Anderson and R. L. Kovach, The Internal Structure of the Moon and the Terrestrial Planets . . . . .	84
J. A. O'Keefe and I. Adler, Lunar Structure as Deduced From Muong Nong Tektites . . . . .	92
H. S. Brown, Summary Remarks on the Moon . . . . .	101

### PART II. JUPITER

M. M. Komesaroff, Recent Radio Observations of Jupiter . . . . .	107
G. L. Berge, Interferometry of Jupiter in the Decimeter Range . . . . .	117
J. W. Warwick, Theory of the Jovian Structure . . . . .	122
A. G. Smith et al., Jovian Rotation Periods and the Origin of the Decametric Burst Structure . . . . .	128

## CONTENTS (Cont'd)

G. A. Dulk, The Effect of Io on the Radio Emission of Jupiter . . . . .	134	—
L. Davis, Jr., Comments on the Discussion of Jupiter . . . . .	137	—
G. B. Field, Remarks on Jupiter . . . . .	141	AC
G. J. Stanley, Summary Remarks on Jupiter . . . . .	143	pl

## PART III. VENUS

J. Strong, Balloon Telescope Studies of Venus . . . . .	147	—
D. Deirmendjian, Comments on the Detection of Water and Ice Clouds on Venus . . . . .	150	—
C. Sagan and J. B. Pollack, Properties of the Clouds of Venus . . . . .	155	—
D. O. Muhleman, Venus Radar Investigations . . . . .	164	—
R. B. Dyce, Some Radar Characteristics of Venus at 430 MHz . . . . .	172	—
J. H. Thomson, Radar Observations of Venus at Jodrell Bank . . . . .	178	—
F. D. Drake, Recent Radio Observations of the Planet Venus . . . . .	180	—
A. D. Kuzmin, Some Remarks Concerning the Radioastronomical Observations of Venus . . . . .	184	—
A. Dollfus, Contribution au Colloque Caltech-JPL sur la lune et les planètes: Venus . . . . .	187	—
D. O. Muhleman, Summary Remarks on Venus . . . . .	203	—

## CONTENTS (Cont'd)

### PART IV. MARS

D. G. Rea, The Atmosphere and Surface of Mars— A Selective Review . . . . .	209	—
R. Goldstein, JPL Radar Observations of Mars . . . . .	239	AD
D. M. Hunten, CO <sub>2</sub> Bands and the Martian Surface Pressure . . . . .	240	—
H. Spinrad, Spectroscopic Observations of Mars, 1964-5 . . . . .	245	—
T. Owen, Recent Observations of the Photographic Spectrum of Mars—A Preliminary Report . . . . .	247	—
R. L. Younkin, A Search for Limonite Near-Infrared Spectral Features on Mars . . . . .	252	AD
R. B. Dyce, Recent Radar Observations of Mars . . . . .	253	AD
C. Sagan and J. B. Pollack, Radio and Radar Evidence on the Structure and Composition of the Martian Surface . . . . .	255	—
A. J. Kliore et al., Preliminary Results of the <i>Mariner IV</i> Occultation Measurement of the Atmosphere of Mars . . . . .	257	—
G. Fjeldbo et al., Preliminary Results of the <i>Mariner IV</i> Radio Occultation Measurements of the Upper Atmosphere of Mars . . . . .	267	—
R. B. Leighton, Comments on the <i>Mariner IV</i> Photographs of Mars . . . . .	273	—
C. Sagan, High-Resolution Planetary Photography and the Detection of Life . . . . .	279	—
A. Dollfus, Contribution au Colloque Caltech-JPL sur la lune et les planètes: Mars . . . . .	288	—
G. Münch, Summary Remarks on Mars . . . . .	306	AD

## PREFACE

The conference which is described in these proceedings was jointly sponsored by the California Institute of Technology and the Jet Propulsion Laboratory as a symbol of the close scholarly relationships between the two organizations, which have been administratively linked for so many years. With the help of the National Aeronautics and Space Administration, the conference was held at the California Institute of Technology, Pasadena, California, September 13-18, 1965, and brought together more than 130 scientists to discuss recent and current studies of the Moon, Jupiter, Venus, and Mars. Conference participants came from many centers of scientific activity in the United States, England, France, Israel, and the USSR.

The Conference was organized under the capable administrative leadership of Dr. Albert Hibbs, and was divided into the following sessions:

- |               |   |                             |
|---------------|---|-----------------------------|
|               | The Moon                                    | Harrison Brown, Chairman    |
| Session I:    | Recent Development                          |                             |
| Session II:   | Earth-Based Observations: Radio and Optical |                             |
| Session III:  | Lunar Structure                             |                             |
|               | Jupiter                                     | Gordon J. Stanley, Chairman |
| Session IV:   | Recent Observations                         |                             |
| Session V:    | Theory of Jovian Structure                  |                             |
|               | Venus                                       | Duane O. Muhleman, Chairman |
| Session VI:   | Recent Observations                         |                             |
| Session VII:  | Radio and Radar Observations                |                             |
|               | Mars  | Guido Münch, Chairman       |
| Session VIII: | Current Problems                            |                             |
| Session IX:   | Spectroscopic Observations of Mars          |                             |
| Session X:    | Results from the <i>Mariner</i>             |                             |
| Session XI:   | Conference Review                           |                             |

The Conference was sponsored by the National Aeronautics and Space Administration under Contract No. NSR 05-002-050. Papers given by employees of the Jet Propulsion Laboratory reported on research carried out under Contract No. NAS 7-100, also sponsored by the National Aeronautics and Space Administration.

These Proceedings contain all papers\* given at the Conference, except for those by Walter E. Brown, Jr., JPL (Session II); Fred T. Haddock, University of Michigan (Session IV); Alan Barrett, Massachusetts Institute of Technology (Session VII); and James Ring, The

\*Some of the papers are given in abstract form in the *Proceedings*.

## PREFACE (Cont'd)

University, Hull, England (Session IX). Also not included is the address given at the banquet meeting by Dr. Colin Pittendrigh, Department of Biology, Princeton University, who eloquently answered the question "Why Go to Mars?"

We appreciate the privilege of using material from other sources, and we should like to thank the University of Chicago Press, the Sky Publishing Company, and the editors of *Science*, *Nature*, *Radio Science*, *Annales d'Astrophysique*, and *Comptes Rendus*, as well as other individuals and publishers cited individually in the text.

Harrison Brown  
*Conference Chairman*



## LIST OF PARTICIPANTS

- ADAMCIK, DR. J. A.  
Texas Technical College  
Lubbock, Texas
- ANDERSON, DR. DON L.  
Seismological Laboratory  
California Institute of Technology
- BACHER, DR. R. F.  
California Institute of Technology
- BARRETT, DR. ALAN H.  
Massachusetts Institute of Technology  
Cambridge, Massachusetts
- BEER, DR. REINHARD  
Jet Propulsion Laboratory
- BELTON, DR. M. J. S.  
Kitt Peak National Observatory  
Tucson, Arizona
- BERGE, GLENN L.  
California Institute of Technology
- BRERETON, ROY G.  
Jet Propulsion Laboratory
- BROWN, DR. HARRISON S.  
California Institute of Technology
- BROWN, WALTER E., JR.  
Jet Propulsion Laboratory
- BRUNE, DR. JAMES N.  
Seismological Laboratory  
California Institute of Technology
- BRUNK, DR. W. E.  
National Aeronautics and Space  
Administration Headquarters
- BULL, HAROLD T.  
Jet Propulsion Laboratory
- CAMPEN, CHARLES F., JR.  
Jet Propulsion Laboratory
- CARPENTER, ROLAND L.  
Jet Propulsion Laboratory
- CHAMBERLAIN, DR. JOSEPH W.  
Kitt Peak National Observatory  
Tucson, Arizona
- CHANG, DR. DAVID B.  
General Atomic Division of  
General Dynamics  
San Diego, California
- CHAPMAN, DR. DEAN R.  
National Aeronautics and Space  
Administration  
Ames Research Center  
Moffett Field, California
- COLE, CHARLES W.  
Jet Propulsion Laboratory
- CONEL, DR. JAMES E.  
Jet Propulsion Laboratory
- DAVIES, RICHARD W.  
Jet Propulsion Laboratory
- DAVIS, DR. LEVERETT, JR.  
California Institute of Technology
- DAVIS, DR. MILFORD H.  
The RAND Corporation  
Santa Monica, California
- DEIRMENDJIAN, DR. DIRAN  
The RAND Corporation  
Santa Monica, California
- DOLLFUS, PROF. AUDOUIN  
Observatoire de Paris  
Meudon (Seine & Oise), France
- DRAKE, DR. FRANK D.,  
Cornell University  
Department of Astronomy  
Ithaca, New York
- DUBRIDGE, DR. LEE A.  
California Institute of Technology
- DUKE, DR. MICHAEL  
United States Geological Survey  
Washington, D. C.
- DULK, DR. GEORGE A.  
University of Colorado  
Boulder, Colorado
- DWORNIK, STEPHEN E.  
National Aeronautics and Space  
Administration Headquarters
- DYCE, DR. ROLF B.  
Cornell University  
Arecibo Ionospheric Observatory  
Arecibo, Puerto Rico
- EPSTEIN, DR. EUGENE  
Aerospace Corporation  
Los Angeles, California
- FIELD, DR. G.  
University of California  
Berkeley, California
- FJELDBO, DR. GUNNAR  
Stanford University  
Stanford, California
- FLOURNOY, DR. JOHN M.  
Jet Propulsion Laboratory
- FRANZGROTE, DR. E.  
Jet Propulsion Laboratory
- GARY, BRUCE  
Jet Propulsion Laboratory
- GILL, MICHAEL R.  
National Aeronautics and Space  
Administration Headquarters
- GIVER, LAWRENCE P.  
University of California  
Berkeley, California
- GODDARD, DR. FRANK E., JR.  
Jet Propulsion Laboratory
- GOLDREICH, DR. PETER  
University of California  
Los Angeles, California
- GOLDSTEIN, DR. RICHARD  
Jet Propulsion Laboratory
- GRAY, FRANK B.  
Jet Propulsion Laboratory
- GRAY, DR. LOUISE D.  
University of California  
Los Angeles, California
- GREENFIELD, DR. STANLEY  
The RAND Corporation  
Santa Monica, California
- HADDOCK, DR. FRED T.  
University of Michigan  
Radio Astronomy Observatory  
Ann Arbor, Michigan
- HAPKE, DR. BRUCE  
Cornell University  
Ithaca, New York
- HERR, DR. KENNETH  
University of California  
Berkeley, California
- HIBBS, DR. ALBERT R.  
Jet Propulsion Laboratory
- HOROWITZ, DR. NORMAN H.  
California Institute of Technology
- HUNTEN, DR. D. M.  
Kitt Peak National Observatory  
Tucson, Arizona
- JAFFE, DR. LEONARD D.  
Jet Propulsion Laboratory
- JAMES, JACK N.  
Jet Propulsion Laboratory
- JONES, DR. DOUGLAS E.  
Jet Propulsion Laboratory
- KAPLAN, DR. LEWIS D.  
Jet Propulsion Laboratory
- KAULA, DR. WILLIAM M.  
University of California  
Los Angeles, California
- KAVANAGH, RALPH  
California Institute of Technology
- KELLERMANN, DR. K. I.  
National Radio Astronomy Observatory  
Green Bank, West Virginia
- KLIORE, DR. ARVYDAS J.  
Jet Propulsion Laboratory
- KOCHER, GEORGE  
The RAND Corporation  
Santa Monica, California
- KOMESAROFF, DR. MAX M.  
University of Maryland  
College Park, Maryland
- KOPAL, DR. ZDENEK  
University of Manchester  
Manchester, England
- KOVACH, DR. ROBERT L.  
California Institute of Technology
- KUIPER, DR. GERARD P.  
Lunar and Planetary Laboratory  
University of Arizona  
Tucson, Arizona

## LIST OF PARTICIPANTS (Cont'd)

- KUZMIN, DR. A. D.  
Physics Institute imeni P. N. Lebedev  
Moscow, USSR
- LAWRENCE, HAROLD R.  
Jet Propulsion Laboratory
- LEIGHTON, PROF. ROBERT  
California Institute of Technology
- LEVIN, DR. B. J.  
Schmidt Institute of Physics of the Earth  
Academy of Sciences of the USSR  
Moscow, USSR
- LEVIN, DR. GILBERT V.  
Hazleton Laboratories, Inc.  
Falls Church, Virginia
- LEVINTHAL, DR. ELLIOTT C.  
Stanford University School of Medicine  
Palo Alto, California
- LEVY, GERALD S.  
Jet Propulsion Laboratory
- LYTTLETON, DR. RAYMOND A.  
Jet Propulsion Laboratory
- MACDONALD, DR. GORDON J. F.  
University of California  
Institute of Geophysics and Planetary Physics  
Los Angeles, California
- MCCLATCHEY, ROBERT A.  
Jet Propulsion Laboratory
- MEGHREBLIAN, DR. R. V.  
Jet Propulsion Laboratory
- MENZEL, DR. D. H.  
Harvard College Observatory  
Cambridge, Massachusetts
- METZGER, DR. ALBERT  
Jet Propulsion Laboratory
- MILLER, DR. JACOB  
National Aeronautics and Space Administration  
Ames Research Center  
Moffett Field, California
- MOFFET, DR. ALAN T.  
California Institute of Technology
- MORSE, GEORGE A., JR.  
Jet Propulsion Laboratory
- MUHLEMAN, DR. DUANE O.  
Jet Propulsion Laboratory
- MÜNCH, DR. GUIDO  
California Institute of Technology
- MUNRO, RICHARD  
Jet Propulsion Laboratory
- MURRAY, DR. BRUCE C.  
California Institute of Technology
- NEUGEBAUER, DR. GERRY  
California Institute of Technology
- NEWBURN, RAY L., JR.  
Jet Propulsion Laboratory
- NOYES, DR. JOHN C.  
Boeing Scientific Research Laboratories  
Seattle, Washington
- OHRING, DR. GEORGE  
Geophysics Corporation of America  
Bedford, Massachusetts
- O'KEEFE, DR. JOHN A.  
Goddard Space Flight Center  
Greenbelt, Maryland
- O'LEARY, BRIAN  
University of California  
Space Sciences Laboratory  
Berkeley, California
- OWEN, RAY D.  
California Institute of Technology
- OWEN, DR. TOBIAS  
IIT Research Institute  
Chicago, Illinois
- PITTENDRIGH, DR. COLIN  
Princeton University  
Princeton, New Jersey
- RANK, PROF. DAVID  
Pennsylvania State University  
University Park, Pennsylvania
- REA, DR. DONALD G.  
University of California  
Space Sciences Laboratory  
Berkeley, California
- READ, DR. RICHARD B.  
California Institute of Technology
- REIFF, GLENN  
National Aeronautics and Space  
Administration Headquarters
- RING, PROF. JAMES  
The University  
Hull, England
- RYAN, DR. J. A.  
Douglas Aircraft Company, Inc.  
Missile & Space Systems Division  
Santa Monica, California
- SAARI, JOHN M.  
Boeing Scientific Research Laboratories  
Seattle, Washington
- SADEK, DR. D.  
University of Israel
- SAFFREN, DR. M. M.  
Jet Propulsion Laboratory
- SAGAN, DR. CARL  
Harvard College Observatory and  
Smithsonian Astrophysical Observatory  
Cambridge, Massachusetts
- SCHILLING, DR. G. F.  
The RAND Corporation  
Santa Monica, California
- SCHORN, DR. RONALD  
Jet Propulsion Laboratory
- SCHURMEIER, HARRIS M.  
Jet Propulsion Laboratory
- SCULL, JOHN R.  
Jet Propulsion Laboratory
- SHOEMAKER, DR. EUGENE M.  
U. S. Geological Survey  
Branch of Astrogeology  
Flagstaff, Arizona
- SHORTILL, DR. RICHARD W.  
Boeing Scientific Research Laboratories  
Seattle, Washington
- SISCOE, DR. GEORGE L.  
California Institute of Technology
- SIX, DR. N. F.  
Scientific Research Laboratories  
Brown Engineering Company  
Huntsville, Alabama
- SMITH, DR. ALEX G.  
University of Florida  
Gainesville, Florida
- SMITH, BRADFORD A.  
New Mexico State University Observatory  
University Park, New Mexico
- SMITH, DR. HARLAN J.  
University of Texas  
Austin, Texas
- SPEED, DR. ROBERT C.  
Jet Propulsion Laboratory
- SPINRAD, DR. HYRON  
University of California  
Berkeley, California
- STANLEY, DR. GORDON J.  
California Institute of Technology
- STEWART, DR. HOMER J.  
Jet Propulsion Laboratory
- STRONG, PROF. JOHN  
The Johns Hopkins University  
Laboratory of Astrophysics and  
Physical Meteorology  
Baltimore, Maryland
- SUESS, DR. HANS  
Scripps Institute of Oceanography  
La Jolla, California
- THOMSON, DR. J. H.  
University of Manchester  
Nuffield Radio Astronomy Laboratories  
Jodrell Bank  
Macclesfield, Cheshire, England
- TOMBAUGH, CLYDE  
New Mexico State University Observatory  
University Park, New Mexico
- TROITSKY, DR. V. S.  
Scientific Research Radiophysics Institute  
Arzamasskoye shosse  
Gorky, USSR

## LIST OF PARTICIPANTS (Cont'd)

TURKEVICH, DR. ANTHONY  
University of Chicago  
Chicago, Illinois

UREY, DR. HAROLD C.  
University of California  
La Jolla, California

VANGO, STEPHEN P.  
Jet Propulsion Laboratory

VREBALOVICH, DR. THOMAS  
Jet Propulsion Laboratory

WARWICK, DR. JAMES W.  
University of Colorado  
Boulder, Colorado

WELCH, DR. W. J.  
University of California  
Radio Astronomy Laboratory  
Berkeley, California

WESTON, DR. C. R.  
University of Rochester  
Department of Biology  
Rochester, New York

WILDT, PROF. R.  
Yale University Observatory  
New Haven, Connecticut

YOUNG, DR. ROBERT  
National Aeronautics and Space Administration  
Ames Research Center  
Moffett Field, California

YOUNKIN, ROBERT L.  
Jet Propulsion Laboratory

## OPENING REMARKS

*Lee A. DuBridge, President*

*California Institute of Technology  
Pasadena, California*

It is a very great pleasure to welcome you to this conference on lunar and planetary science. I think you will agree that the last couple of years have been pretty exciting ones in what we have been learning about the solar system. Hence this seems a most appropriate time to try to bring the results of our experiments and our speculations together and to see what we know, where our knowledge is still incomplete or fuzzy, and what our future program of experimental work should be.

I am sure it is correct to say that there has not been so much progress and so much excitement in the field of planetary science since the days of Galileo, Kepler, and Newton. The work of these giants opened up the whole new field of celestial mechanics (as well, of course, as ordinary mechanics), a field in which lively interest was maintained for two centuries.

Toward the end of the 19th century, however, interest in this field was declining. This was partly because the essential problems seemed to have been solved except for the puzzling phenomenon of the precession of the perihelion of Mercury, which remained a mystery until

Albert Einstein came along. The decline in interest in the planets was partly attributable to the fact that nearly all the observations had been made that could be made with the instrumentation then available. More importantly, however, the development of very large telescopes extended the astronomers' field of view far beyond the solar system into our galaxy and later into the most distant reaches of space. With the development of the concept of the expanding universe, through the work of Hubble and Humason, a new era in cosmology came into being, which has captured the attention of astronomers for the past 40 years and whose mysteries still occupy a major share of their attention. I do not need to recite here all the exciting discoveries and speculations that have been taking place in galactic astronomy during the past 20 years, with new mysteries having opened up in the past two years.

However, the past few years have also seen a tremendous rebirth of interest in the solar system. Without doubt the major cause for this new interest was the coming of the space age and the opening up of possibilities of sending spacecraft to the Moon, to the nearby

planets, and the intervening interplanetary space. At the same time, however, there have been other important developments to reopen solar system investigations; namely, the radio telescope, new techniques of making radar observations on the Moon and the nearby planets, new instrumentation for infrared measurements and for infrared and optical spectroscopy. In addition to this, the work of the astronomers, the nuclear physicists, and the geochemists has given us new insight into the origin and history of the universe and of the solar system, and these theoretical considerations are a spur to new experiments and new observations.

What we have learned about the Moon and planets during recent years surely makes an impressive catalogue of items that will be given extensive discussion during the coming days. We have obtained closeup views of the Moon's surface, revealing craters and other surface features down to a scale size of less than two feet. We have obtained our first good look at the surface of Mars—and have been astounded by its similarity to the Moon. The Earth, with its relatively violent actions of erosion and geologic activity, can have its surface features changed radically in a few million years. The Moon and Mars have changed almost not at all, retaining the scars of meteoric impacts for several billion years.

We have found that Venus and Mars have no detectable magnetic fields; Venus because of its slow spin, Mars because its low mass has not produced a liquid metallic core—further evidence of its internal deadness. Venus has been found to have a surprisingly high surface temperature. Mars has an even lower atmospheric pressure than we had previously thought, and our plans for landing capsules on its surface have had to be changed. We have discovered the Van Allen layer around the Earth—and have measured the radiation from the far more dense ionized layers around Jupiter. We have learned about solar winds and accompanying magnetic fields—and their extraordinary interaction with the Earth's field.

We have measured the distance to the planets far more accurately than ever before and have determined the masses of the Moon, Venus, and Mars to much greater precision. Centimeter-wave doppler measurements can determine the relative positions of a spacecraft to a fraction of a wavelength—but converting these numbers into centimeters or kilometers is limited by the uncertainty in our value of the velocity of light. Can some one think of a way of measuring that quantity to a precision 100 times better than heretofore?

Yes, our list of new information is an impressive one. Yet we have not scratched the surface. We have not scratched the surface of the Moon and we are still quite ignorant about its texture and composition. More so for Mars. The surface of Venus seems out of reach of our instruments for a long time to come. What about Mercury? Is it like the Moon and Mars? That is now a question that is surely within our capabilities to answer.

Most important of all, the question of life on Mars remains unanswered. Mars looks like a pretty inhospitable place for human beings from Earth. It is not a good place to which to export our excess population! Certainly the method of origin and evolution of life on that planet is hard for us to visualize at present. But even if we can't visualize, we can do experiments—and that is the only way we can know.

In short, there are some pretty interesting years ahead.

Caltech, the Jet Propulsion Laboratory, and NASA are sponsoring this five-day conference to try to bring into focus this new information and these new ideas that have emerged about our solar system in recent years and to examine carefully the gaps in our knowledge that should be filled in the years that lie ahead. It is clear that the exploration of the solar system has now become a vast and a very expensive scientific enterprise. It is therefore evident that our explorations and our observations, both from spacecraft and from the Earth, need to be given careful scientific analysis and need to be subjected to extensive scientific planning. Such planning must be preceded by critical examination of what we now know, what we partly know, and what we do not know at all, and this must lead to sound scientific judgments on which things are most important to find out soon, and which can be deferred.

This is intended to be a working conference. We have selected our list of invitees with great care, confining it to those with an active interest and active participation in scientific observations relating to the Moon and the planets. We hope that by having kept the group down to a moderate size and confining it to those with competence in the field that we can have full, frank, and critical discussions of the exciting scientific problems of the solar system.

I want to thank all of you for coming. I want to thank especially Professor Harrison Brown, who has been the chairman of the committee to arrange this event, and Dr. Al Hibbs, who has been the active and energetic manager of the conference.



*I. THE MOON*

## PART I. THE MOON

- H. C. Urey, Observations on the *Ranger VIII* and *IX* Pictures
- G. P. Kuiper, Interpretation of the *Ranger* Records
- E. M. Shoemaker, Progress in the Analysis of the Fine Structure and Geology of the Lunar Surface From the *Ranger VIII* and *IX* Photographs
- B. C. Murray, Current Problems in the Interpretation of Lunar Physical Observations
- V. S. Troitsky, Investigation of the Surfaces of the Moon and Planets by the Thermal Radiation
- V. S. Troitsky, Some Remarks on New Measurements of Lunar Temperature at the Antisolar Point
- B. J. Levin, The Structure of the Moon
- G. J. F. MacDonald, On the Constitution and Origin of the Moon
- D. L. Anderson and R. L. Kovach, The Internal Structure of the Moon and the Terrestrial Planets
- J. A. O'Keefe and I. Adler, Lunar Structure as Deduced From Muong Nong Tektites
- H. S. Brown, Summary Remarks on the Moon

The papers given by Dr. Gerard P. Kuiper and Dr. Eugene M. Shoemaker are presented here in abstracted versions. The complete papers appear in *Ranger VIII and IX, Part II: Experimenters' Analyses and Interpretations*, Technical Report No. 32-800, Jet Propulsion Laboratory, Pasadena, California, March 15, 1966. Other reports published by the Jet Propulsion Laboratory on the results of the *Ranger* flights include the following:

*Ranger VII, Photographs of the Moon, Part I: Camera "A" Series*, August 27, 1964; *Part II: Camera "B" Series*, December 15, 1964; *Part III: Camera "P" Series*, February 10, 1965; *Ranger VIII, Photographs of the Moon*, December 15, 1965; *Ranger IX, Photographs of the Moon*, December 15, 1966.

*Ranger VII, Part II: Experimenters' Analyses and Interpretations*, Technical Report No. 32-700, February 10, 1965.

N66 31 447

## OBSERVATIONS ON THE RANGER VIII AND IX PICTURES

*Harold C. Urey*

*University of California, San Diego  
La Jolla, California*

Pictures are a limited way of investigating a physical problem. On the other hand, in many ways they are a good beginning for the investigation of a subject which cannot otherwise be seen in detail, such as the Moon at a distance of 384,000 km from the Earth. However, the picture should be judged in relation to other physical evidence. It is the purpose of this introductory statement to outline some of the physical evidence secured by other methods which bear on the problem of interpreting the photographs of the lunar surface.

I have assumed that the Moon was captured by the Earth and that it is thus a more primitive object than the Earth and the planets. It is assumed to have accumulated from materials of solar composition and hence to contain less iron than typical meteorites and the terrestrial planets. It is also assumed to have had a molten layer on its surface at one time, with a layer of iron-nickel below. However, it moved about the Sun in the neighborhood of the Earth and accumulated a surficial layer of material of terrestrial composition. The thickness of the layer has not been estimated, but a depth of kilometers or tens of

kilometers of broken-up material is predicted on the basis of this model.

Some favor the view that the Moon escaped from the Earth, although most experts regard this theory as improbable or impossible. If the Moon is of terrestrial origin, then all evidence of the violent separation process has been covered up by subsequent collisional processes. In this case, the surface will be badly broken up for some depth and, in fact, may have the same sort of structure as that outlined for the previous model.

Another school assumes that the Earth and the Moon have the same chemical composition and that the core of the Earth consists of high-density silicates and not of iron-nickel. It is then assumed that the Moon was formed in the neighborhood of the Earth. I have rejected this model because of the fundamental hypothesis on which it is based. The density of Mars and Mercury and the composition of the meteorites do not agree with this postulate. There remains the difficulty of the differing compositions of the Sun and terrestrial planets. Some



believe that the solar composition is the primitive composition, that the Earth has this composition, and that its core is not iron-nickel. Others believe that the Earth and the meteorites have the primitive composition and that astronomers are in error in regard to the solar composition. I argue that the Sun and terrestrial planets have different compositions and, hence, that involved cosmic chemical engineering processes are needed to produce the differences in composition of the planets and the Moon. But if I had to select one or the other model, I would prefer the assumption that the solar values are incorrect. In this case, the Moon must have escaped from the Earth. Although I reject the assumption that the Moon accumulated near the Earth, the model may be accepted by others; again, this would require that the surface of the Moon consist of highly broken and fragmented material.

In any case, great crevasses and cavities probably existed beneath the surface and have been modified to some extent, though not removed completely, during the life of the Moon.

The Moon is a triaxial ellipsoid with three moments of inertia whose values are not consistent with the forces acting upon the Moon at the present time. These values have been reviewed by astronomers for many years, with little change resulting in the final values. When the moments of inertia are converted to radii, assuming uniform density of the Moon, it is found that there are projections toward and away from the Earth about 1 km in height as compared with the polar radius, and the radius is perpendicular to these two radii, whereas the equilibrium height should be in the neighborhood of 60 m. This implies one of two possibilities: a substantial stress of about 20 bars must exist at the center of the Moon if the Moon has strength throughout; or an outer shell of the Moon must have sufficient strength to support the nonequilibrium shape.

The suggestion that the Moon has sufficient strength throughout to support the difference in elevation seems unlikely when one considers the great length of time that is to be taken as a reasonable age of the Moon.

A second suggestion was made by Urey *et al.* (Ref. 1), namely, that there is a variation of density with angle in the body of the Moon, the least dense material being distributed along the axis pointing toward the Earth, the densest material in the polar direction, and a material of intermediate density along the axis perpendicular to these. This hypothesis requires much less strength than

the first, and it requires a mechanism for the origin of the Moon which would produce the difference in density distribution with angle.

A third explanation is that slow convection occurs on the interior of the Moon, with rising currents of matter toward and away from the Earth along the axis pointing toward the Earth, and falling currents in the regions of the limb of the Moon. This theory is favored by Runcorn (Ref. 2).

It would seem to this author that the first suggestion is unlikely but that the latter two are possibilities. In any case, all three of them require a relatively cold Moon to account for the triaxial ellipsoidal shape.

The differences in elevation on the lunar surface, with comparatively deep areas in the region of the maria and rather high mountainous areas in other regions, have been studied by Baldwin (Ref. 3), but there is some disagreement in regard to his results. Watts (Ref. 4) has found differences in elevation on the limb of the Moon, with one case on the eastern limb amounting to some 10 km. Rather simple calculations show that if the Moon had the rigidity of the Earth, such differences in elevation would have decreased considerably in comparatively short periods of time (say, a quarter of a billion to a billion years). This again speaks for a cold interior of the Moon.

These arguments have been revived recently by Urey and are considered pertinent to the problem of lava flows on the Moon. It is surprising that very little attention has been given to these considerations by other students of the *Ranger* pictures.

Proceeding on the basis of such observational facts, Urey (Refs. 5 and 6) and MacDonald (Ref. 7) have tried to construct thermal histories for the Moon that would be consistent with these observations. They assumed low temperatures for the Moon at origin ( $0^{\circ}\text{C}$  for example), and found that only the deep interior of the Moon should have melted. Slightly different physical constants were used, but the results were in substantial agreement. Urey in particular concluded that if a thermal diffusivity of 0.005 in cgs units and calories were assumed, if the abundances of K, U, and Th in the chondritic meteorites were used, and if an initial temperature of  $0^{\circ}$  were postulated, then complete melting would occur only near the center of the Moon. MacDonald obtained similar values, starting with an initially cold Moon, and showed that the values would be considerably higher if some  $600^{\circ}\text{C}$  were assumed for the initial condition. There is no basis for

choice of the initial conditions except the evidence that the Moon has irregular shapes that favor a low temperature.

The Russian school has assumed a higher temperature for the interior of the Moon, and consequently, a highly melted core. This assumption seems quite unreasonable to the writer. Since silicate liquid is less dense than its solid, a melted interior would be unstable, and outer parts of the Moon should sink to the interior. Hence, enormous lava flows would be characteristic if this were the correct thermal history. Of course, convection in the Moon would probably transport heat more rapidly to the surface than thermal conductivity, in which case a colder Moon again would be expected. No more than slight melting seems likely in any case, which is the situation that exists in the mantle of the Earth. It seems most unlikely that the Moon would possess a higher temperature distribution than does the Earth and it seems equally unlikely that the silicate materials of the Moon can be melted more than to a slight extent.

In very general considerations, one should expect that small planetary objects will be colder than large ones because (1) the rate of heat generation is proportional to the volume, and the loss of heat is proportional in some way to the surface; and (2) the energy of accumulation per unit mass is less for the smaller objects, and hence, initial temperatures would probably be less. Thus, we would expect the Earth to have a high general temperature, Mars, for example, to have a lower temperature, and the Moon to be still cooler. It therefore seems reasonable to believe that the smaller planetary objects in the solar system are likely to have less volcanic activity than the larger ones. Also, it seems likely that lava flows and volcanic activity on the Moon have been substantially less than those on Mars and on the Earth. The recent *Mariner* photographs of Mars, though they supply us with only a small sampling of the surface, are nevertheless consistent with very limited volcanic activity over the area explored, a result which was expected and is reasonable. Dr. H. Brown of CIT and I pointed out some 15 years ago that the Clairaut constant of Mars was consistent with a smaller core than that of the Earth or no core at all, in agreement with the *Mariner IV* conclusions. It therefore seems appropriate to suggest that *possibly* the smooth areas of the Moon are not due to lava flows, as has been traditionally assumed for many years. I believe that this assumption was based on completely inadequate evidence, and that the people who proposed it long ago did so because no other explanations of the extensive smooth areas occurred to them. Were they living today, they might agree with the reasoning presented above.

Difficulties in regard to the lava hypothesis have been recognized in the past. The lava flows, if such they are, have apparently traveled over great distances. If they resemble such phenomena on the Earth in any way, they must have been very fluid (Ref. 8). Also, it is indeed surprising that so many separate lava flows should have occurred in the mountainous areas of the Moon, since one must assume that a pipe extending down 100 km or so in the interior of the Moon would bring lava out in many small pools, within craters and between craters, in all of the land areas of the Moon. This is a point brought to our attention by T. Gold (Ref. 9).

We also owe to Gold the suggestion that dust, which he first ascribed to erosion processes on the mountainous areas of the Moon (a postulate which does not seem to have stood up with time), was responsible for the smooth filling of the older craters and the great maria. Urey (Ref. 10) suggested that highly fragmented material was created by the great collisions that produced the maria and the large craters. He also suggested that perhaps temporary rains washed the dust off the mountainous areas into the neighboring regions. A number of people have discussed the dust problem since it was introduced by Gold, and much detailed argument has been devoted to the method of transport of the dust. It does seem to the author that Gold's suggestion of dust and the extension by Urey to fragmented material from the great collisions might well be considered as an alternative explanation for the smooth areas on the Moon, or that such material contributes to the phenomena to some extent.

In recent years, Gold in particular has emphasized the possible importance of water in the subsurface regions of the maria and has suggested specifically that some of the phenomena of permafrost regions of the Earth are in evidence in the lunar mare areas. The question of the origin and composition of the maria is so complicated at the present time because of what I believe is good evidence for erosion by micrometeorites, possible proton bombardment, small and large macrometeorites, cometary collisions, possible evaporation of water from beneath the surface, probable lunar seismic activity, and other processes that it is too much to expect that pictures of the Moon, even those taken by the *Rangers*, would be able to provide a decisive answer.

There have been discussions of meteorites coming from the Moon, a suggestion which I believe goes back to the last century but which was reconsidered by the present author on what appear to be modern physical bases (Refs. 11 and 12). The stone meteorites have spent only

relatively short times in space (from some 25,000 up to perhaps 100 million years, with a rather large concentration of ages at 20 million years), whereas the iron meteorites are often hundreds of millions of years old, although some cosmic-ray ages are in a lower range. Therefore, it appeared possible that they were coming from two sources: the stones from the Moon and the irons from the asteroidal belt. Considerable study has been devoted to this subject in recent years, but the validity of the hypothesis is certainly not clear on the basis of meteorite studies, although a number of arguments are currently being presented which favor it. Because of the difference in composition of the meteorites and the nonvolatile fraction of the Sun, as reported by astronomers, it appears that the stone meteorites are some special sample of matter which probably originated in some specialized region such as the surface of the Moon or the surface of the larger asteroids, and that these materials do not represent a true average primordial composition. It is not unreasonable to consider the possibility that the stone meteorites do indeed come from the Moon, and it might even be that some of the irons also originated on this body. There are pros and cons to this problem (which will not be reviewed at this point) that will probably not be resolved until samples from the lunar surface are secured.

There have been persistent assumptions that tektites come from the Moon since the suggestion was made by Dr. Nininger some years ago which the present writer considered seriously on the occasion of an invitation to speak before the American Physical Society 10 years ago. However, the suggestion was rejected for reasons that still appear to be valid (Refs. 13 and 14). The tektites have a chemical composition which is very similar to that of certain granites or mixtures of sedimentary rocks or so-called ash flows on the Earth. They are high in silica and alumina, low in magnesium, and have other characteristics of this acid form of rock. Rocks of this composition are believed to be produced on the Earth mostly by remelting of sedimentary rocks that come from the water erosion of basalts, which in turn have been produced by extensive lava flows. It is difficult to conceive of a prominent fraction of the Moon's surface being of this composition. Furthermore, the tektites are observed only in limited areas of the Earth. One group arrived in southeast Asia and Australia 600,000 years ago; another group arrived in Europe about 15 million years ago, still another in North America some 30 million years ago, and a group in west Africa some 15 million years ago. In addition, there are fused silicas in the Libyan Desert and on the island of Tasmania that are very difficult to account for on the basis of melting processes on the Earth. It

seems highly unlikely that batches of material of this kind could have been thrown from the Moon to the Earth and could be located in these small patches only, and not spread uniformly all over the Earth. Also, some should have missed the Earth entirely and returned to collide with it again in a uniformly distributed pattern over the surface of the Earth. Experienced physical scientists will recognize the inherent probability of this type of collision, but although rather unusual and remarkable postulates have been made in regard to this problem, to the author's knowledge, no model of high probability has been devised. It seems likely that if material of approximately the composition of the tektites occurs on the Earth, it would be much more probable, and involve a much less energetic process, for such material to have been melted and scattered comparatively short distances over the Earth than to assume that similar collision and melting processes produced the objects on the Moon and distributed them only in localized areas 384,000 km away. I am rejecting the tektite hypothesis as I have rejected it in the past, but I believe that the meteorite hypothesis is not unreasonable. Incidentally, no one has suggested that the meteorites could not have come from the Moon because they fell uniformly over the Earth's surface and not in localized areas on a few distinct occasions.

The next item of consideration appears more doubtful, although during recent years considerable interest has been manifested in it. It has been reported that biological material exists in the carbonaceous chondrites. The possible existence of fossils in chondrites has been reported by reputable micropaleontologists, as has the existence of compounds characteristic of living things, such as the fatty acids, hydrocarbons, optically active compounds, and other materials of this sort. To me, possibly the most convincing evidence offered by micropaleontologists is their discovery of the residue of organisms that are very similar in many ways to well established microfossils on the Earth. If biological material is indigenous to these objects, the most reasonable postulate would be that they are coming from the Moon. If this should prove to be true, it seems very likely that the maria of the Moon consist partly of carbonaceous chondritic material, possibly mixed with water below the surface, and that the highlands consist of meteoritic material of the non-carbonaceous kind. I do not wish to present this possibility as a firmly established fact but only to say that I have been considering it for some years and have kept it in mind as I studied the *Ranger* pictures of the Moon.

In summary, there is considerable evidence that the lunar maria may not be the result of traditional lava flow

but may be filled with dust or fragmented material mixed with water. Also, the entire surface may consist of fragmented materials from many collisions for which evidence exists on the surface, as well as possibly many collisional layers below the visible one. It was with this background in mind that I approached the pictures taken by *Ranger VII*, as well as those obtained by *Rangers VIII* and *IX*. It is my firm conclusion in regard to the general problem that it is not possible, on the basis of pictures alone and what we can deduce from them, to decide firmly what the maria and the highland areas of the Moon consist of. They may be lava, or they may be fragmented material, and water may have played a part in the history of the Moon for a short period of time.\*

### A. Summary of the Ranger VII Observations

There are several very interesting features in the *Ranger VII* photographs which the author mentioned in the *Ranger VII* report (Ref. 16) and which have been discussed by others. During the past year, since the *Ranger VII* mission, the writer has had considerable occasion to think over his statements concerning these pictures.

It seems certain that considerable smoothing of the smaller craters has occurred, which seems to have very nearly obliterated craters as large as 300 to 400 m in some cases. This interpretation indicates that the fragmented material on the inside of these craters is some 30 to 40 m deep. Related to the interpretation of this smoothing effect is another observation, namely, that there appear to be crevasses in certain areas consisting of very smooth material covered only slightly with finely divided matter. It is difficult to understand how comparatively small features of this kind could have been preserved if a considerable transport of fragmented material occurred. As far as I know, no satisfactory explanation of this apparent contradiction has been advanced.

There is certainly considerable evidence for collapse features of various kinds, as was pointed out in the *Ranger VII* report (Ref. 16) by the present author. Upon further consideration, I am still of the opinion that at least some of these features are indeed due to collapse into crevasses below the surface.

\*Gilvarry (Ref. 15) suggested that seas existed on the Moon for billions of years. In this case, extensive river systems should have been present, and extensive erosion should have occurred. Since no evidence exists for such effects, we must conclude that free water had no more than a very temporary existence on the Moon.

The explanation of the dimple craters as being the result of material draining through a hole at the bottom of the crater or of the scattering of material leaving a dimple-like depression seems reasonable, although L. Jaffe's alternative observation (Ref. 16) that finely divided material on a laboratory scale will in some cases settle down into an approximate dimple shape is worthy of serious consideration. It may be that the dimples, in some cases at least, were caused by the walls of a collision crater moving in slowly, that is, by a flow in the surface regions of the Moon. Gault has observed that dimple craters of small size sometimes are produced by high-velocity projectiles in loosely divided solid materials.

The "crater with the rocks," in which a fairly large object is suspended in the crater, was explained as possibly being due to the escape of water from the interior of the Moon or perhaps to some collisional effect. Since this hypothesis was put forward in the Experimenters' meeting last fall, my attention has been drawn to Gold's early discussions with his colleagues to the effect that this phenomenon was similar to the pingos of the frozen North of the Earth, and observations by Smalley and Ronca (Ref. 17), who also concluded that it might be due to water. I believe that water is the most reasonable explanation of the crater with the rocks.

The many secondary craters have attracted the attention of observers of the *Ranger* photographs. Clusters of craters appear to be definitely due to secondaries from large craters, though other small craters may, of course, also be secondaries. Certain of these secondaries appear to have come from Tycho, 1000 km away, or from Copernicus, some 600 km distant, the latter assumption having been made by Gault, Quaide and Overbeck (Ref. 18). In either case, this theory speaks for the projection of very large objects across the surface of the Moon for very substantial distances and suggests definitely that much smaller objects were probably thrown off the Moon when a crater such as Tycho was produced. Also, it may be that in the production of smaller craters, objects of the size of meteorites might indeed leave the Moon. The rows of craters that appeared in the *Ranger VII* photographs and the elongated gashes may be due to secondaries or they may, in some cases, be the collapse features previously suggested.

These *Ranger VII* photographs would indicate that friable material probably covers the Moon to depths of as much as 20 m and possibly even greater. There seems to be very little evidence supporting the view of extensive

lava flows in the photographs, although they do not exclude this possibility.

## B. The Ranger VIII Pictures

The landing area of Mare Tranquillitatis was chosen to make possible comparison with another mare area, and because Mare Tranquillitatis looks more like a lava flow than many other parts of the Moon. The mare has an irregular area and is very dark, as though a liquid of some kind had flowed back into all the bays. It has been my contention for many years that the lava produced during the fall of the planetesimal that created Mare Serenitatis flowed out over the neighboring areas of Mare Tranquillitatis. This lava appeared to be of a very dark kind. I have not abandoned this suggestion, even though others have pointed out that collisions of objects of this kind do not in general produce much liquid. However, arguments against the production of lava are based upon the assumption that one pure crystalline solid collides with another. If, on the other hand, the objects which fell on the Moon were not pure but heterogeneous in density and perhaps not well compacted, then sufficient heat might well have been generated throughout the colliding bodies to produce the lava flows.

A-camera photographs 46 to 51 show areas which appear to be slightly elevated with respect to neighboring regions, and there seem to be terminal walls at the edges of the more elevated smooth areas (Fig. 1). At first glance, these appear to be lava flows, but on closer examination, it is difficult to decide where the lava flows originated and in what directions they flowed. It seems possible that they are not lava flows at all. Note that the rilles appear to be sunken areas which for some reason have collapsed below the general level of the mare; irregular areas may be phenomena of the same sort. As pointed out above, the idea of recent lava flows on the Moon does not seem reasonable on energetic grounds.

There are many collapse features in the area covered by the *Ranger VIII* pictures. There is a beautiful dimple on B-camera photograph 90 (Fig. 2), a "square brick" depression, and the irregular and complicated "bathtub" on B86 (Fig. 3), all of which may well be collapse features which were not produced by simple collisions alone. There are also several lines of craters and shallow linear depressions. Dr. Shoemaker argues that these are due to the effects of objects projected from neighboring craters; that is, they are secondary craters of a certain kind. I find it difficult to be sure that this is the case and believe that some of them may indeed be collapse features.

The *Ranger VIII* pictures show many secondaries of a kind similar to those observed in the *Ranger VII* photographs. Undoubtedly, these can be assigned to secondaries from various large craters in the neighborhood, and the assignment to any particular crater in many cases can hardly be expected to be unique. There is a very interesting group of secondaries in Delambre, on the outside of the western wall and on the inside of the eastern wall, which could well be due to objects thrown from Langrenus in a single swarm, for example. The individual small craters have an elongation that suggests that they may have been formed by ejecta from Theophilus; but if this were the case, there would have had to be two groups of objects. It is difficult to choose between these possibilities. However, throughout the region photographed by *Ranger VIII* there are many craters that can undoubtedly be assigned to secondaries, and they seem to have been produced by large objects similar to those that produced the craters recorded by *Ranger VII*. Thus, it appears that very large objects have been thrown from these craters to considerable distances, just as was the case in the regions observed by *Ranger VII*.

There are projections above the surface shown in the pictures taken by *Ranger VIII*. In the lower right-hand corner of B-camera photograph 90 (Fig. 2), one sees very definite projections on the wall of the very nearly obliterated crater that look as though they may have been eroded from the wall. One, however, seems to be perched on the side of a small crater, and it would be quite easy to assume that the projection is the result of the collision that produced the crater. No "rocks in craters" of the type seen in the *Ranger VII* photographs have been observed in the *Ranger VIII* pictures.

The rilles are quite prominent and seem to be linear depressed areas, possibly similar to graben on the Earth. There is some disagreement in regard to the origin of the terrestrial graben, some maintaining that it is the result of a block being depressed by pressure from the sides, and others that the depression is due to expansion of the sides. The rilles would indicate that there has been some very general and large-scale movement of the lunar surface. However, it is difficult to see any evidence for this kind of movement. The rilles, of course, were seen in terrestrial photographs, and the *Ranger VIII* pictures add only minor details and therefore raise no new problems.

There are many ridges in the region covered by the *Ranger VIII* pictures, radiating from the collision of Mare Imbrium, that were seen in less detail in terrestrial photographs.





*I. THE MOON*

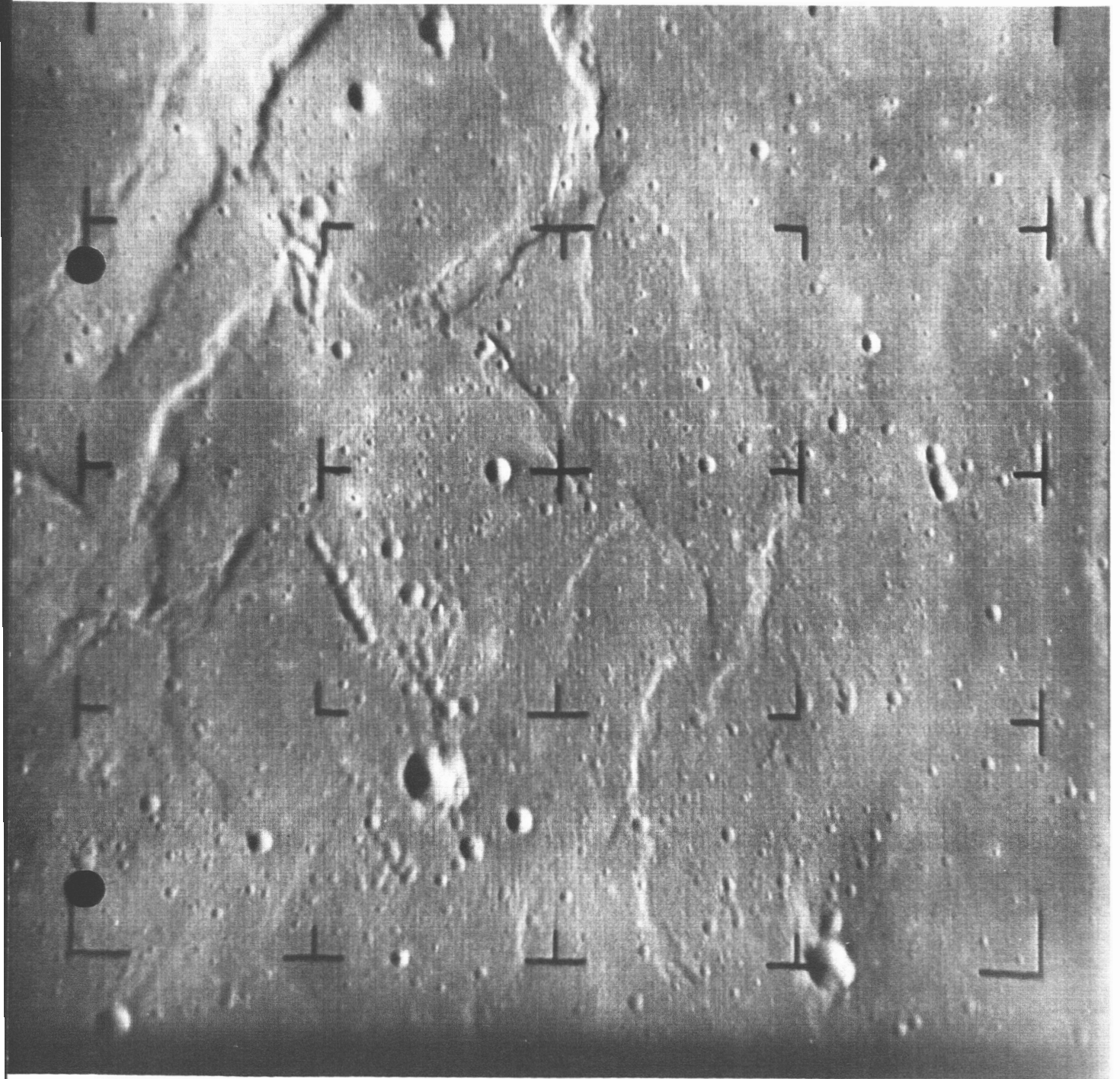


Fig. 1. *Ranger VIII* A-camera photograph 46, showing slightly elevated areas and apparent terminal walls at edges of more elevated, smooth regions.



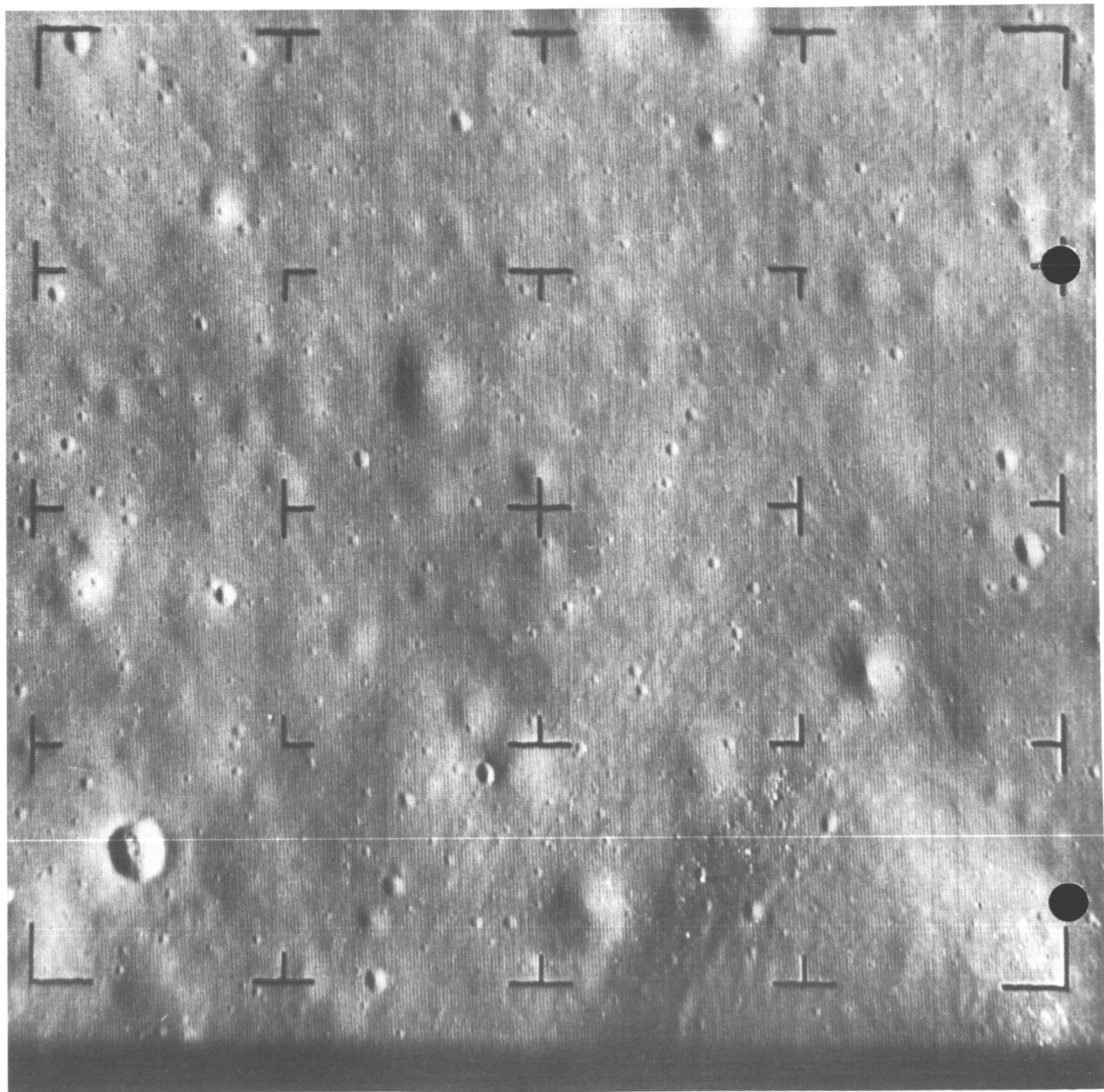


Fig. 2. *Ranger VIII* B-camera photograph 90, showing dimple crater as an example of collapse features found in the area.



Definite evidence for different types of collisional processes is found on these photographs, confirming similar evidence provided by terrestrial photographs. Thus, Delambre is known to be an older crater in the mountainous areas, with slump features in its walls and a rough floor and with no central peak. It is undoubtedly of collisional origin. On the other hand, Theon Junior and Theon Senior are two nearby collisional craters which have been formed in similar lunar material and have very smooth interiors. I suggest that Delambre was produced by a high-density object, and that the Theons were produced by low-density objects such as comet heads. (Photograph B22 [Fig. 4] shows these craters and features very well.) Other examples of both types are evident. A high-density object would penetrate into loosely conglomerated material and cause slumping, whereas a low-density object such as a comet head would produce a high-density, high-temperature mass of gas which could blow out smooth craters such as the Theons. These smooth craters are smaller than the craters with slumped walls, but I doubt that the difference can be ascribed entirely to size.

In general, little new information was obtained from the *Ranger VIII* pictures. They were unsatisfactory, in my opinion, because there was no nesting of the frames, so that the landing site was not present in any of the pictures. It was not possible, especially toward the end of the flight, to compare one picture with another in a satisfactory way. Comparison of the photographs is a feature I found particularly valuable in the *Ranger VII* series and very interesting in the case of *Ranger IX*.

### C. The *Ranger IX* Pictures

The *Ranger IX* landing area in Alphonsus is in a region of the Moon believed for various reasons to be of volcanic origin. Kozyrev (Refs. 19 and 20) reported the escape of gases from the neighborhood of the central peak, and Earth-based photographs showed halo craters (craters surrounded by dark areas) in considerable numbers within the crater Alphonsus. It had been supposed for a long time that the halos of darker material in the neighborhood of these craters were an indication of the escape of gases from the interior of the Moon. Kozyrev claimed to have detected the spectrum of  $C_2$ , but band spectroscopists are very skeptical about this interpretation. On the basis of Kozyrev's suggestion, I made the proposal that the dark areas were due to graphite because of the deposit of  $C_2$  on the surface. Of course, if Kozyrev's observation is not correct, this suggestion is not correct either. It has been pointed out that high-energy protons

would probably remove graphite in any case. The dark areas are quite similar in general appearance to dark areas on other parts of the Moon. This evidence for some sort of plutonic activity was an important reason for selecting Alphonsus for the *Ranger IX* landing site. It might be noted that Alphonsus is also a large crater filled with smooth material, and it was of interest to see whether this smooth material has characteristics similar to those of the mare areas. The B-camera took pictures to the east of Alphonsus, while the A-camera photographs covered the western areas predominantly; the landing area was to the north and east of the central peak.

Alphonsus is a very large crater, undoubtedly produced by the fall of a great object at some time in the past. The floor of the crater has been filled with smooth grey material, superimposed upon which are numerous craters and a central distribution of material oriented north and south, approximately in a direction toward the center of the Imbrian collision. This central region, which falls slightly to the west of the central peak, must have been produced during the formation of Mare Imbrium and consists either of material from the Imbrian collision itself or of material driven from the wall of Alphonsus by ejecta from the Imbrian collision. It will be noted, for example on photograph A55 (Fig. 5), that rather high cliffs occur on the western edge of this central mass, indicating that when it fell, it depressed the floor of the crater. This implies that the smooth material of the crater floor was in position before the Imbrian collision occurred; it also suggests that the smooth material of the crater floor was capable of considerable compaction, that is, that it is composed of unconsolidated material with ample pore space.

One of the marked general features which is immediately evident is that the number of craters per unit area within Alphonsus is greater than the number of craters on the Alphonsus crater walls. This indicates a very distinct difference between the kinds of material which make up the walls and those of the crater floor. It is also true that the number of craters within Alphonsus is different from the number of craters in the neighboring smooth areas to the west of the crater, and even the western part of Alphonsus has a lower crater density than the eastern part. It is probable that several different explanations of these phenomena will be advanced.

It appears evident that there is some difference between the composition of the Alphonsus crater wall material and that of the smooth material of the interior. This might be explained as being due to a difference in the number of objects falling within the crater to produce

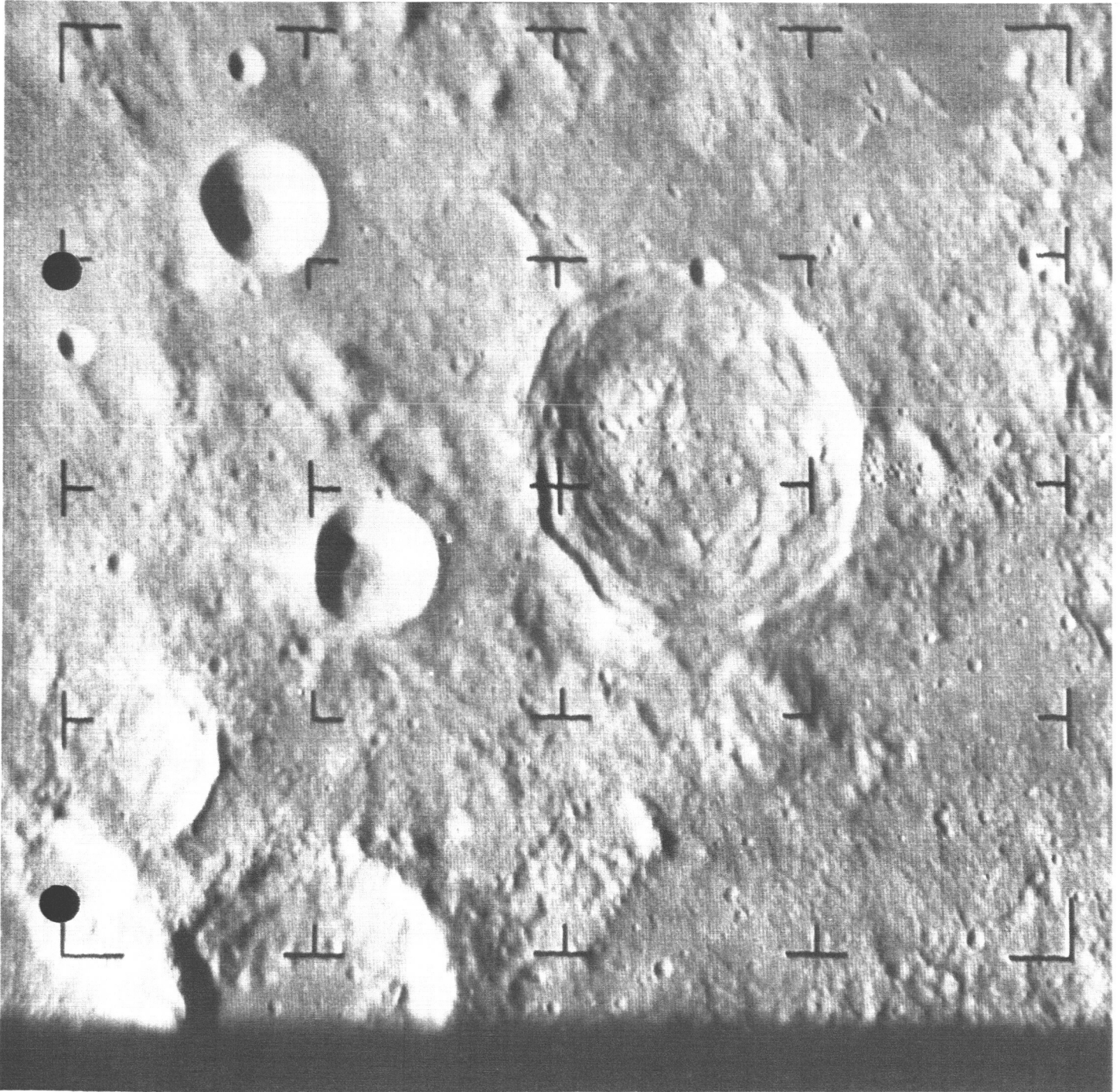


Fig. 4. *Ranger VIII* B-camera photograph 22, showing evidence for different types of collisional processes. (Delambre has slump features in its walls, a rough floor, and no central peaks; Theon Junior and Theon Senior have smooth interiors.)

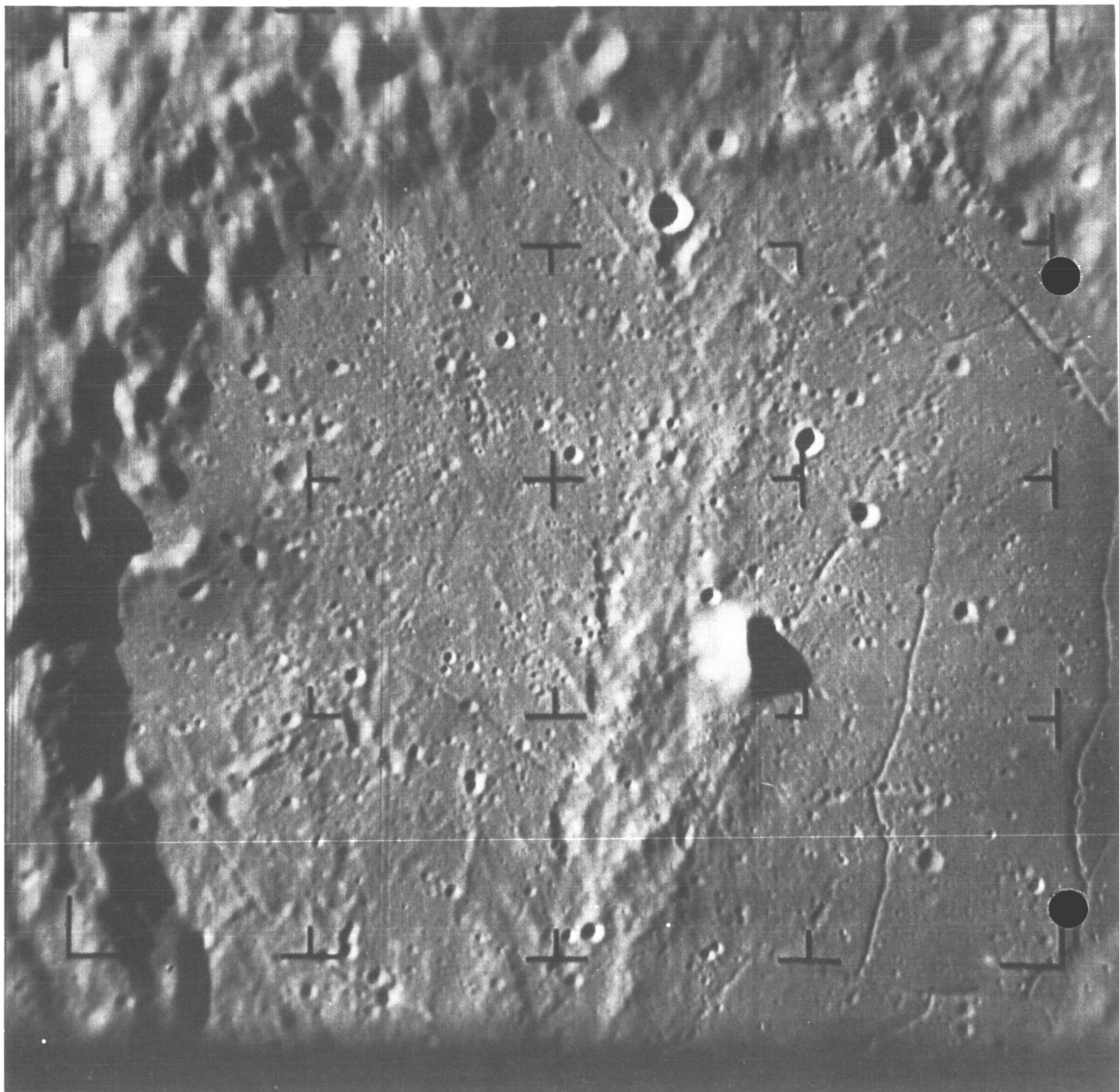


Fig. 5. *Ranger IX* A-camera photograph 55, showing high cliffs on W edge of central mass of Alphonsus. (Cliffs indicate that smooth crater-floor material was in position prior to Imbrian collision.)

small craters, in which case one would expect that most of them are secondaries and that for some reason an accidental variation occurred in the distribution of the falling objects. Another possible explanation is that the material within the crater was much more subject to the production of collapse craters than the material in the walls and outside. Undoubtedly, another explanation that will be offered is that more recent lava flows have occurred outside Alphonsus than within the crater. In regard to this last suggestion, it is curious that there is evidence for plutonic activity within Alphonsus, namely, the escape of gases from the interior of the Moon, whereas evidence of this kind outside the crater is far less obvious, if it exists at all. Some explanation for this apparent discrepancy can undoubtedly be given. It is difficult to arrive at a definite conclusion, except that there does seem to be evidence for a difference in physical properties of the crater walls and the floor regions.

Several kinds of craters are evident from the *Ranger IX* photographs. Many of the larger craters within Alphonsus are of the collisional type, and this type of crater also occurs to a considerable extent on the crater walls. Collisional craters appear to be approximately uniformly distributed between the interior of Alphonsus and the neighboring smooth areas, as well as in the mountainous regions. I believe that these craters are due to collisional effects that have been occurring since the general features were formed at some remote time.

Eruptive craters are characteristic of the Alphonsus floor and have been recognized on terrestrially obtained photographs for a good many years. They are in general surrounded with dark halos. Two in the west part of Alphonsus, beautifully shown on many A pictures (A46 [Fig. 1], for example) near the western wall, are quite obvious. One might think that these craters are primarily collisional in origin, but one of them is elliptical, lies on a crevasse, and is probably not collisional at all. Both craters are surrounded by the dark halos which are believed to consist of ash-like thrown-out material. This material obliterates some of the numerous craters in their neighborhood. Another eruptive crater lies just west of the central peak, again on a crevasse. These craters seem to be of a type that is quite distinct from most of the volcanic craters on Earth. Geologists whom I have consulted have confirmed this impression.

Other craters of the eruptive type can readily be seen on many other photographs. There are some eight, and possibly more, craters of this kind, most of which were detected on terrestrial photographs but are seen more clearly in the *Ranger IX* pictures. In general, they occur

on great crevasses. They appear to be due to the loss of gas from the interior of the Moon in an explosive or near-explosive type of eruption, and are surrounded by dark halos.

There appears to be no doubt but that many craters within the Alphonsus floor are collapse features. Great crevasses extend across the floor of the crater, in some cases terminating in rows of depressions which are probably craters of a collapse nature. For example, A46 (Fig. 1) gives a suggestion of this feature. It appears that many similar features in other areas of the Moon may indeed be due to collapse and not to secondary collisions. Other examples of features of this kind can be found in the *Ranger IX* photographs, as for instance in A26 (Fig. 6) near the northern part of the picture, just west of Davy. This particular depression might be interpreted as being due to a collision phenomenon, i.e., a group of objects having fallen in such a way as to produce the slightly curved linear feature, but because of the large size of the craters in the chain, it seems improbable that this is a correct explanation. The *Ranger IX* pictures have supplied a great deal of evidence for collapse features, which also seemed evident in *Ranger VII*. *Rangers VIII* and *IX* have reinforced my previous conclusion in this regard.

The paucity of craters on the mountainous areas and their mottled character have been mentioned previously. This is best seen on the B-camera photographs, ranging from about 45 down through 74 (Fig. 7). In the region shown in these pictures, the mountainous walls are covered with very poorly formed craters and with patches that reflect light more readily than the smooth crater floor. There are small craters in the relatively level mountainous regions, but craters on the walls are badly formed. This indicates that the crater walls consist of rather soft material, which slides down the hill in a collision. Gault and Quaide have made experiments on sloping loose material which suggest this explanation.

On the other hand, there are bright peaks in the crater walls, as seen in the east walls of Alphonsus, which extend above the surrounding areas as though they consisted of more durable material than the surroundings and therefore were able to maintain themselves on the top of the peak as other material was eroded to lower levels. It comes to mind immediately that this material may be iron-nickel or that it contains considerable amounts of iron-nickel. Material of the iron-nickel kind would be unlikely to retain its brightness under bombardment by protons from the Sun and by micrometeorites, but these brighter spots are actually only slightly brighter than their surroundings, though they do appear to be



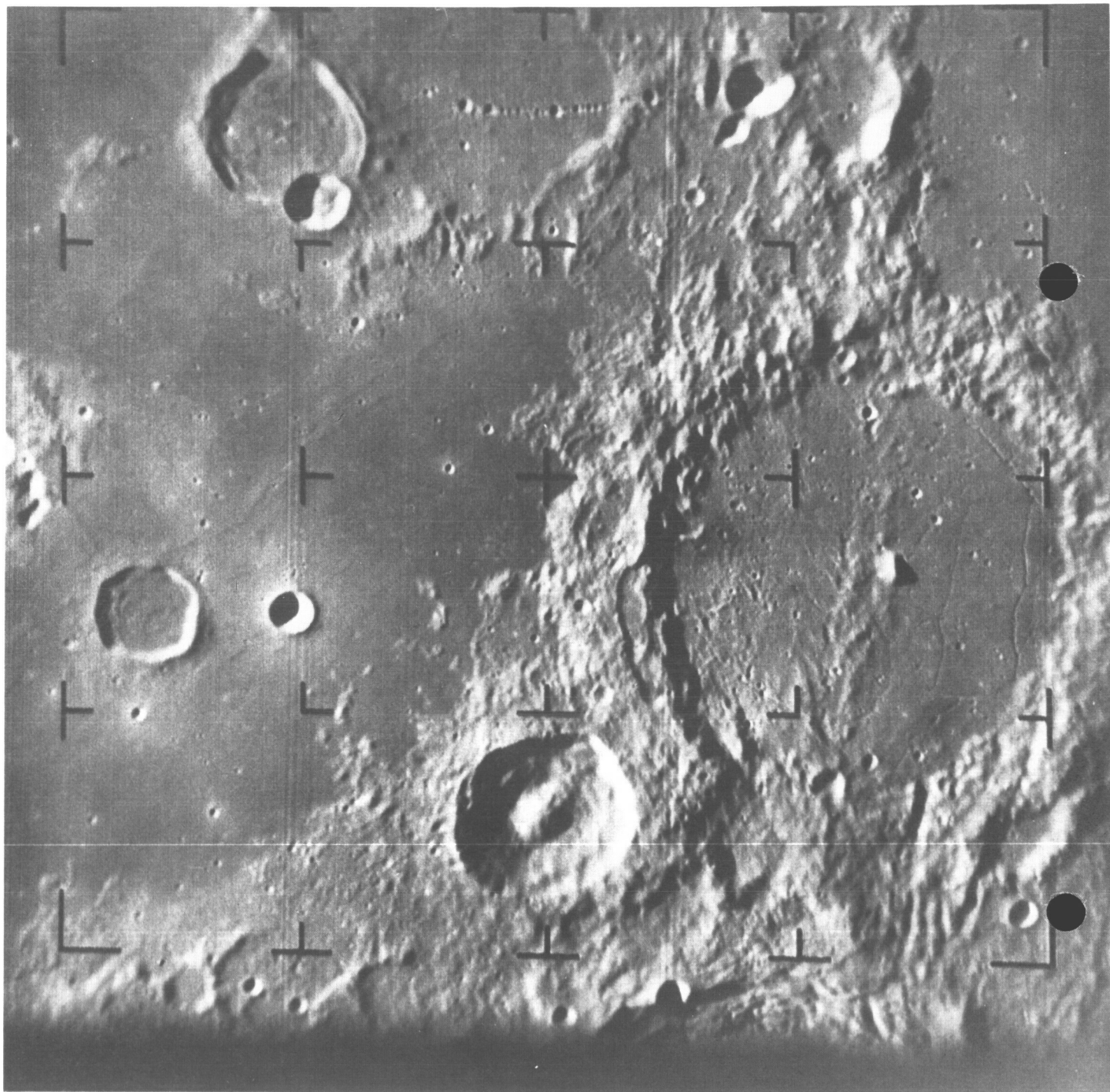


Fig. 6. *Ranger IX* A-camera photograph 26, showing example of collapse feature just W of Davy.

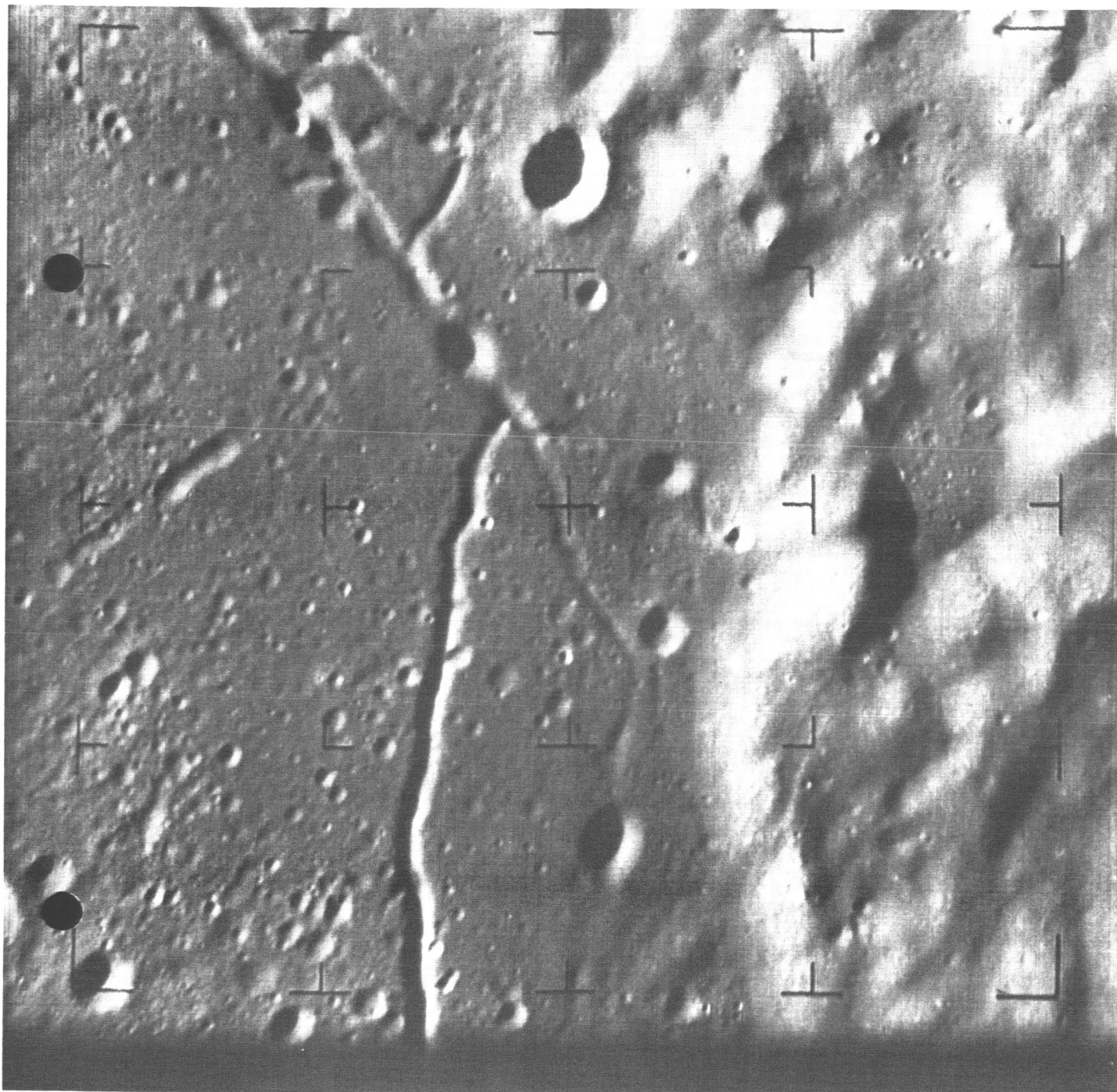


Fig. 7. *Ranger IX* B-camera photograph 74, illustrating paucity and mottled character of craters in mountainous areas.

considerably stronger. One would certainly expect, on almost any grounds, that some iron-nickel would be present on the lunar surface because of the bombardment by meteorite type of material during geologic time and probably during the terminal stage of the formation of the Earth-Moon system. One might call to attention that Urey's model for the Moon, as a primary object which developed substantial masses of iron-nickel below its surface (Ref. 12), is of precisely the nature needed to produce substantial masses of iron-nickel in the walls of a large crater such as Alphonsus. If the primitive Moon had a layer of iron-nickel at some unknown but, let us assume, short distance below the surface, then a massive collision such as that required to produce Alphonsus could well have lifted metallic iron-nickel from beneath the surface and left some masses distributed on the high areas of the crater walls.

There is a question as to whether or not the smooth areas within Alphonsus and neighboring craters, in patches within the crater walls and in the neighborhood of the craters, are lava flows, as many undoubtedly believe. As Gold remarked some 10 years ago, and as mentioned earlier, it seems odd that lava flows should have come up through all of this region of the Moon within craters, between craters, and in small areas in crater walls and outside them, and have left smooth lava flows sometimes apparently with approximately the same level as the large crater floor and sometimes with markedly different levels in the smooth areas. This theory assumes a very substantial volcanic activity, which, as explained in the introduction to this Part, seems improbable on energetic grounds. There are other reasons for questioning this interpretation. For example, photograph B74 (Fig. 7) shows a smooth dark area in the crater wall region at the right and, as a matter of fact, at the south end, a line leaving this region and extending southward to the crater floor. When I first saw this picture as it was being transmitted during the flight, it occurred to me that the dark patch might be the bottom of a dried-up lake and that the line at the south was the path of the overflow. Almost immediately thereafter, however, this initial explanation did not seem very probable, one of the reasons being that lower overflow regions might have existed through other paths from the postulated lake-bed area. But after a number of months of consideration, I am convinced that the postulate that such smooth areas as the one in question are indeed the bottoms of dried-up lake beds is probably just as reasonable as the postulate of lava flows, if not more so. On B35 (Fig. 8), for example, there are other areas in this region that might be discussed on a similar basis.

The high flat area on the western wall of Alphonsus, which Mr. Whitaker facetiously labeled "Lake Titicaca" as the pictures were arriving, is shown in A61 (Fig. 9) and neighboring pictures. This elevated smooth area on the western wall seems to have a slight rim around it on the east side and a higher wall in the west, and possibly an overflow region in the shadow toward the north. The area is approximately  $1\frac{1}{2}$  km above the floor of the crater. Is it not astonishing that a lava flow would come up through the broken and fragmented materials of the walls to a high level and not find some crevasses, some openings through the material of the crater wall to a lower level? It strikes me that the explanation of "Lake Titicaca" as a lava flow is unreasonable and that the possibility that it is indeed the remains of a temporary lake area is worthy of consideration.

The great crevasses within the floor of Alphonsus are, of course, obvious and were indicated in terrestrial photographs, although they can be seen in much greater detail in the *Ranger IX* pictures (for example, A61 [Fig. 9]). There is a concentration of them near the walls, and most follow the walls of the crater to some extent. There are others that have general directions across the crater floor, with possibly some preferred directions, which, however, are not sufficiently consistent to make it possible to draw any important conclusions relative to them.

Because of the illumination, there is always a tendency to see north and south crevasses of this kind more readily than east and west ones, though I do find two such lines of craters on A61 (Fig. 9) in the southeast region, running almost due east and west. The crevasses are evidently collapse features of a marked kind, and they often terminate in rows of craters extending from the crevasse area. In some cases, they cross the central Imbrian deposit, indicating that they were formed after this deposit was laid down on the crater floor. Some, I am sure, will maintain that these crevasses are of the same character as crevasses due to lava flows found on the Earth; I am skeptical of this explanation for reasons explained in the introduction to this Part. The highly broken and fragmented outer layers of the Moon due to its terminal collisional history also provide an adequate explanation. Again, they might well be the result of the evaporation of subsurface water along the lines suggested by Gold, Kopal, and myself, especially if evaporation occurred from solid water. One argument against the water hypothesis is that some of these crevasses enter the mountainous regions, such as the line of craters in the northern crater walls seen in A61 (Fig. 9) and the prominent line of craters mentioned earlier, lying to the west of Davy. A line of craters



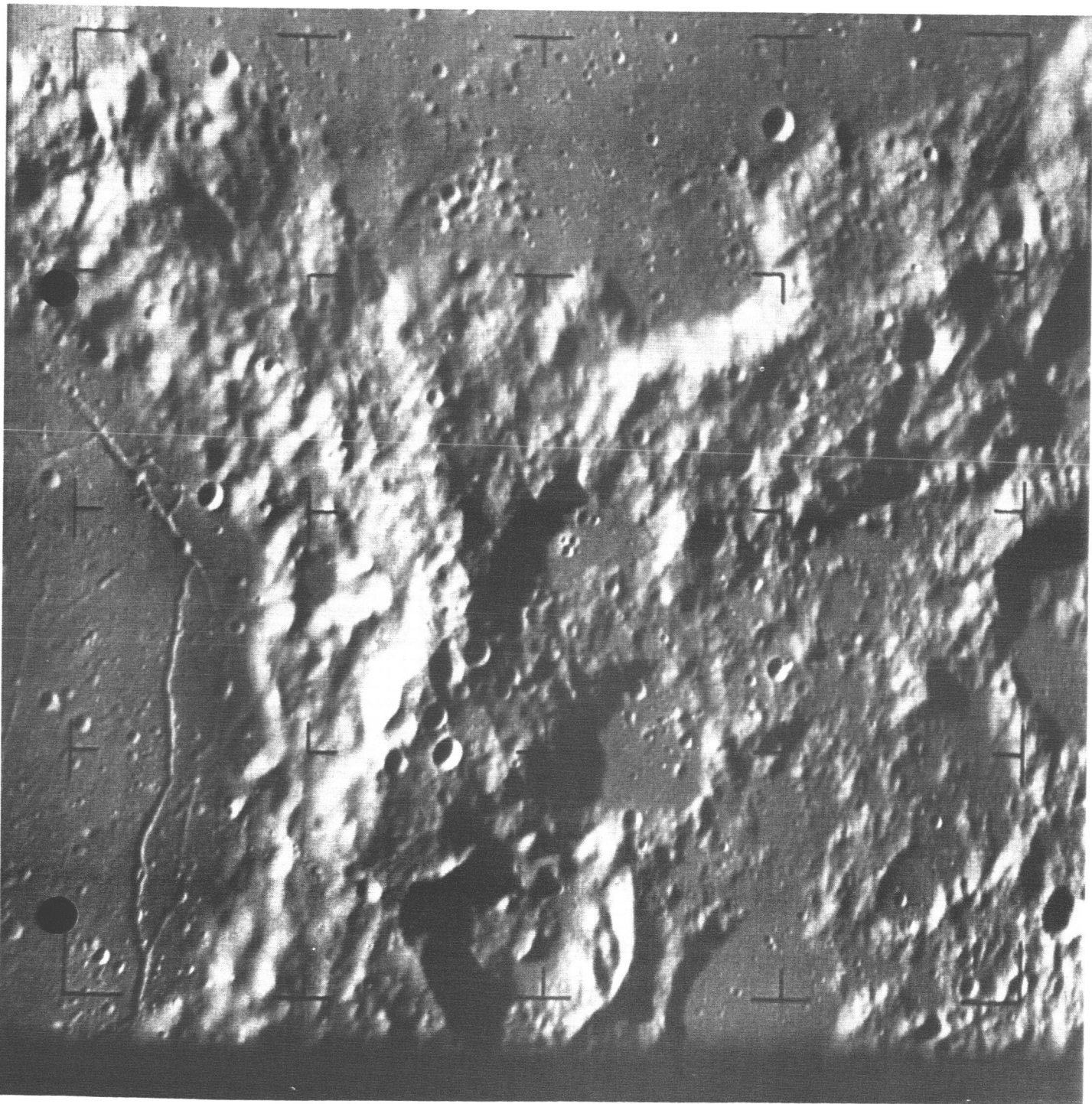


Fig. 8. Smooth areas such as those in *Ranger IX* B-camera photograph 35 support the postulate that these regions may be the bottoms of dried-up lake beds.



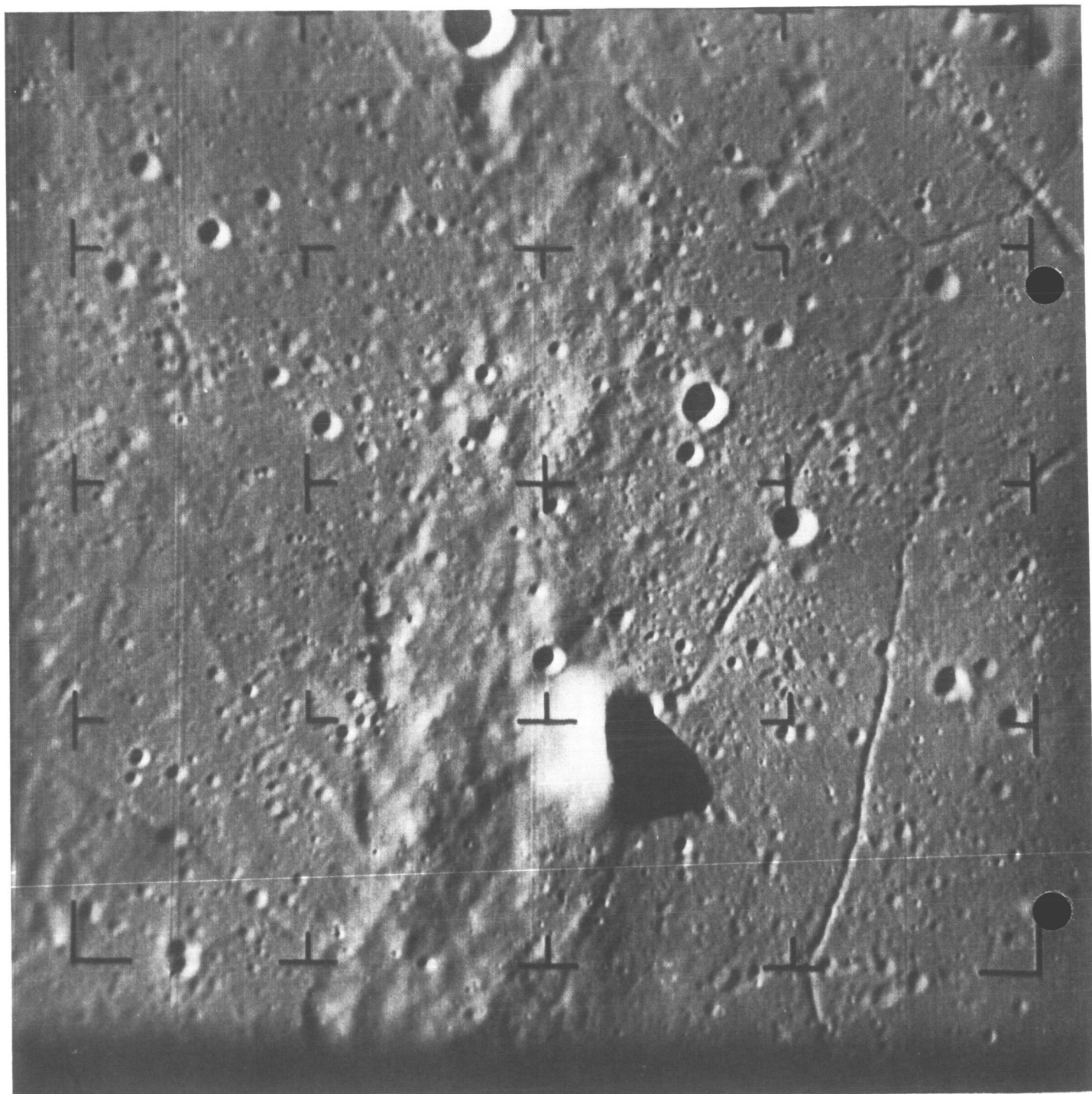


Fig. 9. *Ranger IX* A-camera photograph 61, showing "Lake Titicaca" on W wall of Alphonsus.

such as that in A61 also indicates that the source of the crevasses is not entirely related to the smooth material within the crater floors regardless of its origin or character. It is very likely that no particular single explanation will account for all of these features, and possibly more than one suggested mechanism has contributed to the final result.

At this point, it is appropriate to note Alpetragius and its curious peak, which has puzzled people for a long time. Gold (Ref. 22) and MacRae (Ref. 23) have suggested that this peak is related to the pingo phenomenon in regions where permafrost exists on the Earth. Of course, it is much larger than the usual pingo formations, which resemble the whole structure—crater wall and central rounded peak—in many ways. More specifically, the explanation suggests that in the collision which produced Alpetragius, an opening to lower sources of water was produced through which water flowed to the surface and froze, creating the curious rounded mass in the middle of the crater. I am not convinced of the validity of this explanation, but as far as I am aware, no other suitable explanation of this unusual peak has been offered. It just may be that it is another rare modification of a central peak produced by the collision phenomena that produced the craters on the Moon and, incidentally, apparently the central peaks of some of the craters on Mars.

It should also be noted that there are ridges in the floor of Alphonsus to the west of the central line of Imbrian debris which have a predominantly northwest-southeast orientation. These may be related to the fall of the Imbrian debris, which came from the north and fell with a component of velocity toward the south, possibly producing this effect.

The P pictures and the last B and A pictures show regions where smooth, pillowy masses appear in crevasses of moderate size (i.e., meters to tens of meters in width). These features are found in all three of the *Ranger* series of photographs. They are interpreted by Dr. Kuiper as conclusive evidence for the lava-flow hypothesis and for lava flows so recent that little dust has accumulated on the surface. If such lava flows are very ancient, i.e., 4.5 billion years old, then no fragmentation of the surface has occurred in all geologic time. This is highly improbable, for there is good reason to believe that much fragmentation due to micro- and macrometeorite infall, atomic-ion bombardment, etc., has occurred. The assumption of recent lava flows meets also with many difficulties when one considers the entire history of the lunar surface,

with its superimposed craters, maria, more craters, mountainous masses, etc. I have no specific solution to this difficulty, but if the permafrost hypothesis emphasized by Gold should be correct, it may be that an explanation of the pillow structures will be found in some movement of the permafrost.

## D. Summary

The *Ranger* pictures give considerable evidence supporting the view that the whole lunar surface—maria and terrae—consists of highly unconsolidated material. In the first place, because of the erosion caused by micrometeorites, small macrometeorites, bombardment with ionized atoms from the Sun, and heat and light and effects, we expect that some layer of fragmented material will be present. The fact that craters up to approximately 300 or 400 m appear to be smoothed over indicates that this erosion may be at least as deep as some 20 or 40 m in places.

The conclusions of Gault and Quaide, based upon their laboratory studies, are in accord with this general conclusion. There is, however, an element not consistent with this view, namely, the very smooth, rolling character of some of the crevasses in the lunar surface. No entirely satisfactory explanation of this inconsistency has occurred to the writer, but it is not certain at all that such features must be ascribed to lava flows upon which there had been no erosional effects of any kind since they were formed.

There is extensive evidence for slump features on the Moon. The dimple effect may indeed indicate that there is a hole at the bottom of the crater through which material drains, although I believe that this is not necessarily the only explanation for these objects. There are extensive crevasses in the maria and terrae. Large crevasses have been evident for years from Earth-based photographs, both in the smooth regions and in the mountainous regions. The *Ranger* pictures show many such features on a smaller scale. The slump features range from some tens of meters in size up to kilometers, with various sizes spanning the whole range almost continuously. These features are very similar in some ways to slump features on the Earth, mostly seen in connection with lava flows, although such slump features are rather small on the Earth, where they are due to the draining of lava from crusted-over channels. One of the major problems in ascribing the slump features on the Moon to similar phenomena is that it is difficult to see from what point the lava flowed and where it went, if it is actually lava.

There are extensive rows of slump features evident in the *Ranger VII*, *VIII*, and *IX* pictures. Sometimes it is difficult to distinguish between these and the elongated features that may have been produced by collisions.

Several sources for the crevasses below the surface can be postulated. (1) The cavities below the surface are the residue of such features produced by the original intense collisional processes that formed the surface of the Moon. (2) They may be due to the collapse of cavities left by lava flows (though I find it difficult to take this suggestion seriously). (3) If water was once present in the maria of the Moon below the surface, if it froze, and if it has evaporated over geologic time, it can be expected that great subsurface cavities and low-density material would exist. I feel sure that the first source of crevasses is present, and I am uncertain as to the others.

It has been evident that there are marked differences in nature as well as appearance between the maria and other smooth surfaces of the Moon and the mountainous areas. There is, for example, the difference in color. The mare areas in general are darker than the mountainous regions. Lava flows on the Earth are generally darker than the areas upon which they flow; but we must keep in mind that terrestrial areas are subject to the effects of water and oxygen in the air, which produce sediments and eroded material of lighter color than the lava flows. Such effects should not be present on the Moon. The mountainous areas can hardly be claimed to be light for the same reason that sedimentary and other rocks subjected to the action of water on the Earth have a light character. Studies made on the effect of proton bombardment on silicate materials indicate that all such materials turn dark under these conditions, some more so than others. Possibly Gold's suggestion of erosion from the mountainous masses to materials below has some merit in explaining the differences in color.

There are greater crater densities in Alphonsus than is generally true in the mountainous areas. The craters are mostly small and much more densely distributed than had been suspected from terrestrial photographs. The increased density of craters suggests to me that they are collapse features in many cases. In Alphonsus, at least, the greatly increased number of craters may be due in part to this effect.

The mottled character of the crater walls of Alphonsus indicates some inhomogeneity of composition, with some material having darkened less than other material. These are markedly brighter peaks than have been referred to,

which indicates that they erode less rapidly than neighboring material and have remained as rather definite projections on the tops of certain mountainous areas. Since, according to all suggested theories of the origin of the Moon, iron-nickel should be present on the lunar surface, it seems likely that these stronger masses consist of such material. Indeed, the mottled character of the mountainous crater walls may be due in part to this same composition.

The greatest source of controversy in regard to the surface of the Moon is, of course, the presence of lava in the maria and its origin, the possible presence of finely divided material, and the possible presence of water within this material as an explanation of the great smooth areas. Two sources of lava have been suggested. The first is internal, which postulates a high-temperature interior; for the various reasons outlined above, this appears to me to be quite improbable. But it would be reasonable to suppose that in the early history of the Moon, as it was accumulating and the intense bombardment of the surface took place, substantial temperatures existed below the surface even if it were not melted. Collisional effects of solid materials of a poorly consolidated character occurring at moderate temperatures could well have produced a considerable conversion of kinetic energy to heat energy and perhaps some melting. The origin of lava on the Moon was ascribed to the collisional processes by Gilbert some 72 years ago. In my early studies on this subject, I accepted Gilbert's conclusions. They have been criticized in subsequent years by people who maintain that collisional processes will not produce melting. There are difficulties with their arguments, in that collisional processes on the Moon of a sufficient magnitude to produce the maria probably did not involve materials of uniform composition and of highly consolidated character; hence, more heat may have been produced in such collisions than would be expected in collisions involving uniform and compact materials. There are also important difficulties with the origin of lava by melting deep in the lunar interior which, it seems to me, the proponents of the lava hypothesis have not tried to solve. However, I would not be willing to maintain that no lava flows of any kind have occurred on the Moon. I have thought that Mare Tranquillitatis looked like a large lava flow, and I still do; and there are a few terminal wall effects shown in the *Ranger VIII* pictures that would confirm this point of view.

That the maria of the Moon consist of dust or fragmented material is a hypothesis that goes back again to the early years of this century but which was brought forward in modern form by Gold some 10 years ago. It

seems to me that the processes postulated by him should be present to some extent. But I do believe that the great collisions that have produced the maria and the great craters of the Moon should have produced enormous quantities of fragmented material. Assuming temporary atmospheres during the enormous collisions that produced the maria, one would expect that substantial amounts of fragmented material would have fallen in localized areas of the lunar surface. Also, the larger collisions could well have penetrated below the outer surface of the Moon to regions where mixtures of gases, presumably mostly water, and solids similar to ignimbrite flows on the Earth could have been produced, accompanied by outwelling of enormous masses of finely fragmented material. Such flows on the Earth are of a very acid character, consisting of the granitic type of material. To postulate that material of this kind exists on the Moon implies some way of producing such material by processes presumably similar to those that have produced them on Earth. It is very difficult to believe that granites, which are the result of active and complicated igneous processes on the Earth, should be present as a prominent feature on the surface of the Moon. But possibly finely divided material of nongranitic composition may have been produced by different processes, such as the great collisions penetrating deep below the surface.

It would be difficult to prove the existence of water in the surface regions of the Moon from the results of these studies. It would be equally difficult to maintain definitely that it is not present. Escape of the Moon from the Earth might well have been accomplished by some retention of water on its surface. We know so little about the processes by which water is captured on planets during their formation that the possible capture of water on planetary objects is not necessarily excluded.

The halo craters in Alphonsus and elsewhere on the Moon are most readily explained as being due to the escape of gases from the interior which carry with them dust and ash-like material; the most likely gas to be expected is water. In fact, it is a general belief that the surface water of the Earth has come largely from the interior as a result of volcanic action. The halo craters do not look to me like typical Earth volcanoes, and they indicate a much milder type of plutonic activity than that characteristic of the Earth. Otherwise, I can find no reliable evidence from the *Ranger* pictures for the escape of water from the interior of the Moon.

Gold's explanation of Alpetragius' peak being related to the terrestrial pingo phenomenon is interesting, but of course, the evidence was present before the *Ranger* pictures were taken. The "crater with the rocks" of the *Ranger VII* pictures may be due to a similar effect, and there is a second crater shown in the *Ranger VII* series, with two black dots in it, that may indicate another crater of this kind. However, this sort of effect is not evident in any of the craters of the *Ranger VIII* and *IX* series.

Much has been learned about the lunar surface as a result of the *Ranger* pictures, but the interpretations are very controversial in character. It is to be hoped that actual samples of the lunar surface will be returned to the Earth. When this occurs, many of the postulates that are made in this discussion and others will be subjected to serious re-evaluation. A few samples taken almost at random on the Moon will settle the questions of whether differentiation of the lunar surface has occurred, whether granites and basalts are present, and thus, whether lava flows of a terrestrial type exist, and whether free water has had any part in shaping the surface. It is to be hoped that such chemical tests will be made in the future.

## REFERENCES

1. Urey, H. C., Elsasser, W. M., and Rochester, M. G., "Note on the Internal Structure of the Moon," *Astrophysical Journal*, Vol. 129 (1959), pp. 842-848.
2. Runcorn, S. K., "Convection in the Moon," *Nature*, Vol. 195 (1962), pp. 1150-1151.
3. Baldwin, R. B., *The Face of the Moon*, Chicago: University of Chicago Press (1949).
4. Watts, C. B., Private communication and address before AAAS meeting, Washington, D.C. (1958).
5. Urey, H. C., "Origin and History of the Moon," Chap. 13, *Physics and Astronomy of the Moon*, ed. by Z. Kopal, London: Academic Press (1962).
6. Urey, H. C., "Age of the Moon, Chemical Composition, Geological Aspects, Stress and Cooling History," *Proceedings of the Conference on Lunar Exploration*, Virginia Polytechnic Institute, Blacksburg, Va., August 1962 (1963), pp. III-1-III-31.
7. MacDonald, G. J. F., "Calculations on the Thermal History of the Earth," *Journal of Geophysical Research*, Vol. 64 (1959), pp. 1967-2000.
8. Dietz, R. S., "The Meteoritic Impact Origin of the Moon's Surface Features," *Journal of Geology*, Vol. 54 (1946), pp. 359-375.
9. Gold, T., "The Lunar Surface," *Monthly Notices of the Royal Society*, Vol. 115 (1955), pp. 585-604.
10. Urey, H. C., "The Origin of the Moon's Surface Features," *Sky and Telescope*, Vol. 15, Nos. 3 and 4 (1956), pp. 108-111 and 161-163.
11. Urey, H. C., "Primary and Secondary Objects," *Journal of Geophysical Research*, Vol. 64 (1959), pp. 1721-1737.
12. Urey, H. C., "Meteorites and the Moon," *Science*, Vol. 147 (1965), pp. 1262-1265.
13. Urey, H. C., "On the Origin of Tektites," *Proceedings of the National Academy of Sciences*, Vol. 41 (1955), pp. 27-31.
14. Urey, H. C., "Origin of Tektites," *Science*, Vol. 137 (1962), pp. 746-748.
15. Gilvarry, J. J., "The Nature of the Lunar Maria," *Astrophysical Journal*, Vol. 127 (1958), pp. 751-762.
16. *Ranger VII: Part II. Experimenters' Analyses and Interpretations*, Technical Report No. 32-700, Jet Propulsion Laboratory, Pasadena, California, February 10, 1965.
17. Smalley, V. G., and Ronca, L. B., Abstract, *Transactions of the American Geophysical Union*, Vol. 46 (1965), p. 138.
18. Gault, D. E., Quaide, W. L., and Overbeck, V. R., *Interpreting Ranger Photographs from Impact Cratering Studies*, Preprint, Goddard Space Flight Center, April 15-16, 1965.

## REFERENCES (Cont'd)

19. Kozyrev, N. A., "Observation of a Volcanic Process on the Moon," *Sky and Telescope*, Vol. 18 (1959), pp. 184-186.
20. Kozyrev, N. A., *The Moon*, ed. by Z. Kopal and Z. Mikhailov, New York: Academic Press (1959), p. 263.
21. Urey, H. C., "The Early History of the Solar System as Indicated by the Meteorites," *Proceedings of the Chemical Society*, London (March 1958), pp. 67-78.
22. Gold, T., Private communication (1965).
23. MacRae, D. A., paper presented at the American Astronomical Society Meeting, Montreal, Dec. 28-30, 1965.

## Acknowledgment

I wish to thank Dr. Alexander R. McBirney for interesting conversations in regard to this report. Following are some general comments made by him.

"I find no unequivocal evidence for lava flows. There is a scarcity or total lack of such features as broad lava shields with summit craters, fissure vents with lines of spatter cones, contrasting textures resulting from slight differences of vesiculation and oxidation, and fumarolic alteration in possible vent areas. Depressions thought by some workers to be collapsed lava tubes are too large to be compared with terrestrial lava tubes. There are few if any pressure ridges, flow lines, kipukas, and many other features that are also ubiquitous in lavas.

On the other hand, there is certainly evidence for mantle bedding by aerially deposited fragmental debris. It is difficult to state whether the debris results from collision or has been carried to the surface in gaseous eruptions. One would expect that if the cones were actually volcanic pyroclastic cones formed by gaseous eruptions, there would be a few recognizable lava flows

coming from the same vents. These cones could possibly be formed by gas discharges through a thick dust layer without any magmatic activity.

"In view of the present popularity of the theory that ignimbrites fill the maria, I have tried to find evidence for this, either pro or con. If magmatic activity has resulted in volcanism on the Moon, it would seem that ignimbrites of rhyolitic composition would be easier to produce than lavas of basaltic composition, provided the appropriate composition is available to be melted. Ignimbrites tend to produce very flat surfaces lacking the textural features of lava flows, and many of the maria fillings could well be composed of fragmental debris transported and deposited by 'nuées ardentes' or 'ash flows.' I do not believe that this question can be decided on the basis of the photographs alone, however.

"Many craters seem to be caused by subsidence or collapse. They are identical to collapse pits in volcanic regions or over large mine cavings. These are quite distinct in form from the more common bowl-shaped craters which are presumably impact scars."

N66 31448

## INTERPRETATION OF THE RANGER RECORDS

Gerard P. Kuiper

Lunar and Planetary Laboratory  
University of Arizona, Tucson, Arizona

### I. Ranger VIII and IX Coverage

The *Ranger VIII* and *IX* missions have enriched science with two massive files of pictorial documents of remarkable quality and immense value. Their influence will be felt for many years as supporting investigations progress. In this report, a full assessment of the scientific implications cannot yet be given.

*Ranger VIII* impacted in Mare Tranquillitatis on February 20, 1965, 01:58 GMT, at  $24.8^{\circ}$ E longitude and  $2.6^{\circ}$ N latitude, after having transmitted back to Earth over 7000 pictures. The high-resolution coverage occurs in typical mare terrain, crossed by a complex system of ridges already well recorded by Earth-based photography. This part of Mare Tranquillitatis is on the blue end of the scale of mare colors in contrast to Mare Cognitum, which is on the yellow end. The color differences between and within the maria are not large; but they are distinct and important, associated as they are with the process of mare deposition. The *Ranger VIII* records thus cover one extreme of the mare color scale, those of *Ranger VII* the other. The similarities between these maria (as noted below) are therefore likely to extend to all lunar maria.

The vertical path of *Ranger VIII* over the lunar surface and the directions of the A- and B-camera axes were such that the same terrain features were viewed with the B camera at two to three times the distance of the A camera; but since the focal length of the B camera is three times that of the A camera, the scales of corresponding photographs are similar, making possible stereoscopic viewing right up to impact. This expected application was a factor in the decision not to change the orientation of the spacecraft before impact by performing a terminal maneuver. *Ranger VIII* covered both upland and mare terrain, doing double duty in that sense, and its records have provided a very rich source of information.

*Rangers VII* and *VIII* having covered the range of mare colors, it appeared opportune to direct *Ranger IX* to one of the several large lunar craters. Among the obvious candidates was Alphonsus, whose central peak had been suspected of emitting gases, and which had eight prominent dark-halo craters on its floor, all but one associated with peripheral rilles on the crater floor. The impact (March 24, 1965, 06:08 GMT) was planned for an area between the central peak and a group of prominent dark-halo craters at  $2.4^{\circ}$ W longitude,  $12.9^{\circ}$ S latitude, with the A camera sweeping in from the side of

Mare Nubium and the B camera from the opposite direction. This configuration was achieved by commanding the spacecraft to execute its "nominal" terminal maneuver, which at the same time assured a minimum of image trailing close to the lunar surface. Thus, while in the case of *Ranger VIII*, the highest resolution in one coordinate was traded for increased overall coverage, the geometry of the *Ranger IX* approach favored the camera orientations provided by the nominal terminal maneuver and also yielded maximum attainable camera resolution.

The floor of Alphonsus was found to resemble mare-type terrain in almost every respect. All three *Ranger* missions, including *Ranger IX*, achieved maximum resolution for maria; in addition, good records of intermediate resolution were obtained for uplands and crater rims.

The emphasis in the *Ranger* program on mare-type terrain reflects the conviction that the maria are more likely to be comparatively "simple" and interpretable, since they are less precipitous than the uplands and have a shorter and less complex history. Because of the absence of large mountain systems, and a dense, overlapping distribution of craters, the maria also seemed to be the logical initial choice for unmanned and manned landings. In retrospect, these estimates appear to have been valid, although there are some reservations concerning the "simplicity" of the mare surface, owing to the discovery of the prevalence of collapse depressions, first detected by *Ranger VII* and later confirmed by the *Ranger VIII* and *IX* records.

## II. Summary of Results and Conclusions

The *Ranger* missions are among the Nation's most brilliant scientific achievements. Each of the last three flights carried out flawlessly its over 100 commands, and each returned a vast collection of photographic records of incomparable resolution and quality. These records have closed the worst information gap extant concerning the Moon, covering dimensions from about  $\frac{1}{2}$  m to  $\frac{1}{2}$  km in the widely separated areas of Mare Cognitum, Mare Tranquillitatis, and the Alphonsus floor.

The *Ranger* records supply data that help answer some basic questions about the nature of the mare surface. It is inferred from them that the maria are lava deposits overlain with a layer of low-density rock froth a few meters thick, the uppermost part of which has been eroded by micrometeorite impacts and sputtering. From the radar-reflection data, it is inferred that the mare surface becomes very rough at 1 cm. This critical dimension is

assumed to be due to the "bubble" size of the rock froth, effective not only in the original deposit, but in its eroded form due to sputtering and its fragmented form due to impacts. The dust layer on this rough material is well below 1 cm. Beneath the visible cover of rock froth, an intricate system of tunnels developed in the lava deposits through drainage and relocation, which caused the surfaces of the maria and the mare-type terrain to exhibit near-circular collapse depressions. A number of identifiable caves have been found among these depressions. The close parallels noted between the lunar collapse features and those observed in terrestrial lava flows have opened up a wide field for further investigation and have suggested the development of field methods for lunar-surface exploration.

The sources and modes of deposition of the mare lavas have long been uncertain, but some answers to these questions have now emerged. Telescopic observation of Mare Imbrium provided the first good information not only on the existence of a succession of major lava flows on the maria but also on a likely source of the lavas. Apparently, the sources of the last phases of the mare flooding were associated with the ridges.

The Marius field of lava domes appears to have been a very active volcanic field. The field, with its system of major flows, illustrates (1) many typical volcanic vents and associated lava channels, bearing witness to the extraordinary local volcanic activity, and (2) the tremendous gains in resolution that must still be made before one can hope to understand the Moon adequately.

The deposition of the lavas and their solidification and cooling were accompanied by several groups of phenomena that have left observable marks on the surface: the sinuous rilles, the domes, the lineaments, the tree-bark structure on all three maria, and the many outcroppings, such as those on the Alphonsus floor. These phenomena, together with the collapse depressions, the ridges discussed in the *Ranger VII* Report, and the observed lava flows and their probable sources on Imbrium (referred to above), round out the interpretation of the maria as lava deposits.

With this explanation now well established, further research can be directed toward the determination of the individual sources for each of the maria and the details of the flooding process. Inspection of some of the *Ranger* photographs showing the Marius volcanic field suggests that part of this investigation can be accomplished from the Earth, provided an intensive effort is made at the best astronomical site available.



After the deposition of the mare floors and the formation of the many associated features (drainage tunnels, collapse structures, domes, faults, ridges, dark-halo craters, rilles, and other lineaments), meteoritic impacts added *primary-impact craters*. Their frequencies have been derived and tentatively interpreted, and their numbers are found to be *consistent with the meteorite counts*. Down to diameters of 22 m, these craters cover about 2.2% of the mare surface and down to 1-m diameters about 18%. However, among the post-mare craters, some very large objects occur, such as Archimedes and Plato, with flooded floors, clearly formed immediately post-mare. In addition, there are several moderate-size craters whose central mountains indicate that the subsurface layers of the mare were still hot when they were formed. The latter group is characterized by having central *vents* instead of central peaks: Timocharis, Lambert, Euler, and Pytheas in Mare Imbrium, and Plinius and Maskelyne in Mare Tranquillitatis. The unusual frequency of these two classes of large and very large post-mare craters formed within a comparatively short interval implies that they were the concluding phase of the initial intense (mostly pre-mare) bombardment of the Moon (attributed to impacts by *circumterrestrial* rather than asteroidal bodies), which included the phase of mare formation itself. The asteroidal impact rate increases with time because each collision in the asteroid ring increases the total exposed cross section of the asteroids.

The interpretation above has recently received support from two sources: (1) the primary crater counts and their explanation by Le Poole<sup>1</sup> confirm the increase in asteroid-type impacts during geologic time by at least one order of magnitude, and (2) the *Mariner IV* data indicate that the crater-forming rate on Mars has been about 15 times that on the lunar maria, which is consistent with the greater impact rate expected on Mars because of its greater proximity to the asteroid ring. On the other hand, the lunar pre-mare crater density appreciably exceeds that on Mars and clearly has a cause (impacts by circumterrestrial bodies) not operative on that planet.

Although the interpretation of the larger telescopically observed craters being due to primary impacts is widely accepted, efforts to discover alternative explanations for some of the large craters may prove fruitful. There are a number of puzzling cases among the large craters that appear to involve additional mechanisms. The *Ranger*

data are a vast source of information also for the investigation of large craters. Time has not permitted the inclusion of such studies in this report; in fact, except for a few experimental runs, the basic photogrammetric evaluations have not yet been made. The ACIC mapping program referred to earlier, coupled with photogrammetry, will in time supply a foundation for quantitative studies of the three *Ranger* impact areas.

The analysis of the ridges on Mare Tranquillitatis, which were well covered by *Ranger VIII*, is another important unfinished item in the *Ranger* evaluation program. A third is the discussion of the results of the picture analysis and clean-up performed by JPL, a process that has led to improved representation of the pictures themselves and has made possible the preparation of photometrically calibrated contour maps.

If allowance is made for the different Sun angles, it is seen that the *Ranger VII* and *IX* impact areas do not vary appreciably in their populations of small craters, but that the *Ranger VIII* impact area deviates. There are two known causes for this deviation: image motion during exposure (1.1 m), and differences in aspect and illumination. The second effect causes all craters to appear shallower in the *Ranger VIII* pictures than they do in the *Ranger VII* and *IX* records. Le Poole estimates that, for this reason, a crater with a true depth-to-diameter ratio of 1:5 appears as 1:8 in the *Ranger VIII* frames. Also, the image motion will transfer an increasing fraction of craters with  $D = 8$  m and less into the "soft" class. There seems to be a third effect, however, which is probably *local* in nature, and may be the result of a small local "deposition" effect (of recent date, to explain the absence of sharp craters).

The linear pattern was recognized in Strom's<sup>2</sup> discussion, although the prints used by him showed the system less clearly and included only a few lineaments. The directions noted are the same, however, as those found in earlier pictures; i.e., *they belong to the global lunar grid pattern*. This is very remarkable in view of the smallness of the features observed here, and implies considerable cohesiveness of the lunar crust even in the upper meter or so.

Another problem briefly considered in the *Ranger VII* Report is the nature of the long, narrow valleys ("grooves" or "scars") in Mare Cognitum, which are approximately oriented toward Bullialdus. With the additional evidence now available, the interpretation of these valleys may be

<sup>1</sup>Rudolph S. Le Poole, in Section III, *Ranger VIII and IX, Part II: Experimenters' Analyses and Interpretations*, Technical Report No. 32-800, Jet Propulsion Laboratory, Pasadena, California, March 15, 1966.

<sup>2</sup>Robert G. Strom, op. cit.

improved. A comparison of the Bullialdus features and others like them with the *Ranger VIII* and *IX* linear depressions leads to the conclusion that they all have basically the same kind of structure, namely, that they consist of aligned groups of from three to six adjacent or merging round collapse depressions, often around 0.6 km in width and 3 km long but sometimes having only half or a third these dimensions. The high-resolution *Ranger* pictures show sharp folds and furrows on the floors and walls of the depressions, quite like those found in the larger isolated collapse depressions; most of them belong to the lunar grid system.

The linearity of the beaded troughs observed on the Moon as well as their directions and their distinguishable fine structure all indicate that the collapses took place along dynamically determined structural lines or planes (not lava tunnels). There remains the question of whether the collapses resulted from the withdrawal of magma in these planes or occurred much later in the solid state. The presence of domes in some of these depressions favors the former explanation; also, the soft outlines of the troughs suggest that the collapse took place when the top layers were still in a *plastic state* and draped themselves over the cavities.

Rille-like depressions and beaded troughs occur also as part of the radial systems surrounding Langrenus, Aristoteles, Aristillus, and other craters. These radial systems have often been regarded as "scars" or "gouges," but their interpretation as collapse troughs over fissures appears more plausible. One argument is that the radial troughs are by far the strongest where their direction coincides with other known grid directions. To what extent the weaker and shorter grid troughs are due to collapse only, collapse stimulated by impact, or pure impact, cannot readily be ascertained from the present data.

On this connection, the Copernican system of beaded valleys presents some special aspects. The apparent increased frequency of the valleys within the large rays crossing Mare Imbrium and the roughness of the rays seen on the terminator would suggest the cause to be impact, unless the excess is due to photometric causes only. Stimulated collapses propagating along pre-existing structural lines of weakness are known to occur over subsurface mines; since they occur in cold and brittle rock, they lead to rougher interior contours. Information on the structural and engineering properties of the mare crust can probably be derived with the aid of existing studies of mine stopes and the causes of surface subsidence over mines.

The fracture systems seen over mines are similar to those of the depressions in lava fields, except that the latter appear less brittle and blocky. As has been stated, this is presumably due to the somewhat plastic nature of the crust that still prevailed at the time the collapses in the lava fields occurred.

Yet another approach to the investigation of the nature of the mare surface is to study the effects of surface texture on *crater ray deposits*. Recently, considerable progress has been made in recording these deposits through the program of full-Moon photography with the 61-in. telescope at the U. S. Naval Observatory near Flagstaff, Arizona, using long exposures (30–60 sec) on exceedingly fine-grain plates of high contrast.

The Copernicus field is especially instructive. It contains hundreds of what appear to be dark-halo craters, most of which are so small that only their dark, fuzzy nimbi are visible. The location of these craters with respect to the exceptionally dark volcanic fields bordering Sinus Aestuum is interesting. They do not coincide with the summits of the dark domes and mounds (seen clearly in *Photographic Lunar Atlas*, Sheets D4a, b, and e) but seem to be randomly distributed on their lower slopes and in the valleys. There is some evidence of the steeper mounds having a deposit of ray material from Copernicus on the exposed side. This, together with the varying degrees of contrast shown by the dark spots and the strong rays partly covering some halos, indicates that the dark-halo craters as a class are *older* than the Copernicus rays. Their present visibility is attributed to the *roughness* of the ejecta of the dark-halo craters. Differential sputtering will then, after some time, expose the nimbi.

The same differential effect is operative on ordinary impact craters such as Eratosthenes C, D, and E (all about 3.5 km in diameter) and Draper C ( $D = 7$  km) in Mare Imbrium, as well as Eratosthenes itself. In each case, the ejecta blanket has a fairly sharp outer boundary, which is about 1 crater diameter away from the crater rim for the four smaller craters. The ejecta belts are markedly darker than the surroundings wherever the ray deposit is moderate or light; however, heavy ray deposits are not visibly reduced by the ejecta belts. The dark belts are quite pronounced for Eratosthenes A and B ( $D \simeq 6$  km each) where the Copernicus ray deposit is thin (*Rectified Lunar Atlas*, Sheets 12c and d). Inspection of the Saari-Shorthill heat map<sup>3</sup> indicates that Eratosthenes A + B and D + E are "hot spots"; i.e., they have better than average conduction to the deeper layers of the mare. This

<sup>3</sup>Fig. 11, op. cit.

is consistent with the concept of a broken, rocky surface deposit.

The concept that *differential denudation of ray deposits yields a measure of the roughness of the lunar surface in the decimeter range* has application also to Mare Nubium and Mare Cognitum. In the *Ranger VII* pictures, a dark mountain range attracted attention and had been suspected to be of recent origin. This conclusion now appears unwarranted. The evidence indicates that the range is pre-Tycho, just like the dark portions of the crater floor of Pitatus, the dark, split dome on the rille west of Birt, and several other features whose age is almost certainly essentially that of Mare Nubium itself. The outlines of the dark patch in Mare Cognitum on a full-Moon photograph are soft like a crater halo and unlike the sharp outlines of the mountain range inside it, as observed by *Ranger VII*.

The *bearing strength of the typical mare surface* is of concern for both instrumented and manned soft-landing operations. Two aspects of this problem have become apparent during the *Ranger* photographic reduction program. First, the widespread occurrence of collapse depressions and the caves observed in some of them are indications of the fragile and unstable nature of much of the mare surface and, therefore, of the obvious risks to landing operations. There are, however, identifiable areas on the maria that appear to be free from the collapse depressions—i.e., *the ridges* and at least *some portions of Mare Nubium*. The surface distribution of such regions ought to be more fully explored before landings are attempted.

The second aspect of the soft-landing problem is the bearing strength on the "micro" scale, which involves not the easily identified terrain features but the nearly level terrain between obstacles. In the *Ranger VII* Report, an estimate was given on the basis of a probable identification of the uppermost mare surface with rock froth, somewhat compacted by particle impact. The *Ranger IX* impact area afforded the opportunity to determine the limiting bearing strength directly and an order-of-magnitude value ( $1 \text{ kg/cm}^2$  or  $1 \text{ ton/ft}^2$ ) consistent with the *Ranger VII* discussions was obtained.

After detailed lunar studies have clarified the post-mare developments, the *pre-mare* period will come into better focus, and the great problems of the origins of the Moon and the Earth will become more tractable. One aspect of these problems is the early thermal history of the Moon and, in particular, any observable effects that

might still remain of a high solar-luminosity phase assumed to have immediately followed the period of pre-solar contraction. A direct tie-in of the solar and lunar time scales would be of vast scientific importance. It may be possible also to arrive at some prediction of the water content of the uppermost layers of the terrae; they may be very dry because of the hot vacuum treatment. In this connection, efforts must be made to analyze spectroscopically the reddish glow of the gases that are expelled from the lunar crust from time to time.

The terrae and maria are sometimes thought to parallel the continents and ocean basins of the Earth, but this analogy is almost certainly in error. The terrestrial continents appear to be blocks 35–40 km thick, floating plastically in the mantle from which they were apparently differentiated during geologic time. The 5- to 6-km-thick basaltic ocean floors likewise originated during geologic time as a result of repeated volcanism. The lunar terrae, on the other hand, are not differentiation products but appear to be surface residues of the accreted material that initially formed the entire Moon. (The closest views of this type of material are found in the *Ranger IX* coverage of the Alphonsus wall and the *Ranger VIII* coverage of the Delambre region.) This pre-mare material appears to have been very severely shaken by gigantic impacts such as those that caused Mare Imbrium (reducing all original steep slopes) and metamorphosed by hydrothermal action during the period of maximum subsurface melting. It is therefore not surprising that no visible fissures exist that are definitely pre-mare, although the presence of a pre-mare lineament system is indicated by the numerous polygonal pre-mare craters and ridges in the terrae. As Strom has pointed out, the fact that at least the Nectaris and Imbrium lineament systems cut the global system (shown by ridges) indicates that the latter must be older. The maria themselves were caused by the flooding of pre-existing basins (the most prominent of which were due to impacts of circumterrestrial bodies).

Unlike the deposition of basalt on the floors of the terrestrial oceans, the lava deposition in the maria did not occur sporadically all through geologic time but appears to have taken place during a limited interval some  $4.5 \times 10^9$  years ago. Conclusions that have occasionally been drawn about the maria being much younger (a few times  $10^8$  years) are based on the facile assumption that the age of a lunar province is proportional to its crater density.<sup>4</sup>

<sup>4</sup>This assumption ignores such evidence as that which has led to the concepts represented in Fig. 134, op. cit.

Lineaments disclose roots leading to the deeper crustal layers and are thus potentially important sources of information. The fact that the global grid system of the Moon can be traced to the submeter crustal properties is very remarkable. On the Earth, very prominent lineaments have been discovered not only on the continents but also, e.g., on the Pacific floor. Some of these are over 4000 km in length, and together they represent, at least in the eastern Pacific, a roughly zonal system. Parallel to these lineaments, large displacements of the crust (wrench faults) have been found, which have alternately been interpreted as being due to (1) polar displacements within the body of the Earth, causing sheer forces through zonal changes in the linear velocity of rotation which act on a crust supported by a plastic base, and (2) convection currents in the Earth's mantle, with drag forces exerted on the overlying crust. The equivalent of either of these processes is likely to be nonexistent on the Moon: (1) the inertial ellipsoid of the Moon's body has a forced rotation in the tidal field of the Earth, whereas the position of the axis of rotation within the body of the Earth is in indifferent equilibrium; (2) because the Moon is much less massive than the Earth, its internal temperature will be less and its body more rigid, as is in fact demonstrated by the considerable deviation of the Moon from hydrostatic equilibrium. Consistent with, and thus confirming, the conclusions above, one finds no substantial displacements along any of the lunar lineaments. Furthermore, unlike the Pacific floor lineaments, which appear to be of comparatively recent geologic age ( $\leq 10^8$  years), the lunar grid system probably dates from the pre-mare to the early post-mare period, and must be related to the thermal and tidal properties pertaining at that time. Yet another difference between the Moon and the Pacific floor system is that the grid lines on the Moon are not normally divisions between different physiographic provinces. On the Pacific floor, the opposite is frequently the case. A preliminary study made by Strom of the Martian grid system observed in the *Mariner IV* records indicates that the Mars system somewhat resembles that of the Moon.

The terrestrial continents have lineament systems that are more similar to those found on the Moon and on Mars. Reference is made to a study of the Australian

lineaments which are much older than the very prominent system in the northeastern Pacific, and along which no displacements have been noted. Similar results have been derived for the Canadian Shield, among others.

A practical as well as a scientific objective must finally be to determine more precisely the nature of the upper 1 cm–1 m of the lunar maria. The radar and optical evidence indicates strongly that outside craters larger than 1 m and outside the ejecta belts immediately surrounding large impact craters, the surface is comparatively smooth down to dimensions of 1–3 cm, where the surface becomes extremely rough and vesicular. It appears further that the importance of ejecta from primary craters has been overrated and that, in particular, many long valleys attributed to ejecta (scars) are in reality depressions along fractures.

The dynamics and engineering aspects of the lunar collapse depressions occurring in the honeycombed and vesicular mare deposits are likely to develop into a major subject of scientific interest as well. The problem of finding shelter will be paramount after landing operations. The *Ranger* records have shown that the lunar maria are honeycombed with accessible cavities that might serve this purpose.

### Acknowledgments

The Principal Investigator wishes to record his gratitude for the privilege of participating in the *Ranger* program. This has been an unmatched scientific challenge and opportunity. His personal thanks go to Dr. Homer Newell and his staff at NASA Headquarters for providing this opportunity and for their guidance; and to the *Ranger* Team at JPL, especially Messrs. Schurmeier, Smith, Willingham, and Vrebalovich, for their unfailing friendship and cooperation. The extraordinary competence of the *Ranger* Team which made the missions a success has been a constant source of inspiration. This report is also the result of a group effort at the Lunar and Planetary Laboratory, and all who have been associated with it join in expressing their thanks to NASA and JPL.

## PROGRESS IN THE ANALYSIS OF THE FINE STRUCTURE AND GEOLOGY OF THE LUNAR SURFACE FROM THE RANGER VIII AND IX PHOTOGRAPHS

*Eugene M. Shoemaker*

*United States Geological Survey  
Flagstaff, Arizona*

The pictures acquired from the *Ranger VIII* and *IX* missions contain a wealth of new data about the lunar surface and supplement our knowledge of the Moon in several ways.

First, the *Ranger VIII* and *IX* pictures greatly augment the information about the fine structure of the lunar surface obtained from the *Ranger VII* mission. Other parts of the Moon were shown to be similar to the part first photographed with high resolution by *Ranger VII* in Mare Cognitum, and, in a general way, predictions based on the data obtained in this mission were confirmed. In addition, certain features, such as the small lineaments, that were only faintly discernible in the *Ranger VII* pictures, were found to be more prominent and much more widespread than had been anticipated. The improved portrayal of small features of low relief is due mainly to the fact that the *Ranger VIII* and *IX* target areas were closer to the terminator at the time of impact than was the target area of *Ranger VII*.

Both the *Ranger VIII* and *IX* pictures contain much new information as to the detailed topography of the lunar plains. In the *Ranger VIII* mission, the decision was made to maintain the cruise-mode orientation of the spacecraft during the final approach to the Moon's surface, specifically for the purpose of obtaining good stereoscopic coverage along the surface trace of the trajectory. The pictures thus acquired provide the best material for photogrammetric measurement of the shape of small features on the Moon among all of the photographs obtained from the entire *Ranger* series.

Inasmuch as the *Ranger VIII* and *IX* pictures cover major samples of the lunar highland areas as well as of the plains, they contain a great deal of new information on areas of complex geology. It is possible to map the geology of selected areas from these photographs at many different scales, ranging from 1:1,000,000 (the scale employed in the Earth-based telescopic mapping program) up to approximately 1:10,000 (a scale typically employed for highly detailed geologic mapping on Earth).

Finally, the *Ranger VIII* and *IX* data, combined with those from *Ranger VII*, provide the basis for preliminary planning and evaluation of the scientific tasks that may be successfully executed by astronauts in the early landings on the Moon of Project *Apollo*. On the basis of the high-resolution *Ranger* pictures, it is now possible to identify many of the types of geologic features that will be of specific interest and to estimate the time and evaluate the activities that will be required for the astronauts to conduct meaningful investigations.

The reduction and synthesis of the data obtained from the *Ranger VIII* and *IX* missions is still in a preliminary stage. This report presents an analysis of the data, as it bears upon the above categories, based largely upon qualitative considerations. The quantitative analysis, for the most part, must await completion of the detailed photometric and photogrammetric reduction of the pictures that has just begun. However, many general conclusions can be drawn at this time which are expected to be modified or refined only slightly by the final program of analysis.



N66 31450

## CURRENT PROBLEMS IN THE INTERPRETATION OF LUNAR PHYSICAL OBSERVATIONS\*

Bruce C. Murray

California Institute of Technology  
Pasadena, California

An extensive review of the physical observations of the Moon and of current interpretations was presented orally. The present brief paper summarizes a part of that presentation and ensuing discussion that has not been published before—the apparent contradiction between recent infrared results and those to be expected on the basis of the theoretical model of V. S. Troitsky and others. This model is based primarily on an interpretation of precise observations of the integral brightness of the Moon at radio wavelengths.

There are two main inconsistencies. First of all, as Troitsky discusses elsewhere in this volume, the 100° K (or lower) midnight temperature on the lunar surface reported from recent infrared observations is incompatible with the mean radio temperature averaged over the disk of  $207 \pm 2^\circ \text{K}$  used by Troitsky and others to infer physical parameters of the lunar surface. Certainly, the new infrared observations need confirmation at other wavelengths and, most important, over a substantial range of phase angle. However, if the observational discrepancy persists, as the recent work of Low at  $20 \mu$  and 1.4 mm indicates, then the resolution of the infrared vs radio discrepancy must be sought in the relationship between observed brightness temperature and actual surface and subsurface lunar temperatures; the problem may be geophysical rather than astronomical.

---

\*Summary of remarks.

The second major inconsistency between the radio and infrared data may provide a clue to a difficulty associated with passing from integral radio brightness temperature to actual lunar temperatures. The infrared eclipse and nighttime observations illustrate an enormous number of thermally "anomalous" regions of the lunar surface where consolidated rock is evidently at or just barely beneath the surface. These anomalous areas are distributed on a scale of 10 to 100 km. In addition, there are characteristic differences between individual maria in the abundances of such anomalies and also in the presence or absence of broad, low-level enhancements of infrared emission. Thus it is clear that the physical properties of the lunar surface are quite *heterogeneous* horizontally and that the radio observations must refer to some *average* radio emission emanating from significantly different surface structures. Hence, it may be hazardous to attribute to a hypothetically uniform lunar surface layer the properties arising from the blending of individual contributions from numerous geophysically distinct areas on the lunar surface.

New high-resolution radio observations at 3.4 and 8 mm, corresponding to several hundred kilometers resolution on the lunar surface, indicate a significant difference between maria and upland areas and, possibly, between individual maria as well. If this pattern persists as the geographic resolution of radio frequency observations is increased, the apparent discrepancy may be resolved by recognition that there are no meaningful *average* lunar surface properties for regions hundreds of kilometers or more in diameter; instead, the Moon must be recognized as having a complex geophysical structure both horizontally and vertically, and detailed mapping of that structure is required before actual physical parameters can be inferred.

## INVESTIGATION OF THE SURFACES OF THE MOON AND PLANETS BY THE THERMAL RADIATION\*

V. S. Troitsky

Scientific Institute of Radiophysics  
Gorky, USSR

In the present paper, the attempt is made to summarize the numerous data, experimental and theoretical, of the investigation of the lunar and planetary surfaces based on their thermal radiation and to consider the data from a common standpoint following from the physical principles discussed in this study. Accordingly, in the first part a brief theory is set forth of the methods for investigating the properties of planetary material. In the second, the results are given as obtained by the application of these methods to the emission of the Moon.

### 1. Physical Grounds for Studying the Material Properties and Thermal Regime of Planets' Surfaces by the Thermal Radiation

#### A. General Statements

The investigation of solid properties by the thermal radiation is based on the measurement of the radiation flux emitted by a body, usually from the surface layer of a material.

As is known, the spectral density of a flux is equal to

$$e(\nu, T) = [1 - R(\nu, r)] \int_0^\infty E(\nu, T) I(x) e^{-\tau(x)} \frac{dx}{\cos r'}, \quad (1)$$

\*Essentially the same paper appeared in *Radio Science*, Vol 69D, No. 12, December, 1965, pp. 1585-1611.

where  $R(\nu, r)$  is the reflection coefficient,  $E(\nu, T)$  is the function of a black-body emission at the frequency  $\nu$ ,  $T = T(x, t)$  is the temperature at the depth  $x$  at the moment of time  $t$ ,  $I(x)$  is the coefficient of wave absorption,

$$\tau(x) = \int_0^x I(\xi) \frac{d\xi}{\cos r'}$$

is an optical thickness,  $r'$  is the angle of incidence of emission out of the Moon's interior, and  $r$  is the angle of refraction (the angle between the normal to the surface and the observational direction). At the stationary conditions and thermal equilibrium inside the layer,  $T(x, t) = T = \text{constant}$  and

$$e(\nu, T) = [1 - R(\nu, r)] E(\nu, T). \quad (2)$$

For radio emission of the bodies of the solar system, ordinarily  $h\nu \ll kT$  and  $E(\nu, T) = kT/\lambda^2$ ; then  $e(\nu, T) = kT_e/\lambda^2$ , where

$$T_e = [1 - R(\nu, r)] T \quad (3)$$

is the effective temperature of radiation.

Thus, the measurement of the radiation flux  $e(\nu, T)$ , or of the effective temperature in the case of stationary conditions, enables one to estimate  $T$ , or, when  $T$  is known, one may find  $R(\nu, r)$ .

## B. The Dielectric Constant and the Density of Material

The value  $R(\nu, r)$  is determined by the medium's properties and their distribution to the depth of penetration of a corresponding wave  $l_e = 1/I$ , as well as by the geometry of the surface (roughness). An estimate of  $R(\nu, r)$  allows a determination of the definite properties, but at present this method is developed only for the material with a smooth surface, the reflection from which is described by Fresnel's relations. The material of the surface is assumed to have a sufficiently small loss angle that there is no influence on  $R(\nu, r)$ . It is generally accepted that the permeability is equal to unity. Under these assumptions the dielectric constant  $\epsilon$  of the material is evaluated, by which one can find the density  $\rho$  of the material (Troitsky, 1961a, 1961b, 1962a).

For this, one may use the relation

$$\epsilon = \epsilon_0 \left( 1 - \frac{3p}{\frac{2\epsilon_0 + 1}{\epsilon_0 - 1} + p} \right), \quad (4)$$

where  $p = 1 - \rho/\rho_0$  is a porosity value,  $\rho_0, \epsilon_0$  being the known density and dielectric constant, respectively, of a rock in a nonporous state.

An empirical formula having an accuracy of 5 to 10% is more suitable for practically all terrestrial silicate rocks (Krotikov, 1962a)

$$\epsilon^{1/2} - 1 = g\rho, \quad (5)$$

where  $g = 0.5 \text{ cm}^3\text{g}^{-1}$ .

The spectrum of the reflection coefficient permits a determination of  $\epsilon(\nu)$  which may bring out a real change of the electric properties of the material with the frequency. However, for silicate rocks,  $\epsilon$  remains unchanged over a wide range of microwave frequencies. Therefore, at the smooth surface of a dielectric having small absorption, the spectra  $R(\nu)$  and  $\epsilon(\nu)$  indicate the inhomogeneity of the material properties in depth, particularly the density  $\rho$ , at least in the layer of the order of the depth of penetration of an electromagnetic wave.

The measurement of the spectrum  $\epsilon(\nu)$ , and hence  $\rho(x)$  as well, may be carried out by polarization studies of radiation by the object (Troitsky and Tseytlin, 1962).

## C. The Variable Thermal Regime and the Measurement of Thermal Parameters

In the case of the variable thermal regime of the surface, new possibilities arise for determination of properties. For the bodies of the solar system the value of energy  $S_0 f(t)$  falling on the unit of the surface per unit of time is known, where  $S_0$  is the solar constant, and  $f(t)$  is the function depending on the position of a given point on a body surface. In this case the temperature  $T(x, t)$  at the moment  $t$  at the depth  $x$  may be calculated from the equation for a semi-infinite body if the medium's properties, their change with depth, and temperature dependence upon the temperature and depth (a homogeneous medium) has been considered. Then

$$\frac{\partial T}{\partial t} = a^2 \frac{\partial^2 T}{\partial x^2} \quad (6a)$$

$$(1 - R_i) \sigma T_s^4 - [(1 - R_c) S_0 f(t)] = \kappa \left( \frac{\partial T}{\partial x} \right)_{x=0}, \quad (6b)$$

where  $R_i$  is a mean reflection coefficient or albedo in the range of reradiated waves (for the bodies of the solar system in the range of infrared waves),  $R_c$  is the reflection coefficient or albedo of light waves,  $a^2 = \kappa/\rho c$  is the diffusivity,  $\kappa$  is the thermal conductivity, and  $c$  is the specific heat capacity.

For a homogeneous model the surface temperature  $T_s(t) = T(0, t)$  is proved to depend more considerably on the parameter value  $\gamma = (\kappa \rho c)^{-1/2}$  (Wesselink, 1948; Jaeger and Harper, 1950; Jaeger 1953).

Consequently, if the function of the surface temperature is known experimentally, one can find the value  $\gamma$  even with rather inaccurate data for  $R_c$  and  $R_i$ . Generally,  $R_c$  is known and the value  $R_i$  (for silicate rocks) is small enough ( $R_i = 0.15 \pm 0.15$ ) (Burns and Lyon, 1964), that inaccurate knowledge of it does not add error to the measurement of the infrared temperature or to the calculation (Troitsky, 1964a, b).

The insolation  $f(t)$  may be periodic or nonperiodic. For the Moon both the regimes take place. The first has a period of 29.53 days, the second, during the lunar eclipse, lasts only 4 to 5 hours. The layer thickness at which the temperature variation takes place will be, obviously,

different for different time duration of the insolation changes. Hence, it follows that, with an inhomogeneous layer, for short-time regimes we shall obtain information about  $\gamma$  of the upper layers, but for slow variations we shall obtain information about the lower layers.

For the determination of  $\gamma$  from observations of a periodic regime, one may sometimes not use the function  $T_s(t)$  itself but its Fourier coefficients (Krotikov and Troitsky, 1963a). Experimentally, the surface temperature is usually based on infrared waves, since these are emitted by solid surfaces.

#### D. The Radio Emission of the Surface of a Planet in a Nonperiodic Thermal Regime

The radio emission out of a layer compared with the depth of penetration of temperature variation enables one to measure the surface parameters. At the present time the radio emission has been considered for a homogeneous model (Piddington and Minnett, 1949; Troitsky, 1954) and for an inhomogeneous two-layer one when a thin upper layer is considered to be absolutely transparent for radio waves (Piddington and Minnett, 1949). These cases correspond to the periodic regime of the Moon and describe the dependence of radio emission on its phase. This theory is extended to the radio emission observed of the surfaces of Venus and Mars (Troitsky, 1964a).

Only recently has the radio emission of the homogeneous model been considered in the nonperiodic regime of the temperature variation during a lunar eclipse (Troitsky, 1965).

All calculations of radio emission for the bodies of the solar system must begin with the solution of the thermal problem (Eqs. 6) with the corresponding forms of the insolation function  $f(t)$ , depending on coordinates  $\phi$  and  $\psi$  on the surface of a planet. Then, by using the solution  $T(x, t, \phi, \psi)$ , one may evaluate the intensity of the thermal radiation according to (1). The solution of (1) with

Planck's function  $E(\nu, T)$  has not yet been obtained. Since  $h\nu \ll kT$ ,  $E(\nu, T) = kT(x, t)/\lambda^2$  and a flux will be proportional to the effective temperature

$$T_e = (1 - R) \int_0^\infty T(x, t, \phi, \psi) I(x) e^{-\tau(x)} \frac{dx}{\cos r'} \quad (7)$$

where  $e(\nu, T) = kT_e/\lambda^2$ .

In a general case, however, an analytical form of the solution (6a) for  $T(x, t, \phi, \psi)$  at the boundary conditions (6b) has not yet been found. Therefore, one uses the fact that (6) may be solved numerically, for example on a digital computer by which it is possible to estimate the surface temperature  $T_s(0, t)$  (Krotikov and Shchuko, 1963). Utilizing  $T_s(t)$  as boundary conditions in (6a) one may obtain the analytical solution.

At present, let us consider the heating and radio emission of an idealized planet represented as an ideal smooth sphere rotating near its axis with the angular velocity  $\Omega^*$  with respect to the stars. The Sun and the observer are considered to be in a plane normal to the rotation axis passing through a planet. Their visible velocities of rotation around the planet are equal to  $\Omega = 2\pi/t_0$  and  $\Omega^*$ , respectively, where  $t_0$  is the period of rotation of the planet (the period of insolation variation  $f(t)$ ).

The coordinate system is generally connected with the planet. One introduces the longitude  $\phi$ , read from the central meridian, and the latitude  $\psi$  from the equator. In this system the positions of the Sun and the observer are determined by the longitude of a subsolar point  $\phi_s = \Omega t$  (its latitude  $\psi = 0$ ) and that of the planet under the observer  $\phi_E$  (the observer is assumed to be on the Earth, though it may also be an equatorial satellite of the planet). In a common case the angular velocity of the observer is not constant; therefore,  $\phi_E = \int \Omega_E(t) dt$  as takes place, for example, with Earth observations of Venus.

The surface temperature in any point of the planet may be expressed in the form

$$T_s(\phi, \psi, t) = T_{s0}(\psi) + \sum T_{sn}(\psi) \cos(n\Omega t - \phi_{sn} - n\phi), \quad (8)$$

where  $\phi_{sn}$  is the phase lag of the temperature with respect to the insolation phase.

The solution (6a) with the boundary condition (8) gives

$$T(x, t) = T_{s0} + \sum T_{sn} e^{-\beta_n x} \cos(n\Omega t - \beta_n x - \phi_{sn} - n\phi), \quad (9)$$

where

$$\beta_n = \frac{1}{a} \left( \frac{n\pi}{t_0} \right)^{1/2}$$

is the coefficient of harmonic attenuation of a temperature wave. If, besides the solar heating, there is heat flux out of the interior, it gives an additional temperature increase with the depth. Owing to the smallness of this flux, the temperature increase on the surface itself will approximate zero and we may write  $T(x) = ax$ . Adding it together with (9) and substituting into (7), one can obtain the radio temperature distribution over the planet

$$T_e(\phi, \psi, t) = [1 - R(r)]T_{s0}(\psi) + [1 - R(r)]a l_e \cos r' + [1 - R(r)] \sum \frac{T_{sn} \cos(n\Omega t - \phi_{sn} - \xi_n - n\phi)}{(1 + 2\delta_n \cos r' + 2\delta_n^2 \cos^2 r')^{1/2}} \quad (10)$$

which periodically changes at each point near some constant component  $T_{e0}$ . Here

$$\delta_n = \frac{\beta_n}{I} = \frac{(n\pi)^{1/2}}{Ia(t_0)^{1/2}} \quad (11)$$

$$\xi_n = \arctg \delta_n \frac{\cos r'}{1 + \delta_n \cos r'}. \quad (12)$$

The value  $1/\beta_1 = l_T$  is the depth of penetration of a temperature wave; therefore, the value  $\delta_1 = l_e/l_T$  is the electrical and thermal wave-penetration ratio. For a dielectric with the loss tangent  $\operatorname{tg} \Delta \ll 1$ , as is known,  $I = 2\pi(\epsilon)^{1/2} \operatorname{tg} \Delta/\lambda$ , following (11),

$$\delta = \frac{1}{Ia} \left( \frac{n\pi}{t_0} \right)^{1/2} = \frac{\lambda c \gamma}{b(\epsilon)^{1/2}} \left( \frac{n\pi}{t_0} \right)^{1/2} = m\lambda; \quad l_e = m\lambda l_T, \quad (13)$$

where  $b = \operatorname{tg} \Delta/\rho$ .

Thus, with increasing wavelength and hence  $l_e$ , the constant component of the radio temperature [as it is seen from (10)] may increase due to temperature increase with depth of the body. For a two-layer model with the first harmonic only taken into account

$$T_e = (1 - R)T_{s0} + (1 - R)al_e \cos r' + (1 - R) \frac{T_{s1} \cos(\Omega t - \phi_{s1} - \xi_1 - \xi_s - \phi)}{N(1 + 2\delta_1 \cos r' + 2\delta_1^2 \cos^2 r')^{1/2}} \quad (14a)$$

where  $N$  and  $\xi_s$  are an additional attenuation of the temperature wave and the phase lag in the upper layer with

$$N = (1 + 2\delta_s + 2\delta_s^2)^{1/2} \quad \xi_s = \arctg \frac{\delta_s}{1 + \delta_s},$$

where  $\delta_s = \Delta x \beta_s \gamma_1^2/\gamma_2^2$ ;  $\Delta x$  is the thickness of the upper layer; and  $\gamma_1$  and  $\gamma_2$  are the values of  $\gamma = (\kappa\rho c)^{-1/2}$  for the upper layer and sublayer, respectively. From the relative measurements of  $T_e(t)$  during the whole period of insolation (e.g., during lunation) one may find  $\delta_1/\lambda = m$  or  $Ia$ .

When the observer is rotated around the planet it is possible to observe the surface radiation only for the longitudes  $\phi = \phi_E \pm \tilde{\phi}$ , where  $0 < \tilde{\phi} \leq \pi/2$  are the longitudes read from the point under the observer coinciding with a visible disk of the planet. For a uniform motion of the observer,  $\phi_E = \Omega_E t$ . By substituting it into (10) we



obtain for the argument  $n(\Omega - \Omega_E)t - \phi_{sn} \pm n\tilde{\phi}$ . Here  $(\Omega - \Omega_E)t = \Phi$  is a phase angle of the planet. But  $\Omega = \Omega^* \pm \Omega_s^*$  and  $\Omega_E = \Omega^* \pm \Omega_E^*$ , where  $\Omega_s^*$  and  $\Omega_E^*$  are the angular velocities of the Sun and observer rotation among the stars (as seen from the sphere). The minus sign corresponds to a direct rotation of the sphere with respect to the Sun, and the plus sign corresponds to a retrograde rotation. Thus, the phase angle  $\Phi = \phi_s - \phi_E = (\Omega - \Omega_E)t = \pm (\Omega_s^* - \Omega_E^*)t$ . For a nonuniform motion of the observer (e.g., observation of Venus from the Earth),  $\Phi = \pm (\Omega_s^* t - \int \Omega_E(t) dt)$ . In a general case, the expression for radio emission takes the form of

$$T_e(\phi, \psi, t) = (1 - R)T_{s0} + (1 - R)a l_e \cos r' + (1 - R)\Sigma \frac{T_{sn} \cos(\pm n\Phi - \phi_{sn} - \xi_n - n\tilde{\phi})}{(1 + 2\delta_n \cos r' + 2\delta_n^2 \cos^2 r')^{1/2}} \quad (14b)$$

When observing the Moon from the Earth, the libration being neglected, one may consider  $\phi_E = 0$  and  $\phi = \tilde{\phi}$ ,  $\Phi = \Omega t$  to have "+" as the directions of the proper lunar rotation and around the Sun coincide.

### E. A Temperature Gradient to the Depth and Heat Flux out of the Interior

Carrying out the measurement of the constant component of radio temperature for two waves  $\lambda_1$  and  $\lambda_2$  when observing normal to the surface of a body and using (10) and (14) (Troitsky, 1962 a, b, c) we obtain

$$\text{grad } T(x) = a_1 = \frac{dT_e}{d\lambda} \frac{1}{(1 - R_\perp)ml_r}. \quad (15a)$$

Multiplying it with the thermal conductivity, we shall have, for the heat flux density

$$q_s = \frac{dT_e}{d\lambda} \frac{\pi^{1/2}}{(1 - R_\perp)m\gamma(t_0)^{1/2}}. \quad (15b)$$

### F. The Temperature of the Surface of a Planet

In the foregoing, temperature distribution over the planet is determined by a set of independent solutions of a plane one-dimensional thermal problem with a semi-infinite layer for the surface elements with coordinates  $\phi, \psi$ . The effect of horizontal fluxes, which may be important at the poles, is not taken into consideration. Equation (6) was solved on the digital computer, enabling one to find the time dependence of the surface temperature for each point of the surface  $\phi, \psi$  in the form (Krotikov and Shchuko, 1963):

$$T_s(\phi, \psi, t) = T_{s0}(0) \cos^{0.2} \psi + T_{s1}(0) \cos^{0.33} \psi \cos(\Omega t - \phi - \phi_{s1}) \\ + T_{s2}(0) \cos^{0.27} \psi \cos(2\Omega t - 2\phi - \phi_{s2}) - T_{s3}(0) \cos^{0.44} \psi \cos(3\Omega t - 3\phi - \phi_{s3}). \quad (16)$$

Here  $T_{sn}$  is the amplitude of harmonics for the equator,  $\phi_{sn}$  is the phase lag between harmonics of the temperature and those of a falling flux. The value of the amplitude  $T_{sn}$  and phase lag  $\phi_{sn}$  depending on the value  $\gamma$  are cited in Table 1. The mean disk surface temperature has the form of

$$\bar{T}_0 = T_{s0}(0) \cdot 0.962 + T_{s1}(0) \cdot 0.741 \cos(\Omega t - \phi_{s1}) + T_{s2}(0) \cdot 0.315 \cos(2\Omega t - \phi_{s2}). \quad (17)$$

At present there is a wide use of the distribution adopted earlier (Piddington and Minnett, 1949; Troitsky, 1954).

$$T_s(\phi, \psi, t) = T_{sn} + (T_{sm} - T_{sn})\eta(\Omega t - \phi)\eta(\psi), \quad (18a)$$

where  $T_{sm}$  and  $T_{sn}$  are the temperatures of the subsolar and the antisolar point of a spherical surface. It was found (Troitsky, 1956) that  $\eta(\Omega t - \phi) = \cos^{1/2}(\Omega t - \phi)$  or  $\eta(\psi) = \cos^{1/2} \psi$ . Then (18a) is represented as a series

$$T_s(\phi, \psi, t) = [T_{sn} + a_0(T_{sm} - T_{sn}) \cos^{1/2} \psi] + a_1(T_{sm} - T_{sn}) \cos^{1/2} \psi \cos(\Omega t - \phi), \quad (18b)$$

**Table 1. Numerical values of the terms of Fourier expansion of the surface temperature in the center of the lunar disk and  $\phi$ , as a function of  $\gamma$**

$\gamma$	$T_{1n}$	$T_{2n}$	$T_{3n}$	$T_{4n}$	$T_{5n}$	$\phi_{1n}^\circ$	$\phi_{2n}^\circ$	$T_{10}/T_{11}$	$T_{20}/T_{21}$
125	390	158	247	132	34	5	-7	1.86	7.27
250	391	136	237	146	35	4	-7	1.62	6.77
400	392	123	230	156	36	3	-7	1.48	6.40
500	392	117	227	159	36	3	-7	1.42	6.30
700	393	109	223	165	36	3	-6	1.35	6.20
1000	393	100	219	170	36	2	-6	1.29	6.10
1200	393	96	217	173	36	2	-6	1.26	6.03

where  $a_0 = 0.382$ ,  $a_1 = 0.56$ . Here, the first term is the constant component and the second one is the first harmonic of the temperature variations. The mean disk value of the constant component is equal to (Krotikov and Troitsky, 1962)

$$\bar{T}_{s0} = T_{sn} + (T_{sm} - T_{sn}) (0.92) (0.382). \quad (19)$$

Both the distributions give similar results, but for the temperature in a polar zone the first term is zero and the second term is equal to  $T_{sn}$ . At present, more accurate data for temperature in the polar zone are needed; this requires the solution of the thermal problem for the whole sphere (the horizontal heat fluxes being taken into account).

### G. The Integral Radio Emission

Recently, for interpretation of measurements, a theory of an integral radiation was developed (Krotikov, 1963a, 1965). If the properties of the material of the planet's surface are homogeneous, the full radiation of the mean disk effective temperature may be expressed by that of the disk center, by introducing averaging coefficients. Therefore, instead of (10) and (14b) we obtain

$$\bar{T}_e(t) = (1 - R_\perp) T_{s0}(0) \beta_0 + (1 - R_\perp) \sum \frac{T_{sn}(0) \beta_n \cos(n\Omega t - \phi_{sn} - \xi_n(0, 0) - \Delta\xi_n)}{(1 + 2\delta_n + 2\delta_n^2)^{1/2}}. \quad (20)$$

Here  $\beta_0$  and  $\beta_n$  are the averaging coefficients, being approximately unity with  $0.91 \leq \beta_0 \leq 0.96$  and dependent only on  $\delta$ . In addition,  $\beta_n$  depends on  $\delta$ ; in particular,  $0.75 \leq \beta_1 \leq 1$ , and  $0.25 \leq \beta_2 \leq 0.35$ . As expected, when averaging, the second harmonic is heavily attenuated. In most cases it will be valid for the higher harmonics. Consequently, the integral radiation, in practice, is of a sinusoidal form. It is interesting that when averaging, an additional phase lag  $\Delta\xi_n$  occurs which, for the first harmonic, does not exceed  $5^\circ$ . For the case of an arbitrary relationship of the pattern width with angular dimensions of a planet's disk, the values of averaging coefficients have been calculated as well. It turns out that when the pattern width is equal to the angular dimensions of the planet, the mean disk effective temperature is actually determined.

### H. The Radio Emission of the Surface of a Planet at the Nonperiodic Thermal Regime (the Lunar Eclipse)

Now let us give briefly the results of the theory of the radio emission of the Moon during an eclipse (Troitsky, 1965). In order to calculate the lunar emission during an eclipse it is necessary to know the function of the surface temperature variation. As is known from the measurements during the interval  $t_2 - t_1$  corresponding to the beginning and the end of the penumbral stage of eclipse, the surface temperature falls almost linearly from the value  $T_1$  to  $T_2$ .

Then during the whole umbral phase up to the time  $t_3$ , the temperature slowly falls almost linearly to  $T_3$  and, finally, in the last penumbral period it linearly increases to the value  $T_4 = T_1$  at the time of the end of eclipse  $t_4$ . In accordance with this, a real function of the surface temperature is represented as a broken line drawn through the points  $t_k$ ,  $T_k$  as

$$T_s(0, t) = \psi(t) = T_k + \alpha_k(t - t_k)$$

$$\alpha_k = \frac{T_{k+1} - T_k}{t_{k+1} - t_k} \quad k = 1, 2 \dots 4.$$

The initial temperature  $T_s(x, t_1)$  is deduced from the solution (9) at  $\Omega t = 0$  (the full Moon) for the central part of the lunar disk. First, the thermal problem of  $T(x, t)$  estimation was solved, expressed by (6a), with the boundary and initial conditions above. Then the value of the effective temperature was obtained from (7), which in the interval of the penumbra is equal to

$$T_{e1}(t) = T_v(q_1) + T_1(t, q_1) \quad t_1 \leq t \leq t_2. \quad (21)$$

During the penumbral phase

$$T_{e2}(t) = T_{e1}(t) - T_1(t, q_2) + T_2(t, q_2) \quad t_2 \leq t \leq t_3. \quad (22)$$

During the second penumbral phase

$$T_{e3}(t) = T_{e2}(t) - T_2(t, q_3) + T_3(t, q_3) \quad t_3 \leq t \leq t_4. \quad (23)$$

Finally, after the end of eclipse,

$$T_{e4}(t) = T_{e3}(t) - T_3(t, q_4) + T_4(t, q_4) \quad t_4 \leq t \leq \infty, \quad (24)$$

$$\text{where } \frac{T_v(q_1)}{1 - R} = T_{s0}[1 - \Phi(z_1)]e^{z_1^2} + \frac{T_{s1}}{2} A_-[1 - \Phi(y)]e^{y^2} + \frac{T_{s1}}{2} A_+[1 - \Phi(z_1)]e^{z_1^2} \cos 2yz_1$$

$$- \frac{T_{s1}}{\pi^{1/2}} D_+ y \cos 2yz_1 + \frac{T_{s1}}{2} D_-[1 - \Phi(z_1)]e^{z_1^2} \sin 2yz_1, \quad (25)$$

$$\text{and } \frac{T_k(t, q_n)}{1 - R} = \left\{ T_k + \alpha_k(t - t_k) + \frac{\alpha_k}{I^2 a^2} \right\} \{1 - e^{z_n^2} [1 - \Phi(z_n)]\}$$

$$- \frac{2}{\pi^{1/2}} \alpha_k(t - t_n)z_n^{-1} + \alpha_k(t - t_n)e^{z_n^2} [1 - \Phi(z_n)]. \quad (26)$$

Here  $q_n = 1/2a (t - t_n)^{1/2}$  is analogous to the coefficient of the thermal-wave attenuation during the eclipse and  $z_n = 1/2q_n = Ia (t - t_n)^{1/2}$  is the ratio of electrical and thermal-wave attenuations.

$$\Phi(z_n) = \frac{2}{\pi^{1/2}} \int_0^{z_n} e^{-\xi^2} d\xi, y = \beta/2q_1; A_- = \frac{1 + \delta}{B} - \frac{1 - \delta}{B_1}; A_+ = \frac{1 + \delta}{B} + \frac{1 - \delta}{B_1}; D_+ = \frac{\delta}{B} + \frac{\delta}{B_1};$$

$$D_- = \frac{\delta}{B} - \frac{\delta}{B_1}; B = 1 + 2\delta + 2\delta^2; B_1 = 1 - 2\delta + 2\delta^2; \delta = \beta/I.$$

As one can see, the temperature variations during the eclipse are determined by the values  $z_n$  and  $y$ , i.e., by the value  $Ia$ . For waves longer than  $\lambda = 0.1$  cm, the value  $Ia$  is very small,  $z_n$  and  $y$  being small as well. It permits one to use the relations (25) and (26) in a series expansion over these parameters. By restricting with the second approximation over  $Ia$  we obtain for each  $k$  interval of the eclipse

$$T_{ek}(t) = T_{em} + (1 - R) \frac{4Ia}{3(\pi)^{1/2}} \sum_1^k (\alpha_n - \alpha_{n-1}) (t - t_n)^{3/2} - (1 - R) \frac{I^2 a^2}{2} \sum_1^k (\alpha_n - \alpha_{n-1}) (t - t_n)^2 \quad k = 1, 2 \dots 4, \quad (27)$$

with  $\alpha_0 = \alpha_4 = 0$ .

The value of the initial effective temperature is equal to

$$T_{em} = \left( T_{s0} + T_{s1} \frac{1 + \delta}{B} \right) (1 - R)$$

and coincides with that which follows from (10) for the full Moon. In practice, the maximum radio temperature variation appears exactly at the moment  $t_3$ . According to (27) it is equal to

$$\frac{1}{M(\lambda)} = \frac{\Delta T}{T_{em}} = - (1 - R) \frac{4Ia}{3(\pi T_{em})^{1/2}} \{ \alpha_1(t_3 - t_1)^{3/2} + (\alpha_2 - \alpha_1)(t_3 - t_2)^{3/2} + (1 - R) \frac{I^2 a^2}{2T_{em}} \{ \alpha_1(t_3 - t_1)^2 + (\alpha_2 - \alpha_1)(t_3 - t_2)^2 \} \}. \quad (28)$$

From (25) to (28) one can see that the measurements of relative changes of the radio emission intensity permit an estimation of the value of  $Ia$  during both eclipse and lunation,

$$Ia = \frac{1}{\lambda} \cdot \frac{b(\epsilon)^{1/2}}{c\gamma}. \quad (29)$$

For the measurements during eclipse this value characterizes the upper layer of the material and for those during lunation it characterizes a layer approximately 10 times deeper. In Fig. 10, the families of curves for the radio eclipse of December 30, 1963, are given, calculated in accordance with the formulae (21) to (26) at different values of  $\gamma/b(\epsilon)^{1/2}$ . From (27) and (29) it is obvious that a reciprocal value of maximum relative changes of radiation  $M(\lambda)$  is almost a linear function versus the wavelength. The spectrum incidence is defined by the value  $c\gamma/b(\epsilon)^{1/2}$ . Consequently, the experimental study of the spectrum of radio-temperature fall during the eclipse, as well as for a periodic case, may give only the relation  $c\gamma/b(\epsilon)^{1/2}$ . In Fig. 11, the spectrum  $M(\lambda)$  is shown calculated from (21) to (26) for the eclipse of December 30, 1963, and the experimental points are plotted.

## I. Investigation of Material Microstructure of a Layer

The conclusions concerning the microstructure may be derived from the value of the volumetric density  $\rho$ , because when  $\rho_0$  is known, one can estimate the degree

of body porosity. However, two bodies, one of powder and the other solid-porous, may have an identical overall apparent porosity. Apparently, these cases may be distinguished when comparing the value  $\kappa$  with  $\rho$ . The value of thermal conductivity of one and the same material

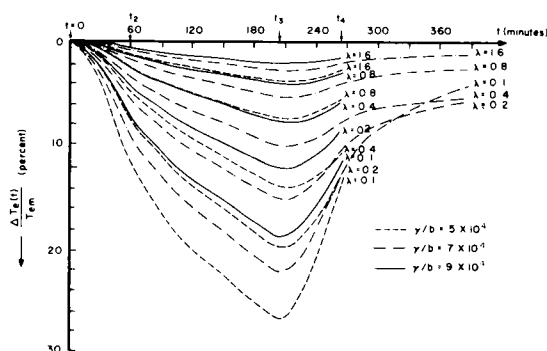


Fig. 10. The families of curves for the radio eclipse of December 30, 1963, at different values of  $\gamma/b$

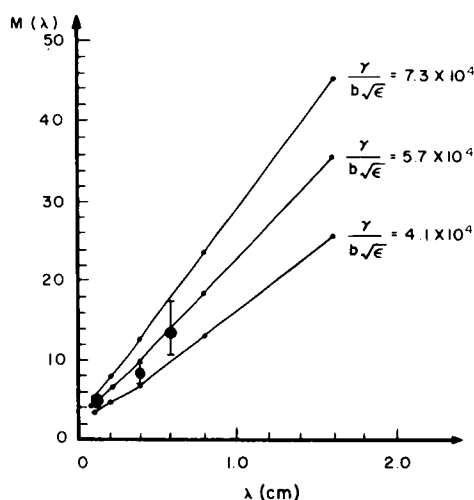


Fig. 11. The spectrum  $M(\lambda)$  for the eclipse of December 30, 1963, at different  $\lambda/b(\epsilon)^{1/2}$ . The dots correspond to the experimental data.

may differ considerably at the equal volumetric density  $\rho$  (and porosity), either for a powder or solid-porous state of a body in vacuum. Otherwise, the function of  $\kappa$  dependence upon  $\rho$  must be different for these media and, besides, may be dependent on grain size or pores.

It was shown (Troitsky, 1962a) that, in the air, for all porous solid and powder silicate materials, the following relation may be used with an accuracy of 10 to 20%:

$$\kappa = \alpha\rho = 0.6 \times 10^{-3}\rho \quad 0.4 \leq \rho \leq 1.5. \quad (30)$$

This relation of  $\kappa$  and  $\rho$ , as was shown by experimental investigations, also holds in a high vacuum, but for the fine powder materials with grains of about several

microns, the value  $\alpha$  turns out to be 50 times less (Bernett, Wood, Jaffee, and Martens, 1963):

$$\kappa_c = \alpha_c\rho \simeq 10^{-5}\rho \quad 0.2 \leq \rho \leq 1.5. \quad (31)$$

For a solid-porous body, accurate measurements have not yet been made. Probably, one may expect (Woodside and Messmer, 1961) that

$$\kappa_r = \alpha_r\rho \simeq 5 \times 10^{-5}\rho. \quad (32)$$

There are data on the influence of gas composition filling the pores (Woodside and Messmer, 1961).

Therefore, a knowledge of  $\kappa$  and  $\rho$  and the use of  $\kappa/\rho$  permits us to draw a conclusion about the structure of the material and, perhaps, about the nature of gas filling the pores and its pressure. The latter is especially valuable for the investigation of Venus and Mars. The dependence between  $\kappa$  and  $\rho$  is discussed in the same way as in Halajian's work (1964). It should be noted that for different dispersity and pore sizes the question of the dependence between  $\kappa$  and  $\rho$  has not yet been studied, either theoretically or experimentally.

## J. The Nature of Material: Mineralogical Composition

The investigation of a chemical composition is based on comparison with the Earth's rocks for the definite parameters. Neither density nor thermal conductivity is suitable for this purpose. Attempts are made to identify the material by the loss angle at the microwave frequencies; as is known, this angle is mainly determined by the chemical material composition. However, there is no full identification of the relation between the loss angle and chemical composition. One and the same loss angle may correspond to rather different natural materials. But if we take a definite group of materials (e.g., silicate rocks), such a comparison will not be so hopeless. However, the value  $\tan \Delta$  by itself depends not only on a rock type but also on its density  $\rho$ . Therefore, for identification a value invariant from the density is suggested for use (Troitsky, 1961a). Theoretically, such a value is the specific tangent of the loss angle:

$$b = \frac{\tan \Delta}{\rho}.$$

The independence of this value to within  $\pm 15\%$  of the density has been shown experimentally when  $0.1 \leq \rho \leq 1.5$  for different Earth rocks (Krotikov, 1962a). This justifies the introduction of it in the expressions for  $\delta$  and  $Ia$  as a basic electric characteristic of the material.

## K. Main Conclusions

Let us draw some conclusions from which we shall be able to learn about the properties of a body by its radiation, assuming, for simplicity, that the layer of material is homogeneous, the surface is smooth, and the material is a dielectric. As a result of measurements, we have three known relations,  $\epsilon = \epsilon(\epsilon_0, \rho)$ ,  $\gamma = (\kappa \rho c)^{-1/2}$ , and  $c\gamma/b(\epsilon)^{1/2}$  between six unknowns,  $\epsilon_0$ ,  $\rho_0$ ,  $\kappa$ ,  $\rho$ ,  $c$ , and  $b$ . Three of them are immediately determined in practice if the rocks are considered to belong to a silicate group. Then  $c = 0.2$ ,  $\epsilon = \epsilon(\rho)$ , but  $\kappa$ ,  $\rho$ , and  $b$  remain unknown, being connected with three known equations. In the case of a density change with depth, for example, one more unknown is added that is characteristic scale of inhomogeneity. Therefore, a measurement of new independent relations of parameters is required. The radar investigations of the spectrum of the reflection coefficient may give the important data of the degree of inhomogeneity of properties with depth.

## II. Investigation Results of Properties of the Surface Cover and Its Temperature Regime

In this section the experimental data of the lunar investigation on infrared and radiowaves are considered. A theoretical interpretation is given of experimental data obtained in accordance with the methods above in order to obtain information about the material parameters of the upper layer.

The order of analysis corresponds to the general scheme of investigation mentioned in the first section.

### A. The Temperature of the Lunar Surface

The surface temperature of the Moon is ordinarily measured on infrared waves in the atmosphere window 8 to 12  $\mu$ . At present, the temperature measurement for different regions and details of the Moon have been carried out during both lunations and eclipses. An estimate of the temperature of a subsolar point  $T_{sm}$  by many authors is in rather good agreement, being equal to 407°K (Pettit and Nicolson, 1930) or 389°K (Geoffrion et al., 1960). The recent measurements on the wavelength 4  $\mu$  gave  $400 \pm 10^\circ\text{K}$  (Moroz, 1965). The measurements on this wavelength are especially important for  $h\nu = 15kT$ , and an error because of the infrared albedo not being taken into consideration, even if the latter is equal to 20 to 30%, affects the result less than 2%. The absence of difference in the results of measurements at 4  $\mu$  and

10  $\mu$  suggests a small infrared albedo of the Moon's surface which, apparently, is not more than the optical albedo. A theoretical value of the temperature of the subsolar point is equal to  $T_{sm} = 395^\circ\text{K}$ , the visible and infrared albedo being equal. Thus, one may take

$$T_{sm} = 400 \pm 10^\circ\text{K}$$

The situation is much worse when measuring the temperature  $T_{sn}$  at an antisolar point. According to Pettit and Nicolson's measurements (1930) and Geoffrion et al. (1960),  $T_{sn} = 120 \pm 2^\circ\text{K}$ . Recently Murray and Wildey (1964) have obtained  $T_{sn} = 106^\circ\text{K}$  and Saari and Shorthill (1964) have obtained  $T_{sn} = 100^\circ\text{K}$ . It should be noted that such a low night temperature leads to a value of the constant component that appears to be equal to or far less than that of the radio temperature, an impossibility. Below we shall take some mean value

$$T_{sn} = 115^\circ\text{K}$$

In accordance with the results of measurements (Pettit and Nicolson, 1930), (Saari and Shorthill, 1962), the temperature during the eclipses in different parts of the disk with the exception of crater bottoms has, on the average, a similar relative change. So  $T_2/T_1 = 0.53$ ,  $T_3/T_1 = 0.46$ ; that gives  $T_1 = 400^\circ\text{K}$ ,  $T_2 = 210^\circ\text{K}$ , and  $T_3 = 185^\circ\text{K}$  for the central part of the disk. Recently Saari and Shorthill (1965) have discovered that, during the umbra, the Mare Humorum is warmer than others and that over the entire disk there are about a hundred observable warm points. Some of them are identified with small rayed craters. The distribution of the surface temperature over the disk is estimated only for the full Moon along the equator (Pettit and Nicolson, 1930). Instead of the expected law  $\cos^{1/4}r$ , one obtains  $T = T_{sm} \cos^{1/6}r$ . It is explained by the roughness influence not taken into account in the theory. The distribution measurements of the surface temperature on radio waves confirmed the correctness of the theoretical distribution (18b) (Kaydanovsky and Salomonovich, 1961; Saari and Shorthill, 1962). But more valuable measurements of isotherms for a night Moon have not yet been made.

### B. Experimental Data on Radio Emission of the Moon

At present, the radio emission of the Moon has been studied in the range of waves 0.13 cm and 168 cm, both during lunations and eclipses. The dependence of radio emission intensity on phase cannot be measured on a wavelength of 20 cm or longer, and the eclipse changes are not noticeable even on the waves 2 cm and longer.



All the experimental dependences of radio temperature upon the lunar phases are approximated rather well by a sum of a constant component and a sinusoidal one, thus,  $T_e = T_{e0} + T_{e1} \cos(\Omega t - \xi_1)$ . In Table 2, the measurement results have been cited during a phase cycle of the Moon, and, in Table 3, during the eclipses.

In Table 2, the values of a constant component  $T_{e0}$ , the amplitude of the first harmonic  $T_{e1}$ , the phase lag  $\xi_1$ , the beam width of the radiotelescope, and the accuracy of measurements are given. In Table 3, the maximum values are given of the relative temperature variations at the moment of the end of the umbral phase of the corresponding eclipse. It is interesting to note that in a set

Table 2. Experimental results of the radio emission of the Moon during lunations

	$\lambda$ cm	$T_{e0}$ °K	$T_{e1}$ °K	$\xi$ deg	Error of measure- ment $\pm$ %	Half beam width $\theta$	References
1	0.13	219	120	16	15	10'	Fedoseyev, 1963.
2	.18	240	115	14	20	6'	Naumov, 1963.
3	.40	230	73	24	10	25'	Kislyakov, 1961.
4	.40	228	85	27	15	1'6	Kislyakov, Salomonovich, 1963.
5	.40	204	56	23	4	36'	Kislyakov, Plechkov, 1964.
6	.8	197	32	40	10	18'	Salomonovich, 1958.
7	.8	211	40	30	15	2'	Salomonovich, Losovsky, 1962.
8	.86	180	35	35	15	12'	Gibson, 1958.
9	1.25	215	36	45	10	45'	Piddington, Minnett, 1949.
10	1.63	224	36	40	10-15	26'	Zelinskaya et al., 1959.
11	1.63	208	37	30	3	44'	Kamenskaya et al., 1962.
12	1.63	207	32	10	3	44'	Dmitrenko et al., 1964.
13	2.0	190	20	40	7.5	4'	Salomonovich, Koshchenko, 1961.
14	2.3			35		$2 \times 40'$	Kaydanovsky et al., 1961.
15	3.15	195	12	44	15	9'	Mayer et al., 1961.
16	3.2	223	17	45	15	6'	Koshchenko et al., 1961.
17	3.2	245	16	41	15	40'	Strezhnyova, Troitsky, 1961.
18	3.2	210	13.5	55	2.5	1°12'	Krotikov et al., 1961.
19	3.2	213	14	26	2	1°27'	Bondar' et al., 1962.
20	3.2	216	16	15	3	40'	Bondar' et al., 1962.
21	9.4	220	5.5	5	5	2°20'	Medd, Broten, 1961.
22	9.6	230			15	19'	Koshchenko et al., 1961.
23	9.6	218	7	40	2.5	1°40'	Krotikov, 1962b.
24	10.3	207			15	18.05'	Sloanaker, 1962.
25	11	214			12	17'	Mezger, Strassl, 1960.
26	14.2	221			3.5	2°	Krotikov et al., 1965.
27	20.8	205	5			36'	Waak, 1961.
28	21	250	$\leq 5$		15	35'	Mezger, Strassl, 1959.
29	22	270			20	15'	Davies, Jenisson, 1960.
30	22	270					Westerhout, 1958.
31	23	254	$\leq 6.5$		15	38'	Castelli, 1961.
32	32.3	233			2.5	3°00'	Razin, Fyedorov, 1963.
33	33	208				3°06'	Denisse
34	35	236			4		LeRoix.
35	36	237			3	3°10'	Krotikov, Porfiriyev, 1963.
36	50	240			5	4°40'	Krotikov, 1963b.
37	70.16	217			8	1°30'	Krotikov et al., 1964.
38	75	185			20	2°00'	Seeger et al., 1957.
39	168	233			4	$13.6 \times 4^\circ$	Baldwin, 1961.

Table 3. Experimental measurement results of the radio emission of the eclipsed Moon.

$\lambda$ , cm	$\frac{\Delta T_e}{T_{em}}$ %	$T_{em}$	$\Delta\phi$	$(\gamma/b\sqrt{\epsilon}) \cdot 10^{-4}$		Date of eclipse	$t_2 - t_1$		$t_3 - t_1$		References
				Center	Disk		Center	Disk	Center	Disk	
0.12	17*	315	7	6.2		6-7/7/63	85		175 <sub>min</sub>		Kamenskaya et al., 1965.
.12	22.5 ± 2	315	7	4.7		30/12/63	60		204		
.21	8*	300	10	10.0		6-7/7/63	85		175		
.32	6 ± 2	277	2.9	10.5		30/12/63	60		204		Jacobs et al., 1964.
.4	8 ± 2	270	20	8.3	9.7	6-7/7/63	85	75	175	255	Kamenskaya et al., 1965.
.4	12 ± 2	270	20	4.5		30/12/63	60		204		
.4	10 ± 2	270	20	4.5		19/12/64	60		194		Plechkov, Porfirjev, 1965.
.43	4 ± 1	268		12.9		26/8/61	63		182		Tolbert et al., 1962.
.6	8 ± 2	257	35	4.5		30/12/63	60		204		Kamenskaya et al., 1965.
	5 ± 2	253	36	7.5	8.7	6-7/7/63	85	75	175		
.86	7	247		3.9		5/9/60	60		211		Gibson, 1961.
1.6	3 ± 2	235	44	6.4	7.5	6-7/7/63	85	75	175		Kamenskaya et al., 1965.
1.6	6 ± 3	235	44	3.3		25/6/64	71		239		Plechkov, 1965.
2.2	1	228	58	15.6		19/12/64	60		194		Plechkov, Porfirjev, 1965.

\*The value of radiotemperature drop in 60 min after the beginning of the umbral eclipse of the center of disk.

of measurements carried out by the usual methods (Table 2) the difference of values given by different authors exceeds twice the error of the measurement and is equal to 30%. In a set of precision measurements made by the method of the "artificial Moon" the difference on each wavelength is far less than the error of each measurement, i.e., not more than 1 to 2%.

The important first detailed observations of radio emission of the Moon during lunations and eclipses on wavelengths of 0.2 and 0.13 cm were carried out by Naumov (1963), and Fedoseyev (1963). Since the main results of the lunar properties have been obtained from the precision measurements, we shall consider the method in more detail.

This method is based on the comparison of the radio emission of the Moon or planets with etalon radiation of an absolutely black disk placed in the Fraunhofer zone of an antenna at a sufficient elevation. This method was called the method of the "artificial Moon," as the disk is arranged to have the same angular dimensions as the Moon viewed from the radiotelescope.

In order to eliminate the diffraction of the radio emission of the Earth around the disk, which contributes some power to the antenna, a second pattern was used in a shape of an opening in the plane that covers the main lobe of the polar diagram of the antenna and is inserted

into the place formerly occupied by the disk. The opening repeats strictly the dimensions of the disk. In this case, the signal pattern formed with emission of the disk inserted into the opening appears to be weakened by the magnitude of power of the Earth emission (diffraction powers are equal in value). Consequently, the mean signal value from a free disk and from that in the opening will be strictly equal to the known black-disk emission (Krotikov, Porfirjev, and Troitsky, 1961). Later, by applying the second disk, the conditions of the disk model were found under which the diffraction effect for the given wave and disk diameter could be disregarded. Finally, the diffraction error was computed theoretically (Tseytlin, 1963). Figures 12 and 13 show the model of an artificial Moon installed on the mountain Khara-Dag in the Crimea.

As a result of adopting the method above, measurements of the radio temperatures of the Moon are possible with an error not exceeding 2 to 3%, in a wide range of wavelengths.

### C. Investigation of the Distribution of Material Properties With Depth, Using the Spectrum of Periodic Variations of the Radio-emission Intensity

The data obtained for the spectrum of the variable part of the radio emission of the Moon enable one to explore the character of the distribution of material

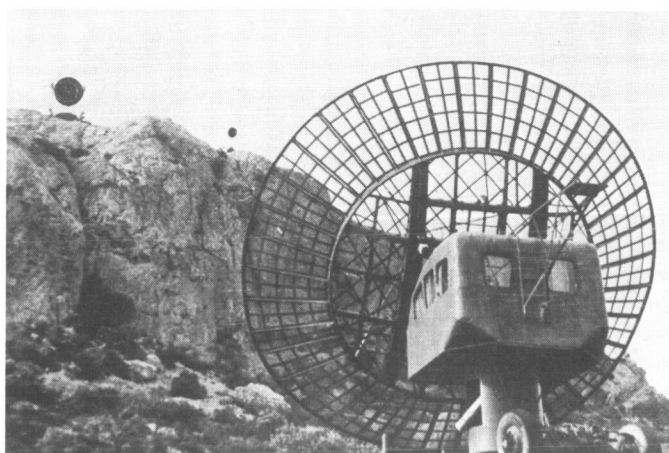


Fig. 12. Artificial Moon installed on the mountain Khara-Dag in the Crimea, viewed from the antenna

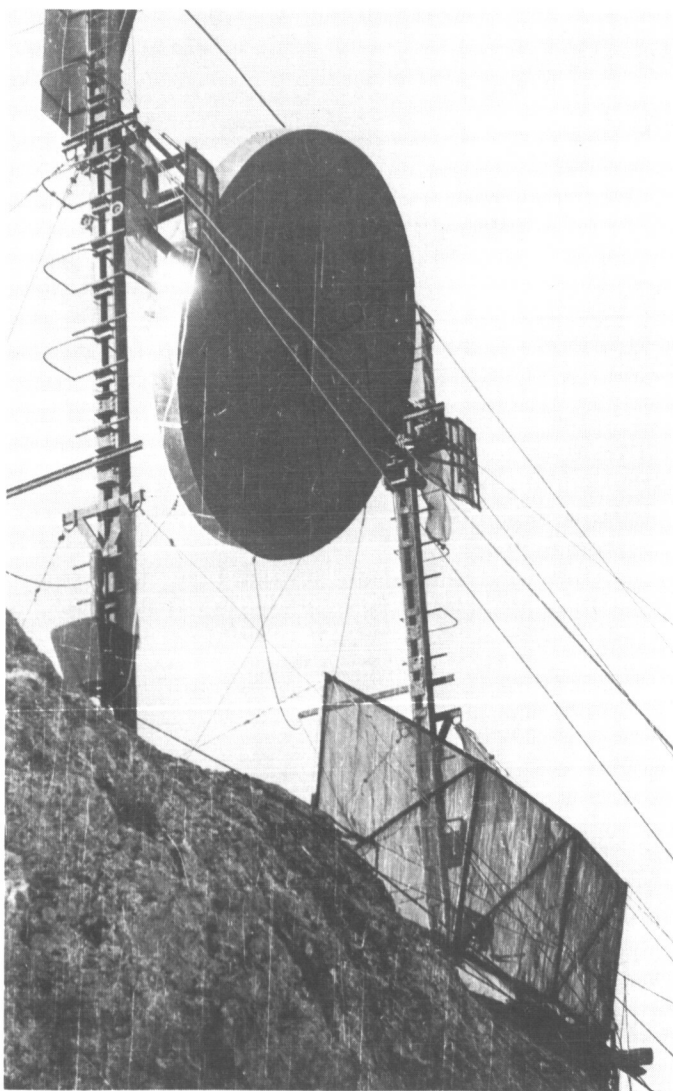


Fig. 13. Closeup of artificial Moon and mounting

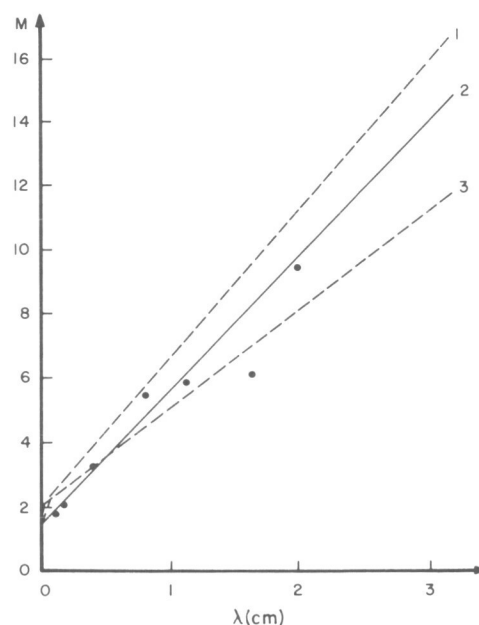


Fig. 14. The dependence of  $M$  on  $\lambda$ . Curve 2 corresponds to a homogeneous model ( $m = 1.0$ ,  $\delta_1 = 2\lambda$ ). Curve 1 corresponds to a two-layer model ( $m = 1.5$ ,  $\delta = 1.5\lambda$ ), Curve 3, to a model with  $m = 1.5$ ,  $\delta = \lambda$ .

properties with depth. At present, the experimental results are compared with two extreme idealizations of the distribution of properties: a homogeneous model and a sharply inhomogeneous one with a nonabsorbing upper layer (Troitsky, 1961a, 1962a, 1964b). Figures 14 and 15 present the results of this comparison.

In Fig. 14 are plotted the theoretical curves of dependence of the inverse magnitude  $M(\lambda) = T_{e0}/T_{e1}$  of relative variations of the radio temperature, in the function  $\lambda$ , equal, in accordance with (20) and (14), to

$$M_1(\lambda) = N \frac{T_{s0}(0) \beta_0}{T_{s1}(0) \beta_1} (1 + 2\delta_1 + 2\delta_1^2)^{1/2}; \quad \delta_1 = \nu \quad (32a)$$

Curve 2 corresponds to the single-layer model, and curves 1 and 3 to the two layer model by the  $N = 1.5$ ,  $\delta_1 = 1.5\lambda$ , and  $N = 1.5$ ,  $\delta_1 = \lambda$ . The circles indicate the experimental points which lie on a straight line for the homogeneous model ( $N = 1$ ) plotted for  $\delta/\lambda = m = 2$ . The value  $M$  and the retardation  $\xi$  are functions of the model.

Figure 15 gives the theoretical dependence between  $M$  and  $\xi$  for the assumed models and presents the experimental points. Curve 1 corresponds to the homogeneous

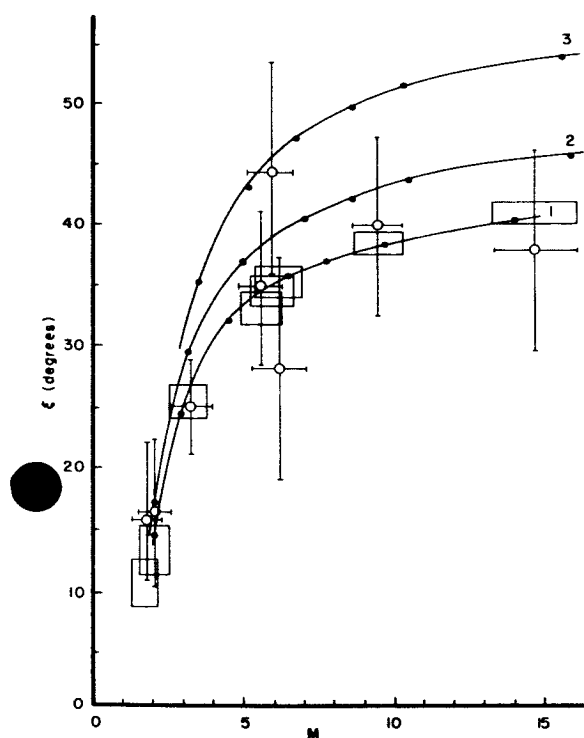


**Fig. 15. Theoretical dependence of the phase lag of the first harmonic of the radio emission of the Moon on the ratio of the constant component to the amplitude of the first harmonic of the emission for a cycle. 1, Homogeneous structure of the surface ( $m = 1.0$ ,  $\xi = 0$ ,  $\delta = 2\lambda$ ). 2–3, Two-layer dust ( $m = 1.0$ ,  $\xi = 5^\circ$ ,  $\delta = 2\lambda$ , and  $m = 1.4$ ,  $\xi = 15^\circ$ ,  $\delta = 1.5\lambda$  respectively). Black dots are theoretical values for wavelengths of 0.13, 0.4, 0.8, 1.25, 1.63, 2.0, and 3.2 cm. The circles are the experimental values plotted with indication of errors on  $\xi$  and  $M$ .**

model ( $N = 1$ ,  $\xi = 0$ ); curve 2 corresponds to the two-layer model with a very thin upper dust layer giving  $N = 1.1$  and  $\xi_s = 5^\circ$ . At the thickening of the layer when  $N = 1.4$  and  $\xi_s = 15^\circ$ , one obtains curve 3. Experimental points for the wavelengths 0.13, 0.2, 0.4, 0.8, 1.25, 1.6, and 3.2 cm are marked by circles with indication of the limits of the possible error in  $\xi$  and  $M$ . As is seen from Fig. 15, the experimental points correspond to the single-layer model, and all of them cannot be made to agree simultaneously with the two-layer model having even a very thin layer of dust. Rectangles mark the values  $M$  and  $\xi$  when  $M$  is derived from the experiment and  $\xi$  is computed from the value  $\delta_1$  (found by the value of  $M$ ) by the formula for the homogeneous model. If the model were inhomogeneous, these values would not fall on the

curve which corresponds to the homogeneous model. Thus, in the limits of the investigated spectrum of the value  $M$ , the upper layer behaves as a homogeneous medium in radio emission. This enables one to draw a conclusion of a quasi-homogeneity of layer properties with depth. The result obtained does not contradict the assumption of a smooth, slight inhomogeneity which does not become apparent either due to inaccuracy of measurements, or due to insufficient coverage of the spectrum.

Investigation of the model of the superficial cover structure by the spectrum of a variable part of the radio emission of the Moon is, for the present, unique. Often, in the works on the measurements at one wavelength, conclusions are drawn about the model, but, as shown by analysis, the data at one wavelength may be interpreted loosely enough. This is not surprising, as only the spectrum of radio emission values satisfies the exploration of different depths. In most works the statements about the model are simply drawn without any analysis (Garstang, 1958; Giraud, 1962).

It should be noted that the generally adopted two-layer model is self-contradictory (Troitsky, 1964b). Generally the layer in this model has  $\gamma_1 = 1000$ , and the lower  $\gamma_2 = 100$ , the density being admitted as equal to  $\rho_1 = \rho_2$ . Therefore it turns out that thermal conductivities differ from each other by  $\kappa_2/\kappa_1 = \gamma_1/\gamma_2^2 = 100$  times! Taking into consideration  $\kappa = \alpha\rho$ , we find that the model with given values  $\gamma_1$ ,  $\gamma_2$  cannot have the arbitrary relationships of thermal conductivity and density; it must have the following correct relations of parameters:

$$\kappa_2/\kappa_1 = \gamma_1(\alpha_2)^{1/2}/\gamma_2(\alpha_1)^{1/2}, \quad \rho_2/\rho_1 = \gamma_1(\alpha_1)^{1/2}/\gamma_2(\alpha_2)^{1/2}.$$

In the case of the identical structure type ( $\alpha_1 = \alpha_2$ ), the relation of thermal conductivities and densities in the adopted model ought to be identical and equal to 10. By different structures of the sublayer is solid and of the upper layer, as for example when the sublayer is solid and somewhat porous, and the upper layer is thin dust.

$$\alpha_2 \simeq 4\alpha_1$$

$$\kappa_2/\kappa_1 = 20$$

$$\rho_2/\rho_1 = 5$$

#### D. Spectrum of Reflection Coefficient. Dielectric Constant and Density of Material of the Upper Layer. Model of Layer

Four methods are offered for measuring the reflection coefficient and dielectric constant of the planet material:

(1) measurements of the constant component of radio temperature (Krotikov and Troitsky, 1962); (2) measurement of the polarization of radio emission (Troitsky, 1954; Troitsky and Tseytlin, 1960); (3) measurements of distribution of radio brightness at the disk (Salomonovich, 1962a); (4) measurements of the amplitude distribution and phase lag of variations of radio temperature on the equator of the Moon (Troitsky, 1961a).

The precision measurements of radio emission enable one to determine the constant component of the brightness radiotemperature on the disk. Measurements at a number of centimeter wavelengths, which will be described below, with gradient correction, give the following value for the constant component:

$$T_{e0} = 207 \pm 2^\circ \text{K}.$$

Comparison with the mean value of surface temperature gives us the mean hemisphere reflection coefficient  $\bar{R} = 0.04 \pm 0.02$ . This gives (Krotikov and Troitsky, 1962)

$$R_{\perp} \approx 1\% \quad \epsilon = 1.5 \pm 0.3.$$

Polarization measurements carried out at wavelengths of 3.2 and 2.05 cm (Soboleva, 1962; Baars, Mezger et al., 1963) give the value for dielectric constant

$$\epsilon = 1.5.$$

In both works the roughness of the surface was taken into account; in the second, the value  $\pm 15^\circ$  was taken for the slopes as the closest to that derived from the radar. For distribution of radio brightness, one value only is obtained:  $1 \leq \epsilon \leq 2$  (Salomonovich, 1962). Thus, by means of radio astronomical methods,  $\epsilon = 1.5 \pm 0.3$  and  $R \approx 1\%$  were obtained for the centimeter wavelengths. Knowing the dielectric constant and assuming the silicate structure of rocks, the density of the material on the Moon surface layer, in accordance with (5), is equal to  $\rho = 0.5 \pm 0.3$ . Meanwhile, the radar investigations give, at the same wavelengths, the average from all the existing measurements,  $R_1 = 4\%$  and  $\epsilon = 2.25$ . The difference is probably associated with roughness leading to the formation of sufficiently plane reflection surfaces creating a similarity to a polyhedron inscribed into the sphere of the Moon. On radio emission where the phase relationships play no part, such a form of the surface will have no influence. It is interesting that the same radar measurements give, for the  $\lambda = 30\text{--}75$  cm, the average reflection coefficient value, for all the data, of

twice as much, i.e.,  $R_1 = 8\%$  and  $\epsilon = 3.2$ . Of course, the spectrum of the reflection coefficient is not associated with a real change of  $\epsilon$  with the frequency, and appears as a result of inhomogeneity of the properties with depth. This problem was considered in one of the works (Matvejev, Suchkin, and Troitsky, 1965), the results of which are reduced to the following: As for initial data, one may safely adopt the values  $R$  and  $\epsilon$  at the centimeter waves, measured radio-astronomically, and at the decimeter waves, the value 2.5, i.e.,

$$\begin{aligned} R_1 = 1.7\% \quad \epsilon_1 = 1.7 \quad \rho_1 = 0.6 \quad 0.8 \leq \lambda \leq 12 \text{ cm} \\ R_2 = 4\% \quad \epsilon_2 = 2.25 \quad \rho_2 = 1.0 \quad 33 \leq \lambda \leq \infty \text{ cm} \end{aligned} \quad (33)$$

(values for  $R_1$  and  $R_2$  correspond to the normal incidence of waves).

The range, where the transition from one series of values to another one is being achieved, makes up about 15 to 50 cm. The medium-frequency wave in this range,  $\lambda_m = 30\text{--}35$  cm, is not determined with certainty.

The most probable explanation of the dependence  $R(\lambda)$  consists in the assumption of the changing of density and  $\epsilon$  with depth. Here two cases may be noted: the change occurs at the depth of the order of wave penetration (Gold, 1963), or the density is changing on the surface itself. In both cases one should assume that the properties of the layer are varying for the length which presents portions of the length of the wave  $\lambda_m$ . The first version should be excepted as it does not explain the difference between the eclipse and lunation values of  $\gamma$  (see below). The second case is probable. Therefore, if the properties vary smoothly from the surface to the depth  $l$ , then, for  $\lambda \gg l$ , the lower dense layer of the material will mainly reflect, and, for  $\lambda \ll l$ , the boundary of the upper layer for this wave will become deeper as  $\lambda$  increases.

The following law of density variation with depth was adopted:

$$\rho(x) = \rho_2 - (\rho_2 - \rho_1)e^{-x/x_0}, \quad (34)$$

where  $\rho_1$  and  $\rho_2$  are the density values of lunar material at the surface and at the depth  $x$ , respectively. At the depth  $l=2.5x_0$ , later called the thickness of an inhomogeneous layer, the density attains its limiting value,  $\rho_2$ .

In the case of one-dimensional inhomogeneity, the coefficient of reflection is determined, as is known by the Ricatti equation. Its solution under conditions (33), (34) was carried out on a digital computer. As a result, it turned out that the experimentally known medium-frequency wave of the transition range depends on the thickness of inhomogeneity, in the following way:

$$l = \frac{\lambda m}{8}.$$

Taking into account the experimental value of  $\lambda_m = 30$  cm, we find that the observed spectrum of the reflection coefficient will take place if the thickness of the inhomogeneous layer is

$$l = 4 \text{ cm} \quad x_0 = 1.5 \text{ cm}.$$

Thus, the radio-astronomical and radar investigations of the reflection coefficient lead to the conclusion about density changing of the material to the depth by 1.5–2 as much for the distance of 3 to 4 cm. The thermal conductivity probably varies in the same proportion, as well, (if  $\alpha(x) = \alpha = \text{const}$ ).

A final judgement still necessitates the accurate measurement of the spectrum of reflection in the range of 10 to 50 cm, both by radar and radio-astronomical methods.

### E. Thermal Properties of the Surface Cover

Let us apply the above-considered methods of determining the value  $\gamma$ . Let us first consider the eclipse regime. To determine  $\gamma$ , the different curves of temperature falls obtained at the time of the eclipses in 1927 and 1939 were used (Pettit and Nicolson, 1930; Pettit, 1940). Comparison with the computation for the homogeneous model (Wesselink, 1948; Jaeger and Harper, 1950) leads us to the value

$$\gamma_1 = 1000.$$

However, the optimum coincidence of the theoretical curve in the zone of shade is obtained, for the two-layer dust model (Jaeger, Harper, 1950) considered above. Recently, for the eclipse on September 5, 1960, the measurements of cooling curves and of the  $\gamma$  of five radiant craters, with their environment, were carried out (Saari and Shorthill, 1962). On the average, with the exception of the bottoms of craters,  $\gamma = 1000$ . However, the extreme need for more precise and reliable measurements

of temperature slope at the time of the eclipses for different formations should be noted. The case is somewhat worse with the measurement of the  $\gamma_2$  in the lunation regime. Here the complete cycle does not yet exist. Theoretical curves for the homogeneous model are presented in Fig. 16 (Krotikov and Shchuko, 1963). As can be seen from this figure, the most effective measurements to determine the  $\gamma_2$  are measurements by the transition from day to night. Recently such measurements were carried out (Murray and Wildey, 1964), giving the value  $\gamma_2 = 700$ . The periodic regime permits another method of determining  $\gamma_2$ —not by the curve of the surface temperature, but by its Fourier components. This method has the advantage that we can use the data on radio measurements which do not give the absolute values of the surface temperatures, but allow the Fourier components to be determined without requiring a knowledge of electrical properties of the model. For such a determination, the related values  $T_{sn}$ ,  $T_{s0}(0)$ ,  $T_{s0}(0)/T_1(0)$  in the function  $\gamma_2$  are given in Table 1 for the homogeneous model (Krotikov and Shchuko, 1963). Disposing of experimentally known values  $T_{s0}$ ,  $T_{s0}/T_{s1}$ , and  $T_{sn}$ , one finds the value of  $\gamma_2$  (Krotikov and Troitsky, 1963a). Here we present the value  $\gamma$  corrected according to more precise

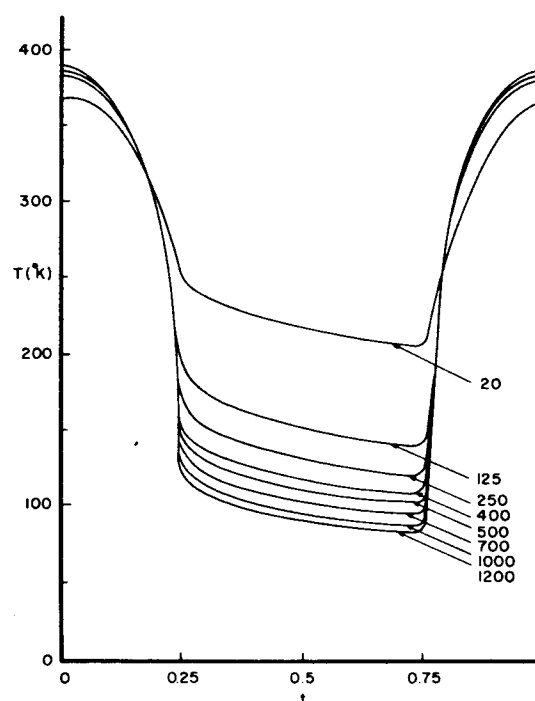


Fig. 16. The surface temperature measurement in the center of the lunar disk in the dependence of the given lunation period for different values of the parameter  $\gamma$



initial data. Plotting curve  $M(\lambda)$ , according to the measurements of radio emission, one can find that by letting  $\lambda \rightarrow 0$ , then  $T_{s0}/T_{s1} = 1.35 \pm 0.1$ . This gives, in accordance with Table 1,  $400 \leq \gamma_2 \leq 800$ . The value of the night temperature  $T_{sn} = 115 \pm 5^\circ$  leads to the same value. For the constant component of the center at the disk, according to the measurements of mean radio temperature for the disk and after a corresponding recomputation, one obtains  $T_{s0}(0) = 226^\circ \pm 5^\circ$ , which gives  $\gamma_2 = 600-800$ . Thus, the present data lead to the value

$$\gamma_2 = 600 \pm 200.$$

This difference between the eclipse and lunation values is naturally explained by inhomogeneity of the density of the material in the superficial layer. Realizable dependency of the material properties on temperature (Buettner, 1963), as computations show (Aljeshina and Krotikov, 1965), cannot explain the observed difference. The assumption of a linear dependence of  $\kappa$  and  $c$  on the temperature, made by Munsey (1958) seems to us to be very unlikely. It should be noted that, in the case of an existing inhomogeneity and with the adoption of the theory of a homogeneous model for the determination of  $\gamma$ , we can obtain an overestimation of  $\gamma_2$  lying between that at the surface and the true value at a depth. Using the values for defined parameters at the surface  $\gamma_1 = 1000$  and  $\rho_1 = 0.5$ , we obtain, for the thermal conductivity,

$$\kappa_1 = (1 \pm 0.5) \times 10^{-5} \text{ cal/cm deg sec.}$$

The structural parameter is equal

$$\alpha_1 = \kappa_1/\rho_1 = (2 \pm 1) \times 10^{-5} \text{ cal cm}^2/\text{sec deg.}$$

At the depth of 3-4 cm or more,  $\gamma_2 = 600$  and  $\rho_2 = 1$ ; hence  $\kappa_2 = (1.7 \pm 1) \times 10^{-5}$  for the same structural parameters. It remains to evaluate the depth of the penetration of a temperature wave. As for both media  $\kappa = \alpha\rho$ , the value

$$l_T = \left( \frac{\kappa}{c\rho} \cdot \frac{t_0}{\pi} \right)^{1/2}$$

should be identical for both media too. But in the case of the inhomogeneous layer composed of those media, this expression is now untrue for the  $l_T$ . However, a small inhomogeneity will not change the value  $l_T$  substantially, and it will be

$$l_T = \left( \frac{\alpha t_0}{c\pi} \right)^{1/2} = (10 \pm 5) \text{ cm.}$$

For the eclipse, a similar value at the moment of the end of the umbral phase is equal to

$$l_{ec} = \left( \frac{\alpha}{c} \right)^{1/2} (t_3 - t_1),$$

where  $t_3 - t_1$  is a time-interval from the beginning of the eclipse up to the umbral phase; this time interval is equal to about 3 hours. Hence,

$$l_{ec}/l_T = \left[ \frac{(t_3 - t_1)\pi}{t_0} \right]^{1/2} \simeq 0.1$$

and  $l_{ec} \simeq 1 \text{ cm.}$

## F. Absorption Spectrum of Electromagnetic Waves in the Material of the Moon

In order to determine the absorption spectrum, it is necessary to determine  $\delta_1$  from the experimental data. The best way is to compare the experimental value  $M$  with the theoretical one (32a) for the homogeneous model. It is apparently safe to use the theory of the homogeneous model in spite of the existence of some inhomogeneity; as we have seen, the experiment satisfies this model to within the measurement accuracy. Determination of  $\delta$  at the wavelengths of 0.13 to 3.2 cm has shown that it is changing in proportion to the wavelength  $\lambda$  (Troitsky and Zelinskaja, 1955; Zelinskaja, Troitsky, and Fedosejev, 1959; Krotikov and Troitsky, 1963b)

$$\delta = m\lambda \quad 0.1 \leq \lambda \leq 3.2 \text{ cm.}$$

The value of the coefficient of proportionality is found to be equal to  $m = 2$ . Figure 17 shows the spectrum  $\delta/\lambda = m$ , including all available data. Some deviation from a linear dependence takes place in the vicinity of  $\lambda = 1.6 \text{ cm}$ , which can be interpreted as absorption in the lunar material near that wavelength. Taking the

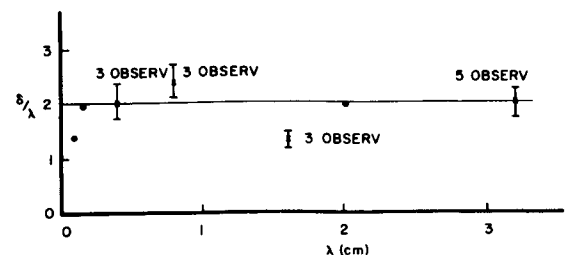


Fig. 17. The dependence of  $\delta/\lambda$  on wavelength  $\lambda$ . Black dots correspond to the experimental data.

value of  $l_r = 10$  cm, we obtain depth of the penetration of electromagnetic wave of

$$l_e = (20 \pm 10) \lambda.$$

This dependence between  $l_e$  and  $\lambda$  confirms the dielectric nature of the Moon material. The unknown relationship of the heat and electric parameters is equal to

$$\frac{c\gamma_2}{b_2(\epsilon_2)^{1/2}} = 5.6 \times 10^3 m = 11.2 \times 10^3,$$

where the points indicate parameters most likely to concern the layers deeper than 3 to 4 cm ( $3 \leq l_e \leq 60$  cm). Contrary to this, the eclipse measurements give the value for the parameters of the upper layer and are marked by the  $x$ 's. All present data on the magnitude of the relative drop in radiation temperature at the time of the eclipse are given in Table 3.

In the same table are presented the values  $\gamma_1/b_1(\epsilon_1)^{1/2}$  computed in accordance with the above theory (Troitsky, 1965).

Figure 14 gives the theoretical curves  $M(\lambda)$  for the eclipse of December 30, 1963, with different values for  $\gamma/b(\epsilon)^{1/2}$ , computed by exact formulas, together with the experimental points. According to the data presented in Table 3 (except the data on the partial eclipse of February 7, 1963), one may take

$$\frac{c\gamma_1}{b_1(\epsilon_1)^{1/2}} = (11.4 \pm 3) 10^3.$$

This value concerns the layer less than  $l_{ec} \simeq 2 - 3$  cm. In accordance with this it is necessary to adopt the values  $\epsilon$  and  $\gamma$  for the corresponding depths, for the determination of  $b_1$  and  $b_2$ ; i.e.,  $\epsilon_1 = 1.5$ ,  $\gamma_1 = 1000$ ; and  $\epsilon_2 = 2.25$ ,  $\gamma_2 = 600$ . As a result we obtain

$$b_2 = (7.5 \pm 1.5) \times 10^{-3} \quad b_1 = (14 \pm 4) \times 10^{-3}.$$

A comparison of these data suggests that, together with a certain inhomogeneity as to the density of the material, an inhomogeneity apparently occurs with depth of the electrical properties, i.e., of the nature of the material. The increase in a specific loss angle to the surface may be associated with saturation of the surface layer by meteoric material having the  $b \simeq 2 \times 10^{-2}$ .

### G. Spectrum of the Constant Component and Heat Flux From the Depths of the Moon

As shown above, the constant component of radio emission is determined by a constant portion of the layer temperature at the depth of the penetration of the wave. The repeated attempts to discover the anticipated systematic rise of the constant component with the wavelength turned out to be unsuccessful due to poor precision of usual radio measurements. In order to discover the effect, special measurements of radio emission were carried out at the 168-cm wavelength (Baldwin, 1961.) However, neither precision of measurements, nor assumptions made by working out the results (linear rise in temperature up to the wavelength 168 cm) allowed the gradient and flux to be determined with sufficient safety. One has estimated the flux,  $q_s = 0.25 \times 10^{-6}$  cal/cm<sup>2</sup> sec, that coincides with the theoretical values (Jaeger, 1959; McDonald, 1959; Levin and Majeve, 1960; Majeve, 1964). As a result of using the precision method of measurements, the growth of the constant component of radio temperature of the Moon was soundly established (Krotikov and Troitsky, 1963c). Figure 18 presents the spectrum  $\bar{T}_{ec}(\lambda)$ , obtained by the above measurements of the wavelengths of 0.4, 1.6, 9.6, 14, 32.5, 35, and 50 cm, carried out in the Research Institute of Radio Physics in 1961–1964. The observed effect cannot be explained by any overlooked errors of measurements or such causes as roughness or reflection by the Moon of galactic and solar radiation. Reflected by the Moon, the galaxy radiation appears at those wavelengths so small that it may be disregarded (Starodubstev, 1964). The only way to explain the observed effect is to admit a real rise in the deep temperature due to flux of internal heat. However, the question of the origin of such a flux remains. In principle, two possibilities exist. Either the flux is of a solar origin, or, just as for the Earth, it is caused by dissociation of radioactive elements, contained in all of the rocks. The first assumption requires very unnatural suppositions about light penetrating to depths of up to 10 m, and so on. The least contradictory explanation is that the flux of heat comes from great depths. Figure 18 shows the almost linear rise in radio temperature of the Moon with wavelength up to  $\lambda = 30$  cm, which suggests an approximately constant thermal conductivity to the depth of penetration of each wavelength. There are far more dense layers at greater depth with thermal conductivity close to the terrestrial value (100 times greater than the lunar), giving, therefore, a temperature rise with depth hundreds of times smaller. Thus, the thick porous layer of the material lies, apparently, on a dense rock base. The thickness of this layer may be evaluated. As the thermal conductivity in the layer is equal throughout,

the density is equal as well. If the parameter  $b$  is not changed, the value of electromagnetic wave attenuation is equal in the total layer, as well as in its upper part,  $l_e = 20\lambda$ . Consequently, the thickness of the porous layer, corresponding to depth of penetration of waves of  $\lambda = 30$  cm, is equal approximately to

$$l_{\text{por}} \simeq (3 \text{ to } 10) \text{ m.}$$

As seen from Fig. 18,  $dT_{e0}/d\lambda \simeq 1$  deg/m. Hence, from the theoretical computations above, where  $l_T = (10 \pm 5)$ , we obtain for the gradient of temperature in the 6-m layer,

$$\text{grad } T(x) = (4 \text{ to } 2) \text{ deg/m.}$$

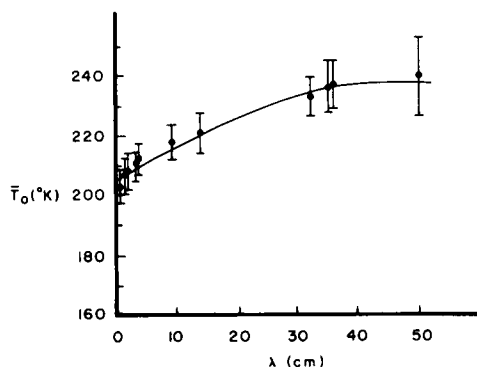


**Fig. 18. The dependence of the mean disk constant component of the effective temperature on wavelength, from the data of precision measurements of lunar radio emission**

Accepting  $\gamma_2 = 600$ , the density of the flux, according to (15), turns out to be equal to

$$q_s = (1 \pm 0.3) \times 10^{-6} \text{ cal/cm}^2 \text{ sec.}$$

As we have seen, the theoretical values for the flux density give a value 4 to 5 times less. The total heat flux from the depths of the Moon is

$$Q = (1 \pm 0.3) \times 10^{19} \text{ cal/deg.}$$

If a heat equilibrium is set up, then it follows from the value  $Q$  that per 1 g of the lunar material there is educed per year

$$q_v = 1.7 \times 10^{-7} \text{ cal/g year}$$

of radiogenic heat.

This value is 4 to 5 times greater than that for the Earth and suggests that the mean concentration of radioactive elements in the Moon material is much higher than their mean concentration for the Earth. This fact will require the radical revision of existing ideas about the heat history of the Moon, based on low content of radioactive elements.

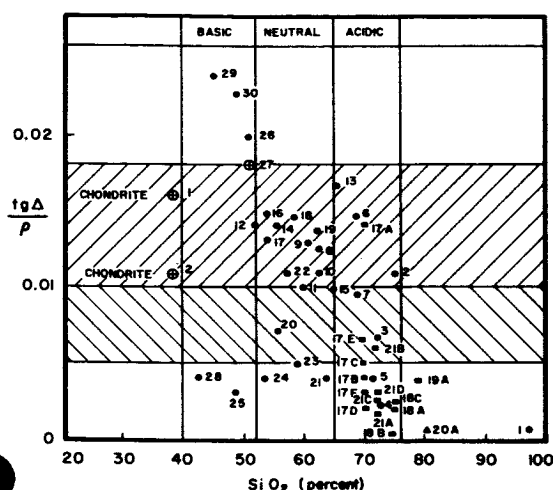
## H. Microstructure: Nature of the Material

The microstructure of the obtained porous layer is still very obscure. In the main, one has to choose between a fine dispersed dry (dust) and a solid porous structure. However, the parameter  $\alpha_L$  for the Moon appears so well determined for this purpose. Its value, as we have seen, for both parts of the layer is approximately  $\alpha_L \simeq 2 \cdot 10^{-5}$ . This value lies between the values  $\alpha$  for the dust and the solid porous medium in vacuum, which are composed of terrestrial rocks. Unreliability of the latter numbers, and of the value  $\alpha_L$ , too, for the Moon makes the conclusion about the microstructure very tentative. It is possible that the vicinity of  $\alpha_L$  to the value for the dust points to the character of origin of the upper porous layer by means of cohesion and adhesion of dust particles arising by meteoric bombardment of sufficiently loose structures. This gives an intermediate structure between a solid-porous and a dry-dust structure, when the heat contacts are weaker than in the first one, and stronger than in the second, as the pores are opened. A similar structure was investigated at optical wavelengths and was found to correspond, as to the scattering, to the superficial layer of the Moon (Hapke and Van Horn, 1963).

To draw some conclusions about the nature of the material, according to the method above, values of  $\text{tg } \Delta/\rho$  for various rocks are given in Fig. 19. In the diagram are plotted two shaded bands corresponding to likely lunar values of parameters. The upper band corresponds to the measurements to the time of the eclipse that give a value for the layer at a depth of the order of 1 to 2 cm. The lower band corresponds to the values  $b_2$  derived from the lunar measurements for underlying depths. As seen from Fig. 19, the upper layer of the material may be a volcanic slag, meteoric material and tuff, the lower layers, tuff, pumice, ashes, etc.

## I. Distribution of Properties on the Surface of the Moon

A number of investigators repeatedly affirm a considerable difference in properties of the material over the lunar surface. Thus, for example, the maria have



- |                    |                       |
|--------------------|-----------------------|
| 1 quartz sand      | 23 diorite            |
| 2 obsidian         | 24-25 gabbro          |
| 3 ignimbrid        | 26-27 basalts         |
| 4 liparite         | 28 iolite             |
| 5 granite          | 29 dunite             |
| 6-7 pumice stone   | 30 dolerite           |
| 8-10 tuffs         | 17A-17F australites   |
| 11 trachytic lava  | 18A-18C indochinites  |
| 12-19 volcanic ash | 19A moldavites        |
| 10-21 simtes       | 20A silica glass      |
| 22 andesitobasalt  | 21A-21D philippinites |

Fig. 19. The dependence  $\text{tg } \Delta/\rho$  on the percent content  $\text{SiO}_2$  for different rocks, meteorites, and tektites

been claimed to be formed of basalt, and the continents of granite.

Quantitative investigation of different characteristics of reflected light (polarization, index of reflection, albedo, color) lead, as is known, to the conclusion of a high photometric homogeneity of the Moon's surface (Barabashov et al., 1959). However, this does not give sufficient arguments in favor of the homogeneity of such properties as density, thermal conductivity, and chemical and mineral composition.

The author (Troitsky, 1964c) considered in his work the methods to determine the variations of values  $\gamma$ ,  $\rho$ , and  $b$  on the disk of the Moon. Briefly the results are reduced to the following:

One can determine variations of the value  $\gamma$  on the disk of the Moon by spatial distribution of the temperature of the night Moon or at the time of an eclipse. Fluctuations of temperature can be determined by deviation of observed isotherms from the ideal ones. Approximately, the relationship connecting the variations  $\gamma$  with those of the night temperature has a form

$$\frac{\Delta T_{sn}}{T_{sn}} = \frac{1}{16} \frac{\Delta \bar{\gamma}^2}{\gamma^2} + \frac{1}{16} \frac{\Delta \bar{R}_i^2}{(1 - R_i)^2}.$$

Spatial distributions of infrared temperature in the sunlit zone, when the incidence angle of the Sun's rays is  $i \leq 70-80^\circ$ , are equal to

$$\frac{\Delta \bar{T}^2}{T^2} = \frac{1}{16} \text{tg}^2 i \Delta \bar{i}^2 + \frac{1}{16} \frac{\Delta \bar{R}_c}{(1 - R_c)^2} + \frac{1}{16} \frac{\Delta \bar{R}_i^2}{(1 - R_i)^2}.$$

The fluctuations of temperature in the subsolar zone ( $i = 0$ ), as one can see from the expression, allow a determination of the sum of mean squares of relative fluctuations of an optical and infrared albedo. Measurements at low angles of the Sun determine the fluctuations of surface slopes. The investigation of infrared isotherms for the sunlit zone using a resolution of about 20 km (Saari and Shorthill, 1962) have shown that for the subsolar point, variations of  $(\Delta \bar{T}^2)^{1/2} = \pm(1 - 1.5)$ . This corresponds to albedo variation of the order of  $(\Delta \bar{R}_c^2)^{1/2} = (\Delta \bar{R}_i^2)^{1/2} \simeq 10^{-2}$ . Variations of the value  $\gamma$  at present can be evaluated only roughly, as a map of the night isotherms of the Moon does not yet exist. Individual measurements of the night temperature all along the trajectory (Murray and Wildey, 1964; Saari and Shorthill, 1964) prove that its variations do not exceed, apparently,  $\pm 15^\circ$ , i.e., about 1/20 of the average value. Hence we obtain

$$\frac{\Delta \gamma_s}{\gamma_s} = \pm 0.25; \quad 750 \leq \gamma_s \leq 1250.$$

The direct measurements of  $\gamma_1$  for different points on the Moon's disk (with the exception of the bottom of radiating craters) show the same scattering (Saari and Shorthill, 1962). Thus, we come to the conclusion that thermal conductivity and density of the lunar material, when averaging over a region of about 20 km, are varying on the surface (except at the bottoms of craters) hardly more than by 1.5 to 2 times. Notice that the depth of the penetration of heat wave will be identical, independent of the value of  $\rho$ . By measuring the radio emission with a sharp beam, the possibility arises of evaluating the

distribution of values of  $\gamma/b (\epsilon)^{1/2}$  on the disk. The measurements carried out at 0.4 cm (Kisljakov and Salomonovich, 1963) testify to a considerable constancy of that value in the equatorial zone when averaging over a region having a linear dimension of the order of 150 km. No difference was observed in this value for maria and continents. This indicates the unchanging nature of the material that forms the lunar superficial layer. At least, the data definitely deny the hypothesis of basalt rock for the material of maria and that of granite for continents. The measurements of radio emission at the  $\lambda = 3.2$  mm at the time of the eclipse were recently carried out for different points, including the bottoms of craters, as well (Jacobs et al., 1964). The analysis carried out by us shows that the value  $\gamma/c (\epsilon)^{1/2}$  turns out to be in the limits of precision of measurements ( $\pm 20\%$ ) identical for all of those formations. Thus, besides the photometric homogeneity, there exists the radiometric homogeneity of the material of the first decimeter of the lunar surface, associated with a high degree of the homogeneity of thermal and electric properties of the material on the Moon surface.

#### J. Properties of the Venus Surface

The radar investigations have shown that for Venus,  $R_{\perp} \simeq 0.1$ . This gives  $\epsilon = 4$ , and, if the material of the surface is composed, just as at the Earth, of silicate rocks, then the density  $\rho = 2$  g/cm<sup>3</sup>. The dependence of radio emission on the phase, according to measurements at  $\lambda = 3.2$  cm and 10 cm, respectively, has a form  $T_{e1} = 621 + 73 \cos (\Phi - 12)$  and  $T_{e1} = 622 + 39 \cos (\Phi - 17)$ . This phase dependence proves that the axis of rotation of Venus does not lie in the plane of its orbit, and the rotation is retrograde. We assume for the material of Venus, as well as for all the silicate dielectrics, that  $\delta = m\lambda$ . Equating the relations  $M(3) = 621/73$  and  $M(10) = 622/39$  with their theoretical value (32a) for integral flows and solving the equations with two unknown quantities by the  $\beta_0 = 0.92$ ,  $\beta_1 = 0.73$ , we obtain (Troitsky, 1964)

$$\delta = 0.14\lambda, T_{s0}(0)/T_{s1}(0) = 4, T_{s1}(0) = 150^\circ \text{K}.$$

$$\frac{\gamma c}{b(\epsilon)^{1/2}} = 2m(\pi t_0)^{1/2}$$

The duration of a solar day, according to radar measurements, is of the order of 100 days. Accepting  $c = 0.2$ , we have  $\gamma/b = 1.5 \times 10^4$ . Accepting, as for terrestrial rocks, the mean value  $b = (1 \pm 0.5) \times 10^{-2}$ , we obtain

$$\gamma = 150.$$

This value is too high, and by  $\rho = 2$  leads to the value  $\alpha = 0.6 \times 10^{-4}$ , which is one order less than the value for porous rocks in the atmosphere of the Earth. To solve the problem of determination of a period, adopting the  $\gamma/b = 50/10^{-2} = 5 \times 10^3$  as a initial value close to the terrestrial one, we obtain  $t_0 \simeq 10$  days. It is necessary to carry out more precise measurements of phase dependence of radio temperature of Venus.

### III. Conclusions

As the considerations above show, the investigation of the proper thermal radiation from solid bodies, particularly by existing variable thermal regimes of different periodicity and duration, allows us to obtain substantial information on physical parameters of the layer and the temperature regime. However, the experimental initial data obtained for the Moon are still not sufficiently complete and precise. There continues to be considerable uncertainty in our knowledge of the parameters of the Moon layer material. Essentially, at present we have the values only for those magnitudes. For a more precise determination of parameters of the Moon layer, further investigations on infrared radiation and radio emission of the Moon are needed in both thermal regimes: the lunation and the eclipse. Precise measurements of the night infrared temperature are particularly needed; the absolute measurements of surface temperatures depending on time for different formation on the Moon are also necessary. The relative measurements of temperature distribution on the Moon disk at night and at the time of the total phase of the eclipse are needed as well.

At present, the radio experiments are more advanced, perhaps, than those in the infrared field. In any case, the quantity and precision of radio data on integral emission do not limit the possibility of drawing conclusions. However, at present, it is clearly necessary to measure the radio emission at short millimeter waves in order to determine the inhomogeneity of the layer with depth. Especially advisable is the measurement of the polarization spectrum in the range from millimeter up to decimeter wavelengths. Practically speaking, only the first steps have been made here. Finally, a large remaining field is the investigation at radio wavelengths of separate zones of the Moon. It is extremely advisable here to use wavelengths in the decimeter range. However, here one meets with difficulties in obtaining sufficient resolving power. Possibly such investigations can be made from satellites placed around the Moon.

## REFERENCES

- Alyeshina, T. H., and Krotikov, V. D., 1965, *Izv. VUZ'ov, Radiofizika*.
- Baars, J. W. M., Mezger, D. G., Savin, N., and Wendkel, H., 1963, *URSI Symposium Proceedings, Tokyo, 1963*.
- Baldwin, I. E., 1961, *Monthly Notices Roy. Astron. Soc.* Vol. 122, p. 513.
- Barabashev, N. P., Ezerskaya, V. A., Ezersky, V. I., and Ishutina, T. I., 1959, *Izv. Comm. on Planet Physics*, Vol. 1, p. 67.
- Bernett, E. C., Wood, H. L., Jaffe, L. D., and Martens, H. E., 1963, *AIAA (Amer. Inst. Aeron. Astronaut. J.)*, Vol. 1, pp. 6, 1402.
- Bondar, L. N., Zelenskaya, M. R., Porfiryev, V. A., and Strezhneva, K. M., 1962, *Izv. VUZ'ov, Radiofizika*, Vol. 5, p. 802.
- Buettner, K. J. K., 1963, *Planetary Space Sci.*, Vol. II, p. 135.
- Burns, E. A., and Lyon, R. J., 1964, *J. Geophys. Res.*, Vol. 69, pp. 18, 3771.
- Castelli, J. P., and Ferioli, C. P., 1962, *AF CRL*, pp. 62-882, Bedford, Mass.
- Davies, R. D., and Jenisson, R. C., 1960, *Observatory*, Vol. 80, p. 74.
- Denisse, J. F., and de Roux, E., (unpublished).
- Dmitrenko, D. A., Kamenskaya, S. A., and Rakhlin, V. L., 1964, *Izv. VUZ'ov, Radiofizika*, Vol. 7, pp. 5, 55.
- Fedoseyev, L. N., 1963, *Izv. VUZ'ov, Radiofizika*, Vol. 6, pp. 4, 655.
- Garstang, K. H., 1958, *J. Brit Astron. Associat.*, Vol. 68, pp. 4, 155.
- Geoffrion, A. R., Corner, M., and Sinton, W. M., 1960, *Low. Obs. Bull.*, Vol. 71, p. 102.
- Gibson, J. E., 1958, *Proc. IRE*, Vol. 46, p. 280.
- Gibson, J. E., 1961, *Astrophys. J.*, Vol. 133, p. 1072.
- Giraud, A., 1962, *Astrophys. J.*, Vol. 135, p. 175.
- Gold, T., 1963, *Structure of the Lunar Surface*, Center for Radiophysics and Space Research, Cornell Univ., Ithaca, N.Y.
- Halajian, J. D., 1964, *The Case for a Cohesive Lunar Surface Model*, Grumman Aircraft Engineering Corporation, Report No. ADR-04-04-64.2.
- Hapke, B., and Van Horn, H., 1963, *Photometric Studies of Complex Surfaces, with Application to the Moon*, Center for Radiophysics and Space Studies, Cornell Univ., CRSR, p. 139.
- Jacobs, E., King, H. E., and Stacey, J. M., 1964, *Lunar Eclipse Observations at 3.2 mm With a 2.9 Arc Minute Beamwidth Antenna*, Aerospace Corp., Los Angeles, Calif.
- Jaeger, J. G., 1953, *Australian J. Phys.*, Vol. 6, p. 10.
- Jaeger, J. G., 1959, *Nature*, Vol. 183, p. 1316.

## REFERENCES (Cont'd)

- Jaeger, J. G., and Harper, F. A., 1950, *Nature*, Vol. 166, p. 1026.
- Kamenskaya, S. A., Kislyakov, A. G., Krotikov, V. D., Naumov, A. I., Nikonov, V. N., Porfiryev, V. A., Plechkov, V. M., Strezhneva, K. M., Troitsky, V. S., Fedoseyev, L. I., Lubako, L. V., and Sorokina, E. P., 1965, *Izv. VUZ'ov, Radiofizika*.
- Kamenskaya, S. A., Semyenov, V. I., Troitsky, V. S., and Plechkov, V. M., 1962, *Izv. VUZ'ov, Radiofizika*, Vol. 5, p. 882.
- Kaydanovsky, N. L., and Salomonovich, A. E., 1961, *Izv. VUZ'ov, Radiofizika*, Vol. 4, p. 40.
- Kaydanovsky, N. L., Iskhanova, V. N., Anushinsky, V. A., and Shivrish, O. N., 1961, *Izv. VUZ'ov, Radiofizika*, Vol. 4, p. 428.
- Kislyakov, A. G., 1961, *Izv. VUZ'ov, Radiofizika*, Vol. 4, p. 433.
- Kislyakov, A. G., and Plechkov, V. M., 1964, *Izv. VUZ'ov Radiofizika*, Vol. 7, p. 1.
- Kislyakov, A. G., and Salomonovich, A. E., *Izv. VUZ'ov, Radiofizika*, Vol. 6 (3), p. 431.
- Koshchenko, V. N., Losovsky, B. Ya., and Salomonovich, A. E., 1961, *Izv. VUZ'ov, Radiofizika*, Vol. 4, p. 596.
- Koshchenko, V. N., Kuzmin, A. D., and Salomonovich, A. E., 1961, *Izv. VUZ'ov, Radiofizika*, Vol. 4, p. 425.
- Krotikov, V. D., 1962a, *Izv. VUZ'ov, Radiofizika*, Vol. 5, p. 1057.
- Krotikov, V. D., 1962b, *Izv. VUZ'ov, Radiofizika*, Vol. 5, p. 604.
- Krotikov, V. D., 1963a, *Izv. VUZ'ov, Radiofizika*, Vol. 6, pp. 5, 889.
- Krotikov, V. D., 1963b, *Izv. VUZ'ov, Radiofizika*, Vol. 6, pp. 6, 1087.
- Krotikov, V. D., 1965, *Izv. VUZ'ov, Radiofizika* (in print).
- Krotikov, V. D., Porfiryev, V. A., and Troitsky, V. S., 1961, *Izv. VUZ'ov, Radiofizika*, Vol. 4, p. 1004.
- Krotikov, V. D., Troitsky, V. S., and Tseytlin, N. M., 1964, *Astron. Zh.*, Vol. 41, p. 5.
- Krotikov, V. D., and Porfiryev, V. A., *Izv. VUZ'ov, Radiofizika*, Vol. 6, p. 242.
- Krotikov, V. D., and Troitsky, V. S., 1962, *Astron. Zh.*, Vol. 39, p. 1089.
- Krotikov, V. D., and Troitsky, V. S., 1963a, *Astron. Zh.*, Vol. 40, p. 158.
- Krotikov, V. D., and Troitsky, V. S., 1963b, *UFN*, Vol. 81, pp. 4, 589.
- Krotikov, V. D., and Troitsky, V. S., 1963c, *Astron. Zh.*, Vol. 40, pp. 6, 1076.
- Krotikov, V. D., and Shchuko, O. B., 1963, *Astron. Zh.*, Vol. 40, pp. (2) 297.
- Levin, V. Yu., and Mayeva, S. V., 1960, *Dokl. Akad. Nauk SSSR*, Vol. 133, pp. 4, 243.
- Mayeva, S. V., 1964, *Dokl. Akad. Nauk SSSR*, Vol. 159, pp. 2, 294.
- Matveyev, Yu. G., Suchkin, G. L., and Troitsky, V. S., 1965, *Astron. Zh.*
- Mayer, C. D., McCullaugh, R. M., and Sloanaker, R. M., 1961, *The Solar System*, Vol. 3, Univ. of Chicago.



## REFERENCES (Cont'd)

- McDonald, G. J. F., 1959, *J. Geophys. Res.*, Vol. 64, p. 1957.
- Moroz, V. P., 1965, *Astron. Zh.*
- Medd, W. J., and Broten, N. W., 1961, *Planetary Space Sci.*, Vol. 5, p. 307.
- Munsey, R. W., 1958, *Nature*, Vol. 181, No. 4621, pp. 1458-1459.
- Murray, C., and Wildey, R. L., 1964, *Astrophys. J.*, Vol. 139, No. 2, p. 734.
- Naumov, A. P., 1963, *Izv. VUZ'ov, Radiofizika*, Vol. 6, No. 4, p. 848.
- Pettit, E., 1940, *Astrophys. J.*, Vol. 91, p. 408.
- Pettit, E., and Nicolson, S. B., 1930, *Astrophys. J.*, Vol. 71, No. 2, p. 102.
- Piddington, J. H., and Minnet, H. C., 1949, *Australian J. Sci. Res.*, Vol. 2A, p. 63.
- Piddington, J. H., and Minnet, H. C., 1951, *Australian J. Sci. Res.*, Vol. 4A, p. 459.
- Razin, V. A., and Fedorov, V. T., 1963, *Izv. VUZ'ov, Radiofizika*, Vol. 6, p. 5.
- Saari, J. M., 1964, *Icarus*, Vol. 3, pp. 2, 161.
- Saari, J. M., and Shorthill, R. W., 1962, *Infrared Mapping of Lunar Craters During the Full Moon and the total Eclipse of September 5, 1960*, Boeing Sci. Res. Lab.
- Saari, J. M., and Shorthill, R. W., 1964, *Lunar Temperature Program*, Boeing Sci. Res. Lab.
- Saari, J. M., and Shorthill, R. W., 1965, *Thermal Anomalies on the Totally Eclipsed Moon of December 19, 1964*, Boeing Sci. Res. Lab. Rept. D1-82-0404.
- Salomonovich, A. E., 1958, *Astron. Zh.*, Vol. 35, pp. 1, 129.
- Salomonovich, A. E., 1962, *Astron. Zh.*, Vol. 39, p. 79.
- Salomonovich, A. E., and Koshchenko, B. N., 1961, *Izv. VUZ'ov, Radiofizika*, Vol. 4, pp. 4, 591.
- Salomonovich, A. E., and Losovsky, B. Ya., 1962, *Astron. Zh.*, Vol. 39, pp. 6, 1047.
- Seeger, C. L., Westerhout, G., and Conway, K. G., 1957, *Astron. J.*, Vol. 126, p. 585.
- Sinton, W. M., 1955, *J. Opt. Soc. Am.*, Vol. 45, p. 975.
- Sloanaker, R. M., 1962, *The Solar System, Vol. III, Planets and Satellites*, Univ. of Chicago Press.
- Smoluchowski, M., 1911, *Bull. Acad. Sci. Cracowi, A.*, p. 548.
- Soboleva, N. S., 1962, *Astron. Zh.*, Vol. 39, pp. 6, 1124.
- Starodubtsev, A. M., 1964, *Izv. VUZ'ov, Radiofizika*, Vol. 7, p. 3.
- Strezhneva, K. M., and Troitsky, V. S., 1961, *The Moon*, Academic Press, London, New York; *Izv. VUZ'ov, Radiofizika*, Vol. 4, pp. 4, 600.
- Sytinskaya, N. N., 1959, *Astron. Zh.*, Vol. 36, pp. 2, 315.
- Tolbert, C. W., Krause, L. C., and Dickenson, 1962, *Proc. National Aerospace Electronics Conference*, p. 733.

## REFERENCES (Cont'd)

- Troitsky, V. S., 1956, *Proc. V Conf. on Space Problems*.
- Troitsky, V. S., 1954, *Astron. Zh.*, Vol. 31, pp. 6, 511.
- Troitsky, V. S., 1961a, *Izv. Comm. Planet Phys.*, Vol. 3, p. 17.
- Troitsky, V. S., 1961b, *Astron. Zh.*, Vol. 38, p. 1001.
- Troitsky, V. S., 1962a, *Izv. VUZ'ov, Radiofizika*, Vol. 5, pp. 5, 855.
- Troitsky, V. S., 1962b, *Astron. Zh.*, Vol. 39, p. 73.
- Troitsky, V. S., 1962c, *Izv. VUZ'ov, Radiofizika*, Vol. 5, pp. 3, 602.
- Troitsky, V. S., 1964a, *Izv. VUZ'ov, Radiofizika*, Vol. 7, pp. 2, 208.
- Troitsky, V. S., 1964b, *Astron. Zh.*, Vol. 41, pp. 4, 724.
- Troitsky, V. S., 1965, *Astron. Zh.*
- Troitsky, V. S., and Zelinskaya, M. R., 1955, *Astron. Zh.*, Vol. 32, pp. 6, 550.
- Troitsky, V. S., and Tseytlin, N. M., 1962, *Izv. VUZ'ov, Radiofizika*, Vol. 5, pp. 4, 623.
- Woodside, W., and Messmer, J. H., 1961, *J. Appl. Phys.*, Vol. 32, pp. 9, 1688-1699.
- Waak, J. A., 1961, *Astron. J.*, Vol. 66, pp. 7, 298.
- Wesselink, J. C., 1948, *Bull. Astron. Inst. Neth.*, Vol. 10, p. 351.
- Westerhout, G., 1958, *Bull. Astron. Inst. Neth.*, Vol. 14, p. 215.

## SOME REMARKS ON NEW MEASUREMENTS OF LUNAR TEMPERATURE AT THE ANTISOLAR POINT

V. S. Troitsky

*Scientific Institute of Radiophysics  
Gorky, USSR*

I should like to call attention to the fact that the new value of midnight temperature of the lunar surface,  $T_{sn} \simeq 100^\circ\text{K}$ , cited in B. Murray's paper, sharply contradicts the results of precision measurements of the constant component of the mean disk radio temperature of the Moon  $\widetilde{T}_e$ . In fact, as is known (Krotikov, Troitsky, 1962, *Astron. J.*, Vol. 40, No. 1, 1963, p. 1089),

$$\widetilde{T}_e = (1 - \bar{R}) [T_{sn} + a_0 (T_{sd} - T_{sn}) 0.92],$$

where  $T_{sd}$  and  $T_{sn}$  are the noon and midnight temperatures of the disk center, respectively;  $a_0 = 0.382$  is the Fourier coefficient of the time variation of the temperature; and  $\bar{R}$  is the mean hemisphere coefficient of reflection. The value in square brackets denotes the temperature averaged over the disk and time.

According to numerous measurements and calculations,  $t_{sd}$  is not greater than  $400 \pm 10^\circ\text{K}$ . Assuming that  $T_{sn} = 100^\circ\text{K}$ , one may obtain for the mean disk constant component of radio temperature

$$\widetilde{T}_e = (1 - \bar{R}) 205^\circ\text{K}. \quad (1)$$

By using the "artificial Moon" method, the multiple precision measurements  $\widetilde{T}_e$  at centimeter and decimeter wavelengths lead to the value

$$\widetilde{T}_e = 207 \pm 2^\circ\text{K}. \quad (2)$$

The comparison with (1) shows that  $\bar{R}$  must be equal to zero, i.e., for centimeter waves the Moon is an absolutely black body. This can be true only if the material in the top surface layer, whose thickness is on the order of  $\lambda/8 \simeq 1$  cm, has an extremely low density. Calculations show that, when  $\bar{R} = 5\%$ , the coefficient of reflection for the normal incidence is equal to  $R_{\perp} \simeq 1\%$  and the dielectric constant  $\epsilon = 1.5$ . The new value of the night temperature requires that  $\epsilon \simeq 1$ , but for  $\epsilon = 1.1$  the density is  $\rho = 0.01$  g cm<sup>-3</sup>. Such small  $\epsilon$  and density contradict the polarization and radar measurements.

The contradiction revealed is rather important for all considerations about the parameters of the upper layer of the Moon, and if confirmed, may lead to reconsideration of the data obtained.

I believe that the precision of the lunar infrared night temperature measurements is inferior to that of the radio measurements. Therefore, additional infrared measurements are necessary. In my opinion the inaccuracy of the determination of midnight temperature is connected with incorrect identification of space night temperature distribution with the time one for the center of the lunar disk. Here, the effect of infrared radiation directivity caused by the roughness of the lunar surface may be of great importance. Probably, Lambert's law, which is accepted as valid when passing from space to time distribution, is not applicable to the infrared radiation of the lunar surface. A comparison of direct measurements of midnight lunar temperature in the center of the disk with those that have been carried out will make it possible to obtain the real law of infrared radiation.

## THE STRUCTURE OF THE MOON

B. J. Levin

*Schmidt Institute of Physics of the Earth  
Academy of Sciences of the USSR, Moscow, USSR*

The problem of the structure of the Moon—of its present-day internal constitution and composition—is intimately connected with the much wider problem of the origin of the Moon and of its further evolution.

I am a representative of a group of Soviet scientists who are developing the ideas on the origin of the planetary system, and in particular of the Earth, proposed about 20 years ago by the late Professor O. J. Schmidt. Our results embrace also the origin, evolution, and structure of the Moon. Although the idea that the planets were accumulated from cold matter is now generally accepted, there are important differences in the individual points of view of students in this field upon the details of this process. In my review I will, of course, give due attention to the presentation and defense of ideas developed by our group.

### **1. Origin of the Moon and the Tidal Evolution of the Earth-Moon System**

Three hypotheses of the origin of the Moon are discussed in the scientific literature: the old Darwin hypothesis of its separation from the Earth owing to rotational instability; the capture of an already-formed

Moon; and the accumulation of the Moon from a circumterrestrial swarm of bodies. The last hypothesis was proposed by Schmidt in 1950, and some of its aspects were developed by Ruskol a few years ago.

At the Lunar Symposium at Pulkovo in 1960, all participants agreed that the revival of the hypothesis of the separation of the Moon from the Earth was impossible. However, a month before the Symposium, a paper by Ringwood (Ref. 1) was published, which already contained an attempt at such a revival. Ringwood suggested a rapid segregation of the iron core in a rapidly rotating Earth and mentioned that the acceleration of rotation due to decrease of the moment of inertia could have led to the separation of the Moon. Three years later, Wise (Ref. 2) defended the same idea. He simply mentioned the existence in the literature of opposite points of view on this subject; he neglected the fact that important errors are found in Darwin's and Jeans's calculations which seemed to prove the possibility of the smooth separation of a rotating fluid mass (Ref. 3). Liapunov and Cartan were right when they denied such a possibility.

The separation hypothesis is favorably mentioned in the latest papers and reports by Professor Urey (Ref. 4),

although a few years ago he definitely rejected it (Ref. 5), referring to objections put forward by Jeffreys and Nölke. Along with many other astronomers and geophysicists, Urey now favors the old hypothesis that the Earth's core is composed of iron. In such a case, the difference in the densities of the Earth and the Moon indicates an important difference in their composition, namely, in their iron content. If the Moon originated from some material of the outer shells of the Earth, separated after the segregation of the core and mantle, the difference in composition would be explained.

The alternative explanation favored by Urey is the capture of the already-formed Moon (Refs. 5-7). It is suggested that the Moon was formed at some other distance from the Sun, in an environment that caused its depletion in metallic iron. Urey does not specify the capture process, but in any case its probability is extremely low. Moreover, the orbit of the captured body can have any orientation and eccentricity. The nearly circular orbit of the Moon, lying near the plane of the ecliptic, argues against its capture.

Two years ago, Alfvén (Ref. 8) proposed another version of the capture hypothesis, based on Gerstenkorn's calculations of the tidal evolution of the Earth-Moon system. According to the mathematical calculations carried out by Gerstenkorn (Ref. 9) and also by MacDonald (Ref. 10), the epoch of the closest approach of the Moon to the Earth was preceded by an evolutionary branch when, to go into the past, the size, eccentricity, and inclination of the lunar orbit had to increase rapidly. Alfvén suggested that the Moon was captured on a nearly parabolic orbit with retrograde motion and that its orbit contracted later and became nearly circular, changing its inclination at the same time. At the time of the minimum size of the orbit, the motion became direct, and then began the recession of the Moon from the Earth, which has continued up to now. According to Gerstenkorn's calculations, the distance of the closest approach  $a_{min}$  is insignificantly smaller than the Roche limit, and therefore Alfvén regards the preceding branch of evolution as real. However, according to MacDonald's (Ref. 10) and Sorokin's (Ref. 11) calculations,  $a_{min}$  lies substantially inside the Roche limit (Table 4). Also, in respect to variations of the inclination, Gerstenkorn's results differ markedly from those of Darwin (Ref. 12), Slichter (Ref. 13), MacDonald (Ref. 10), and Sorokin (Ref. 11) (see Fig. 20). The branch of tidal evolution of the Earth-Moon system preceding the closest approach has no real meaning; it is a mathematical result for a point-mass, but not for a real Moon.

**Table 4. Semimajor axis and inclination of the lunar orbit at closest approach**

	Gerstenkorn (Ref. 9)	MacDonald (Ref. 10)		Sorokin (Ref. 10)
		Circular orbit	Elliptic orbit	
$a_{min}$ , Earth radii (taking no account of solar tides)	2.89	2.78	2.78	2.37, for $C = \text{const}$ 2.43, for $C = C(\Omega)$
$a_{min}$ , Earth radii (taking account of solar tides)	2.86	2.72	2.72 <sup>a</sup>	2.40
$\varepsilon$ , deg (at $a = a_{min}$ )	45.7	~10	~10	12.5

<sup>a</sup>2.50, according to MacDonald's letter to Ruskol (1965).

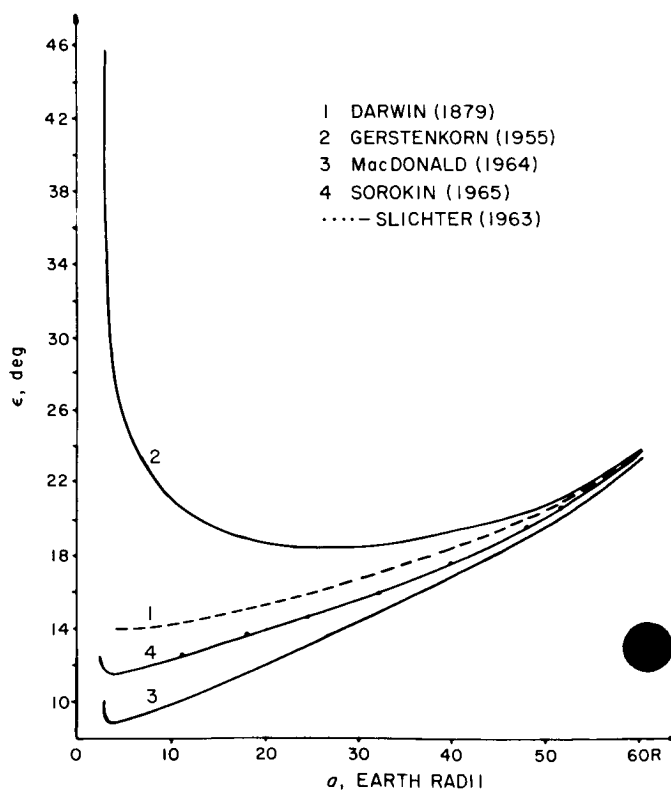


**Fig. 20. The change of the inclination of the orbit of the Moon vs its distance from the Earth**

It is worth mentioning that no existing calculations take into account the fact that the proper plane of the lunar orbit, which coincides at present with the ecliptic, had to coincide with the equatorial plane in the past, when the Moon was close to the Earth.

The change of the eccentricity of the lunar orbit during the recession of the Moon from the Earth depended substantially on the dissipation of the energy of radial tidal deformations of the Moon. If the radial tides did not exist, the eccentricity would have increased with time. Using the numerical value of the parameter  $Q$  he found for the Earth, MacDonald (Ref. 10) concluded that the eccentricity must increase. However, the calculations by Petrova, supervised by Ruskol, (Ref. 14) show that if  $Q$  for the Moon is 2-4 times greater than for the Earth, the lunar eccentricity will remain almost constant or will even decrease with time (Fig. 21).

The curves in Fig. 21 are calculated for four values of the present-day rate of energy dissipation in the Moon ( $\Delta E_0$ ). The change of  $\Delta E_0$  in the course of orbital evolution was taken according to Kaula (Ref. 15). The lag angle of lunar tide on the Earth was taken to be  $\delta = 1^\circ = \text{const}$ , giving the time-scale of tidal evolution of about  $4 \times 10^9$  years.

Because a substantial volume of the lunar interior is partially melted, it seems probable that the Moon is less

rigid than the Earth. As was correctly indicated by Kopal (Ref. 16), the absence of the free libration of the Moon provides confirming observational evidence.<sup>1</sup>

Some years ago, the possibility that the Moon was captured by the Earth was mentioned by MacDonald (Ref. 18), but on quite different grounds. Regarding  $Q$  as constant, he concluded that the Moon must have been close to the Earth less than 2 billion years ago. At that time, the solar system was already formed, and the only possible way for the Earth to obtain a satellite seemed to be a capture of the Moon. In a later paper (Ref. 10), MacDonald proposed another hypothesis: a multi-moon hypothesis. He suggested the existence in the past of several small moons, which accumulated into the present-day Moon less than 2 billion years ago. For small bodies, the tidal evolution proceeds extremely slowly, so that the recession would have to begin only after the accumulation. However, it is hard to understand how several bodies could turn close to the Earth for several billion years, within a small volume of space, without accumulation.

The escape from the difficulty with the time-scale of tidal evolution must be sought for in another direction. MacDonald suggests that in the past the tidal dissipation of energy in the Earth was greater than it is now, and, therefore, that the calculations for constant  $Q$  give the upper limit for the time of evolution. However, when the Earth was still cold, the dissipation of energy by body tides must have been smaller than it is now. The role of sea tides must also have been smaller in the past, because water escaped only gradually from the interior in the course of its heating. As was shown by Ruskol, (Ref. 19), rather plausible assumptions concerning the gradual increase of the effective phase lag of tides permit the time-scale of the tidal evolution to increase up to the age of the solar system (Fig. 22). Therefore, one can consider that the origin of the Moon as the Earth's satellite coincided with the formation of the whole solar system.

Just such an origin of the Moon was suggested in the hypothesis proposed by Schmidt (Ref. 20) and developed by Ruskol (Refs. 21, 22). During the accumulation of the Earth, inelastic collisions of solid bodies in the vicinity of the growing Earth must have produced fragments, some of which moved along elliptic circumterrestrial orbits. Therefore, a circumterrestrial swarm of

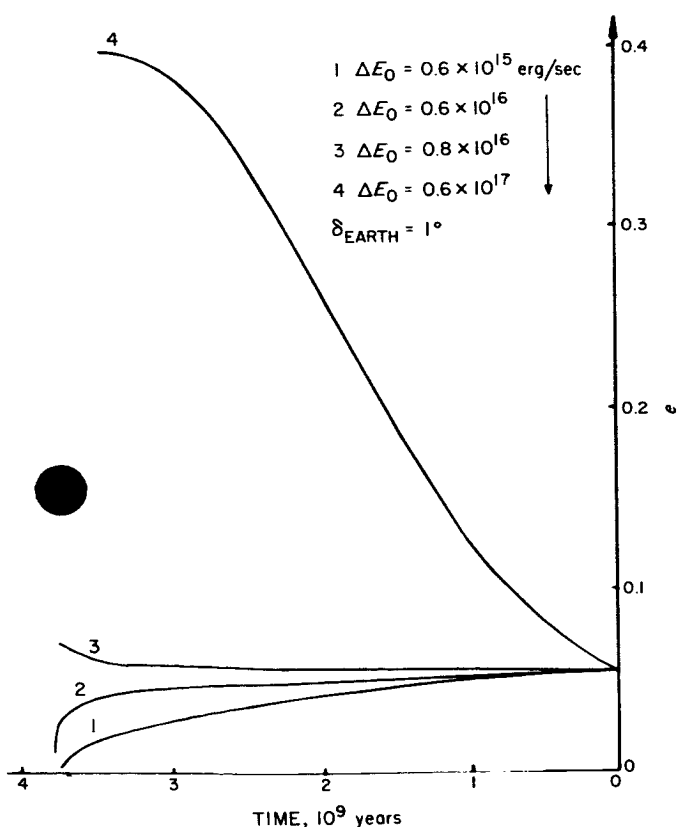
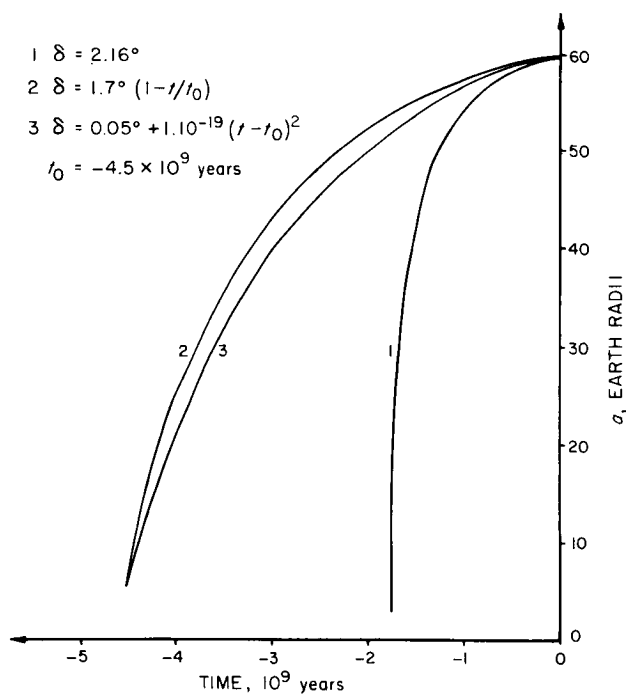


Fig. 21. The dependence of the eccentricity of the lunar orbit on time in the past

<sup>1</sup>Later, Koziel (Ref. 17) found the constants of free libration in longitude but the errors of constants of forced libration turned out to be somewhat greater than in calculations without free libration.





**Fig. 22. The change with time of the Moon's distance from the Earth for different variants of phase-lag  $\delta$  of the lunar tide on the Earth**

bodies must have been formed. Its density rapidly increased toward the Earth, and, when the mass of the Earth increased, the inner parts of the swarm fell on the Earth. As was shown by Ruskol, the mass of the swarm that remained when the accumulation of the Earth was almost ended must indeed have been of the order of the lunar mass, if the largest bodies from which the Earth accumulated were about 100 kilometers in size (for the size distribution usually adopted). If the Earth had accumulated from small bodies, the number of their collisions in the vicinity of the Earth would be too large, and therefore the mass of the swarm would also be too large. But other approaches studied by Gurevich and Lebedinskij (Ref. 23) and by Safronov (Refs. 24, 25) also indicate that a substantial part of the Earth's mass must have been contributed by bodies of about 100 kilometers in size.

The Moon accumulated in the dense inner part of the swarm, at the distance of 5–10 Earth radii, and then receded, owing to tidal friction, sweeping up the outer parts of the circumterrestrial swarm. In order not to be pulled inside the Roche limit, the Moon must have been formed when the Earth's mass reached  $\frac{1}{4}$  or  $\frac{1}{2}$  of its present value. This means that the age of the Moon must

be  $10^8$  years less than that of the Earth, measuring from the beginning of their accumulation.

If the formation process of the Moon was as described above, the Moon must have had practically the same composition as the Earth, not to speak of differences in volatile content. This is incompatible with the hypothesis of the iron core of the Earth. But several serious objections from the cosmogonical and geophysical points of view can be raised against this old hypothesis. These objections can be found in my report presented some years ago to the Liège symposium on planets (Ref. 26). But if the Earth's core is regarded as composed of metallized silicates, then the composition of the Earth and the Moon is almost the same. Unfortunately, the experiments on shock compression of rocks give no abrupt change in their density at the pressure of 1.5 million atmospheres, and this is the main objection raised against the hypothesis of metallized silicates. However, Professor Libby (Refs. 27, 28) has recently shown that for some substances the pressure needed for the phase transition is much larger for shock compression than for static ones.

Thus I regard the idea of the common formation of the Earth and Moon about 5 billion years ago not only to be a natural consequence of the modern ideas on the accumulation of the Earth but also to be in accord with the geophysical data on the structure of the Earth.

## II. The History of Lunar Bombardment

All students of the lunar surface distinguish three main types of structural features: pre-mare, mare, and post-mare. Some proponents of the volcanic origin of lunar craters, for example, Khabakov (Refs. 29, 30) suggested that the epochs of formation of these three types of features were separated by quiet periods when no changes in the surface relief occurred. However, I see no indications for these interruptions in the formation of craters and regard the above-mentioned three periods as a continuous sequence.

The approximately equal surface density of the post-mare craters on different lunar "seas" indicates that all mare were formed at the same epoch. This applies also to circular maria whose origin was obviously not a spontaneous one but resulted from impacts of large bodies up to hundreds of kilometers in size. Hence, the bombardment of the Moon by such large bodies occurred not only during its main accumulation, which lasted about  $10^8$  years, but also up to the epoch when the lunar interior reached maximum heating and melting. The

calculations of the thermal history of the Moon show that this occurred 1–2 billion years after its accumulation (depending on its content of radioactive elements). But later the bombardment by such large bodies ceased.

The idea of the common origin of the Earth and the Moon, followed by the recession of the latter owing to tidal friction (which lasted not 2, but 5 billion years), permits reconciliation of the history of lunar bombardment with the thermal history of the Moon.

It is expedient to separate the bombardment of the lunar surface into three main stages (Ref. 31):

1. The bombardment in the final stage of the main accumulation of the Moon, which occurred at a distance of 5–10 Earth radii. It must have died down after  $3 \times 10^8$  to  $5 \times 10^8$  years after the beginning of accumulation, owing to exhaustion of matter in the inner part of the circumterrestrial swarm—in the “feeding zone” of the Moon.
2. The bombardment during the increase (due to tidal friction) of the radius of the lunar orbit, which led to the sweeping up of the outer part of the circumterrestrial swarm. This stage lasted 1–2 billion years and ended when the Moon came outside the swarm. At the end of this stage, the matter in outer parts of the swarm had already accumulated into large bodies, and the lunar interior had already become heated and partially melted, which led to the formation of lunar maria and of lava-flooded craters.
3. When the second stage ended, the main role passed from the bombardment by bodies of the circumterrestrial swarm to the bombardment of the Moon by bodies moving along circumsolar orbits and accidentally hitting the Moon. These bodies—asteroids, meteorites, cometary nuclei—also hit the Moon during the two first stages, but then they played only a subordinate role.

During the first two stages, when the Moon was bombarded by bodies from the circumterrestrial swarm, the mean velocity of impacts was small ( $2\frac{1}{2}$ –4 km/sec), but in the third stage, which is still continuing at present, the mean velocity has increased up to 10–15 km/sec. The pre-mare craters were formed during the first stage and the first half of the second stage; the maria and the mare craters at the end of the second stage; and the post-mare craters were formed and continue to form in the course of the third stage. During all these stages the formation of primary craters was accompanied by the formation of secondary craters.

The possibility of such a reconciliation of the history of lunar bombardment and of the lunar thermal history seems to me to confirm indirectly the large time-scale of the tidal evolution.

### III. The Thermal History of the Moon

Mathematical calculations of the thermal history of the Moon were made by several authors. The most extensive calculations by Kopal (Ref. 32) were made for a uniform model with a constant coefficient of heat conductivity. However, in the previous calculations by MacDonald (Refs. 33, 18) and by Levin and Majeve (Ref. 34), the radiative heat transfer, which plays a substantial role even at temperatures reached in the lunar interiors, was also taken into account. Later, Kopal (Ref. 35) developed another extreme case: a complicated mathematical theory of thermal conditions in a sphere irradiated from outside and possessing only a radiative heat transfer. Although some numerical examples refer to a body of lunar dimensions, I see no possibility of applying Kopal's results to a real Moon.

The latest calculations by Majeve (Ref. 36) were made for lunar models, which are closest to the reality. She has taken into account the dependence of the lattice conductivity on temperature, the radiative conductivity, and the melting temperature and heat of melting. With the meteoritic content of radioactive elements, the lunar interior must have been heated up to partial melting. Therefore, besides the heating of the Moon by uniformly distributed radioactive elements, Majeve also calculated the cooling of the Moon, which must have begun after the differentiation of the interior and the transfer of the major part of radioactive elements towards the surface.

Even adopting for the Moon the minimum values of uranium and thorium content in chondritic meteorites (and a “normal” meteoritic content of potassium), MacDonald (Refs. 33, 18, 37, 38), Urey (Ref. 5), and Kopal (Ref. 32) obtained, for uniform lunar models, interior temperatures for the present time exceeding the melting temperature. MacDonald, as well as Urey, (Refs. 39, 40, 5) believes that a molten state for the lunar interior is not compatible with the observed disequilibrium figure of the Moon. To obtain a Moon that was (and is) solid throughout, MacDonald, in one series of models, rejected the data on the content of radioactive elements in meteorites and made calculations for a content several times lower. In another series of models, he assumed that the radioactive elements were contained from the very beginning *only* in the thin outer shell.

These models seem to me to be very formal. It seems to me that the calculations must be made for models that take into account as completely as possible the formation process and the further evolution of the Moon and of other related bodies. An attempt to achieve this is contained in the calculations by Majeva. Unfortunately, the existing ideas on the differentiation process, which begins with the partial melting of the interior, are so indefinite that it is impossible to include them in mathematical calculations. We are forced to study separately the stage of heating and the stage of cooling. Some arbitrary "initial" temperature distribution is used in the calculations of cooling, but as the cooling lasts long enough, the temperature distribution for the present moment is almost independent of this "initial" distribution. Even the total content of radioactive elements, which determines their contents in the outer "sialic" layer and determines the surface heat flow, does not substantially affect the temperature of the interior. The latter is determined mainly by the content of radioactive elements that remain in the interior after the differentiation, and also by the heat conductivity.

For most models, the calculations by Majeva show that the central part of the Moon is in a partially molten state, but the outer layer of 500–700 km is in a solid state (Table 5). As the constant subsurface temperature on the Moon

decreases from the equator to the poles, the thickness of the solid layer increases toward the poles for 50–100 km. Unfortunately, the constant subsurface temperature for the polar regions, which depends on the macrorelief and on librations, is unknown. Probably it is about 90–100°K.

Only if one supposes a high heat conductivity inside the Moon, larger than that regarded at present as the maximum possible, can one obtain a Moon that is solid throughout. However, this model is of no interest in explaining the nonequilibrium shape of the Moon: the solidification of the central part would have occurred in this model only recently, while the free rotation of the Moon, which could explain the flattening of its dynamic figure, must have been decelerated long ago by tidal friction.

The values of the heat flow through the surface (for the present moment of time), calculated by Majeva for models with approximately the meteoritic content of radioactive elements, are given in Table 6. These heat flows are 2 to 3 times smaller than the value of  $1.0 \pm 0.3 \mu\text{cal/cm}^2 \text{ sec}$  obtained by Krotikov and Troitsky (Ref. 41) from radio-observation on different wavelengths. It is still unclear how to reconcile these data. The assumption on higher heat conductivity for the lunar interior will reduce, but not eliminate, this discrepancy.

It is worthwhile to note that there is a similar discrepancy between the observed and calculated heat flows for the Earth. In this case, the observed heat flow is rather well known, and therefore the discrepancy is more serious than it is for the Moon. If one suggests a larger content of radioactive elements than is found in meteorites, or a larger initial temperature, one obtains a molten upper mantle, but this contradicts the seismic data. Therefore the increase of adopted values of heat conductivity seems to be very probable.

**Table 5. Present-day thickness  $\Delta l$  of the outer solid layer of the Moon**

$n_i^a$	0.2		0.8	
$\varepsilon, \text{cm}^{-1}$	10	40	10	40
$\Delta l, \text{km}$	700	500	600	450

<sup>a</sup>For the differentiated lunar interior, U content =  $n_i \times 10^{-8} \text{ g/g}$ ; Th content =  $4 n_i \times 10^{-8} \text{ g/g}$ ; K content =  $2.5 \times 10^{-4} \text{ g/g}$ .  $\varepsilon$  denotes opacity.

**Table 6. Present-day heat flow  $q$  through the surface of the Moon**

$n_i^a$	0.2				0.8				Equilibrium heat flow	
$\varepsilon, \text{cm}^{-1}$	10		40		10		40			
$n$	1	2	1	2	1	2	1	2	1	2
$q, 10^{-6}, \frac{\text{cal}}{\text{cm}^2 \text{ sec}}$	0.37	0.46	0.35	0.45	0.34	0.44	0.32	0.41	0.23	0.33

<sup>a</sup>The average content of radioactive elements in the Moon is: U content =  $n \times 10^{-8}$  g/g, Th content =  $4 n \times 10^{-8}$  g/g; K content =  $8 \times 10^{-4}$  g/g.

Summing up, one can say that the Moon, after a stage of differentiation of the interior and a transfer of radioactive elements toward the surface, had to pass from heating to cooling, and at present it is solid at least down to a depth of 500–700 km. But the central part, embracing 20–40% of its mass, must have been in a partially molten state up till the present time.

Because the melting of silicates is accompanied by a decrease in their density, the existence in the Moon of the central semimolten region means the absence of hydrostatic equilibrium. In the solid layer, a tendency must exist toward separation and the sinking of humps, or subregions of greater density. Probably the strength of the layer is enough to withstand this tendency.

The conclusion on the existence of the semimolten core in the Moon will be experimentally tested when apparatus for gravimetric and seismic observations will be delivered on the Moon. The tidal deformations of the lunar globe and the associated variations of gravity depend on the strength of the outer layer and the size of the molten core. However, most precise observations are necessary to obtain reliable results (Refs. 42, 43). The first model calculations of seismic characteristics of the Moon were published some years ago by Press et al. (Ref. 44) and Bolt (Ref. 45). Recently, similar calculations were published by Berikashvily, Zharkov, and Janovskaya (Ref. 46). They have taken into account the existence in the Moon of the thick low-velocity layer and of a molten core. Seismic observations on different epicentral distances are necessary to choose a correct model of the internal constitution of the Moon.

Ten years ago, Lubimova and I, in a note (Ref. 47) containing some preliminary considerations upon the thermal history of the Moon, mentioned the importance of the increase of its radius in the course of the heating and melting of its interior. Five years ago, this problem was considered by MacDonald (Ref. 48). He accepted a low value for the coefficient of the thermal expansion,  $1 \cdot 10^{-5}$ , and, for different models, he obtained an increase in radius of 3–5 km. Although the central temperatures in his models were high, the expansion that accompanies melting was not taken into account. The differentiation of the interior, accompanied by cooling of the Moon, was not taken into account either. Nevertheless, considering the last 1–2 billion years, MacDonald obtained a small decrease in radius, which was due to a cooling of the outer layers. When the differentiation and the general cooling is taken into account, the decrease in radius is much greater.

Calculations of radial shifts of matter at different depths, owing to thermal expansion, are given by Kopal (Ref. 32). But, as was already mentioned, a rather formal model of the Moon is treated in his work.

We are indebted to MacDonald (Ref. 48) for calculations of thermal stresses in the Moon produced by changes in the temperature distribution with time. The energy of these stresses is rather large—of the order of  $10^{24}$  erg/year. A more precise treatment of this problem is necessary, which will take into account the concentration of all stresses in the outer solid layer, while the semimolten central part is free of stress. It is possible that thermal stresses are the main source of seismic activity on the Moon. Another important source can be the impacts of meteorites (Ref. 44).

#### IV. The Figure of the Moon

It is often believed that the deviation of the dynamic figure of the Moon from the equilibrium one consists in the existence of a bulge directed toward the Earth. This conviction is, to a large extent, due to the fact that in the two first editions of Jeffreys' book *The Earth*, which appeared in the 1920's, erroneous values were given for differences in the principal axes of inertia. As was noted in the 1950's by Jeffreys himself (Ref. 49), the values were already obsolete in the 1920's.

Attempts were made to explain the supposed existence of such a bulge as due to the solidification of the Moon at a shorter distance from the Earth, when such a bulge could have been formed by tidal forces. At the present distance of the Moon from the Earth, the equilibrium bulge must be small, giving the following differences of principal moments of inertia:

$$\frac{C - A}{C} = 0.0000375 \quad \frac{B - A}{C} = 0.0000281$$

The ratios

$$\frac{C - A}{B - A} = \frac{4}{3} \quad \text{or } f = \frac{C - B}{C - A} = 0.25$$

are constants that do not depend on the distance between the Earth and the Moon.

Modern determinations give (Ref. 50)

$$\frac{C - A}{C} = 0.000627 \pm 0.000003$$

$$\frac{B - A}{C} = 0.000118 \pm 0.000057$$

Thus the observed value of  $f$  is about 0.6–0.7 instead of 0.25, and this definitely excludes the possibility of explaining the disequilibrium figure of the Moon as due to a fossil tidal bulge. Only if one rejects the value of  $f$  obtained from observations and adopts that of  $f = 0.25$  can one say that the observed value of  $(C - A)/C$  corresponds to the equilibrium shape of a synchronously rotating Moon at the distance of 140,000 km from the Earth. But it is a purely formal statement, which has no bearing on the reality.

The observed differences of the principal moments of inertia indicate that the main deviation of the Moon from the equilibrium shape consists in its oblateness, with a small elongation along the radius vector superimposed. In 1937, Jeffreys realized that the observations give a large value of  $f$ , so that the lunar equator can be regarded as nearly circular, and calculated that the observed value of  $(C - A)/C$  corresponds to a free rotation of the Moon with a period of about 3.5 days (Ref. 49, p. 159). Some years ago I tried to reconcile the hypothesis that the Moon solidified during free rotation with its thermal history (Ref. 51). But the subsequent calculations of the latter showed that it is impossible.

The disequilibrium figure of the Moon, independent of its origin, indicates that stresses of the order of 10 kg/cm<sup>2</sup> exist in the lunar interior. For a spherically symmetrical distribution of density, the maximum stress is in the centrum of the Moon; thus it occurs where the temperature is maximum and the bearing strength is minimum. Even below the melting temperature, the diffusive viscosity must lead to a rapid relaxation of stresses. Therefore, the attempts by MacDonald (Ref. 37) and by Urey (Ref. 5) to calculate the models of a Moon that is solid throughout do not eliminate the difficulty raised by its nonequilibrium shape.

In a molten or semimolten substance, the relaxation of stresses occurs practically immediately. To reconcile the molten state of the lunar interior with the nonequilibrium figure, Runcorn (Ref. 52) suggests that the Moon has a shape distorted by convection. Runcorn even admits the superposition of two convective currents—one with the axis along the polar axis of the Moon, and another with the axis along the radius vector. As to myself, I cannot understand the possibility of such superposition of convective currents.

Kopal, who also mentioned such a convection explanation some years ago, (Ref. 16) recently (Ref. 53) considered this problem strictly mathematically, on the basis of the convection theory developed by Chandrasekhar, and showed that this explanation is incompatible with the properties of the lunar matter. The latter permits only such convective motions as are described by high-order harmonics. However, this conclusion is based on the convection theory for a uniform viscous fluid, while the lunar interior should undergo differentiation. Even a small chemical differentiation is enough to stop convection. Therefore, I doubt very much whether convection exists in planetary interiors, including those of the Earth and the Moon.

Urey, Elsasser, and Rochester (Ref. 54) had looked for another escape from the difficulty presented by the nonequilibrium figure of the Moon. They showed that if one rejects the assumption of spherical symmetry in density distribution, a model can be proposed in which a nonequilibrium figure will be accompanied by zero stress in the centrum. In such models, the stresses are of course not eliminated totally, but their maximum is shifted from the centrum into some layer that is nearer to the surface and therefore has a lower temperature and greater strength.

Following this path and taking into account the results of calculations of the thermal history of the Moon, one can suggest that all stresses connected with the nonequilibrium figure of the Moon are concentrated in the outer, coldest part of the solid layer and that the value of these stresses does not exceed the bearing strength of matter in this outer part.

Last year I put forward a hypothesis explaining the flattening of the figure of the Moon as due to effects connected with a decrease of surface temperature from the equator to the poles (Ref. 55). This decrease of temperature leads to a greater thickness of the solid layer near the poles. Because solid silicates are more dense than molten ones, an isostatic adjustment must have produced the flattening of the Moon. Besides, the *mean* temperature of the outer solid layer near the equator is approximately 200° higher than the temperature near the poles. This leads to some thermal expansion of the equatorial belt. If the excess temperature decreased toward the poles according to the  $\cos \phi$  law, the thermal expansion could explain about  $\frac{1}{3}$  of the observed difference in  $C - A$ , but for the  $\cos^{1/2} \phi$  or  $\cos^{1/4} \phi$  laws, the effect will be smaller. But a very rough estimate showed that the effect of different thickness of the solid

layer is several times larger, and therefore it is probably adequate to explain the observations.

Both these effects were indicated in a note published in Russian in the *Astronomical Zircular*. Unfortunately, this note was written so badly that when it was published in *Nature*, the principal effect (for which no calculations were given) disappeared in the course of improvement of the English translation of my text by Lyttleton. Therefore, when Kopal (Ref. 56) made a complicated mathematical analysis of the temperature distribution in a sphere with a surface temperature decreasing toward the poles down to  $0^\circ\text{K}$  and then calculated its flattening which is due to thermal expansion of the equatorial zone, he was sure that he had analyzed and disproved my hypothesis: for this model  $(C - A)/B = 0.000045$ , i.e., about 14 times smaller than the observed value. But Kopal studied a uniform solid sphere heated from outside by the Sun, with the initial temperature taken to be zero. However, the radiogenic heat cannot be ignored, because it produces a partially molten core surrounded by a solid outer layer with a constant temperature at the bottom that is equal to the melting temperature. Kopal admits a constant heat conductivity for his sphere. But, for lattice conductivity inversely proportional to absolute temperature, the difference of mean temperatures in the solid layer at the equator and at the poles is even larger than the difference of surface temperatures. Thus, calculations by Kopal cannot be regarded as a strict analysis of the thermal effect on the figure of the Moon.

An approximate quantitative analysis was made by Safronov. He suggests that the upper and lower boundaries of the solid layer have a spheroidal shape and he requires that columns from the centrum to the surface along polar and equatorial radii have equal weight. He finds that for the explanation of the observed value of  $(C - A)/C$ , the 20- to 30-km increase in thickness of the solid layer toward the poles is enough if the density of this layer is 3% greater than that of partially molten inner parts. If the deviations of boundaries from spheroidal shape are taken into account, the necessary variation of thickness of the solid layer is smaller. As was already mentioned, the thermal calculations by Majeve show that the variation in thickness can amount to 50-100 km, and therefore the density difference between the solid and partially molten matter can be no more than 1 to 2%. The smaller the density difference, the smaller are the stresses in the solid layer due to the fact that this layer lies on less dense, semifluid matter.

The difference of the principal moments of inertia  $A$  and  $B$  is known with a 50% error. If it turns out that the difference is smaller than is now accepted, it will probably be possible to explain such a smaller difference as due to variation of the constant term of the surface temperature along the lunar equator. Indeed, different parts of the equatorial belt have different reflectivities and thermal properties. But if the modern value of  $(B - A)/C$  is close to reality, the main role must probably be ascribed to the inhomogeneity inside the solid layer.

The geometrical figure of the Moon is not well known. As a result of the incorrect assumption that dynamic data indicate the existence of a bulge directed toward the Earth, attempts are still made to find this bulge in the hypsometric data on the heights of separate points on the lunar surface. However, the errors of these height determinations are large—about 1 km—and there is no correlation between data obtained by different authors (Ref. 57). The lines of equal height do not correspond to contours of lunar maria and highlands, and the data by different authors give different deviations (Refs. 57, 58). Nevertheless, Goudas published a series of papers in which several sets of data on the topography of the visible lunar hemisphere and marginal zone were developed in spherical harmonics (Refs. 59, 60) and then the principal moments of inertia were calculated on the assumption that the Moon is a homogeneous body (Ref. 61). From my point of view it is a mathematical exercise.

It must be added that in drawing the contour lines, as well as in spherical analysis, no attention is paid to the lunar relief, i.e., to the position of measured points relative to the surrounding terrain, although some of them belong to central peaks or to rims.

The measurements of the shape of the lunar disk, analyzed all together, without elimination of mountain ranges and maria, failed to give any indications of its oblateness corresponding to the observed value of  $(C - A)/C$ . According to Yakovkin (Ref. 62) the northern and southern parts of the disk are unsymmetrical. According to Weimer's measurements (Ref. 63) the smoothed lunar contour is a circular one; on the contrary, from the measurements of a single photograph of the full Moon, Potter (Ref. 64) found a slight ellipticity of the disk, with the axis inclined at  $36^\circ$  to the polar axis of the Moon. This result is now confirmed by several authors (Ref. 65). But, as was shown by Baldwin, the highest and the lowest parts of the limb coincide with mountain ranges and maria situated in the marginal zone

(see Ref. 57, Fig. 40A). Using Watt's limb-height measurements, which were remote from mountain ranges and maria, Baldwin found that the equatorial axis (in the plane of the sky) is 1250 m longer than the polar axis. If the Moon were a homogeneous triaxial ellipsoid this difference should be  $900 \pm 100$  m, according to the observed values of  $(C - A)/C$  and  $(B - A)/C$ . Thus the agreement is very good. The Moon indeed has a flattened shape, as is suggested in all explanations of its disequilibrium figure.

## V. Density Distribution in the Moon

The size of the Moon is just such that the increase of density due to pressure and the decrease due to thermal expansion are almost equal, and it is difficult to decide which of these two effects is more important. The answer depends on precise values for coefficients of compressibility ( $\beta$ ) and thermal expansion ( $\alpha$ ) of lunar matter.

When the Moon reached the stage of partial melting of its interior, an almost complete chemical and then gravitational differentiation of matter had to occur. This meant the formation of a thick "sialitic" crust that was less dense than the subcrustal matter. Up to 7% of  $\text{SiO}_2$  can be smelted from silicates similar to those in meteorites, or up to 15% of sialitic matter (Ref. 66). This means that the thickness of the crust on the Moon can be as much as 100–110 km. Besides, if the Moon retained in its interior a substantial amount of volatiles, it can also contain some percent of metallic iron (see Section VI), which, upon differentiation, had to form an iron core.<sup>2</sup>

Although Kuiper's suggestion that the so-called continental parts on the Moon are remnants of the primordial outer layer not replaced by lava flows seems to be very probable, this scarcely can substantially affect our ideas on the mean density distribution along the radius. One can conjecture that under continental areas there exists a *thick* layer of sialitic crustal matter, almost the same as under maria areas.

According to a calculation by Kozlovskaja, (Ref. 68), in isothermal models of the Moon containing no iron core the central density is 3–5% higher than the density of the uncompressed subcrustal matter (Fig. 23, curves 1 and 2). But taking into account the increase of tempera-

- |                         |   |
|-------------------------|---|
| ISOTHERMAL<br>MODELS    | $\left\{ \begin{array}{l} 1. \beta = 1 \times 10^{-12} \text{ cm}^2/\text{dyne} \\ 2. \beta = 0.5 \times 10^{-12} \text{ cm}^2/\text{dyne} \end{array} \right.$   |
| NONISOTHERMAL<br>MODELS | $\left\{ \begin{array}{l} 3. \beta = 1 \times 10^{-12} \text{ cm}^2/\text{dyne}; \alpha = 3 \times 10^{-5} \text{ deg}^{-1} \\ 4. \beta = 0.5 \times 10^{-12} \text{ cm}^2/\text{dyne}; \alpha = 3 \times 10^{-5} \text{ deg}^{-1} \\ 5. \beta = 1 \times 10^{-12} \text{ cm}^2/\text{dyne}; \alpha = 6 \times 10^{-5} \text{ deg}^{-1} \\ 6. \beta = 0.5 \times 10^{-12} \text{ cm}^2/\text{dyne}; \alpha = 6 \times 10^{-5} \text{ deg}^{-1} \end{array} \right.$ |

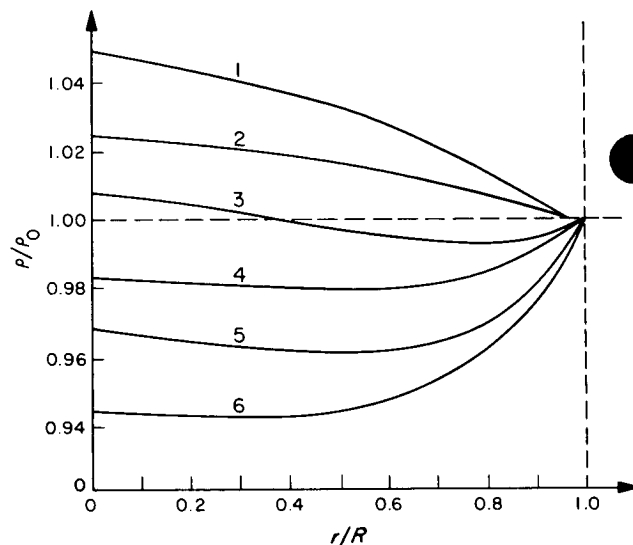


Fig. 23. The density changes along the radius for different models of the Moon

ture with depth, one can obtain different models, depending on the numerical values of the compressibility and thermal expansion coefficients. The decrease in density by 1–6% in the outer layer changes into a small increase in the central, nearly isothermal region (Fig. 23, curves 3, 4, 5, and 6). Density curves for nonisothermal models are calculated for a homogeneous Moon—without crust and differentiation of the interior—and they do not take into account the partial melting of matter in the central region. If one takes all this into account, it will complicate the details of density distribution, but one important conclusion will remain: under the lunar crust, within the lunar mantle, the variations in density are very small—only about 2–4%. There is nothing similar to the large increase in density with depth that is characteristic of the Earth and other massive planets. If the explanation of the disequilibrium figure of the Moon as due to latitude variation of thickness of the outer solid layer proves to be correct, this will indicate that the decrease of density caused by melting is not compensated by its increase due to differentiation and concentration toward the center of the more dense substances. (The theoretical

<sup>2</sup>Kovach and Anderson (Ref. 67) in their calculations of models of the Moon, formally placed the crust-mantle boundary at the depth where the pressure is 9000 bars. This led to a light lunar crust 200 km thick, which required about 8% of metallic iron to obtain the observed mean density of the Moon.



possibility of such compensation is favored by the fact that the lunar matter has no definite melting point, but there is a rather large range of melting temperatures of different minerals.) It is possible that in the subcrustal part of the solid layer the density slightly decreases with depth, less than 1%, owing to a large temperature gradient, and then more sharply decreases (1 to 2%) at the transition to a partially molten interior. Inside the nearly isothermal central region of partially molten substance, the density probably increases with depth, owing both to the increase of pressure and to gravitational differentiation. If the Moon contains only a few percent of metallic iron, it must form a core of several hundred kilometers in size.

## VI. The Composition of the Moon

The only basis for our judgment on the composition of the Moon is its mean density, which we must interpret using cosmogonic ideas.

As was stated in Section I, if one regards the Earth's core as composed of metallized silicates, the large difference in the mean densities of the Earth and Moon can be readily explained as due to differences in pressure combined with identical or similar composition. Unfortunately, we have only a poor knowledge of the composition of the whole Earth, because more than 99% of its substance is inaccessible for direct analysis. Usually one judges from the composition of meteorites, because the Earth and the meteorite parent bodies both are members of the inner zone of the planetary system containing bodies of rocky composition. However, the comparative analysis of the mean densities of the terrestrial planets and the Moon definitely indicates that there are variations of composition within this group, most conspicuously demonstrated by the high density of Mercury. Besides, if one can calculate a model of the Moon composed only of silicate matter similar to that of the Earth's mantle, for the models—for example, of Mars—more dense silicates are necessary, or an iron core, or both (Ref. 69).

Meteoritic matter contains about 10% of metallic nickel-iron. However, according to modern ideas on the origin and evolution of meteoritic matter, the metallic iron in meteorites is not their primary component, but was formed by reduction of iron oxides during the heating of meteorite parent bodies. The carbonaceous meteorites of the Orgueil type are regarded as the closest approach to the primordial solid matter in the asteroidal zone of the solar nebula. They contain iron only in an oxidized form, but they also contain carbon and organic

compounds, which can reduce these oxides under appropriate conditions. At the same time, the condensation of only oxidized forms of iron in the asteroidal zone seems to be natural because, at the low temperatures in this zone, the iron must remain oxidized even in the presence of large amounts of hydrogen.

On the other hand, the high density of Mercury, which indicates a large content of metallic iron, is probably due to the presence of iron in primordial solid grains in the inner part of the nebula. At temperatures above 400°K, which existed at the inner edge of the nebula, iron in the presence of hydrogen must have been condensed in metallic form. In the Earth's zone, the temperature was below 400°K, and therefore there must be no primordial metallic iron in the Earth and the Moon.

It is possible that, in the Earth and the Moon, there is only a small amount of metallic iron of secondary origin, formed by reduction of oxides, or that such metallic iron is not present at all. The temperature in the Earth's zone of the nebula was higher than that in the zones of Mars and the asteroids, and thus the environment was less favorable here for the condensation of organic matter. Therefore the reduced iron was not formed in the Earth and Moon in the amounts that are observed in meteorites and, judging from the density of Mars, are present there also.

Such is a hypothesis I proposed a year ago (Ref. 70). According to this hypothesis, the Moon, as well as the Earth, was formed of matter similar to that of carbonaceous meteorites, i.e., containing a large quantity of hydrated silicates. During the heating of the lunar interior, the dehydration of these silicates occurred, perhaps accompanied by reduction of some part of the iron, if carbon and organic compounds were also present. The density of hydrated silicates is low. Therefore, assuming that some part of them continues to exist in lunar interiors, or assuming that some hydration of silicates in the outer layer occurred during the degassing of the interior, one can accept the presence in the Moon of some metallic iron without contradiction with its observed mean density. Although the so-called ordinary chondrites represent the most abundant type of meteorites, I see no reason to regard them as the best sample of terrestrial and lunar matter in all respects.

Unfortunately, without knowledge of the fraction of hydrated silicates in the Moon, it is impossible to evaluate its content of metallic iron from its mean density only.

Moreover, it remains very unclear what fraction of volatiles that were evolved from the interior during its heating remained captured on the surface and in the surface layer. For a long time it was accepted that neither water nor ice could exist on the lunar surface deprived of atmosphere. But in 1961, Watson, Murray, and Brown (Ref. 71) showed that in the polar regions of the Moon, in the cavities always shadowed from solar rays, the temperature is so low that even bare ice can exist there. However, the number and size of these traps must be small, and the amount of stored ice would be correspondingly small.

In the same year, Kopal (Refs. 72, 16) remarked that because the temperature at about 1 meter under the surface is about  $-30$  to  $-40^{\circ}\text{C}$  and remains negative for at least several tens of meters, the ice must be accumulated here during the degassing of the interior. Ice can be present here in the form of permafrost filling the pores in the rocky ground or in the form of ice lenses. Kopal suggested that perhaps the features usually called lava domes and extinct volcanoes are really domes of ice covered by rubble and dust protecting them from evaporation.

One must remark that as long ago as 1956, Lebedinsky (Ref. 73) pointed out that large amounts of water could exist on the surface of Mars in a frozen form buried under a dust layer. Later, Davydov (Ref. 74) put forward the hypothesis that internal basins of water could exist on Mars below the layer of ice. In 1962, DuFresne and Anders (Ref. 75) made a most interesting suggestion of a *continuous* permafrost layer on the parent bodies of meteorites, with a warmer layer below containing liquid water. Moreover, because the fractures in the ice are self-healing, the permafrost layer is impermeable to gases and makes possible the existence of an "internal atmosphere." Similar suggestions on the existence of an "internal atmosphere" and "internal water basins" on the Moon were recently made by Gold (Ref. 76).

I shall permit myself a most cautious suggestion that perhaps the puff of gas near the centrum of Alphonsus, observed in 1958 by Kozyrev (Ref. 77), escaped from such an "internal atmosphere" of the Moon.

Thus there is a great uncertainty about the content of metallic iron, of hydrated silicates, and of frozen and nonfrozen volatiles in the Moon. This uncertainty is perhaps the most important gap in our knowledge of the structure of the Moon.

The question of the abundance of hydrated silicates and of volatiles in the outer layers of the Moon is most

important in understanding their tectonic development. Although the melting of silicates is accompanied by a decrease in density, even at the stage of maximum melting of the Moon there was no general sinking of all the outer solid layer and replacement by lava flows. Probably Kuiper is correct when he states that continental parts are remnants of the primordial accumulated matter, more or less altered by the degassing process. At the same time, the circular lunar maria and the surrounding regions give evidence of sinking of some parts of the crust, sometimes bordered by circular or arcuate clefts. Perhaps the hydrated silicates and ices are present mainly in the oldest parts of the outer layer, and decreasing its density decreases or eliminates the tendency toward sinking.

## VII. The History of the Lunar Atmosphere

Most students of the Moon believe not only that the Moon has no atmosphere at the present time, but also that it never had any appreciable atmosphere. This point of view seems to me to be correct. However, Gilvarry (Refs. 78, 79) recently argued that if a rapid degassing of the Moon had occurred and a hydrosphere and dense atmosphere had been formed, they would have had to survive for several billion years, because in this case the dissipation must have proceeded slowly. Therefore he tried to explain the form of some lunar craters as being due to their formation by underwater explosions. He even found traces of erosion of the Moon by water.

As was noted by Safronov and Ruskol (Ref. 80), the height of the dissipation layer accepted by Gilvarry does not correspond to a suggested atmosphere of great density, and therefore he underestimates the rate of dissipation by several orders of magnitude. According to Safronov and Ruskol, for the content of volatiles in the Moon similar to that accepted by Rubey (Ref. 81) for the Earth, if their exhalation lasted about one billion years the maximum density of lunar atmosphere near the surface was  $10^{-8}$ – $10^{-9}$  of the present-day density of the Earth's atmosphere, or was equal to the present-day density of the Earth's atmosphere at the height of 150 km. Thus the Moon indeed never had either a substantial atmosphere or a hydrosphere. Its surface was never protected from the influence of most types of cosmic radiations or from impacts of even the smallest meteor particles.

How disagreeable the absence of atmosphere on the Moon may be at present we will soon know, not only from theoretical considerations, but also from the personal sensations of astronauts visiting the Moon.

## REFERENCES

1. Ringwood, A. E., *Geochimica and Cosmochimica Acta*, Vol. 20, No. 3/4, November 1960, pp. 241–259.
2. Wise, D. U., *Journal of Geophysical Research*, Vol. 68, No. 5, March 1963, pp. 1547–1554.
3. Lyttleton, R. A., *Transactions of the IAU*, Vol. 8, 1952, pp. 717–721.
4. Urey, H. C., *Science*, Vol. 147, No. 3663, March 1965, pp. 1262–1265.
5. Urey, H. C., in *Physics and Astronomy of the Moon*, ed. Z. Kopal, New York–London, Academic Press, 1962, pp. 481–523.
6. Urey, H. C., *Proceedings of the First International Space Science Symposium*, North-Holland Publishing Company, Amsterdam, 1960, pp. 1114–1122.
7. Urey, H. C., in *The Moon*, eds. Z. Kopal and Z. Kadla Mikhailov, Academic Press, London–New York, 1962, pp. 113–148.
8. Alfvén, H., *Icarus*, Vol. 1, No. 4, January 1963, pp. 357–363.
9. Gerstenkorn, H., *Zeitschrift für Astrophysik*, Vol. 36, 1955, pp. 245–274.
10. MacDonald, G. J. F., *Reviews of Geophysics*, Vol. 2, No. 3, August 1964, pp. 467–541.
11. Sorokin, N. A., *Astronomicheskij Zhurnal*, Vol. 42, No. 5, September–October 1965, pp. 1070–1074.
12. Darwin, G. H., *Philosophical Transactions of the Royal Society*, Part II, Vol. 170, 1879, pp. 447–530.
13. Slichter, L. B., *Journal of Geophysical Research*, Vol. 68, No. 14, July 1963, pp. 4281–4288.
14. Ruskol, E. L., *Icarus*, Vol. 5, 1966 (in press).
15. Kaula, W. M., *Reviews of Geophysics*, Vol. 2, No. 4, November 1964, pp. 661–685.
16. Kopal, Z., *Planetary and Space Science*, Vol. 9, October 1962, pp. 625–638.
17. Koziel, K., *Report of Commission 17 of the IAU* (Draft Reports, p. 217, XIIth General Assembly, Hamburg, 1964).
18. MacDonald, G. J. F., *Science*, Vol. 133, No. 3458, April 1961, pp. 1045–1050.
19. Ruskol, E. L., *Izvestia Akademii Nauk SSSR, Ser. Geofiz.*, No. 2, February 1963, pp. 216–222 (translated in *Bull. Acad. Sci. USSR, Geophys. Ser.*, Vol. 2, 1963, pp. 129–133).
20. Schmidt, O. J., *Izvestia Akademii Nauk SSSR, Ser. Fizich.*, Vol. 14, No. 1, January–February 1950, pp. 29–45. See also *A Theory of the Origin of the Earth (Four Lectures)*, Lawrence and Wishart, London, 1959.
21. Ruskol, E. L., *Astronomicheskij Zhurnal*, Vol. 37, No. 4, June–July 1960, pp. 690–702 translated in *Soviet Astron.–A.J.*, Vol. 4, 1961, pp. 657–668; Vol. 40, No. 2, March–April 1963, pp. 288–296 (translated in *Soviet Astron.–A.J.*, Vol. 7, 1963, p. 221).

## REFERENCES (Cont'd)

22. Ruskol, E. L., in *The Moon*, eds. Z. Kopal and Z. Kadla Mikhailov, Academic Press, New York-London, 1962, pp. 149-155.
23. Gurevich, L. E., and Lebedinskij, A. I., *Izvestia Akademii Nauk SSSR, Ser. Fizich.*, Vol. 14, No. 6, November-December 1950, pp. 765-799.
24. Safronov, V. S., *Voprosy Kosmogonii*, Vol. 7, 1960, pp. 121-141.
25. Safronov, V. S., *Tectonophysics*, Vol. 1, No. 3, October 1964, pp. 217-221.
26. Levin, B. J., in *La Physique des Planètes*, Université de Liège, 1962, pp. 39-46.
27. Libby, W. F., *Proceedings of the National Academy of Sciences*, Vol. 48, No. 9, September 1962, pp. 1475-1480.
28. Libby, W. F., *Physical Review*, Vol. 130, No. 2, April 1963, pp. 548-549.
29. Khabakov, A. V., *On Basic Problems of the History of Evolution of the Lunar Surface* (in Russian), Geografis, Moscow, 1949.
30. Khabakov, A. V., Ch. 7 in *The Moon*, ed. A. Markov, Pergamon Press, London, 1960.
31. Levin, B. J., *Bulletin Vsesojusnogo Astronomo-Geodesicheskogo Obshestva*, No. 30(37), 1961, pp. 6-19; *Proceedings of the XIIIth International Astronautical Congress* (Varna, 1962), Springer-Verlag, Vienna and New York, 1964, pp. 11-20.
32. Kopal, Z., *Thermal History of the Moon and of the Terrestrial Planets: Numerical Results*, Technical Report No. 32-225, Jet Propulsion Laboratory, Pasadena, California, 1962.
33. MacDonald, G. J. F., *Journal of Geophysical Research*, Vol. 64, No. 11, November 1959, pp. 1967-2000.
34. Levin, B. J., and Majeva, S. V., *Doklady Akademii Nauk SSSR*, Vol. 133, No. 1, July 1960, pp. 44-47; see also Levin, B. J., in *The Moon*, eds. Z. Kopal and Z. Kadla Mikhailov, Academic Press, London-New York, 1962, pp. 149-155; for correction, see Levin, B. J., and Majeva, S. V., *Astronomicheskij Zhurnal*, Vol. 41, No. 5, September-October 1964, pp. 997-998.
35. Kopal, Z., *Icarus*, Vol. 3, No. 1, 1964, pp. 8-44.
36. Majeva, S. V., *Doklady Akademii Nauk SSSR*, Vol. 159, No. 2, November 1964, pp. 294-297; *Izvestia Komissii po Physike Planet*, No. 5, 1965.
37. MacDonald, G. J. F., *Journal of Geophysical Research*, Vol. 67, No. 7, July 1962, pp. 2945-2974.
38. MacDonald, G. J. F., *Space Science Reviews*, Vol. 2, No. 4, 1963, 473-557.
39. Urey, H. C., *The Planets*, Yale University Press, New Haven, 1952, p. 245.
40. Urey, H. C., *Journal of Geophysical Research*, Vol. 65, No. 1, January 1960, pp. 358-359.
41. Krotikov, V. D., and Troitskij, V. S., *Uspekhi Fizicheskich Nauk*, Vol. 81, No. 4, December 1963, pp. 589-639.
42. Sutton, G. H., Neidell, N. S., and Kovach, R. L., *Journal of Geophysical Research*, Vol. 68, No. 14, July 1963, pp. 4261-4267.

## REFERENCES (Cont'd)

43. Harrison, J. C., *Journal of Geophysical Research*, Vol. 68, No. 14, July 1963, pp. 4269-4280.
44. Press, F., Buwalda, P., and Neugebauer, M., *Journal of Geophysical Research*, Vol. 65, No. 10, October 1960, pp. 3097-3105.
45. Bolt A., *Journal of Geophysical Research*, Vol. 66, No. 10, October 1961, pp. 3513-3518.
46. Berikashvili, V. S., Zharkov, V. N, and Janovskaya, T. B., *Izvestia Akademii Nauk SSSR, Ser. Fiziki Zemli*, No. 7, July 1965, pp. 9-21.
47. Levin, B. J., and Lubimova, E. A., *Priroda*, No. 10, October 1955, pp. 81-84.
48. MacDonald, G. J. F., *Planetary and Space Science*, Vol. 2, No. 4, January 1960, pp. 249-255.
49. Jeffreys, H., *The Earth*, 3rd ed., Cambridge University Press, 1952.
50. Jeffreys, H., Ch. 2 in *The Solar System*, Vol. 2, ed. G. P. Kuiper, University of Chicago Press, 1954, pp. 42-56.
51. Levin, B. J., *Voprosy Kosmogonii*, Vol. 6, 1958, pp. 56-61.
52. Runcorn, S. K., *Nature*, Vol. 195, No. 4847, September 1962, pp. 1150-1151.
53. Kopal, Z., *Icarus*, Vol. 4, No. 2, May 1965, pp. 173-176.
54. Urey, H. C., Elsasser, W. M., and Rochester, M. G., *Astrophysical Journal*, Vol. 129, No. 3, April 1959, pp. 842-848.
55. Levin, B. J., *Astronomicheskij Zircular*, No. 285, February 1964, pp. 2-3; *Nature*, Vol. 202, No. 4938, June 1964, pp. 1201-1202.
56. Kopal, Z., *Icarus*, Vol. 4, No. 2, May 1965, pp. 166-172.
57. Baldwin, R. B., *The Measure of the Moon*, The University of Chicago Press, 1963.
58. Goudas, C. L., *Icarus*, Vol. 3, No. 5-6, December 1964, pp. 476-485.
59. Goudas, C. L., *Icarus*, Vol. 2, No. 5-6, 1963, pp. 423-439.
60. Goudas, C. L., *Icarus*, Vol. 4, No. 2, May 1965, pp. 188-206.
61. Goudas, C. L., *Icarus*, Vol. 3, No. 5-6, 1964, pp. 375-400.
62. Jakovkin, A. A., *Izvestia Astronomicheskoy Observatorii imeni Engelgardta*, No. 29, 1955.
63. Weimer, T., in *The Moon*, eds. Z. Kopal and Z. Kadla Mikhailov, Academic Press, London-New York, 1962, pp. 55-58.
64. Potter, H. J., in *The Moon*, eds. Z. Kopal and Z. Kadla Mikhailov, Academic Press, London-New York, 1962, pp. 63-66.
65. Goudas, C. L., *Icarus*, Vol. 4, No. 2, May 1965, pp. 218-220.
66. Vinogradov, A. P., *Khimicheskaja Evoluzia Zemli (Chemical Evolution of the Earth)*, Publishing House of the USSR Acad. Sci., Moscow 1959; *Izvestia Akademii Nauk SSSR, Ser. Geol.*, No. 10, October 1959, pp. 5-27.

## REFERENCES (Cont'd)

67. Kovach, R. L., and Anderson, D. L., *Journal of Geophysical Research*, Vol. 70, No. 12, June 1965, pp. 2873–2882.
68. Kozlovskaya, S. V., *Voprosy Kosmogonii*, Vol. 8, 1962, pp. 145–149.
69. Kozlovskaya, S. V., *Doklady Akademii Nauk SSSR*, Vol. 92, No. 5, October 1953, pp. 903–906.
70. Levin, B. J., *Icarus*, Vol. 3, No. 5–6, December 1964, pp. 498–499.
71. Watson, K., Murray, B., and Brown, H., *Journal of Geophysical Research*, Vol. 66, No. 5, May 1961, pp. 1598–1600; Vol. 66, No. 9, September 1961, pp. 3033–3045.
72. Kopal, Z., *Discovery*, Vol. 22, No. 4, April 1961, pp. 143–146.
73. Lebedinskij, A. I., *Doklady Akademii Nauk SSSR*, Vol. 108, No. 5, July 1956, pp. 795–798.
74. Davydov, V. D., *Voprosy Kosmogonii*, Vol. 7, 1960, pp. 142–166.
75. DuFresne, E. R., and Anders, E., *Geochimica and Cosmochimica Acta*, Vol. 26, November 1962, pp. 1085–1114; Ch. 14 in "The Solar System", Vol. 4, eds. B. Middlehurst and G. P. Kuiper, 1963, pp. 496–526.
76. Gold, T., In *The Origin and Evolution of Atmospheres and Oceans*, eds. P. F. Brancazio and A. G. W. Cameron, J. Wiley and Sons, London–New York–Sydney, 1964, pp. 249–256.
77. Kozyrev, N. A., (a) *Priroda*, No. 3, March 1959, pp. 84–87; (b) in *The Moon* (Symposium No. 14 of the IAU), eds. Z. Kopal and Z. Kadla Mikhailov, Academic Press, London–New York, 1962, pp. 263–271; (c) in *Physics and Astronomy of the Moon*, ed. Z. Kopal, 1962, pp. 361–384.
78. Gilvarry, J. J., *Nature*, Vol. 188, No. 4754, December 1960, pp. 886–891.
79. Gilvarry, J. J., *Publications of the Astronomical Society of Pacific*, Vol. 76, No. 451, 1964, pp. 245–253.
80. Safronov, V. S., and Ruskol, E. L., *Proceedings of the XIIIth International Astronautical Congress* (Varna, 1962), Springer-Verlag, Vienna–New York, 1964, pp. 42–53.
81. Rubey, W. W., in *Crust of the Earth*, ed. A. Poldervaart (The Geological Society of America, Special Paper 62), July 1955, pp. 631–650.

## ON THE INTERNAL CONSTITUTION AND ORIGIN OF THE MOON

Gordon J. F. MacDonald

University of California  
Los Angeles, California

Both ground-based telescopic and *Ranger* photographs reveal a surface on the Moon covered with meteoritic craters having dimensions ranging from 1 meter and less to several hundred kilometers. Is this surface representative of deeper surfaces in the sense that the buried surfaces retain evidence of the long and complex aggregational history? Or is this surface superimposed on a highly organized and differentiated interior in which the details of the accumulation process have long since been erased by internal thermal processes? In the first case, we would expect an interior in which the rubble of collision has been consolidated by the overlying pressure but in which chemical disequilibrium prevails, since partial melting and differentiation have played a minor role. In the alternative model, the Moon has undergone extensive reorganization with abundant volcanic activity accompanying the large-scale differentiation.

In the following, I will argue that the evidence we have on the Moon's interior supports the view of an inhomogeneous, nondifferentiated Moon. I will then briefly consider the relevance of dynamical arguments to question of how the Moon may have formed. Since the data are few, the discussion is necessarily highly speculative.

### 1. Data on the Moon's Interior

Inferences regarding the internal structure of the Moon follow from data on the orbital and rotational motion of that body. Since the data are limited in number and in quality, a wide variety of models of the Moon that do not violate present information can be constructed.

The mass and the mean density of the Moon are the quantities for which the uncertainty is least. The mass has been determined by the lunar inequality, the amount an observation from the Earth is shifted by the rotation of the Earth and the Moon about their common center of mass. Determination of the lunar inequality has depended on observations taken during the close approach of the minor planet Eros. More recently, observations of the *Mariners* have substantially improved the data. The mean density of the Moon is  $3.34 \text{ g cm}^{-3}$ . The reduced density at  $25^\circ\text{C}$  and one bar pressure is uncertain both because of the unknown thermal conditions within the Moon and the possibilities of phase transformations. Urey (1960) estimates a density of  $3.4 \text{ g cm}^{-3}$ , while the thermal calculations to be discussed later lead to values of 3.3 to  $3.45 \text{ g cm}^{-3}$ . Urey (1960) notes that the density

is significantly less than the density of chondritic meteorites ( $3.5$  to  $3.8 \text{ g cm}^{-3}$ ) as well as less than the mean density of the Earth. The density alone suggests that the Moon differs in major element chemistry from both chondritic meteorites and the Earth.

The second-degree harmonics of the Moon's gravitational field are conventionally expressed in terms of the moments of inertia, since their determination is dependent on measurements of the Moon's librations. The moment of inertia about the axis of rotation is denoted by  $C$ , and the least moment of inertia  $A$  is about an axis along the line of centers of the Earth and the Moon, while the moment  $B$  is about the axis tangent to the orbit.

From the inclination of the axis of rotation of the Moon to the pole of its orbit, Jeffreys and Habibullin (1958) find  $(C - A)/B = 0.0006279 \pm 0.0000015$ . From the forced physical vibration in longitude arising from the attraction of the Earth on the Moon's equatorial bulge, Jeffreys (1961) derives from Yakovin (1952) data  $(B - A)/C = 0.0002049 \pm 0.0000009$ .

Observations of the secular motion of node and perigee of the Moon's orbit can be used to estimate

$$\frac{C - A}{MR^2}, \quad \frac{B - A}{MR^2}$$

where  $M$  and  $R$  are the lunar mass and radius respectively (Jeffreys, 1961). The reduction of the data requires a subtraction of the effect of the Sun, Earth, and planets. The effect of the Sun is large, contributing about  $1.46'' \times 10^5$  per year, while about  $1''$  per year is due to the lunar figure. Thus, the solar terms must be precisely evaluated and there is controversy as to the quality of the theory on which the evaluation depends.

Table 7 lists the various observed quantities relating to the Moon's gravitational field. In addition, theoretical values are given, where the theory assumes a hydrostatic Moon rotating at its current angular velocity and tidally deformed by the Earth. The values in Table 7 clearly illustrate the well known fact that the Moon's moments of inertia do not correspond to a body in hydrostatic equilibrium. The Moon's equatorial bulge is much too large for its present rate of rotation and the bulge toward and away from the Earth is much greater than would be expected from tidal theory.

## II. Interpretation of the Moon's Moments of Inertia

Urey (1952) and MacDonald (1962) have argued that the nonhydrostatic figure of the Moon sets important limits on the possible internal configuration. Urey and MacDonald suggest that the equilibrium figure is due to density inhomogeneities and that the inhomogeneities are supported by the finite strength of the rigid material making up the Moon. An alternative view expressed by Runcorn (1962) is that the inequalities in figure are due to internal convection, with the surface bulging outward under the rising currents. Runcorn's models have recently been criticized by Kopal (1965), who points out that the proposed convection would not be a steady process but would be turbulently unstable. Under the conditions presumed by Runcorn there would be no large-scale organized flow capable of providing the non-equilibrium gravitational potential.

Urey, Elsasser, and Rochester (1959) note that the interpretation of the nonequilibrium harmonics in terms of density inhomogeneities sets limits on the manner of formation of the Moon. Urey et al. suggest, on the basis of a qualitative statistical argument, that if the Moon

Table 7. Observed and theoretical values relating to the Moon's gravitational field

Ratios of moments of inertia	Observed value	Theoretical values		Ratio of observed to theoretical values
		Hydrostatic equilibrium	Uniform density	
$(B - A)/C$	0.000205	0.0000281	—	7.3
$(C - A)/B$	0.0006279	0.0000375	—	16.7
$(C - A)/Ma^2$	0.000364	—	0.000251	1.45
$(B - A)/Ma^2$	0.000071	—	0.000084	0.84
$C/Ma^2$	0.56	—	0.4	1.4



accumulated from about  $10^4$  objects of varying density, the moments of inertia of the Moon could be accounted for.

The conclusion that the statistical aggregation of a number of small particles could yield a nonequilibrium second-order harmonic is important and requires close examination. I represent the random density field  $\rho$  as the sum of a mean density  $\rho_0$  and a variable density  $\rho$  which is expanded in a series of spherical harmonics

$$\rho'(x_i) = \sum_{l=0}^{\infty} \sum_{m=0}^l \left[ A_{lm}^{(\gamma)} \cos m\lambda + B_{lm}^{(\gamma)} \sin m\lambda \right] P_{lm}(\cos \theta)$$

where  $\gamma$ ,  $\theta$ , and  $\lambda$  are the radial coordinate, the co-latitude and the longitude respectively.

Let us suppose that on a given spherical surface the correlation of the variable density field depends only on the spherical distance between the two points. Such a condition on the density would result from an isotropic accumulation process. In this case Yaglom (1961) shows that

$$E \{A_{lm} A_{pq}\} = \delta_{lp} \delta_{mq} a_l$$

The covariance of the variable density field

$$E\{\rho'(x_i) \rho'(x_{i'})\}$$

on a given spherical surface then becomes

$$E\{\rho'(x_i) \rho'(x_{i'})\} = \sum_{m=0}^{\infty} \sum_{l=0}^{\infty} \sum_{m=m}^{\infty}$$

$$[a_{lnm} \cos m(\lambda - \lambda') + b_{lnm} \sin m(\lambda - \lambda')]$$

$$P_{lm}(\cos \theta) P_{nm}(\cos \theta') \quad (1)$$

where (Jones, 1963)

$$E\{A_{lm} A_{np}\} = E\{B_{ln} B_{np}\} = \delta_{mp} a_{lnm} \quad (2)$$

$$E\{B_{lm} A_{np}\} = -E\{A_{lm} B_{np}\} = \delta_{mp} b_{lnm}$$

Of the quantities observed for the Moon, we consider  $C-A$ . The expected value of the square of  $C-A$  is then

$$E\{(C-A)^2\} = E\{\iint \rho'(x_i) (x_1^2 - x_3^2)$$

$$\rho'(x_{i'}) (x_1'^2 - x_3'^2) d\tau d\tau'\}$$

$$= \iint E\{\rho'(x_i) \rho'(x_{i'})\}$$

$$(x_1^2 - x_3^2) (x_1'^2 - x_3'^2) d\tau d\tau'$$

(3)

From this equation we note that if the variation in density is uncorrelated,

$$E\{\rho'(x_i) \rho'(x_{i'})\} = 0 \text{ if } x_i \neq x_{i'}$$

then

$$= \gamma \text{ if } x_i = x_{i'}$$

The term  $E\{(C-A)^2\}$  vanishes and the nonequilibrium values of the second harmonic terms in the gravitational field vanish. Thus an aggregation of many small particles will not give rise to a density variation that leads to nonequilibrium values of  $(C-A)/B$ .

That the variations in density must contain power at the second harmonic in order to account for the observed moment follows from noting that

$$x_j^2 - x_3^2 = r^2 \left[ 1/6 P_{22}(\cos \theta) \cos^2 \lambda - P_{20}(\cos \theta) \right]$$

and introducing this expression into Eq. 3 where Eq. 1 is used for the covariance of the density field. The only nonvanishing terms involve  $a_{222}$  and  $a_{220}$  when account is taken of the orthogonality of the associated Legendre functions. From Eq. 2 we note that finite values of  $a_{222}$  and  $a_{220}$  require finite values for the second-order coefficients in the expansion of the variable part of the density field.

From Table 7 we note that the nonequilibrium part of  $(C-A)/MR^2$  and  $(C-A)/B$  equals  $1.5 \times 10^{-4}$  and  $6 \times 10^{-4}$  respectively, so that  $(C-A)^2/M^2R^4$  is of order  $10^{-7}$  to  $10^{-8}$ . If the density field is correlated over a distance  $L$ , then from Eq. 3

$$\frac{E\{(C-A)^2\}}{M^2R^4} < \frac{\gamma}{\rho_0^2} \left( \frac{L}{R} \right)^3$$

so that for a mean density of  $3.34 \text{ g cm}^{-3}$  and a correlation distance of  $0.1 R$ ,

$$\frac{E\{(C-A)^2\}}{M^2 R^4} < 1 \times 10^{-4} \gamma$$

If the spread in densities in stony meteorites of about  $0.3 \text{ g cm}^{-3}$  is used to estimate  $\gamma$ , then the correlation distance must be greater than  $0.1 R$ .

Thus if random density variations in density give rise to second-order harmonics in the Moon's gravitational field, then the correlation distance for the density field must be greater than one tenth of a lunar radius. This implies that if the density variations are due to the process of aggregation, then fewer than 1000 objects participated. In particular, the observed nonequilibrium gravitational harmonics could be accounted for if a small number participated in the accumulation of the Moon. In addition, a rain of much smaller masses may have participated, but these would contribute only to much higher harmonics in the gravitational field.

### III. Thermal Constitution of the Moon

Considerations of the internal temperature distribution are usually based on the assumption that the nonequilibrium figure implies a rigid and therefore relatively cold interior. Urey (1952, 1957, 1962), Levin (1960), and MacDonald (1959, 1962) have carried out extensive calculation on thermal models of the Moon. These studies show that if the Moon is chemically homogeneous and is like chondritic meteorites in chemical composition ( $U = 1.1 \times 10^{-8} \text{ g/g}$ ,  $K = 8.0 \times 10^{-4} \text{ g/g}$ ,  $Th = 4.0 \times 10^{-8} \text{ g/g}$ ), then the melting temperature of silicates is exceeded over much of the Moon's interior. MacDonald (1962) and Urey (1962) show that the internal temperature would be reduced below the melting curve if the percentage of radioactive materials within the Moon were lowered or if the Moon were highly differentiated, with radioactive materials concentrated near the surface as the result of a partially molten stage early in the Moon's history.

If thermal conduction plus radiation transports heat within the Moon, the internal temperatures are determined primarily by the assumed distribution of temperature in the initial stages of formation and the concentrations of radioactivity. In the past it has been customary to assume a chondritic composition in discussions of the thermal development of the Moon and planets. This assumption was based on a rough agree-

ment of chondritic and solar abundances, the consistency of the meteoritic model of the Earth's interior with seismic evidence, the approximate uniformity of chemical composition of many chondrites, and the approximate equality of surface heat flow and the present rate of heat production in a chondritic Earth. The last argument is usually given most weight. Recently Wasserberg et al. (1964) and MacDonald (1964a) pointed out that the ratio of K/U (and also Th/U) is nearly constant in a wide variety of terrestrial materials of varying composition. The ratio of K/U in rocks is about  $10^4$ , while in chondrites it is  $8 \times 10^4$ ; the ratio is variable in achondrites (see Table 8). MacDonald (1964a, 1965) has shown that a number of models of the Earth can be constructed with a K/U ratio of  $10^4$  that yields the observed heat flow of about  $64 \text{ ergs cm}^{-2} \text{ sec}^{-1}$ . The average U concentration for the whole Earth in the acceptable models varies from about  $2.6$  to  $3.1 \times 10^{-8} \text{ g/g}$ . These new results for the Earth suggest that the internal temperature conditions for the Moon be reexamined with a greater variety of radioactive compositions.

**Table 8. Potassium and uranium ratios in meteorites and terrestrial materials (Wasserburg et al., 1964)**

Source	$10^4 \text{ K/U}$
Chondrites	6.7-7.7
Achondrites	
High calcium	0.5
Low calcium	0.4
Granites	0.8
Basalts	1.4
Eclogites	0.8

As an indication of the concentrations of radioactivity that would be permitted without melting, we consider the total heat production over  $4.5 \times 10^9$  years. If the Th/U and K/U ratios are 3.7 and  $1 \times 10^4$  respectively, then one gram of material will produce  $7.2 \times 10^9$  ergs in  $4.5 \times 10^9$  years. Assuming a heat capacity of  $1.3 \times 10^7$  ergs/g  $^\circ\text{C}$ , we see that such a concentration of radioactivity would raise the temperature of the material by  $553^\circ$  in  $4.5 \times 10^9$  years if there were no heat losses. If conduction and radiative transfer are the chief means of heat transport, the central portions of the Moon are insulated and thus a rough estimate of the central temperature follows from the heat production and assumed initial temperature. We note that if the melting temperature is as low as  $1500^\circ\text{C}$ , then the concentration of U in the Moon must be less than  $3 \times 10^{-8} \text{ g/g}$  (see Table 9).

**Table 9. Central temperature for radioactive models of the Moon with initial temperature of 0° C**

Concentration of U, g/g ( $K/U = 10^4$ )	Temperature °C
$2 \times 10^{-8}$	1106
$3 \times 10^{-8}$	1659
$4 \times 10^{-8}$	2212
$5 \times 10^{-8}$	2765
Chondritic ( $K/U = 8 \times 10^4$ )	1900

The effects of varying the radioactivity on the internal temperature field of the Moon have been investigated in a number of numerical models. The numerical techniques are similar to those used in earlier studies (MacDonald, 1959, 1962). The equation governing the transfer of heat is:

$$b(r) \frac{\partial T(r)}{\partial t} = \frac{1}{r^2} \frac{\partial}{\partial r} \left[ r^2 K(r) \frac{\partial T}{\partial r}(r) \right] + A(r, t)$$

where  $b(r)$  is the product of the density  $\rho$  and the heat capacity  $cp$ . The thermal conductivity is taken to be of the form

$$K = C + \frac{16 n^2 S T^3}{3 \epsilon_0}$$

where  $C$  = ordinary lattice conductivity ( $2.5 \times 10^5$  ergs/cm sec °C),  $N$  = the refractive index of the material (1.7),  $C - \epsilon_0$  = the sum of absorption and scattering coefficients averaged over all wavelengths ( $10 \text{ cm}^{-1}$ ), and  $T$  = temperature.

Figure 24 shows the temperature field for the Moon after  $4.5 \times 10^9$  years, provided the Moon were initially at 0°C. The radioactivity is uniformly distributed and the concentrations of uranium are shown ( $U = 2 \times 10^{-8}$  g/g and  $3 \times 10^{-8}$  g/g) with  $K/U = 10^4$  and  $Th/U = 3.7$ . Also shown is the melting curve for diopside, which Boyd and England (1963) have experimentally determined up to a pressure of  $5 \times 10^4$  bars. The melting interval for basalt at low pressures and eclogite at high pressures is also shown (Yoder and Tilley, 1962).

From these calculations, I conclude that if the Moon has the average concentration of radioactive elements

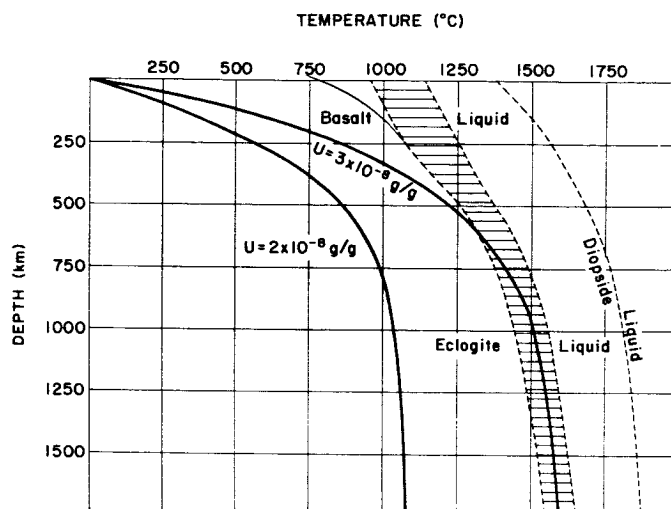


**Fig. 24. Calculated temperature distribution for the Moon.  $K/U = 10^4$ ,  $Th/U = 3.7$ . Initial temperature = 0°C. The melting curve of basalt/eclogite after Yoder and Tilley, 1962, the melting curve of diopside after Boyd and England, 1963**

about equal to that of the Earth ( $U = 2.6$  to  $3.1 \times 10^{-8}$  g/g), then the Moon is solid or nearly so to the center, provided the initial temperature was low (0°C). A chondritic composition would lead to a molten Moon (central temperature = 1900°C if initial temperature = 0°C). Once the Moon was molten, the low rate of thermal transfer would allow even a minor amount of deeply buried radioactivity to keep the Moon at its melting temperature. Thus if density inhomogeneities arising from the initial aggregation are responsible for the figure of the Moon, then the radioactivity of the Moon is as low as the average radioactivity of the Earth and substantially less than that of chondritic meteorites.

#### IV. On the Origin of the Moon

The discussion of the previous sections provides a basis for one possible model for the origin of the Moon. In this model the Moon aggregated from a number of objects of size comparable to the present Moon. In addition, a very much larger number of small objects would have been involved. The chemical composition of the major portion of the Moon must differ from that of chondritic meteorites but could be similar to that of the Earth. In this section I review certain dynamical considerations and suggest how these can be combined with the model for lunar formation outlined above.

The present orbital elements of the Moon and the rotational parameters provide serious limitations to theories of the origin of the Moon. In particular, at present the eccentricity of the Moon's orbit is low ( $5.2 \times 10^{-2}$ ) and is increasing at a rate  $(1/e) (de/dt) = 3.8 \times 10^{-8} \text{ sec}^{-1}$  even when account is taken of the radial tides in the moon, which tend to decrease the eccentricity. In addition,  $(1/e) (de/dt)$  depends on  $\alpha^{-13/2}$  where  $\alpha$  is the semimajor axis of the orbit. Thus the eccentricity was smaller in the past and the rate of increase greater. This observation would appear to rule out any simple capture process for the Moon. Any many-body capture would almost certainly lead to an orbit more eccentric than the present orbit. The tidal processes would only further increase the eccentricity. The tidal capture in a retrograde orbit suggested by Gerstenkorn (1955) could yield the present eccentricity. However, MacDonald (1964b) has indicated a number of very great difficulties with this theory, including energetic and angular momentum considerations.

A second restriction on the theory of lunar origin arises from consideration of the time scale required for the development of the present Earth-Moon system. If the present rate of tidal dissipation has not altered, then the Moon and Earth were close only  $1.8 \times 10^9$  years ago. This restriction is less severe than that placed by the eccentricity, since it is possible that the rate of tidal working has altered in time, though preliminary paleontological evidence argues against such a variation (MacDonald, 1964b). I have suggested that the time scale difficulty can be overcome if it is assumed that the present Moon accumulated out of several smaller moons. The rate of change of the orbital elements of a satellite depends on the force per unit mass of the satellite. For a tidal interaction, the disturbing force is a linear function of the mass of the satellite, so that the rate of change of the orbital elements depends linearly on the mass, with a time scale for a given rate of change in an orbital element varying inversely with the mass. Whereas the rate of change of the orbital elements varies as the mass of the disturbing body, the torque acting on the Earth varies as the square of the mass of the disturbing body. The time scale in the many-moon case is determined by the mass of the largest moon with a multi-moon system tidally evolving more slowly than the present system.

An additional restriction follows from the fact that the orbital plane of the Moon is inclined to the ecliptic, while the tidal torque tends to reduce this inclination. Thus in the near past the Moon's orbital plane was farther out of the ecliptic than it is now.

The combined gravitational, thermal, and dynamic considerations suggest the following model for the formation of the Moon. The Earth and a proto-moon aggregated as a binary system, with the proto-moon having a mass on the order of  $1/4$  to  $1/2$  that of the present Moon. The orbit of the proto-moon was regular and nearly circular, with a low inclination and a semimajor axis substantially less than the present. Associated with the original binary system were a large number of smaller masses, which were gradually swept up by both the Earth and Moon. The binary system also captured a small number of objects with masses comparable to the proto-moon but having orbits of varying inclination and eccentricity level, with semimajor axes larger than that of the proto-moon. No detailed calculations of the capture process have been carried out but it would appear more likely than an initial binary system would be more successful in capturing other objects than would the Earth alone. The multi-moon system thus developed would evolve under tidal forces with the most massive proto-moon moving out more rapidly. Collision and capture of the smaller moons by the proto-moon would increase the mass of the largest moon, which in turn would move out more rapidly. The collisional processes between the large objects would lead to the large-scale density inhomogeneity inferred from the orbital and rotational data.

The many-moon hypothesis outlined above could account for both the time scale deduced from the present rate of tidal deceleration and for the present orbital elements. The many-moon hypothesis, unlike other hypotheses of lunar origin, supposes that the surface of the Moon is relatively young, with the last major collision having taken place  $1.5$  to  $2.0 \times 10^9$  years ago.

The complex model outlined above has within it numerous problems. What are the details of a capture by a binary system: Can a tidally displaced object collide and aggregate with another object somewhat smaller in mass? Can the present remarkably regular orbit of the Moon result from such a series of events?

Observations to be made in the near future are certain to provide critical data in testing the many-moon model as well as other models. The age of the outer surface of the Moon is of critical importance. The determination of the gravitational field will allow us to decide whether the observed gravitational irregularities are due to an irregular aggregation or to internal processes. If the nonequilibrium form is due to random density variations, then the higher terms in the gravitational field should be of the same order as the nonequilibrium second-order

terms. Seismic observations will lead to an estimate of the radioactivity of the interior of the Moon and provide information as to the degree of differentiation. This list

of important new observations is long and it is certain that in ten years our models of the Moon will be much more sophisticated than the present primitive versions.

## REFERENCES

- Gerstenkorn, H., *Z. Astrophys.* Vol. 26, pp. 245–274, 1955.
- Habibullin, S. T., *Soviet Astron. AJ*, Vol. 2, pp. 622–637, 1958.
- Jeffreys, H., *Mon. Nat. Roy. Astr. Soc.*, Vol. 122, pp. 421–432, 1961.
- Jones, R. H., in *Times Series Analyses*, ed. M. Rosenblatt, J. Wiley, New York, pp. 119–124, 1963.
- Kopal, Z., *Icarus*, Vol. 4, pp. 173–176, 1965.
- Levin, B. J., in *The Moon*, ed. by Z. Kopal, Proc. of Symp. No. 14 of IAU, Academic Press, pp. 157–167, 1962.
- MacDonald, G. J. F., *J. Geophys. Res.*, Vol. 64, pp. 1967–2000, 1959.
- MacDonald, G. J. F., *J. Geophys. Res.*, Vol. 67, pp. 2945–2974, 1962.
- MacDonald, G. J. F., *J. Geophys. Res.*, Vol. 69, pp. 2933, 2946, 1964a.
- MacDonald, G. J. F., *Rev. Geophysics*, Vol. 2, pp. 467–541, 1964b.
- MacDonald, G. J. F., in *Terrestrial Heat Flow*, Geophysical Monograph No. 8, Amer. Geophys. Un., pp. 191–210, 1965.
- Runcorn, S. K., *Nature*, Vol. 195, pp. 1150–1151, 1962.
- Urey, H. C., *The Planets, Their Origin and Development*, Yale University Press, New Haven, 1952.
- Urey, H. C., in *Physics and Chemistry of the Earth*, Vol. 2, Pergamon Press, New York, pp. 46–47, 1957.
- Urey, H. C., Elsasser, W. M., and Rochester, M. C. *Astrophys. J.*, Vol. 129, pp. 842–848, 1959.
- Urey, H. C., Lines of Evidence in Regard to the Composition of the Moon, in *Space Research*, Vol I, North-Holland Publishing Co., Amsterdam, 1960.
- Urey, H. C., in *Physics and Astronomy of the Moon*, ed. by Z. Kopal, Academic Press, New York, pp. 481–523, 1962.
- Wasserburg, G. J., MacDonald, G. J. F., Hoyle, F., and Fowler, W. A., *Science*, Vol. 143, pp. 465–467, 1964.
- Yakovkin, A. A., *Trans. IAU*, Vol. 8, pp. 231–232, 1952.
- Yaglom, A. M., *Proc. Fourth Berkeley Symp. Math Statistic Probability*, Vol. 2, pp. 593–622, University of California Press, Berkeley, 1961.
- Boyd, F. R., and England, J. L., *J. Geophys. Res.*, Vol. 68, pp. 311–324, 1963.
- Yoder, H. S., and Tilley, C. E., *J. Petrol.* Vol. 3, pp. 342–532, 1962.

N66 31455

## THE INTERNAL STRUCTURE OF THE MOON AND THE TERRESTRIAL PLANETS

*Don L. Anderson*

*California Institute of Technology  
Pasadena, California*

*and*

*Robert L. Kovach*

*Stanford University  
Stanford, California*

### **1. Introduction**

The known internal structure of the Earth is the logical starting point for discussions of the terrestrial planets and the Moon. Until we have direct data, the most reasonable assumption regarding these bodies is that they are similar in composition to the Earth.

Several recent developments in geophysics have immediate implications for the other planets. These are:

1. The evidence that the upper mantle low-velocity zone is essentially a world-wide phenomenon, is more pronounced, and extends much deeper than previously supposed.
2. The development of techniques to detect and interpret the free oscillations of the Earth, thus permitting a direct determination of density.
3. Shock-wave data on rocks at pressures in excess of those existing in the Earth, thereby permitting the free oscillation densities to be interpreted in terms of composition.
4. Laboratory and seismic evidence for abrupt phase changes in the upper mantle, indicating that planetary models based on self-compression equations of state are invalid.
5. The now conclusive evidence favoring an iron-rich core rather than a silicate phase change.
6. The redetermination of the average radioactive abundances in the Earth, which suggest that the chondritic analogy is not appropriate for the Earth and, presumably, also not appropriate for the inner planets and the Moon.

Any one of the developments listed above would justify a re-examination of present conclusions regarding the structure and composition of the inner planets. By combining all of this new information into the discussion to follow we hope to update the study of planetary interiors to the present level of knowledge regarding the interior of the Earth.

The Moon is of particular interest because of the apparent paradox of its observed high mean moment of inertia. Surprisingly enough, however, if conditions within the Moon are comparable to those at the same pressure level within the Earth, then a density decreasing with depth is predicted for the lunar interior.

## II. Equation of State

An equation of state for the Earth, which does not depend on the Adams-Williamson adiabatic and hydrostatic assumptions, has been determined from free oscillation and shock wave data. The equation implies that low densities are associated with low seismic velocities; this is also implicit in the velocity density relation of Birch. The study of the upper mantle of the Earth is particularly pertinent to the problem of planetary interiors since pressures at the center of the Moon and Mars correspond, respectively, to depths of only about 150 and 650 km within the Earth. This region of the Earth is anomalous on all counts, involving reversals of seismic velocities, densities, and probably the maximum departures from adiabaticity and hydrostaticity and the closest approach to the melting point. It is only at a depth below some 1000 km that the Earth starts to behave as a self-compressed ball.

The low-velocity, low-density zone is an important feature of the upper mantle of the Earth but its contribution to the overall mass and moment of inertia are slight. If conditions in the Moon are comparable to those at the same pressure level in the Earth, then the lunar low-density zone will dominate the properties of the Moon. In fact, a density *decreasing* with depth in the Moon is a feature that is difficult to avoid.

Figure 25 shows the free oscillation equation of state in terms of density vs pressure. For comparison we show the standard Bullen density models and the shock wave equation of state for iron. Below the curve for iron is a curve that shows the equation of state for the core, which represents a mixture of pure iron and mantle silicates. Note the discontinuities, which represent upper mantle phase changes. The arrows at the top of the figure are the minimum central pressures in the Moon, Mars, and Venus.

Figure 26 shows how the free oscillation equation of state is used with shock wave data to determine composition in the Earth. The curves are in terms of the seismic parameter,  $\Phi$ , which is a measure of compressibility and density.

## III. Application to the Moon

The simplest assumption regarding the Moon is that the physical properties are identical to those at corresponding pressure levels in the Earth. Figure 27 shows the equation of state variable  $\Phi$ , which is directly measured for the Earth and its implied variation with depth in the Moon under the assumption above. Note that the pressure at the center of the Moon, about 52 kilobars, corresponds to a depth of about 150 km within the Earth. The seismic velocities in the Moon are related to the square root of  $\Phi$  and the density is some fractional power of  $\Phi$ . A low-velocity, low-density region is then immediately predicted for the interior of the Moon.

An alternate approach to the density structure of the Moon is to estimate the present temperature from thermal history calculations and allow for the effects of thermal expansion and compression. Figure 28 shows the condition for a constant density in the Moon. The change of density with depth is due to increasing pressure (first term, line 1) and increasing temperature (second term, line 1). Together this leads to an estimate of 0.8 C/km as the critical temperature gradient for constant density. Thermal history calculations suggest that this gradient is exceeded, at least to a depth near 400 km, where the melting curve is intersected. One can see that the melting point gradient itself is less than the critical gradient. Any partial melting and consequent upper migration of molten material will tend to smooth out the gradient and it is possible to exceed the critical gradient throughout the Moon, giving a decreasing density from the near surface to the center.

Table 10 gives the density gradients and the total change of density in the upper and lower Moon which result from thermal history calculations. The density decreases by about 4% in the upper 400 km and increases by about 3% from 400 km to the center, thus never recovering its initial value.

Table 10. Density gradients in the Moon<sup>a</sup>

	Upper Moon (0-400 km)	Lower Moon
$\frac{d\rho}{dh}$	-0.32 (g/cm <sup>3</sup> )/1000 km	+0.064 (g/cm <sup>3</sup> )/1000 km
$\Delta\rho$	-0.128 g/cm <sup>3</sup>	+0.086 g/cm <sup>3</sup>
<sup>a</sup> If partial melting occurs, the densities in the Moon will be lower than the values presented here.		

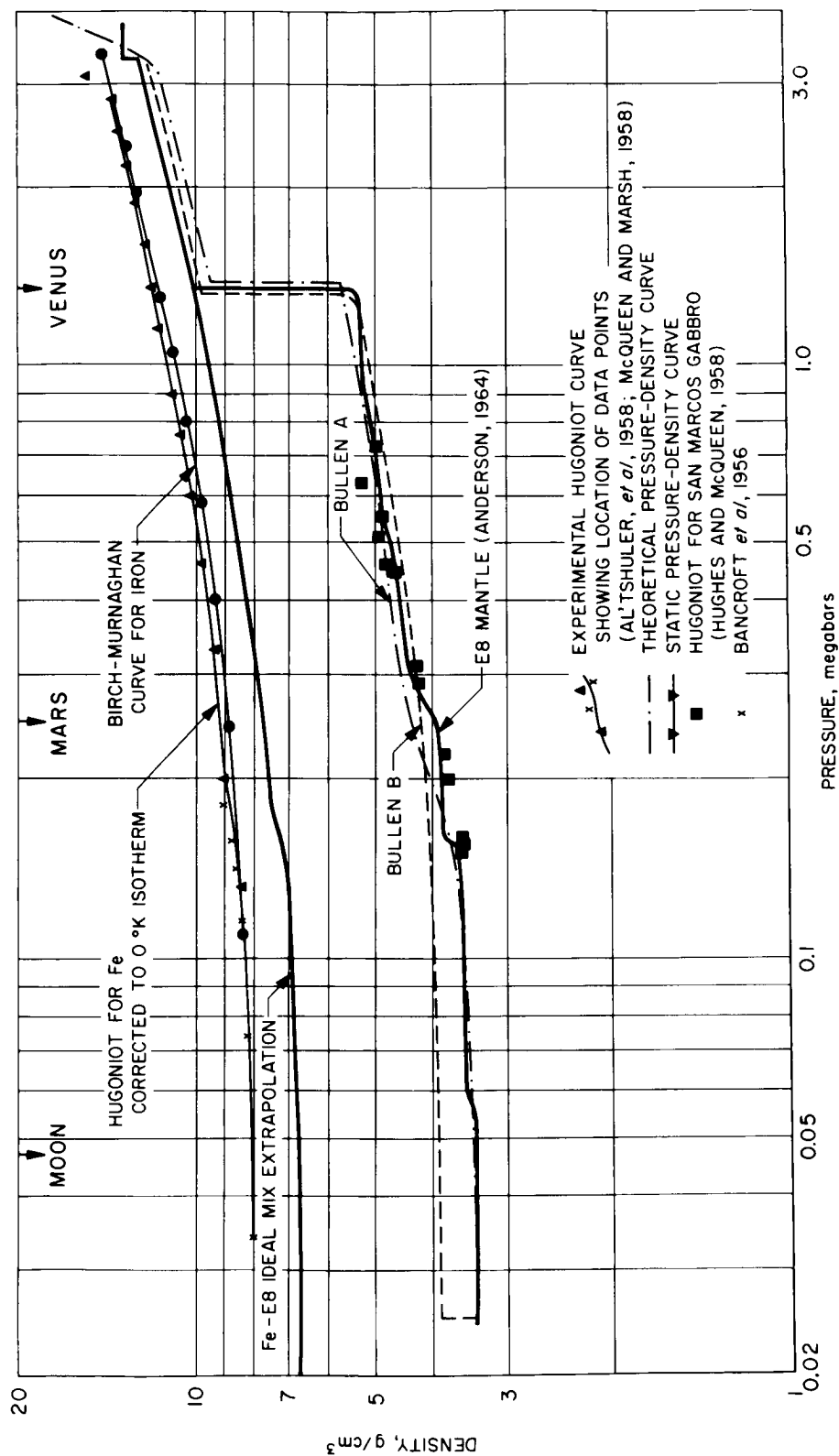


Fig. 25. Equations of state for the mantle and core of the Earth, as determined from seismic and shock wave data



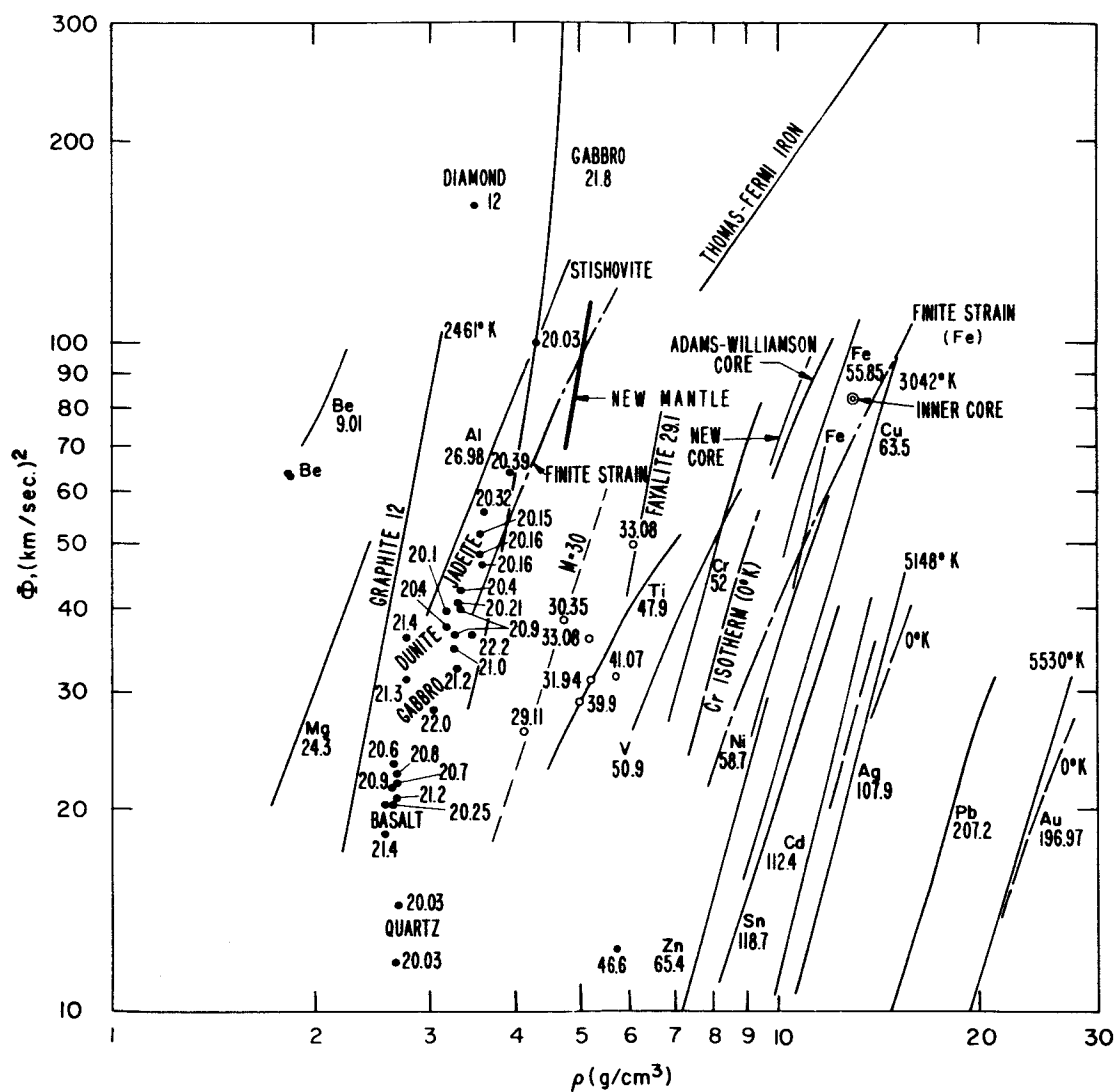


Fig. 26. Equations of state for metals and rocks as a function of mean atomic weight. Also shown are the free oscillation results for the mantle and the core

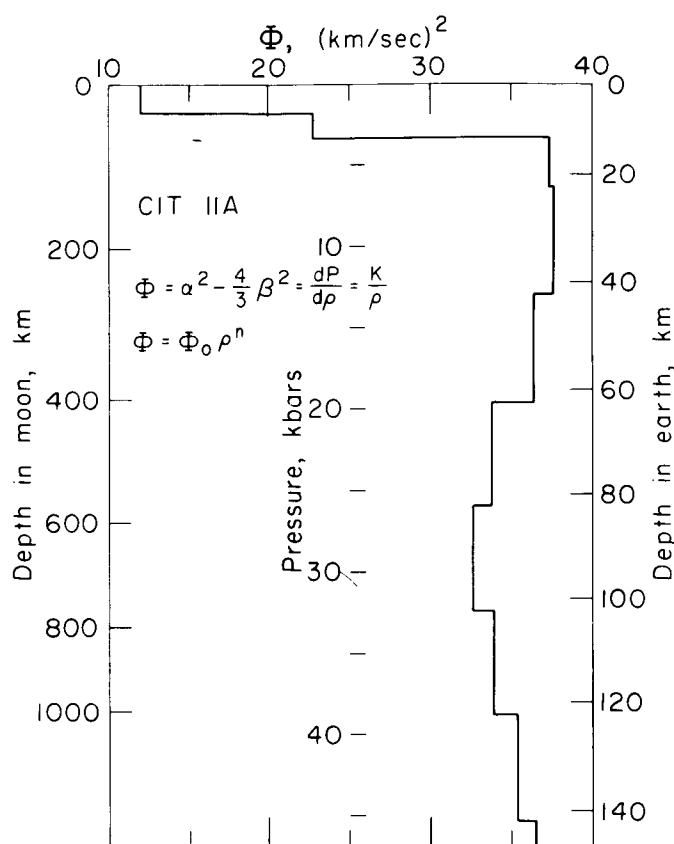


Fig. 27. The equation of state variable  $\Phi$  in the Earth and in the Moon under the assumption that  $dT/dP$  is identical in these two bodies

#### CONDITION FOR CONSTANT DENSITY

$$\frac{d\rho}{dh} = -\frac{g\rho^2}{K_T} + \rho\alpha \frac{dT}{dh} = 0$$

$$\frac{dT}{dh} = \frac{g\rho}{\alpha K_T} = 0.8^\circ\text{C/km}$$

#### CRITICAL GRADIENT

If  $\frac{dT}{dh} > 0.8^\circ\text{C/km}$  density will decrease with depth

$$\frac{dT}{dh} \sim 3^\circ\text{C/km} \quad (400 > h > 0\text{km}) \quad \text{Thermal history calculations}$$

$$\frac{dT}{dh} \sim 0.1-0.2^\circ\text{C/km} \quad \text{Melting point gradient}$$

Fig. 28. Condition for constant density in the Moon

The densities that result from the two approaches above are shown in Fig. 29. The solid curve represents basically a decompressed Earth and involves only an implicit effect of temperature, i.e., the assumption that the change of temperature with pressure is the same in the Moon as it is in the Earth. The dashed curve is the density estimated from an explicit allowance for the temperature from thermal history calculations. The results are similar and both require an extensive low-density region in the Moon and central densities that are less than the near surface densities.

Seismic experiments will supply the most direct evidence regarding the interior of the Moon. However, the decrease in velocities with depth that are predicted in the Earth-decompression analogy will make interpretation

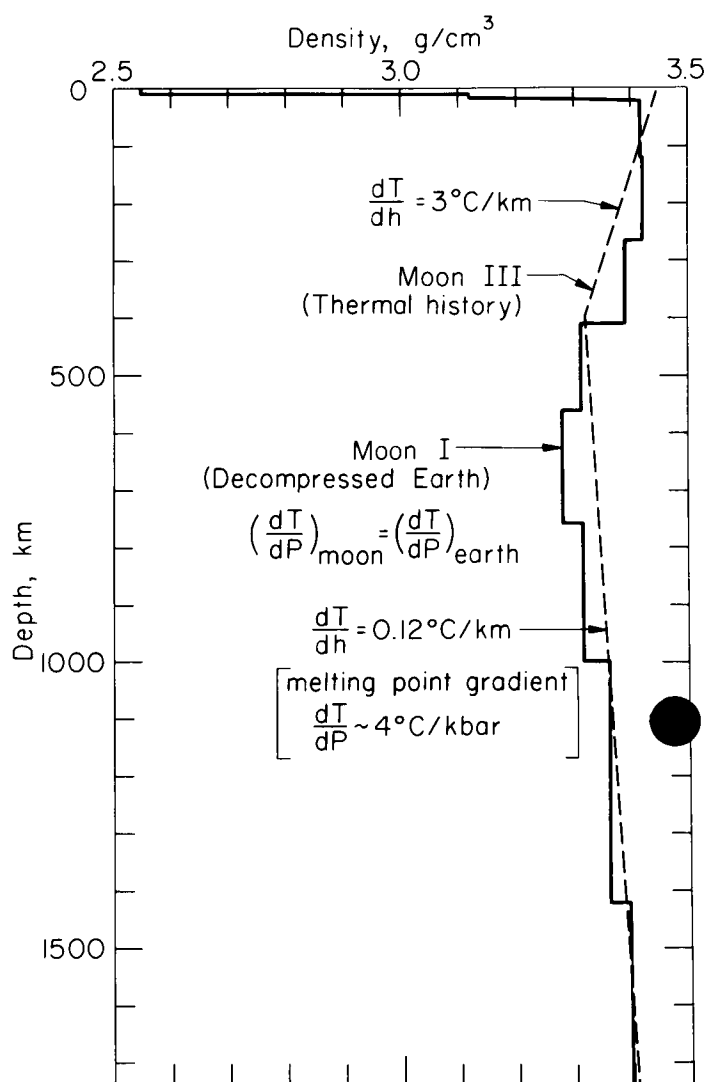


Fig. 29. Density vs depth in the Moon

of standard seismic body wave data less straightforward than for 'standard' Moon models that have previously been discussed. In regions where the velocity decreases inward, the seismic ray paths will be bent downward and defocused.

The theoretical periods of free oscillation of our new Moon model are important in the design of a lunar seismic experiment. These periods are shown in Table 11. These periods, when observed, will clearly differentiate between various models. Our new model has periods significantly longer than the others shown. A long-period lunar seismometer should, therefore, have a capability of detecting oscillations as long as about 16 min in period.

**Table 11. Theoretical periods of free spheroidal oscillations of the Moon for several models**

Order, $n$	Periods of spheroidal oscillations, minutes			
	Homogeneous	Self-compression	Density reversal	Heavy core
2	14.6	15.1	15.7	12.5
3	9.8	10.2	10.6	8.8
4	7.7	8.0	8.2	7.2
6	5.6	5.8	5.9	5.5

#### IV. Thermal History Calculations

Wasserburg et al. (1964) have recently shown that the radioactive abundances in the Earth are quite different from those in chondritic meteorites. Chondritic abundances have previously been used in thermal calculations for the other planets. However, the potassium-uranium ratio is eight times smaller and the uranium content is possibly four times larger in the Earth than in chondrites. To be consistent, therefore, with our general approach, we must redo the thermal history calculations. This has recently been done by Phinney and Anderson (1965) and the results are shown in Fig. 30, along with results for a chondritic Moon. Note that the Moon heats up more rapidly with the new abundances, intersecting the melting curve at a time  $1.6 \times 10^9$  years after formation, assuming that it started at a constant temperature of  $273^\circ\text{K}$  throughout. These calculations are incomplete in the sense that the latent heat of melting and heat transferred by mass movement during the source of differentiation are ignored. For the present, however, we are simply comparing Moons of differing radioactivities. The conclusion is simply that a Wasserburg Moon will start to melt and differentiate earlier and more completely

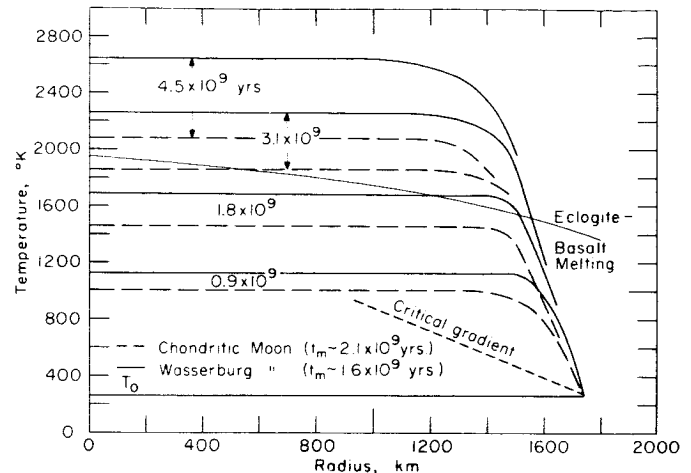


**Fig. 30. Thermal history calculations for initially cold ( $273^\circ\text{K}$ ) chondritic and Wasserburg Moons. Extensive melting at depth is predicted for both models.**

than a chondritic Moon. The surface features of the Moon are therefore probably older than would be assumed with the chondrite analogy. The effect of the latent heat of fusion would be to keep the temperatures at depth on the melting curve; the effect of heat transfer by mass movement would be to smooth out and lower the gradient in the upper part of the Moon.

The calculations indicate that the Moon underwent severe radial differentiation some 3 billion years ago. Partial melting or differentiation does not imply homogenization of the lunar interior or large-scale regular convection cells. The Moon probably has an irregular sialic crust approximately 10 km thick in the highlands, overlying a more basic mantle. This estimate is based on the observed relief on the Moon's surface and is consistent with a degree of differentiation comparable to that having occurred on the Earth.

#### V. The Terrestrial Planets

It is commonly maintained that the differences in the mean densities of the inner planets imply that they all have different compositions.

Ramsey (1948), Bullen (1949, 1957), Lyttleton (1963), and Levin (1963) have maintained that the terrestrial planets have the same composition, but their conclusion requires that if any internal core is present it is composed of a high-density modification of the mantle silicates rather than an iron-rich alloy. On the other hand, Urey (1952), MacDonald (1962) and others have presented

detailed calculations supporting the view that the Moon and the terrestrial planets differ markedly in composition. These calculations suppose that any planetary cores are chemically distinct from the mantle material.

Using the seismic equations of state for the Earth's mantle and core, it is possible to design undifferentiated protoplanets by mixing the iron core into the silicate mantle and suitably combining the individual equations of state. The resulting body, of course, has the same average composition as the Earth. It can be shown that the mean density and moment of inertia of Mars are satisfied by an Earth-like protoplanet that has undergone no differentiation.

Table 12 shows the ellipticities for Mars that result from various degrees of differentiation. Only the undifferentiated Mars gives the proper mean density and ellipticity.

Table 12. Properties of partially differentiated Mars models

Distribution of material	Radius, km	C/MR <sup>2</sup>	η	e <sup>-1</sup>
Differentiated	3309	.3449	.4568	231.2
80% core into mantle	3306	.3784	.1686	205.0
90% core into mantle	3305	.3828	.1332	201.7
80% mantle into core	3307	.3787	.1664	204.3
97% mantle into core	3309	.3836	.1289	200.3

\*The "differentiated" model is geometrically similar to the Earth and represents a chemically differentiated model. The observed inverse ellipticity for Mars is 200, indicating that it is a chemically undifferentiated body; i.e., there is no core.

Thermal history calculations, Fig. 31, show that temperatures in the Earth will exceed the melting point of iron early in its history, thereby producing a heavy central core. The melting points of the silicates are exceeded later, thus giving a crust and a differentiated mantle. However, temperatures in Mars with the new radioactive abundances will never exceed the melting point of iron. Mars, therefore, will not be able to differentiate its iron into a central core. Since dynamo action in a molten iron core is believed responsible for the Earth's magnetic field, by analogy, Mars will have no magnetic field.

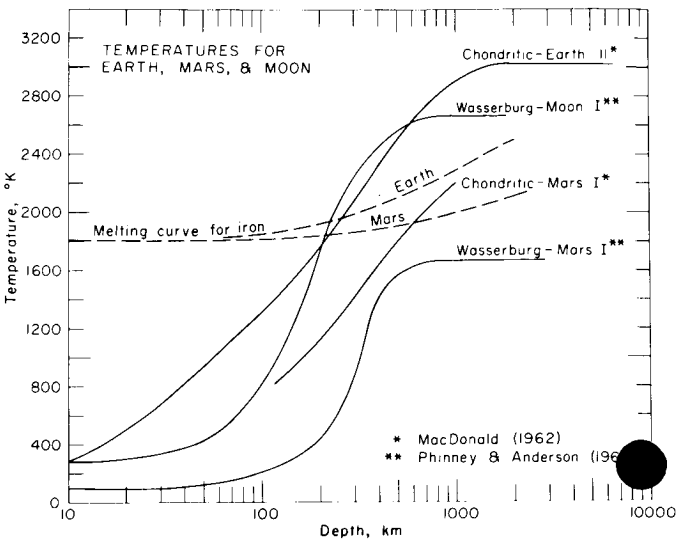


Fig. 31. Present-day temperatures from thermal history calculations for Mars, Moon, and Earth. Mars will not melt or differentiate a core downward nor continents upward. Both the Earth and the Moon go through a hot stage and will differentiate.

VI. The Strength of the Moon

It is often asserted that the irregular shape of the Moon requires great strength and therefore the Moon must be a cold body. Caputo (1965) has recently computed the strength required to support the lunar bulge under various assumptions regarding the size of a possibly liquid core. If the Moon is a solid body throughout, a strength of 18 bars will support the figure; if 75% of the Moon is molten, a strength of 28 bars is required in the remaining solid portion of the Moon. Similar calculations for the Earth show that the mantle is supporting stress differences on the order of 30-160 bars. If the Moon has the same strength as the Earth, it should be able to support stress differences at least 12 times larger than those existing on the Earth, or about 360-2000 bars. This is due to the lower gravity on the Moon. The fact that less than 30 bars is required to support the irregular shape of the Moon implies that it is a weaker, presumably hotter, body than the Earth.

VII. Summary

The differences in the mean densities of the terrestrial planets is usually taken as a compelling argument for the inhomogeneity of this part of the solar system. This conclusion is re-examined in the light of the latest information regarding the distribution of density in the interior

of the Earth. Mars must have its iron more evenly distributed than the Earth but it is not necessary to conclude that Mars differs from the Earth in overall composition. It is possible to design models for Mars and Venus that have the same uncompressed density as the Earth and that satisfy the available data concerning these planets without assuming that the Earth's core is a phase change of the silicate mantle, as argued by Levin, Bullen and Ramsey. Thermal history calculations show that an undifferentiated protoplanet having the composition of the Earth and the dimensions of Mars will not heat up to the melting point of iron or silicates in  $4.5 \times 10^9$  years and will, therefore, not differentiate an iron core or a crust. Mars will, therefore, have no magnetic field and no continents or mountains.

The pressure at the center of the Moon is about 52 kilobars, which corresponds to a depth of about 150 km in the Earth. Conditions down to this pressure level in the Earth are anomalous—namely, the seismic velocities and the density *decrease* with depth. Conditions in this region are not adiabatic nor hydrostatic and the viscosity is anomalously low. The low-velocity zone is an im-

portant feature of the upper mantle of the Earth but its contribution to the overall mass and moment of inertia is slight. If conditions in the Moon are comparable to those at the same pressure level in the Earth, then the low-velocity zone controls the overall properties and the Moon will appear to be a very anomalous body.

An equation of state that is appropriate for the Earth predicts a density decreasing with depth in the lunar interior, thereby giving a high moment of inertia. Thermal history calculations using the new Wasserburg radioactive abundances also predict a density decreasing with depth and, in addition, suggest that the Moon is a differentiated body.

Seismic travel-time curves and periods of free oscillation are computed for the new Moon model. The decreasing seismic velocities with depth make the standard seismic ray methods difficult to apply and interpret because of the defocusing effect. The periods of free oscillation will be the most important data to attempt to obtain in any seismic experiment designed to determine the internal structure of the Moon.

### Acknowledgments

The thermal history models in this paper were computed by Dr. Robert A. Phinney. They form part of a more complete study of thermal history entitled "Internal Temperatures of the Moon" in preparation by R. A. Phinney and Don L. Anderson. We are grateful to Dr. Phinney for permission to use these calculations in advance of publication.

N66 31456

## LUNAR STRUCTURE AS DEDUCED FROM MUONG NONG TEKTITES

J. A. O'Keefe and I. Adler

*Laboratory for Theoretical Studies, Goddard Space Flight Center  
Greenbelt, Maryland*

One avenue toward the exploration of the Moon's surface is undoubtedly furnished by the fragments of that surface which, on any theory, must fall on the Earth. Because it has no atmosphere, the Moon is exposed to bombardment by particles at velocities up to nearly 80 km/sec. Laboratory experiments show that at these velocities, ejecta will be produced which will travel at speeds in excess of the escape velocity from the Moon, 2.3 km/sec, and which, in the absence of an atmosphere, will leave the Moon and eventually, at least in part, find their way to the Earth.

Since the time of the Dutch mining engineer R. D. M. Verbeek (1897), it has been suspected that tektites form a portion of the debris from the Moon. The idea has been advanced in recent years by the discovery of E. C. T. Chao et al. (1962, 1964) that the nickel-iron spherules that are the hallmark of impact in some terrestrial glasses are also present in tektites. It has also been advanced by the work of D. R. Chapman and H. K. Larson (1963) and E. W. Adams and R. M. Huffaker (1962), who have deduced from the forms of the australites that the bodies arrived in the Earth's atmosphere with trajectories that are inconsistent with a terrestrial origin but not inconsistent with an origin on the Moon.

Recently, important new light has been shed on the problem by the study of the Muong Nong-type tektites. This name was given by Virgil Barnes (1961a) to a class of tektites, found chiefly in Thailand and Indo-China,

that have the characteristic that the internal structure is layered. The layering is of somewhat the same nature as the contorted, fluidal structure seen in almost all tektites; but in the Muong Nong material, the structure is arranged in parallel layers and is accompanied by a remarkable appearance within each layer to which Barnes has given the name of "shimmering." The Muong Nong materials have been clearly shown by analysis by Barnes and Pitakpaivan (1962) to be chemically identical with the other tektites (to which Barnes has, for contrast, given the appropriate name "splash-form tektites") except for a minor difference in a state of oxidation of the iron. The resemblance is close enough so that we may be sure not only that the Muong Nong materials are genuinely tektites, but even that they belong to the Far Eastern strewn field. Barnes (1961a) further found that the splash-form tektites, when examined as whole bodies between crossed nicols, show a pattern of strain birefringence that indicates that each one cooled as a unit. There is no such overall strain pattern associated with the Muong Nong material. This fact suggests that Muong Nong tektites are fragments of larger bodies. The same idea is suggested by the fact that Muong Nong tektites are generally found in large associations (Barnes, 1963) weighing tens of kilograms and covering a few tens of square meters. Further support comes from the external shapes of the Muong Nong tektites, which are generally chunky fragments and contrast sharply with the splash-form tektites. The latter, when complete, normally take the forms found in liquid rotating masses: spheres, spheroids, rods, dumbbells, tears, and so forth.

There is every reason to subscribe, therefore, to Barnes's thesis that, in a fundamental way, the Muong Nong materials are more primitive than other tektites and point the way to their origin.

Recently, Barnes (1964) drew attention to the presence of angular voids in some of the Muong Nong tektites, particularly those from Kan Luang Dong. His photograph is shown in Fig. 32. The voids appear black because

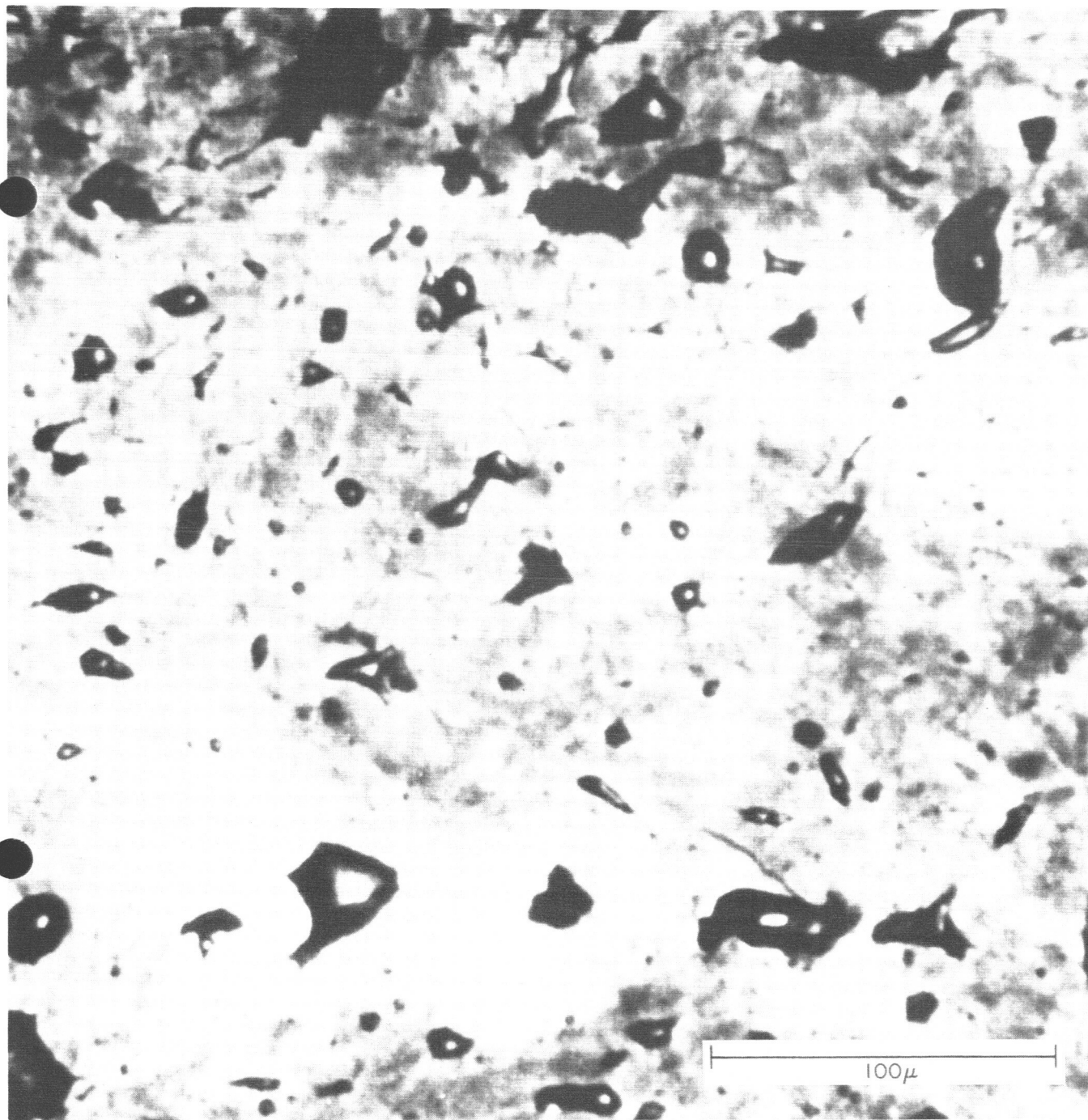


Fig. 32. Angular bubbles observed in a Muong Nong tektite from Kan Luang Dong. Courtesy of V. Barnes. The black marks are voids.

the light is deflected by the bubble surface, except for the central part of some of them, where light can enter the bubble. The significance of the angular voids was pointed out by Barnes, who remarked that they clearly indicated that these tektites had once been some kind of clastic, that is, fragmental material whose grains had been incompletely welded together. The angular voids, therefore, represent the spaces between grains. Barnes pointed out that this implied that these tektites had never been thoroughly melted, since it is well known that voids in a liquid, even a viscous liquid, are spherical or ellipsoidal.

Now this at once opened the way for a decisive test of the theories of the origin of tektites. If tektites are fused sandstone as claimed by Barnes himself (1958), by H. C. Urey (1959), and by S. R. Taylor (1965), then in the Kan Luang Dong tektites we would expect to find the minerals that normally compose a sandstone (Pettijohn, 1957, p. 318), namely, quartz, chert, feldspar, mica, clay, and other minerals existing as separate chemical entities. It is, of course, entirely possible that each of these minerals might have been converted to a glassy form; for instance, quartz to lechatelierite or feldspar to maskelynite as a result of shock. But these materials should,

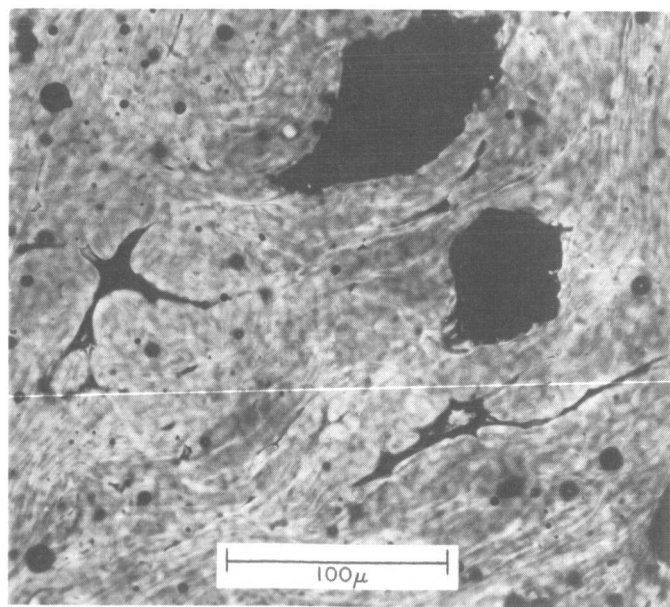


Fig. 33. Microphotograph of a portion of a Muong Nong tektite from Phaeng Dang, showing internal structure. The two large black spots are inclusions.

The small, streaky black lines are voids between shard-like glass bodies. The voids do not extend through the section.

nevertheless, remain chemically distinct. From the appearance of Fig. 32, it is clear that the grain size of the source material was on the order of  $50\ \mu$ . In Fig. 33, we see an enlarged portion of a similar Muong Nong tektite, from Phaeng Dang. It is evident that this tektite is composed of separate pieces of material that were pressed together while soft. The region chosen contains two inclusions; these permit easy orientation in the subsequent figures. Actually such inclusions cover about 15% or less of the area of this portion of this tektite.

In Fig. 34, we see the results of a microprobe scan, using the  $K_\alpha$  line of potassium over the region between the two large spots. (The region was chosen so as to permit easy orientation; the inclusions actually cover about 15% of the section.) The uniform nature of the material is obvious. Remelted bits of feldspar would have shown up as bright spots. Figure 35 is the same kind of thing for silicon; here the silica in the inclusions shows up. Figure 36 is for aluminum; it is uniform outside the black spots (in the inclusions, the voids have become filled with grinding compound,  $Al_2O_3$ , which thus

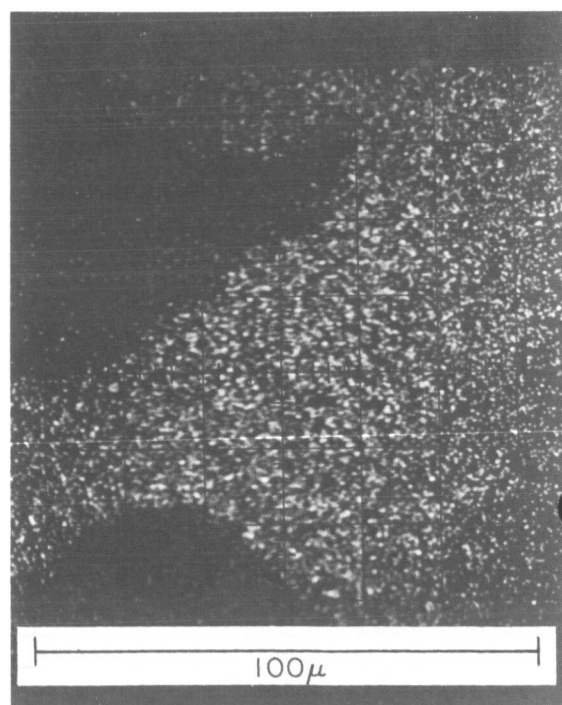


Fig. 34. A portion of the same region as Fig. 33 in the line of the potassium  $K_\alpha$  line prepared by microprobe scanning using X-ray fluorescence. The image is reversed compared with Fig. 33.

Note the homogeneity of the material outside the black inclusions.



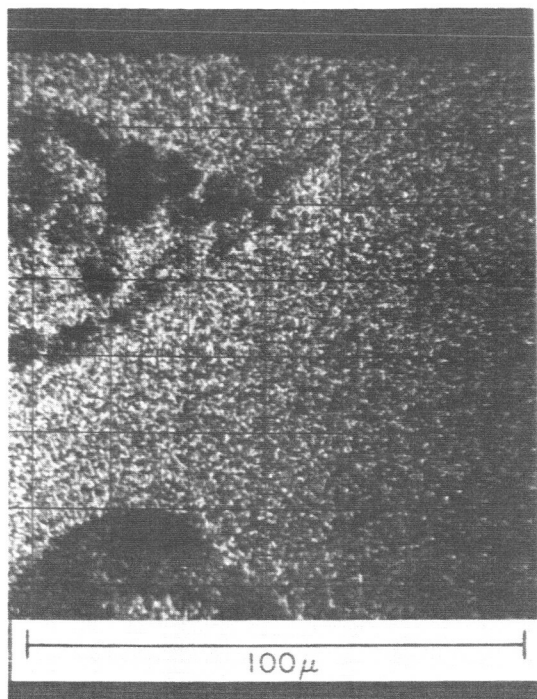


Fig. 35. The same as Fig. 34, for silicon. A network appears in the spots because these are largely composed of vesicular  $\text{SiO}_2$  (frothy lechatelierite).

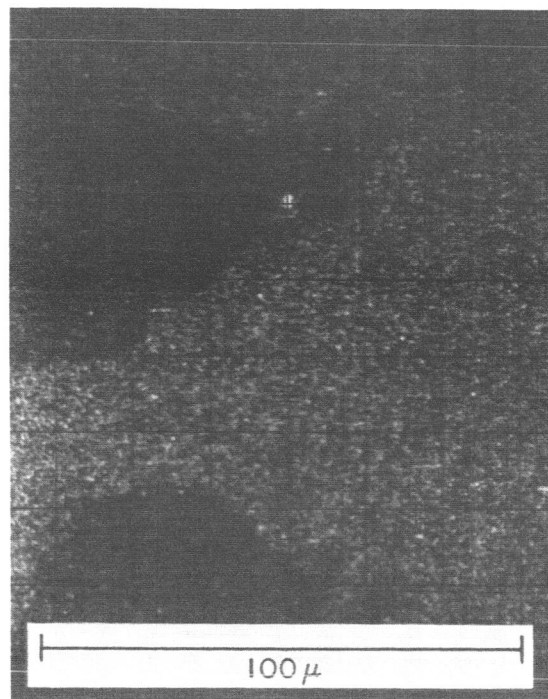


Fig. 37. The same as Fig. 34, for calcium

forms a pattern complementary to the silicon). Figure 37 shows a similar pattern for calcium; a similar pattern for iron is too faint to reproduce.

For comparison, the same techniques were employed on a chemically similar terrestrial specimen kindly supplied by E. A. King, Jr. It is a portion of a tuffaceous sandstone or siltstone, baked by natural fires in an underlying lignite bed. The chemical composition is given by King (1962), who pointed out that it resembles the composition of a tektite (in particular, a bediasite).

In Fig. 38 are similar cathode ray displays for K, Fe, Si, and Al on the Texas siltstone. Each figure is  $90\ \mu$  across. It is evident that the microprobe has more than enough resolution to show the heterogeneous character of this material, if the grain size is of the order of  $50\ \mu$ .

We see that the Kan Luang Dong material is chemically homogeneous and unlike fused soil.

While these studies were going on, Dr. L. Walter (Walter, 1965) at the Goddard Spaceflight Center made what is perhaps the most fundamental discovery in the tektite problem. He examined some small inclusions to which Barnes has given the name "frothy lechatelierite," which are found in the Muong Nong material and which, in the specimens he examined, formed perhaps 1% or less

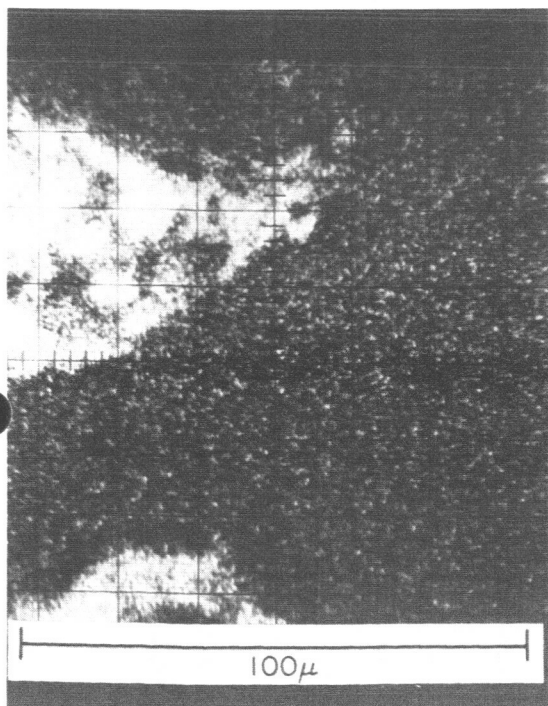


Fig. 36. The same as Fig. 34, for aluminum. Note that the voids in the silica have become blocked up with alumina from the grinding powder.

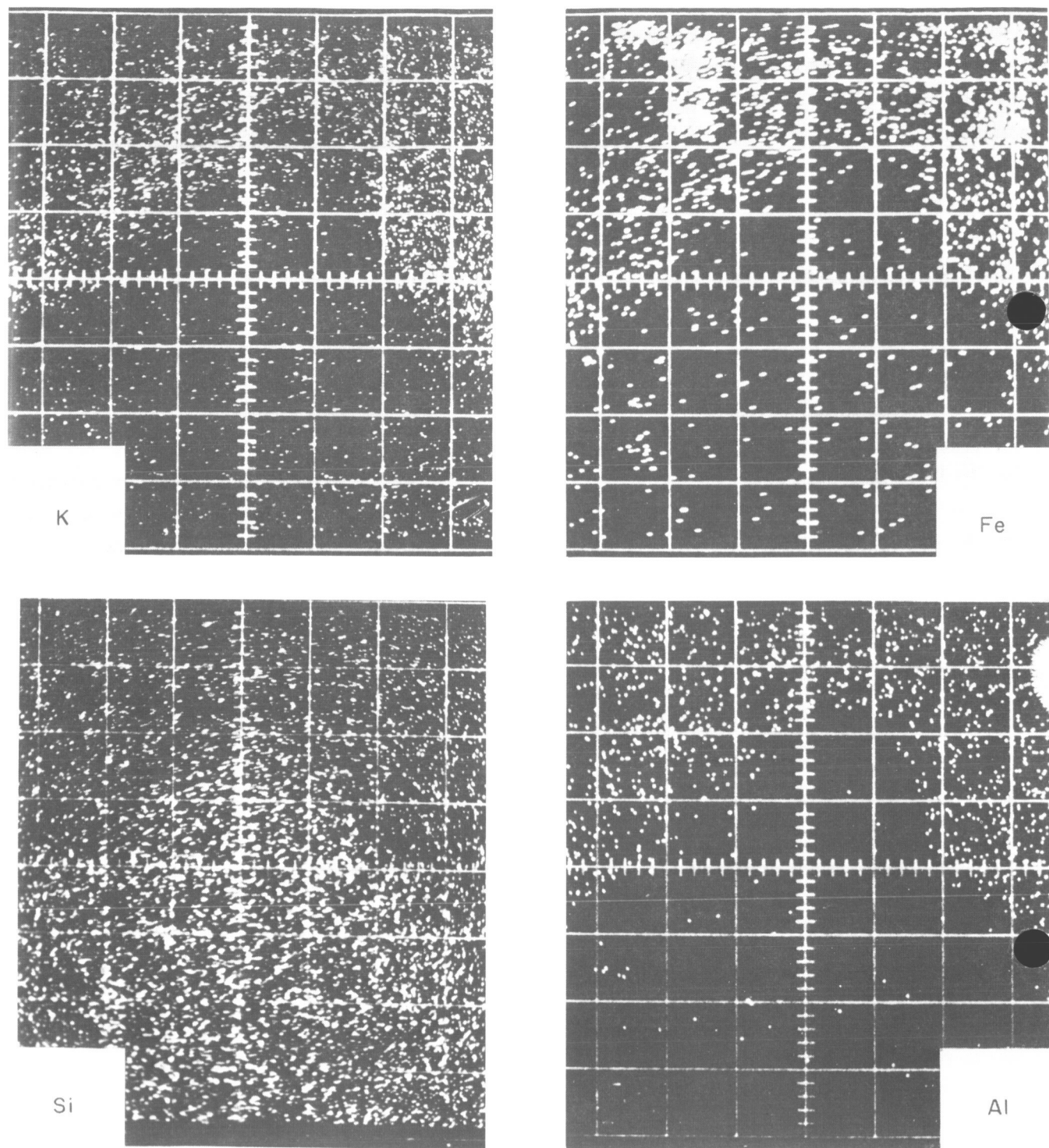


Fig. 38. Microprobe scans for the elements potassium, iron, silicon and aluminum on a sample of Texas siltstone. Note the inhomogeneity as compared with the tektite. Each figure is 90  $\mu$  across.

of the total volume. Walter discovered that the brown central portions of these inclusions contain coesite, which is a high-pressure form of silica, unstable at ordinary temperatures. Since the pioneer work of Chao, Madsen, and Shoemaker (1960), it has been believed that the presence of coesite in a natural rock is an indicator of impact by a meteorite. This interpretation is a very natural one in the present case because of the already-mentioned existence of the nickel-iron spherules. It constitutes a welcome confirmation and eliminates for good the arguments of some doubters who thought that perhaps the nickel-iron spherules were the result of some process of chemical reduction in the glass.

● the coesite has a more fundamental significance because of its instability and especially its tendency to turn into cristobalite. The presence of coesite and the absence of cristobalite constitute, in Walter's phase, a "seal" that guarantees that the material has not been substantially altered since the impact. The kind of heating that would be required to convert a sandstone, for example, into the kind of glass that we observe in the Muong Nong material would convert some of the coesite to cristobalite. In Fig. 39, we show a theoretical calculation

of the rate at which a grain of tektite glass would diffuse into a glass matrix compared with some measures by Dachille et al. (1963), of the rate at which coesite disappears. A single observation by Barnes that lechatelierite particles in bediasites are half gone in  $\frac{1}{2}$  hour at  $1600^{\circ}\text{C}$  is plotted as a cross. It is clear that we are not likely to get rid of the quartz grains without producing cristobalite.

This theoretical conclusion is fully substantiated by experiment. The problem of dissolving quartz grains in a glassy melt is one of the fundamental problems of glass making. It is known to be a difficult problem, especially in a viscous melt, and one that requires hours, if not days. Recently, Corning Glass Works prepared an artificial tektite glass; it is my understanding that they employed a temperature of  $1900^{\circ}\text{C}$  for 16 hours. By contrast, the maximum quench time permitted by the studies of Muong Nong coesite is about 10 sec at  $1700^{\circ}\text{C}$ . This conclusion is certainly what we would expect. The destruction of the coesite demands no more than the disordering of a crystal lattice, while the dissolving of the quartz grains demands migration of the silica molecules through distances of tens of microns.

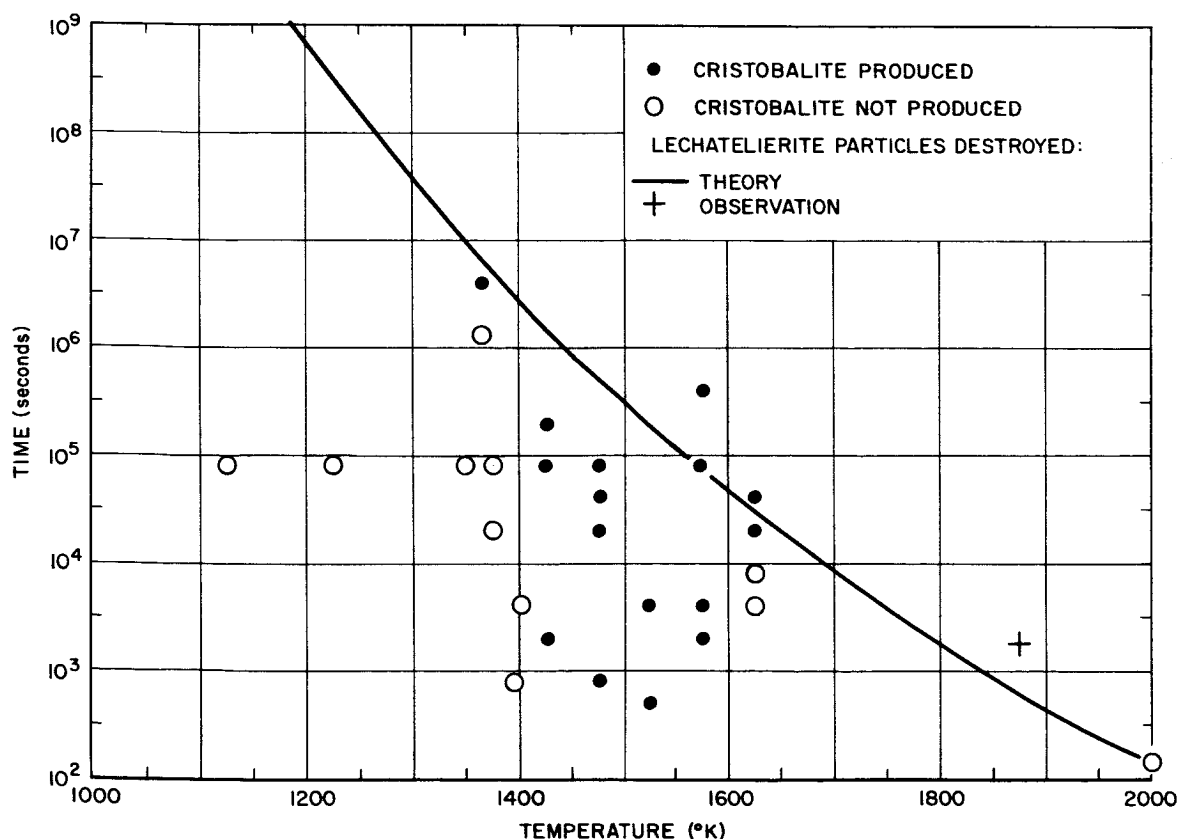


Fig. 39. Production of cristobalite vs destruction of lechatelierite particles

In fact, this migration has not even begun, as can be seen by examination of the borders of these inclusions, (see Walter, 1965, *Science*, p. 1029); the transition from tektite glass to silica glass takes place in a very short distance, much less than the diameter of the particle.

From these data, Walter (1965) drew the vitally important conclusion that the Muong Nong material was glass or finely crystalline before the impact took place. This conclusion is, as Walter has pointed out, difficult to reconcile with the origin of tektites from terrestrial material. Glasses of tektite chemistry are not found at the surface of the Earth. The kind of major changes that would be required to convert a terrestrial rhyolite into a tektite, are, if anything, more difficult to reconcile with the presence of coesite than the melting process that we have already discussed. It is highly probable that, as Taylor (1965) has pointed out, an impact by itself has little effect on the chemistry of the struck material and, in particular, is not competent to convert a rhyolite into a tektite glass. We are thus led to conclude that the impact took place on a glass whose composition was not that found on the Earth.

There is a chain of argument that says that if the tektites are not from the Earth, they must be from the Moon. The argument is based first, on the lack of Al 26 (Viste and Anders, 1962), which should have been produced by primary cosmic ray bombardment if the tektites had been in space for a long time. It is also based on the distribution of tektites, which is best understood as the result of fallout from an orbiting satellite. It is extremely difficult to see how a body could get into a satellite orbit around the Earth unless it were an impact fragment from the Moon. In what remains, we shall therefore discuss the Muong Nong tektites as samples of the lunar surface.

What was the nature of the glass that formed the Muong Nong tektites? From the remarks of Barnes about the angular voids, we are led, in a logical way, to suppose that the glass consisted of some kind of fragmental or clastic material. Clastic glass is called by geologists a tuff. Thus the Muong Nong material is a tuff.

In most specimens of Muong Nong material there are few voids. This could logically be explained if we imagined that the fragments have been welded together as sometimes happens with terrestrial tuff. Then the shimmery structure, to which Barnes has drawn attention, would represent the former boundaries of the bits of glass that formed the ash. If the material is tuffaceous and welded, then it is what we call a welded tuff.

It is possible to make direct comparisons between Muong Nong material and terrestrial welded tuff. In the Muong Nong material, the glass particles are rounded, and the voids are spiny, while in terrestrial welded tuff, it is the glass particles which are spiny.

On the Earth, welded tuffs are normally produced by a process known as ash flow (Ross and Smith, 1961), a volcanic eruption in which the tiny ash particles, instead of floating downward through the cold air and arriving at the ground in the solid state, are immersed in the hot gas and arrive at the final point of deposition still hot. Two modes of transport are possible. In some ash flows, such as the great explosion of Mont Pelée in 1902 (Lacroix, 1904) there is a great volume of gas and very little ash. The small amount of ash, nevertheless, provides coherence for the gas by impeding the spread of the gas molecules in all directions and provides weight for the gaseous mass. The mixture of gas and dust behaves like a fluid, moves toward the lowest point of the topography, and there settles out. Deposits of this kind on the Earth are not normally welded and are, on the Earth, relatively unimportant.

A second mode of transport may be called the dense phase. In the dense phase, we have mostly solids and very little gas. The gas is just sufficient to separate the particles from one another so that the friction is greatly reduced or disappears. The mass behaves like a liquid with a more or less definite upper surface and a density of the order of 1 or  $1\frac{1}{2}$  g/cm<sup>3</sup>. This pseudo-liquid moves across the topography, finds a suitable bed, stops, and then collapses, first through the escape of gas from the solid particles and then through the compression of the solid particles one on the other. The solid particles when emplaced are still at a temperature of 850°C, according to the estimates of Boyd (1961). They are still plastic; welding can and does take place.

The application of these ideas to the Moon might at first sight, seem impossible since it might seem that in a hard vacuum, the gas would immediately escape. It was first pointed out by Lyman Spitzer (1941), that the escape of gas from particles in a vacuum is a much slower process than we would have thought. It is delayed, in part, by the charging up of the solid particles at the expense of the gas. The resulting difference in charge means that very large voltages will develop if there is any significant separation of solids from gas. The internal particles, therefore, in seeking to escape from the gas, will encounter not only the solid particles but also the charged gas molecules to obstruct their way.

A physical analysis by O'Keefe and Adams (1965) shows that the behavior in the dense phase is not unlike that in the terrestrial fluidized material. The differences between the lunar and the terrestrial case are mostly in favor of the process of fluidization. The lower gravity means that the solid particles are more easily carried. It also means that as we go down through the ash flow, the pressure increases less rapidly than in a terrestrial flow. Hence the density also increases less rapidly. Now it is a paradox of the kinetic theory of gases that the viscosity of a gas is independent of its density. Since the gas viscosity is the principal agent responsible for supporting the particles, it follows that a low-density gas can support as much solid matter as one of higher density. There is, of course, a limit. When the mean free path becomes of the same length as the width of the passages between solid particles, the viscosity and thus the supporting power of the gas breaks down. But for ordinary levels of density, the lower pressures of the Moon and the resulting lower densities are pure gain. That, in conjunction with the lower weight of the particles, means that then a given amount of gas will fluidize about 30 times as much solid matter on the Moon as on the Earth.

As we approach the top of the densely fluidized layer, the diminishing pressure and diminishing density must be compensated by an increasing gas velocity in order to carry off the flux of gas that has been generated below. Hence the gas density cannot go to zero; if it did, the velocity would have to go to infinity. The limit is reached when the upward velocity of the gas exceeds the terminal velocity of the small solid particles, which are then carried upwards from the dense phase into the dilute phase we previously mentioned. Because of the absence of a lunar atmosphere, we will always have a dilute phase above a lunar ash flow; calculations seem to show that this dilute phase may carry a substantial amount of the material.

Now this gives us a fairly good explanation of the softening that has been observed in the outlines of lunar craters from the *Ranger* photographs. This softening is often attributed to erosion but there are powerful numerical reasons for thinking that erosion will not do the trick. We need at least 20 or 30 m of softening power even over craters that must be relatively recent; but from considerations of the radiation darkening of the Moon (Wehner, 1965) it appears unlikely that the Moon's surface is being eroded at a rate greater than about 1 meter per billion years. It is of no use to say that the erosion rate might have been more rapid in ancient times, because the cratering rate would also have been greater in

those ancient times. What we observe on the *Ranger* photographs is that there have been 20 or 30 m of softening since the majority of craters in the range of 50 to 500 meters were formed. It is quite logical to explain this softening in terms of a layer some 20 or 30 m thick spread over the existing craters. Quite possibly this layer is not unique; no doubt there were a number of layers, as, in general, there are a number of separate flows in any large deposit of welded tuff. The important point is that the flows had a definite and limited thickness so that large craters in this region retained their original shape while the middle-sized craters were softened or even partly destroyed. Craters of less than 50 m in diameter are, it appears, completely obliterated by the flow. You will see that this implies that the flow was of the type that I have called a dilute flow, that is to say, it was a dusty gas. Had it been a dense flow of the nature of a liquid, then the hollows would have been completely filled with liquid as long as there was enough to cover the highlands. If, however, we are dealing with a pseudo-gas, then the amounts of solid material per square centimeter would be approximately the same, over the smaller terrain features. The amount of gas in a crater 2 or 3 hundred meters deep would be only a few times the amount on the level ground if the scale height in the gas were a few hundred meters as calculated by O'Keefe and Adams (1964).

After the deposit of the ash, new craters were formed that were naturally unaffected by it. We see these as the smaller craters on the lunar surface simply because there are always more little craters than big ones, but the little craters that occurred before the ash flow have been effaced. It is a striking phenomenon in the study of the *Ranger* photographs that craters in the range of a few meters look more like those in the range of a kilometer or so than like those in the range of a few hundred meters. The large craters were too big to be smoothed; the little ones, too recent.

In connection with ash flows, we should like to draw attention to the interesting possibility that the red spots, which have been observed by Kozyrev, Greenacre (1963), and others, on the Moon, may be manifestations of a sort of lunar lightning. There are two observations of the spectra of these spots, both by Kozyrev. The first of these (Kozyrev, 1958) indicated a spectrum that might be explained by  $C_2$ . The second (Kozyrev, 1963) was considerably more detailed and indicated the presence of the molecule  $H_2$ . The latter is in all ways more plausible, especially because it gives rise to a red illumination. Water is the principal gas emitted in volcanic outbursts. In his 1963 paper, Kozyrev stated that the source of the

H<sub>2</sub> could not be water since this would dissociate into H and OH, while he did not observe the lines of H. On the other hand, the excitation of water vapor is one of the standard methods of producing the H<sub>2</sub> spectrum. The OH bands are not obvious in the visible spectrum. It appears possible, in spite of the absence of atomic hydrogen lines, that the H<sub>2</sub> is due to water vapor, provided that we can find a suitable method of excitation.

On the other hand, there is a serious problem arising from the fact that the bands of the H<sub>2</sub> molecule that are visible in this spectrum come from levels 15 v above the ground. The production of such a large amount of high-energy quanta is a genuine puzzle. The difficulty can perhaps best be seen by keeping in mind that the red spots have been seen on the bright portion of the Moon's surface. It follows that, over the areas on which they are seen, the amount of light coming from the red spots was a substantial fraction of the total amount of sunlight being reflected by the Moon at these points. It is known that the reflection efficiency of the Moon is on the order of 7%. The energy supplied by the Sun is on the order of 1.3 million ergs/sec cm<sup>2</sup>. The light reflected by the Moon is therefore perhaps 100,000 ergs/sec cm<sup>2</sup> and the light supplied by the red spots would have to be a substantial fraction of this. The total amount of radiation supplied by the Sun in the ultraviolet region where 15-v quanta are available is of the order of 10 ergs/sec cm<sup>2</sup>. The energy supplied by particles in the form of the solar wind is likewise of the order of 1 or 2 ergs/sec cm<sup>2</sup>. Thus

the Sun is utterly incapable of supplying the necessary energy. If, however, we suppose that the source of the energy is some kind of volcanic outburst, then it is obvious from terrestrial experience that the energy flux may greatly exceed the flux from the light of the Sun. In a terrestrial volcanic outburst, a portion of the energy goes into lightning through mechanisms which are interpreted as static electricity but whose precise nature is not known. It turns out that whenever a suspension of small solid particles is produced in a gas we are very likely to have manifestations of static electricity. Examples, in addition to thunder storms and volcanic lightning, are the lightning associated with dust storms and the manifestations of static electricity in dusty factories.

It is perhaps significant that the observations of the red spots are associated with regions that appear to exhibit contemporary volcanism. These morphological intimations are so strong that Mrs. Cameron (Cameron, 1964) predicted the appearance of red spots near the Cobra head in advance of Greenacre's report. Near Alphonsus, the *Ranger IX* photographs show plainly that recent volcanism has been at work.

We conclude therefore by suggesting that the hypothesis of ash flow processes on the Moon provides at the same time a reasonable explanation of the structure of the Muong Nong tektites, the morphology of some lunar craters, and the observations of lunar red spots.

## REFERENCES

- Adams, E. W., and R. M. Huffaker, *Nature*, Vol. 195, pp. 681-684, 1962.
- Barnes, V., in *Tektites*, ed. by J. A. O'Keefe, Ch. 2, pp. 25-50, University of Chicago Press, Chicago, Illinois, 1963.
- Barnes, V., *Geochim. et Cosmochim. Acta*, Vol. 14, pp. 267-278, 1958.
- Barnes, V., *GeoTimes*, Vol. 6, pp. 8-12, 38, 1961a.
- Barnes, V., *Scientific American*, Vol. 205, No. 5, pp. 58-65, 1961b.
- Barnes, V., *Geochim. et Cosmochim. Acta*, Vol. 28, pp. 1267-1271, 1964.
- Barnes, V., and Pitakpaivan, K., *Proc. Nat. Acad. Sci.*, Vol. 48, pp. 947-955, 1962.
- Boyd, F. R., *Welded Tuffs of the Rhyolite Plateau, Yellowstone Park, Wyoming*, Geological Society of America, Bulletin 72, pp. 387-426, 1961.



## REFERENCES (Cont'd)

- Cameron, W. S., *J. Geophys. Res.*, Vol. 69, No. 12, pp. 2423–2430, 1964.
- Chao, E. C. T., Adler, I., Dwornik, E. J., and Littler, J., *Science*, Vol. 135, pp. 97–98; also *Geochim. et. Cosmochim. Acta*, Vol. 28, pp. 971–980, 1962.
- Chao, E. C. T., Shoemaker, E. M., and Madsden, B. M., *Science*, Vol. 132, pp. 220–222, 1960.
- Chapman, D. R., *Nature*, Vol. 188, p. 353, 1960.
- Chapman, D. R., and Larson, H. K., *J. Geophys. Res.*, Vol. 68, pp. 4305–4358, 1963.
- Dachille, F., Zeto, R. J., and Roy, R., *Science*, Vol. 140, pp. 991–993, 1963.
- Greenacre, A., *Sky and Telescope*, Vol. 26, pp. 316–317, 1963.
- King, E. A., Jr., *Nature*, Vol. 196, pp. 569–570, 1962.
- Kozyrev, N., *Sky and Telescope*, Vol. 18, pp. 184–186, 1958; translated by L. G. Jacchia.
- Kozyrev, N., *Nature*, Vol. 198, pp. 979–980, 1963.
- Lacroix, A., *La Montagne Pelée et ses Eruptions*, Paris, Masson et C<sup>ie</sup>, 1904.
- O'Keefe, J. A., and Adams, E. W., *J. Geophys. Res.*, Vol. 70, pp. 3819–3829, 1965.
- Pettijohn, F. J., *Sedimentary Rocks*, 2nd ed., Harper and Row, New York, 1957.
- Ross, C. S., and Smith, R. L., *Ash Flow Tuffs, Their Origin, Geologic Relations and Identification*, Geological Survey, Professional Paper 366, Gov't Printing Office, Washington, D. C., 1961.
- Spitzer, L., *Astrophys. J.*, Vol. 94, pp. 232–244, 1941.
- Taylor, S. R., *Science*, Vol. 149, pp. 658–659, 1965.
- Urey, H. C., *Nature*, Vol. 183, p. 1114, 1959.
- Verbeek, R. D. M., *Jaarb. Mijnwesen in Ned. Indië*, 1897, pp. 235–272, 1897.
- Viste, E., and Anders, E., *J. Geophys. Res.*, Vol. 67, pp. 2913–2919, 1962.
- Walter, L. S., *Science*, Vol. 147, pp. 1029–1032, 1965.
- Wehner, G. K., Rosenberg, D. L., Kenknight, C. E., *Investigation of Sputtering Effects on the Moon's Surface*, 8th Quarterly Status Report on Contract NAS w-751, Litton Systems, Inc., Minneapolis, Minnesota, 1965.

## SUMMARY REMARKS ON THE MOON

*Harrison Brown*

*California Institute of Technology  
Pasadena, California*

In spite of the beauty and remarkable clarity of the *Ranger* photographs, the attitudes of the eleven invited speakers on the Moon differed markedly, indicating the truth of Professor Gold's remark (as quoted by Professor Urey) to the effect that the *Ranger* pictures are a mirror in which every man sees himself. The participants in the discussion appeared to agree that there really is a Moon. But beyond that single statement of fact, near-unanimity of opinion was not often evident.

Concerning the great majority of lunar craters, it is now widely agreed that they were formed by meteorite impact. The curve of frequency of craters as a function of size follows, in a general way, that which one would expect on the basis of the observed sizes of terrestrial meteorite falls. It was emphasized, however, that among the smaller craters there are large numbers of secondaries presumably formed by ejected material. It was also emphasized that, in some areas, the numbers of smaller craters appear to be in a "steady state"—that is, old ones are disappearing as rapidly as new ones are being formed.

There was considerable discussion and debate concerning a variety of other lunar surface features including crevasses, dimple-craters, features thought to result from collapse, and features thought to result from erosion, as well as some that might have had their origin in tectonic activity. The existence of caves at the bottoms of some of the *Ranger* photo craters was suggested. Lava flows were discussed at some length as possibly accounting for certain apparently smooth areas, but in general it was conceded that it is difficult to prove beyond reasonable doubt the volcanic origin of any particular lunar surface feature. This listener emerges from the discussions with the distinct impression, however, that with the exception of impact craters and related features, it will be some time before the scientific community achieves something approaching a consensus concerning the origin and evolution of a substantial fraction of those surface features of the Moon that can now be identified in photographs.

The fragmentary nature and diversity of the formations on the lunar surface are emphasized by Earth-based radio and optical observations. Heat scans of the Moon



during eclipses and during the lunar night show that on the whole the lunar surface is highly insulated, but that there are wide variations in conductivity. Different maria appear to have different thermal properties. Numerous "hot spots" have been found that do not necessarily correspond to the distribution of craters. Craters that appear exactly the same in photographs may have quite different thermal properties. There are also systematic differences between maria and highlands.

The thermal behavior of the Moon indicates that although the surface is very heterogeneous, about 99% of it must be covered by at least 1 mm of dust. Lunar radio emission, too, shows that there is a systematic difference in emissivity between the maria and highlands.

Measurements of radar scatter as a function of polarization indicate that there is a layer, in most areas 25 cm or more in thickness, of dielectric constant much lower than that of solid rock. It was stressed, however, that radar scattering data from the Moon can often be interpreted to support almost any model.

Recent researches reported by colleagues from the USSR suggest a porous layer on the Moon some 3–10 m in depth and an internal heat generation per unit mass some 4–5 times greater than that from the Earth.

This great heat generation, if it is real, can only be accounted for if it is assumed that the concentration of radioactive elements in the Moon is 4–5 times greater than in the Earth.

Conflicting views were presented concerning the nature of the lunar interior. Two views were expressed to the effect that a molten state of the lunar interior is incompatible with the observed deviation of the figure of the Moon from hydrostatic equilibrium. On the other hand, new thermal history calculations using revised abundances for radioactive elements in the Earth indicate that the Moon might have started melting fairly early in its life and that it might have undergone severe, radical differentiation some 3 billion years ago. An equation of state appropriate for the Earth predicts a density decrease with depth in the lunar interior.

One participant believes that the Moon and Earth have identical compositions and that Earth's core is composed of liquid silicates. Another has given evidence strongly indicating that the Earth's core is metal and that

the Moon and Earth are quite different in their chemical make-up.

There was no consensus as to the mode of origin of the Moon. Participants agreed that it could have been formed elsewhere, then captured by the Earth; that it might have escaped from the Earth; or that it might have been formed together with the Earth in a two-body system.

In short, the participants raised questions far more than they indicated generally acceptable answers.

In the view of this participant many of the questions that were raised and that are still with us will not be answered satisfactorily until we make new kinds of observations with new lunar probes. Some of the questions that badly need answering include:

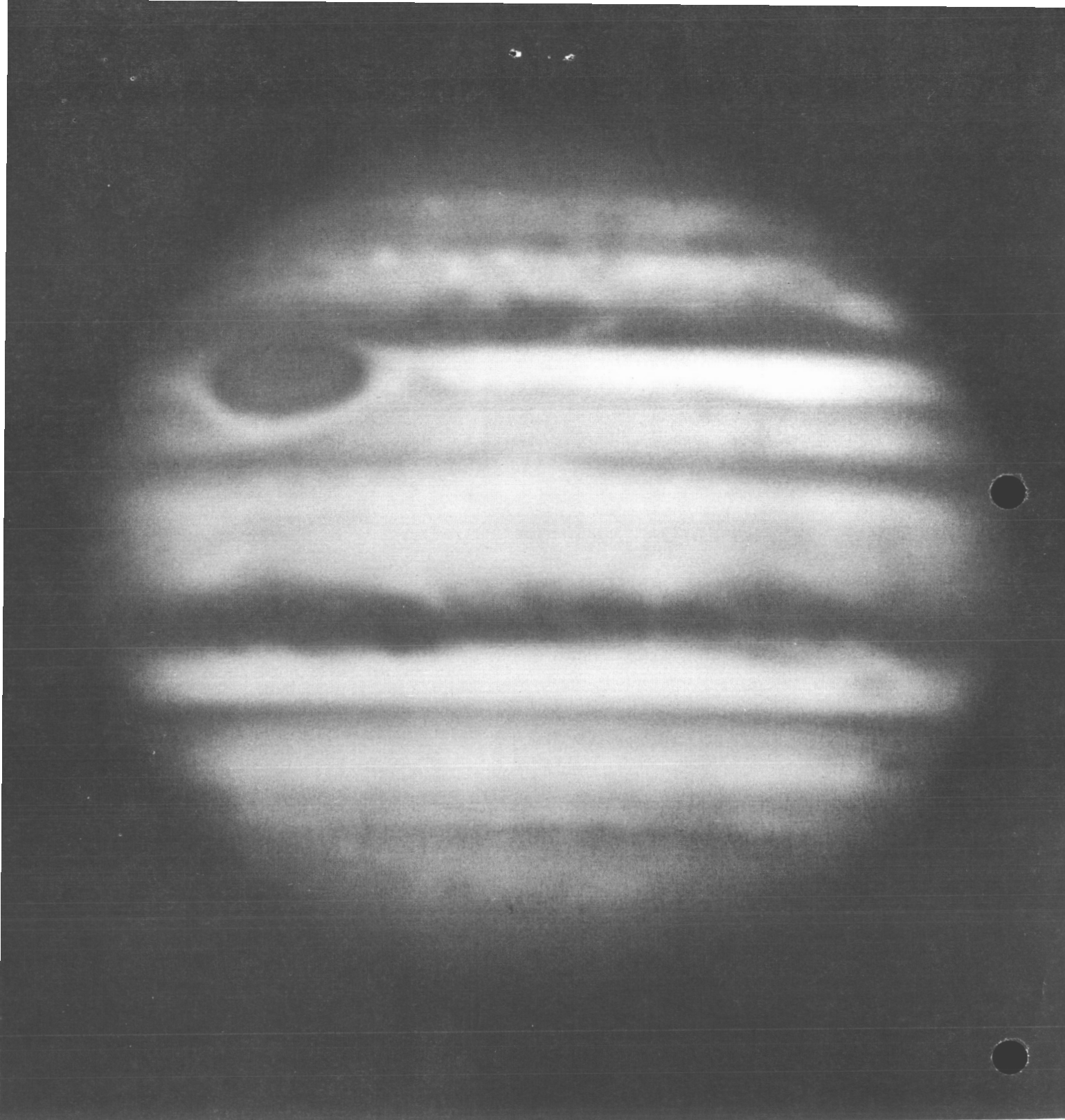
1. What do lunar landscapes look like in selected maria and in selected areas of the highlands?
2. How old are the major lunar features?
3. How thick are the layers of lunar dust and porous unconsolidated materials?
4. Is there really volcanic activity of sorts on the Moon as indicated by observations in the USSR?
5. What is the chemical composition of the lunar crust and how does it vary?
6. Do one or more groups of meteorites have their origin in the Moon, ejected by collision with asteroidal or cometary bodies?
7. Is it possible, as suggested by one participant, that tektites come from the Moon?
8. What are the causes of the color differences noted on the Moon?
9. What is the heat flow through the lunar crust?
10. Is there seismic activity on the Moon?
11. Will seismic experiments reveal that the Moon is differentiated?
12. Will we find that the density within the Moon increases or decreases with depth?

Not until we answer such questions will we really understand the Moon in relation to the Earth and the other terrestrial planets.

## PART II. JUPITER

- M. M. Komesaroff, Recent Radio Observations of Jupiter  
G. L. Berge, Interferometry of Jupiter in the Decimeter Range  
J. W. Warwick, Theory of the Jovian Structure  
A. G. Smith et al., Jovian Rotation Periods and the Origin  
of the Decametric Burst Structure  
G. A. Dulk, The Effect of Io on the Radio Emission of Jupiter  
L. Davis, Jr., Comments on the Discussion of Jupiter  
G. B. Field, Remarks on Jupiter  
G. J. Stanley, Summary Remarks on Jupiter

OVERLEAF: *The planet Jupiter, in blue light (200-inch photograph). (Courtesy of Mount Wilson and Palomar Observatories)*



## *II. JUPITER*

N66 31457

## RECENT RADIO OBSERVATIONS OF JUPITER

Max M. Komesaroff

University of Maryland  
College Park, Maryland

### I. Introduction

During the ten years that have elapsed since it was discovered that Jupiter has unexpected properties when observed at radio frequencies, a considerable amount of observational data has accumulated. In describing some of the more recent results, it is convenient to discuss the observations below 40 Mc/sec separately from those made above about 200 Mc/sec, since the characteristics of the radiation in the two frequency ranges are markedly different.

In the decameter wavelength range the radiation is sporadic, elliptically polarized, and frequently extremely intense. At any one time the radiation source is considerably smaller in angular size than the planetary disk. By contrast, from about 200 Mc/sec to several thousand megacycles, the nonthermal intensity component is steady and amounts to only a few flux units. The predominant polarization is linear, and the radio source is several times more extended than the planet. The high-

frequency radiation is thought to be fairly well understood, but this is not so for the decameter bursts.

### II. The Decameter Radiation

#### A. Time Variations

1. *Dependence on System III longitude.* Soon after Burke and Franklin (1955) discovered the decameter radiation, their discovery was confirmed by Shain (1955 and 1956). Using records going back to 1951, Shain was also able to demonstrate a periodicity in the Jovian emission only some seconds shorter than the optically determined System II period, which corresponds to the observed movement of clouds in the nonequatorial belts of Jupiter. Carr et al. (1961) and Douglas (1960) have used data extending over nine years to derive a more accurate period, and their estimates differ from one another by only 0.02 sec. Commission 40 of the International Astronomical Union (IAU) has recommended the use of System III longitudes for the presentation of Jovian data. This system has a rotational period

of  $9^h55^m29^s.37$  and coincides with System II at  $0^h$  UT on January 1, 1957. Observations of the Jovian microwave source have indicated that it, too, rotates with the System III period, which is taken to be the rotation period of the planetary magnetic field.

Figure 1 shows the frequency of occurrence of Jupiter activity as a function of  $\lambda_{III}$  for several frequencies. It is due to Smith et al. (1965), and indicates that near 20 Mc/sec the greatest probability of Jupiter's radiation occurs when the longitude range  $220^\circ$  to  $260^\circ$  is presented towards the Earth. Subsidiary peaks occur for  $\lambda_{III} \approx 130^\circ$  and  $\lambda_{III} \approx 330^\circ$ . The three peaks on this

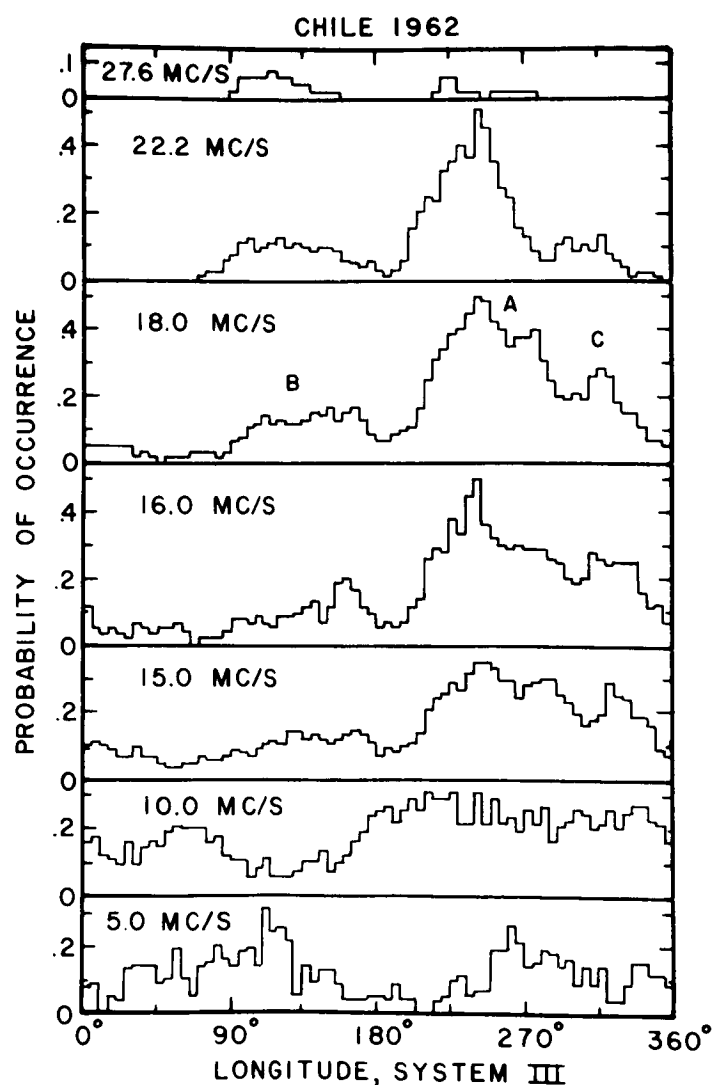


Fig. 1. Histograms of probability vs System III (1957.0) longitude for the 1962 observations made in Chile (Smith et al., 1965). (From *The Astrophysical Journal*, 1965, Vol. 141, p. 463)

histogram will be subsequently referred to as the "main peak," the "early peak," and the "late peak."

Figure 2, also due to Smith et al. (1965), shows the System III longitude of the main peak at 18.0 Mc/sec since 1952. It would seem to indicate that in early 1960 a substantial change occurred in the rotation rate.

**2. Short-period fluctuations.** On a much shorter time scale, fluctuations are observed whose durations vary from several milliseconds (Kraus, 1956; Douglas and Smith, 1961) to some minutes. More usually the durations are between a few tenths of seconds and several seconds.

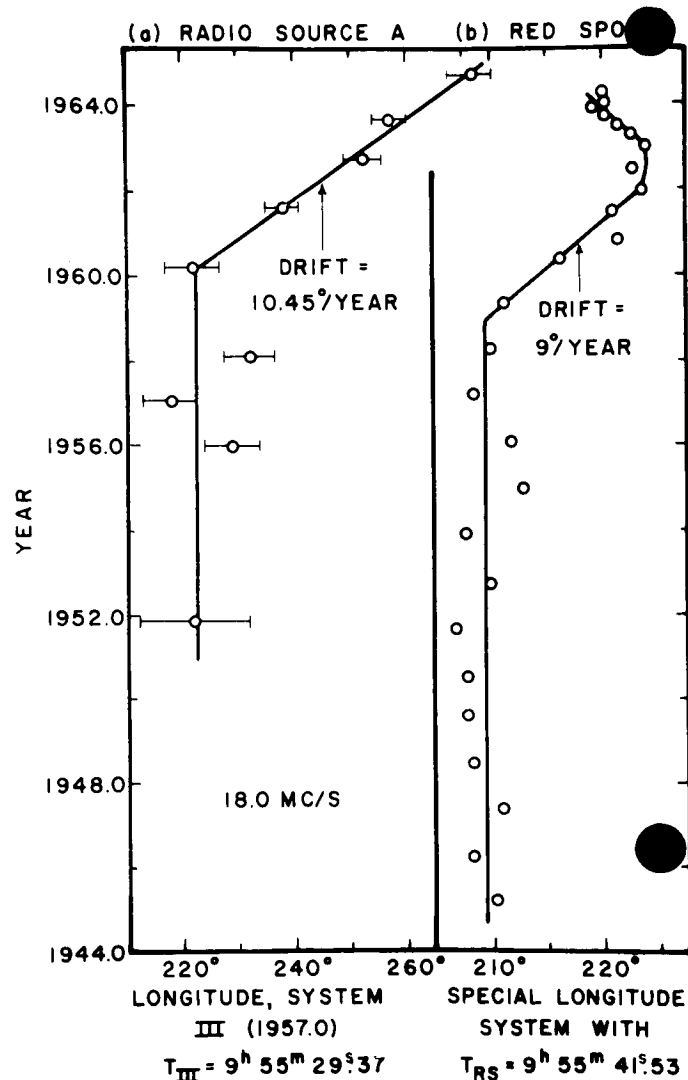


Fig. 2. (a) Drift of main source in System III (1957.0) coordinates; (b) drift of the Great Red Spot in a special longitude system designed to minimize its motion from 1945 to 1959 (Smith et al., 1965). (From *The Astrophysical Journal*, 1965, Vol. 141, p. 471)

Simultaneous observations at different observing sites (Gardner and Shain, 1958; Douglas and Smith, 1961; Smith et al., 1960) have indicated that some of this structure is imposed by the terrestrial ionosphere. However, the results of Douglas and Smith (1961) indicate that the radiation contains at least some of the burst structure when it impinges on the ionosphere.

Recent observations reported by Smith and Douglas (1962) and Douglas (1964) indicate that many of the bursts may represent an effect due to the interplanetary medium. At times when there was good general correlation between the burst structure recorded at separate sites, they found a consistent relative delay in the arrival time of the bursts at the two sites. Furthermore, they found that the sense of this delay reversed near opposition. Their interpretation is that pulses of duration of about one second are produced by diffraction in interplanetary electron clouds. Near opposition the clouds' component of drift velocity perpendicular to the Earth-Jupiter line might be expected to reverse.

### B. Source Size Measurements

The evidence for interplanetary scintillations implies a small angular diameter for the source. Slee and Higgins (1963) have made source size measurements using a wide-based radio link interferometer. The most recent set of observations, reported by J. A. Roberts at the Arecibo Symposium on Planetary Atmospheres and Surfaces, was made with a base line of 12,700  $\lambda$ . They found that the apparent source size varied between 5 and 15 seconds of arc.

### C. Spectral Characteristics

Referring again to Fig. 1, we see that the main peak of emission, which is very pronounced near 20 Mc/sec, decreases at the lower frequencies, and that at 5 Mc/sec there are two peaks of roughly equal amplitude separated by about  $180^\circ$  in longitude. Similar results have been obtained by McCulloch and Ellis (as reported by Ellis at the Arecibo Symposium). Ellis has shown that if the quantity plotted is mean power rather than occurrence probability, the histograms are similar, except that the peaks are more pronounced.

Detailed spectral studies have been made by Warwick (1961, 1963) using a dynamic spectrum analyzer. His records show that at any one time the Jupiter radiation may extend over a frequency bandwidth as wide as 20 Mc/sec, and that within this band short-lived features

can be discerned (presumably corresponding to the "bursts" seen on single-frequency records), usually extending over only a few megacycles.

Warwick found that the whole band of activity may drift with time toward higher or lower frequencies and that this drift depends on the central meridian longitude. For longitudes above  $200^\circ$  the drift is toward lower frequencies, whereas for  $\lambda_{III} \approx 140^\circ$  the drift is in the opposite sense. Warwick (1963) found that individual spectral features (or "landmarks") tend to recur at the same longitudes, so that records taken on different days can be superimposed on the basis of these "landmarks" to yield surprisingly good coincidence in their longitude scales. Figure 3 shows the longitudes of radio "landmarks" plotted as a function of time from opposition

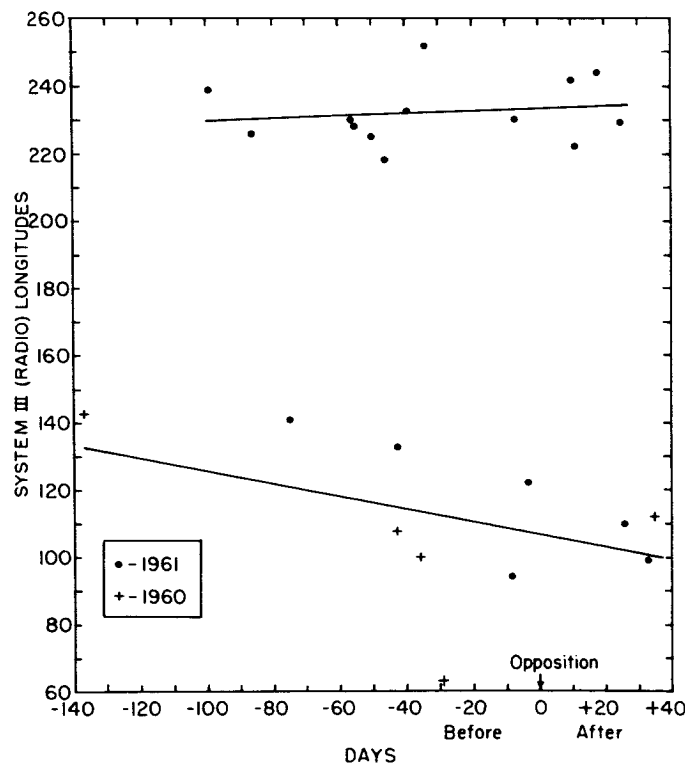


Fig. 3. Relation between  $\lambda_{III}$  (1957.0) longitudes of radio special landmarks and time in days from opposition. Only 1961 data enter the relation for negative-drift emission, the upper of the two groups of points. The negative drifts define a horizontal line within the precision of measurement, while the positive drifts define a line of decreasing longitude as time increases during the apparition (Warwick, 1963).

(From *The Astrophysical Journal*, 1963, Vol. 137, p. 45)

for data taken in 1961 and 1962. It illustrates two interesting facts:

1. The scatter of points about the least-squares lines shows that the radiation is sharply beamed into a cone of half angle only about  $9^\circ$ .
2. Whereas features in the main peak ( $\lambda_{III} \simeq 230^\circ$ ) remain essentially fixed in longitude, those in the early peak drift toward lower longitudes through the time of opposition.

Point 2 presumably explains the broadness of the early peak as shown in Fig. 1. It should be noted that the sense of the drift in longitude is opposite to what would be expected if the radiation were stimulated by solar radiation as suggested by Shain (1956).

Warwick (1963) has pointed out that the stability of the spectra evidently rules out an explanation of the spectral features in terms of plasma frequencies in an assumed Jovian ionosphere. Such an explanation would imply that Jupiter's ionosphere is vastly more stable than the Earth's. Thus, current theories (Ellis and McCulloch, 1963; Ellis, 1965; Warwick, 1961, 1963) have related the frequencies of emission to the gyrofrequencies of electrons streaming along the Jovian magnetic field lines.

#### D. Polarization

Observations showing a high degree of circular or elliptical polarization support the idea that magnetic fields are intimately connected with the radiation process. Above about 20 Mc/sec, the sense of rotation is almost exclusively right-handed circular. This is true whether the measurements are made in the northern or southern hemisphere, indicating that the polarization is not imposed by the terrestrial ionosphere. Franklin and Burke (1958) found some 22 Mc/sec bursts associated with the early longitude source that had the left-handed sense of rotation. Barrow (1962, 1963) and Sherrill and Castles (1963) found an increasing proportion of left-handed bursts below 20 Mc/sec. At 10 Mc/sec, Dowden (1963) recorded both senses, the right-handed sense being associated with the main peak and the left-handed predominantly with the early peak.

#### E. Solar Correlations

There have been several reports (Kraus, 1958; Carr et al., 1960; Warwick, 1963) suggesting a positive correlation of Jupiter emission with solar activity occurring some days previously. However, there is some conflict between conclusions drawn by the various observers, and it seems

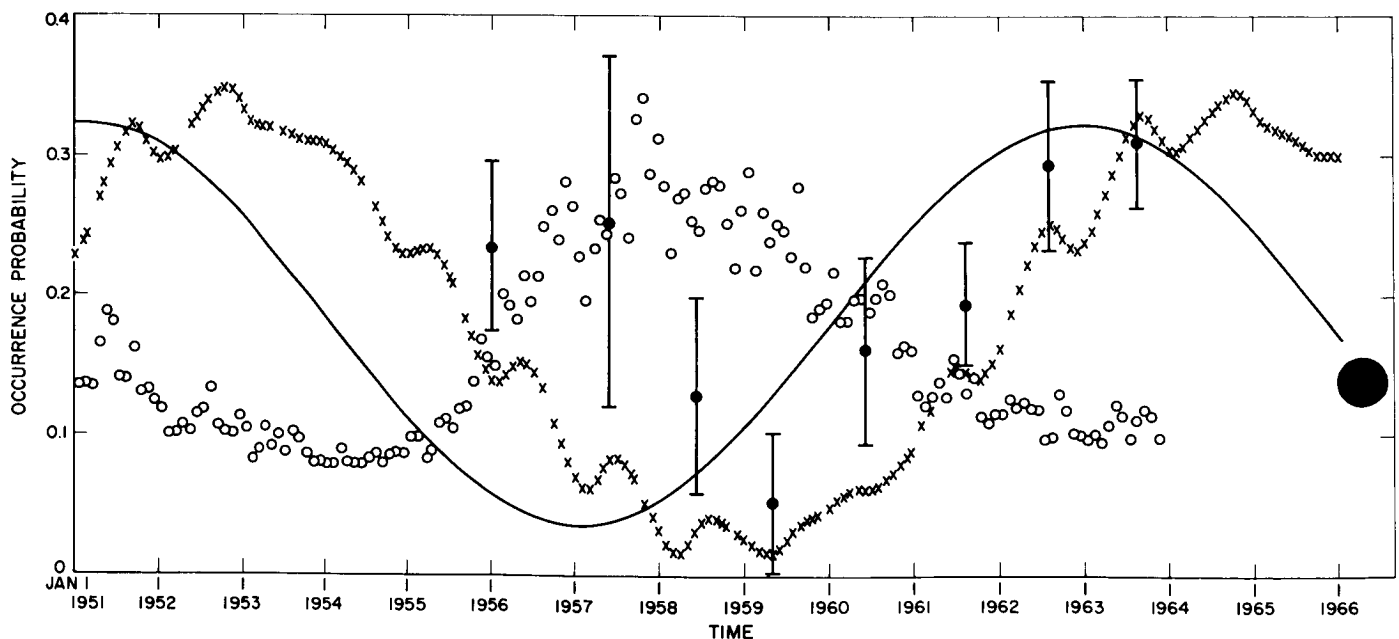


Fig. 4. 22.2-Mc/sec main source occurrence probability (heavy dots with error flags) compared with provisional sunspot number (open circles). Also shown (without ordinate scales) are declination of Earth seen from Jupiter (x's) and sub-Jovian latitude on the Sun (line). Range of sub-Jovian latitude on the Sun is about  $\pm 9^\circ$ ; range of declination of Earth is about  $\pm 3^\circ$  (Douglas, 1964).

that insufficiency of data prevents firm conclusions being drawn.

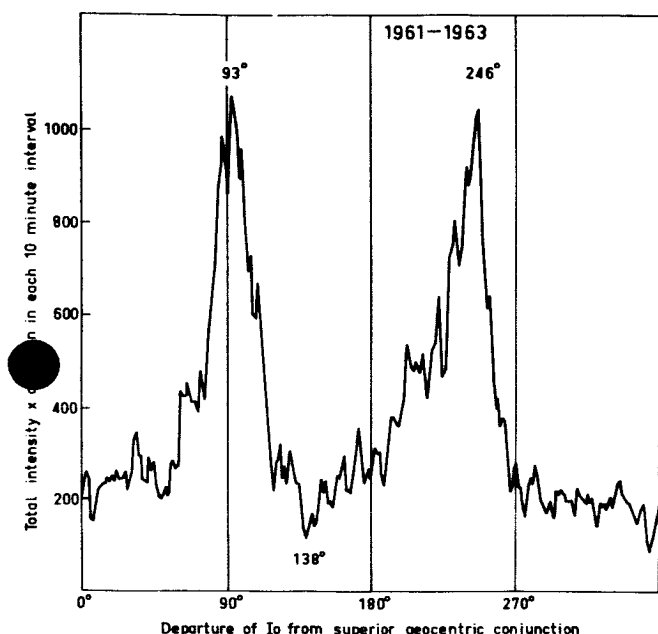


Fig. 5. Dependence of Jupiter's decametric radio emission on the position of the satellite Io (Bigg, 1964).

On the other hand, as shown in Fig. 4 (due to Douglas, 1964), there seems to have been a long-term anticorrelation between Jupiter activity and sunspot number. As Douglas (1964) has pointed out, however, this result must be treated cautiously since the sunspot cycle and Jupiter's period of revolution are almost equal. Fig. 4 indicates that over the same period there is a positive correlation between Jupiter's activity and the Earth's declination as seen from Jupiter. It should also be remembered that the Sun's declination, as viewed from Jupiter, is very similar to that of the Earth, so that the data could also be taken to indicate solar stimulation of a Jovian source.

#### F. Correlations With Io

Perhaps the most unexpected recent discovery was that made by Bigg (1964), who showed that the probability of emission is a strong function of the position of the satellite Io relative to the Earth-Jupiter line. (Io is the innermost of the large satellites.) The occurrence probability has two maxima, one when Io's longitude is about 90° earlier than its passage across the Earth-Jupiter line, and the other 60° after it has passed this line. Bigg's results are shown in Figs. 5, 6, and 7. He has shown that the effect of Io is even more marked if only events showing emission above 30 Mc/sec are included (Fig. 7).

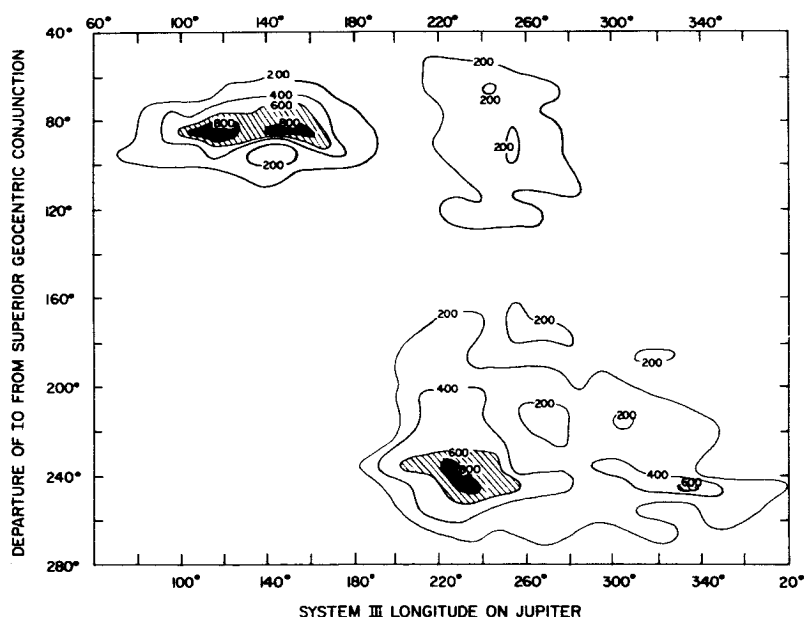
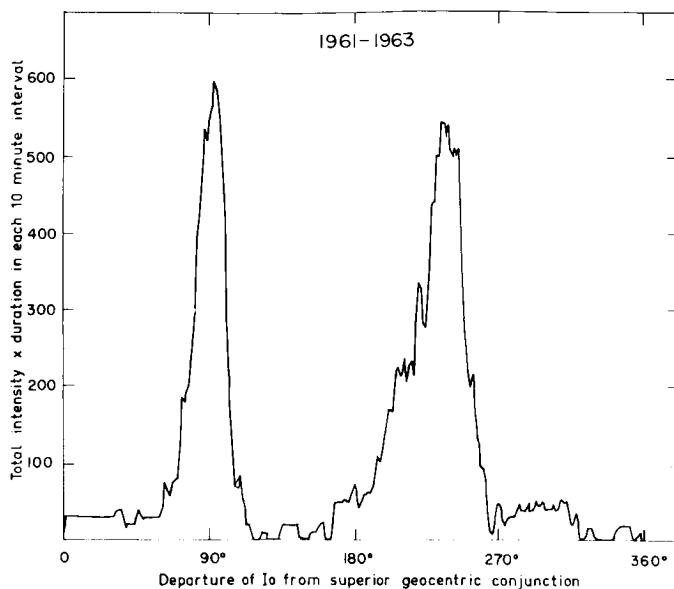


Fig. 6. The relationship between the position of Io and the orientation of Jupiter for the reception of decametric emission at the Earth (Bigg, 1964).





**Fig. 7. Dependence of Jupiter's emission on the position of Io when only cases having top frequencies  $> 30$  Mc/sec are considered (Bigg, 1964).**

### III. The Decimeter Radiation

#### A. Discovery

A few years after the discovery of the decametric emission by Burke and Franklin, Sloanaker (1959) of the U.S. Naval Observatory measured unexpectedly intense radiation at 10 cm. Sloanaker had previously measured an apparent disk temperature of  $145 \pm 20^\circ\text{K}$  at 315 cm, which was in good agreement with the infrared temperature, but at 10 cm he found the disk temperature to be about  $600^\circ\text{K}$ , or more than four times greater.

Subsequent measurements (Drake and Hvatum, 1959; McClain, 1959; Epstein, 1959; Roberts and Stanley, 1959) confirmed this result and also indicated that the flux remains substantially constant from 10 to 70 cm, so that the effective disk temperature appeared to increase with wavelength, apparently exceeding  $5 \times 10^4^\circ\text{K}$  at 70 cm.

It seemed unlikely that the high temperature could result from thermal processes alone, and suggestions were advanced that the radiation was produced by electrons spiralling in the assumed magnetic field of the planet. Drake and Hvatum (1959) suggested, by analogy with the terrestrial Van Allen Belt, that the radiating electrons were moving at relativistic velocities and emitting synchrotron radiation. Field (1959, 1960, 1961) also discussed this case, but considered in greater detail the

possibility that the electron energies were subrelativistic and that the electrons were emitting the local cyclotron frequencies in a dipole magnetic field.

Later observations of the polarization and angular extent of the radio source have supported the synchrotron rather than the cyclotron model, but, as will be shown, the observations still show a number of features that await explanation.

#### B. Spectrum

The combined observations of a number of observers (Gower, 1963; Golnev et al., 1964; Haddock and Dickel, 1963; Kazes, 1964; Mayer, 1961; Roberts and Komesaroff, 1965; Roberts and Ekers, 1965; and Thornton and Welch, 1963) show that between 178 Mc/sec and nearly 3000 Mc/sec the flux density has a substantially constant value of between about 5 and 7 flux units. Beyond 3000 Mc/sec the flux density rises to some hundreds of flux units at 37,000 Mc/sec.

On the assumption that the radiation combines two components, a thermal contribution from the disk at a temperature of  $130^\circ\text{K}$ , and a nonthermal component with a flat spectrum from the Van Allen Belt, we should expect a rise at the higher frequencies, but in fact the observed rise is too great to be explained in this way. However, Berge (1965) has reported evidence that the disk component at 10 cm is about twice as high as would be expected from the infrared temperature of  $130^\circ\text{K}$ .

The flat spectrum below  $3000^\circ\text{K}$  also presents a problem. Assuming that the major part of the radiation comes from relativistic electrons that have an isotropic velocity distribution and gyrate in the planet's magnetic field, and making the usual assumptions of synchrotron theory, we require that the electrons have a differential energy spectrum proportional to  $E^{-1}$  (where  $E$  is the electron energy). For the Earth's Van Allen Belt, the spectrum is proportional to  $E^{-5}$ . It is not clear why there should be a relative deficiency of low-energy electrons in the Jovian Belt.

#### C. Polarization

**1. Linear polarization.** If the Jupiter radiation is produced by electrons gyrating in a magnetic field, a high degree of linear polarization might be expected, and so, following the suggestions made by Drake and Hvatum and by Field, linear polarization studies were undertaken at the California Institute of Technology. Radhakrishnan and Roberts (1960) found that the radiation was about 30% linearly polarized at 31 cm, with the maximum

*E*-vector in the planetary equatorial plane. Morris and Berge (1962) confirmed the 31-cm result and found a similar result at 22 cm. They also found that the more extended components of the source are more highly polarized.

Subsequent observations by Roberts and Komesaroff (1965) showed that the degree of polarization is essentially constant between 300 and 2650 Mc/sec at about 22%, or somewhat lower than reported previously. Above 3000 Mc/sec, the polarized component decreases.

The constancy of polarization with frequency up to 3000 Mc/sec certainly contradicts predictions based on a model depending on cyclotron radiation from nonrelativistic electrons. However, even using synchrotron theory, which predicts a broad spectrum of emission from the individual electrons, it is difficult to construct a plausible model that gives a spectrum of polarized emission as broad as that observed.

Another important discovery by Morris and Berge was that the direction of polarization rocks through about  $\pm 10^\circ$  as the planet rotates. This finds a ready explanation if it is assumed that Jupiter's magnetic axis, like that of the Earth, is tilted with respect to the rotational axis, since synchrotron theory predicts that the direction of polarization is determined by the directions of the magnetic field lines.

Detailed polarization studies by Roberts and Komesaroff (1965) using the Parkes pencil-beam instrument have confirmed the Morris and Berge result and have also shown that the period of the rocking agrees with the IAU System III (1957.0) period to within 0.5 sec. Roberts and Komesaroff also find that the dependence of position angle on  $\lambda_{\text{III}}$  shows distinct departures from the sinusoidal form that would be predicted from a simple dipole model. At both 21 and 11 cm, the second harmonic term in the "rotation curve" has an amplitude of between 5 and 10% of the fundamental. The most plausible explanation of this effect at the moment is in terms of nondipolar components in the magnetic field configuration. Explanations of the decametric burst characteristics have also required nondipolar field components.

**2. Circular polarization.** Roberts and Komesaroff (1965) attempted to detect circular polarization at 960 Mc/sec, using circularly polarized feeds based on a design developed by the Jet Propulsion Laboratory. The technique involved observing one sense of circular polarization, then changing the feed and observing the other sense.

One set of measurements occupied 2 to 3 hours. Although the observations indicated that the long-term mean circular polarization does not exceed about 1%, they did not exclude the possibility of a component varying with the planetary rotation and having an amplitude of up to 3%.

Some recent observations by Berge and Morris (1964), appear to have demonstrated the existence of such a variable component. The aim of the measurements was to investigate the possibility of a displacement in position between the visible planet and the radio source. Their technique was to measure the interferometer visibility function, first with parallel feeds having their *E*-vectors parallel to Jupiter's rotational axis, and then with crossed feeds at  $45^\circ$  to the axis. The first configuration accepts almost exclusively unpolarized radiation, which includes thermal radiation from the disk. The observers were able to determine the spacing at which the fringe amplitude with this feed orientation corresponds to the first null in the visibility function of the nonthermal component alone. At this spacing the fringe amplitude corresponded to the disk component alone, which was unresolved.

In the crossed horn configuration the only contribution must come from the polarized, nonthermal radiation. Therefore, assuming all the polarization is linear, any difference in the phase of the patterns in the two configurations at the spacing described above must be due to a spatial displacement between the disk and the nonthermal source. In fact, Berge and Morris found such a phase difference; it comprised both a constant component and a component that varied quasi-sinusoidally with  $\lambda_{\text{III}}$ . They initially interpreted this as a displacement of the radio source from the center of the planet, the constant component representing a shift in declination and the variable component representing a shift (of about 0.4 of the planetary radius) from the axis of rotation. However, Roberts and Ekers (1965) measured the position of Jupiter relative to a nearby radio source and concluded that any displacement of the radio centroid from the axis of rotation is less than 0.15 radii.

As reported at the Arecibo conference, Berge now believes that the interferometer result may be due to a small component of circular polarization, a result that would explain the variation with  $\lambda_{\text{III}}$ . On this interpretation, Jupiter's magnetic moment has the opposite orientation to that of the Earth, in agreement with a result deduced by Warwick (1963) from decametric burst observations.

### D. Variability

A number of authors have reported long-term variations in the Jupiter radiation, and some have suggested variations that correlate with solar activity.

From observations at 11 and 21 cm made between 1962 and 1964, Roberts and Komesaroff (1965) found no long-term variations in the total flux greater than the possible experimental error. They did find a distinct variation of about 15% with planetary rotation. However, for the same values of  $\lambda_{III}$ , the total flux remained constant to within 4%.

The variation with  $\lambda_{III}$  showed two minima per revolution, one near  $\lambda_{III} = 198^\circ$  and a shallower one near  $18^\circ$ . Between November 1963 and November 1964 the period of the variation agreed with the System III period to within 0.8 sec.

This variation can be explained if it is assumed that a beaming process causes the radiation to be emitted in the direction of the magnetic equator (Gary, 1963; Bash et al., 1964; Roberts and Komesaroff, 1965). In that case the tilt of the rotational axis toward the Earth, as well as the inclination of the magnetic axis with respect to the rotational axis, would account for the main features of the variation. Since the beaming of synchrotron radiation depends on the electron pitch angles, these data, together with the polarization data, provide information about the pitch angle distribution. Roberts and Komesaroff have shown that the observations are consistent with a two-component model of the electron population, one component having very flat helices (and therefore being concentrated toward the magnetic equator), and the other much more widely distributed. Measurements of the detailed brightness distribution made by Berge also seem to point to such a two-component model.

The simple analysis above does not explain all features of the observations. It is found that the observed degree of beaming with magnetic latitude depends on whether the Earth is north or south of the magnetic equator. This is additional evidence supporting the idea of nondipolar terms in the Jovian magnetic field.

### IV. Conclusions

The following rather general conclusions may be drawn:

1. Both the decameter bursts and the decimeter radiation indicate the existence of a Jovian magnetic field. The decimeter radiation shows that the dipolar component of the field has its axis inclined at about  $10^\circ$  to the planetary rotational axis, but both types of observation indicate substantial non-dipolar terms.
2. The electrons responsible for the decimeter emission appear to occur in two distinct belts, one widely distributed in latitude, and the other more closely confined to the magnetic equator.
3. The decameter observations seem to provide the best chance of estimating the magnetic field strength. The observed elliptical polarization and the constant association of spectral features with System III longitudes strongly suggest that the emission frequency is close to the local electron gyrofrequency. This would imply that field strengths in the emitting regions are as large as 10 to 20 gauss.
4. The following argument suggests that the decameter emission originates in the planetary exosphere. Both the burst occurrence probability histograms and the dependence of polarization axial ratio on System III longitude show a greater degree of symmetry at 10 Mc/sec and below than they do at 20 Mc/sec. These effects would be expected if the lower frequencies originate at greater distances from the surface of the planet, where the total magnetic field strength is lower and where the dipolar component predominates over the higher-order field terms.

The development of large decametric arrays may provide an answer to this question by permitting measurements of the burst source position relative to the planetary disk.

## REFERENCES

- Barrow, C. H., 1962, *Astrophys. J.*, Vol. 135, p. 847.
- Barrow, C. H., 1963, *Nature*, Vol. 197, p. 180.
- Bash, F. N., Drake, F. D., Gunderman, E., and Heiles, C. E., 1964, *Astrophys. J.*, Vol. 139, p. 975.
- Berge, G. L., and Morris, D., 1964, *Astrophys. J.*, Vol. 140, p. 1330.
- Berge, G. L., 1964 (reported at the Symposium on Planetary Atmospheres and Surfaces, May 24-27, Dorado, Puerto Rico), *Radio Science*, Vol. 69D, p. 1552.
- Bigg, C. H., 1964, *Nature*, Vol. 203, p. 1008.
- Burke, B. F., and Franklin, K. L., 1955, *Nature*, Vol. 175, p. 1074.
- Carr, T. D., Smith, A. G., and Bollhagen, H., 1960, *Phys. Rev. Letters*, Vol. 5, p. 418.
- Carr, T. D., Smith, A. G., Bollhagen, H., Six, N. F., and Chatterton, N. E., 1961, *Astrophys. J.*, Vol. 134, p. 105.
- Douglas, J. N., 1964, *IEEE Trans. Ant. and Prop.*, Vol. AP-12, p. 839.
- Douglas, J. N., and Smith, H. J., 1961, *Nature*, Vol. 192, p. 741.
- Dowden, R. L., 1963, *Australian J. Phys.*, Vol. 15, p. 490.
- Drake, F. D., and Hvatum, S., 1959, *Astron. J.*, Vol. 64, p. 329.
- Ellis, G. R. A., and McCulloch, P. M., 1963, *Australian J. Phys.*, Vol. 16, p. 380.
- Ellis, G. R. A., 1965 (reported at the Symposium on Planetary Atmospheres and Surfaces, May 24-27, Dorado, Puerto Rico), *Radio Science*, Vol. 69D, p. 1513.
- Epstein, E. E., 1959, *Nature*, Vol. 184, p. 52.
- Field, G. B., 1959, *J. Geophys. Res.*, Vol. 64, p. 1169.
- Field, G. B., 1960, *J. Geophys. Res.*, Vol. 65, p. 1661.
- Field, G. B., 1961, *J. Geophys. Res.*, Vol. 66, p. 1395.
- Franklin, K. L., and Burke, B. F., 1958, *J. Geophys. Res.*, Vol. 63, p. 807.
- Gardner, F. F., and Shain, C. A., 1958, *Australian J. Phys.*, Vol. 11, p. 55.
- Gary, B., 1963, *Astron. J.*, Vol. 68, p. 568.
- Golnev, V. Y., Lipkova, N. M., and Pariiski, Yu. N., 1964, *Dok. (1964) Akad. Nauk, SSSR*, Vol. 157, p. 554.
- Gower, J. F. R., 1963, *Nature*, Vol. 199, p. 1273.
- Haddock, F. T., and Dickel, J. R., 1963, *Trans. Am. Geophys. Union*, Vol. 44, p. 886.
- Kazes, I. N., 1964, Cornell University, Research Report, RSGI, p. 48.
- Kraus, J. D., 1956, *Astron. J.*, Vol. 61, p. 182.

## REFERENCES (Cont'd)

- Kraus, J. D., 1958, *Proc. IRE*, Vol. 46, p. 266.
- Mayer, C. H., 1961, *The Solar System, Vol. III, Planets and Satellites*, ed. by G. P. Kuiper and B. M. Middlehurst, p. 442 (Univ. of Chicago Press, Chicago).
- Mayer, C. H., McCullough, T. P., and Sloanaker, R. M., 1958, *Astrophys. J.*, Vol. 127, p. 11.
- McClain, E. F., 1959, *Astron. J.*, Vol. 64, p. 339.
- Morris, D., and Berge, G. L., 1962, *Astrophys. J.*, Vol. 136, p. 276.
- Radhakrishnan, V., and Roberts, J. A., 1960, *Phys. Rev. Letters*, Vol. 4, p. 493.
- Roberts, J. A., and Stanley, G. J., 1959, *Publ. Astron. Soc. Pacific*, Vol. 71, p. 485.
- Roberts, J. A., and Komesaroff, M. M., 1965, *Icarus*, Vol. 4, No. 2, p. 127.
- Roberts, J. A., 1965 (reported at the Symposium on Planetary Atmospheres and Surfaces, May 24-27, Dorado, Puerto Rico), *Radio Science*, Vol. 69D, p. 1543.
- Shain, C. A., 1955, *Nature*, Vol. 176, p. 836.
- Shain, C. A., 1955, *Australian J. Phys.*, Vol. 9, p. 61.
- Sherrill, W. M., and Castles, M. P., 1963, *Astrophys. J.*, Vol. 138, p. 587.
- Slee, O. B., and Higgins, C. S., 1963, *Nature*, Vol. 197, p. 781.
- Sloanaker, R. M., 1959, *Astron. J.*, Vol. 64, p. 346.
- Smith, A. G., Carr, T. D., Bollhagen, H., Chatterton, N., and Six, F., 1960, *Nature*, Vol. 187, p. 568.
- Smith, A. G., Lebo, G. R., Six, N. F., Carr, T. D., Bollhagen, H., May, J., and Levy, J., 1965, *Astrophys. J.*, Vol. 141, p. 457.
- Smith, H. J., and Douglas, J. N., 1962, *Astron. J.*, Vol. 67, p. 120.
- Thornton, D. D., and Welch, W. J., 1963, *Icarus*, Vol. 2, p. 228.
- Warwick, J. W., 1961, *Annals N.Y. Acad. Sci.*, Vol. 95, p. 39.
- Warwick, J. W., 1963, *Astrophys. J.*, Vol. 137, p. 41.
- Warwick, J. W., 1963, *Astrophys. J.*, Vol. 137, p. 1317.

## INTERFEROMETRY OF JUPITER IN THE DECIMETER RANGE

Glenn L. Berge

*California Institute of Technology  
Pasadena, California*

In the last few years a great deal of information has been obtained about the integrated source behavior for Jupiter: for example, the very complete and accurate data of Roberts and Komesaroff (1965). On the other hand, high-resolution information about the source has been lacking. Until two years ago, only a rough angular size determination was available. Because the source is small, the only type of instrument capable of resolving it in the decimeter-wavelength region is an interferometer such as we have at the Owens Valley Radio Observatory. Through the use of this instrument, a large amount of long-baseline, high-resolution work at 10.4 and 21.2 cm has been done on Jupiter in the last two years. Most of the observations were made in late 1963 and early 1964.

Some of the results were mentioned in the review paper, but I would like to discuss them in more detail. Most observations were made using east-west baselines ranging up to 4800 wavelengths. In addition, some observations were made with north-south baselines between 3000 and 4000 wavelengths. The object was to determine the angular brightness distribution and the polarization distribution of the source. The observations,

usually made over a large range of hour angles, consisted of repetitions of successive orientation combinations of the linearly polarized feeds. The data consisted of the fringe amplitudes and the relative fringe phases of successive observations. The main difficulty was that the source changes in orientation, in flux density, and probably in apparent structure as Jupiter rotates. Therefore, the data are divided according to the longitude of the central meridian.

The visibility functions obtained indicate qualitatively that there is a significant thermal contribution from the planetary disk at 10.4 cm, that the nonthermal emission has a very symmetric distribution, which, however, may not be centered exactly on the disk, and that the polarization properties are roughly what one would expect for synchrotron emission in a dipole magnetic field. In order to determine the brightness distribution from the visibility functions, a rather elaborate model-fitting procedure was used. This procedure used the visibility functions for all the feed combinations and assumed that the orientation of the plane of polarization across the source is indeed what one would expect if the radiation were produced in a dipole magnetic field.

Figure 8 shows the result of this work for a wavelength of 10.4 cm and  $l_{III}$  (longitude of the central meridian in System III) =  $20^\circ$ .

In general, the distribution of the emission among various regions and the overall dimensions shown are probably quite accurate. However, the smaller details are not so well determined. The resolution available is indicated by the brackets. They represent the separation of a double source, in the direction of the baseline orientation used, whose visibility function would be at its first null at the largest baseline.

It is not possible to say much about the change of apparent structure as Jupiter rotates, because the effect that this would produce is masked by the effects of the changing source orientation and changing flux density. The brightness distribution at 21.2 cm seems to be nearly identical with that found for 10.4 cm except for differences that are obviously due to the disk emission.

One rather unexpected result concerned the disk emission: at these wavelengths it seems to be about twice as large as would be expected for the disk temperature inferred from infrared and 3-cm measurements. In order to explain the parallel feed horn observations at 10.4 cm it is necessary to have more emission from the central regions of the source than can be explained by the radiation belt emission. At 21.2 cm, however, this problem is

hardly noticeable, and the conclusion is that the extra central emission has a thermal spectrum. Thus it was identified with the thermal disk emission, making an equivalent disk temperature of about  $260^\circ\text{K}$ . The situation may be similar to that of Saturn, where the 10-cm disk temperature is about twice the infrared temperature.

The last major result of this investigation was the detection of a small and variable circularly polarized component in Jupiter's decimeter emission. If there is such a component, the interference fringes it produces with crossed horns are  $90^\circ$  out of phase with respect to those produced by a linearly polarized signal and also  $90^\circ$  out of phase with respect to the fringes produced with parallel horns. The phase can either lead or lag  $90^\circ$ , depending on the sense of the circular polarization.

Figure 9 shows the data from which the existence of the circularly polarized component was first recognized. The points were obtained for a wavelength of 21.2 cm and an antenna spacing of  $290 \lambda$  east-west. They represent the difference in phase between a crossed-horn measurement with the  $E$ -vectors of the feed horns at  $45^\circ$  on either side of Jupiter's equatorial direction and a parallel-horn measurement. Two different cases are shown, one with the parallel-horn arrangement aligned along the polar axis and the other with it aligned along the equatorial direction. The systematic deviation of the phase difference from zero is interpreted as being due to a

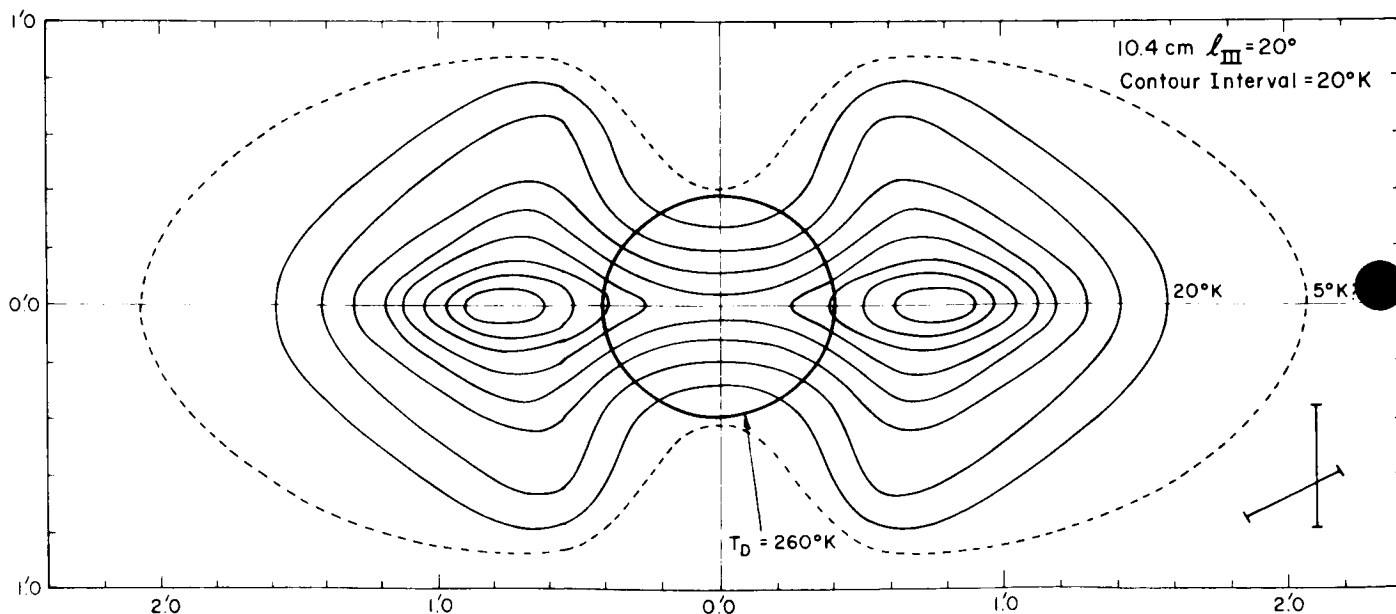
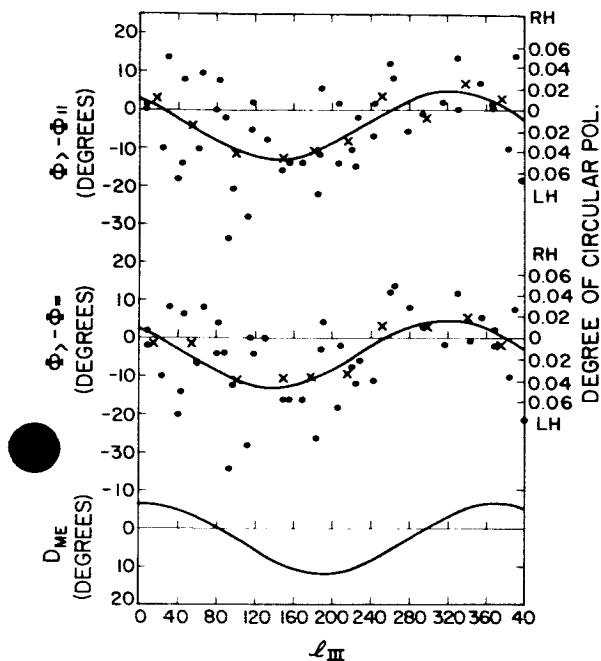


Fig. 8. The 10.4-cm brightness distribution determined for  $l_{III} = 20^\circ$ . The scales, in minutes of arc, refer to a distance for Jupiter of 4.04 AU.



**Fig. 9.** The upper graphs show the evidence for circular polarization at 21.2 cm ( $290 \lambda$  E-W, January–February, 1964). The filled circles are the data points, the x's are means for each  $40^\circ$  of longitude, and the curves are least-squares fits of a sinusoid to the data. The lower curve shows the magnetic declination (or latitude) of the Earth.

small, variable amount of circularly polarized radiation adding in phase quadrature to the linearly polarized radiation. The variation is due to the rocking to and fro of the magnetic axis as Jupiter rotates. Similar measurements made since at 10.6 cm have shown a similar effect.

It is very difficult to explain this result by instrumental effects or by an intrinsic asymmetry of the source rotating with the System III period. A similar effect has been reported by Berge and Morris (1964) for a wavelength of 10.4 cm and an antenna spacing of  $2200 \lambda$  east-west. It was found that the effect could be explained by having a displacement of the radiation belt away from the center of the planet by almost 0.7 radii. However, there are now several reasons for rejecting this explanation in favor of the circular polarization interpretation. One is that the suggested displacement cannot explain the short-baseline observations, but the presence of circular polarization can explain both the short- and long-baseline observations. The long-baseline observations indicate

that the circularly polarized component, when it appears, is a rather well-defined double source with a separation of about 5 equatorial radii.

From a knowledge of the place of origin, the sense of the circularly polarized radiation, and the direction in which the magnetic axis is tipped, all at some given longitude, we can determine that the magnetic pole in Jupiter's northern hemisphere is a north magnetic pole. This is opposite the polarity of the Earth's field.

For a synchrotron emission source one expects an appreciable degree of circular polarization only when the width of the emission cones for the electrons is not negligible compared with the scale of variation of the pitch angle distribution. For Jupiter the relativistic energies are comparatively low so that the emission cones are of the order of degrees in width. It is also known that the pitch angle distribution of the electrons is sharply peaked at  $90^\circ$ . Using the analysis of Roberts and Komesaroff (1965) for monoenergetic electrons and the pitch angle distribution given by Thorne (1965) we can solve for the field strength and electron energy. The results are about 1.7 gauss in the regions of interest and 12 Mev for the 21-cm radiation. The errors are large and we must allow an uncertainty of a factor of ten each way in the value for the field strength. Despite this large uncertainty, the result is of interest because the method used is the most direct one available for measuring the field strength. The range obtained agrees with what was previously suspected for the field strength from other considerations.

When the present investigation was begun, the previously determined size information, although sketchy, proved to be very useful in deciding what sort of measurements to make. In the same way, future observations with high resolution will be guided by what is now known about the source. In order to visualize this point, see Fig. 10, for example. Here we have a contour diagram of the visibility function for the Stokes parameter  $Q$  as predicted from Fig. 8, assuming a dipole magnetic field. The baseline components  $s_x$  and  $s_y$  are measured along the major and minor axes of the source, respectively. The heavy straight lines show the baselines used in the present study. This visibility function is almost what is obtained with crossed feed horns with the  $E$ -vectors at  $45^\circ$  on either side of the equatorial direction. However, because of the existence of some circular polarization, the nulls will, in general, be filled in a bit and the phase differences will not be exactly  $180^\circ$  when this



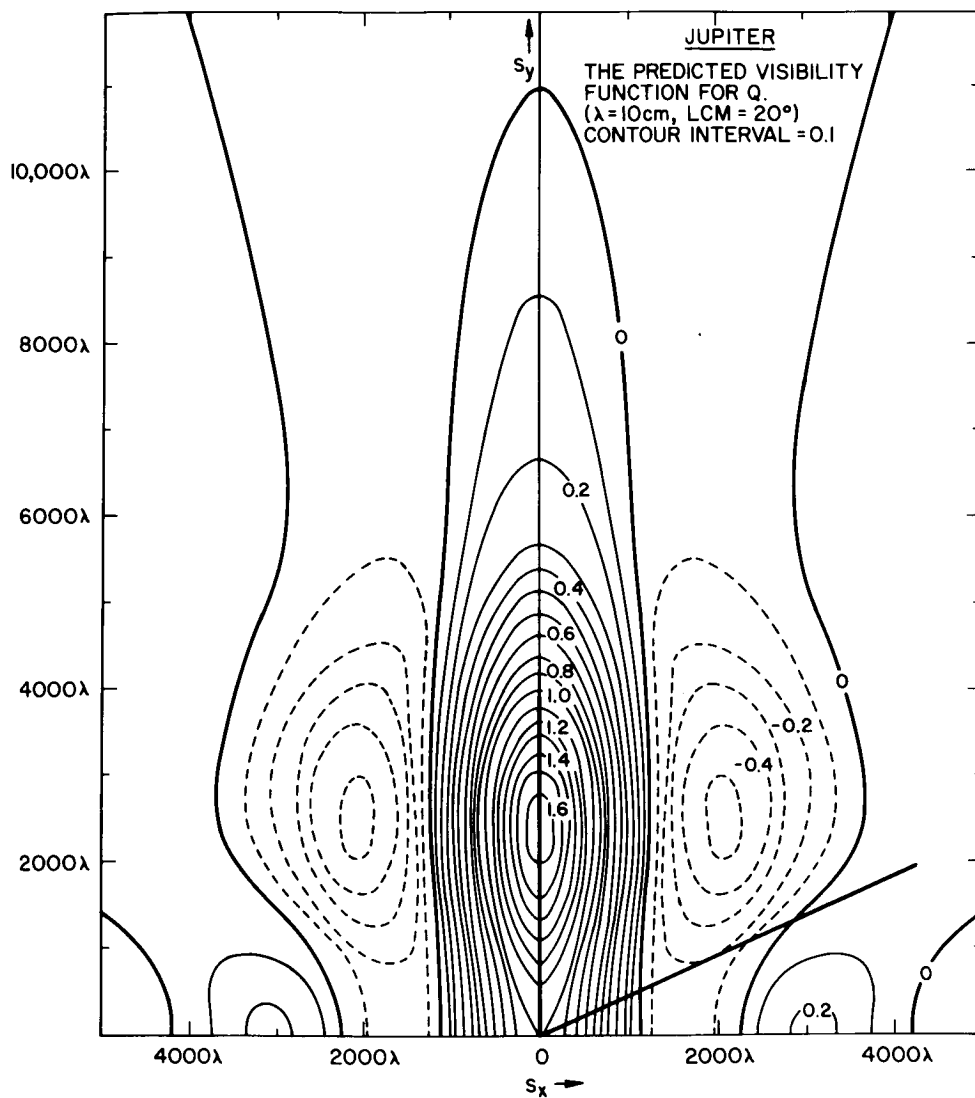


Fig. 10. A contour diagram of the two-dimensional visibility function for the Stokes parameter  $Q$ , as predicted from Fig. 8, assuming a dipole magnetic field. The baseline components  $s_x$  and  $s_y$  are measured along the major and minor axes of the source, respectively. The normalization is such that the contour at the origin is 1.0.

horn combination is used. Future observations in which the baseline range cuts the diagram in other ways will yield new information. It appears, for example, that it would be valuable to use large north-south baselines and track over a large hour angle range. Any deviations

from this diagram will enable one to improve the details of the distribution shown in Fig. 8. The corresponding visibility functions for other horn combinations also have regions of special interest when plotted in the manner of Fig. 10.

## REFERENCES

Berge, G. L., and Morris, D., 1964, *Astrophys. J.*, Vol. 140, p. 1330.

Roberts, J. A., and Komesaroff, M. M., 1965, *Icarus*, Vol. 4, p. 127.

Thorne, K. S., 1965 (reported at the Symposium on Planetary Atmospheres and Surfaces, May 24-27, Dorado, Puerto Rico), *Radio Science*, Vol. 69D, p. 1557.

N66 31459

## THEORY OF THE JOVIAN STRUCTURE

*James W. Warwick*

*University of Colorado  
Boulder, Colorado*

As J. N. Douglas puts it, "theory and observations [of Jupiter's decametric emission] are . . . difficult to compare . . . because of the great complexity of the observational problem." In one hour's time, I can't hope to do justice to all the facets of Jupiter radio structure. Furthermore, I'm not quite sure what meaning we can place on "theory" in this context, where we are at present, and are likely to be for a long time to come, far from a deductive formalism based on simple physical premises.

Rather than even attempt that sort of thing, I've tried to organize my remarks around my own appraisal of the quality of the largely heterogeneous facts now available about Jupiter's radio phenomena. We can have great confidence concerning quite a few observations and derivative "theoretical" conclusions. Other data are still not completely confirmed, and some deductions are, as well, not unassailable. Finally, some results are, to a greater or lesser extent, extrapolations at present. Beyond that, I will conclude by commenting on a number of studies that may suggest fruitful researches to come.

Often I will have to mention decimetric radio emission as well as decametric radio emission. These are mouthfuls in which so much has the same flavor that you might not

quickly sense the difference. To distinguish them sharply, I am going henceforth to refer to them as DIM and DAM respectively.

### ***1. Well-Established Phenomenology***

With supreme confidence we know that Jupiter has a magnetic field; equally confidently, we assert that Jupiter's field is not that of a centrally located dipole, nor even azimuthally symmetric (e.g., poloidal). The rotation rate of this field is close to System II, and defines a radio period and longitude scale, called System III (1957); the period is  $9^h55^m29.4^s$ . This value (actually with 2.37 instead of 29.4 sec) is the conventional one adopted by radio astronomers for ephemerides, and corresponds to the average over the decade 1950 to 1960.

There is energetic particle "radiation" trapped within the magnetic field.

The satellite Io, at  $6R_J$ , interacts observably with DAM.

DIM is produced by synchrotron emission from highly relativistic trapped electrons.

DAM is coherent emission produced either by bundles of particles or through interactions of nonelectromagnetic waves that produce electromagnetic waves. The emission source is small, less than 5 seconds of arc.

DAM lies below about 40 Mc/sec; its lower spectral limit is certainly no higher than 4.8 Mc/sec, and may be much lower. Its flux roughly parallels the increase of galactic noise towards low frequencies. The spectrum can be broadband, often with a sharp high-frequency cutoff; especially above 15 Mc/sec it is frequently narrowband, with bandwidths of only a few per cent of the central frequency. At high DAM frequencies the spectrum is characteristic of the radio longitude at central meridian passage ( $\lambda_{\text{III}}\text{-CMP}$ ), and to a lesser extent, of the aspect of Io in its orbit. Positive spectral drifts tend to occur in the range of 0 to 180°, and negative ones from 180 to 360°.

DAM is right-handed elliptical at all  $\lambda_{\text{III}}\text{-CMP}$ . This holds above 15 Mc/sec; below 15 Mc/sec, DAM becomes left-handed in the range of 300 to 120° (the early part of the early source) and right-handed the rest of the way. DAM contains very little randomly polarized component (< 10%).

DAM occurrences fall in peaks at  $\lambda_{\text{III}}\text{-CMP}$  values near 130, 240, and 300°. Another peak appears in dynamic spectra from 050°. These peaks are narrow in longitude, spanning perhaps 40° between half-intensity points (for the peak at 240°). Spectral structure indicates still narrower peaks, less than 10 or 20° broad.

DAM shows terrestrial quasi-longitudinal (QL) Faraday effect. The fact that a similar Faraday effect at Jupiter lies unobserved below the low threshold of detection sets limits on the region of generation and/or the mode of propagation of the radiation at Jupiter. DAM often shows burst-like time variations reminiscent of terrestrial radio star scintillations. Customarily there appear 1- to 10-sec bursts (decasecond bursts), but occasional millisecond bursts are recorded, and, especially at superior conjunction, decaminute bursts.

We must assume that whenever Jupiter's magnetic pole swings past Io there is DAM in both sources, inasmuch as during these times DAM is then practically a certainty, in both the early and main sources (i.e., 130 and 240°  $\lambda_{\text{III}}\text{-CMP}$ ). It would be incredible to assert that Io creates whatever instability process leads to DAM only when Io and Jupiter face, so to speak, the Earth. Furthermore, there is no real reason to suppose that the

slightly tilted moment should be nodded towards Io for the instability to occur. The instability must continuously be generated as Io moves around Jupiter.

The  $\lambda_{\text{III}}\text{-CMP}$  range associated with Io is broader by a factor of 4:1 than the range of Io's position over which Io is effective. The Io mechanism, by strong implication, generates a sheet of emission, rather than pencils of emission. This sheet wraps around Jupiter in longitude, but covers only a narrow range in latitude. That is, it is not a thick sheet, or we would see continuous emission from early through main sources. In other words, the steady Io effect leads to emission falling in general above or below the ecliptic direction containing the Earth.

Within the global pattern there exists a subtle, but definite, fine structure of emission in longitude and frequency, which depends sensitively on the position of Io. This is shown both by sequential dynamic spectra with Io longitude as the parameter, and by comparison of the contour plots of DAM occurrence on Io- $\lambda_{\text{III}}$  coordinates. These plots, for data at single frequency, characteristically exhibit lanes that can be described as the locus of a point moving in real time across the Io- $\lambda_{\text{III}}$  plane. These lanes do not appear on similar plots of dynamic spectral data.

## II. Strong Conclusions

A very strong, but not rigorous, case can be made for the assertion that at high frequencies DAM originates in and near Jupiter's ionosphere. The argument is similar in character to, but stronger than, the arguments in the original literature, which were based on the narrow peaks in the DAM profile. The permanent dynamic spectrum describes emission occurring repeatedly at the same frequency and  $\lambda_{\text{III}}\text{-CMP}$ . The available parameter to provide the necessary stability would be the magnetic field. However, the magnetosphere lines of force cover a great range of field strength and direction. At Jupiter's surface the field has a unique and nearly permanent value at a given zenographic position.

A further argument tending to confirm this analysis is the change in DAM polarization to right-handed elliptical, at all  $\lambda_{\text{III}}\text{-CMP}$ , for high enough frequencies.

The frequency of DAM is the electron gyrofrequency  $\omega_{pe}$  for similar reasons. The electron gyrofrequency is well-defined, must play a prominent role in plasmas undoubtedly involved in DIM and DAM, and is permanent, that is, independent of plasma density. Harmonics or subharmonics of  $\omega_{pe}$  are not involved.

DAM data from Arecibo showed a few cases (out of a total of 19) where right-handed and left-handed waves alternated with each other as a function of frequency (and time as well). The right-handed waves showed stronger fringes than the left-handed ones. Also, simultaneous observations with a rotating linear antenna disclosed the characteristic terrestrial Faraday effect. The effect can be synthesized if we assume DAM propagates in a region where the magneto-ionic modes are substantially elliptical (NB, not linear). When the wave frequency  $\omega \gg \omega_{pe}$  ( $Y < 1$ ), as for these waves in our ionosphere, the modes are either circular (QL case) or linear, the quasi-transverse (QT) case. The transition region is very thin, and, furthermore, QT is restricted (on our nights at Arecibo), to within a few minutes of arc of the perpendicular to the lines of force. Elliptical modes at Jupiter must in general represent an extremely specialized angular relation to the lines of force. Just the fact of elliptical radiation carries the same implication.

On the other hand, if  $\omega \sim \omega_{pe}$  ( $Y \sim 1$ ), QT and QL are not restrictive, nor especially significant. There is a broad region over which the ellipticity changes gently. I propose to call the resulting Faraday effect the  $Y$ -One effect.

DIM is consistent with a poloidal field; the source is 3 times wider in the equatorial than in the polar direction. There are no links or sharp discontinuities in DIM's profile in longitude.

For DAM, the asymmetries are more pronounced; for example, the radiation is right-handed at all longitudes, and has a one-peaked occurrence histogram in longitude. My argument for a dipole field, whose source was displaced from Jupiter's center, depended on the wide longitude range through which the dynamic spectrum exhibits a consistent drift pattern, first positive, then negative, and spanning ranges of as much as  $100^\circ$  of  $\lambda_{III}$ -CMP.

Rather than conclude now on a displaced dipole, I think it is more rigorous to conclude merely that the data show a nearly axisymmetric field, e.g., a poloidal field, for which the dipole is only one of many cases (see the discussion under Section V).

DAM must be sharply directive, if the longitude profile is so finely determined by the dynamic spectrum. The plasma cutoff beaming discussed ten years ago does not appear effective; instead, we are dealing with the electromagnetic generation mechanism, including especially the coherence properties of the source. Two special

directions lie naturally at hand. They are the equatorial plane of the field and the field direction itself. With a poloidal field, equatorially beamed radiation must propagate into a wide longitude range. If there is a slight tilting or distortion of the field, as Jupiter rotates the equatorial sheet will cross the direction of the Earth and be visible for a moment whose duration depends on the angular width of the sheet in the co-latitude direction and on the angle between the local field and the rotation axis of Jupiter. For example, if the field line were parallel to Jupiter's rotation axis, and if it lay in the plane of the sky, we'd see the emission for  $\geq 180^\circ$  of longitude.

If we assume that a typical angle between field and rotation directions is  $10^\circ$ , and that the range of  $\lambda_{III}$ -CMP for which a given point is visible is  $10^\circ$  also, the emission must have been beamed into a sheet of width  $10^\circ \sin 10^\circ \sim 2^\circ$ . In other words, equatorial emission stresses an extremely narrow beaming.

It may be easier to explain the beaming effect along the field lines, where the pencil of radiation would cover  $10^\circ$ , instead of  $2^\circ$ .

DAM must involve two physical processes, generation of the phenomena—particles or waves—that excite the electromagnetic radiation, and secondly, the wave excitation itself. The existence of the Io effect reinforces this argument.

Most dynamic spectra made with sufficient resolution show the QL-Faraday effect, but do not show the  $Y$ -One Faraday effect. Instead, the right-handed and left-handed channels show fringes that coincide in frequency. The effect may be generated through interaction of direct and reflected modes at Jupiter. It is not an antenna mismatch or local ground reflection effect.

### III. Somewhat Hypothetical Conclusions

While Io certainly creates a disturbance in Jupiter's magnetosphere, the detailed type will depend on unknown parameters, such as Io's conductivity, possession of insulating surface material (if any), and inherent magnetism, and the long-term properties of Jupiter's field. (Does it reverse? How rapidly?)

Io, one will hazard, does not have a fluid core. Its field comes to it rather through a diffusion process such as described for the Moon by Gold. With the same constants as Gold used, we conclude, as he did, on a diffusion time constant of a few years. If Jupiter's field variations are only small-scale ones over periods like those in which

the Red Spot rotation varies, then we ought to conclude that Io moves in a region of nearly constant field strength and direction. (Almost certainly it lies within Jupiter's magnetosphere.) A major problem is to establish the size and shape of this equilibrium field.

The observed DIM lies within  $3R_J$  of Jupiter. My estimate of the magnetic moment of Jupiter sets the value of the field there at about 1/2 gauss, corresponding to a gyrofrequency of about 1 Mc/sec. This may be the lower limit of DAM. Observational confirmation would be important.

Io lies on dipole field lines that intersect Jupiter's surface at high magnetic latitudes,  $\geq 70^\circ$ . The fact that Io influences DAM at 90 and 240°, Io longitude, suggests that the centroid of the active lines of force lies nearly in the plane of the sky. If the emission occurs equatorially, this geometry may be plausible. If the emission propagates along the lines of force, it will not be observed on the Earth. In the latter case, we should assume that somehow the excitation moves from the high L-shell containing Io to a lower one more likely to emit towards the Earth. In other words, sharp L-shell crossing may be involved (see Section V below).

One of the merits of the displaced dipole theory is that it predicts 0.5 gauss in the DIM source. If we had a strong higher-order pole, then DIM's field might turn out to be much less. The theory of DIM is, however, sufficiently open at present to allow considerable latitude of this type.

Another merit of the displaced dipole model is the fact that, with a southern displacement, it gives qualitatively the right kind of asymmetry shown by the polarization profile of DIM. Quantitative results still await computations based on DIM's brightness distribution, etc.

However, there is a tendency for the centroid to appear displaced, in the average around all longitudes, towards the south. This tends to emphasize the physical distortion. This is a result of the displacement of the near side belt emission towards the south, when the dipole is tipped towards us at clockwise cross-over, and towards the north at 180° later. Since less of the far side emission is occulted at clockwise cross-over than at counterclockwise cross-over, the *average* effect is to shift the emission centroid towards the south.

Near-side belt emission shifts towards the north when the dipole's north end is tipped towards us (clockwise crossover), and towards the south 180° later. Since more far-side emission is occulted at clockwise crossover, the

average effect is to shift the apparent centroid northwards.

Europa, Ganymede, and Callisto move in orbits farther from Jupiter, but perhaps still within the magnetosphere. They are dynamically a unit, linked by strong perturbations that include Io. The Io effect extends at least as far back as 1956. In the High Altitude Observatory at Boulder we have not found effects from the other Galilean satellites.

That such effects may occur is reasonable and may eventually clarify some important points, for example, concerning L-shell drifts. Because the Io effect is so strong, a cautious, long-term analysis will be required.

Io affects a wide longitude range of  $\lambda_{III}$ -CMP values. At the same time, Io must lie within a much narrower longitude range (by three or four to one; this is *not* an effect of the 4:1 ratio of  $P_{Io}$  to  $P_{III}$ ). Io's influence from time to time can cover different longitudes than it occupies itself. Gradient drifts of electrons (proportional to  $B \times \Delta B$ ), are only a few cm sec<sup>-1</sup> at Io, and are wholly inadequate to explain the effect. Does Io distort the field over a 40° range of its orbit? If it did, we would hardly find that it influenced DAM only within a 10° range.

In Boulder, we have again observed steady, low-frequency emission (below ~20 Mc/sec) this summer. In 1960 we reported similar emissions, but we had not seen them since. Is this a broad source, not sensitive to scintillation phenomena?

#### IV. Suggestions For Further Studies

Important questions on the variation of rotation rates of DAM have recently been discussed. It is now important to relate these questions to the rate of DIM as well. DAM surely slowed, by about a second, in the early 1960's, and is now back almost to where it was before. DIM's rate has been reported now by several workers. These data need systematic intercomparison to establish differences, if any, between DIM and DAM rotation.

Suppose that DAM originates in a quadrupole component of Jupiter's field, and DIM in a dipole. We shouldn't assume that their rotation rates will vary identically.

Our Arecibo data are beautiful to behold, but on three occasions were made with perhaps one order of magnitude too slow a sweep rate. It is important to repeat this experiment with good sensitivity, complete polarimetry, a broader sweep range, and a 1-msec sweep rate.

Low-frequency data, to establish the lower cutoff value, should be made from the Moon, eventually, or by satellite. They should extend below 1 Mc/sec, should have positive identification, and should include polarization.

Jupiter flyby data become of highest solar system priority, it seems to me. They should measure the dipole field strength, the trapped spectrum, and Io's perturbation of the magnetosphere.

For DIM the clear essentials now are high-resolution observations made in real time with pencil beams, including full determinations of the polarization. If we start immediately, we may have these data in 10 years.

### V. Speculative Discussion

The decasecond bursts are very likely produced from originally smooth radiation, perhaps the decaminute structures, through a scintillation mechanism in the space between Jupiter and our receivers.

Direct source-size measures of DAM show it to lie in the range of 5 to 15 seconds of arc, the apparent size of a source already broadened through scintillations. The few degrees width of the dynamic spectra can be translated into a source size, a  $10^\circ$  source subtending about 4 seconds of arc at CMP.

With this size of source,  $T_B$  for DAM is  $10^{13}$  to  $10^{14}$  K;  $10^8$ -ev electrons, the most energetic perhaps to be found in the DIM source, correspond to only  $10^{12}$  K. DAM therefore is highly collimated and highly intense, and must be coherently excited. Further evidence in this direction comes from its narrow bandwidth and its fixed spectrum and polarization.

The millisecond bursts pose a puzzle, unless they measure the basic instability time of the electromagnetic generator or exciter generator. However, not many DAM events have millisecond structure, which implies that the majority of DAM does not consist of overlapping myriads of these short bursts. The millisecond bursts are so intense that, with their short duty cycle taken into account, they still have the same average power as the longer bursts.

Suppose the basic exciter fluctuates on a decaminute scale, corresponding to the superior conjunction data. The decasecond bursts are produced by scintillation effects. The millisecond bursts, we shall assume, are produced when coherent excitation of a large area of the

planet takes place. The speed of the bursts then measures the angular spacing between the "side lobes," so to speak, of a gigantic natural antenna near the surface of Jupiter. Its dimensions are measured in thousands of kilometers. (Fortunately, they are not bigger than Jupiter itself.)

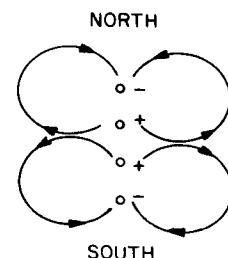
The Y-One effect seems to have appeared only on these millisecond burst records. The present explanation for the bursts offers a natural reason why this is so. A Faraday effect at Jupiter, which involves 10,000 km across the planet's face, requires a constant radiofrequency phase over this large an area. If the phase were not coherent, then different parts of the wave front would suffer different Faraday effects, not in average total rotation so much as in exact phase of rotation at a given frequency. This would destroy the effect we observe.

My final remarks concern magnetic field asymmetries. I have argued for a displaced dipole model of the field and tried to show just how the observations might fit such a model. The DIM measurements made at present do not yet, in my opinion, disprove the model, as I mentioned earlier. Time will, I hope, eventually give us definitive answers.

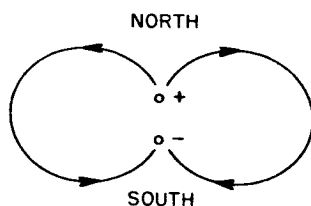
The spirit I had in mind in advancing the model was that since DIM and DAM suggest a dipole, we should work hard with a dipole model, all the more so since this represents the simplest field that nature can produce. In fact, as I also mentioned earlier, the evidence bears really on a poloidal field, that is, a field that is azimuthally symmetric in some modest approximation.

Going to more complicated matters, we might introduce on top of our dipole a certain amount of axisymmetric quadrupole. Beyond that, we have the horror of unsymmetric quadrupoles, and even still higher poles, which I shall not contemplate at all.

An axisymmetric quadrupole will have lines of force like this:



which are to be added to dipole lines of force like this:



I have labeled North and South on both diagrams to indicate the positions I will give these poles to represent Jupiter. For the indicated orientations, the total field will be relatively weak in the north and strong in the south (if the quadrupole is sufficiently small), while the centroid of DIM, which depends sensitively on field strength, should be shifted south by a small amount. This then should represent the displaced dipole picture, but in terms of central multipole fields.

The detailed structure of the total field has some curious features worth mentioning here. Suppose that the quadrupole is strong enough so that at or near Jupiter's surface, quadrupole and dipole are in a rough balance with one another. This will occur, of course, only within a thin stratum. Along the northern polar axis there will occur a zero of the field, which is a singular point (see Fig. 11). The lines of force avoid this singularity and concentrate instead into a belt lying in equatorial latitudes. This would give an alternative to the L-shell drifts I mentioned earlier.

I have prepared this review not for publication as a formal paper, but just as a verbal report to be given at this conference. The style at times is therefore quite

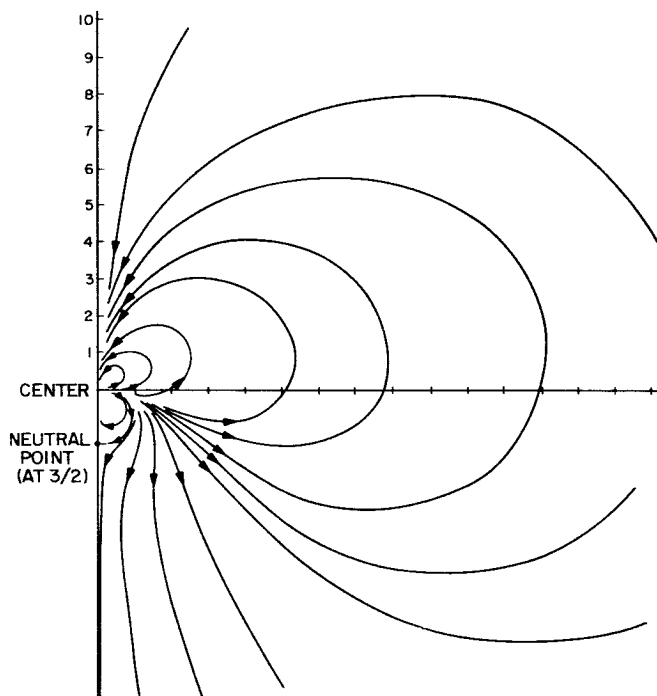


**Fig. 11. Lines of force, dipole plus axisymmetric and parallel quadrupole (the unit of distance is the ratio of quadrupole to dipole moment strengths)**

informal, and the argumentation often suggestive. Also, as is appropriate to a paper read under these circumstances, I have not included a bibliography. Many people have made the researches that I have summarily reported here. Finally, I would like to single out my own two immediate co-workers, Mark Gordon and George Dulk, whose efforts underlie much of my report, and who have been a source of continuing inspiration to me.



N66 31460

## JOVIAN ROTATION PERIODS AND THE ORIGIN OF THE DECAMETRIC BURST STRUCTURE\*

Alex G. Smith, G. R. Lebo, C. N. Olsson,  
W. F. Block,\*\* N. F. Six,† and T. D. Carr

University of Florida  
Gainesville, Florida

### 1. Rotational Periods

Considerable interest was aroused by the discovery that Jupiter's decametric sources had increased their apparent period of rotation near 1960 (Douglas and Smith, 1963). This interest was heightened when one of us (A.G.S.) called attention to the fact that a similar change had occurred slightly earlier in the period of the Great Red Spot (Smith, 1964; Smith et al., 1965). Because most theories of the radio sources link them to the planetary magnetic field, and thus by presumption to Jupiter's core, such changes are of obvious significance in formulating models of the planet.

For example, Hide proposes that the Red Spot is the visual manifestation of a hydrodynamic vortex or "Taylor column" generated by the slippage of Jupiter's atmosphere over an irregularity in the mantle (Hide,

1963). To account for the pronounced long-term variations in the Spot's period of rotation (Fig. 12), Hide suggests that the core and the mantle undergo opposed torsional oscillations. Clearly this would lead one to suspect that changes in the radio period and the Red Spot period should be in opposite directions, a prediction not borne out by our earlier investigations. Recently Runcorn (1965) and Dulk (1965) questioned this finding, claiming from optically derived rotational periods that the period of the Red Spot had in fact altered in the opposite sense from that of the radio sources. It is the purpose of the present note to re-examine this important point more critically.

To establish long-range perspective, note in Fig. 12 that during the past 134 years the Red Spot has oscillated more than  $\pm 600^\circ$  in the most favorable longitude system that can be devised, reflecting fluctuations of as much as 17 sec in its rotational period. The accelerations of current interest appear only as an almost imperceptible "wiggle" at the upper end of this long-term curve. When we turn to the other extreme, Fig. 13 presents a very short-term picture of the Spot's motion. Evidently

\*Sponsored by the National Science Foundation, the Army Research Office (Durham), the Office of Naval Research, and the National Aeronautics and Space Administration.

\*\*Now at Florida Presbyterian College, St. Petersburg.

†Now with the Brown Engineering Co., Huntsville, Alabama.

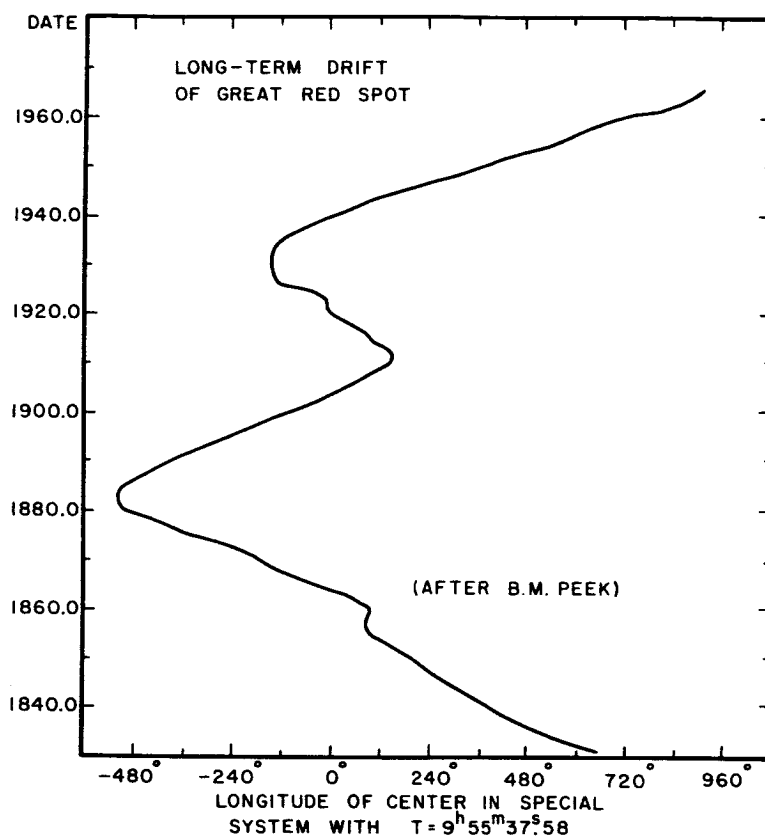


Fig. 12. Long-term oscillations in the longitude of the Great Red Spot (updated from Peek, 1958).

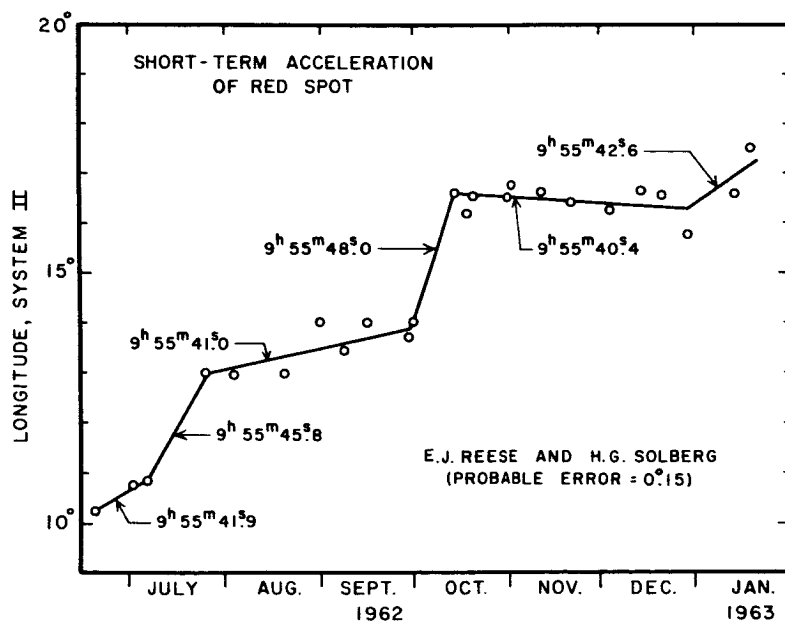
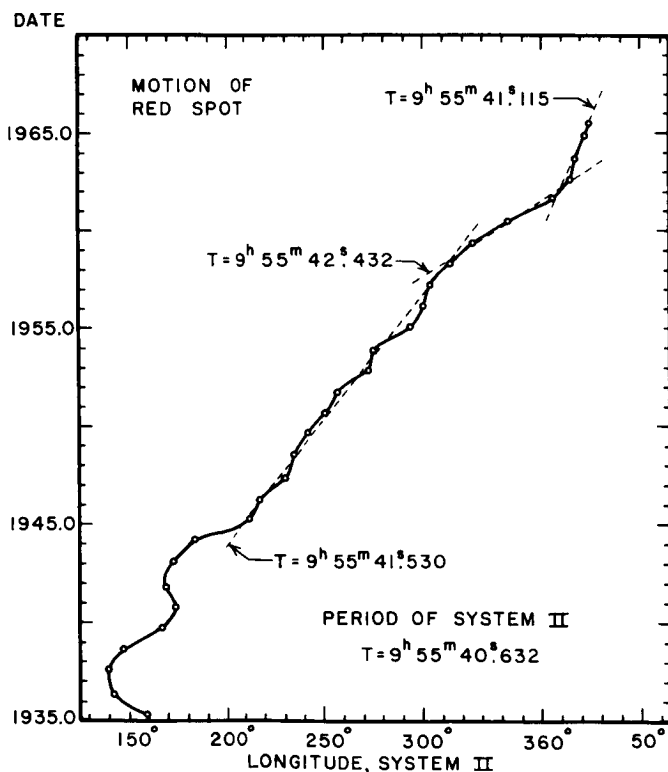


Fig. 13. Short-term accelerations of the Great Red Spot (after Reese and Solberg, 1965). These photographic measurements are probably the most accurate yet available.

the Spot is subject to rapid accelerations that can produce six "periods" differing by as much as 8 seconds, all within a span of 7 months. There is visual evidence (Peek, 1958) that such accelerations can be caused by temporary interactions with other atmospheric features, which is to say that these accelerations may well be superimposed on a long-term drift of entirely different origin. Presumably it is this long-term drift that would be of interest to radio observers, rather than the brief meteorological effects.

Figure 13 illustrates the hazard associated with accepting an instantaneous "period" as representative of the Spot's motion over even a moderate interval of time. (Perhaps some of the recent questions have arisen through a tendency to confuse the behavior of the first derivative with that of the function itself!) We have felt that a sounder approach is that of systematically plotting the longitude of the Spot from the best available data,



**Fig. 14. Recent movements of the Red Spot in System II coordinates.** The points through 1952 are from Peek (1958); the remainder are from W. E. Fox; E. J. Reese; Reese and Solberg; P. W. Budine; H. P. Squyres and Reese; and Reese and R. G. Brooke. In a number of instances the later points represent weighted averages from several different references.

as in Fig. 14. Such a plot can be compared directly with the motions of the radio sources; or if desired, average periods can be derived for intervals long enough to permit meaningful comparison with the radio observations.<sup>1</sup> Notice that the pertinent part of Fig. 14 can be approximated by three periods, with breaks near 1959 and 1962.

Figure 15a shows the Red Spot data since 1945 replotted in a special longitude system rotating at the mean period of the interval 1945–1958. Here the breaks near 1959 and 1962 are more conspicuous. For comparison, the location of the principal radio source, A, is shown in Fig. 15b in System III coordinates. The increase in the Red Spot period near 1959 was followed rather closely by a similar *increase* in the radio period. However, the abrupt decrease in the Red Spot period in 1962 does not

<sup>1</sup>The deviation  $\Delta T$  of the period from System II is given by  $\Delta T = 0.1124 \Delta \lambda$  sec, where  $\Delta \lambda$  is the drift in degrees per year in System II coordinates (Smith, 1964; Smith et al., 1965).

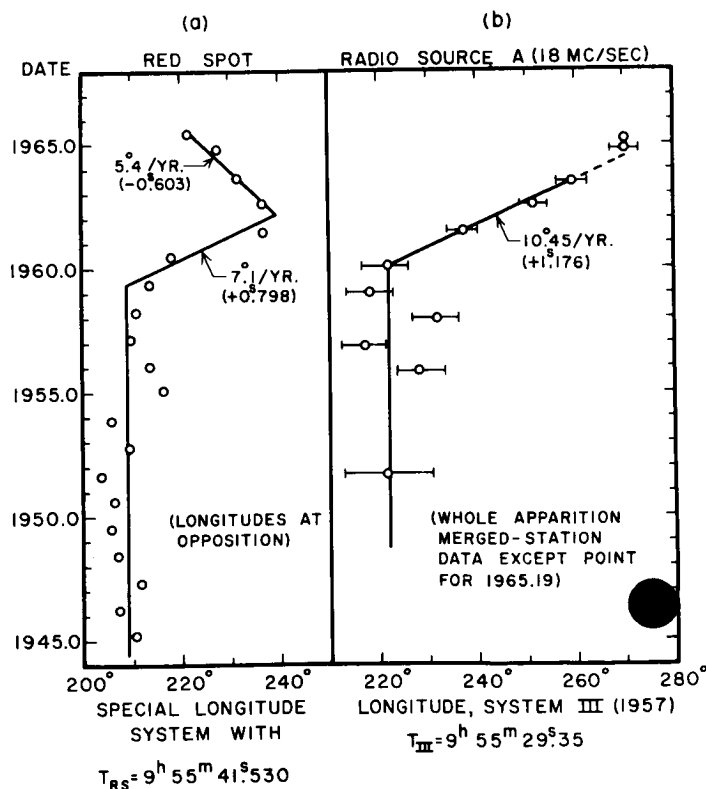


**Fig. 15. A comparison of Red Spot drift with the drift of the principal radio source.** The radio data for 1951 are those of C. A. Shain, while the data for 1955 are from K. L. Franklin and B. F. Burke. The remainder of the radio data are from the University of Florida.

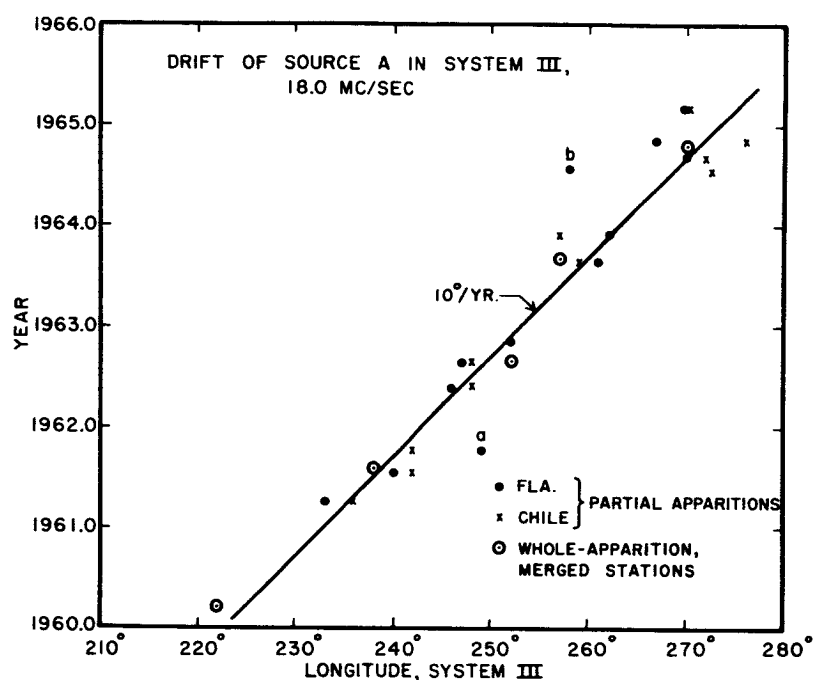


Fig. 16. Drift of source A based on partial-apparition histograms. Point "a" is given low weight because of poor statistics in the data; there is no obvious explanation for the unusually large deviation of point "b."

seem to be reflected in any significant change in the subsequent motion of the radio source. The radio points in Fig. 15b are derived from statistical analyses of entire apparitions. Fig. 16 shows the results of a study in which the radio data were broken down into shorter intervals of time; there is no convincing evidence of short-term drifts exceeding the scatter of the points.

While the preceding work was based on the 18-Mc/sec observations, which are the most numerous and most reliable, similar investigations have been made at several other frequencies. Fig. 17 shows the mean rate of drift of source A in System III coordinates for 15, 18, 22.2, and 27 Mc/sec. The solid curve is based on least-squares solutions for all data up to 1965, while the dashed curve was derived earlier from visual fitting of a smaller quantity of data. In both cases there is evidence that the observed source drift is frequency-dependent, implying that the drift may be a virtual effect, perhaps related to the mechanism of escape of the radiation.

## II. Origin of the Burst Structure

We now turn to a different investigation, aimed at throwing light on the origin of the well-known burst structure in the Jovian decametric radiation. Since the earliest observations there has been evidence of a strong

ionospheric influence (Gardner and Shain, 1958; Smith et al., 1960) and some workers have even attributed the entire burst structure to the local ionosphere. We have now compared the Jovian radiation with scintillation phenomena known to be local in origin—in this case, signals from radio stars and from the S-66 beacon satellite. A Jovian "pulse character,"  $C$ , was defined in such a way that  $C = 1$  corresponds to very long pulses (duration  $\sim 10$  sec),  $C = 2$  to normal pulses (duration  $\sim 0.5$  sec), and  $C = 3$  to the rapid "spitting" pulses (duration  $\sim$  millisec). A comparable index,  $S$ , was defined for the S-66 data:  $S = 0$  corresponds to no scintillation, while  $S = 2$  represents scintillation strong enough to obliterate the normal periodic modulation due to Faraday rotation. Comparisons were also made with the radio star data of Hewish (1952) and of Koster and Wright (1963).

Figure 18 shows the usual diurnal variation of radio star and satellite scintillation. On the other hand, the Jovian index follows no such trend. In other studies,  $C$  failed to display the normal seasonal and zenith angle effects found in the S-66 and radio star data. The most direct comparison involved simultaneous 20-Mc/sec observations of Jupiter and S-66 when the two were near appulse; Fig 19 shows that once more  $C$  and  $S$  appear to be uncorrelated. All of these comparisons suggest that

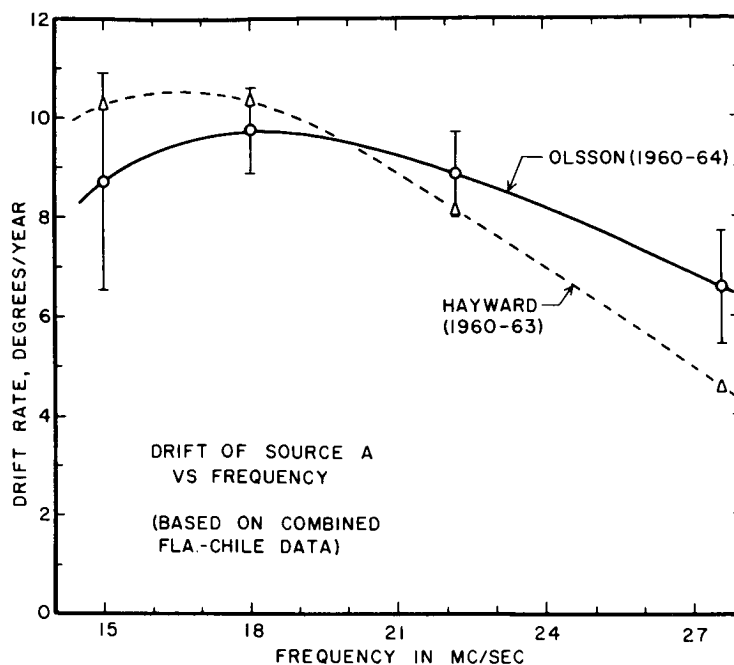


Fig. 17. Frequency dependence of radio source drift rate since 1960—two studies.

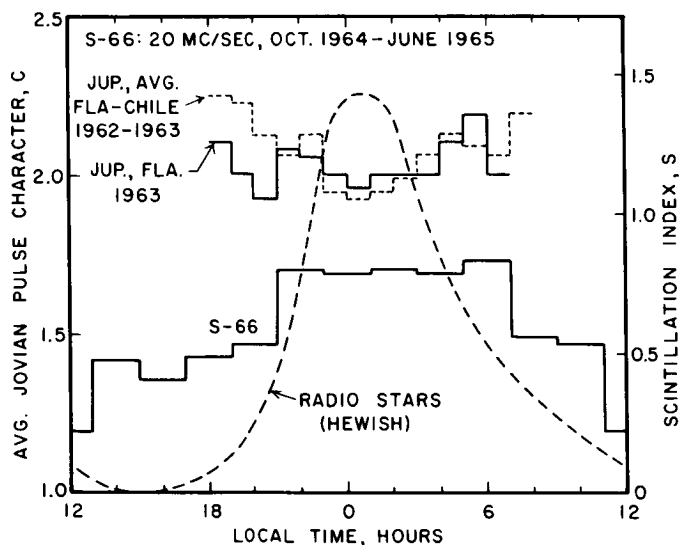


Fig. 18. Diurnal variation of Jovian pulse character  $C$ , S-66 scintillation index  $S$ , and radio star scintillation.

$C$  and  $S$  are University of Florida data, while the radio star measurements are from Hewish, 1952.

Jovian pulse character is not determined by the same factors that control the scintillation of satellite and radio star signals. This conclusion is consistent with the suggestion of Douglas (1965) that the pulses are formed in interplanetary space. However, it is important to note that our study shows for the one year thus far analyzed

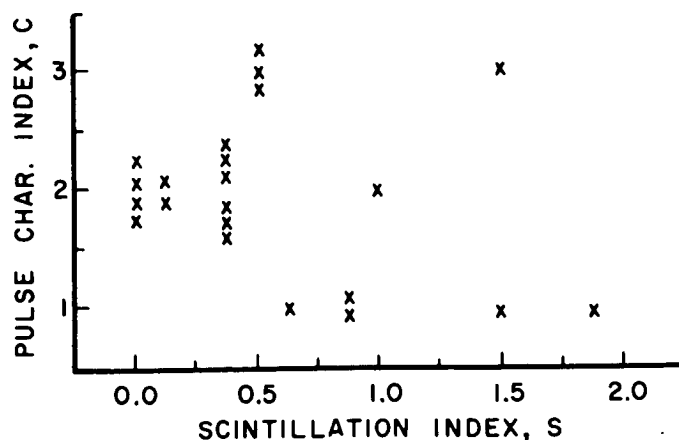


Fig. 19. Comparison of Jovian pulse character  $C$  and S-66 scintillation index  $S$  near appulse, October 1964-June 1965

a marked dependence of  $C$  on System III longitude (Fig. 20). The principal effect is a tendency for the milli-second pulses to occur when source B is on the central meridian.

On the assumption that these pulses originate at Jupiter, an effort is being made to determine the mean electron density of the intervening interplanetary medium by measuring the delay in arrival time between two frequencies 200 kc apart at 18 Mc/sec. The initial result

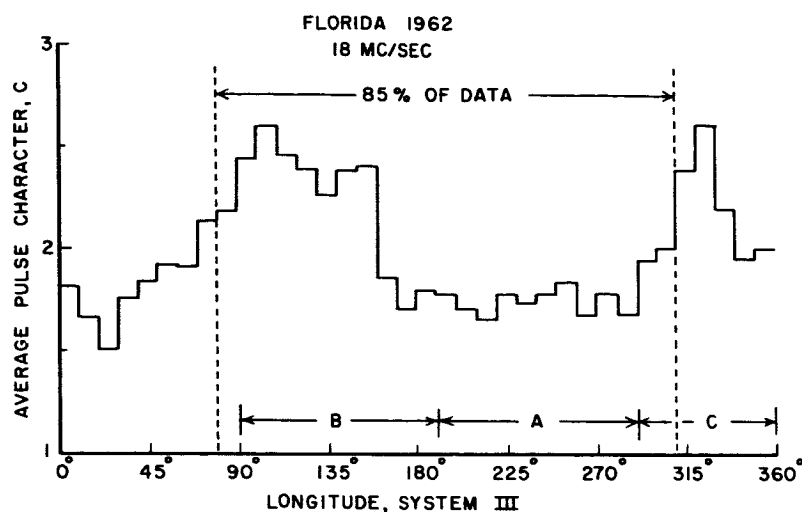


Fig. 20. Jovian pulse character as a function of System III longitude

of 23 electrons/cm<sup>3</sup> is clearly high in comparison with other methods. It is possible that a substantial part of this dispersion occurs as the radiation escapes along ion ducts in the Jovian magnetosphere.

We are indebted to W. A. Morton for most of the S-66 observations. R. Hayward and J. May contributed to the Jupiter data, while W. W. Richardson and H. W. Schrader prepared the figures.

## REFERENCES

- Douglas, J. N., 1965, *Magnetism and the Cosmos* (Proc. NATO Advanced Study Inst. on Planetary and Stellar Magnetism, Univ. of Newcastle upon Tyne), ed. by S. K. Runcorn (Olive & Boyd, Edinburgh, in press).
- Douglas, J. N., and Smith, H. J., 1963, *Nature*, Vol. 199, p. 1080.
- Dulk, G. A., 1965, Ph.D. thesis, Univ. of Colorado, p. 33.
- Gardner, F. F., and Shain, C. A., 1958, *Australian J. Phys.*, Vol. 11, p. 55.
- Hewish, A., 1952, *Proc. Roy. Soc.*, Vol. A214, p. 494.
- Hide, R., 1963, *La Physique des Planetes* (Mem. Soc. R. Sci. Liege, Ser. 5, Vol. 7), pp. 481–505.
- Koster, J. R., and Wright, R. W., 1963, in *Radio Astronomical and Satellite Studies of the Atmosphere*, ed. by J. Aarons (North-Holland Publ. Co., Amsterdam).
- Peek, B. M., 1958, *The Planet Jupiter* (Macmillan Co., New York).
- Reese, E. J., and Solberg, H. G., 1965, TN-557-65-7, New Mexico State Univ.
- Runcorn, S. K., 1965, *Magnetism and the Cosmos* (Proc. NATO Advanced Study Inst. on Planetary and Stellar Magnetism), Univ. of Newcastle upon Tyne (Oliver & Boyd, Edinburgh, in press).
- Smith, A. G., 1964, paper presented to the American Physical Society, April 27.
- Smith, A. G., Carr, T. D., Bollhagen, H., Chatterton, N. E., and Six, N. F., 1960, *Nature*, Vol. 187, p. 568.
- Smith, A. G., Lebo, G. R., Six, N. F., Carr, T. D., Bollhagen, H., May, J., and Levy, J., 1965, *Astrophys. J.*, Vol. 141, p. 457.

N66 31461

## THE EFFECT OF IO ON THE RADIO EMISSION OF JUPITER

George A. Dulk  
University of Colorado  
Boulder, Colorado

I will discuss Io's effect in somewhat more detail and present some ideas on how Io could exert its effect. This will then serve as a basis for further discussion by Dr. Davis and Dr. Field.

Io seems to induce about 50% of the radio emission at high decameter frequencies (16 to 40 Mc/sec) and almost 90% of the emission above 35 Mc/sec. That is, 50% of the 16- to 40-Mc/sec emission occurs when Io is within  $\pm 20^\circ$  of either of two favorable points in its orbit. The emission probability approaches 100% when Io's position and Jupiter's longitude are simultaneously favorable. I will not discuss the emission that occurs independently of Io's position.

The geometry of the emission pattern is important to the interpretation of the Io effect. The emission seems to leave Jupiter's vicinity in two cones. As is shown in Fig. 21, one cone is centered  $90^\circ$  to one side of Io, and the other cone is centered  $60^\circ$  to the other side of Io. As we heard this morning, the Jupiter longitude  $\lambda_{JII} = 200^\circ$  contains the north end of Jupiter's tilted

magnetic dipole. That longitude is important in the Io effect. We now consider what occurs if we take the point of view of an observer on Io and watch Jupiter rotate: When the  $200^\circ$  meridian reaches a position  $90^\circ$  ahead of Io (labeled "a" in Fig. 21), 4th source emission begins in the early and 4th source cone. Slightly later, main source emission begins in the other cone. Emission then goes simultaneously into the two cones until the  $200^\circ$  meridian approaches a position  $90^\circ$  behind Io (labeled "b") and then it ceases. Positions of the  $200^\circ$  meridian when there is maximum emission probability for the four sources are labeled in Fig. 21. (Because of the low frequency of 3rd and 4th source emission and the existence of interference, emission from these sources is seen on spectrograph records less often than is main and early source emission. It remains possible that 3rd and 4th source emission occurs each time that conditions are favorable.)

The sequence just described recurs every 13 hours as Jupiter rotates under Io. There is no corresponding emission associated with the opposite ( $20^\circ$ ) meridian of Jupiter.

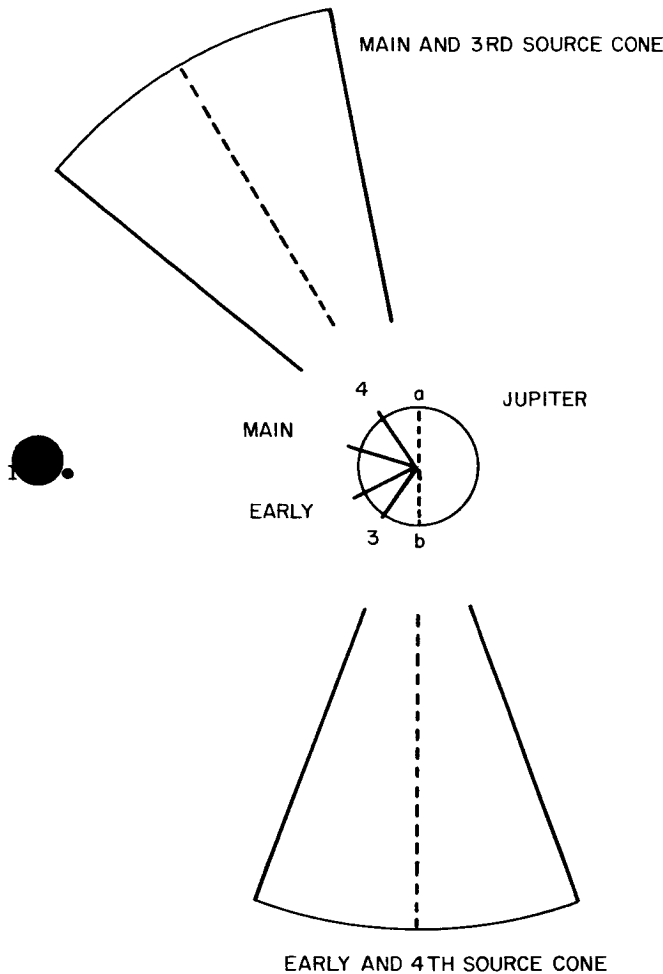


**Fig. 21. Emission pattern of Io-related emission from the four sources as seen by an observer on Io. Fourth source radiation starts when, as Jupiter rotates, the 200° meridian reaches "a;" the radiation reaches its peak when the 200° meridian is near "4," and ends when the 200° meridian is near "main." Main source emission begins when the 200° meridian is near "4," reaches its peak near "main," and ends near "early." Similar sequences occur for the early and third sources. Emission ceases when the 200° meridian reaches "b."**

More details of geometry and spectrum of main and early source emission are shown in Fig. 22, again from the point of view of an observer on Io. In Fig. 22,  $\psi$  is the angle from the Jupiter-Io line to the direction of emission, and  $\alpha$  is the angle from the Jupiter-Io line to the 200° meridian (labeled "magnetic axis"). The spectrum of emission into the two cones is shown for values

of  $\alpha$  between  $-60^\circ$  and  $+60^\circ$ . Note that the direction of the emission cones as seen by our observer on Io is fixed, even though Jupiter rotates by  $70^\circ$ . This indicates that the direction of the emission cones is controlled by Io, but since the spectrum changes considerably as Jupiter rotates, the spectrum is controlled by conditions on or near Jupiter.

Now I turn to means by which Io may exert influence on the decameter emission. I will list a few parameters important to the discussion:

1. Io has a circular orbit at  $6 R_J$  in the equatorial plane of Jupiter, and hence is nearly in the ecliptic plane (within  $3.5^\circ$ ). Io's period is approximately 42 hours and Jupiter's rotational period is approximately 10 hours.
2. The sunward boundary of Jupiter's magnetosphere is somewhere near  $50 R_J$ , so that Io is well inside.
3. In Io's vicinity,  $B \approx 0.1$  gauss, the Alfvén velocity is  $\approx 10^{10}$  cm/sec, Io's velocity is  $\approx 50$  km/sec relative to the field lines of Jupiter, and the particle drift velocity is  $\approx 1$  m/sec.

Several means have been suggested by which Io might influence the radio emission:

1. Io distorts Jupiter's field lines in its vicinity, thus disturbing the orbits of particles trapped on these field lines and causing them to precipitate into Jupiter's ionosphere or atmosphere, where they generate the radio emission. The radio emission is beamed into a conical sheet and is observed at the Earth only where the sheet intersects the ecliptic. Io would affect a larger volume of space if it had its own magnetic field, the existence of which seems unlikely, but judging from results presented at the lunar sessions of this conference, not impossible. A difficulty of this explanation lies in the tight binding of particles to the local field lines, so that it may be difficult to continually resupply the depleted field lines near Io. J. W. Warwick has calculated that large regions of the magnetosphere must be replenished every 6 min during a radio event lasting a few hours.
2. Shock waves emanate from Io and disturb trapped particle orbits in regions remote from Io. This mechanism was suggested by James Witting, who considered the hydromagnetic wave velocity as it varies with direction in the magnetic field. Despite



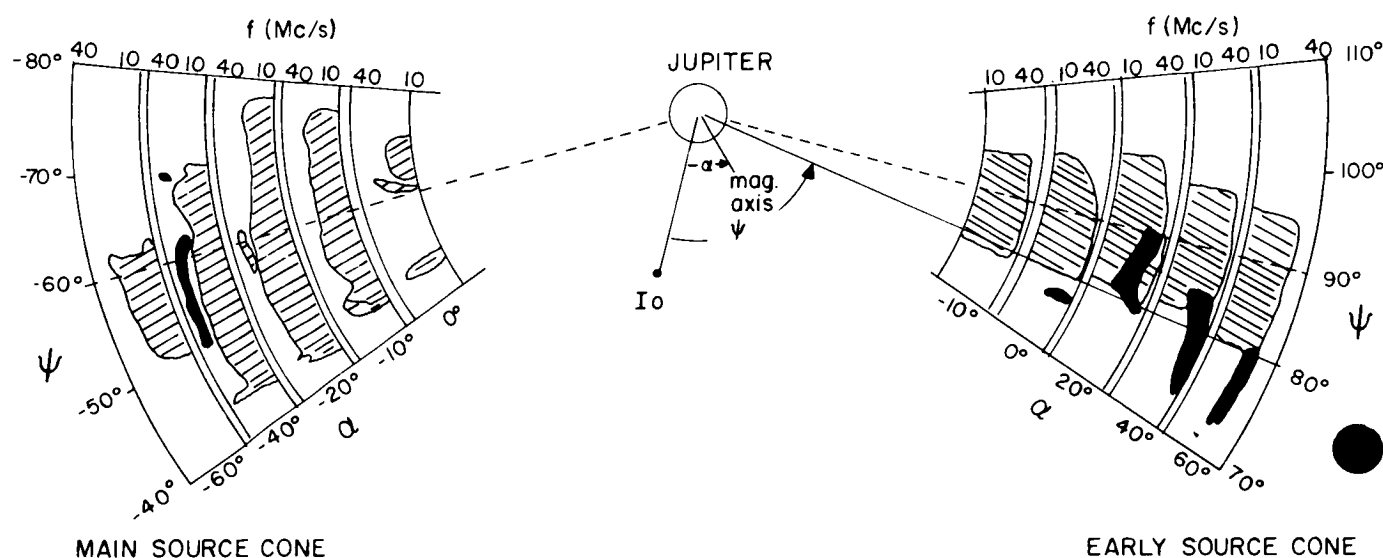


**Fig. 22.** The permanent spectrum of emission into the emission cone for Io-related early and main source emission as Jupiter rotates under Io. The spectrum of emission of each source is shown as a function of  $\psi$  (the angle between the Io-Jupiter line and the direction of emission) for five different values of  $\alpha$  (the angle between the Io-Jupiter line and the 200° meridian of Jupiter). The frequency scale for each spectrum runs from 10 to 40 Mc/sec, and the relative intensity is shown by shading.

Io's sub-Alfvénic velocity, Witting found that shock waves can propagate in some directions. G. R. A. Ellis proposed a similar mechanism to bring Io's effect to the central meridian, where, according to his theory, the radiation is generated.

3. George Lebo and A. G. Smith proposed tidal effects to explain Io's influence. Since Dr. Smith is here, I will let him explain this mechanism if he desires.
4. Io might act to accelerate particles in its vicinity rather than simply to disturb them. In a manner similar to the one Gold suggested for the Moon, Io may collect a magnetic tail by dragging out field

lines during its motion through Jupiter's field. Near the end of the tail, a neutral point may exist where magnetic field energy may be dissipated into particle energy, which in turn goes partly into radio energy. Adequate energy is available in the form of Io's potential energy in its orbit.

5. Finally, an electric field may exist between Io and Jupiter, which could accelerate particles as they travel along field lines between the bodies. The potential difference might be maintained by the accumulation of protons at Io. Because of their larger gyroradii, more protons than electrons would collide with Io.

## COMMENTS ON THE DISCUSSION OF JUPITER\*

Leverett Davis, Jr.

California Institute of Technology  
Pasadena, California

This afternoon I would like to present a complete explanation of all these interesting observations; but, unfortunately, no matter how much I would like to, I do not know how to do it. But the patterns that are beginning to emerge, particularly those connecting the position of the satellite Io with the decametric radio emission, seem to be so full of information that it should not be long before the basic mechanisms begin to be discovered. To start the discussion, I would like to present yet another way of organizing the data, although at present it enables us only to ask questions, not answer them.

Initially, it was natural to describe the phenomena as seen from the Earth and to use coordinate systems based on the position of the Earth and the Sun. But, as we have just seen from Dr. Dulk's beautiful work, if we look at the decametric radiation from the point of view of an observer on Io as it moves in orbit around Jupiter, we discover a very significant effect. The radiation in the Jovian equatorial plane tends to be concentrated in directions that are either  $90^\circ$  ahead of the position of Io or  $60^\circ$  behind it. Whether or not radiation is emitted depends also on the position of Jupiter's magnetic axis.

Dr. Dulk has a beautiful diagram that shows this very clearly. It contains all the geometric information and even contains the spectral information. However, in its frame of reference, Jupiter, with its eccentric magnetic field and all its belts of trapped radiation, rotates. This gives us a very complicated moving structure. It seems better to take the point of view of a hypothetical inhabitant of Jupiter and use a coordinate system in which Jupiter and its basic magnetic field are stationary. In this system a variety of things do move, but they are mostly simple things that are relatively easy to keep track of. In the first place, Io moves around in an essentially circular equatorial orbit. We can think of this as a moving source of excitation. The Earth also travels around, making one revolution in about 12 hours, and slowly scanning over a zone extending  $3.5^\circ$  on each side of the equator. We can think of this as a means of sampling the radiation emitted under all circumstances and in all directions in this zone. But we display the statistical results developed in this way in the Jovian reference frame. We must not forget that there is one more thing that moves rapidly in this coordinate system, and this is the outermost part of Jupiter's magnetic field, its magnetopause, magnetic tail, and bow shock. These are essentially stationary in a system oriented toward the Sun, and they rotate in the Jovian system. Since

\*This work has been supported in part by the National Aeronautics and Space Administration under Grant NsG 426.

the Earth is always nearly in the direction of the Sun, we have no observational way of knowing whether this outer structure affects the radiation pattern. However, this outer structure should begin to be apparent only beyond a distance of 25 to 30 Jupiter radii from the planet, and since it appears very plausible that all the phenomena we are considering originate well within 10 or 15 radii, this complication can be ignored for the present.

Now consider Fig. 23, which is redrawn from one of Dr. Dulk's figures to show how the main decametric radiation appears in this Jovian coordinate system. Let  $\phi$  be the angle from the plane containing Jupiter's magnetic axis around to the position of Io. As Io moves in its orbit in the range from  $\phi = 300^\circ$  (or  $-60^\circ$ ) on around to  $60^\circ$  (it appears to move backward because Jupiter rotates more rapidly than Io revolves), radiation is emitted in the equatorial plane relatively infrequently. But when Io comes to where  $\phi = +60^\circ$ , decametric radiation is usually emitted in the equatorial plane in the

directions and over the frequency range indicated by the spectrum labeled  $\phi = +60^\circ$ . As Io moves along to  $\phi = +40^\circ$ , the spectrum moves over to the position correspondingly labeled. With continued motion of Io, the radiation continues to be emitted about  $60^\circ$  ahead of Io until  $\phi = 10^\circ$ , when radiation begins to appear  $90^\circ$  behind Io as well as  $60^\circ$  ahead, the diagram showing two regions marked  $\phi = 10^\circ$ . This double pattern slides around with Io until after it passes  $\phi = 0^\circ$ ; but over the range  $-20^\circ > \phi > -60^\circ$ , radiation in the equatorial plane is only found regularly  $90^\circ$  behind Io. Thus there is a shift from radiation ahead of Io to radiation behind it.

Observations from the Earth let us check the emission in the equatorial plane, but tell us nothing about radiation in directions well out of this plane, although presumably there is radiation in some of these directions. The fact that radiation is observed in two directions for  $\phi = 0$  to  $10^\circ$  suggests that it is emitted in a curved sheet that connects the two observed directions. It can not be

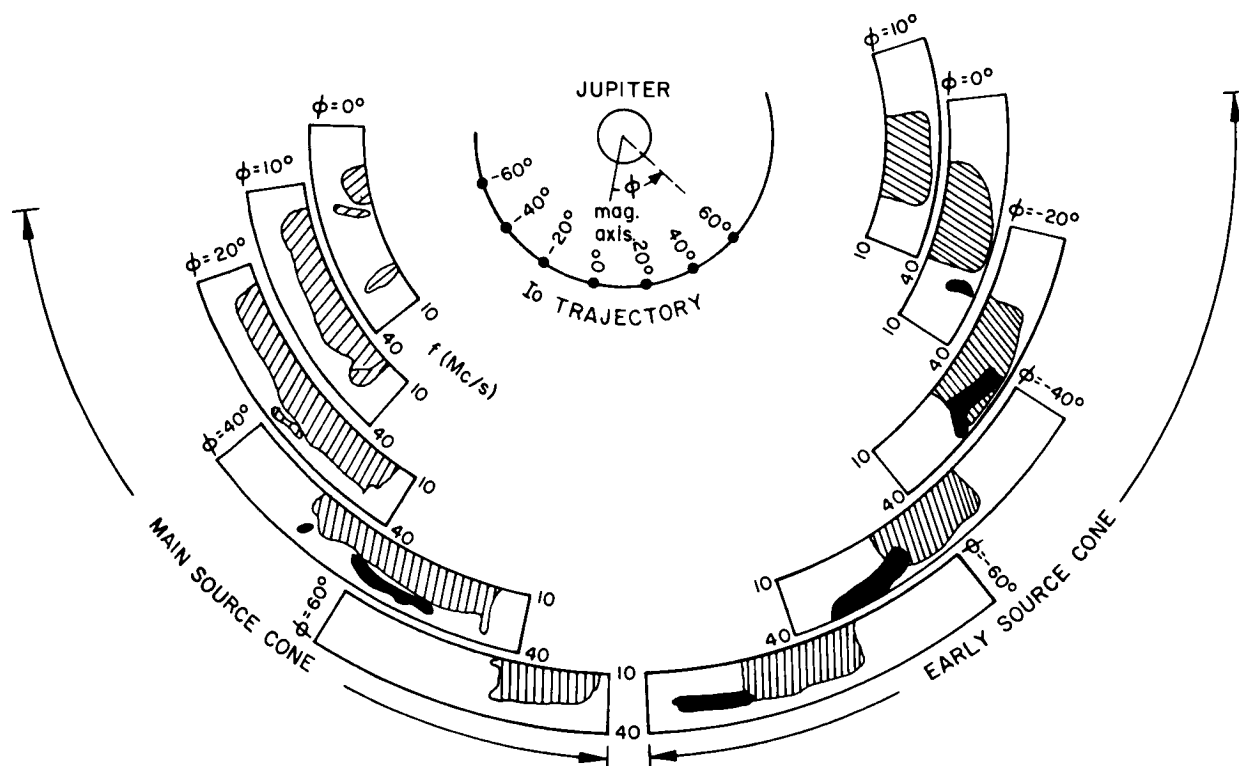


**Fig. 23.** The permanent spectrum of emission into the emission cones as Io rotates around Jupiter. The spectra of early and main source emissions are shown for eight different positions of Io, each spectrum showing the direction of emission in the plane of the ecliptic with respect to Jupiter's System III and its magnetic axis plane. The positions of Io are indicated by value of the angle  $\phi$ . The relative intensity of the emission is shown by the shading, and the frequency range, on a scale running from 10 to 40 Mc/sec, is denoted by the radial extent of the shading.

emitted in a complete cone more or less centered on Io and moving continuously, perhaps northward and southward as well as in longitude, since there would then be either two or zero directions in which radiation could be observed in the equatorial plane for most positions of Io.

Since Io is clearly connected with the radiation, one might think that the radiation is emitted from the neighborhood of Io or from its wake in the magnetosphere. But out at the Io orbit, six Jupiter radii from the center of the planet, conditions should be reasonably uniform all the way around Jupiter and it is difficult to see why radiation is not emitted nearly as copiously from points on the back side of Jupiter or why, when it is beamed into directions 60 or 90° away from the radius to Io, it doesn't always appear on both sides when it appears on one. Even a long wake does not appear to give an obvious answer to these questions.

Alternatively, consider the possibility that the radiation originates near the surface of the planet but only on the feet of the lines of force that pass through Io, or through a short section of its wake near Io. This model has a number of attractive features already pointed out by Dr. Warwick. Among other things, the radiation can now take place in a region where the field is reasonably strong and the radiation can be emitted at the cyclotron frequency. Thus as Io moves around in the equatorial plane, there will be a small radiating spot, or perhaps two, one in each hemisphere, moving around in the (magnetic) polar regions. If Jupiter has a reasonably eccentric and inclined dipole field, it is easy for phenomena to be quite different at different longitudes and for the radiation to come from only one hemisphere.

Now consider some questions that can be asked concerning this model. Is the radiation produced in a narrow beam, perhaps along the field lines, and do we see it only when the field lines are directed toward the Earth? Or does the radiation start in this way but then get refracted by the inhomogeneous magnetoactive plasma? In either case, the answer is likely to be "No," since it appears improbable that such a beam would be directed into the equatorial plane so much of the time. The presence of two beams when  $\phi$  is near 0° could be explained by supposing that they originate in opposite hemispheres, but it would still be very hard to explain the observed directions.

Suppose next that the radiation is emitted nearly normal to the field lines at a level relatively close to Jupiter. When the source region is in the plane of sym-

metry containing the magnetic axis and the rotation axis, the disk of directions normal to the field lines will not be parallel to the equatorial plane. It will be more nearly parallel to the surface just below, although tipped down on the side away from the magnetic pole. Thus radiation in the plane of symmetry will go out of the equatorial plane and can not be observed at the Earth. But in the directions normal to the plane of symmetry, the radiation will be emitted roughly parallel to the equatorial plane as observed. As Io moves around Jupiter, this emitting disk moves around correspondingly. Why do we not continue to see radiation in two directions in the equatorial plane? As Io moves away from the plane of symmetry, the emitting region tends to circle the magnetic pole rather than Jupiter's spin axis. The geometry is somewhat complicated, but when it is disentangled, one finds that one of the two directions that are both normal to the field direction and in the plane of the ecliptic now passes through Jupiter. The remaining direction in which radiation can escape and be detected at the Earth lies in approximately the right direction. It is both on the proper side of Io's position and, by a cancellation of various disturbing factors, appears to move around more nearly at the same rate as Io than would appear possible at first glance. So this model does seem to explain some features of the observations. The fact that the two beams in the equatorial plane are separated by 150° rather than 180° might be explained by refraction, or it might be that the radiation is emitted in a shallow cone rather than a disk. The fact that Io does not lie just halfway between the two beams could be explained if the excitation involves a wake of Io in the more rapidly rotating Jovian magnetosphere.

Among the questions that still remain are whether one or both polar regions are involved, and why no radiation is emitted when Io is on the opposite side of Jupiter. It may be that the eccentricity, tilt, and quadrupole terms in the field could explain these features. Because of the 3.5° inclination of Jupiter's axis of rotation, the Earth scans a zone 7° wide during the 11.8-year Jovian orbital period. This could produce systematic changes in the angle from Io to the beams of radiation observed at the Earth. These changes could serve as a test of the model if it is not too difficult to disentangle them from effects related to the solar cycle.

The main questions, of course, are "What is the mechanism of radiation?" and "What does Io do to the magnetic tubes of force that it passes through to produce the radiation?" It has been suggested that the energetic particles trapped on the magnetic L-shells may be

involved, and the question has been raised whether diffusion across the L-shells is rapid enough to replenish the particles if they are used up or lost. The rate of diffusion can well be large since it depends more on the amount and kind of perturbations that are present than it does on the drift velocity, which can be slow for the high field strengths involved. If Jupiter has a nearly static field, the diffusion is likely to be slow and it will be difficult to maintain a high trapped-particle density if there is a substantial loss rate. But if the field is frequently disturbed by fluctuations in the density and velocity of the solar wind, by fluctuations in conditions in Jupiter's magnetic tail, by waves generated by the rotation of Jupiter inside its magnetosphere, or by the irregularities in the transition region between Jupiter's bow shock and magnetopause, there may be enough perturbations to produce substantial diffusion. In any case, Jupiter's magnetosphere does not appear to be a particularly

quiet place and the possibility of a considerable amount of diffusion seems quite plausible. I think that this problem should be turned over to those who study similar phenomena in the Earth's magnetosphere, where we can get more information on what is happening. It is a very significant and important problem in both regions.

Let me make one last speculative comment in closing. In its outer regions, Jupiter's magnetic field is certainly swept back by the solar wind and there must be some kind of enormous tail behind the magnetosphere that we have heard discussed so much. It may not be hard to arrange the geometry of the tail of a planet with a skew magnetic axis so that the lines of force in the tail come close to those that make up the L-shell that passes through Io's orbit on the front side. In this case one might have a copious source in the electrons that come in from the tail.

## REMARKS ON JUPITER

George B. Field  
University of California  
Berkeley, California

The interaction of Io with Jupiter's magnetosphere has been discussed by Dulk at this meeting. It appears to me that a model in which the lines of force in the wake of Io's motion are severely distorted from the vacuum field is untenable, since such distortions could occur only by virtue of currents in the medium. Such currents would lead to forces that would modify the hypothetical distortion very rapidly, at speeds approaching the Alfvén speed (several thousand kilometers per second). Since this speed is far higher than the motion of Io with respect to the field, a large distortion could not persist in the steady state.

John Rather, a graduate student at Berkeley, has discussed with me some calculations he has made on the simple assumption that the interaction is a direct one resulting from the collisions of trapped particles with the satellite. Because the bounce period for electrons is less than the time for the satellite to move through its own diameter, the lines of force intersecting Io are quickly drained of electrons. In this way, a barrel-shaped shell at about  $L = 6$ , whose radial width equals the diameter of the satellite, is cleaned out in one revolution of Io in the  $\lambda_{III}$  coordinate system (which takes about 13 hours). If

the dipole field of Jupiter is eccentric, the width of the shell is increased to twice the displacement of the dipole in the equatorial plane of the planet, which may be as much as  $0.1 R_J$ .

The "moat" in the radiation belt that is thereby set up would not appear to be of great interest for the decameter problem unless we postulate that the energetic electrons observed through their decimeter emission around  $L = 3$  in fact got there by crossing the moat from parts of the radiation belt outside Io. That this may indeed be the case is suggested by two things: that the boundary of the magnetosphere, where solar wind energy disturbs the magnetic field, is at  $L \simeq 50$ , and that some current theories ascribe particle acceleration to diffusion of particles into the higher fields near the planet, with accompanying increases in energy by the betatron effect. The diffusion is postulated to be due to disturbances in the magnetic field.

Rather accepts the basic Warwick model, which ascribes the decameter radiation to instabilities near the gyrofrequency in the energetic electron population. He further postulates that the field lines active at 20 Mc/sec

are primarily at  $L \leq 6$ . The intensity of 20-Mc/sec radiation should then reflect the density of electrons on such field lines, and this in turn is to some degree affected by the ability of electrons to cross the moat at Io.

One way of interpreting the emission data is to say that emission occurs at times when both the Earth and Io are at certain favorable values of  $\lambda_{III}$ . This suggests that one should look to the diffusion across the moat in the wake of Io's passage as the effect that introduces Io into the probability of emission. If the diffusion time across the moat is of the same order as Io's period in  $\lambda_{III}$  coordinates (13 hours), the particle density in the moat would be greatest just before Io's passage, and zero just after. Although the diffusion problem for the magnetosphere inside Io's orbit has not been investigated, it appears that the asymmetry at  $L = 6$  would be propagated, in attenuated form, down into the region nearer the planet, resulting in a nonaxisymmetric density distribution on the field lines that radiate at 20 Mc/sec, the maximum in this distribution rolling around the planet with the same period in  $\lambda_{III}$  coordinates as Io.

One specific prediction can be made. Since the net effect of diffusion is an inward flux of electrons, the shells outside Io would be less affected by that satellite, so that if there is a tendency for lower (or higher) frequencies than 20 Mc/sec to originate on shells with  $L > 6$ , the Io modulation would be reduced for such frequencies. It would then be interesting to see if Europa modulates them in turn. If this picture is correct, we may find out something about diffusion rates at various distances.

The small satellite V would produce a sweeping effect similar to that of Io with two exceptions. First, its small size would provide a greater chance for high-energy par-

ticles with large Larmor radii to miss the satellite. Secondly, the satellite never reaches the magnetic equator, owing to its proximity to Jupiter. Hence particles with mirror points near the magnetic equator are contained with impunity. This is consistent with the observation of the plane-polarized component of the decimeter emissions.

One other point, concerning the nature of Jupiter's magnetic field. I believe that it cannot be primordial because an estimate of the electrical resistivity of impure metallic hydrogen due to the presence of helium gives a Joule dissipation time of about  $10^7$  years. How, then, does it arise? One possibility is that the mechanism is related to that described by Babcock for the Sun. A poloidal field is stretched by differential rotation into a poloidal one. If convection exists (and Peeble's interior models are consistent with this assumption) it can perhaps twist the toroidal field and realign it poloidally, at least locally. Reconnection of field lines then reestablishes the original relatively weak poloidal field. Since the basic mechanism is axisymmetric, there seems to be no way for the poloidal field to be grossly eccentric, as suggested earlier by Warwick. We are therefore interested that the recent measurements imply a smaller eccentricity.

If this mechanism is to operate on Jupiter we require differential rotation—and indeed we have it in the form of a considerable relative velocity between Systems II and III (meters per second). We may expect cyclic variations in the configuration of matter and magnetic field, and these may be present in the wanderings of the Red Spot with a period of 50 years and the accelerations of the magnetic field configuration implied by changes in  $P_{III}$ . It is interesting to note that the time for an Alfvén wave to cross Jupiter is 50 years if the field strength is 50 gauss.

## SUMMARY REMARKS ON JUPITER

G. J. Stanley

*California Institute of Technology  
Pasadena, California*

The discussions at this meeting were largely confined to the various aspects of radio emission from Jupiter and their interpretation. Much of the material was also presented at the very recent conference in Puerto Rico, sponsored by the International Scientific Radio Union and the International Astronomical Union, and there were few new developments to report since that date. I can add very little to the excellent general presentations of the various aspects of the centimeter and decameter radiation and their interpretations presented by Komesaroff, Smith, Warwick, and Haddock.

In the afternoon discussions, some attempts were made by Dulk, Davis, and Field to interpret the recent discovery of the influence of the satellite Io on Jupiter's decameter radiation. Much of this discussion would seem to be of a tentative nature, as it would appear that more experimental evidence is needed before a satisfactory explanation of the effect can be advanced.

Most of the discussion of the other features of Jupiter's radiation was surprisingly unanimous. In the discussion one was more conscious of problems that had not yet been attempted rather than those for which the solution

was arguable. A few such problems, selected at random, might be:

1. The influence of Io on decimeter radiation.
2. The relationship between the decimeter and decameter rotation periods.
3. The influence of solar radiation on the decameter emission.
4. The explanation and further investigation of the abnormally high disk temperature at 10 cm.
5. A more accurate measurement of the displacement of the magnetic dipole.
6. The explanation of the asymmetrical curve of plane of polarization vs  $l_{III}$  found by Komesaroff and Roberts.
7. Higher-resolution studies of the planet at decimeter and centimeter wavelengths.

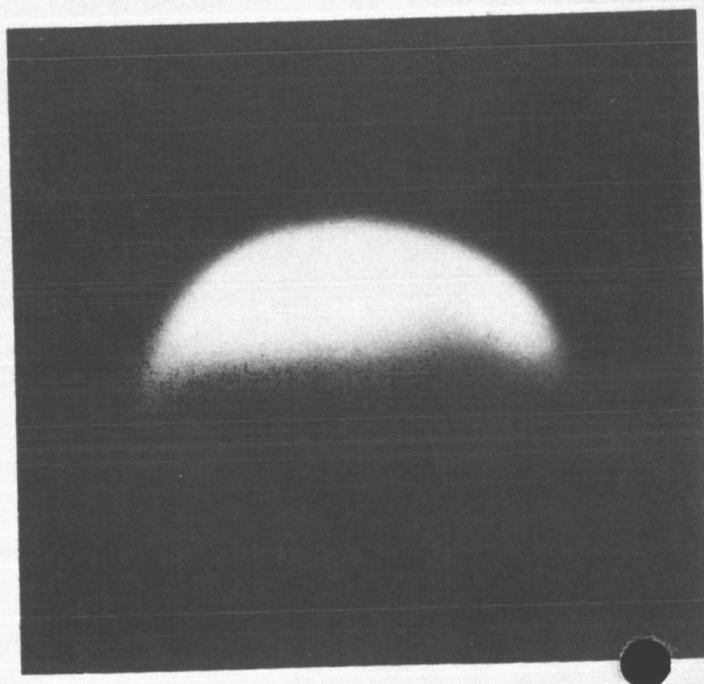
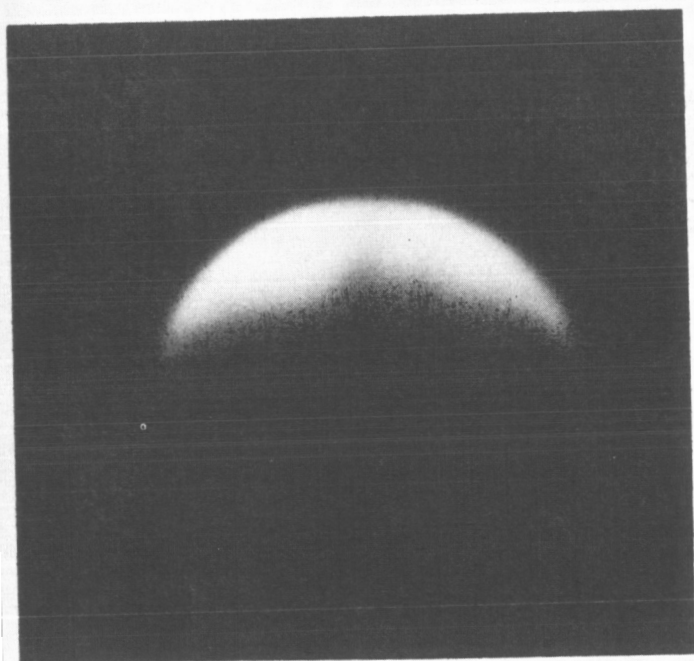
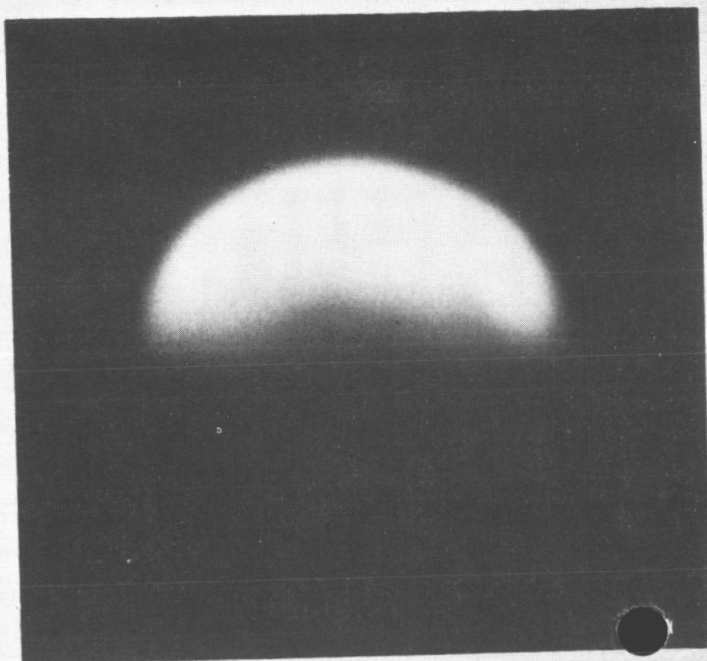
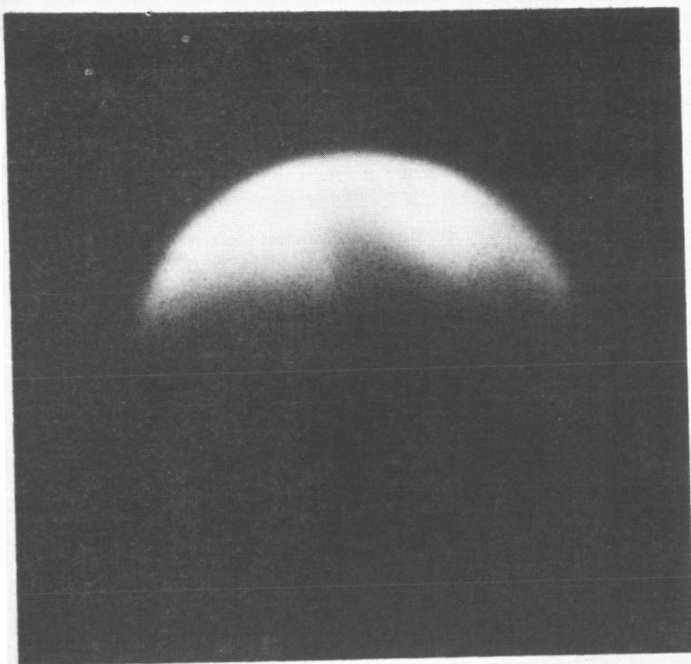
These are a few random examples of the problems that I hope we will have at least partial answers to in the next few years.



### PART III. VENUS

- J. Strong, Balloon Telescope Studies of Venus
- D. Deirmendjian, Comments on the Detection of Water and Ice Clouds on Venus
- C. Sagan and J. B. Pollack, Properties of the Clouds of Venus
- D. O. Muhleman, Venus Radar Investigations
- R. B. Dyce, Some Radar Characteristics of Venus at 430 MHz
- J. H. Thomson, Radar Observations of Venus at Jodrell Bank
- F. D. Drake, Recent Radio Observations of the Planet Venus
- A. D. Kuzmin, Some Remarks Concerning the Radioastronomical Observations of Venus
- A. Dollfus, Contribution au Colloque Caltech-JPL sur la lune et les planètes: Venus
- D. O. Muhleman, Summary Remarks on Venus

OVERLEAF: *Four 100-inch photographs of the planet Venus. (Courtesy of Mount Wilson and Palomar Observatories)*



### *III. VENUS*

PRECEDING PAGE BLANK NOT FILMED.

## BALLOON TELESCOPE STUDIES OF VENUS

*John Strong*

*Johns Hopkins University  
Baltimore, Maryland*

In this presentation I intend to review the work on Venus carried out by the Johns Hopkins University balloon astronomy group. This work has been reported by Bottema et al. (1964a and 1964b).

My approach to the problem of Venus represents a minority opinion about the interpretation of the available data, the radio emission data in particular. I would like to keep open the question of the origin of the radio emission because I believe that it is not entirely surface emission but that some nonthermal process such as that suggested by Tolbert and Straiton (1962) is active. However, before going into this question, I wish to describe the evidence for the existence of ice-crystal clouds in the upper Venusian atmosphere as obtained by our balloon astronomy group.

### **1. Determination of Water Vapor in the Atmosphere of Venus**

Venus was observed with a 30-cm telescope suspended from a balloon at an altitude that was above 99.9% of the Earth's water vapor and 97% of the Earth's CO<sub>2</sub>. The telescope was oriented with a Sun tracker and a star

tracker. Radiation was measured in the band at 1.13  $\mu$ , with a grating spectrometer of 2 Å resolving power. This portion of the spectrum was scanned once every 10 sec with a set of 21 exit slits arrayed to match 21 H<sub>2</sub>O absorption line groups. The radiation passing through was received by a chilled photomultiplier with S-1 surface, and its response was recorded on paper.

From 120 such records we have determined that the modulation produced by the water absorption, when the line groups were scanned, was  $10.5 \pm 0.5$  %. By calibration, this modulation is the same as that produced by  $9.8 \times 10^{-3}$  gm/cm<sup>2</sup> of water vapor at atmospheric pressure. We were also able to measure the influence of the doppler shift on our recorded data. At one point in each scan cycle a mercury-discharge spectral line at 11287 Å was passed through one of the exit slits and was recorded as a modulation in the reference-level spectrum. Measurements from this fiducial line to the Venus water dips, taken from 20 scans, exhibit a doppler shift of  $0.49 \pm 0.05$  Å, in agreement with a shift of 0.495 Å calculated from the orbital motions of Venus and the Earth.

The pressure at the cloud level is poorly known but is thought to range between 90 and 600 mb. The amounts of water vapor calculated from our data for gravitational atmospheres at these base pressures are:

$$22.2 \times 10^{-3} \text{ gm/cm}^2 \text{ for the 90-mb case}$$

$$5.2 \times 10^{-3} \text{ gm/cm}^2 \text{ for the 600-mb case}$$

The respective mixing ratios would be  $2.5 \times 10^{-4}$  and  $0.87 \times 10^{-5}$ .

## II. Determination of the Existence of Ice Clouds

A second balloon experiment was carried out in October 1964 with a low-dispersion grating, utilizing three detectors in place of slits. The following scans were carried out:

- 40 scans of the Venus spectrum
- 12 scans of the spectrum of adjacent sky
- 10 scans of a tungsten lamp
- 18 scans of the solar spectrum

The spectra, which covered a range from 1.7 to  $3.4 \mu$ , were corrected for water vapor using the results of our previous measurements to obtain an absorption spectrum of water vapor above the cloud tops. The work of Kuiper was used to correct for the  $\text{CO}_2$ . Our observed and corrected spectra are indicated by the solid line in Fig. 1. Also shown in Fig. 1 is the reflection spectrum of a  $-39^\circ\text{C}$  laboratory ice cloud. The agreement is excellent!

These corrections not only strengthen our inference that the Venus clouds consist of ice but also confirm our prior determination of the quantity of water vapor above them.

The existence of water vapor and ice clouds allows an explanation of one of the mysteries of the observations of Venus: namely, that the temperature of the shady side of the planet does not fall more than a few degrees short of the temperature of the sunny side as measured in the 8 to  $14 \mu$  band, even though the shady side has several months to cool off. This is a circumstance that model builders have been somewhat more complacent about than we have. The failure to cool is due to the

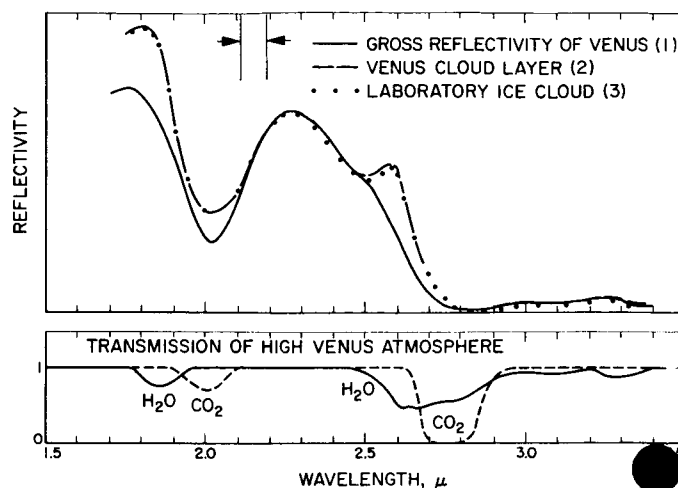


Fig. 1. Reflection spectrum of Venus clouds, showing correction for upper Venusian atmosphere. (From the *Journal of Geophysical Research*)

liberation of latent heat of  $\text{H}_2\text{O}$  vapor, of about 620 calories per gram, as that vapor condenses to form clouds.

Menzel and Whipple (1955) have pointed out in their discussion of the atmosphere of Venus that the Schaefer point is  $-39^\circ\text{C}$ , the temperature below which saturated water vapor cannot be cooled without spontaneous nucleation and crystallization. This temperature is precisely the temperature assumed by many high-level cumulus clouds on Earth. Menzel and Whipple calculate  $13.0 \times 10^{-3} \text{ gm/cm}^2$  of saturated water vapor above the Venus clouds.

We interpret the work of Clark and Kuzmin on the radio emission of Venus assuming that the measured brightness temperature is due in part to surface emission and in part to emission of the clouds. Our calculations show that  $T_b$  would be reduced by  $168^\circ\text{K}$  and the average temperature would be  $238^\circ\text{C}$ .

In summary, it seems to us that Venus is becoming a more interesting planet now that the *Mariner IV* photographs have lessened the romance that Lowell had fastened so securely on Mars. The data that are now coming in must be criticized harshly, and modern methods should be used to consider all possibilities, or we will not be on time or even live to see the day when the mysteries of Venus are resolved.

## **REFERENCES**

- Bottema, M., Plummer, W., and Strong, J., 1964a, *Astrophys. J.*, Vol. 139, No. 3.
- , ———, ———, and Zander, R., 1964b, *Astrophys. J.*, Vol. 140, No. 4.
- Menzel, D. H., and Whipple, F. L., 1955, *Publ. Astron. Soc. Pacific*, Vol. 67, p. 161.
- Tolbert, C. W., and Straiton, A. W., 1962, *J. Geophys. Res.*, Vol. 67, p. 1741.

N66 31464

## COMMENTS ON THE DETECTION OF WATER AND ICE CLOUDS ON VENUS

*Diran Deirmendjian*

*The RAND Corporation  
Santa Monica, California*

Because of circumstances, I have been unable to prepare an adequate discussion of the recent observations described by Dr. Strong. Instead I propose to comment on the detection of Venusian clouds, particularly the problems of interpretation of the data, and to suggest some additional observations that may help clarify the nature of the clouds without recourse to actual sampling.

By now it is generally agreed, I believe, that the Venusian atmosphere contains large amounts of particulate matter that appears to be in permanent suspension. This material must certainly be related to the observed planetary brightness, polarization, and spectrum, not only in the ultraviolet, visible, and infrared region, but in the near microwave region as well.

Two years ago in Liège (Ref. 1), I proposed that this particulate matter could very well be composed of the condensation products of water substance. In a subsequent article (Ref. 2) I elaborated on several lines of reasoning in support of this hypothesis, which I advanced in the face of the then current arguments favoring a

rather dry atmosphere based on the near-infrared spectra of the planet, and prior to the announcement by J. Strong and co-authors (Ref. 3) of their balloon detection of the  $\lambda$  1.13  $\mu$  H<sub>2</sub>O bands.

The more recent balloon detection, also by Strong and his collaborators (Ref. 4), of ice particles in the upper atmosphere of Venus indicates the existence of at least two phases of water substance in the atmosphere of planet. The spectroscopic detection of ice particles appears to be the only *direct* observational evidence of this kind, ever since B. Lyot's (Ref. 5) nearly 40-year-old analysis of the polarization curve in terms of water cloud droplets. If we accept the more recent evidence, the question still remains: how much water is there in the form of vapor and condensation products below the "visible" surface? I assert that this is still very much an open question.

First, let us take at face value the estimate of about 10 mg of water vapor per cm<sup>2</sup> above the "top" of the clouds, assumed to be around 100 mb, according to

the analysis of the  $\lambda$  1.13  $\mu$  observation (Ref. 3). This spectral region seems to be a good choice for the *vapor* detection since liquid water and ice show no strong absorption bands there. We then observe that the 100-mb pressure level is found at a height of about 16 km on Earth, somewhere between the levels of formation of high cirrus clouds and mother-of-pearl clouds. The deduced Venusian water vapor mixing ratios are actually *higher* than those observed for the terrestrial stratosphere above 12 km! On this basis alone, one might surmise that the amounts of atmospheric water substance on Venus and Earth are comparable. However, we note that Chamberlain (Ref. 6), has pointed out some serious uncertainties regarding the level of formation of the  $\lambda$   $\mu$  bands.

Next let us consider the evidence for the existence of ice clouds on Venus. The Johns Hopkins group (Refs. 4, 7) base their deduction mainly on a comparison of the infrared spectrum of ice clouds produced in their laboratory with those of Venus. They have not published details on the laboratory experiment.<sup>1</sup> From our knowledge of the extreme difficulties in reproducing high cirrus cloud particles in the laboratory, and the fact that the infrared optical constants of ice are known only for bulk ice, we have to qualify this kind of experimental evidence. On the other hand, a theoretical prediction of the spectrum of diffusely reflected infrared sunlight on a cloud of nonspherical ice crystals of unknown shape, size, and size distribution is even more difficult. The best kind of test at present would therefore be a comparison with directly observed spectra of actual terrestrial ice clouds under similar conditions. Fortunately, this kind of evidence has just become available.

I refer to sunlit cloud spectra taken from a high-flying aircraft over terrestrial cloud systems, a kind of observation that has only recently been carried out, despite the evident need for it. The results are so far available only in the form of an unclassified report<sup>2</sup> by H. H. Blau and R. P. Espinola (Ref. 8). The work appears to have been carefully conducted, with infrared spectra obtained with resolution as high as, or higher than, those of the balloon instrument, and the well calibrated spectra are given in absolute units and for specified angles of illumination and observation. The most interesting results, for our purposes, are the average of eight spectra of dense cirrus clouds (Ref. 8, p. 102). These are uncorrected for path absorption and solar energy density. To compare them

with the Venusian spectra, I read off the terrestrial values from the published graph and simply divided by the corresponding spectral solar constant values. The result is shown in Fig. 2. The full and dashed curves are the Venusian spectra (Refs. 4, 7), the dashed line as corrected for water vapor absorption by the authors. The dash-dot curve is the terrestrial cirrus spectrum, reduced as above, and plotted in arbitrary units so that the maximum around  $\lambda$  2.3  $\mu$  coincides with the Venusian curve. Considering this very preliminary reduction, the similarities between the terrestrial cirrus cloud and the Venusian features are striking indeed. Note in particular that a water vapor correction around  $\lambda$  1.86  $\mu$  would further improve the similarities.

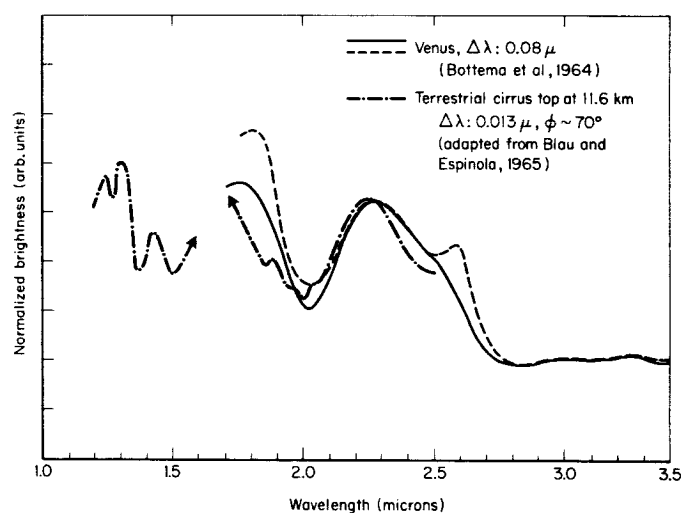


Fig. 2. Comparison of Venusian and terrestrial ice cloud spectra

Other terrestrial spectra in the report (Ref. 8), taken over dense water droplet clouds, are quite different. They show conclusively that in this case the same spectral region is dominated by the water vapor absorption bands around  $\lambda$  1.86  $\mu$ . The difference between the spectra of water clouds and those of ice clouds could be explained in terms of (1) the effects on the albedo of single scattering, (2) the absorption bands in the water or ice phase *depending on the size and size distribution of the responsible particles*, and (3) the abundance of water vapor between particles.

The remarkable thing is that this kind of differentiation between the effects of vapor absorption and particle absorption, in the case of clouds, is likely to occur only in the infrared region in question, i.e.,  $\lambda$  1.5 to 3  $\mu$ . In other words, the Johns Hopkins group, either by design

<sup>1</sup>Added in proof: See, however, R. Zander, 1966, *J. Geophys. Rev.*, Vol. 71, pp. 375-378, which appeared after this Conference.

<sup>2</sup>See, however, R. P. Espinola and H. H. Blau, 1965, *J. Geophys. Rev.*, Vol. 70, pp. 6263-6264, also published after this Conference.

or accident, chose to look at this significant part of the spectrum to obtain clear evidence of the existence of ice particles. Thus from a cursory comparison of the terrestrial and Venusian reflected spectra we can tentatively conclude that the latter represent infrared sunlight diffusely reflected by a dense, unbroken Venusian ice cloud layer. It would be hard to deduce any information on the presence or absence of a lower layer of water clouds from these data alone. I do have some suggestions on how to obtain such information.

First, allow me to make a few statements about the formation of absorption bands by scattering alone, and on cloud scattering in general. You will have to take my word for these until the appearance of detailed work, which I am in the process of preparing, on the nature of the scattering functions for various clouds, inside and outside regions of liquid water absorption.

For a given absorption band in the bulk material (water or ice):

1. The resultant absorption coefficient per particle depends very much on its relative size, the variation not being monotonic as a function of size.
2. The albedo of single scattering and hence the absorption coefficient per unit volume of polydisperse particles changes with the predominant size and the *size distribution* of the particles.
3. Multiple scattering may have two opposing effects on the intensity of an absorption band produced by scattering: In regions of strong absorption, the albedo of single scattering per unit volume is low, multiple scattering is suppressed, and the band will have essentially the central intensity given by the single-scattering process, but may show some broadening. In the region of very weak and narrow bands, the albedo of scattering is high, and multiple scattering will take place to some extent, resulting in some apparent deepening of the band at the center.
4. Since the degree of multiple scattering depends also on the available radiation, and since the scattering of infrared by cloud particles can be highly anisotropic (Ref. 9), there is also a *virtual anisotropy* in the albedo of single scattering and hence in the band shape and intensity. Therefore, for whole-disk spectra, these features will change with the planetary phase. If the disk can be resolved, there will also be a change with position on the disk.

All the remarks above apply to a hypothetical cloud with no humid air between particles; that is, the effects of water *vapor* absorption have not been mentioned. When we consider that in some regions the liquid and ice spectra are displaced with respect to the vapor spectrum, it becomes clear why it would be difficult to deduce liquid water and water vapor amounts from the spectra of sunlit clouds, without some rather sophisticated analysis. Chamberlain (Ref. 6) has recently discussed some of these difficulties in considering the problem of band formation on diffuse reflection.

As regards water droplet clouds, I have shown elsewhere (Ref. 9) that even in polydisperse clouds, certain features in the angular scattering pattern, at wavelengths where there is no absorption, are retained in the integrated single scattering phase function despite the many superpositions. Thus, for example, the cloudbow and the glory. Observation on natural clouds shows that these features are not quite suppressed by multiple scattering either, e.g., the commonly seen glories around the shadow point of aircraft overflying water clouds. I emphasize that these features are *not possible* with nonspherical particles; for example, randomly oriented prismatic ice crystals would not do. Hence, to determine whether the Venusian ice cloud overlies a lower deck of water clouds, I propose the following type of observation.

The object is to detect the glory that occurs in a ring about one degree wide and 2 to 5° radius around the subsolar point. To observe it one must have a large angular field of the medium available; in other words, it would be difficult to detect by terrestrial telescopic because the entire planet would be smaller than the feature. It is here that a flyby platform, similar to *Mariner II* and *IV*, with the planet subtending several tens of degrees rather than seconds of arc, would have a distinct advantage over terrestrial observations. It would be very easy to obtain the subsolar point and have a narrow-aperture photometer scan the area several degrees on either side. With a polarizer in two or three positions the experiment would be even more reliable since the glory has a definite polarization of opposite sign to that of the cloudbow occurring at about 38 deg from the subsolar point (Ref. 9).

As to the question of spectral region, if the visible spectrum is used, the chances of detecting the glory through an upper, optically dense, and unbroken ice cloud layer would be small. However, water-cloud glories exist also in the infrared in nonabsorbing regions. Choosing a narrow region around, say,  $\lambda$  1.6  $\mu$  or  $\lambda$  2.25  $\mu$ ,



where neither vapor nor liquid water has significant absorption bands, the chances of detecting the infrared glory are much improved, particularly in regions and at times of thinning of the Venusian ice cloud.

Such a deceptively simple experiment is well worth trying, because if any kind of glory-like phenomenon is detected, it would supply us with rather reliable evidence of the existence of water droplet clouds below the visible surface, and hence of considerable water substance in the atmosphere. If, on the other hand, the results of the experiment are negative and the existence of ice particles is confirmed, we must conclude that the Venusian ice cloud layer is optically dense in the infrared and we have to think of other methods of finding out what lies below it. We cannot think of alternate methods, however, short of actual probing of the clouds. By terrestrial analogy it is difficult to conceive a dense, unbroken ice cloud surrounding the planet without assuming a lot of water substance in the lower, denser, and warmer regions of the atmosphere.

Finally, let me refer to a recent paper by A. D. Kuzmin (Ref. 10)<sup>3</sup> which has just become available in English translation. In it the author arrives at the conclusion that the particulate matter is composed of aerosols of a polar liquid in the form of "functional derivatives of methane, ethane, and benzene." Considering the complex radiative processes in a sunlit atmosphere containing large particles, we can hardly justify his derivation of fundamental properties of the particulate substance, such as the relaxation time of the assumed organic molecules, on the basis of the observed planetary spectrum unless there are other convincing and concurring pieces of evidence. Granted that the *microwave* region could be thus interpreted, the particles must still act as strong scatterers in the visible and infrared to fit the observations.

In view of our present ignorance of the nature of the Venusian atmosphere, and as I tried to argue elsewhere (Refs. 1, 2), the assumption of water substance (including water drops measuring a few millimeters in diameter) seems to be the most logical and natural one so far, capable of explaining most observables, including the microwave brightness. Extensive and detailed model-making at this stage cannot be very productive without

more reliable data, I therefore merely sketched a tentative concept of the watery atmosphere, suggesting that an overall water content of  $10 \text{ gm cm}^{-2}$  is sufficient as a working hypothesis. I even went so far as to suggest that the existence of three distinct particulate layers would not contradict the observations: a lower, liquid water cloud with an optical thickness of the order of 100 in the visible and infrared; separated from this by a few kilometers of "clear" air, an intermediate ice cloud layer of optical thickness  $10^{-1}$  to 1 in the same spectral region; and a superior layer several tens of kilometers above the ice cloud, in what may be the coldest region of the Venusian atmosphere, with an optical thickness of  $10^{-3}$  or less in the visible, responsible for the well known elongation of the horns of Venus.

Note that the assumption of a certain number of raindrop-size water particles in suspension is an essential feature of our conceptual model (Refs. 1, 2). This assumption, by the way, could provide an alternate explanation for the apparent temperature differences between the sunlit and dark hemispheres, deduced from the microwave brightness, and between the "polar" and "equatorial" regions, deduced from the differential polarization at  $\lambda 10.6 \text{ cm}$ , recently observed by Clark and Kuzmin (Ref. 11). One merely has to consider the temporal or spatial variations in the amount of these larger hydrometeors over the planetary surface and their ability to attenuate and polarize the microwaves emitted at the surface by absorption and scattering (Ref. 12). This is without even considering hailstone-sized particles, which might very well exist under these conditions, and which would further affect the emergent microwave radiation.

In conclusion, may I reiterate my belief that it is not possible to derive the nature of the *gaseous* component of the Venusian atmosphere from the observed spectrum, brightness, and polarization alone, without definite knowledge of the nature of the *particulate* component. Along these lines, and as early as July 1960, we had submitted formal and detailed proposals to the pertinent NASA agencies for a Venus flyby photopolarimetric experiment in narrow spectral bands covering the visible through the infrared up to  $\lambda 2.5 \mu$ . A similar experiment incorporating also the glory scan outlined above should be within the capabilities of a new Venus flyby package and still worth the moderate effort involved, in view of the scientific payoff.

<sup>3</sup> See also Dr. Kuzmin's "Some Remarks Concerning the Radio-astronomical Observations of Venus" in these *Proceedings*.

## REFERENCES

1. Deirmendjian, D., 1964, in *Les Spectres Infrarouges des Astres* (paper presented at 12th International Astrophysical Colloquium, 1963), Université de Liège, pp. 397-405.
2. ———, 1964, *Icarus*, Vol. 3, pp. 109-120.
3. Bottema, M., Plummer, W., Strong, J., 1964, *Astrophys. J.*, Vol. 139, pp. 1021-1022.
4. ———, ———, ———, Zander, R., 1964, *Astrophys. J.*, Vol. 140, pp. 1640-1641.
5. Lyot, B., 1929, *Ann. Obs. Paris*, VIII, No. 1, in NASA Tech. Translation NASA TT F-187, 1964.
6. Chamberlain, J. W., 1965, *Astrophys. J.*, Vol. 141, pp. 1184-1205.
7. Bottema, M., Plummer, W., Strong, J., and Zander, R., 1965, *J. Geophys. Res.*, Vol. 70, pp. 4401-4402.
8. Blau, H. H., Jr., and Espinola, R. P., 1965, *Infrared Spectral Properties of High-Altitude Clouds*, Final Report, A. D. Little, Inc., Cambridge, Mass.
9. Deirmendjian, D., 1964, *Appl. Optics*, Vol. 3, pp. 187-196.
10. Kuzmin, A. D., 1964, *Izvestia VUZ'ov, Radiofizika*, Vol. 7, No. 6, pp. 1021-1031; (in English transl., 1965).
11. Clark, B. G., and Kuzmin, A. D., 1965, *Astrophys. J.*, Vol. 142, pp. 23-44.
12. Deirmendjian, D., 1965, *Radio Science*, Vol. 69D, pp. 893-897.

## PROPERTIES OF THE CLOUDS OF VENUS

**Carl Sagan**

*Harvard University*

*and*

*Smithsonian Astrophysical Observatory*

*Cambridge, Massachusetts*

**James B. Pollack**

*Smithsonian Astrophysical Observatory*

*Cambridge, Massachusetts*

The reflection spectra obtained from dispersed media—both clouds and powders—depend on the monochromatic single scattering albedo, the single scattering phase function, the particle size distribution, the total optical depth, and the albedo of the underlying surface. A successful analysis of observed spectra should extract most of the foregoing parameters from the observations. We now describe a method for calculating the fraction of monochromatic radiation reflected, transmitted, and absorbed by a layer of dispersed particles having arbitrary characteristics; we then apply the method to an examination of the clouds of Venus.

For wavelengths at which the cloud particles are large compared with the wavelength, the particles may scatter a very large fraction of the radiation into the forward hemisphere; in this case, isotropic scattering is a poor assumption. For expected particle sizes of dust grains,

ice crystals, or water droplets, anisotropic scattering will be important in the visible and near infrared. The appropriate equation of radiative transfer for monochromatic radiation nonconservatively and anisotropically scattered by a dispersed medium is

$$\mu \frac{dI}{d\tau} = -I + \int_{\Omega'} I p \frac{d\Omega'}{4\pi} \quad (1)$$

where  $I$  is the specific intensity,  $\tau$  the optical depth,  $\Omega'$  the solid angle,  $\arccos \mu$  the angle between the direction of propagation and the local planetary normal, and  $p$  the scattering phase function (cf., e.g., Chandrasekhar, 1950); the integration is over all solid angles. In the following discussion we will be concerned only with fluxes; i.e., with such quantities as the reflectivity integrated over all angles of incidence and reflection. Accordingly,

it is sufficient to rewrite Eq. (1) in the Schuster-Schwarzschild, or two-stream, approximation, which preserves anisotropies in flux:

$$\begin{aligned} 3^{-1/2} \frac{dI_+}{d\tau} &= -I_+ + I_+ \tilde{\omega}_0 (1 - \beta) + I_- \tilde{\omega}_0 \beta \\ -3^{-1/2} \frac{dI_-}{d\tau} &= -I_- + I_- \tilde{\omega}_0 (1 - \beta) + I_+ \tilde{\omega}_0 \beta \end{aligned} \quad (2)$$

where  $\tilde{\omega}_0$  is the single scattering albedo,  $I_+$  is the average specific intensity in the  $+d\tau$  hemisphere, and  $I_-$  is the average specific intensity in the  $-d\tau$  hemisphere. The factor  $\beta$  is a measure of the fraction of radiation singly scattered into the backward hemisphere of the incident radiation. It equals 1/2 for isotropic scattering and about 1/15 for ice crystals  $\sim 10 \mu$  in radius and for visible radiation;  $\beta$  is related to other scattering parameters below. Note in Eqs. (2) that the backward hemisphere is in the  $-d\tau$  direction for  $I_+$ , but in the  $+d\tau$  direction for  $I_-$ . The factor  $3^{-1/2}$  in Eqs. (2) represents the appropriate average value of  $\mu$  in the two-stream approximation (Chandrasekhar, 1950).

Equations (2) are two coupled, linear, first-order differential equations with constant coefficients and may be solved in closed form by well-known techniques. Let  $\mathcal{A}$ ,  $\mathcal{R}$ , and  $\mathcal{T}$  be, respectively, the fraction of the incident radiation absorbed, reflected, and transmitted by the dispersing medium. For the boundary condition of negligible surface albedo, the solution of Eqs. (2) is

$$\mathcal{R} = \frac{(u + 1)(u - 1) [\exp(\tau_{eff}) - \exp(-\tau_{eff})]}{(u + 1)^2 \exp(\tau_{eff}) - (u - 1)^2 \exp(-\tau_{eff})} \quad (3)$$

$$\mathcal{T} = \frac{4u}{(u + 1)^2 \exp(\tau_{eff}) - (u - 1)^2 \exp(-\tau_{eff})} \quad (4)$$

$$\mathcal{A} = 1 - \mathcal{R} - \mathcal{T} \quad (5)$$

where

$$u^2 = \frac{1 - \tilde{\omega}_0 + 2\beta\tilde{\omega}_0}{1 - \tilde{\omega}_0} \quad (6)$$

and

$$\tau_{eff} = 3^{1/2} u(1 - \tilde{\omega}_0) \tau_1 \quad (7)$$

In Eq. (7),  $\tau_1$  is the total interaction optical depth of the clouds; i.e.,  $\exp(-\tau_1)$  represents the fraction of the incident radiation which experiences neither absorption nor scattering during its traverse of the clouds; when the average particle size exceeds the wavelength, it is a wavelength-independent quantity. When the average particle size is smaller than the wavelength,  $\tau_1$  generally decreases with increasing wavelength. Equations similar to Eqs. (3)–(7) have been obtained previously by Neiburger (1949), who used, however, a factor of 1/2 for the average value of  $\mu$  in Eqs. (2). The factor  $\beta$  takes account of the marked forward-to-backward asymmetry of the phase function.

We now compare our approximate solutions (3) and (4) with exact solutions in a variety of limiting cases. As we have already emphasized, our calculations refer to flux ratios, averages of the specific intensity over all angles of incidence and all angles of reflection. These flux ratios will be related to the actual observations of Venus—which are, of course, not integrated over all angles—below. To exhibit the functional form of the averaging more explicitly, we first consider the fraction of sunlight transmitted and the fraction reflected from the sunlit hemisphere of the planet. The latter is the Russell-Bond albedo. Let  $I_+(\mu, \phi; \mu_0, \phi_0; \tau_1)$  be the specific intensity directed downward at the bottom of the clouds when sunlight falls from the direction  $(\mu_0, \phi_0)$ . Then the flux of sunlight transmitted through a unit area of cloud tilted in the direction  $(\mu_0, \phi_0)$  to the solar beam is given by

$$\mathcal{T}_+(\mu_0, \phi_0; \tau_1) = \int I_+(\mu, \phi; \mu_0, \phi_0; \tau_1) \mu d\Omega \quad (8)$$

The total power of sunlight transmitted through the clouds is the integral of Eq. (8) over the illuminated hemisphere. The transmissivity is then obtained by dividing by the power of sunlight incident. Thus,

$$\mathcal{T} = \frac{\int \mathcal{T}_+(\mu_0, \phi_0; \tau_1) R^2 d\Omega_0}{\pi F \pi R^2} \quad (9)$$

where  $\pi F$  is the flux of incident sunlight passing through a unit area oriented normal to the beam, and  $R$  is the planetary radius. A similar equation holds for the reflectivity  $\mathcal{R}$  and the absorptivity  $\mathcal{A}$ .

In a second case of interest, infrared radiation is emitted by a hot opaque atmosphere below the clouds and is incident on the cloud bottoms. If we adopt an appropriate angular average of the emitted intensity we derive just the same equation—Eq. (9) and its reflectivity and absorptivity analogues—as in the case of incident sunlight.

Employing Eq. (9), we first compare our results with an exact solution for a limiting case of special interest. Piotrowski (1956) has obtained  $\mathcal{I}_+(\mu_0, \phi_0; \tau_1)$  for the special case  $\tilde{\omega}_0 = 1$  and  $\exp[-\tau_1/\mu_0] \ll 1$ . When his solutions are introduced into Eq. (9), we find

$$\mathcal{I} = \frac{1.33}{\tau_1 (1 - \frac{1}{3} \tilde{\omega}_1) + 1.42} \quad (10)$$

where  $\tilde{\omega}_1$  is the coefficient of the Legendre polynomial of first order in a Legendre polynomial expansion of the scattering phase function. For isotropic scattering, Eq. (10) reduces to the result obtained by van de Hulst (1964), employing different methods, for large  $\tau_1$ .

In the same limiting cases that Piotrowski has used, our Eq. (4) reduces to

$$\mathcal{I} = \frac{1.16}{2\beta\tau_1 + 1.16} \quad (11)$$

Because of the difficulty in obtaining appropriate angular averages directly from the Schuster-Schwarzschild approximation, we will infer the relation between  $\beta$  and  $\tilde{\omega}_1$  directly from a comparison of Eqs. (10) and (11). The comparison is constrained by the boundary condition that  $\beta = 1/2$  for the isotropic case  $\tilde{\omega}_1 = 0$ . We then infer

$$2\beta \simeq 1 - \frac{1}{3} \tilde{\omega}_1 \quad (12)$$

To assess the accuracy of our approximations, Eqs. (3)–(7) and Eq. (12), we now compare our results with exact solutions for five special cases, and with two categories of laboratory results. Just as in the preceding discussion, we employ Eq. (9)—or its analogue for  $\mathcal{A}$ —to perform angular averages of known solutions. The results of the comparison—for Rayleigh scattering; for conservative isotropic scattering; for isotropic scattering with infinite optical depth; for the phase function  $p = \tilde{\omega}_0 (1 + \cos \Theta)$  with infinite optical depth; and for the case  $\exp(-\tau_1) \ll 1$  with conservative scattering—are presented in Table 1. This comparison shows that our approximate formulae are accurate to 5 or 10% in

absolute value, and a few percent in relative value. Further, the comparison of Table 1 provides us with correction factors which reduce still further the error in absolute value.

An empirical justification of our approach is given by the good fit of the theoretical reflectivity curves with the corresponding laboratory measurements for ice. This correspondence is displayed in Figs. 3 and 4, and is discussed more fully below.

If the real and imaginary parts of the index of refraction are known for a given material,  $\tilde{\omega}_0$  and  $\tilde{\omega}_1$  can be obtained from Mie scattering calculations. Dr. William Irvine has kindly supplied us with exact values of  $\tilde{\omega}_0$  and  $\tilde{\omega}_1$ , obtained with an IBM 7094 for spherical ice crystals in the 0.2 to 150  $\mu$  wavelength interval (cf Irvine, 1965). The coefficients of the zeroth and first-order Legendre polynomials are functions of both particle radius  $a$  and wavelength  $\lambda$ . When  $a \gg \lambda$ , we find that the exact Mie theory solution for this single scattering albedo is represented to sufficient accuracy by

$$\tilde{\omega}_0 = \frac{1}{2} + \frac{1}{2} \exp(-2k_\lambda a) \quad (13)$$

where  $k_\lambda$  is the volume absorption coefficient of the particle. This equation has physical significance. The first term represents the diffraction part of the scattering, and the exponential factor represents the fraction of radiation that is absorbed while traversing the particle. The geometry of the particle enters only as the coefficient of  $k_\lambda a$  in the exponential, and it is clear that substantially similar results will apply for nonspherical particles as well.

Equation (13) permits us to compare theory and observation for the limiting case  $\tilde{\omega}_0 = 1/2$ . The observed albedo will be a function of  $\tau_1$ , of  $\tilde{\omega}_0(a)$ , and of  $\beta(a)$ . In the 3–3.4  $\mu$  region there is a very strong water absorption band in the spectrum of ice. We therefore expect, from Eq. (13), that  $\tilde{\omega}_0 = 1/2$  at these wavelengths; for any appreciable thickness of ice crystals we also expect  $\tau_1 \rightarrow \infty$ . Thus the albedo will be a function of  $\beta(a)$  alone. In this wavelength range,  $\tilde{\omega}_0$  is varying much more rapidly than  $\tilde{\omega}_1$ . If we adopt the Mie theory value for  $\tilde{\omega}_1$  for spherical ice crystals (where  $a$  is within an order of magnitude of 10  $\mu$ ), use Eq. (12) to obtain  $\beta$ , and insert in Eq. (3), we reproduce the value of the albedo measured in the laboratory at 3–3.4  $\mu$ . This exercise is a test of Eq. (12) and an example of the applicability of Mie theory for spherical particles to other shaped particles—the laboratory ice crystals are probably hexagonal prisms—in problems involving fluxes.

Table 1. Comparison of the approximations of the present paper with exact solutions of the transfer equation

Rayleigh scattering (Coulson, 1959) <sup>a</sup>			Conservative isotropic scattering (Chandrasekhar, 1950) <sup>a</sup>			Isotropic scattering, $\tau_1 = \infty$ (Goody, 1964) <sup>a</sup>			$P = \tilde{\omega}_0 (1 + \cos \Theta)$ $\tau_1 = \infty$ (Goody, 1964) <sup>a</sup>			$e^{-\tau_1} < 1$ $\tilde{\omega}_0 = 1$ (Piotrowski, 1956) <sup>a</sup>			
$\tau_1$	$\mathcal{I}$ exact	$\mathcal{I}$ approx	$\tau_1$	$\mathcal{I}$ exact	$\mathcal{I}$ approx	$\tilde{\omega}_0$	$\mathcal{A}$ exact	$\mathcal{A}$ approx	$\tilde{\omega}_0$	$\mathcal{A}$ exact	$\mathcal{A}$ approx	$\tilde{\omega}_1/3$	$\tau_1$	$\mathcal{I}$ exact	$\mathcal{I}$ approx
0.05	0.955	0.959	0.05	0.955	0.959	0.1	0.021	0.026	0.1	0.013	0.018	0.0	20	0.0620	0.0548
0.10	0.916	0.921	0.10	0.916	0.921	0.5	0.147	0.172	0.5	0.104	0.127	0.7	20	0.179	0.162
0.15	0.881	0.886	0.15	0.881	0.886	0.9	0.479	0.520	0.9	0.409	0.451	0.9	20	0.388	0.367
0.20	0.849	0.853	0.20	0.849	0.853	0.975	0.695	0.727	0.975	0.641	0.677				
0.25	0.820	0.822	0.25	0.820	0.822										
0.50	0.704	0.699	0.50	0.704	0.699										
1.00	0.552	0.537	1.00	0.552	0.537										

<sup>a</sup>Source of the exact solution below.

<sup>a</sup>Source of the exact solution below.

Having discussed the application of our approximations to a case where  $\omega_0 = 1/2$ , we now discuss an application to the opposite extreme,  $\omega_0 = 1$ . Both Rayleigh scattering and conservative isotropic scattering are independent of  $\omega_1$ . However, Rayleigh scattering shows a functional dependence on  $\omega_2$  which conservative isotropic scattering does not. For  $\omega_0 = 1$  and the same value of  $\tau_1$ , we expect, from Eqs. (12) and, e.g., (4), that the transmissivity should be independent of  $\omega_2$ . Comparison of the exact solutions for Rayleigh scattering and for conservative isotropic scattering in Table 1 shows the identity of  $\mathcal{T}$  for these two scattering functions. Thus, the approximations remain valid in this example of vanishing  $\omega_1$  and small optical depth. Because of the success of our approximations in such a wide range of cases, we have some confidence in applying them to Venus.

The quantities  $\mathcal{R}$ ,  $\mathcal{T}$ , and  $\mathcal{A}$ , as given by Eqs. (3)–(5), refer to ratios of fluxes, and, as such, contain no information on the angular variation of reflected or transmitted specific intensities. The quantity  $\mathcal{R}$ , for example, corresponds to the Russell-Bond spherical albedo. Fortunately, however, Russell's phase law implies that the reflectivity of a planet at phase angle  $50^\circ$  is a fixed constant times the Russell-Bond albedo; the constant is very closely independent of the phase law for the albedo (see, e.g., de Vaucouleurs, 1964). Thus the ratio of the reflectivities for two wavelengths at phase angles near  $50^\circ$  is equal to the ratio of the Russell-Bond albedos for these wavelengths. This circumstance allows us to apply Eq. (3) to relative albedo measurements made near phase angle  $50^\circ$ , or, alternatively, to obtain the Russell-Bond albedo at a desired wavelength,  $\lambda_1$ , from the Russell-Bond albedo at another wavelength,  $\lambda_2$ , and a measurement of the ratio of the albedos at  $\lambda_1$  and  $\lambda_2$  measured near phase angle  $50^\circ$ .

Observations of Venus by Moroz (1964) and by Bottema et al. (1965) strongly suggest that the Cytherean clouds are composed of ice crystals, a suggestion made earlier (Sagan, 1961) on other grounds. Excluding for the moment the wavelength interval around  $2.0 \mu$  where the correction for Cytherean  $\text{CO}_2$  is rather uncertain, several features have been observed that are diagnostic for ice: a stepwise decrease of albedo from 1.2 to 1.8 to  $2.3 \mu$ ; a very sharp decline from  $2.3$  to about  $3.2 \mu$ ; and relative maxima at 1.8 and  $2.3 \mu$ . At all these wavelengths gaseous absorption by  $\text{CO}_2$  and  $\text{H}_2\text{O}$  in or above the Cytherean clouds can be neglected; these reflectivity measurements must pertain to the clouds. The identification of the clouds with ice is further supported by Bottema et al.'s (1965) excellent match of the observations with the re-

flectivity of an ice cloud produced in the laboratory. Both the observations of Moroz and those of Bottema et al. were made near phase angle  $50^\circ$ .

These identifications do depend on the assumption that appropriate allowance for the effects of overlying absorption have been made. We now examine this contention in somewhat more detail. Between  $3.0$  and  $3.4 \mu$ , and between  $2.2$  and  $2.5 \mu$ , there is little  $\text{CO}_2$  or water vapor absorption; these segments of the spectra observed by Bottema et al. can be accepted as intrinsic to the clouds, with little reservation. The correction for  $\text{H}_2\text{O}$  vapor near  $1.8 \mu$  can be checked against the work of Moroz (1964), who observed between  $1.7$  and  $1.8 \mu$  and also near  $2.3 \mu$  where there is little gaseous absorption. Moroz' ratio of  $1.8$  to  $2.3 \mu$  albedos agrees with the determination of Bottema et al. This check on the water vapor correction performed by Bottema et al. near  $1.8 \mu$  lends support for the similar correction they performed between  $2.5$  and  $2.65 \mu$ .

The primary remaining ambiguity lies in the region around  $2.0 \mu$ , where absorption by Cytherean  $\text{CO}_2$  is expected. Kuiper's (1962) ground-based near-infrared spectra, performed with a resolution much superior to that of Bottema et al., exhibit prominent carbon dioxide bands at  $1.6 \mu$ . If they originate at about the same atmospheric level as the  $1.6 \mu$  bands, the  $2.0 \mu$   $\text{CO}_2$  bands should appear even stronger in the Venus spectrum. Along with the neighboring hot and isotopic bands, it is possible that they account for the minimum observed near  $2.0 \mu$  by both Kuiper and Bottema et al. On the other hand it is difficult to exclude the possibility that the observed  $2 \mu$  minimum is partially due to carbon dioxide absorption and partially due to a lower intrinsic reflectivity of the clouds. Such a lower reflectivity implies that the  $2 \mu$   $\text{CO}_2$  absorption takes place at higher altitudes than would otherwise be the case.

However, even if we exclude the region around  $2.0 \mu$ , the fit of the laboratory ice cloud to the Cytherean spectrum is very impressive. Both clouds are produced by atmospheric saturation in the presence of condensation nuclei; the detailed correspondence in the wavelengths of dips and rises and in the overall shape of these spectra denotes detailed agreement, not only in the indices of refraction, but also in the particle size distributions of the Venus and the laboratory particles. The influence of size and composition on the reflection spectrum will be discussed below, where we show that several independent methods for determining the mean particle radius from the observations yield very similar results, provided the

clouds are assumed to be composed of ice. In summary, there appears to be good evidence that the clouds of Venus are composed of ice.

The interaction optical depth of the clouds,  $\tau_1$ , can be found from the Venus albedo in the 4000 to 13,000 Å interval. In this wavelength range, the albedo is found to have a high, nearly constant value (Sinton, 1963; Yessipov and Moroz, 1963; Moroz, 1964). These observations are remarkable, because in the same wavelength interval, the absorption coefficient of ice, water, and most other materials is changing by many orders of magnitude. The results can be understood only if  $\omega_0$  is sufficiently close to unity that the cloud albedo is controlled only by  $\tau_1$ ; e.g., a change in  $\omega_0$  from 0.9999999 to 0.99999 would then have little influence on the observed albedo, while a change from 0.99 to 0.50 would have a major influence (see Eqs. 3, 6, and 7, for the case of slowly varying  $\beta$ ). The deduction that  $1 - \omega_0 \ll 1$  at these wavelengths is supported by the values of  $\omega_0$  deduced either from Mie theory or from Eq. (9) for particles in the expected size range. From Eqs. (3), (6), and (7) and the Mie theory values of  $\beta$ , we obtain a value of  $\tau_1$  for Venus between 18 and 43; the uncertainty in  $\tau_1$  is chiefly a consequence of the observational error in the visible and near-infrared cloud albedo. These values of  $\tau_1$  are much larger than the values that would have been obtained for isotropic scattering ( $\beta = 1/2$ ) from the same albedo observations. The difference illustrates the highly forward scattering behavior of ice crystals at these wavelengths.

At longer wavelengths, the single scattering albedo decreases significantly below unity and becomes the dominant factor in Eq. (3). There is then little dependence of overall reflectivity on  $\tau_1$ , since the derived values of  $\mathcal{R}$  are close to the values for a semi-infinite cloud layer. Through Eq. (9), we can then extract from the observations several independent estimates of the mean particle radius  $\bar{a}$ .

We obtain  $\bar{a}$  from (1) the absolute value of the albedo at 2.5  $\mu$ ; (2) the ratio of the albedos at 1.2 and 1.75  $\mu$ ; and (3) the relative albedo variation between 1.75 and 3.4  $\mu$ . The observational value of the Russell-Bond albedo at 2.5  $\mu$  was obtained from the Russell-Bond albedo at 0.55  $\mu$  (Sinton, 1963), the albedo ratio near 50° phase angle of observations at 0.55 and 2.2  $\mu$  (Moroz, 1964), and the albedo ratio near 50° phase angle of observations at 2.2 and 2.5  $\mu$  (Bottema et al., 1965). The observed albedo ratio at 1.2 and 1.75  $\mu$  was obtained from Moroz' (1964) data. Comparisons of theory and observation are provided for the first two methods in Table 2, and, for the

**Table 2. Comparison of theoretical and observed values of the albedo of Venus**

Mean particle radius, $\mu$	A (2.5 $\mu$ )		A (1.75 $\mu$ )/A (1.2 $\mu$ )	
	$\tau_1 = 18$	$\tau_1 = 43$	Minimum $\tau_1$	Maximum $\tau_1$
	Theoretical values			
1	0.41	0.56	0.980	0.958
2	0.61	0.64	0.967	0.933
4	0.51	0.52	0.944	0.894
6	0.44	0.44	0.903	0.832
7.5	0.39	0.40	0.862	0.7
10	0.32	0.32	0.816	0.728
12.5	0.27	0.27	0.773	0.684
15	0.24	0.24	0.737	0.650
20	0.19	0.19	0.666	0.589
	Observed value			
	$0.34 \pm 0.05$		$0.81 \pm 0.04$	

NOTE: Minimum  $\tau_1$  and maximum  $\tau_1$  are the minimum and maximum values for  $\tau_1$  implied by the 0.4 to 1.3  $\mu$  albedo for a given particle size. For  $\bar{a} = 7.5 \mu$ , the values are  $\tau_1 = 18$  and 43. For other particle sizes, the values of  $\tau_1$  are slightly different.

third, in Figs. 3 and 4. In the figures, the region near 2.3  $\mu$  carries little weight, because  $k_\lambda$  is relatively poorly known in this low-absorptivity region. We see from the table and the figures that all three methods yield a mean particle radius for ice crystals,

$$7.5 \mu \leq \bar{a} \leq 10 \mu \quad (14)$$

The mutual agreement of the results of these independent methods supports the identification of ice as the principal constituent of the clouds of Venus. Even liquid water differs significantly from ice in its values of  $k_\lambda$ . Bound water of crystallization should exhibit even larger deviations in absorption coefficient; and while dust containing water of crystallization will exhibit some similarities in reflectivity with ice, a detailed agreement is not to be expected.

Our estimates of  $\bar{a}$  are compatible with the values of  $\bar{a} \simeq 1 \mu$  found from polarization measurements (Dollfus, 1961). We believe the difference in values of  $\bar{a}$  can be attributed to two causes. First, the weighting function in the averaging over the particle size distribution to derive



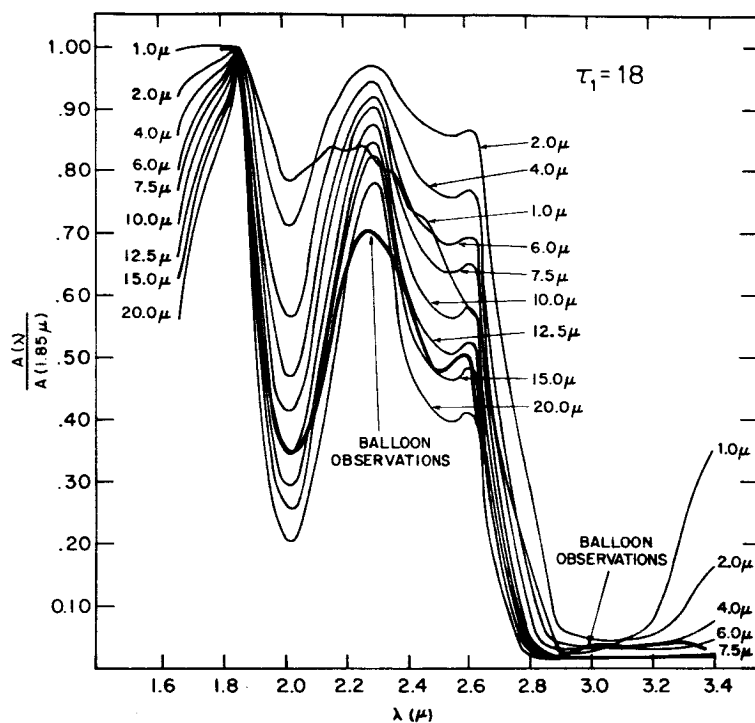


Fig. 3. Comparison of theoretical and observed normalized infrared reflectivities of Venus for particle radii 1–20  $\mu$  and  $\tau_1 = 18$

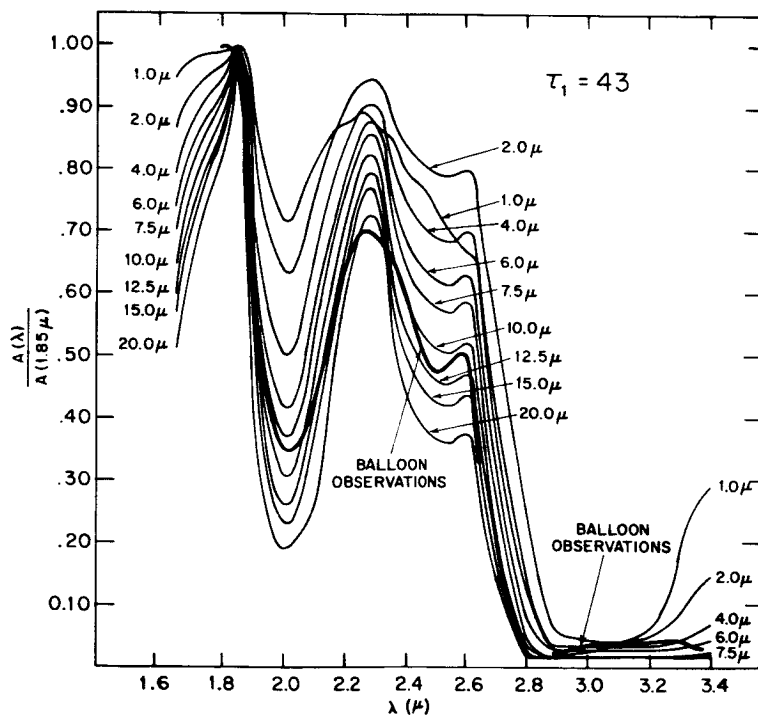


Fig. 4. Comparison of theoretical and observed normalized infrared reflectivities of Venus for particle radii 1–20  $\mu$  and  $\tau_1 = 43$

$\bar{a}$  is different for polarization than for reflectivity and will lead to more of the small end of the distribution function being sampled during polarization measurements. Secondly, since multiple scattering depolarizes, the polarization measurements refer chiefly to photons scattered once, or at most a small number of times. If there is any tendency for particle size sedimentation in the Cytherean clouds, the polarization measurements will refer to higher levels in the clouds, where mean particle sizes are smaller than they are at the levels probed by reflectivity measurements.

The location of relative maxima and minima in the spectra of Bottema et al. (1965) also permits a crude estimate of temperature to be derived. The balloon observations unambiguously show relative maxima at wavelengths of approximately 1.82 and 2.28  $\mu$ . These peaks correspond well to minima in  $k_\lambda$ , and, therefore, maxima in  $\omega_0$  for ice crystals, but are distinctly longward of the corresponding peaks for liquid water (1.67 and 2.22  $\mu$ ) at room temperature. But temperature declines will shift both minima and maxima to longer wavelengths. Thus we may conclude that the observed albedo is a consequence of multiple scattering in regions of the Cytherean clouds that were below 0°C, in agreement with the expected thermometric temperatures of the clouds (Pollack and Sagan, 1965).

The foregoing estimates of composition,  $\tau_1$ , and  $\bar{a}$  permit us to determine the optical properties of the clouds at all wavelengths. We find that between 20 and 50% of the sunlight absorbed by the planet reaches the surface; the remainder of the absorbed sunlight is accounted for in approximately equal parts by the clouds and by the

underlying atmosphere. Owing to absorption by water vapor and carbon dioxide and to the high surface pressures and temperatures, the Venus atmosphere is fairly opaque beyond 1  $\mu$ . The clouds have an enormous opacity beyond 2.65  $\mu$ . Because they are poorly absorbing and anisotropically scattering in the visible and photographic infrared, but strongly absorbing and almost isotropically scattering at longer wavelengths, the clouds provide the additional differential opacity required to establish an effective greenhouse effect and maintain surface temperatures  $\sim 700^\circ\text{K}$  (cf. Sagan, 1960; Ohring and Mariano, 1964). The clouds serve chiefly by plugging holes in the principal atmospheric infrared windows. The value of the surface temperature is determined by the height of the ice clouds in the convective Cytherean atmosphere; this height depends, in turn, on the total atmospheric water vapor content. Our calculations show that the cloud bottoms have a quantity of supercooled water droplets ( $\sim 0.1 \text{ g cm}^{-2}$ ) too small to influence the reflection spectrum significantly, but adequate to account for the general features of the millimeter-wavelength spectrum of Venus. These and related consequences of the water clouds of Venus are discussed in greater detail elsewhere (Sagan and Pollack, 1966).

### Acknowledgments

We are very grateful to Dr. William Irvine for providing us with Mie theory solutions for ice and water under a variety of assumed conditions; to Dr. John Strong for a discussion of his laboratory observations; and to Mrs. Elinore Green for assistance with the calculations. The final phases of this investigation were supported by NASA grant NGR 09-015-023.

### REFERENCES

- Bottema, M., Plummer, W., Strong, J., and Zander, R., 1965, *J. Geophys. Res.*, Vol. 70, pp. 4401–4402.
- Chandrasekhar, S., 1950, *Radiative Transfer*, Oxford University Press, London.
- Coulson, K. L., 1959, *Planet. Space Sci.*, Vol. 1, pp. 277–284.
- Dollfus, A., 1961, "Polarization Studies of Planets," *Planets and Satellites*, ed. by G. P. Kuiper and B. M. Middlehurst, Univ. of Chicago Press, Chicago, pp. 343–399.
- Goody, R. M., 1964, *Icarus*, Vol. 3, pp. 98–102.

## REFERENCES (Cont'd)

- Irvine, W. M., 1965, *J. Opt. Soc. Am.*, Vol. 55, pp. 16-21.
- Kuiper, G. P., 1962, *Communications of the Lunar and Planetary Laboratory*, Univ. of Arizona, Vol. 1, pp. 83-118.
- Moroz, V. T., 1964, *Soviet Astron.-AJ*, English Transl., Vol. 7, pp. 109-115.
- Neiburger, M., 1949, *J. Meteorol.*, Vol. 6, pp. 98-104.
- Ohring, G., and Mariano, J., 1964, *J. Geophys. Res.*, Vol. 69, pp. 165-175.
- Piotrowski, S., 1956, *Acta Astronomica*, Vol. 6, pp. 61-73.
- Pollack, J. B., and Sagan, C., 1965, *J. Geophys. Res.*, Vol. 70, pp. 4403-4426.
- Sagan, C., 1960, *The Radiation Balance of Venus*, Technical Report No. 32-34, Jet Propulsion Laboratory, Pasadena, California.
- Sagan, C., and Pollack, J. B., "On the Nature of the Clouds and the Origin of the Surface Temperature of Venus," to be published.
- Sinton, W. M., 1963, in *The Physics of the Planets*, Proceedings XI International Astrophysical Colloquium, Liège, Belgium, pp. 300-310.
- van de Hulst, H. C., 1964, *Icarus*, Vol. 3, pp. 336-341.
- de Vaucouleurs, G., 1964, *Icarus*, Vol. 3, pp. 187-235.
- Yessipov, V. F., and Moroz, V. I., 1963, *An Attempt at Spectrophotometry of Venus and Mars in the Interval 7000-10,000 Å*, Astron. Tsirkulyar No. 262 (in Russian).

N66 31466

## VENUS RADAR INVESTIGATIONS

Duane O. Muhleman\*

*Jet Propulsion Laboratory,  
Pasadena, California*

Echoes from the surface of Venus were first detected by groups at JPL and Lincoln Laboratory in the spring of 1961. Since that time Venus has been faithfully observed radarmetrically at all times when detection was possible by the JPL group. Considerable information has been obtained from the data concerning the motion and rotation of the planet, the scattering properties of its surface, and the nature of the surface material itself. I shall review these results in this paper.

### **1. The Motion of Venus and the Astronomical Unit**

The motion of Venus relative to that of the Earth is well described by planetary theory, particularly in the work of Newcomb. As is well known, the position of Venus may be found by reference to the Fundamental Ephemerides of Venus and the Earth contained in Newcomb's Tables. These tables allow one to determine the angular coordinates of the planet and distances expressed in astronomical units. The tables were constructed by a theoretical study of all the major bodies

of the solar system in conjunction with the empirical determination of the parameters of the theory from angular observations. The accuracy of the table depends on the mathematical integrity of the theory and the quality of the observations. If the tables were precise the astronomical unit could be determined by measuring the distance between the Earth and Venus in laboratory units such as light seconds or kilometers, a task best carried out with radar. Since the distance in AUs would be precisely determined by the tables, the unit of length is easily determined from a measurement of radar distance or velocity.

However, the tables are not precise. A comparison of the distance or velocity in astronomical units with the radar measurements yields different values of the AU at different times. Consequently, the AU can only be determined after the tables have been corrected with new observations and/or theory. It can be shown that the radar observations themselves, taken over a long arc, can simultaneously correct the ephemerides and yield an estimate of the AU. This is a long and laborious task. Our results to date are shown in Table 3. The determinations

---

\*Now at the Department of Astronomy, Cornell University.

**Table 3. Astronomical unit determinations from radar observations of Venus<sup>a</sup>**

Source of data	AU, km	Other parameters
		$\pi_{\oplus}$ , sec
Good radar methods <sup>b</sup> (1961)		
Muhleman et al.	149,598,640 $\pm$ 250	8.7941379 $\pm$ .000015
Pettengill et al.	149,597,850 $\pm$ 400	8.7941849 $\pm$ .000026
Muhleman (revision of Pettengill's value)	149,598,100 $\pm$ 400	8.7941705 $\pm$ .000026
Marginal radar methods (1961)		
Thomson et al.	149,601,000 $\pm$ 500	
Maron et al.	149,596,000	
Kotelnikov	149,599,500 $\pm$ 400	
USSR (1964) (Kotelnikov)	149,598,000 $\pm$ 400	
		$L_{\odot}$ , sec of arc
Complete parameter solutions <sup>c</sup>		
JPL doppler ('61, '62, '64)	149,598,106 $\pm$ 18	0.86
JPL range ('62, '64)	149,598,333 $\pm$ 10	0.95
JPL doppler and range	149,598,388 $\pm$ 5	0.94
JPL doppler, range, and optical (1934-1949)	149,598,439 $\pm$ 5	0.96

<sup>a</sup> $c = 299,792.5$  exactly.

<sup>b</sup>Good radar methods are those that were used to observe Venus over a sufficiently long arc to remove the major part of the errors of the ephemerides.

<sup>c</sup>Simultaneous solution for AU and corrections to the orbital parameters of the Earth and Venus.

in 1961 were, of course, limited to a short arc and yield somewhat discordant results. However, my present work utilizes the JPL observations from 1961 through 1965 and a stable solution is beginning to appear (the lower part of Table 3. The major error in the ephemerides is in the longitude of Venus relative to that of the Earth,  $L_{\odot}$ , which appears to amount to  $\Delta L_{\odot} \simeq 0.95$ . Corrections to almost all of the orbital parameters of the two bodies have been found, but will not be reported here. The best estimate of the AU is apparently

$$149,598,439 \pm 10 \text{ km}$$

based on  $c = 299,792.5$  exactly. The uncertainty is a formal mathematical result and undoubtedly is at least a factor of 10 too small.

The precise determination of the AU and the orbital elements for the Earth is hardly an academic matter, since precise interplanetary guidance and proposed checks on the general theory of gravitation demand an exact knowledge of the position and motion of the Earth.

## II. Basic Radar Concepts

I believe that it will greatly aid in understanding all the radar discussions of this symposium if I present the fundamental ideas of planetary radar techniques. The radar approach derives its power from its ability to almost completely control the illuminating radiation. This is done, of course, with modulation techniques; a particular scheme of modulation, or coding, being appropriate for a particular experiment. The possibilities range between no modulation at all (CW) to very narrow pulses of width on the order of microseconds. The response of a planet to a narrow pulse is most easily understood and is illustrated in Fig. 5. At a time  $\tau$  after the pulse has encountered the sub-Earth point, the pulse has illuminated an annulus of width  $d\Omega$  in a time increment  $d\tau$  at an angle of incidence  $\Omega$ . Thus the shape of the elongated returned pulse is a direct measure of the backscatter characteristics of the surface as a function of incidence angle. The measured pulse shape is called the backscatter function.

If the planet is illuminated with a pure CW signal, the rotation of the body will spread the signal in frequency,

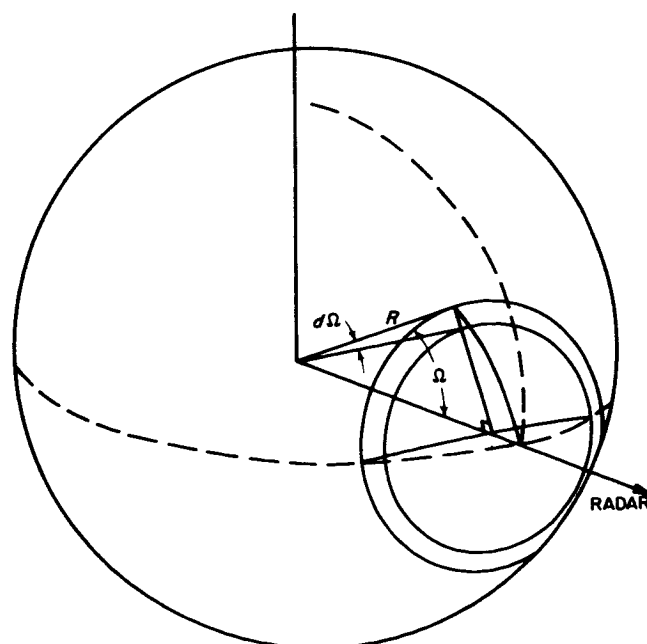


**Fig. 5. Geometry for the planetary pulse response**

creating the CW spectrum. The geometry is illustrated in Fig. 6. The points of constant doppler shift form a semicircle centered on the instantaneous axis perpendicular to the plane formed by the rotation vector and the vector to the radar. Thus, the doppler spectrum is a map of the returned power as a function of equatorial angle for the illumination integrated at angles of incidence from  $\Theta$  to  $\pi/2$ . The CW spectrum is related to the backscatter function by an integral equation and they are equivalent.

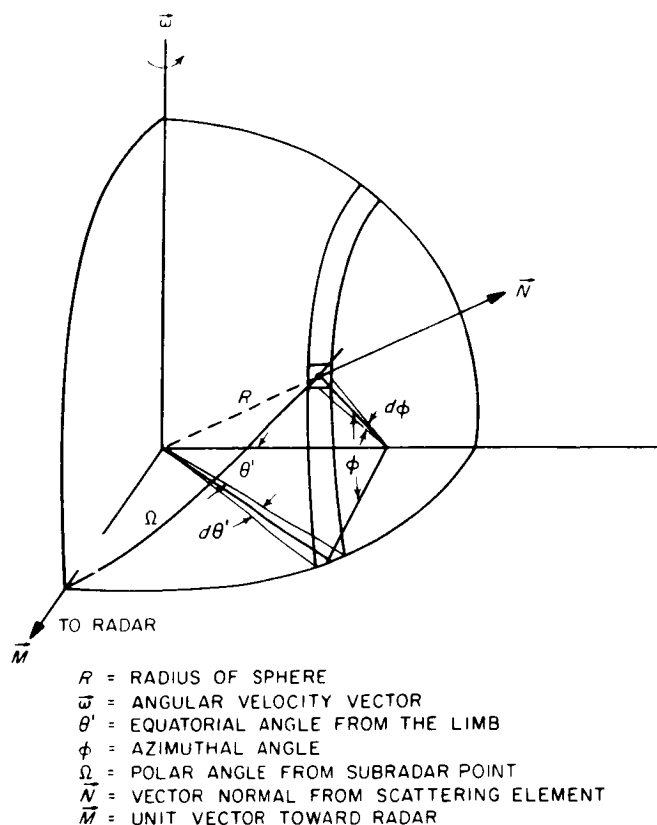


**Fig. 6. Geometry for the planetary continuous-wave response**

In practice, the pulses have finite width and the spectra are measured to a finite frequency resolution. Thus, convolutions with the surface are involved.

If the spectrum and pulse response are measured simultaneously (through modulation techniques) we get the doppler-range maps as shown in Fig. 7. The power at any one frequency on a given spectrum of the set is a measure of the echo from the region corresponding to the intersection of the corresponding range annulus and doppler strip. Resolution on the order of tens of kilometers has been obtained for Venus in this way.

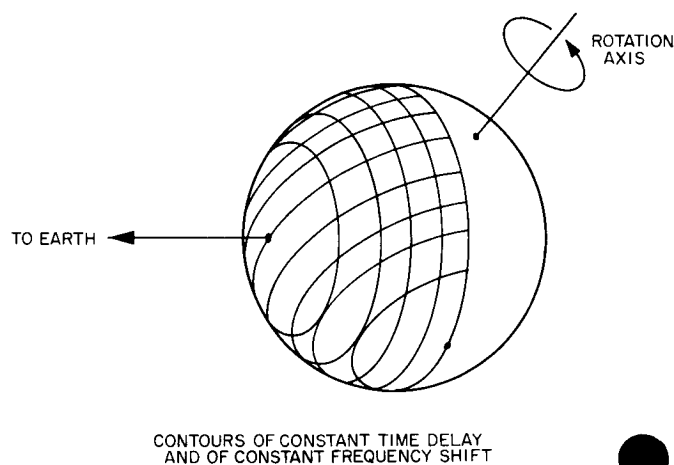


**Fig. 7. Geometry for the simultaneous response in doppler and range**

### III. Power Reflectivity

The power reflectivity is defined as the ratio of the CW power received from the planet to the power that would be received from an equivalent smooth conducting sphere with the same geometry. It is a difficult quantity to measure on an absolute scale since the uncertainties of all of the radar parameters enter, particularly the antenna gain. Published values of the reflectivity are listed in Table 4.

Except for the value at 3.6 cm, the data suggest little if any variation over wavelength. The most reliable results are those at 12.5, 23, and 70 cm, all of which are in excellent agreement. The hypothesis has been put forward by the MIT group (Morrow, 1964) that the very

**Table 4. Published reflectivity values**

Wavelength, cm	Reflectivity, %	Conjunction
3.6 (MIT)	$0.9 \pm 0.3$	1964
12.5 (JPL)	$11 \pm 3$	1961
	$9.5 \pm 2$	1962
	$12.0 \pm 1$	1964
23 (MIT)	13.0	1964
43 (USSR)	12-18	1962
	19	1964
68 (MIT)	10	1961
70 (AIO)	14	1964
6 m (NBS)	20	1962
7.8 m (MIT)	20	1964

low reflectivity at 3.6 cm is due to absorption in the Venusian atmosphere. It is not clear as yet whether or not such an explanation is consistent with the microwave emission observed at that wavelength. I will return to this subject in the section on the backscatter behavior of Venus. The radio brightness temperature of Venus shows a clear indication of falling off in the meter region (Drake, 1965). If the decrease in emission at the long wavelengths is due to surface phenomena we would expect to observe an increase in radar reflectivity. It can be seen from Table 3 that the evidence of such an effect is weak.

significant variation of reflectivity with time or planetary phase angle has been found. The reflectivity with data for the 1962 and 1964 conjunctions is shown in Fig. 8. The data were taken by the JPL group. The difference in mean levels is apparently due to an error in gain calibration for the 1962 system. Thus the results suggest a homogeneous surface structure with a dielectric constant of about 4-5.

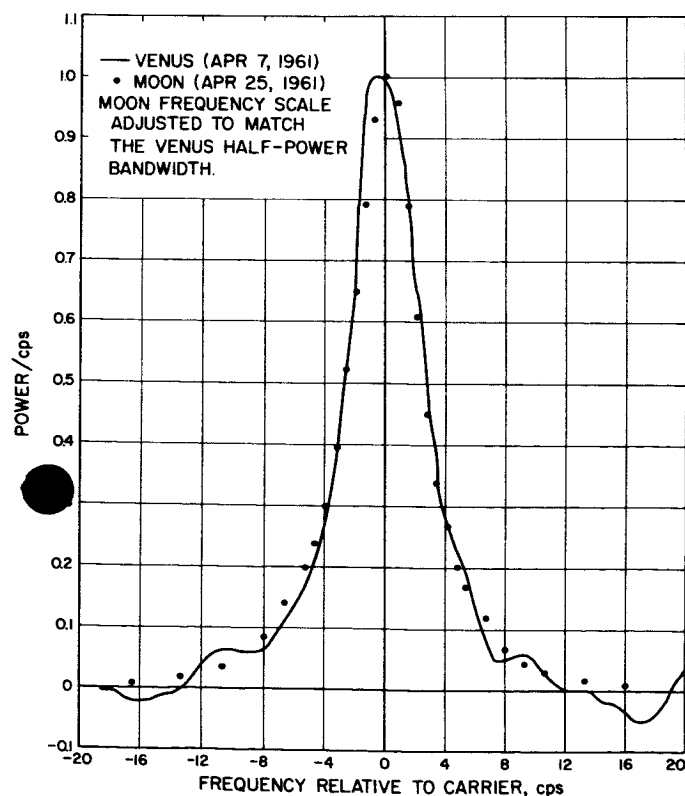


Fig. 8. The comparison of an early Venus spectrum with a lunar spectrum taken with the same radar equipment

#### IV. Planetary Rotation

The first report of a period of rotation on the order of 250 days was made by Muhleman (1961) in collaboration with R. Carpenter of JPL, and was based on the data shown in Fig. 9. The figure shows the overlay of a Venus spectrum with a lunar spectrum taken with the same equipment. The frequency axis of the lunar spectrum was scaled to match the Venus spectrum at 1/2 power and the corresponding lunar libration rate was scaled accordingly. This procedure led to a result of  $250 \pm 100$  days, the uncertainty being related to our confidence in the assumption of the similarity of the lunar and Venus scattering laws. No comment could be made concerning the direction of rotation.

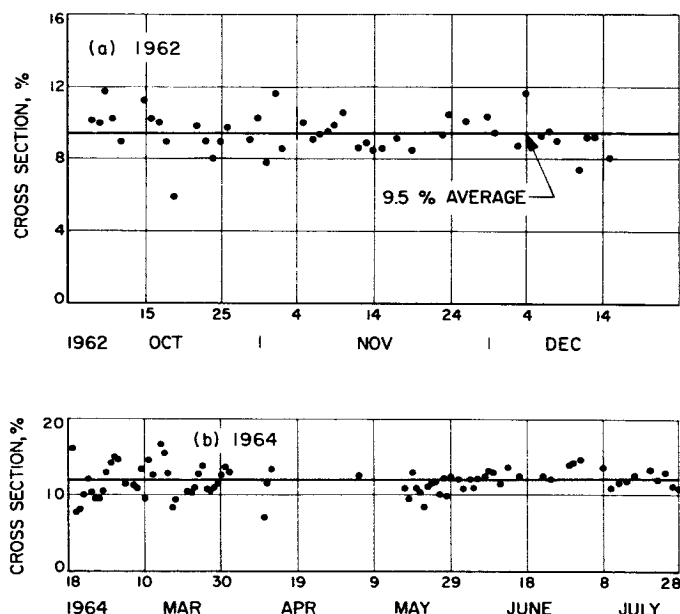


Fig. 9. The 12.5-cm reflectivity of Venus, measured in 1962 and 1964 by the JPL radar group

A plot of total doppler bandwidth with date led R. Carpenter to suggest that the rotation of Venus was retrograde, see Fig. 8. JPL observations of 1962 confirmed this hypothesis (Goldstein, 1964; Carpenter, 1964) and a repeat of the experiment in 1964 led to a reliable determination of the Venusian rotation vector. The best result available at the time of this report is (Carpenter, 1965)

$$P = -250^{+4}_{-7} \text{ days}$$

$$\alpha = 255^{+10}_{-4} \text{ deg}$$

$$\delta = 68 \pm 4 \text{ deg}$$

Essentially identical results have been obtained by Goldstein (1965) and Dyce (1965).

It is of considerable interest to notice that if the period were  $-244$  days, Venus would manage to show the identical face to the Earth at each inferior conjunction.

The study of Venusian surface areas that cause anomalous radar echoes is closely related to the question of the planet's rotational vector. If a local area on the planet were an abnormally strong reflector because of, e.g., a high value of dielectric constant, its presence would be manifested in the observed CW spectra. A region of higher power density would appear in the spectrum on the side corresponding to the approaching limb as the area became visible to us on Earth. Since the area would be sharing the rotation of the planet relative to us, it would appear to move across the face of Venus with time. Correspondingly, the region of high spectral density would move across the observed spectra. The exact motion of the phenomena in the spectra would be due to the following factors: the Venusian latitude of the area, the orientation of the rotational vector and its rate, and the orbital geometry of Earth-Venus. Since the latter is known, the former can be found from such observations.

Indeed, a number of such spectral features have been observed and followed by the JPL group. Carpenter

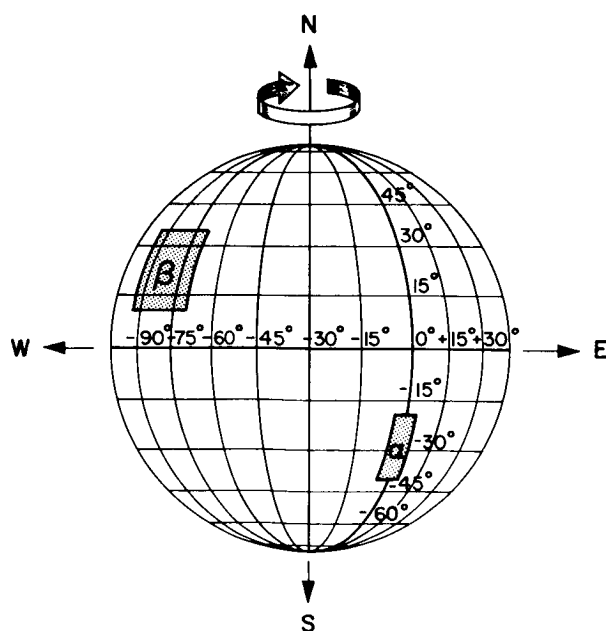


Fig. 10. A preliminary radar map of Venus showing the regions of anomalous reflectivity at 12.5-cm wavelength

(1965) and Goldstein (1965) have discussed these observations in detail. In each case, the observed features have confirmed the rotational vector determinations. Two major anomalous areas have been located in latitude, and a longitude system has been defined for Venus, based on the most prominent feature. A preliminary map, due to Goldstein, is shown in Fig. 10, which shows these features (which have been named "Goldstone  $\alpha$  and  $\beta$ " by persons outside the JPL group). The critical test for this work will occur at the next inferior conjunction of Venus (January 1966) when these features should reappear at predicted positions and times.

The ultimate way to study the anomalous features is to utilize simultaneous range-gating and spectral analysis, which allows one to locate a region in a specified doppler-range box. Data of this type have been obtained by Goldstein, one example of which is shown in Fig. 11.

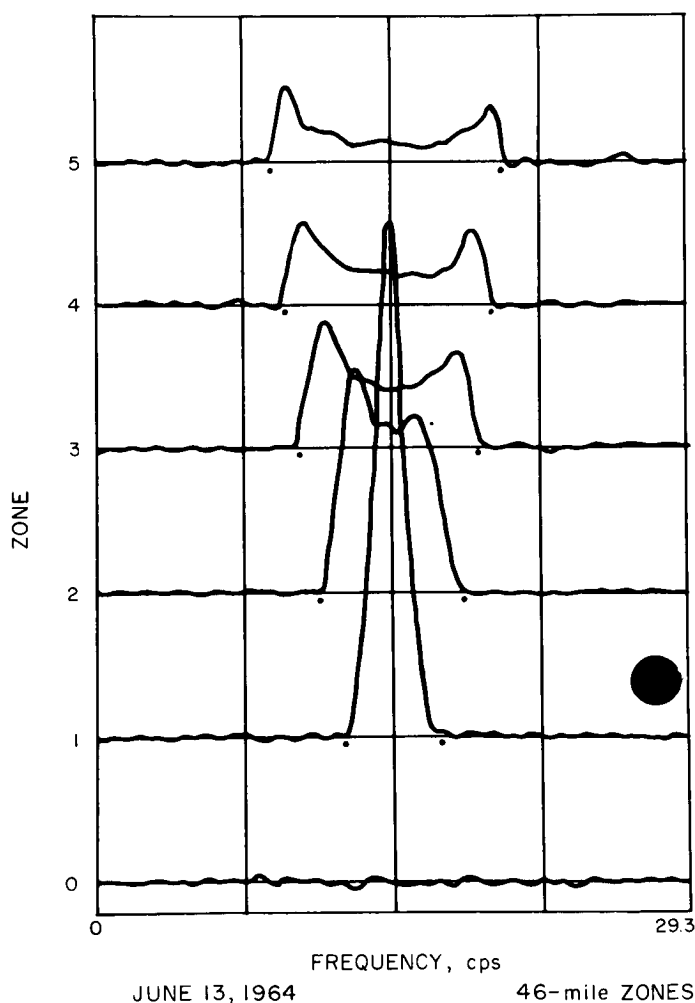


Fig. 11. Typical Venus doppler-range gated spectra showing the spectra at increasing range depths



An asymmetry can be located in both doppler frequency and depth back from the sub-Earth point, which should yield a much stronger and indeed, a unique determination of the rotational vector. These data are being analyzed in detail by Dr. Shalhav Zohar of JPL. Similar measurements are being carried out by Dyce and Pettingill at the Cornell University Arecibo facility. Some of this work is reported in another paper by Dr. Dyce in this symposium.

## V. The Radar Backscatter Function

Perhaps the most difficult problem in the radar studies of Venus is the interpretation of the backscatter function that appears in the measurement of the planet's pulse response or doppler spectrum shape. At present, these curves can only be measured with rather poor range or doppler resolution, e.g., 15 km and 1% of the total spectral width, respectively. Even in the case of the Moon, where work is being carried out with pulses (or the equivalent) of 1- $\mu$  sec width (300 m) the interpretation is far from complete. Numerous workers have

developed statistical theories to explain the scattering behavior of the Moon, but nothing has been published as yet concerning Venus.

The author (Muhleman, 1964, 1965) has been able to show that the scattering behavior of Venus is mathematically similar to that of the Moon at 12.5 cm. However, the statistical parameters from the theory, such as the mean slope, are considerably smaller for Venus.

A typical half-spectrum of Venus is shown in Fig. 12, along with a fit of Muhleman's scattering function

$$F(\tau) = \frac{\alpha^2 \cos \Theta}{(\sin \Theta + \alpha \cos \Theta)^2}$$

where

$$\tau = \frac{2R}{c} (1 - \cos \Theta)$$

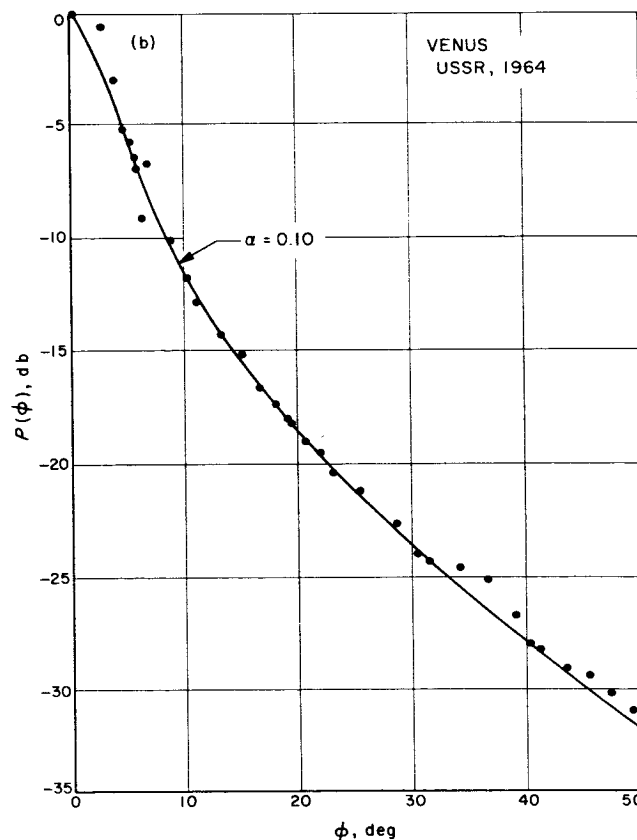
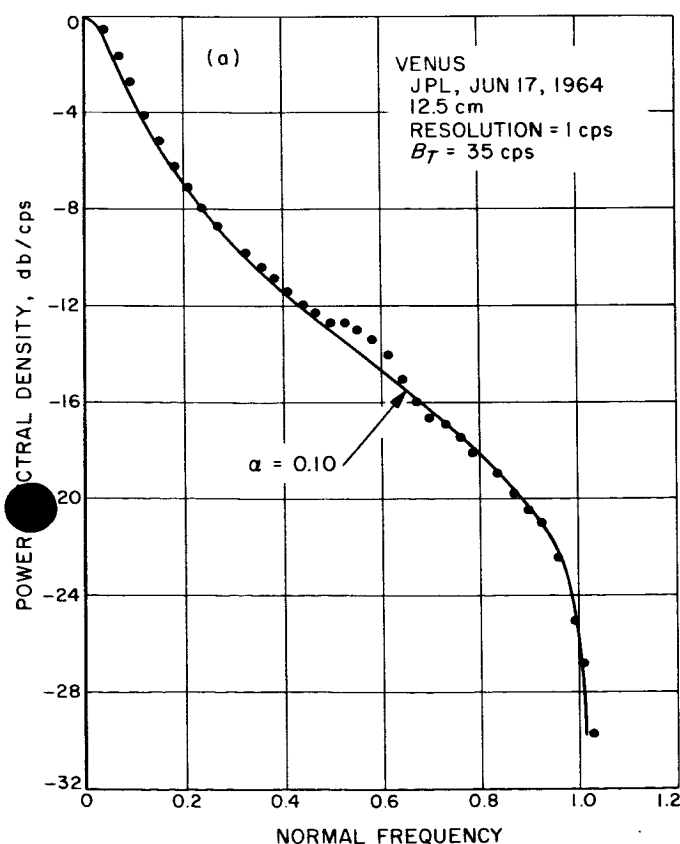


Fig. 12. (a) Typical observed Venus spectrum with a scattering law model; (b)  $\lambda$  43-cm pulse response with the same model

with  $\alpha = 0.10$ . The function appears to fit well across the Venusian disk. The  $\alpha$ -parameter should be interpreted as a one-dimensional mean slope, effective at 12.5 cm.

All of the observed backscatter functions available to the author are shown in Fig. 13. The curve for  $\lambda$  3.6 cm is theoretical and is based on the reported result that Venus appears as a Lambert scatterer at this wavelength. The  $\lambda$  12.5 cm is Muhleman's function as fitted to his observed spectra with  $\alpha = 0.10$ , and then convolved with a 100- $\mu$ sec square pulse. The  $\lambda$  23,  $\lambda$  43, and  $\lambda$  70 cm are 40-, 150-, and 100- $\mu$ sec observed-pulse responses, respectively. It can be seen that they all have the same mathematical form.

One would intuitively expect that Venus would appear smoother with increasing wavelength. The data in Fig. 13 confirm this, but the picture is very much confused by the use of varying pulse widths.

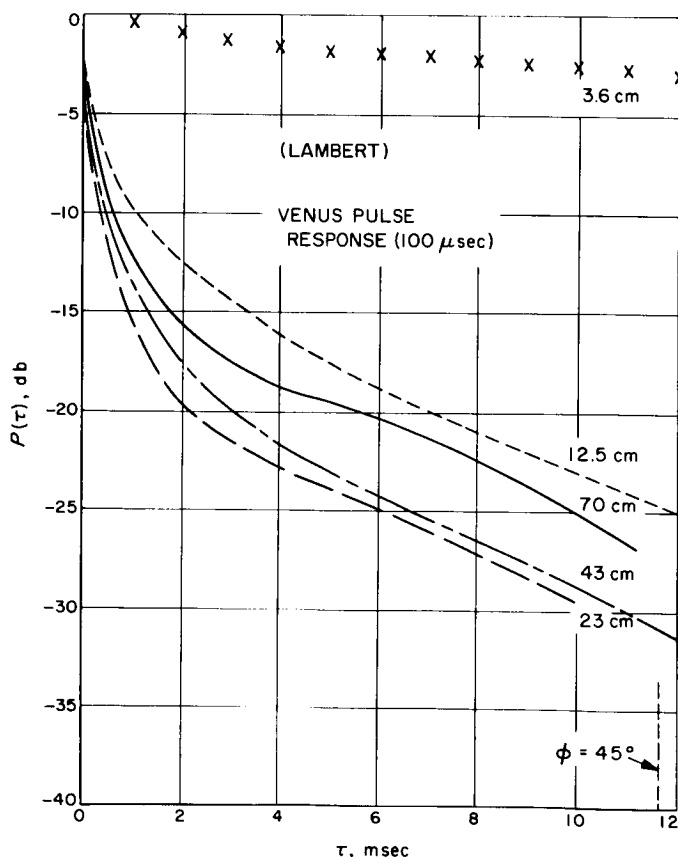


Fig. 13. Venus backscatter functions measured at various wavelengths

The Soviet workers, e.g., Kotelnikov (1965), have actually published two Venus backscatter curves, which are shown in Fig. 14. Kotelnikov has pointed out the difference between these two curves and offers the interpretation that the backscatter function of Venus varies by the amount shown in the picture. This appears completely incorrect to me. A careful study of the Soviet report appears to show that the 1962 curve was obtained with the equivalent of a 500- $\mu$ sec pulse, while the peak for the 1964 curves utilized a 150- $\mu$ sec pulse. My computations show that with this assumption the curves are identical.

It appears that the proper way to obtain the backscatter function, independent of particular pulse shapes, is to hypothesize a backscatter function, which can then be convolved with a specific pulse shape for comparison with the corresponding observations. These computations are in progress.

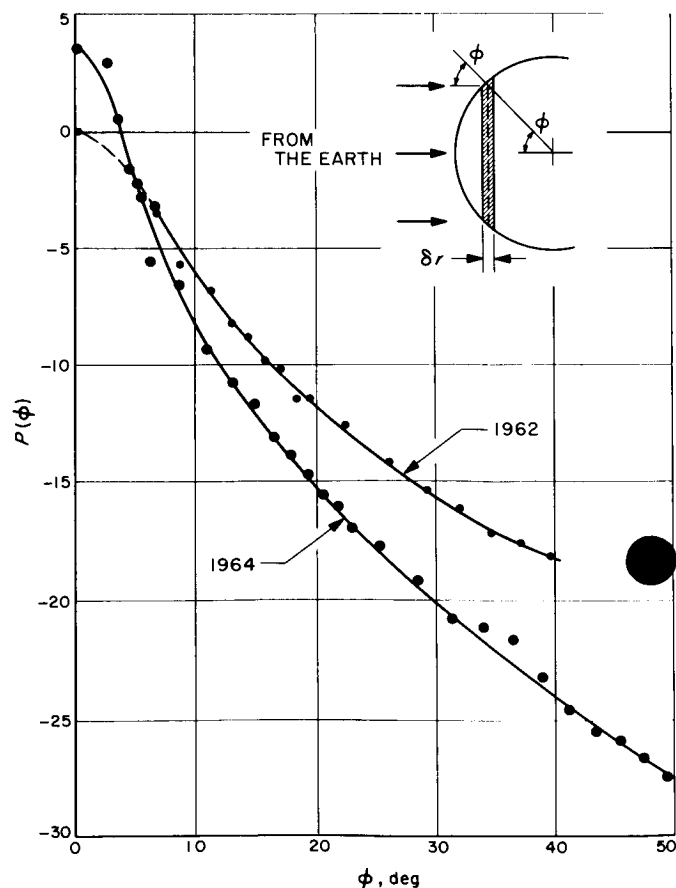


Fig. 14. Venus backscatter functions, as measured by the USSR radar group at  $\lambda$  43 cm

## REFERENCES

- Carpenter, R., 1964, *Astron. J.*, Vol. 69, p. 2.
- Carpenter, R., 1965a, Personal communication.
- Carpenter, R., 1965b, Submitted to the *Astron. J.*
- Drake, F., 1965, *These Proceedings*.
- Dyce, R., 1965, *These Proceedings*.
- Goldstein, R., 1964, *Astron. J.*, Vol. 69, p. 19.
- Goldstein, R., 1965, *Radio Science*, Vol. 69D, No. 12, p. 1623.
- Kotelnikov, V. A., 1965, *Radio Science*, Vol. 69D, No. 12, p. 1634.
- Morrow, W. E., 1964, Unpublished.
- Muhleman, D., 1961, *Astron. J.*, Vol. 66, p. 292.
- Muhleman, D., 1964, *Astron. J.*, Vol. 69, p. 34.
- Muhleman, D., 1965, *Radio Science*, Vol. 69D, No. 12, p. 1630.

N66 31467

## SOME RADAR CHARACTERISTICS OF VENUS AT 430 MHz

R. B. Dyce

Cornell University

Arecibo Ionospheric Observatory, Puerto Rico

### I. Introduction

The observations to be described were made during 1964 at the Arecibo Ionospheric Observatory (AIO) using the 1000-ft-D reflector and a pulsed 430-MHz radar system.

By coincidence the Venus conjunction of June 1964 occurred at a declination that could be ideally viewed within the pointing constraints of the antenna system. Observations were also made from March to August 1965, although the echo was much weaker than in 1964 because Venus was undergoing superior conjunction during the latter period.

The large antenna area is an important asset in the struggle to obtain a strong signal-to-noise ratio for accurate range and doppler measurement over as much of each planetary orbit as possible. A principal purpose of the AIO program has been to measure departures (on the order of 50- $\mu$ sec accuracy) from a working ephemeris so as to improve knowledge of the orbital parameters, the Earth's motion, the planetary radius, and the astronomical unit. This joint AIO-Lincoln Laboratory program will not be treated here.

A second byproduct that will not be discussed here concerns the disruption of Venus and Mercury echoes when they are viewed through the solar corona.

### II. Equipment and Procedure

Although principally intended for ionosphere studies, the Arecibo radar can be employed for radar astronomy and radio astronomy. The principal radar characteristics are given in Table 5.

The antenna is continuously directed at the apparent position of the planet for a period of time that depends upon the declination but can be as long as 2.5 hours. A train of coherent pulses is transmitted for a duration of time equal to the round-trip delay (less than 30 min). The transmitter is then stopped and the receiver turned on for a corresponding period of time. The echo is sampled with respect to a time base that is moved so as to follow the ephemeris position of the planet to an accuracy of a few microseconds. In most cases the receiver was arranged to give two quadrature outputs simultaneously so that the phase as well as the amplitude of each sample could be digitally recorded on magnetic tape. At a later time, samples taken at a given delay with

**Table 5. Characteristics of the Arecibo planetary radar**

Characteristic	Value
Location	18°20'46" N, 66°45'11" W
Antenna diameter	1000 ft (304.8 m)
Gain	56.25 db in zenith
Beamwidth	9 min of arc at half-power points
Sky coverage	Within 20° of zenith (approx $\delta = 0^\circ$ to $\delta = 38^\circ$ )
Transmitted frequency	430.0 MHz ( $\lambda = 0.69$ m) in coherent pulses
Typical peak power	2.0 Mw
Maximum duty cycle	6.25%
Typical pulse width	0.1 to 10 msec
Receiver front-end	Uncooled Adler tube pumped at 862 MHz (1964) Uncooled Varactor Paramp pumped at 4 GHz (1965)
System temperature	220 $\pm$ 40°K (1965)
Doppler compensation	Preset for each run using a local oscillator synthesizer
Range change compensation	Obtained from phase shifter driven by preset digital counter
Data recording	8-bit A/D converter, computer, magnetic tape

respect to the planet were processed for frequency information. This resulted in excellent resolution on the order of 0.1 Hz selectable by choice of computer instructions. For Venus and Mercury the ambiguity at the pulse repetition frequency is of no consequence. By such "coherent processing," both the range and the frequency information are simultaneously available.

### III. Reflectivity

Previous workers have found values for the fractional cross-section lying between 10 and 20%, with the higher values generally associated with longer wavelengths. All the measurements indicate a significantly higher reflectivity than that of the Moon, which is about 7%. If one applies the same analysis used for the Moon, one finds a surface dielectric constant of between 4 and 5, not inconsistent with a surface composed of dry material such as terrestrial rocks. Large areas of liquid water at the surface are apparently ruled out. The AIO data for 1964 are plotted in Fig. 15, showing an average of about 14%.

As was observed by James and Ingalls (1964) the Arecibo data show variation with date that are believed to exceed all equiptmental variations. These variations could be due to differentiation on the planet as various portions of the planet pass across the subradar point on the planet (see Section V).

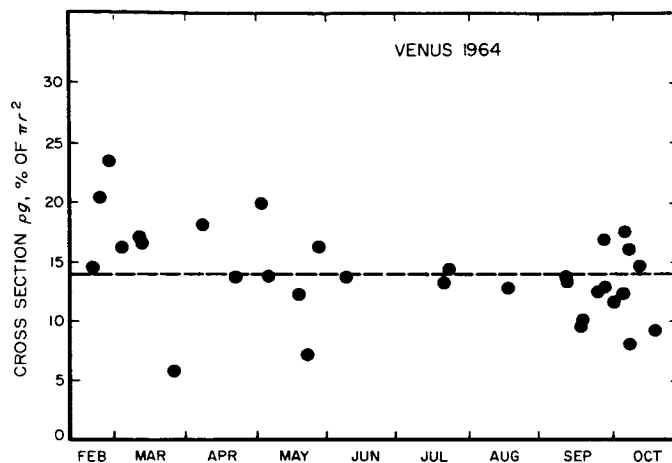


**Fig. 15. Reflectivity of Venus as a function of date, obtained by the 430-MHz Arecibo Ionospheric Observatory radar**

### IV. Angular Scattering Law

A pulse of a width that is short compared with a Venus radius will be returned from the planet with a decay at the tail of the echo. If adequate sensitivity is available, the dependence of the backscatter on the angle of incidence to the planetary surface can be measured. The curve shown in Fig. 16 is typical. (The "planetary radius" scale can, of course, be converted into angle of incidence.) Workers of several countries agree that the Venus echo resembles that of the Moon in the sense that the bulk of the echo is related to quasi-specular or coherent reflection from the smooth areas of the surface near the center of the disk (subradar point). In the case of Venus, the surface appears to be significantly flatter than that of the Moon. For greater delays, the rough scattering component for Venus strongly resembles the lunar law.

Although the Moon shows a sharper angular scattering law at low radar frequencies, the Venus behavior at 430 MHz appears identical to recent data at 1295 MHz (J. V. Evans, private communication).

### V. Surface Markings at 430 MHz

The JPL preliminary data for the Venus conjunction of June 1964 indicate two regions, called "Alpha" and "Beta." Examined in frequency, without range resolution, these features drift across the planet. Their longitude and approximate latitude can be deduced, based on the changing frequency of each feature with respect to the central frequency of the planet (Goldstein, 1965).

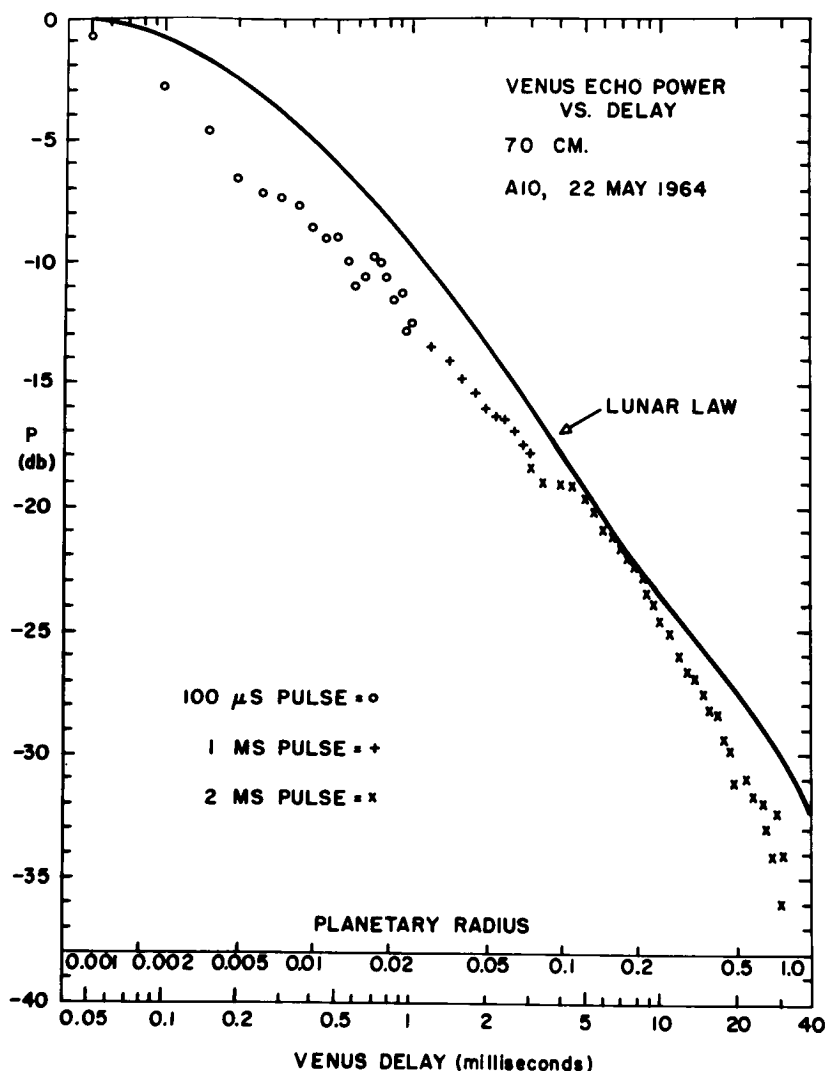


Fig. 16. Venus echo power vs delay observed in 1964 at 430 MHz at the AIO. The solid curve represents the corresponding behavior of the Moon, scaled to the Venus radius. Note the similarity between the two laws, holding except for the region near the center of the disk where Venus appears smoother and more reflective than the Moon.

In the course of range-doppler processing of the Arecibo data, a variety of Venus enhancements have been evident. Specifically, the Arecibo data have been examined for confirming evidence of the Alpha and Beta regions. Region Alpha showed clearly on 23 July, 1964, which, by coincidence, was the day that it passed across the central meridian (see Fig. 17). Region Alpha has some detailed structure but is not wider than 900 km. The longer dimension must be in excess of 3800 km (0.62 of a radius). Note that Alpha is a long, narrow region that happens to be approximately parallel to the frequency strips. On an earlier day (July 9, shown in Fig. 18) the feature was located on the approaching side of the planet, still exhibiting a linear nature. The line might

have been longer on this date but was limited by the unfortunate termination of the sampling at 14.5-msec delay and limited by confusion with the "wing" corresponding to 2-msec delay. (Incidentally, this motion yields about 240 days sidereal period  $\pm 20\%$ .)

Region Beta is more extensive (shown earlier by JPL) and consequently, with 1-msec resolution, appears as a complex region in the Arecibo data. To make this more evident, a contour map of echo strength is presented in Fig. 19 as a function of delay and doppler (viewed from the northern celestial hemisphere). So far, no attempt has been made to resolve the northern and southern hemisphere ambiguity. The JPL study suggests that Region

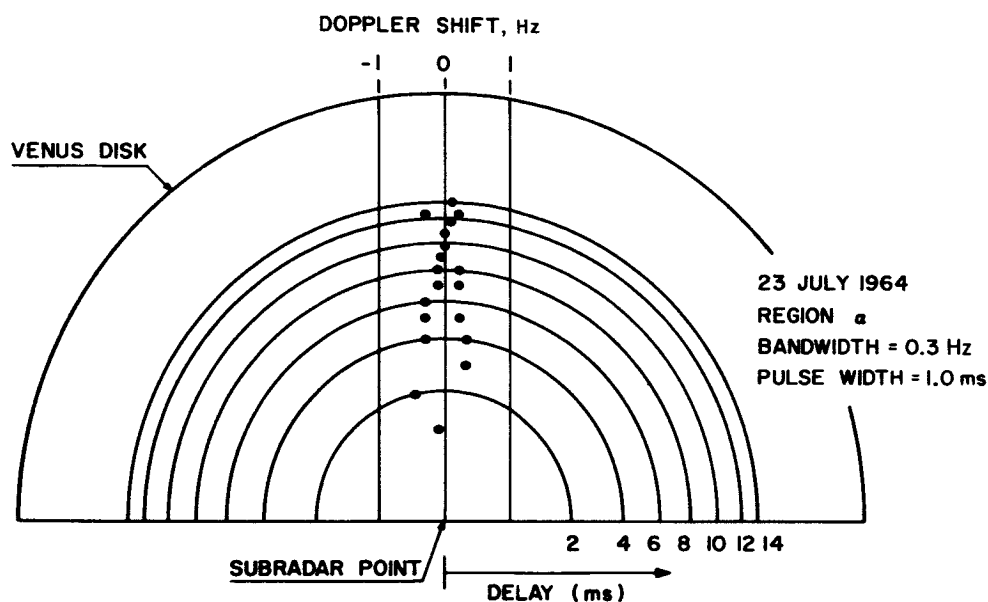


Fig. 17. Appearance of Venus disk to 430-MHz radar with resolution in range and frequency. Peaks of reflectivity are denoted by the dots near the central meridian. This corresponds to the JPL "Region Alpha." Only half of the disk is presented because of the two-fold ambiguity present in a single observation. JPL work indicates that Region Alpha is in a single half of the disk.

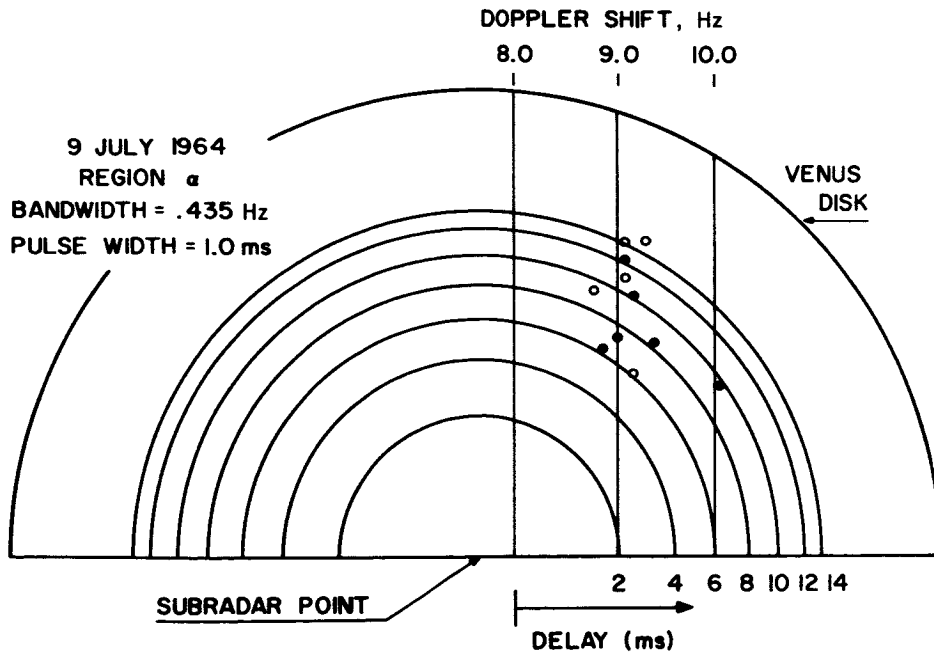


Fig. 18. Appearance of Venus disk showing positions of 430-MHz enhanced echoes associated with Region Alpha. The open circles indicate that the echo strength was less than three standard deviations above the noise level.

Beta lies above 10 deg in the northern hemisphere. Data for June 12, 15, and 30 also should be similarly treated. A cursory examination suggests that the individual

detailed structure had altered with changing orientation, but that Region Beta remained a strongly backscattering area.

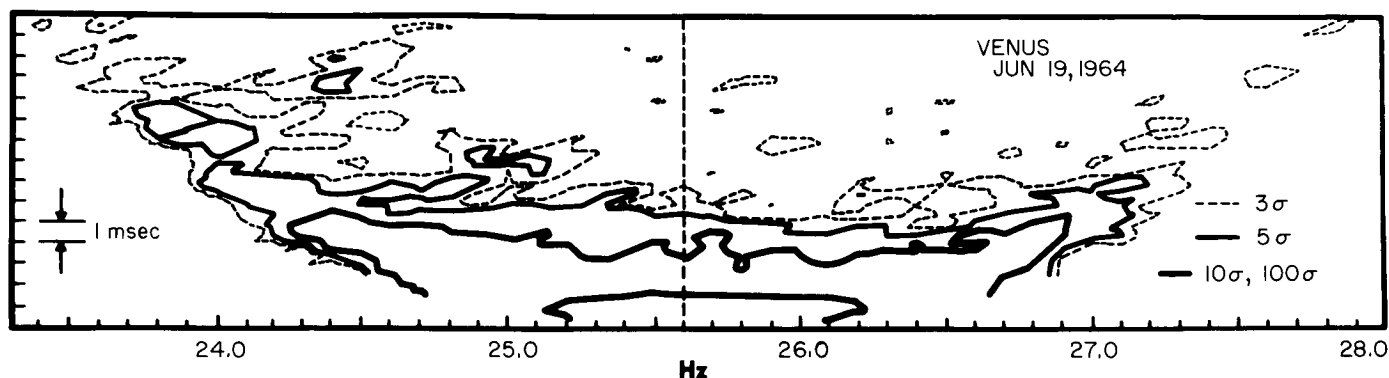


Fig. 19. Contours of echo strength measured in units of standard deviations above system noise level as a function of range and doppler frequency shift. Seventy-two spectra were summed, each with a frequency resolution of 0.2 Hz and a range calculation every 0.5 msec. The curvature of the planet can be readily observed. Region Beta appears as a group of "islands" on the left side of this figure.

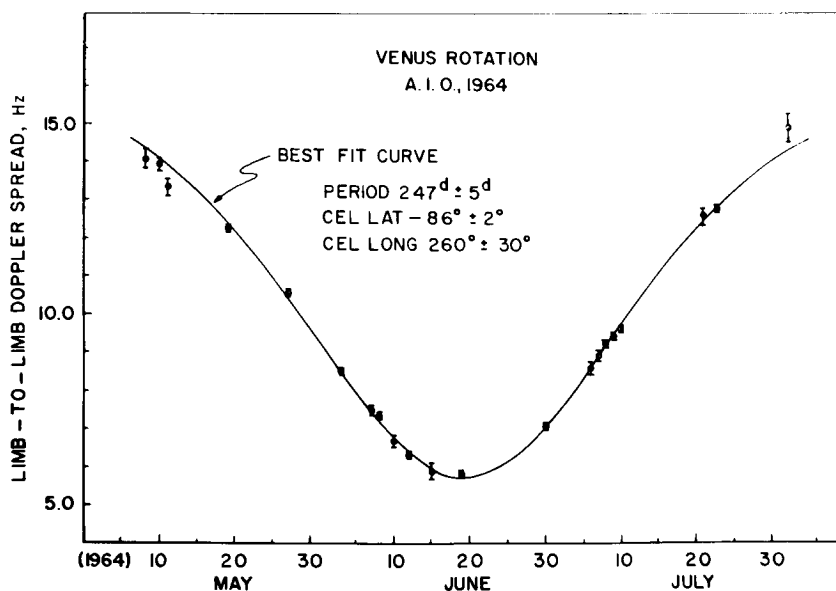


Fig. 20. Plot of limb-to-limb doppler spread vs date observed for Venus at the AIO during the 1964 inferior conjunction. The solid curve represents the least-mean-squares fit to the data and corresponds to the rotation axis specified.

## VI. Rotation Measurements

The apparent rotation rate of a spherical planet at a given time can be unambiguously computed from a measurement of frequency spectra at a known delay (usually measured with respect to the leading edge of the planetary echo). Using this technique, Goldstein (1964) has obtained from the 1962 conjunction observations a retro-

grade rotation of 248 days, with an axis orientation approximately normal to the orbital plane. Data taken at the Arecibo Ionospheric Observatory during the 1964 conjunction confirm the 1962 results and lead to a sidereal rotation rate of  $247 \pm 5$  days retrograde with an axis  $6^\circ$  from normal to the orbital plane. Twenty-one measurements are shown in Fig. 20, together with the curve fitted by the method of least-mean-squares with



three degrees of freedom. This value is preliminary and may be readjusted by as much as 1% in the final analysis (Dyce, Pettengill, and Shapiro, in preparation).

### **VII. Acknowledgments**

These observations were made with the encouragement, suggestions, and participation of G. H. Pettengill.

T. W. Thompson, A. D. Sanchez, D. B. Campbell, and T. Kan contributed their time to specific aspects of these observations.

The Arecibo Ionospheric Observatory is operated by Cornell University with the support of the Advanced Research Projects Agency under a research contract with the Air Force Office of Scientific Research, OAR.

### **REFERENCES**

Goldstein, R. M., 1964, *Astron. J.*, Vol. 69, p. 12.

Goldstein, R. M., 1965, *Radio Science*, Vol. 69D, No. 12, p. 1623.

James, J. C., and Ingalls, R. P., 1964, *Astron. J.*, Vol. 69, p. 19.

N65 31468

## RADAR OBSERVATIONS OF VENUS AT JODRELL BANK

J. H. Thomson

University of Manchester

Nuffield Radio Astronomy Laboratories, Macclesfield, England

Planetary radar at Jodrell Bank has been confined to observations of Venus. Two separate systems have been used, pulse and CW, both with the 250-ft Mk I radio telescope as transmitting and receiving aerial. The pulsed system was operational during the 1959 close approach, but genuine echoes were first obtained in 1961. The CW system was built between the close approaches of 1961 and 1962 and was used in 1962 and 1964. The parameters of both systems are given in Table 6, and the following sections list the operations and main results obtained at each close approach.

### I. 1959 (Evans and Taylor)

The 408-Mc/sec pulsed system with a peak power of 50 kw and a 30-msec pulse length was used. One pulse per second was transmitted for a period of 5 min, followed by 5-min reception. The receiver had eight integrating channels in range moved along the time base to follow the changing range of the planet by a semi-automatic system. As the channels covered 240 msec

and the interpulse period was 1 sec, not all possible ranges could be covered, and ranges corresponding to the value of the astronomical unit obtained in 1958 at MIT were selected. Integration for 58¾ hours of operation revealed a 2½ standard deviation rise in the channel corresponding to this range. It was estimated that there was an 8% chance that noise alone caused this result, and in the light of subsequent work this would seem the probable explanation of this early result.

### II. 1961 (Thomson et al.)

Basically the same system as in 1959 was used, with improvement in noise figure obtained by the use of an electron beam parametric amplifier. Echoes were first detected on April 8, by which time the new MIT value of the AU was available. Nevertheless, 660 msec of the time base was searched, sufficient to cover all likely values of the AU, and the echo was found to confirm the MIT value, giving 149,600,000 ± 5000 km. An attempt to measure the spectral width of the return failed.

Table 6. Radar equipment parameters

Parameter	Value
<b>Continuous wave radar</b>	
Frequency	410.25 Mc/sec
Power	5 kw
Aerial	250-ft, fully steerable paraboloid
Effective area	2500 m <sup>2</sup>
Transmitted polarization	Right circular
Received polarization	Left circular
System excess noise temperature	1100°K (1962), 200°K (1964)
Receiver bandwidth	Eleven channels 1 cps wide and 1 cps apart
Integration time	Up to several hours
Frequency stability	Better than 2 parts in 10 <sup>11</sup>
<b>Pulse radar</b>	
Frequency	408 Mc/sec
Peak power	50 kw
Aerial	250-ft paraboloid
Effective area	2500 m <sup>2</sup>
Transmitted polarization	Right circular
Received polarization	Left circular
System excess noise temperature	1200°K (1959), 200°K (1961)
Receiver system	Eight channels in range, each 30 msec long
Integration time	Several hours

**III. 1962 (Ponsonby et al.)**

The entirely new CW radar system at 410.25 Mc/sec was used with a transmitter of power 5 kw CW. The receiver had eleven integrating channels in frequency, each of 1 cps bandwidth at 1 cps spacing. The central frequency of the receiver was digitally controlled to follow a computed frequency ephemeris to about 0.1 cps. The basic quantities measured were the doppler shift and the spectrum of the returned signal. From the doppler shift a value of the AU of 149,596,600  $\pm$  900 km was computed, and an upper limit of 1 cps was put on the width of the spectrum to half power throughout the observations, which were made for about 6 weeks after closest approach. It was concluded from the spectral width observations that the period of rotation was of the same order of magnitude as the orbital period, and of undetermined sense.

**IV. 1964 (Ponsonby et al.)**

The same CW system was again used, with increased sensitivity obtained by the use of a parametric amplifier, which brought the predetector signal-to-noise ratio to about 1/2. Doppler shift was again measured to about  $\pm$ 0.1 cps, and actual spectral widths, rather than upper limits, were obtained. These showed a minimum at closest approach and confirmed the rotation to be retrograde with a period of between 100 and 300 days. The signal to noise ratio, when corrected for distance, showed an rms deviation of 0.75 db and indicated a radar cross-section compatible with other measurements.

**REFERENCES**

- Evans, J. V., and Taylor, G. N., 1959, *Nature*, Vol. 184, p. 1358.
- Ponsonby, J. E. B., Thomson, J. H., and Imrie, K. S., 1964, *Monthly Notices Roy. Astron. Soc.*, Vol. 128, p. 1.
- Ponsonby, J. E. B., Thomson, J. H., and Imrie, K. S., 1964, *Nature*, Vol. 204, p. 63.
- Thomson, J. H., Ponsonby, J. E. B., Taylor, G. N., and Roger, R. S., 1961, *Nature*, Vol. 190, p. 519.

N66 31469

## RECENT RADIO OBSERVATIONS OF THE PLANET VENUS\*

F. D. Drake

Cornell University  
Ithaca, New York

### I. Introduction

Very significant advances in our observational knowledge and theoretical understanding of the radio emission from Venus have recently occurred. Probably the most significant steps have been (1) A great improvement in knowledge of the Venus radio spectrum; (2) The successful detection and measurement of the polarized radio emission from the Venus surface; (3) Improvements in observational data concerning the variation of the Venus radio emission with time, therefore phase angle, and the development of a successful theory explaining these observations; (4) Broad and sophisticated studies of a multitude of models of the Venus atmosphere and surface, and a critical and enlightening comparison of the results with the observational data.

### II. The Radio Spectrum

The development of large radio telescopes of good resolution for the longer microwave wavelengths, and the construction of high-sensitivity millimeter wave instruments, have made possible the extension of the Venus spectrum to both higher and lower frequencies than heretofore. Accurate measurements of the Venus radio

emission are now available at closely spaced wavelength intervals from 1.3-mm to 68-cm wavelength. (The observed radio spectrum of Venus is shown in Fig. 21.) At the shorter wavelengths, there is a significant drop in the equivalent disk black-body temperature from about 600°K at 2-cm wavelength to about 350°K at

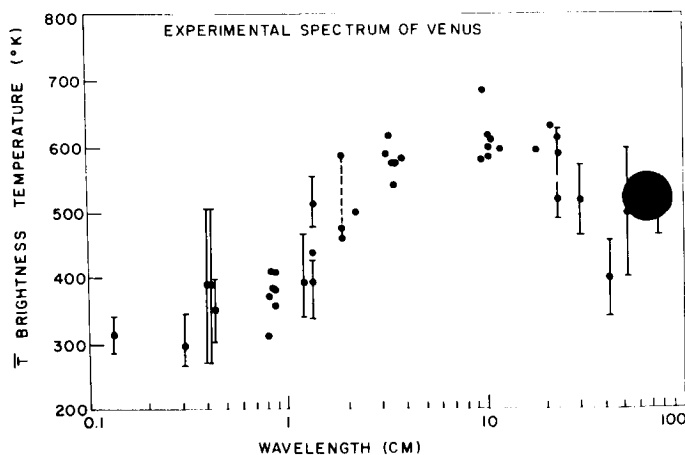


Fig. 21. The observed radio spectrum of Venus. The error brackets are omitted in the regions where the points cluster closely together, but those shown are generally typical.

\* This paper appears here in abstract form.

8-mm wavelength. The disk temperature then falls gradually to about 300°K at 1.3-mm wavelength. This decrease in the equivalent disk temperature is presently ascribed most widely to attenuation by cooler particles in the clouds of Venus.

On the long wavelength end of the spectrum, the data now seem to confirm that the spectrum drops from typically 600°K at 20-cm wavelength to 500°K at 68-cm wavelength. No satisfactory explanation of this phenomenon has been forthcoming. It has been suggested that this behavior may be explained by a model in which the longer-wavelength emission comes from such a depth below the surface that it encounters an interface between two dielectric materials as it approaches the surface. This dielectric interface will reflect some of the radio energy and thus cause the effective emissivity to be less at the longer wavelengths. This possibility is supported weakly by the radar data, but the latter do

not give quantitative agreement with the radio reflectivity implied by this hypothesis and the observed spectrum. Further observations are necessary to clarify this situation.

The abundance of water vapor in the Venus atmosphere plays a key role in the choice of the most plausible model for the Venus atmosphere and surface. Stimulated by this, investigators have conducted many searches for the water vapor line at the 1.35-cm wavelength. All have produced essentially negative results, with an upper limit of about 10% being placed on the strength of the line. This implies, using a reasonable model for the atmospheric temperature profile, a total precipitable water content in the atmosphere of less than a few tens of centimeters. This result constrains many models of Venus and keeps alive the difficulties inflicted on theories of solar system evolution by the apparently very low Venus water abundance (see Fig. 22).

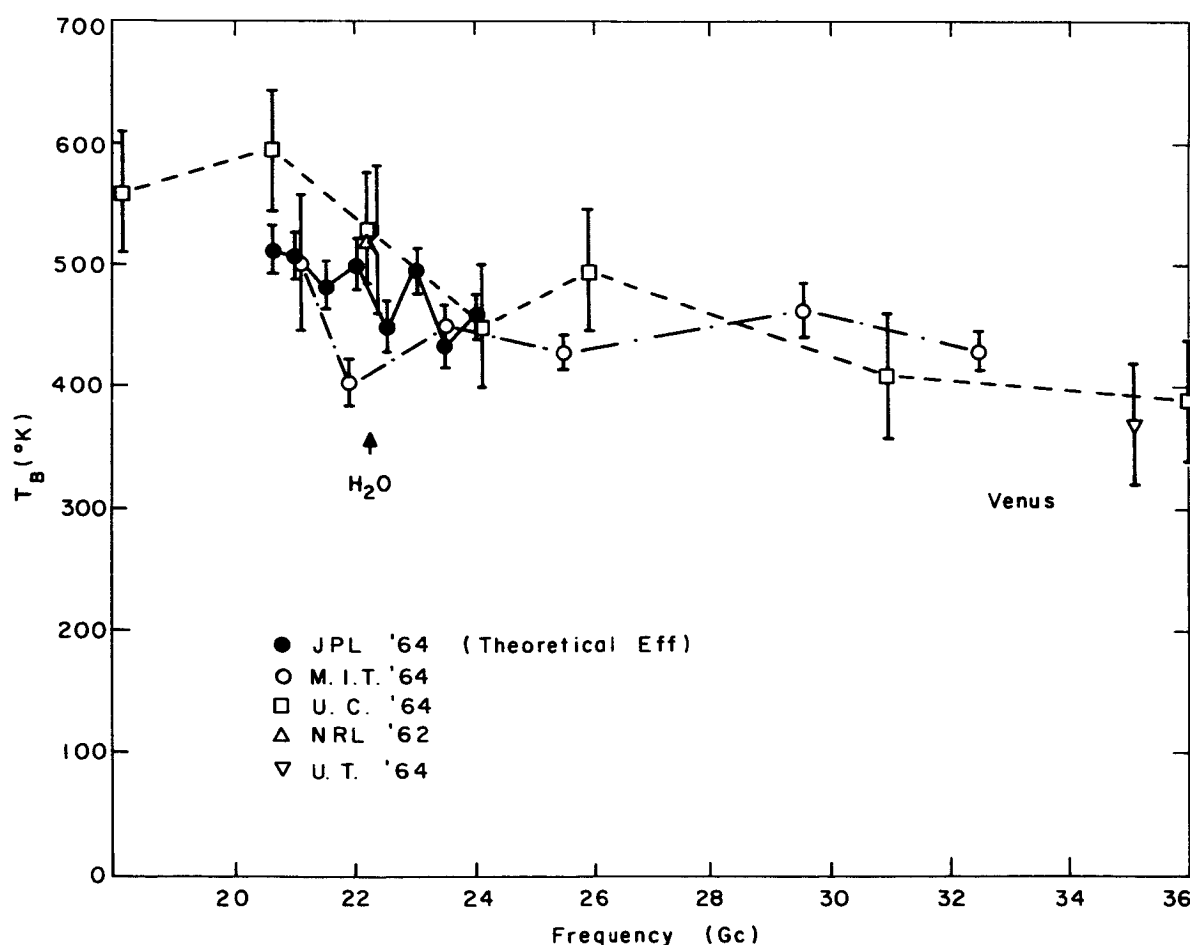


Fig. 22. Radio spectrum of Venus in the vicinity of the 135-cm water vapor line

### III. The Polarized Radio Emission

Despite the intrinsic difficulties of the experiment, accurate measurements have been made by Clark and Kuzmin of the polarized brightness distribution of the decimeter emission. The greatest significance of such emission is that it is the strongest evidence so far gathered that the observed radio emission actually is emitted from the planetary surface. This, in turn, implies strongly that the very high observed disk brightness temperatures are close to the surface thermometric temperature. All models of Venus must account for this high temperature, a difficult feat.

The measurements of the polarized brightness distribution allow a much more accurate picture to be drawn of the temperature distribution over the disk, the size of the radio disk, and the orientation of the rotational pole of the planet. The results of such measurements are consistent with estimates of the same quantities made by other means. The polarized brightness distribution also indicates that the dielectric constant of the surface is 2.5, a value inconsistent with most compacted solid materials, but not inconsistent with the granulated forms of some common terrestrial materials. This suggests that Venus is covered in the main by loose material.

### IV. The Venus Phase Effect

Excellent phase effect data have now been obtained at 8-mm wavelength, providing satisfactory phase effect information on 0.8-, 3- and 10-cm wavelengths. It has been noted that the 3- and 10-cm data correlate with the declination of Venus, suggesting the possibility that the data have been influenced, perhaps strongly, by instrumental effects. However, review of the observations by the observers has shown that the data have not been deteriorated by undetected instrumental effects. Some observations by Dickel have indicated that the 3-cm-wavelength equivalent black-body disk temperature rises sharply when Venus is near superior conjunction; this result would have an important bearing on interpretations of the phase effect. However, because of the difficulties in making such observations, they need confirmation.

Taking the best phase effect information at 0.8, 3 and 10 cm, Muhleman, Pollack and Sagan, and Troitsky have shown that these data are entirely consistent with the thermal and electric behavior of a typical planetary surface as predicted by the theory of Piddington and Minnett. Applying this theory, they show that the behavior of the surface does not define the probable surface material well. However, the data are again most consistent with a surface of expected planetary materials in granulated form. The results also are consistent only with a retrograde sense of rotation for the planet, a situation already indicated by the phase effect and established by the radar data.

### V. Models of the Venus Atmosphere and Surface

Barrett and Staelin, Pollack and Sagan, Basharinov, and Welch have all explored in detail various plausible models of the Venus atmosphere and surface. Perhaps the main point to emerge so far from such studies is that there is a wide range of quite different models that can be adjusted so as to produce observational effects consistent with the actual data. In particular, absorption by carbon dioxide, dust from the surface, or ice crystals can produce the magnitude and spectrum of the attenuation observed at the shorter radio wavelengths. It is clear that the short-wavelength spectrum must be even more accurately defined if this unfortunate situation is to be resolved.

However, perhaps the model that fits best all of the known conditions, particularly the high surface temperature and the greenhouse effect required to sustain it, is the model in which the major role is played by liquid or solid water particles, which are presumed in the model to constitute the well-known Venus clouds. Although this model places a large water abundance in the clouds, with a concomitant appreciable water vapor pressure, the water vapor implied is just permitted by the negative results of the search for the Venus water vapor line. It is clear that it is important to improve the observational data on the strength, if any, of the 1.35-cm line.

## REFERENCES

- Barrett, A. H., and Staelin, D. H., 1964, *Space Science Review*, Vol. 3, p. 109.
- Clark, B. G., and Kuzmin, A. D., 1965, *Astrophys. J.*, Vol. 142, p. 23.
- Muhleman, D. O., 1964, *Space Programs Summary No. 37-26*, Vol. IV, Jet Propulsion Laboratory, Pasadena, California, p. 267.
- Piddington, J. H., and Minnett, H. C., 1949, *Australian Journal of Scientific Research A*, Vol. 2, p. 63.
- Pollack, J. B., and Sagan, C., 1966, *Icarus*, To be published.

N66 31470

## SOME REMARKS CONCERNING THE RADIOASTRONOMICAL OBSERVATIONS OF VENUS

A. D. Kuzmin

*P. N. Lebedev Physical Institute  
Moscow, USSR*

The purpose of my report was to make a comment about Drake's survey report. But Drake's report includes all the statements of B. Clark's and my investigation of Venus' surface, and I have no intention of criticizing this result.

Therefore I would like to add only some short comments about models of Venus' atmosphere. It is well known from optical measurements that in the atmosphere of Venus there are many aerosols and, therefore, I ask myself this question: Is it possible to explain the radar astronomical results of the spectra of Venus by absorption by these aerosols? It seems to me that it is better and more fruitful to solve this question in a general form, i.e., not to investigate, for example, water or some other component to satisfy the radio astronomical data, but rather to investigate what must be the general properties of such aerosols in order to satisfy the data. The results of such an investigation show that the radio astronomical data may be satisfied by aerosols containing polar liquid dielectric if the relaxation time of this dielectric is equal to  $1.5 \times 10^{-12}$  to  $5 \times 10^{-12}$  sec. It is necessary to have about 0.1 to 0.2 g/cm<sup>2</sup> of such an aerosol. The investigation suggests, for example, that if there is one gram

per cubic meter of such an aerosol (which is reasonable) similar to the quantity of water droplets in dense Earth clouds, then heights of such clouds of from 1 to 2 kilometers are obtained, which are not high enough. Then, if we know what types of aerosol satisfy these data, we can easily get some reference book on physics and chemistry and find what substances would satisfy the data. The data are satisfied, for example, by supercooled water and by some types of hydrocarbons such as CH<sub>3</sub>OH, C<sub>6</sub>H<sub>5</sub>Cl, etc. In Fig. 23, theoretical curves are shown, calculated for such an aerosol model. Experimental data are also shown here and they are in good agreement.

I would also like to say a few words about the interpretation of long wave emission. I made an attempt to explain the measurements by Drake and Kellermann at wavelengths from 20 to 48 cm by involving the ionosphere, but such an ionosphere that has an electron temperature less than the temperature of the surface. In Fig. 24 are shown calculated curves for electron temperatures of 400° and 300°K, together with experimental results. Because this wavelength is not long enough, it is necessary to have electron densities that are not so high as those in a classic ionosphere model.



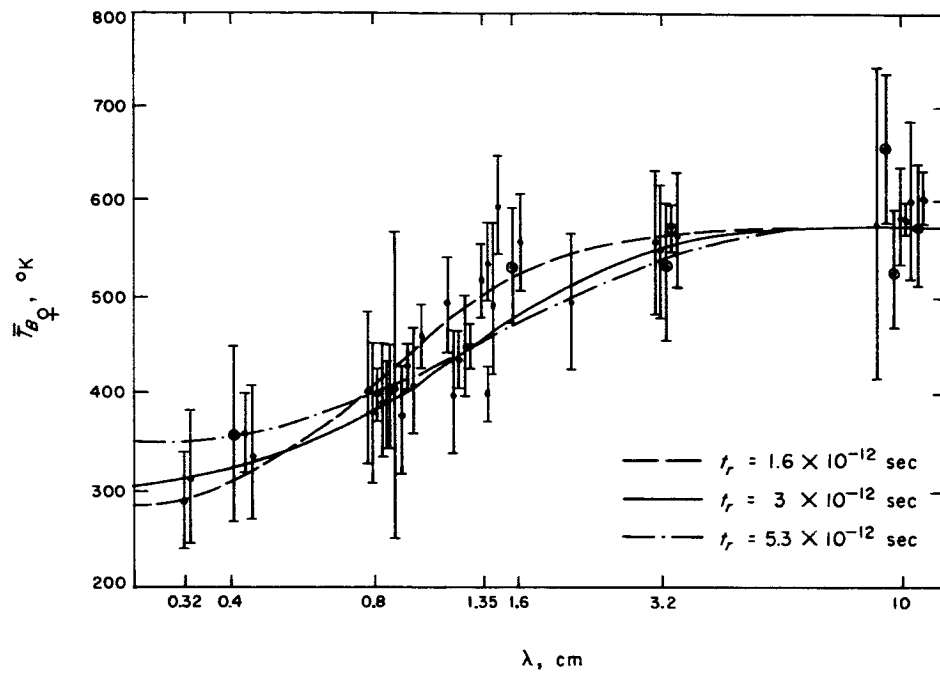


Fig. 23. Theoretical curves for an aerosol model, with experimental results

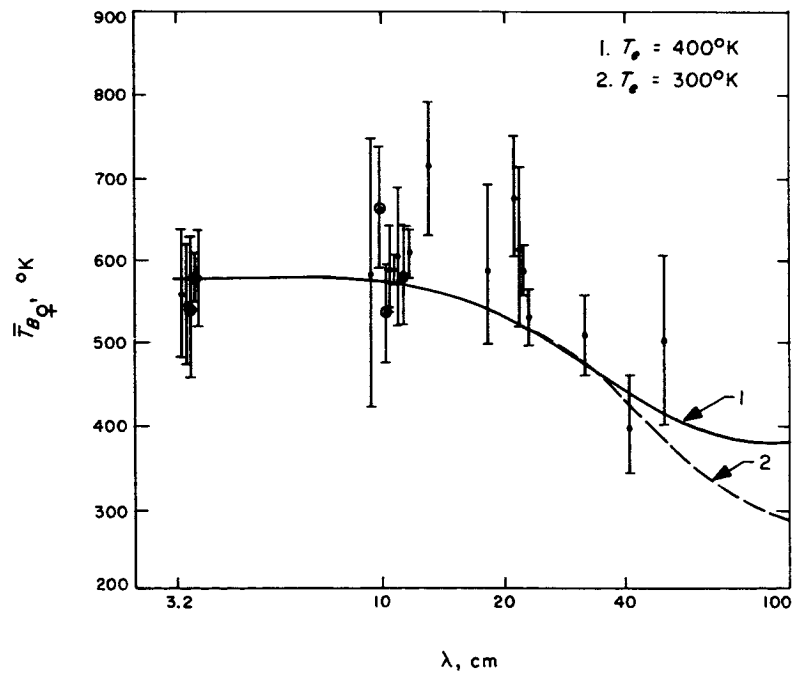


Fig. 24. Calculated curves for electron temperatures of 400 and 300°K, with experimental results

I am more skeptical of the phase variation measurements discussed by Dr. Drake than he is, and I should like to point out a few features. The phase variations cited by Drake were obtained by wide extrapolation of the measurements near inferior conjunction of Venus. It may be expected that the more accurate data will be obtained by direct comparison of Venus' brightness temperature near inferior and superior conjunction. There are a few such measurements near the 10-cm wavelength made by Drake, Kellermann, and myself. The results of this measurement are shown in Table 7.

The table shows that all these measurements are in fair agreement and they show that the temperature difference between the illuminated and unilluminated parts of Venus does not exceed 5%. But all these measurements are in some disagreement with Drake's phase variation, because the difference between illuminated

**Table 7. Measurements of Venus' brightness temperature at 10 cm**

Investigator	$\bar{T}_B, ^\circ\text{K}$	
	Dark hemisphere	Illuminated hemisphere
Drake (Ref. 1)	580	610
Kuzmin (Ref. 2)	580	555
Kellermann (Ref. 3)	605	629

and unilluminated parts in Drake's result (Ref. 4) is about 13%. It seems to me today that this situation is not clear, and it is possible to say only that the temperature difference between illuminated and unilluminated parts is not large. I believe that it is necessary to obtain more observations.

## REFERENCES

1. Drake, F. D., 1962, *Nature*, Vol. 195, No. 4844, p. 894.
2. Kuzmin, A. D., 1965, *Astron. Zh.*, Vol. 42, No. 6.
3. Kellermann, K. I., 1965, *Radio Science*, Vol. 69D, No. 12, p. 1574.
4. Drake, F. D., 1964, *Astron. J.*, Vol. 69, No. 1, p. 62.

## CONTRIBUTION AU COLLOQUE CALTECH-JPL SUR LA LUNE ET LES PLANETES: VENUS

Audouin Dollfus

Observatoire de Paris  
Meudon, France

### **1. Detection de la vapeur d'eau dans la haute atmosphere de Vénus**

La lumière de Vénus est renvoyée par les parties supérieures de la couche nuageuse et elle traverse la haute atmosphère de la planète. J'ai cherché à déceler la vapeur d'eau dans ces régions supérieures de l'atmosphère de Vénus, grâce à la bande d'absorption produite dans le spectre à 1,40 microns.

Le spectrophotomètre photoélectrique à filtre polarisant réalisé dans ce but a déjà été décrit, ainsi que le télescope spécial de 50 cm de diamètre auquel il a été associé (1)(3)(4)(5).

Le filtre polarisant isole, selon le principe de Lyot, la bande 1,4 microns de la vapeur d'eau. Il a été étudié de telle façon que les raies d'absorption du  $\text{CO}_2$  les plus

intenses de l'atmosphère de Vénus ne soient pas transmises par le filtre, et que les plus faibles soient réparties de façon à se compenser. L'instrument n'est donc pratiquement sensible qu'au spectre de la vapeur d'eau. La mesure consiste à annuler le signal grâce à un compensateur étalonné directement en quantité de vapeur d'eau exprimée en  $\text{gr/cm}^2$  à la pression atmosphérique ordinaire. L'étalonnage est peu sensible à la valeur de la pression atmosphérique sur la planète, car l'élargissement de la bande sous l'effet de la pression donne un signal négatif qui compense presque exactement l'accroissement correspondant de l'intensité de la bande.

On mesure la quantité d'eau en observant alternativement Vénus et des astres de comparaison voisins tels que la Lune, et le Soleil convenablement affaibli; les différences caractérisent alors la vapeur d'eau de l'atmosphère de Vénus.

La bande 1,4 microns de la vapeur d'eau se sature toutefois pour une quantité d'eau voisine de  $0,10 \text{ gr/cm}^2$  de sorte qu'il est nécessaire d'observer dans des conditions telles que notre atmosphère contienne moins d'eau que cette limite. Cette condition n'est jamais réalisée au niveau du sol.

J'ai d'abord observé en ballon libre, notamment dans la nuit du 22 au 23 Avril 1959 au cours d'une ascension en cabine étanche jusqu'à l'altitude de 14.000 mètres (6). J'ai observé aussi en haute montagne, en hiver, lorsque la température très basse abaisse la teneur en eau au-dessous de la limite de saturation de la bande. Le meilleur résultat a été obtenu à la faveur de l'occultation de Vénus par la Lune, les 21 et 22 Janvier 1963, à la Station Scientifique du Jungfraujoch en Suisse à l'altitude de 3.000 mètres.

Les résultats des mesures, déjà publiées par ailleurs (2)(3)(6), ont donné la quantité d'eau sur Vénus au-dessus du niveau des nuages, soit  $0,7 \cdot 10^{-2} \text{ gr/cm}^2$ . Cette valeur correspond à 70 microns d'eau précipitable.

Il est vraisemblable que les nuages de Vénus sont constitués de très fines particules d'eau glacée; la réflexion sur les petits cristaux de glace donne un faible signal négatif dans notre instrument: la valeur  $0,7 \cdot 10^{-2} \text{ gr/cm}^2$  devrait être très légèrement augmentée dans ce cas. On peut estimer la quantité d'eau de la haute atmosphère de Vénus comprise *entre 70 et 100 microns* d'eau précipitable, au-dessus de la couche nuageuse visible.

Cette valeur peut être rapprochée de celle que j'avais mesurée pour la stratosphère terrestre au-dessus de l'altitude de 13.000 mètres au cours de mes ascensions en ballon, soit  $1,0 \cdot 10^{-2} \text{ gr/cm}^2$  (1). La teneur en eau de la

haute atmosphère de Vénus est comparable à celle de notre propre stratosphère.

On peut encore comparer cette valeur à celle calculée, en supposant la couche nuageuse formée de cristaux d'eau à une température de  $-40^\circ\text{C}$ , avec saturation, le gradient thermique vertical au-dessus de la couche étant voisin de  $10^\circ/\text{km}$  et l'humidité relative décroissant avec l'altitude. Les valeurs numériques correspondantes sont données dans le tableau 8 et conduisent à une quantité d'eau de 115 microns, dont l'ordre de grandeur est très voisin de celui observé.

Dans la suite, le Prof. J. Strong a réussi à détecter aussi la vapeur d'eau sur Vénus à l'aide d'un instrument automatique porté par ballon (voir le chapitre correspondant du présent ouvrage). La valeur qu'il a obtenue est très voisine de la détermination précédente.

## II. Etude des aérosols en suspension dans la haute atmosphère de Vénus

Au-dessus du niveau supérieur de la couche nuageuse, l'atmosphère de Vénus n'est pas parfaitement limpide, mais elle contient en suspension des aérosols résiduels qui diffusent plus de lumière que les molécules.

Cette légère pollution des couches élevées de l'atmosphère de Vénus s'observe depuis la Terre au moment des conjonctions inférieures, lorsque Vénus est vue sous l'aspect d'un fin croissant très effilé. Les extrémités des cornes du croissant s'allongent alors au-delà de leurs limites géométriques. Lorsque l'angle de phase dépasse  $176^\circ$ , le croissant dégénère en un filin lumineux qui peut devenir une auréole complète (figure 25).

Tableau 8

Tranches d'air au-dessus des nuages, km	Température, $^\circ\text{C}$	Quantité d'eau saturante dans la tranche, $\text{g/cm}^2$	Humidité estimée, %	Quantité d'eau dans la tranche, $\text{g/cm}^2$
0,0 - 0,5	- 40	0,0060	100	0,0060
0,5 - 1,0	- 45	0,0040	60	0,0024
1,0 - 2,0	- 50	0,0040	30	0,0012
2,0 - 3,0	- 55	0,0030	20	0,0006
3,0 - 7,0	(- 60)	(0,0040)	20	0,0008
Au-dessus de 7,0	---	---	---	(0,0005)
Total . . . . . $1,15 \cdot 10^{-2} \text{ g/cm}^2$				

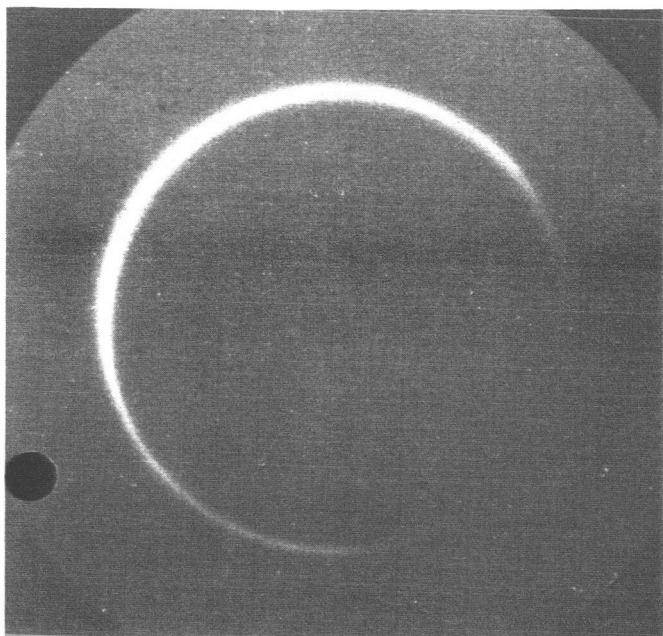


**Fig. 25 : Photographie du croissant de Vénus  
le 21 Juin 1964 à 8h40**

#### Observation à la conjonction inférieure de Vénus en 1964

Les circonstances se présentaient ainsi le 19 et le 20 Juin 1964 : j'ai observé le phénomène à l'Observatoire du Pic-du-Midi avec E. Maurice (7). Nous utilisons le réfracteur de 60 cm adapté spécialement par Lyot à l'étude des planètes en 1943 (figure 26). L'astre étant très proche du Soleil, les observations étaient pratiquées en plein jour, lorsque le ciel était très pur. Un écran circulaire de 80 cm de diamètre a été placé à l'extrémité d'un mat extensible de 13 mètres de longueur maximum fixé au rebord de la coupole (figure 27). Ce grand parasoleil, préparé sous la direction de J. Rösch, était manipulé par un treuil afin de porter ombre sur l'objectif de la lunette. On évitait de la sorte les reflets de la lumière solaire directe entre les faces de l'objectif, ainsi que la diffusion des poussières et les défauts du verre, qui auraient donné un fond lumineux très brillant, perturbant gravement les observations pour les angles de phase inférieurs à  $170^\circ$ .

Entre le 6 Juin et le 4 Juillet 1964, nous avons bénéficié de 20 journées d'observation et recueilli 29 séries de clichés au foyer direct de 1825 cm du réfracteur. (Voir figure 25.) Ces clichés portaient des marques d'étalonnage photométriques exprimées en valeurs absolues de luminances, c'est-à-dire comparées directement à l'éclairement  $E_0$  donné par le Soleil. Dans ce but, après chaque série de poses sur Vénus, l'objectif principal de la lunette

était recouvert d'un petit diaphragme d'environ 2 cm de diamètre seulement, associé à une lame de verre absorbant 99% de la lumière; la lunette était pointée vers le Soleil et des séries d'expositions supplémentaires de durées croissantes étaient effectuées sur la photosphère solaire près du centre du disque.

Soit  $\alpha = 0^\circ$  l'azimuth du rayon du disque planétaire dirigé à l'opposé du Soleil, selon les conventions de la figure 28.  $\alpha = +90^\circ$  correspond à la corne Nord et  $\alpha = -90^\circ$  à la corne Sud. Les clichés ont été mesurés radialement au micro-densitomètre, en même temps que les marques d'étalonnages, pour des angles  $\alpha$  croissant de  $5^\circ$  en  $5^\circ$  tout autour du disque.

L'intensité de l'aurole est exprimée par la largeur équivalente du profil photométrique pour un petit arc  $\Delta\alpha$  sous-tendant  $1^\circ$ ; elle est rapportée à l'éclairement  $E_0$  donné par le Soleil à la distance de la Terre; on obtient le rapport

$$\Phi = 10^{-13} \frac{B(\alpha = 1^\circ)}{E_0 (1 \text{ UA})}$$

La figure 28 donne les mesures obtenues pour ce rapport  $\Phi$ , en fonction de l'angle de phase  $V$ , pour quatre directions de l'azimuth  $\alpha$ , à  $90^\circ$ ,  $80^\circ$ ,  $60^\circ$  et  $45^\circ$ ; on a reporté seulement les moyennes entre les mesures recueillies sur les deux cornes Nord et Sud. Les valeurs de  $\Phi$  se lisent sur l'échelle d'ordonnée de droite.

#### Diamètre des particules en suspension dans la haute atmosphère

Divisons l'atmosphère de Vénus en couches concentriques d'altitudes  $z$  croissantes. L'origine des altitudes  $z = 0$  km correspond au niveau supérieur de la couche nuageuse visible; si les nuages ont une structure complexe, ce niveau correspond aux sommets les plus élevés des formations nuageuses, puisque celles-ci sont vues au bord du disque sous l'incidence rasante. L'aurole provient de la diffusion par les particules résiduelles en suspension dans ces hautes régions de l'atmosphère. Chaque couche contient  $N(z)$  particules par unité de volume; ces particules ont un coefficient de diffusion  $R(V)$  qui dépend de l'angle de phase  $V$  et que nous supposons indépendant de l'altitude. Chaque couche contribue à l'éclat de l'aurole proportionnellement à un trajet  $T(V, \alpha, z)$  que nous avons calculé numériquement en fonction de  $z$  pour différentes valeurs de  $\alpha$  et de  $V$ . Chaque couche donne donc la lumière diffusée

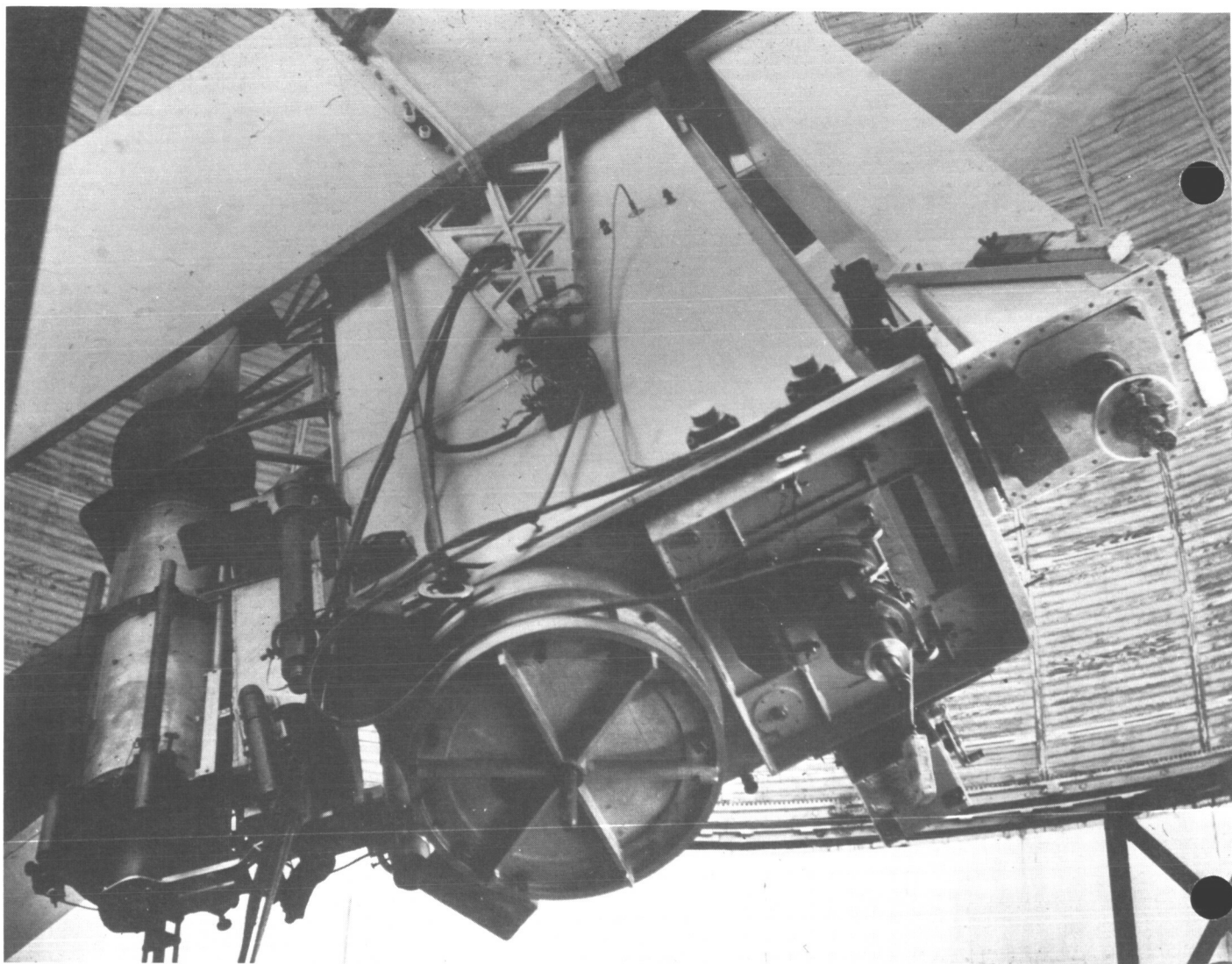


Fig. 26 : Lunette de 60 cm du Pic-du-Midi

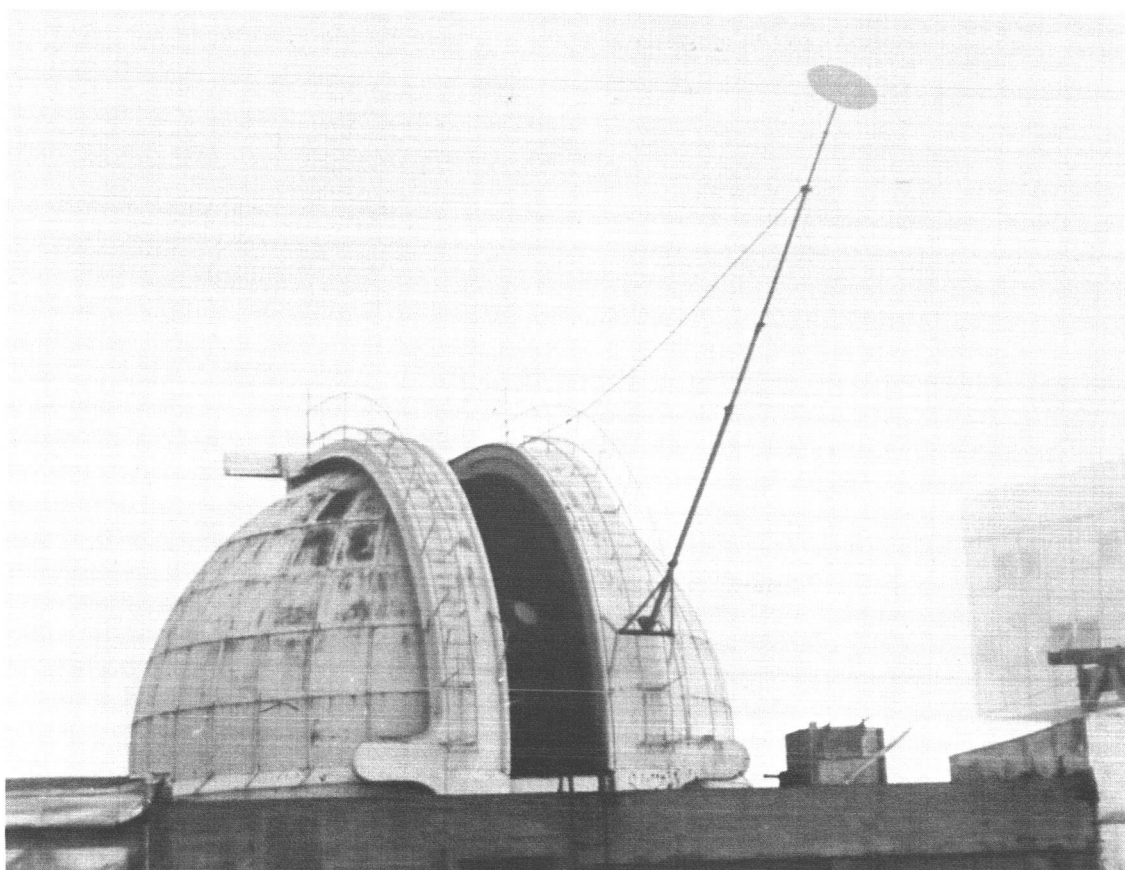


Fig. 27 : Le parasoleil pour l'étude de Vénus au Pic-du-Midi

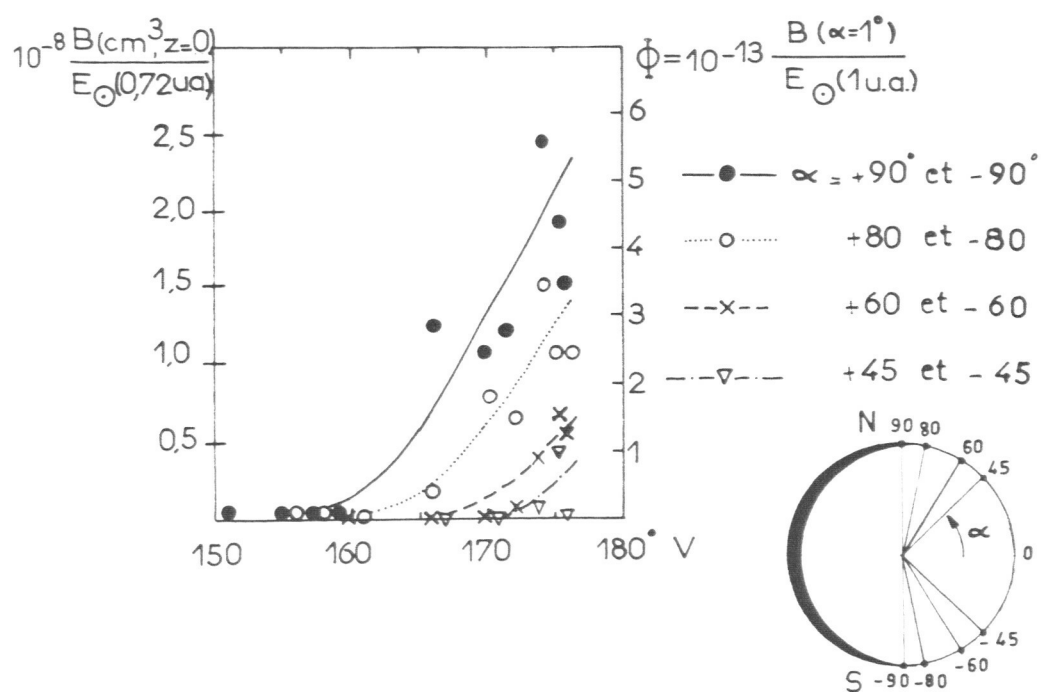


Fig. 28 : Etude photométrique des cornes du croissant de Vénus

$\Phi(V, \alpha, z) = R(V) \cdot N(z) \cdot t(V, \alpha, z)$ . En négligeant l'absorption propre et la diffusion multiple, l'intensité totale de l'aurole sous l'azimut  $\alpha$  vaut:

$$\Phi(V, \alpha) = R(V) \int_{z_0}^{\infty} N(z) \cdot T(V, \alpha, z) \cdot dz$$

avec

$$z_0 = r \left[ 1 - \cos \left( \frac{\pi - V}{2} \cos \alpha \right) \right]$$

$r$  étant le rayon de Vénus.

Pour les cornes exactes du croissant ( $\alpha = +90^\circ$  et  $-90^\circ$ ) le trajet optique s'exprime par  $T = 2\sqrt{2rz}$ . Ce trajet demeure indépendant de l'angle de phase  $V$  de sorte que la courbe en trait plein de la figure 28 reproduit, à un facteur près, l'indicatrice de diffusion moyenne  $R(V)$  des particules en suspension dans la haute atmosphère de Vénus au-dessus du niveau supérieur des nuages.

Cette indicatrice de diffusion moyenne  $R(V)$  révèle une très forte concentration de lumière pour  $V = 180^\circ$ , c'est-à-dire à l'opposé de la direction du Soleil; l'intensité décroît très vite lorsqu'on s'écarte de cette direction privilégiée et tombe déjà à près du centième de sa valeur maximum à  $20^\circ$  de cette direction.

Il est connu que de telles propriétés de diffusion caractérisent des particules de très petites dimensions, dont le rayon ne vaut que quelques longueurs d'onde. Supposons que ces poussières soient opaques; la formule de la diffraction  $S = 1,22 \cdot \lambda / 2a$  donne un diamètre moyen de particules  $2a$  voisin de 2 microns. Supposons les particules transparentes avec un indice de réfraction voisin de 1; la théorie de la diffraction par des petites sphères, donnée par Mie, a été calculée par Van de Hulst (8). On trouve un diamètre moyen  $2a = 1,5$  microns.

Dans tous les cas, les particules en suspension dans la haute atmosphère de Vénus ont en moyenne des diamètres voisins de 1,5 ou 2 microns seulement.

#### Répartition verticale du nombre des particules

Pour les azimuths  $80^\circ$ ,  $60^\circ$  et  $45^\circ$  de plus en plus éloignées de la pointe du croissant géométrique, les intensités diminuent vite selon la figure 28. La lumière

provient en effet de couches de plus en plus élevées dans l'atmosphère de la planète et les particules y deviennent plus raréfiées. Nous avons calculé les parcours et les intensités correspondantes, pour deux valeurs de l'angle de phase  $170^\circ$  et  $175^\circ$ , et pour quatre hypothèses sur la répartition verticale  $N(z)$  du nombre de particules par unité de volume :

1. Le nombre de particules décroît proportionnellement à la pression atmosphérique :

$$N(z) = N_0 \exp [(-mg/KT)z] = N_0 \exp (-z/8 \text{ km})$$

2. Le nombre est constant jusqu'à l'altitude de 10 km et nul ensuite.

3. Le nombre est constant jusqu'à l'altitude de 7,5 km et nul ensuite.

4. Le nombre décroît deux fois plus vite que la pression atmosphérique :

$$N(z) = N_0 \exp [(-2 mg/KT)z] = N_0 \exp (-z/4 \text{ km})$$

Les courbes sont reproduites dans la figure 29; le meilleur accord est obtenu dans le dernier cas.

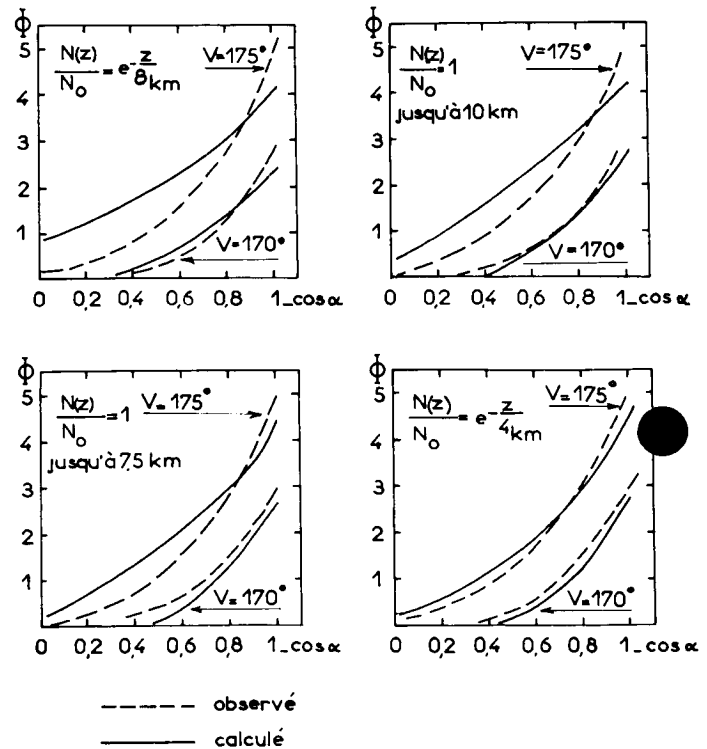


Fig. 29 : Calcul de la répartition des aérosols de la haute atmosphère de Vénus en fonction de l'altitude



Naturellement, les particules peuvent former soit des brumes régulières, soit des voiles clairsemés, soit des colonnes verticales surmontant de part en part la couche nuageuse; mais dans l'ensemble, leur nombre moyen décroît rapidement au-dessus du niveau supérieur des nuages correspondant à  $z = 0$ , dans un facteur  $e$  tous les 4 km, soit à peu près dans un facteur 2 tous les 2,8 kilomètres.

### Coefficient de diffusion par centimètre cube

En supposant la répartition verticale moyenne précédente, l'expression de  $\Phi(V, \alpha)$  donnée ci-dessus s'écrit, pour les cornes du croissant  $\alpha = 90^\circ$  :

$$\Phi(V) = R(V) \cdot N_0 \cdot \int_0^\infty \exp[(-2mg/KT)z] 2\sqrt{2rz} dz$$

L'intégrale, calculée numériquement, donne  $2 \cdot 10^{20} \text{ cm}^3$ .

$R(V)N_0$  est le coefficient de diffusion par  $\text{cm}^3$  à l'altitude  $z = 0 \text{ km}$ , soit

$$\frac{B(\text{cm}^3 z = 0)}{E_0(0,72 \text{ UA})}$$

exprimé en stilb,  $\text{phot}^{-1}, \text{cm}^{-3}$ .  $\Phi(V)$  représente l'intensité globale de l'auréole pour les  $2 \cdot 10^{20} \text{ cm}^3$ , vue de la Terre, rapportée à l'éclairement solaire  $E_0$  (1 UA) à la distance de la Terre. Cette valeur, rapportée à l'éclairement  $E_0$  (0,72 UA) sur Vénus, devient  $\Phi(V) \cdot (0,72)^2$ . Pour  $1 \text{ cm}^3$  à  $z = 0 \text{ km}$ , cette intensité par unité d'éclairement s'écrit :

$$\Phi(V) \frac{(0,72)^2}{2 \cdot 10^{20}} \text{ candela, phot}^{-1}, \text{cm}^{-1}$$

La luminance est l'intensité par unité d'angle solide; on a donc la valeur du coefficient de diffusion par  $1 \text{ cm}^3$  à  $z = 0 \text{ km}$ , en multipliant par le carré de la distance  $d_0$  de Vénus à la Terre exprimée en cm:

$$\begin{aligned} \frac{B(\text{cm}^3 z = 0)}{E_0(0,72 \text{ UA})} &= \Phi(V) \cdot (0,72)^2 \frac{d_0^2}{4 \cdot 10^{20}} \\ &= \Phi(V) \cdot 2,2 \cdot 10^4 \text{ stilb, phot}^{-1}, \text{cm}^{-1} \end{aligned}$$

On a reporté les valeurs correspondantes sur l'échelle d'ordonnée de gauche de la figure 28.

Dans la direction opposée au Soleil,  $\Phi(180^\circ) = 6 \cdot 10^{-13}$  et par suite

$$\frac{B}{E_0}(V = 180^\circ) = 2,6 \cdot 10^{-8} \text{ stilb, phot}^{-1}, \text{cm}^{-1}$$

Le calcul précédent ne donne qu'un ordre de grandeur; les irrégularités variables de l'éclat des cornes et les nodosités lumineuses passagères observées le long de l'auréole indiquent que l'abondance des particules peut varier de plus d'un facteur 5 d'une région à l'autre de la haute atmosphère de Vénus et au cours du temps.

### Conclusions sur la pureté de la haute atmosphère de Vénus

La valeur trouvée  $2,6 \cdot 10^{-8} \text{ stilb, phot}^{-1}, \text{cm}^{-1}$  est très faible. Pour comparaison,  $1 \text{ cm}^3$  d'air parfaitement pur à la pression atmosphérique ordinaire diffuse dans la direction opposée à la source  $1,1 \cdot 10^{-8} \text{ stilb, phot}^{-1}, \text{cm}^{-1}$ .

Comparons la teneur en poussières de la haute atmosphère de Vénus avec celle de notre stratosphère terrestre; les mesures de la luminance du ciel à faible distance du bord solaire, effectuées à différentes altitudes par ballon (9) (10) montrent que notre stratosphère est légèrement polluée par de petits aérosols de diamètres voisins de 1 à 2 microns, comme dans le cas de Vénus. A  $10^\circ$  du bord du Soleil, on aurait sur Vénus, d'après la figure 28,  $B(170^\circ) = 1,0 \cdot 10^{-8} \cdot E_0$  pour 1 cm de parcours à  $z = 0 \text{ km}$ . Pour l'ensemble de l'atmosphère éclairée au-dessus de cette altitude lorsque le Soleil est au zénith :

$$\begin{aligned} \frac{B}{E_0} &= 1,0 \cdot 10^{-8} \cdot \int_0^\infty \exp(-z/4,10^5 \cdot dz) \\ &= 4,0 \cdot 10^{-3} \text{ stilb, phot}^{-1} \end{aligned}$$

Le disque solaire sous-tend  $5,8 \cdot 10^{-5}$  stéradians, et donne une luminance  $B_0 = E_0 (10^5/5,8) \text{ stilb}$ .

L'éclat apparent du ciel à  $10^\circ$  du Soleil pour un observateur situé dans l'atmosphère de Vénus à l'altitude  $z_0$  correspondant au niveau supérieur de la couche nuageuse, serait  $4,0 \cdot 10^{-3} \cdot 5,8 \cdot 10^{-5} = 2,3 \cdot 10^{-7}$  fois la luminance du disque solaire. Cette valeur est très faible; selon les mesures recueillies en ballon pour la stratosphère terrestre par G. Newkirk et J. A. Eddy (9)(10); il faut s'élever dans notre atmosphère jusque vers l'altitude de 10 km pour trouver une brillance du ciel à  $10^\circ$  du Soleil aussi réduite.

On voit donc que la haute atmosphère de Vénus acquiert au-dessus du niveau des nuages la limpidité de la stratosphère terrestre. Une très faible pollution résiduelle est rendue décelable par l'aurole très brillante qu'elle produit lors des conjonctions supérieures de la planète; elle provient de particules de 1 à 2 microns de diamètre, comme dans notre propre stratosphère; la concentration de ces particules décroît verticalement plus vite que la pression atmosphérique et leur éclat global rappelle celui de notre propre atmosphère à l'altitude de 10 km.

### III. Pression atmosphérique au niveau supérieur de la couche nuageuse

La diffusion par les particules devient inappréciable selon la figure 28 lorsque l'angle de phase  $V$  devient inférieur à  $155^\circ$ ; les cornes du croissant cessent alors d'être allongées et deviennent inférieures au seuil de sensibilité photométrique de l'émulsion qui vaut à peu près

$$\Phi_{\text{seuil}} (V=155^\circ) = 0,3 \cdot 10^{-13} \cdot E_0 \text{ (1 cm)} \text{ pour } \Delta \alpha = 1^\circ$$

Cependant l'atmosphère moléculaire pure devrait encore se manifester, si la pression atmosphérique était suffisante.

Soit  $n_0$  le nombre de molécules de gaz à l'altitude  $z = 0$  km correspondant au niveau supérieur de la couche nuageuse observée tangentiellement,  $R$  la constante de Rayleigh-Cabannes de la diffusion par ce gaz et son coefficient de dépolarisation. On a, aux cornes extrêmes du croissant pour lesquelles  $\alpha = 90^\circ$ :

$$B_{\text{atm}}(V) = R \cdot E \cdot n_0 \left(1 + \frac{1-P}{1+P} \cos^2 V\right) \cdot \int_0^\infty \exp[(-mg/KT)z] 2\sqrt{2rz} \cdot dz \text{ stilb, cm}^{-1}$$

L'intégrale vaut numériquement  $4,3 \cdot 10^{20} \text{ cm}^3$  pour un segment d'aurole de  $\Delta \alpha = 1^\circ$ . Pour l'air terrestre,  $1 = 0,04$  et  $R = 5,5 \cdot 10^{-9} \text{ stilb, phot}^{-1}$  dans les conditions normales de pression et température (STP). A la distance 0,72 UA de Vénus au Soleil, on aurait:

$$B_{\text{atm}}(155^\circ) = 5,5 \cdot 10^{-9} \frac{n_0}{n(\text{STP})} 1,85 \times 4,3 \cdot 10^{20} \frac{E_0(1\text{UA})}{(0,72)^2} = 8,5 \cdot 10^{12} \frac{n_0}{n(\text{STP})} E_0 \text{ stilb, cm}^{-1}$$

Vu de la Terre, à la distance  $d_0 = 4,17 \cdot 10^{12} \text{ cm}$ :

$$\begin{aligned} \Phi_{\text{atm}}(155^\circ) &= 8,5 \cdot 10^{12} \frac{n_0}{n(\text{STP})} \frac{E_0}{(4,17 \cdot 10^{12})^2} \\ &= 0,5 \cdot 10^{-12} \frac{n_0}{n(\text{STP})} E_0 \text{ (1 UA)} \end{aligned}$$

Nous avons vu que le seuil décelable était  $0,3 \cdot 10^{-13} E_0$  (1 UA), donc :

$$\frac{n}{n(\text{STP})} \leq \frac{0,3 \cdot 10^{-13}}{0,5 \cdot 10^{-12}} = 0,06$$

La densité de l'air au niveau supérieur de la couche nuageuse de Vénus observée horizontalement est donc inférieure à 6% de celle de notre air au niveau du sol.

L'attraction de la pesanteur étant sensiblement la même que sur Terre, et notre atmosphère ayant une hauteur dans les conditions STP d'environ 8 km, l'épaisseur de l'atmosphère de Vénus au-dessus des nuages correspond à moins de  $0,06 \times 8000$ , soit 480 mètres dans les conditions STP. La pression atmosphérique à ce niveau doit être inférieure à 60 millibars. Cette pression s'observe, dans notre atmosphère terrestre, à l'altitude de 20 km.

Des mesures polarimétriques obtenues par ailleurs indiquent que les valeurs de la densité et de la pression de l'air ne doivent pas être très inférieures aux limites maximales déterminées ci-dessus.

### IV. Etude polarimétrique de la nature des nuages

La nature et les dimensions des particules qui composent les nuages de Vénus peuvent être précisées, dans une certaine mesure, par l'étude de la polarisation de leur lumière. La proportion de lumière polarisée

$$P = \frac{I_1 - I_2}{I_2 + I_2}$$

est mesurée pour différents angles de phase de la planète; on reconstitue finalement la "courbe de polarisation" donnant la variation de  $P$  en fonction de l'angle de phase  $V$ .

B. Lyot (11), à l'aide de son polarimètre visuel à franges, avait donné en 1929 la courbe de polarisation de la planète Vénus pour la lumière de l'ensemble du disque et de l'ensemble du spectre visible. Lyot compara cette

courbe avec de nombreuses déterminations qu'il effectua au laboratoire sur des aérosols artificiels, et montra que les nuages de Vénus pouvaient être constitués de petites particules d'eau mesurant de 2 à 3 microns de diamètre seulement.

En 1955, j'avais publié les premiers résultats d'une étude de la répartition de la lumière sur le disque de Vénus, sous plusieurs angles de phase (12); depuis cette date, j'ai continué à recueillir de nombreuses mesures (18).

La figure 30 donne les courbes de polarisation de Vénus 3 domaines spectraux centrés sur  $0,47 \mu$ ,  $0,55 \mu$  et  $0,65 \mu$ . Ces mesures ont été réalisées avec un polarimètre visuel à franges de B. Lyot, adapté à un réfracteur de

30 cm à l'Observatoire de Meudon, ainsi qu'au réfracteur de 60 cm du Pic-du-Midi (figure 26). Pour les angles de phase inférieurs à  $25^\circ$  et supérieurs à  $155^\circ$ , il faut observer en plein jour, faire usage du parasoleil représenté sur la figure 27 et interposer après le polarimètre le compensateur de polarisation atmosphérique dont j'avais donné la description en 1955 (12).

La polarisation de la lumière est très variable d'un point à l'autre du disque ainsi que nous le verrons plus loin; les mesures de la figure 30 sont localisées dans le plan équatorial de la planète, à mi-distance entre le limbe et le terminateur apparent.

Les observations pour  $V < 25^\circ$  ont été relevées lors de la conjonction supérieure de Vénus en Octobre 1950; on

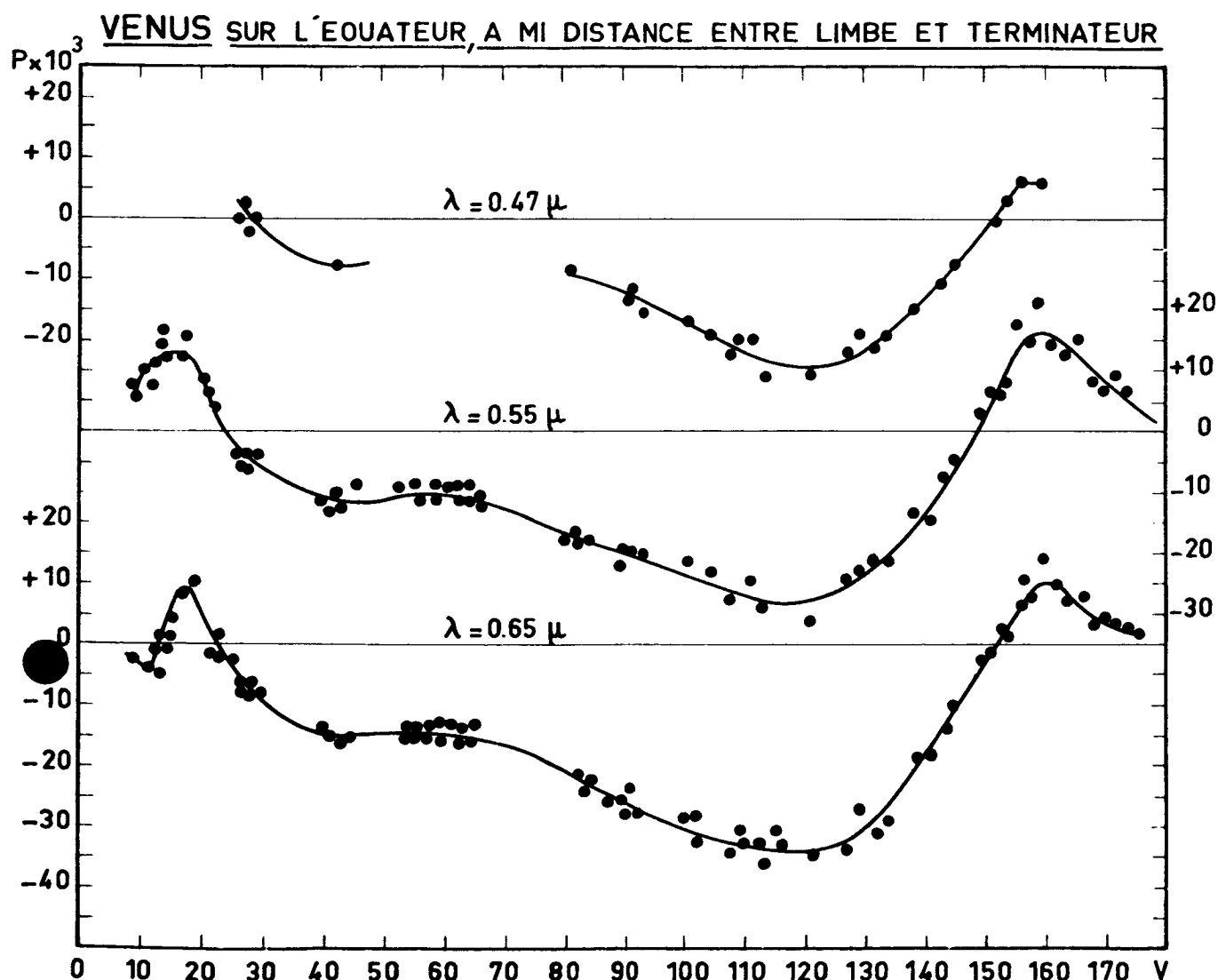


Fig. 30 : Courbes de polarisation de Vénus à  $0,47$ ,  $0,55$  et  $0,65$  microns

remarque une rapide déformation des courbes selon le filtre coloré choisi; de telles variations spectrales caractérisent généralement la diffusion par des particules petites et transparentes.

Les mesures pour  $V > 155^\circ$  furent recueillies à la conjonction inférieure de Juin 1964. La planète se présentait alors comme un très fin croissant, selon les aspects des figures 25 et 34. La polarisation est alors fortement influencée par les diffusions multiples anisotropes dans l'atmosphère de Vénus, selon un mécanisme qui sera expliqué plus loin. Cette diffusion multiple donne, le long de l'équateur, une composante polarisée positive qui doit altérer les mesures; il est possible que les formes de courbes que donnerait la diffusion simple par les

particules ne présentent pas de branches positives vers  $V = 160^\circ$  et possèdent une tangente horizontale avec polarisation nulle pour  $V = 180^\circ$ .

La figure 31 donne les courbes de polarisation de Vénus dans l'infra-rouge pour 3 domaines spectraux centrés sur  $0,84 \mu$ ,  $0,95 \mu$  et  $1,05 \mu$ . Ces mesures correspondent à la lumière globale de l'astre recueillie dans un orifice de diamètre plus grand que celui de la planète et mesuré à l'aide d'un polarimètre photoélectrique. Le principe du polarimètre a déjà été décrit (15)(16). Pour cette application particulière, les cellules étaient des photo-multiplicateurs à cathodes de caesium sur argent oxydé, réalisés à l'Observatoire de Paris par le Prof. Lallemand; elles étaient refroidies avec de la carbo-

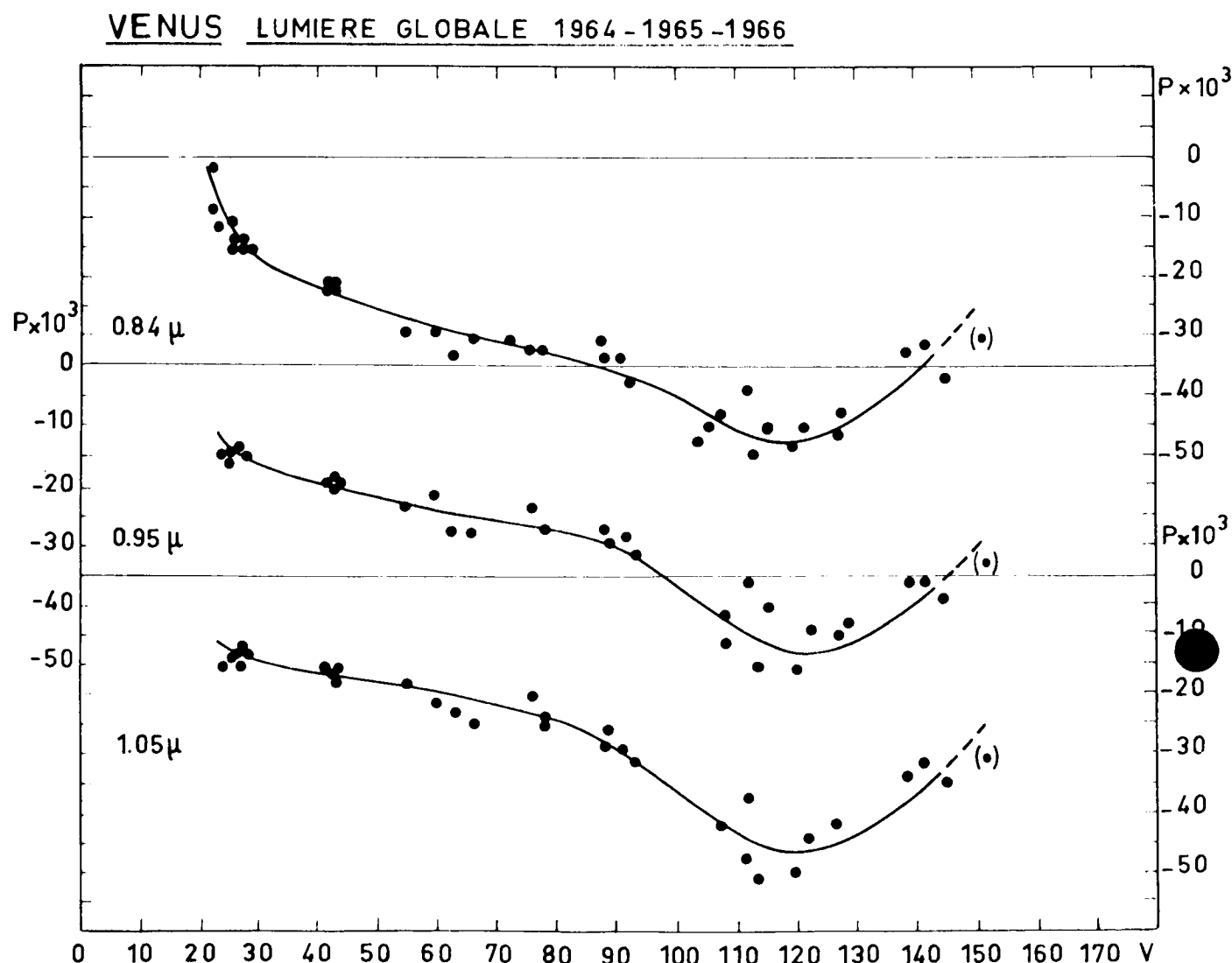


Fig. 31 : Courbes de polarisation de Vénus dans l'infra-rouge à 0,84, 0,95 et 1,05 microns

Ce polarimètre photoélectrique a été utilisé avec le réflecteur de 100 cm de l'Observatoire de Meudon (17) et avec le réflecteur de 107 cm du Pic-du-Midi. Les mesures deviennent assez dispersées lorsque l'angle de phase dépasse  $110^\circ$ , en raison de la difficulté croissante de l'observation dans le crépuscule, et parce que le fin croissant montre des variations locales de polarisations assez fortes.

Les résultats précédents sont résumés sur la figure 32. On y trouve aussi la variation en fonction de la longueur d'onde de l'angle pour lequel la polarisation s'annule (aux environs de  $23^\circ$ ). Cette variation est assez directement liée au diamètre des particules diffusant la lumière.

En 1959 et 1960, T. Gehrels (13) avait recueilli des mesures photoélectriques de la polarisation sur Vénus à travers plusieurs filtres colorés couvrant l'infra-rouge 9.800 Å jusqu'à l'ultra-violet 3.590 Å. Les mesures infra-rouges ne s'accordent pas parfaitement avec les présents résultats qui donnent pour  $V = 60^\circ$  et  $\lambda = 9.500$  Å une polarisation négative plus faible, laquelle diminue encore lorsque la longueur d'onde augmente.

On pourra interpréter les courbes précédentes par le calcul de la diffusion de Mie sur de petites particules; T. Gehrels et J. Coffeen ont déjà entrepris un travail de cette nature. D. Deirmendjian (14) a retrouvé à peu près la courbe de polarisation de Lyot pour un brouillard de petites particules diélectriques légèrement absorbantes ayant un indice de réfraction  $M = 1,353 - 0,0059i$  et différents diamètres voisins de la valeur moyenne  $1,0 \mu$ .

## V. Déviations de la direction de la lumière polarisée

La polarisation de la lumière n'est pas répartie de façon uniforme ou progressive sur la surface du disque; on observe des régions limitées qui manifestent des proportions de lumière polarisée différente des régions voisines.

Ces régions particulières sont temporaires et semblent se modifier rapidement de sorte qu'il n'est généralement pas possible de les reconnaître au bout de 24 heures; leurs comportements rappellent ceux des nuages mobiles et variables que l'on observe en photographiant la planète en lumière ultra-violette. Vers la quadrature, les taches sombres en ultra-violet correspondent quelquefois avec des régions plus fortement polarisées dans le sens négatif mais cette tendance n'est pas toujours confirmée.

Les régions de polarisation anormale montrent souvent des déviations de la direction polarisée. Ces déviations deviennent particulièrement bien visibles lorsque l'angle de phase est voisin de la valeur  $V = 23^\circ$  correspondant à l'annulation de la polarisation moyenne. La figure 33 illustre ce cas et donne les mesures de polarisation relevées en lumière verte (à gauche), en lumière rouge (au centre) et les dessins des taches visibles sur le disque (à droite). Les hachures indiquent la direction de la vibration avantagée; elles sont d'autant plus serrées que la polarisation est plus forte; la proportion de lumière polarisée

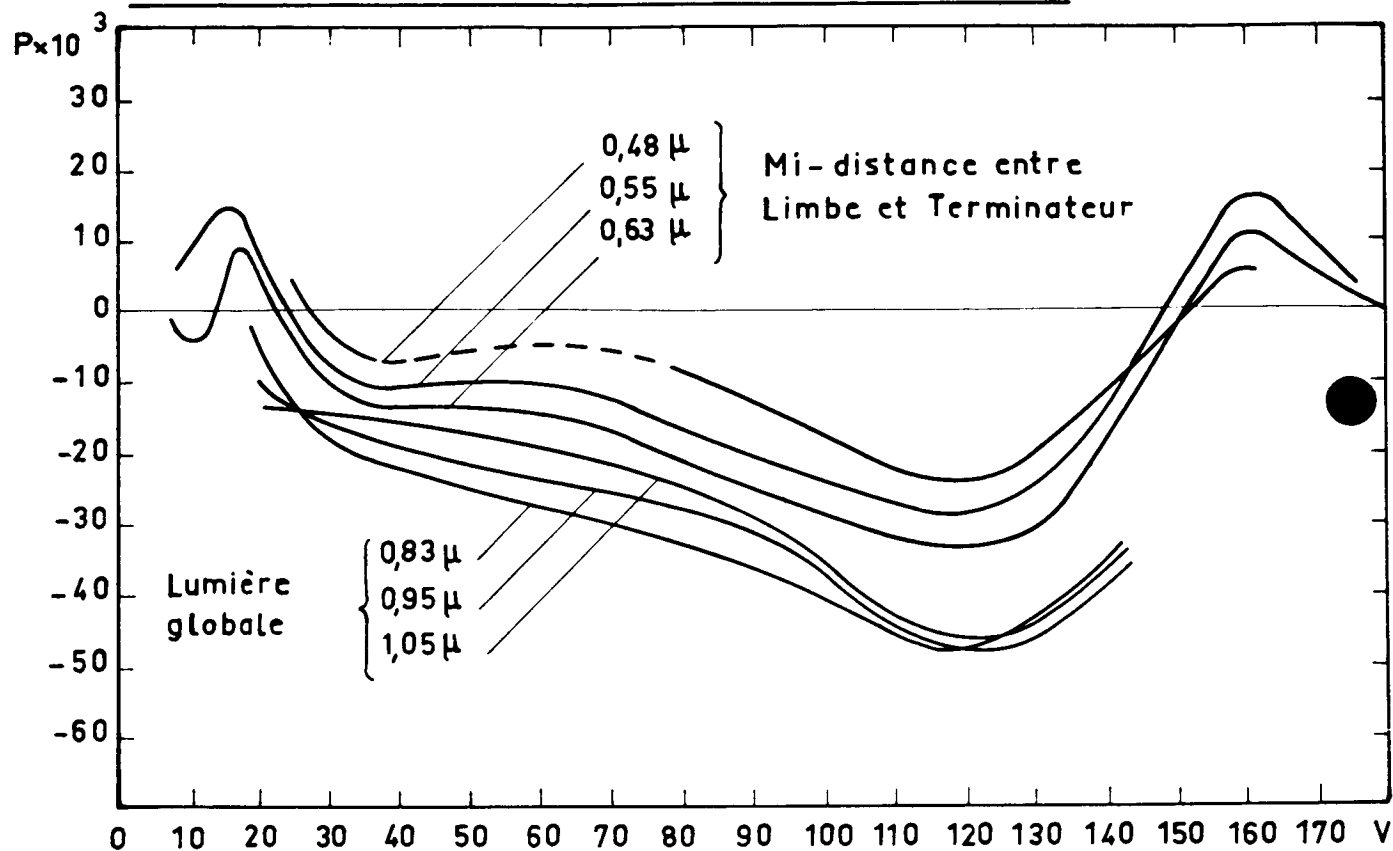
$$P = \frac{I_1 - I_2}{I_1 + I_2}$$

est exprimée en millièmes. On voit que les taches polarisées sont généralement les mêmes en lumières verte et rouge. Sous ces angles de vision, la polarisation de la lumière diffusée une seule fois sur les particules est nulle ou très faible et ne peut donner une direction avantagée que parallèle ou perpendiculaire à la ligne des cornes. Les taches polarisées montrent au contraire des directions privilégiées orientées dans des directions les plus diverses. Cette polarisation ne peut donc provenir de la diffusion simple par les particules composant les nuages; il semble qu'elle provienne de la diffusion multiple entre ces particules, sur des nuages ayant des structures en stries parallèles.

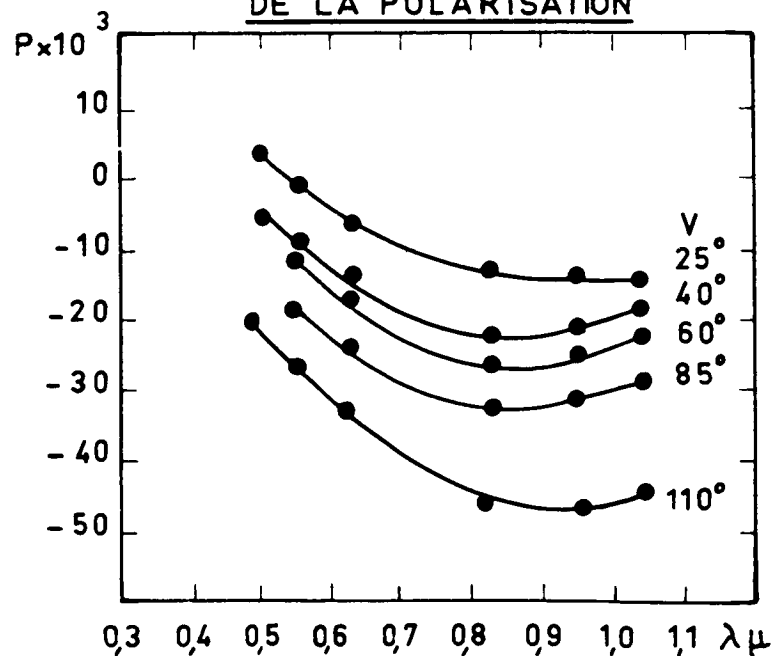
D'autre part, la direction de la lumière polarisée a généralement tendance à être déviée le long du limbe; elle semble pouvoir se décomposer alors en deux polarisations qui se combinent: d'une part une composante principale qui est celle de l'ensemble du disque et dont la direction de vibrations avantagées est, sauf dans les régions où il y a déviation, parallèle ou perpendiculaire à la ligne des cornes. D'autre part, une composante localisée le long du limbe, d'autant plus forte que l'on observe plus près du bord du disque, et dont la direction avantagée est tangente au bord du limbe. Lorsque l'angle de phase devient supérieur à  $165^\circ$ , la planète prend l'aspect d'un très fin croissant, la polarisation principale s'affaiblit et la composante tangente au limbe devient prépondérante. La figure 34 illustre ce cas.

Cette composante tournante ne semble pas pouvoir s'expliquer par la diffusion multiple dans l'atmosphère au-dessus de la couche nuageuse; celle-ci donnerait en effet une vibration perpendiculaire au limbe. La composante observée peut s'expliquer comme il suit: La

COURBE DE POLARISATION DE LA LUMIERE DE VENUS



— VARIATION SPECTRALE —  
DE LA POLARISATION



— ANGLE DE PHASE —  
DE L'INVERSION

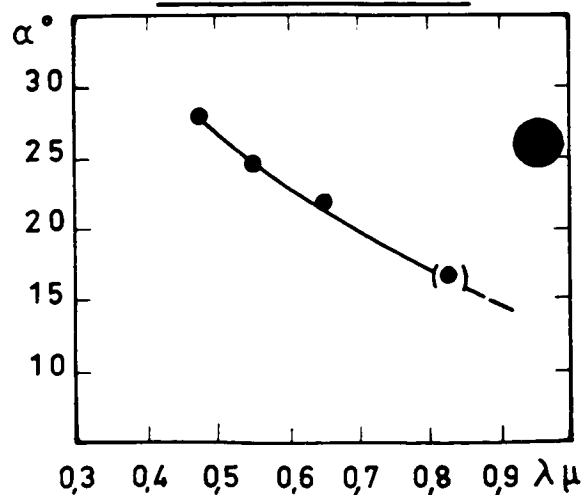
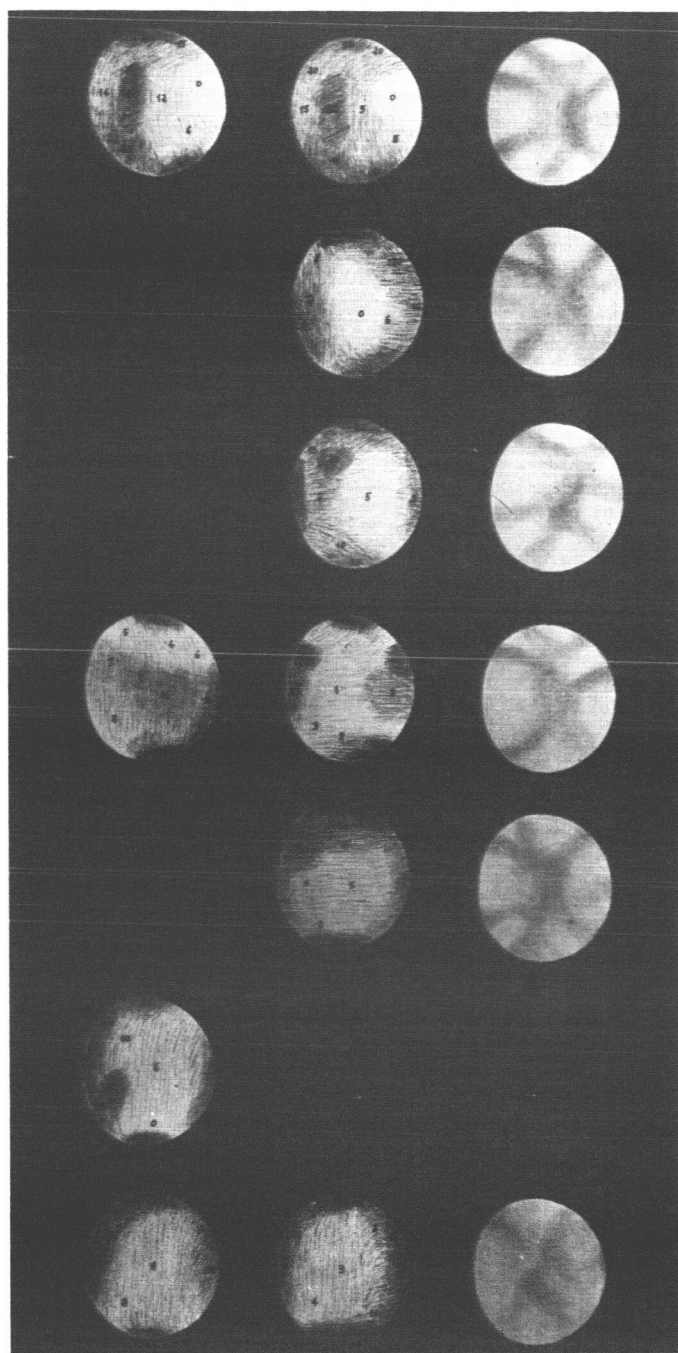


Fig. 32 : Ensemble de courbes de polarisation de Vénus



POLARISATION LUMIÈRE VERTE	POLARISATION LUMIÈRE ROUGE	OBSERVATION VISUELLE
-------------------------------	-------------------------------	-------------------------

5 OCTOBRE 1950 de 8h à 9h		
6 OCTOBRE 1950 de 8h à 9h		
8 OCTOBRE 1950 de 7h30m à 8h30m		
12 OCTOBRE 1950 de 7h30m à 8h30m		
14 OCTOBRE 1950 de 7h30m à 8h30m		
18 OCTOBRE 1950 de 8h30m à 9h30m		
20 OCTOBRE 1950 de 8h à 9h30m		

**Fig. 33 : Répartition de la lumière polarisée sur la surface du disque de Vénus**

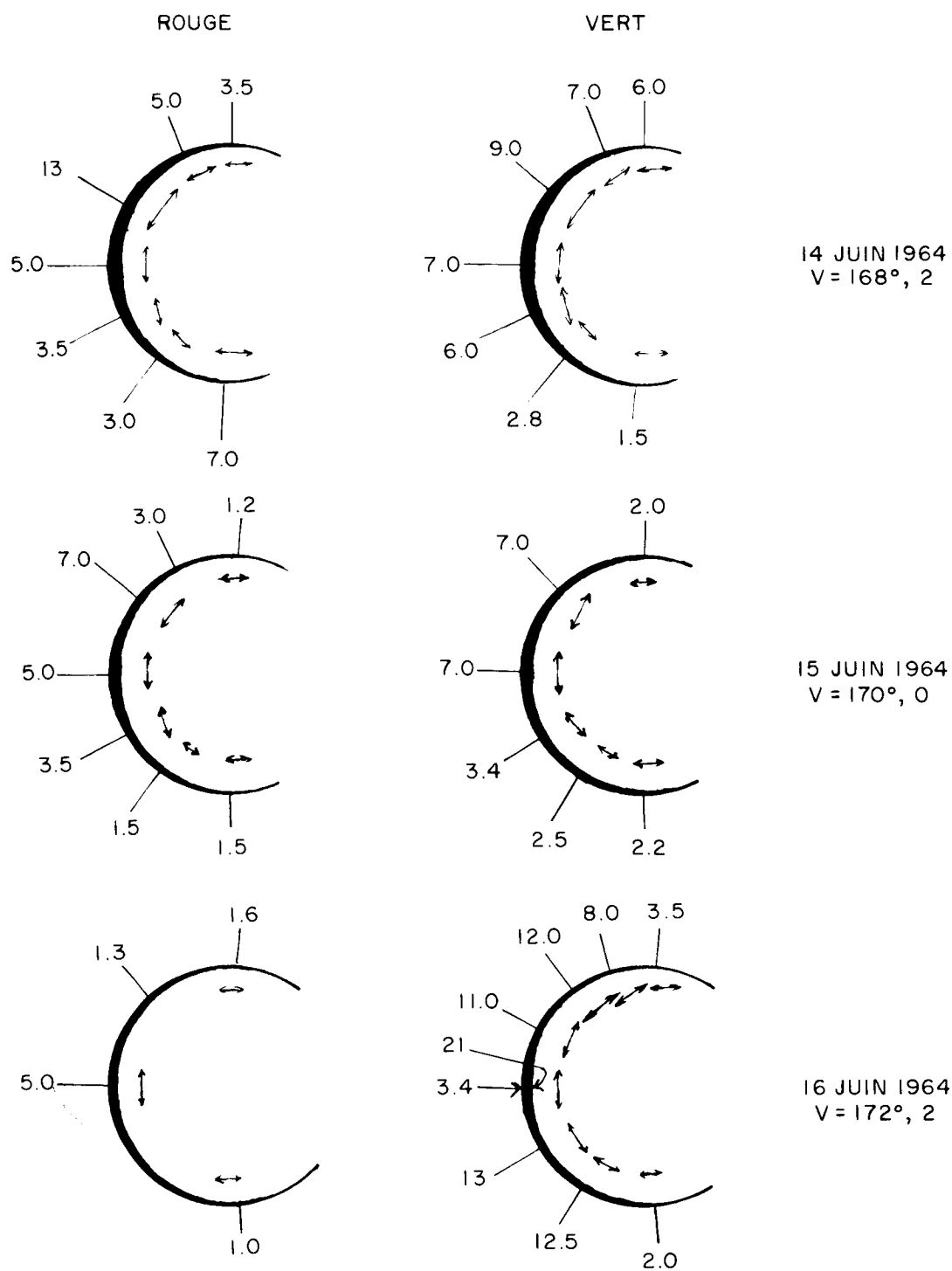


Fig. 34 : Polarisation de la lumière sur les cornes du croissant de Vénus



polarisation des nuages de l'atmosphère de Vénus montre souvent des déviations de direction qui peuvent provenir de la diffusion multiple sur des structures nuageuses en bandes ou en rouleaux. Admettons qu'il en soit ainsi, plus généralement, à une échelle de dimensions inférieure au pouvoir séparateur de notre polarimètre. Au centre du disque, les polarisations diversement orientées se compensent en moyenne et se détruisent; au bord du disque, à la distance planétocentrique  $\theta$  du centre, elles sont vues obliquement, et la résultante est une composante polarisée proportionnelle à  $\cos^2 \theta$ .

Selon les observations précédentes, les nuages de Vénus sembleraient donc présenter très souvent des structures en bandes ou en rouleaux parallèles, soit sur

de très grandes étendues, soit sur des régions plus limitées.

Nos nuages terrestres présentent aussi ce caractère, qui apparaît sur de nombreuses photographies infra-rouges des formations nuageuses terrestres obtenues par les satellites météorologiques. Ces structures résultent des stratifications thermiques dont l'atmosphère est le siège, lesquelles sont provoquées principalement par les changements d'état de l'eau sous forme solide, liquide et vapeur.

De telles structures ne semblent pas pouvoir apparaître dans une atmosphère dont les voiles seraient dus seulement à des poussières solides.

## REFERENCES

1. "L'Astronomie" Décembre 1959, p. 468.
2. C. R. Acad. Sci. 1963, 256 3250.
3. "The Origin and Evolution of Atmospheres and Oceans," chap. 12, p. 257. Pub. Brancazio et Cameron, John Wiley and Son 1964.
4. Mem. Soc. Roy. Liège, Cinquième Série IX 392.
5. AFCRL "Scientific Balloon Symposium" USAF-OAR 409 1964.
6. "L'Astronomie" Février 1964, p. 41.
7. A. Dollfus et E. Maurice, C. R. Acad. Sci. 1965, 260 427.
8. Van de Hulst, "Sight Scattering by Small Particles" John Wiley and Son 1957.
9. G. Newkirk et J. Eddy, JI. of Atmospheric Sci. 1964, 21 35.
10. G. Newkirk et J. Eddy, Nature 1962, 194 638.
11. B. Lyot, "Recherches sur la polarisation de la lumière des planètes et de quelques substances terrestres" Ann. Observatoire Meudon Tome VIII 1929. Traduction en anglais NASA TT F-187.
12. A. Dollfus, "Etude des planètes par la polarisation de leur lumière" Thèse, Paris 1955 et Supplément Ann. Astroph. 1955. Traduction en anglais NASA TT F-188.
13. T. Gehrels et R. E. Samuelson, Astroph. JI. 1961, 134 1022.
14. D. Deirmendjian, JI. Geophysical Res. 1962, 67 1635.

## REFERENCES (Cont'd)

15. A. Dollfus, C. R. Acad. Sci. 1958, 246 2345.
16. A. Dollfus, C. R. Acad. Sci. 1963, 256 1920.
17. M. Marin, Rev. Optique 1965, 44 115.
18. En partie grace à une convention de recherche avec l'U.S. Air Force, Contract AF 61(052)-508.

## SUMMARY REMARKS ON VENUS

Duane O. Muhleman\*

Jet Propulsion Laboratory  
Pasadena, California

The availability of observational data concerning Venus has greatly increased during the period from 1960 to the present. Perhaps 1960 appears to be a turning point in this regard since passive radio emission measurements became available at that time. These measurements by Mayer, McCullough, and Sloanaker at wavelengths of 3 and 10 cm indicated a temperature of  $600^{\circ}\text{K}$  and a thermal-emission spectrum. The radio observations have been extended down to the submillimeter region and up to the meter region with significant variations from  $600^{\circ}\text{K}$  in evidence. The radio observations also showed a strong dependence on the solar phase angle relative to the Earth, particularly at 8 mm.

H. Spinrad, from his study of old Mount Wilson plates, found indications of atmospheric pressures on the order of from 2 to 5 atm deep in the Venusian atmosphere but little trace of water vapor, perhaps less than  $10\ \mu$ . Investigators at Mount Wilson had, of course, reported the apparent lack of water many years earlier. However, A. Dollfus in France and J. Strong's group did find spectral information to suggest about  $100\ \mu$  of water vapor above ice-crystal clouds.

\*Now at the Department of Astronomy, Cornell University.

The question of the rotational rate of Venus was essentially cleared up by the radar work of R. Carpenter, R. Goldstein, and D. Muhleman; a circumstance that now makes it possible to carry out qualitative calculations of heat conduction, cloud building, etc., for the planet. Radio measurements from *Mariner II* supported the wealth of Earth-based radio measurements and gave a clear indication of limb darkening, which, in turn, supports the well established idea that the surface of Venus itself has a temperature on the order of  $600^{\circ}\text{K}$ .

It was in the atmosphere of this information that the symposium on Venus assembled. The discussions began with the presentation of the balloon astronomy work carried out by Strong and his co-workers at Johns Hopkins University. Strong reported that the observations of Venus were made with an automatic 30-cm telescope supported by a balloon at 26.5 km above the Earth. The radiation was measured in the  $1.13\ \mu$  bands with a grating spectrometer of 2 Å resolving power. The effect of the Venus water vapor absorption was the same as the calibrated effect of  $98\ \mu$  of water at 1 atm pressure. The effect of the water in the Earth's atmosphere

above the telescope was just a few percent. Strong's group measured the reflection spectrum from the top of the cloud layer in a subsequent balloon flight within the spectral range from 1.7 to 3.4  $\mu$ . A comparison with the reflection spectrum in the same wavelength interval of an ice-crystal cloud at  $-39^{\circ}\text{C}$  (prepared in the laboratory) was shown to be in excellent agreement with the Venus spectrum. The Venus spectrum was corrected for the amount of water vapor above the Venus clouds found from the previous balloon measurements and for  $\text{CO}_2$  found by earlier investigators. Strong reminded us that the significance of a cloud top temperature of  $-39^{\circ}\text{C}$  was noted by Menzel and Whipple in a 1955 paper: namely, that  $-39^{\circ}\text{C}$  is precisely the temperature assumed by high-level cumulus clouds in the Earth's atmosphere because this temperature is the lowest at which water can still exist in the liquid state.

Strong believes that his results offer an explanation for the observed equality of the dark and light hemisphere infrared temperatures found by early workers and more recently by B. Murray and his co-workers here at Caltech. He believes that the temperature of the dark side is maintained by the heat of condensation. Water vapor from the sunlit hemisphere, as it is carried convectively to the dark hemisphere, will cool, condense, and freeze with the release of over 600 calories per gram.

D. Deirmendjian reported that he has compared Strong's spectrum with spectra obtained from high-flying airplanes over dense cirrus-ice clouds on the Earth and found excellent agreement. It was reported that the observations of Strong suggest that the disposition of water in the high Venus atmosphere is similar to that above 16 km on the Earth. Deirmendjian reiterated his belief "that the Venusian atmosphere contains large amounts of particulate matter that appears to be in permanent suspension." Furthermore, he believes that it is not possible to derive the nature of the *gaseous* component from the observed spectrum, brightness, and polarization alone, without definite knowledge of the nature of the *particulate* matter.

Discussions from the symposium as a whole lead to the general agreement that the work of Spinrad with the early Venus plates was sound. His analysis of the Venus spectral lines yielded a rotational temperature on the order of  $400^{\circ}\text{K}$  and pressures of about 2 atm, which surely must mean that he was looking deeply into the Venusian atmosphere. As is well known, the major result of this work was the identification of only about 10  $\mu$  of water at these depths. This is clearly in conflict with the

information provided by the work of Strong and Dollfus and, in my opinion, a paradox clearly exists.

Dollfus reviewed his 1959 balloon work and reported 70  $\mu$  of water vapor above the clouds. He also reviewed for us a considerable collection of photometric and polarimetric observations of the Venus clouds. The photometric data were shown to match the responses of an atmosphere with a scale height of 2.8 km, a grain size of 2  $\mu$ , and a number density on the order of  $3 \times 10^8 \text{ cm}^{-3}$ . Variations in the polarization of the reflected light suggest to Dollfus the presence of water clouds as opposed to dust clouds.

C. Sagan reported some of the results of extensive calculations, carried out in collaboration with J. Pollack, of a model atmosphere employing water clouds. They performed exact solutions to the Mie theory problem utilizing an arbitrary single-scattering albedo and an *anisotropic* phase function to reconstruct theoretical curves to match the Venus observations. Their calculations support Strong's identification of ice as the "principal constituent" of the clouds. The mean radius of the cloud particles was found to lie between 7.5 and 10  $\mu$ . Clouds with these properties allow a sizable fraction (20 to 50%) of the incident sunlight to penetrate the surface, but are extremely opaque to radiation thermally produced by the planet. Thus, according to Sagan, an efficient greenhouse effect is operative. The calculations of Sagan and Pollack predict a small absorption dip at 1.3 cm in the microwave spectrum that has not been observed in the measurements of Welch, Barrett, Drake, or Jones. This writer believes that this is a true discordance between theory and experiment. The amount of water required by Sagan and Pollack is modest by terrestrial standards but more than that reported by Spinrad.

The radar observations were reviewed by Muhleman, who reported an average reflection of the Venus surface in the wavelength range from 12 cm to 8 m of about 12 to 14% with some indication of increased reflectivity at the long wavelengths. A reflectivity of 1% at 3.6 cm, measured by Karp and coworkers at the Lincoln Laboratory, was reported. They have interpreted this measurement as an indication of a high opacity of the Venus atmosphere in the 3-cm region. Since this result is very important to model calculations and was somewhat marginal owing to the difficulties of the measurement, a confirming experiment is vital.\*

\*Between the time of the symposium and the publication of these *Proceedings*, a confirming radar experiment has been carried out with positive results. This is new information of considerable importance.

Muhleman reported the most current results of the work of Carpenter and Goldstein concerning the rotational rate of Venus as determined by radar. A retrograde rotational period of  $250 \pm 5$  days with the rotational pole at a right ascension of  $80^\circ$  and a declination of  $-68^\circ$  have been obtained (about  $6$  or  $7^\circ$  from the pole of the Venus orbit). Similar results were reported to the symposium by R. Dyce from work at the Cornell Arecibo Observatory and by J. Thomson at Jodrell Bank.

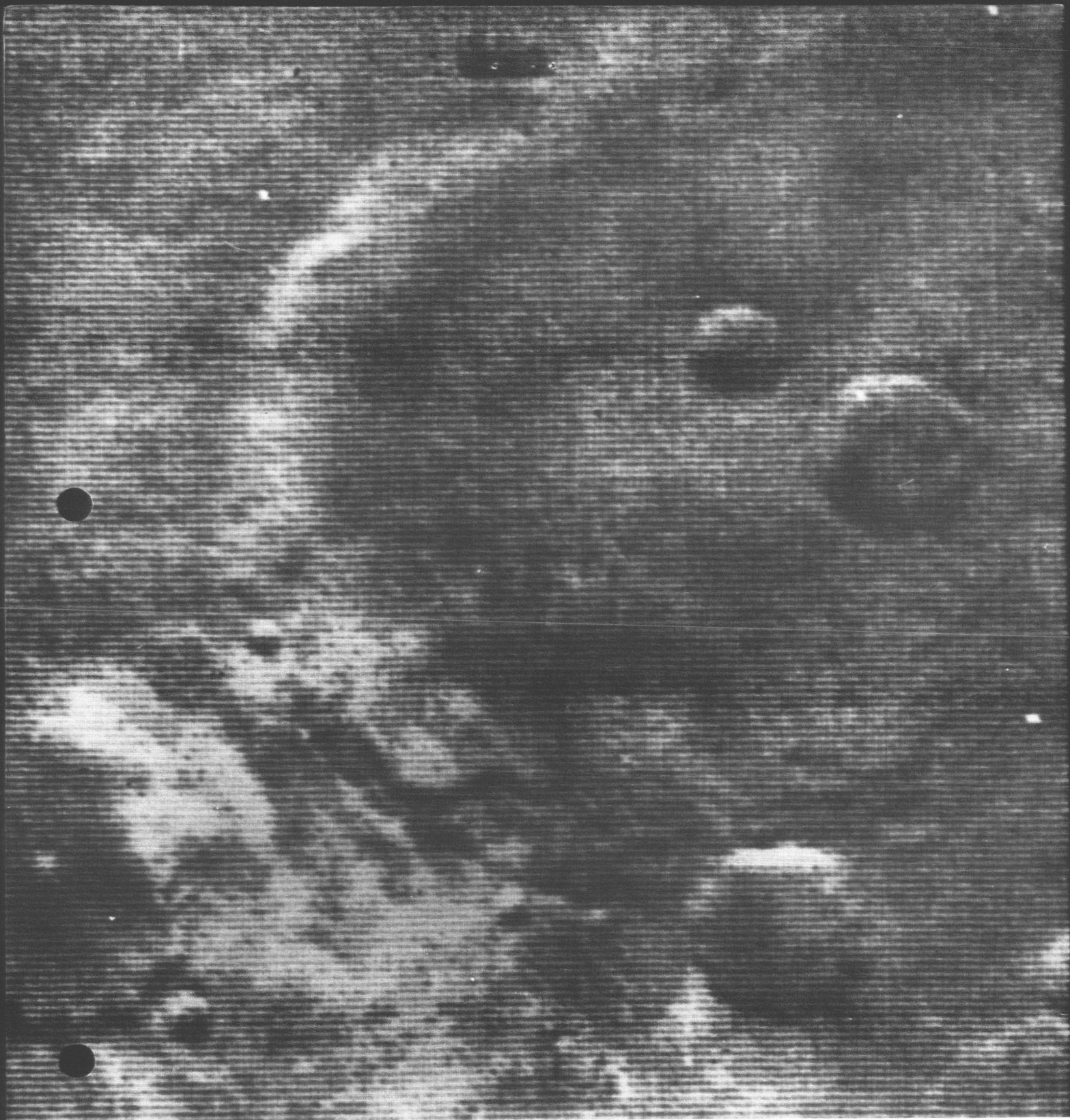
Muhleman's study of the radar backscatter function of Venus from pulse response and radar spectral analysis indicates that Venus is considerably smoother than the Moon at radar wavelengths, perhaps by a factor of 2 in terms of mean slopes. Highly significant surface features have been found by Goldstein and Carpenter and have been verified by Dyce and Pettengill. This work has enabled Goldstein and Carpenter to construct the beginnings of true surface maps of Venus.

The passive radio measurements were reviewed by F. Drake. The microwave spectrum has been extended by F. Low to the submillimeter region, where a temperature of about  $300^\circ\text{K}$  is found to be consistent with the millimeter work. Measurements at wavelengths longer than  $20$  cm indicate that the brightness temperature falls off from the high values of  $600$ – $700^\circ\text{K}$ . Drake reported that the suggested increase in radar reflectivity at these wavelengths would partially explain these effects. A. Kuzmin has proposed a cold ionospheric model as a possible explanation. Detailed measurements around the microwave water vapor line show no clear indication of such a line in the Venus atmosphere. Drake reviewed the radio interferometric work of Clark and Kuzmin, which,

he believes, most strongly supports the conclusion that the high radio brightness temperatures arise in the Venusian surface. Clark and Kuzmin found a temperature of  $630^\circ\text{K}$  at the center of the disk and  $470^\circ\text{K}$  toward the poles. These measurements have been interpreted as the thermal emission from a dielectric sphere with dielectric constant  $\epsilon = 2.2$ – $2.5$ . These values are considerably below the values obtained from the radar reflectivities; this is the *same situation that arises in the case of the Moon*.

Drake also reported the work by Muhleman and by Pollack and Sagan on explaining the microwave phase effect. Their calculations show that the observed effect in the centimeter region is explained by the emission at various depths into the Venusian surface from materials of low thermal conductivity and in a granulated state. The proper delay in the time (phase) of the temperature minimum and the amplitude of the temperature variation under these conditions with a 250-day retrograde rotational period is exhibited. This method offers a powerful tool for the study of the Venusian surface materials.

Finally, A. Barrett reviewed his extensive work on model calculations in an effort to explain the microwave spectrum. He showed that a wide range of models involving high-pressure  $\text{CO}_2$ , dust, water clouds, etc., would explain the observations. Barrett pointed out the great dangers in using laboratory line widths and shapes, etc., for the application to the Venus problem. Furthermore, he expressed the great need for the *close* exploration of Venus by space probes. I believe that the agreement on this point was, for once, unanimous.



#### *IV. MARS*

PRECEDING PAGE BLANK NOT FILMED.

#### PART IV. MARS

- D. G. Rea, The Atmosphere and Surface of Mars—  
A Selective Review
- R. Goldstein, JPL Radar Observations of Mars
- D. M. Hunten, CO<sub>2</sub> Bands and the Martian Surface Pressure
- H. Spinrad, Spectroscopic Observations of Mars, 1964-5
- T. Owen, Recent Observations of the Photographic Spectrum  
of Mars—A Preliminary Report
- R. L. Younkin, A Search for Limonite Near-Infrared Spectral  
Features on Mars
- R. B. Dyce, Recent Radar Observations of Mars
- C. Sagan and J. B. Pollack, Radio and Radar Evidence on the  
Structure and Composition of the Martian Surface
- A. J. Kliore et al., Preliminary Results of the *Mariner IV*  
Occultation Measurement of the Atmosphere of Mars
- G. Fjeldbo et al., Preliminary Results of the *Mariner IV* Radio  
Occultation Measurements of the Upper Atmosphere  
of Mars
- R. B. Leighton, Comments on the *Mariner IV* Photographs  
of Mars
- C. Sagan, High-Resolution Planetary Photography and the  
Detection of Life
- A. Dollfus, Contribution au Colloque Caltech-JPL sur la lune  
et les planètes: Mars
- G. Münch, Summary Remarks on Mars

## THE ATMOSPHERE AND SURFACE OF MARS—A SELECTIVE REVIEW

D. G. Rea

University of California  
Berkeley, California

### 1. Introduction

Our knowledge of the Martian environment has been growing at an ever increasing pace the past few years. This growth is directly related to the major space programs initiated by the United States and the Soviet Union. The plans for observing Mars from flybys, orbiters, and landers have stimulated not only spacecraft experimental development but also ground-based observations. The latter have used traditional astronomical telescopes, in some instances applying recent technological advances, together with the newer radio telescopes. Laboratory studies have helped in interpreting these observations. While the major space programs are essentially localized in only two countries, their stimulus has extended to many others, and significant contributions are coming from scientists in many lands. Today I will gather together the published reports of this work and construct a framework to which the subsequent papers can be related. I will attempt to present a unified picture, but one that includes more than one interpretation for the same phenomenon where the correct one is not clearly indicated. Older data and interpretations, where no longer valid, will be mentioned at most only in passing. Anyone interested in pursuing the historical background

further should consult the excellent book by de Vaucouleurs (Ref. 1). Another fascinating, but less general, work is *Mars, The Photographic Story*, by Slipher (Ref. 2).

Some important characteristics are summarized in Table 1. The mass has been determined by measuring the orbits of the two satellites, Phobos and Deimos. Both are very small and their diameters have perforce been derived from their observed brightness, assuming their reflecting power to be identical to that of the parent planet. The values so found are 23–30 and 11–14 km respectively. Their orbital radii are respectively 9,340 and 23,500 km, and Phobos is distinguished among the planetary satellites by having its orbital period, 7 hours 39 min, shorter than the rotational period of the parent. Phobos has also been singled out for attention as a possibly artificial satellite since its orbital elements appear to indicate a secular acceleration (Ref. 3). This was attributed by Shklovsky (Ref. 4) to atmospheric drag, whose effectiveness is enhanced by a very low density associated with a hollow structure put in orbit by intelligent Martians. This proposal conflicts with the widespread belief that a highly intelligent and technological



Table 1. Some physical properties of Mars and Earth

Property	Mars	Earth
Mass, g	$0.646 \times 10^{27}$	$5.98 \times 10^{27}$
Diameter, km	6800	12,800
Average density, g cm <sup>-3</sup>	3.96	5.52
Surface gravitational acceleration, cm sec <sup>-2</sup>	370	981
Mean distance from Sun, km	$228 \times 10^6$	$150 \times 10^6$
Angle between rotation axis and orbital plane, deg	24.5	23.5
Length of year, days	687	365
Length of southern spring, days	146	91
Length of southern summer, days	160	87
Length of southern fall, days	199	93
Length of southern winter, days	182	94
Length of day, hours	24.6	24

Martian life has never developed. Other explanations proposed for the secular acceleration of Phobos are tidal effects (Ref. 5) and conventional atmospheric drag (Ref. 6). The latter explanation used an atmospheric model with a surface pressure of 85 mb, roughly an order of magnitude higher than our best current estimates. This suggests that the drag theory is probably no longer tenable. The writers on this subject have all recognized the inadequacy of the raw data and have suggested that the effect itself may be fictitious.

The diameters, equatorial and polar, of Mars have been measured by several observers with somewhat discordant results. The most recent determinations, by Dollfus (Ref. 7), using a birefringent micrometer, give  $D_{eq} = 6790$  km and  $D_{pol} = 6710$  km, the optical flattening,  $(D_{eq} - D_{pol})/D_{eq}$ , then being 0.0117. He observed no difference in diameters for red and blue light, in contrast with some previous workers, notably W. H. Wright, who obtained diameters that were 2-3% greater in the blue than in the red. The difference may be due to greater limb darkening in the red, or to a blue scattering haze layer in the atmosphere.

The optical flattening of 0.012 is significantly different from the value of 0.0051 obtained by an analysis of the satellite orbits. MacDonald (Ref. 8) has argued that 0.012 is improbably high for reasonable strengths of the Martian rocks. The possibility that an atmospheric effect is responsible has been advanced by Kuiper (Ref. 9), who

proposed an equatorial haze layer at an altitude of ca 17 km. This idea has been criticized by de Vaucouleurs (Ref. 1) on two counts: (1) the maximum altitude of the haze layer is 17 km, at the estimated tropopause, whereas a layer at 70 km is required to account for the difference, and (2) a haze layer can not affect the flattening measured by Wright's method of following surface features as they cross the disk. Moreover the haze layer should have a greater effect in the blue than in the red, whereas the oblateness is not found to be wavelength-dependent. Another possible explanation is that the optical flattening is real and that the density of the material in the equatorial bulge is lower than that in the polar regions (Ref. 7).

The orbital parameters differ somewhat from Earth's. The mean distance from the Sun is  $228 \times 10^6$  km, compared with  $150 \times 10^6$  km for Earth, resulting in a mean solar constant at Mars which is 0.43 that at Earth. In the course of a Martian year of 687 Earth days, the planet travels an elliptic orbit with an aphelion of  $248 \times 10^6$  km and a perihelion of  $208 \times 10^6$  km. The seasons are accordingly unequal in length, and, since the tilt of the rotational axis is such that summer in the southern hemisphere occurs near perihelion, this season is shorter and hotter than summer in the northern hemisphere. The seasons, however, are essentially similar to ours since the inclinations of the rotational axes of Mars and Earth to their orbital planes are nearly identical.

## II. The Atmosphere

Important properties of the atmosphere of Mars include pressure, composition, and particulate content, as well as the presence of clouds.

### A. Pressure

Early estimates of the surface pressure were drawn principally from photometric and polarization observations. Thus the brightness and polarization were measured as a function of wavelength, position on the disk, and phase angle. Certain assumptions were made about the composition of the atmosphere and the reflecting properties of the surface, and the atmospheric pressure was then derived. A set of such values is given in Table 2, taken from de Vaucouleurs (Ref. 1), p. 124 (the comments in the "Remarks" column are his). After evaluating the various attempts, he decided that the pressure was  $85 \pm 4$  mb. This was the value in general use until 1963, when a new and powerful technique, based on infrared spectroscopy, was applied to the problem.

Table 2. "Old" determinations of the surface pressure

No.	Year	Author	Method	Pressure, mb	Remarks
1	1926	Menzel	Visual and photographic albedo	—	Rejected
2	1929	Lyot	Visual polarimetry	—	Rejected
3	1934	Barabascheff	Photographic photometry	50	Doubtful
4	1940	Barabascheff	↓	116	Doubtful
5	1941	Scharonow		120	Indirect
6	1944	Sytinskaya		112	Doubtful
7	1944	Fessenkoff		125	Illusory
8	1945	Vaucouleurs	Visual photometry	93	Approximate
9	1948	Hess	Theoretical meteorology	80	Illusory
10	1948	Dollfus	Visual polarimetry	80	Preliminary
11	1951	Dollfus	↓	95	Approximate
12	1951	Dollfus		83	Final

On the night of April 12/13, 1963, a high-resolution, near-infrared spectrogram of Mars was obtained by Spinrad on the 100-in. coudé spectrograph at Mount Wilson. He was attempting to detect Martian water vapor and was successful in that quest. But the plate surprisingly showed lines of the  $5 \nu_3$  band of  $\text{CO}_2$  at 8700 Å, Fig. 1. Since the lines were very weak, their equivalent width was affected only slightly by the pressure and a  $\text{CO}_2$  abundance, *essentially independent of the pressure*, could be derived. This was done in an analysis by Kaplan, Münch and Spinrad (Ref. 10) and a value of  $55 \pm 20$  m-atm was found. This abundance was then used to obtain a pressure from the pressure-sensitive  $2 \mu$  bands of  $\text{CO}_2$  as measured previously by Kuiper and by Sinton, Fig. 2. The resultant  $25 \pm 15$  mb was much lower than the previously accepted value of 85 mb and created quite a stir, not only in the scientific community, but also in that part of the NASA charged with landing a laboratory on the surface of Mars. When the pressure is so low, a significant fraction of a lander's weight is consumed by the spacecraft, which must have a large drag coefficient to slow it down so that a

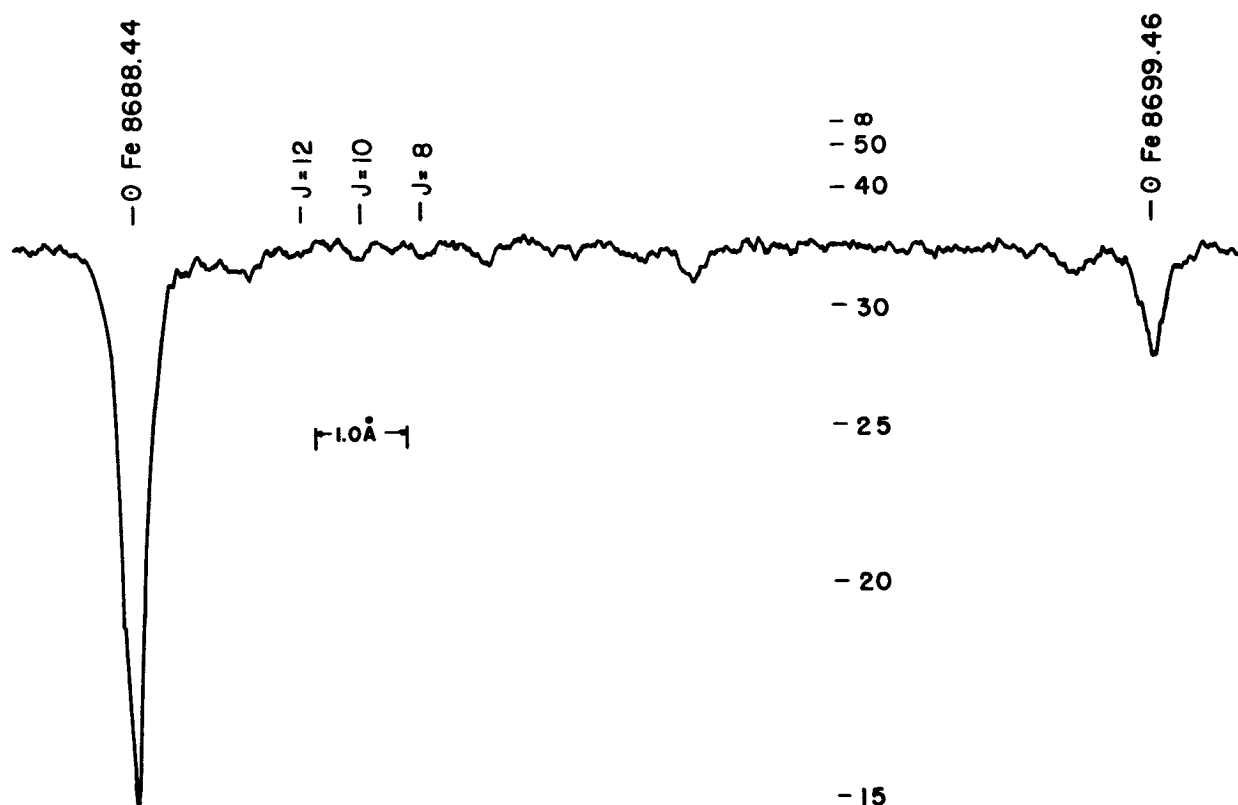


Fig. 1. A microphotometer tracing of the R-branch in the  $5 \nu_3$   $\text{CO}_2$  band of Mars. The measured lines  $J = 8, 10, 12$ , and two solar lines are shown (Ref. 10). (From *The Astrophysical Journal*, 1964, Vol. 139, p. 4)

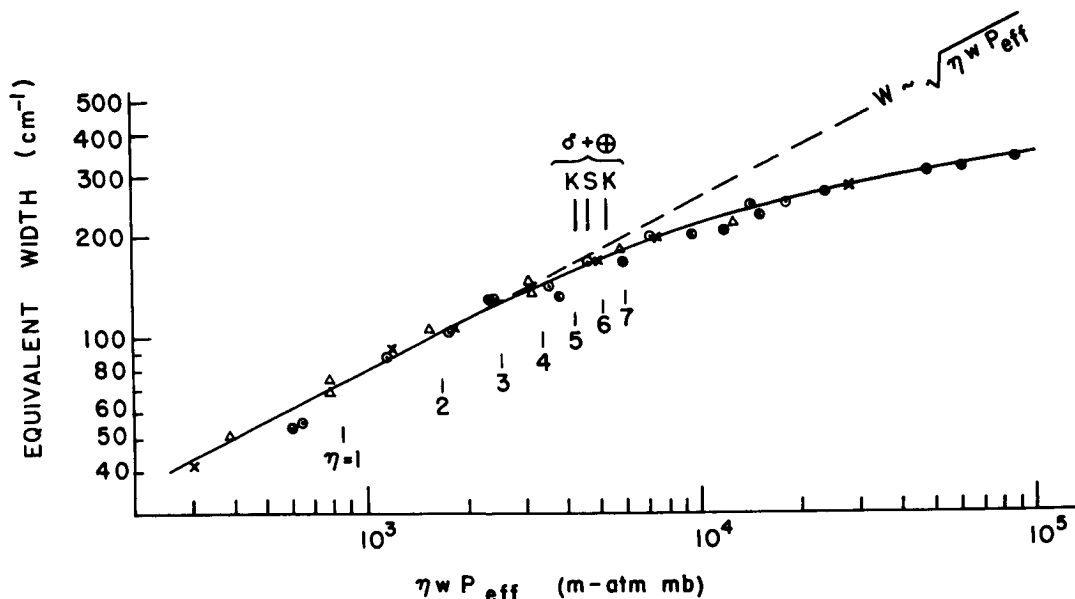


Fig. 2. Equivalent width of  $2 \mu$  band complex vs  $\text{CO}_2$  amount times effective pressure. The abscissa markings below the curve are for various telluric air masses,  $\eta$ , above the curve for Earth plus Mars from Sinton (S) and Kuiper (K), upper and lower limits (Ref. 10).  
(From *The Astrophysical Journal*, 1964, Vol. 139, p. 9)

parachute can be deployed for a soft landing. Since the engineers would, of necessity, be conservative in their design, it was mandatory to confirm this new estimate and to reduce its error limits if at all possible.

The desirability of refining the pressure determination is dramatized in Fig. 3, kindly supplied by C. F. Campen and J. A. Stallkamp (Ref. 11). The weights apply to a particular landed capsule designed to operate with uncontrolled entry orientation, for entry angles from grazing ( $20^\circ$ ) to vertical ( $90^\circ$ ), and with a single subsonic parachute for terminal descent. The useful landed payload includes power, communications, structures, and scientific instruments (ca 5–10% of the useful landed payload). A more precise knowledge of the atmosphere will also permit an orbit to be chosen that has a periapsis closely matched to the actual atmospheric structure and the desired apoapsis and lifetime, Table 3. This clearly facilitates the reconnaissance function of the orbiter, by increasing the spatial resolution attainable.

Accordingly, for scientific and agency reasons, several groups initiated programs to confirm and refine the spectroscopic pressure determination. These efforts have been critically reviewed by Chamberlain and Hunten (Ref. 12) and by Cann, Davies, Greenspan and Owen (Ref. 13). The latter have made some small corrections and have re-evaluated the uncertainties, with the

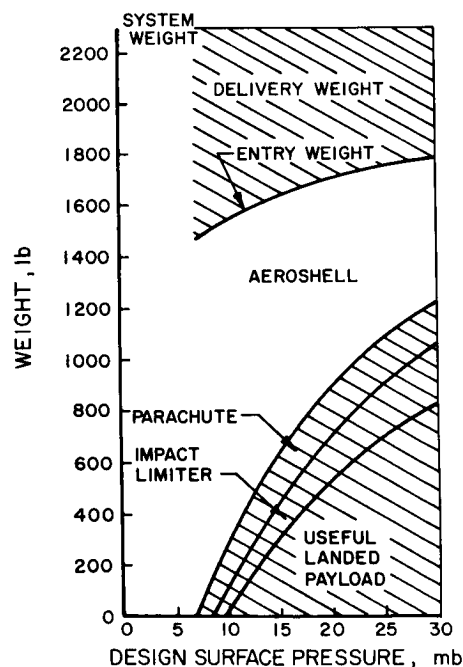


Fig. 3. The effect of atmospheric pressure on a particular capsule design (Ref. 11)

results shown in Table 4. Both groups have re-examined the polarimetric pressure determination and have pointed out the numerous critical assumptions in the deductive

Table 3. Computer periapses for a Martian orbiter

Apoapsis, km	Periapses at designated lifetimes, km				
	50 yr	10 yr	5 yr	1 yr	0.5 yr
<b>"Conservative" atmosphere</b>					
Circular	5500	3100	2400	1600	1400
5,000		2000	1450	850	700
10,000	3100	1400	1100	700	600
20,000	2100	1100	900	625	550
30,000	1800	1000	800	600	500
50,000	1500	900	750	550	450
<b>"Realistic" atmosphere</b>					
Circular	1400	1000	900	650	560
5,000	690	430	350	240	210
10,000	550	350	290	210	190
20,000	460	300	250	190	180
30,000	420	280	230	180	170
50,000	380	240	210	170	160

chain leading from the observational data to the calculated pressure. They are in essential agreement with Dollfus' comment in his original work that his pressure is only "an order of magnitude estimate."

Low pressures have also been derived by Musman (Ref. 14) and Evans (Ref. 15) from Martian ultraviolet albedos. Musman used an albedo for the total disk obtained photoelectrically by de Vaucouleurs. For a phase angle of  $21^\circ$  and  $\lambda = 3300 \text{ \AA}$ , an albedo of 0.032 was found. Assuming that (1) there are no particles in the atmosphere contributing to the albedo, (2) there are no absorbing atmospheric constituents, and (3) the surface reflectivity is zero, Musman calculated surface pressures of 27 mb for a pure  $\text{N}_2$  atmosphere and 19 mb for a pure  $\text{CO}_2$  atmosphere.

Evans has used an *Aerobee* rocket to obtain an ultraviolet spectrum between 2400 and 3500  $\text{\AA}$ , Fig. 4. In deriving a pressure he makes the following assumptions: (1) the surface reflectivity is 1% at 3000  $\text{\AA}$  and 0 at 2500  $\text{\AA}$ , (2) a haze due to ice spheres  $0.2 \mu$  in diameter reflects 2% at 3000  $\text{\AA}$  and 2.5% at 2500  $\text{\AA}$ , and (3) the various reflectivities add. The results are  $6 \pm 3$  mb for pure  $\text{CO}_2$ ,  $9 \pm 4$  mb for pure  $\text{N}_2$ , and  $13 \pm 6$  mb for pure A atmospheres. There is no evidence for band structure

Table 4. Recent spectroscopic determinations of Martian surface pressure

Author	Original estimate, mb	Revised estimate, mb	Remarks
1. KMS*	$25 \pm 15$	$33 \pm 30$	Revision based on Martian $\text{CO}_2$ abundance of $45 \pm 25$ m-atm.
2. OK	$17 \pm 3$ (pe)	37 (upper limit)	
3. Moroz	$15^{+10}_{-5}$	$13^{+25}_{-8}$	
4. Hanst and Swan	$56 \pm 31$	—	Based on Martian $\text{CO}_2$ abundance of $28 \pm 13$ m-atm.

\*KMS—Kaplan, L. D., Münch, G., and Spinrad, H., 1964, *Astrophys. J.*, Vol. 139, p. 1.  
 OK—Owen, T. C., and Kuiper, G. P., 1964, *Communications of the Lunar and Planetary Laboratory*, Vol. 2, p. 113.  
 Moroz—Moroz, V., *Astron. Zh.*, Vol. 41, p. 350.  
 Hanst and Swan—Hanst, P., and Swan, P., 1965, *Avco Report*.

in the spectrum as one would expect if gaseous absorbers were present. If there is atmospheric absorption in this region it would have to be continuous and would

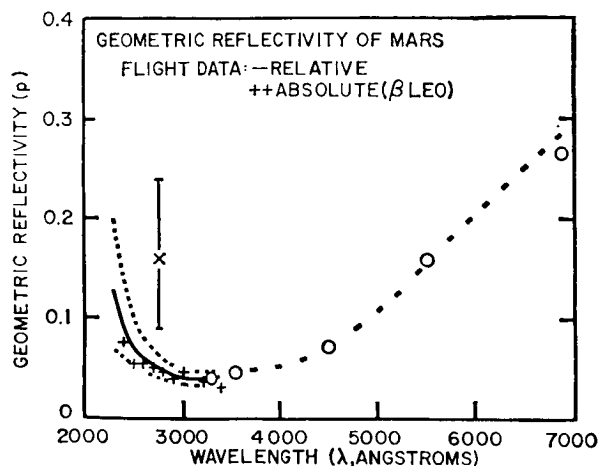


Fig. 4. The geometric reflectivity of Mars. Solid line, relative data adjusted to 0.04 at 3400 Å; +, absolute reflectivity determined by comparison with  $\beta$  Leo, plotted independently. The dashed lines below 3400 Å represent the error range applied to the relative data (Ref. 15).

probably be due to suspended solids. Actually the similarity of the spectrum to that expected from a pure Rayleigh scattering atmosphere suggests strongly that atmospheric absorption, if present, is very slight. This point is reinforced by the close agreement between Evans' results and the most recent ones obtained by the spectroscopic and occultation techniques.

The best pressure estimates, as available in the literature prior to this meeting, are gathered in Table 5.

Table 5. Current literature estimates of Martian surface pressure

Author	Technique	Pressure, mb
Kaplan, Münch, Spinrad (revised by Cann et al.)	Near-infrared spectroscopy	$33 \pm 30$
Owen and Kuiper (revised by Cann et al.)		37 (upper limit)
Moroz (revised by Cann et al.)		$13 \pm 25$ $-8$
Hanst and Swan		$56 \pm 31$
Musman	Ultraviolet albedo (3300Å)	$\left\{ \begin{array}{l} 19 \text{ (pure CO}_2\text{)} \\ 27 \text{ (pure N}_2\text{)} \end{array} \right.$
Evans	Ultraviolet spectrum (2400–3500Å)	$\left\{ \begin{array}{l} 6 \pm 3 \text{ (pure CO}_2\text{)} \\ 9 \pm 4 \text{ (pure N}_2\text{)} \\ 13 \pm 6 \text{ (pure A)} \end{array} \right.$

## B. Composition

The first molecule to be identified in the Martian atmosphere was  $\text{CO}_2$ . Kuiper (Ref. 9) noted that the 1.575 and 1.605  $\mu$   $\text{CO}_2$  bands were stronger in Martian spectra than could be accounted for by the telluric  $\text{CO}_2$ . Early estimates of the abundance were based on the atmospheric pressure of ca 90 mb and have now been superseded by abundances based on the  $5 \nu_3$  band. The initial value of  $55 \pm 20$  m-atm of Kaplan, Münch, and Spinrad (Ref. 10) has been revised by Cann et al. (Ref. 13) to  $43 \pm 24$  m-atm. The latter authors have re-analyzed a determination by Owen and arrived at  $46 \pm 20$  m-atm. It is repeatedly stressed by the workers in this area that all the  $\text{CO}_2$  abundance measurements, and accordingly the pressure determinations, are based on only one part of the  $5 \nu_3$  band of Martian  $\text{CO}_2$ . This situation has been rectified, and additional measurements of the Martian band will be reported later today. Parenthetically it might be noted that 45 m-atm of  $\text{CO}_2$  corresponds to a partial pressure at the surface of 3.3 mb.

The only other molecule yet detected in the gas phase is  $\text{H}_2\text{O}$ . The detection of water vapor is credited to Spinrad, Münch, and Kaplan (Ref. 16) who used the doppler shift, produced by the high relative velocity of Mars with respect to Earth at quadrature, to shift the Martian lines onto the wings of the much stronger telluric lines, Fig. 5. An analysis of the line intensities gave an abundance of  $14 \pm 7 \mu$  precipitable water, averaged over the entire planet. This is not very much and, if present in a constant mixing ratio in the atmosphere, would give relative humidities at the surface of  $8.5 \times 10^{-5}$  and  $1.4 \times 10^{-5}$  at 273 and 300° K respectively, and a dew point of  $-80^\circ$  C. As might be expected, the water vapor abundance is not constant, but varies both in time and space. Observations of these variations will be presented by H. Spinrad at this conference.

For other possible atmospheric constituents, only upper limits are available. A proposal that the oxides of nitrogen system could explain several Martian phenomena (Ref. 17) has provoked a certain amount of debate, and attempts have been made to confirm the initial work. These have failed, but they have served to decrease the upper limit on the  $\text{NO}_2$  abundance to ca 0.01 mm-atm (Ref. 18, 19). This is far below the level necessary to produce the phenomena postulated by Kiess et al., so that their proposal must be rejected.

A pair of molecules whose upper limits have also been recently reduced are  $\text{O}_2$  and  $\text{O}_3$  (Ref. 15). Evans has set an upper limit on  $\text{O}_3$  of 4  $\mu$  atm. Using photochemical

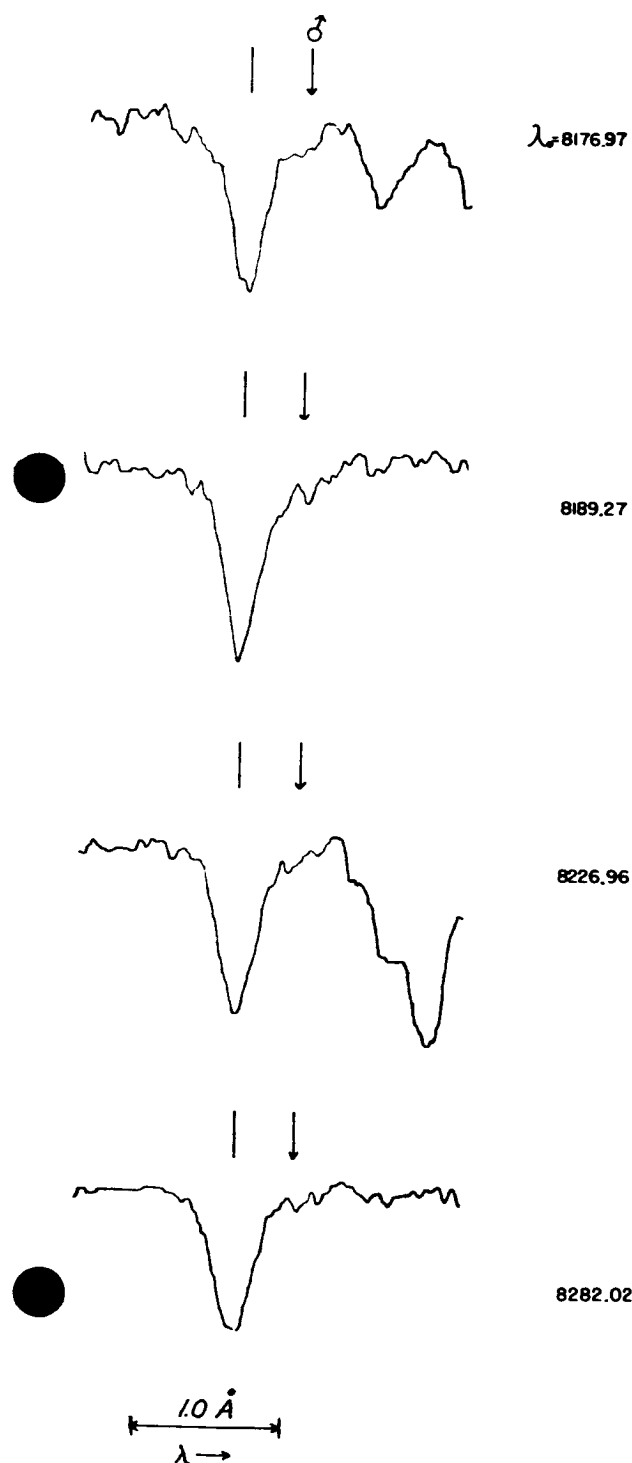


Fig. 5. Doppler-shifted Martian  $\text{H}_2\text{O}$  lines (Ref. 16).  
(From *The Astrophysical Journal*, 1963,  
Vol. 137, p. 1320)

equilibrium calculations of Marmo and Warneck, he then derives an upper limit for  $\text{O}_2$  of 2 cm-atm. This is considerably lower than the 70 cm-atm estimated by

Kaplan et al. (Ref. 10) from the absence of doppler-shifted Martian lines in the 7600 Å band of  $\text{O}_2$ .

Another compound that has been the center of some speculation is acetaldehyde, proposed by Colthup (Ref. 20) to explain certain features of the infrared spectrum. In the subsequent section on the Martian surface, the spectral evidence will be discussed and it will be noted that there is no evidence for ascribing absorption at acetaldehyde frequencies to the Martian atmosphere. This implies an upper limit on this molecule of ca 60  $\mu$  atm (Ref. 21).

Kuiper (Ref. 22) has continued his near-infrared spectrometric studies and determined the following upper limits:  $\text{CO}$ , < 1 cm-atm;  $\text{CH}_4$ , < 1 mm-atm;  $\text{NH}_3$ , < 1 mm-atm;  $\text{N}_2\text{O}$ , < 0.8 mm-atm;  $\text{NO}$ , < 20 cm-atm;  $\text{H}_2\text{S}$ , < 7.5 cm-atm;  $\text{H}_2\text{CO}$ , < 0.3 cm-atm;  $\text{COS}$ , < 0.2 cm-atm. Moreover, he has tentatively determined an  $\text{O}^{18}/\text{O}^{16}$  ratio "larger" than that on Earth and is currently making a precise determination.

The abundances of the various detected and considered components are listed in Table 6. Two molecules,  $\text{N}_2$  and A, are missing from the table, although they have been used frequently to make up the discrepancy between the partial pressure of  $\text{CO}_2$  and the estimated

Table 6. Molecular abundances in the Martian atmosphere

Molecule	Abundance
$\text{CO}_2$	$45 \pm 25$ m-atm
$\text{H}_2\text{O}$	$14 \pm 7$ $\mu$ precipitable $\text{H}_2\text{O}$ (variable in time and space)
$\text{O}_2$	< 2 cm-atm
$\text{O}_3$	< 4 $\mu$ -atm
$\text{CH}_3\text{CHO}$	< 60 $\mu$ -atm
$\text{CO}$	< 1 cm-atm
$\text{CH}_4$	< 1 mm-atm
$\text{NH}_3$	< 1 mm-atm
$\text{NO}_2$	< 10 $\mu$ -atm
$\text{N}_2\text{O}$	< 0.8 mm-atm
$\text{NO}$	< 20 cm-atm
$\text{H}_2\text{S}$	< 7.5 cm-atm
$\text{H}_2\text{CO}$	< 0.3 cm-atm
$\text{COS}$	< 0.2 cm-atm

total pressure. In view of the current state of flux of estimates of these two quantities, it seems preferable to omit them from the table and simply state that they are likely candidates for any difference that may exist.

### C. "Permanent" Particulate Content

The existence of a more or less permanent load of particles in the atmosphere has been suspected as the cause of the lack of contrast in blue pictures, Fig. 6. The most likely prospects for the aerosols are ice or carbon dioxide crystals, or dust particles, with diameters in the submicron region. Recently Kuiper (Ref. 22) has briefly re-examined the problem, noting the unusual polarization effects observed by Gehrels at  $\lambda = 3200 \text{ \AA}$ . For instance, over a 7-day period at a phase angle of  $43^\circ 3'$ , the polarization changed from 1.5 to 9.8%, evidently reflecting a change in the particle size distribution. Kuiper has examined Gehrels' data in conjunction with calculations based on Mie scattering theory and believes that the data favor submicron ice spheres. He stresses that this is only tentative and that extensive photometric and polarization observations at ca  $3200 \text{ \AA}$  are very desirable. This wavelength is particularly appropriate since the surface reflectivity is low and the Rayleigh scattering by the atmosphere has not begun to dominate. Moreover, it is accessible from Earth-based observatories, a very convenient circumstance.

It should be noted that the increased amount of  $\text{CO}_2$  now estimated on Mars increases the probability that the particles are composed of  $\text{CO}_2$ . I know of no observational data that exclude  $\text{CO}_2$ , and a simple calculation indicates that crystallization of  $\text{CO}_2$  at altitudes of ca 20 km is not improbable (Ref. 23). If the particles are ice crystals, then there should be a correlation between the blue clearings and the amount of water vapor in the atmosphere. The latter apparently varies widely so that this correlation should be quite apparent. If one does not exist, then the possibilities can be narrowed to  $\text{CO}_2$  crystals or dust particles.

### D. Clouds

Three types of clouds have been discussed—blue, white, and yellow (Refs. 1, 2). The latter, almost certainly due to dust storms, will be discussed in the Surface section. The blue clouds are evident as bright spots on blue pictures, but are not seen on pictures in the red, while white clouds may be seen throughout the visible range. There seems little doubt that the two are related and are clouds of crystalline  $\text{H}_2\text{O}$  or  $\text{CO}_2$ . A recent survey

(Ref. 24) suggests that white clouds occur most frequently over bright areas and adjacent to dark areas. Wells has proposed that these are analogous to clouds produced on Earth where moisture-laden winds blow at right angles over a mountain range. Downwind of the range there are regions where the air is at a low pressure, and the adiabatic expansion cools it sufficiently to permit condensation. If this is occurring on Mars, it implies that at least some of the dark areas are elevated, and that the winds blow from the dark to the bright areas during the time when clouds are observed.

## III. Surface

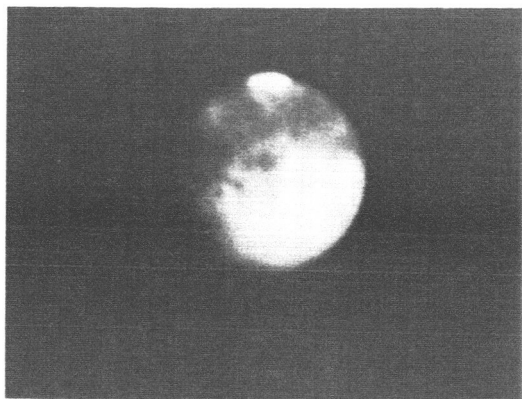
Principal observations and their interpretation are discussed in this section.

### A. Principal Observations

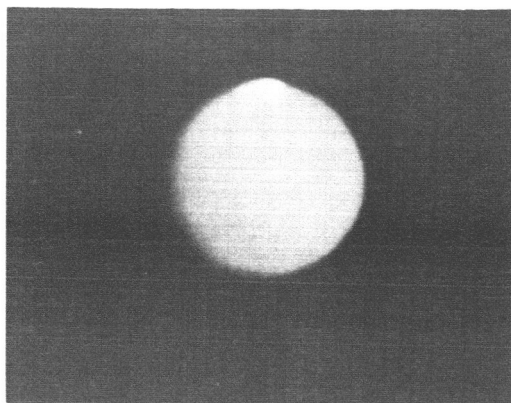
The visual appearance of the planet (Refs. 1, 2) presents areas that are bright ochre, dark, and white, Fig. 7, with the bright areas concentrated in the northern hemisphere, the dark areas in the southern hemisphere, and the white areas near the poles.

1. *The white areas at the poles.* When winter occurs in a particular hemisphere, a white shroud forms about its pole and extends to cover a significant portion of the hemisphere. In southern winter the white cap extends to ca  $42^\circ \text{ S}$  and in the northern winter the corresponding cap goes to ca  $57^\circ \text{ N}$ . As a result of polarization studies by Dollfus, infrared spectral work of Kuiper (confirmed by Moroz, Ref. 38), and considerations based on the local temperature and the partial pressure of gaseous constituents over them, the caps are now believed to be a thin (ca 1 mm) coating of finely divided ice crystals, similar to hoar frost. They wax and wane with the seasons in a manner completely analogous to our own snow caps.

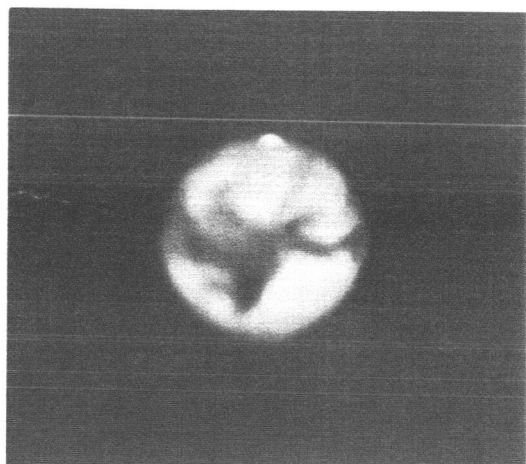
2. *The bright areas.* The hue of the bright areas is generally accepted as reddish or ochre and is close to that observed by the naked eye for the integrated planetary light. Its spectrum, Fig. 8, merely confirms this fact. Not all areas are equally bright, with Hellas being the brightest. Hellas is distinguished by being the southernmost extension of the south polar cap, and is at times very bright, suggesting it is temporarily covered with a deposit (frost?). It has been concluded that Hellas must then be an elevated plateau (Ref. 27), and it is thus one of two areas to which an increased or decreased elevation can be assigned with some degree of certainty. The



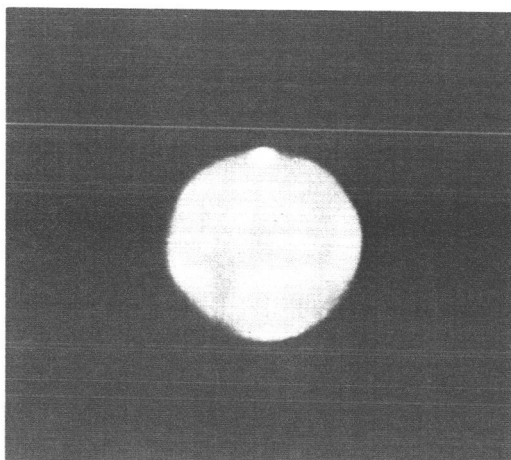
1. 1956 Aug 24  $\lambda 84^\circ$   
U.T. 23:49 R  
May 30 M.D.



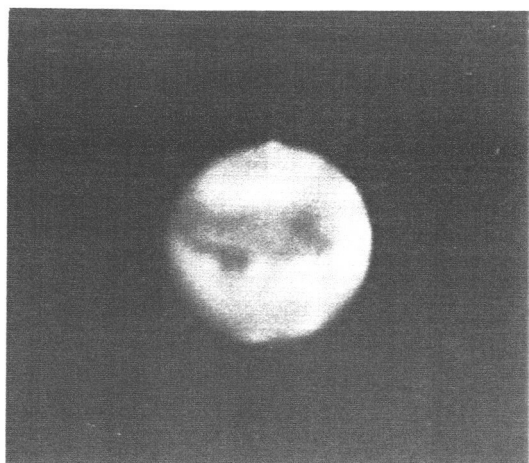
2. 1956 Aug 24  $\lambda 79^\circ$   
U.T. 23:27 B  
May 30 M. D.



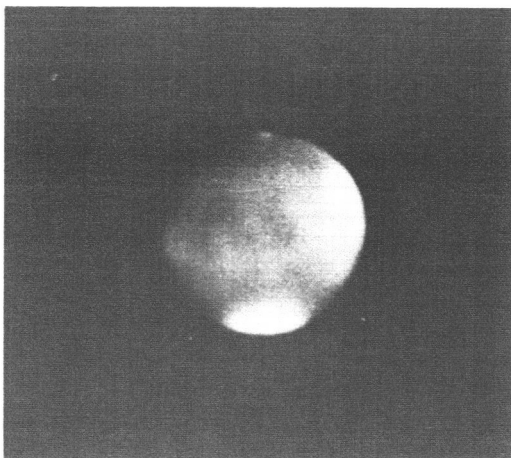
3. 1941 Oct 11  $\lambda 305^\circ$   
U.T. 6:00 O  
July 11 M.D.



4. 1941 Oct 11  $\lambda 320^\circ$   
U.T. 7:07 B  
July 11 M.D.



5. 1926 Oct 27  $\lambda 10^\circ$   
U.T. 6:48 Y  
Aug 1 M.D.



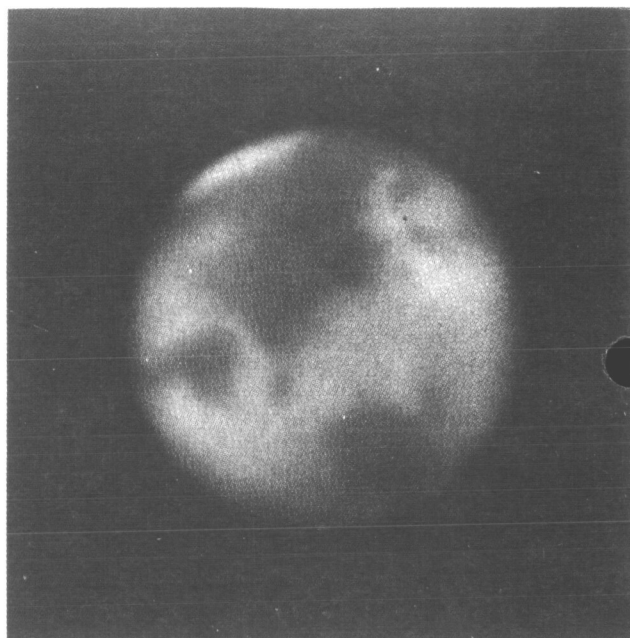
6. 1926 Oct 27  $\lambda 22^\circ$   
U.T. 8:06 B  
Aug 1 M.D.

Fig. 6. Comparisons of yellow and blue photographs showing the presence of the obscuring blue haze together with partial clearing (Ref. 2)





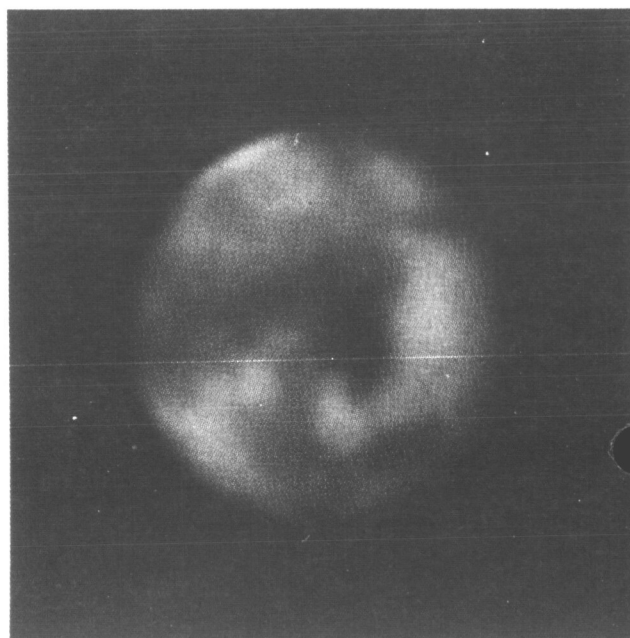
(a) July 1, 1954, 21<sup>h</sup>5<sup>m</sup> U.T.,  $\omega$  75°



(b) July 5, 1954, 20<sup>h</sup>56<sup>m</sup> U.T.,  $\omega$  37°



(c) July 11, 1954, 20<sup>h</sup>16<sup>m</sup> U.T.,  $\omega$  334°



(d) July 14, 1954, 18<sup>h</sup>49<sup>m</sup> U.T.,  $\omega$  286°

**Fig. 7. The visual appearance of Mars in 1954 (Ref. 25)**

other is the Mountains of Mitchel, which manifest themselves as isolated white spots when the south polar cap recedes.

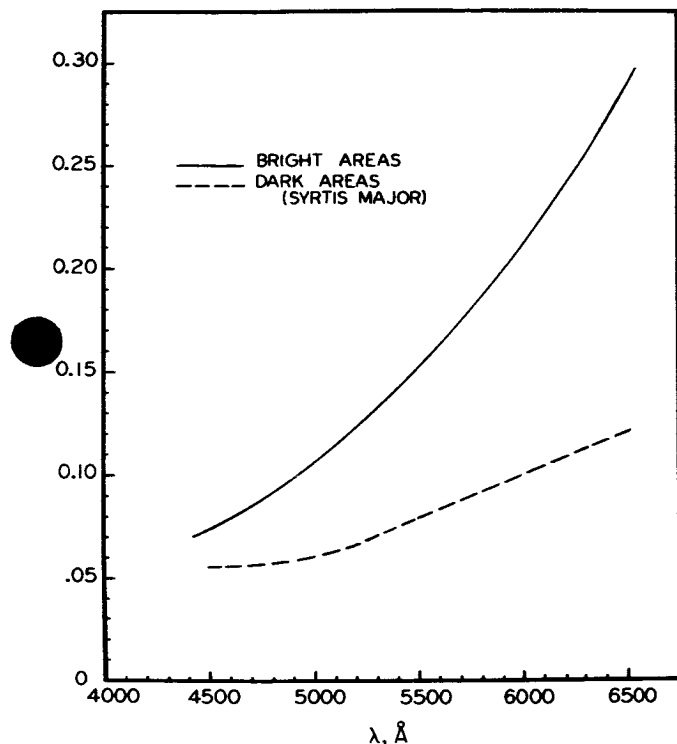


Fig. 8. The spectra of the bright and dark areas (Ref. 26)

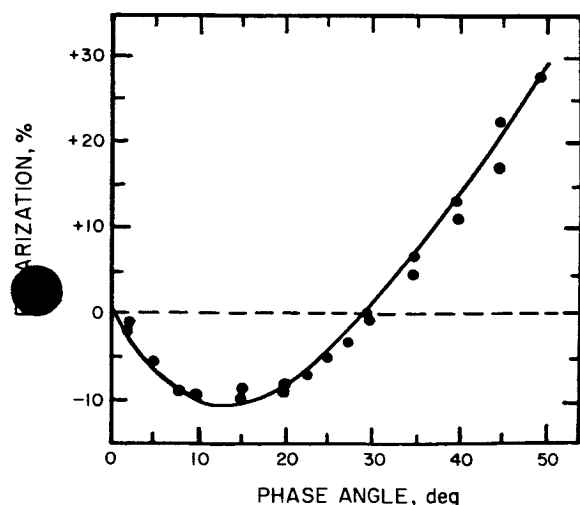


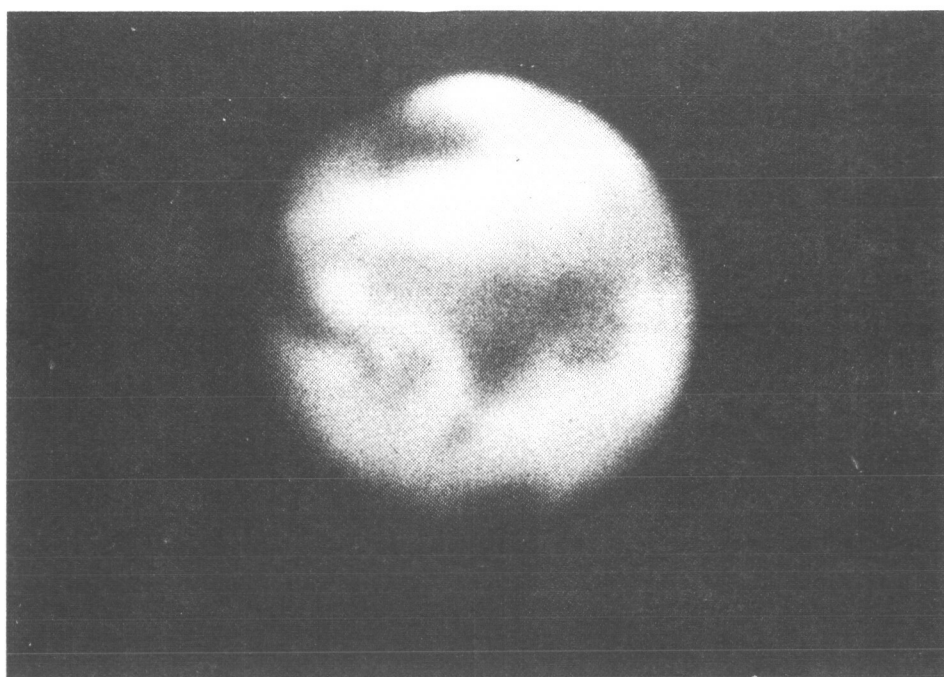
Fig. 9. The polarization of the bright areas vs phase angle as reduced for a Rayleigh scattering molecular atmosphere with a pressure of 90 mb. The dots represent laboratory measurements of pulverized limonite (Ref. 28).

Polarization observations have been carried out by Dollfus (Ref. 28) for the range of accessible phase angles and for the various seasons. No seasonal variation was observed, but a highly characteristic dependence on the phase angle was discovered, Fig. 9.

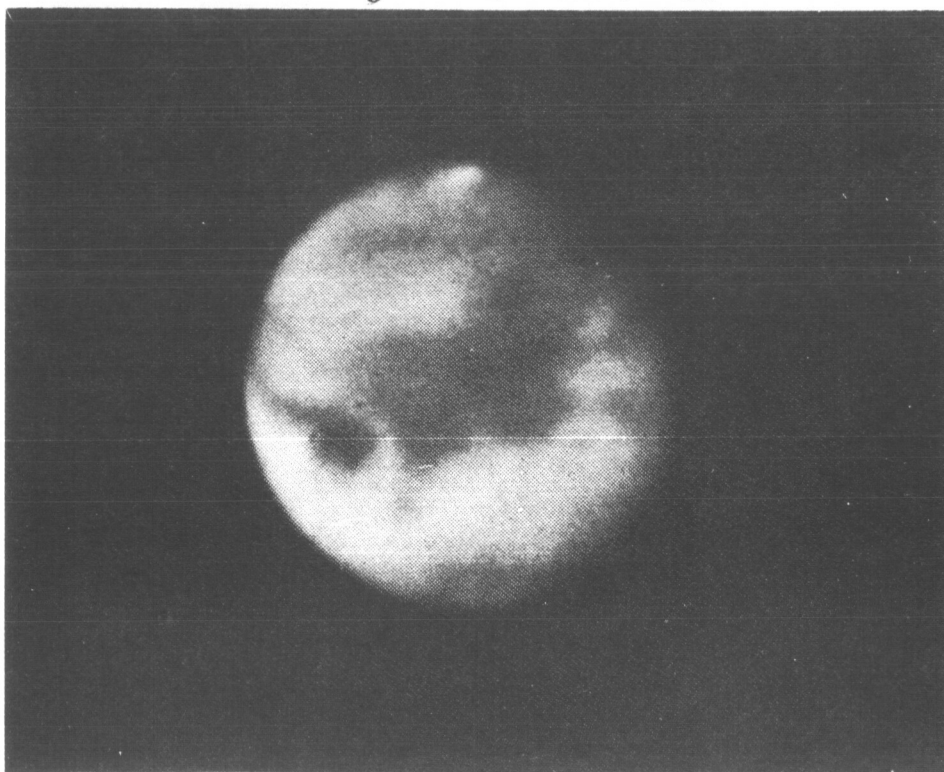
The material covering the bright areas is evidently fine dust, since dust storms of the same color are frequently observed. They may be localized in extent, or cover a major fraction of the planet, Fig. 10. Ryan (Ref. 29) has made a detailed study of some of the problems associated with dust on Mars: (1) the winds necessary to raise dust off the surface, (2) the vertical winds required to elevate the dust into the atmosphere, and (3) the settling time for particles of different sizes. A calculation of particular interest to engineers designing Martian landers is the range of surface wind velocities that may be encountered. For a 25-mb pressure and a model surface that is probably most applicable to Mars, the minimum winds estimated to initiate grain motion are 145–190 km hr<sup>-1</sup> at an altitude of 1 m, and 230–270 km hr<sup>-1</sup> at an altitude of 100 m. These velocities will scale roughly as pressure<sup>-1/2</sup>, so that for a pressure of 10 mb they are ca 230–300 km hr<sup>-1</sup> and 360–430 respectively, and for a pressure of 5 mb ca 320–420 km hr<sup>-1</sup> and 510–600 km hr<sup>-1</sup>. These are all much higher than the winds of up to 100 km hr<sup>-1</sup> deduced from the cloud movements. Assuming the surface model is reasonable, the only explanation is one proposed by Ryan wherein "... the clouds are initiated in transient cyclonic systems."

Temperatures have been measured from the emitted infrared radiation by Lampland (data reduced by Gifford, Ref. 30), Pettit and Nicholson (Ref. 31), and Sinton and Strong (Ref. 32). Maps have been produced by Gifford showing the variation of the noon-time temperatures as a function of latitude, longitude, and season, Fig. 11. The diurnal variation has been measured most precisely by Sinton and Strong, Fig. 12, who deduced therefrom a thermal inertia,  $(k\rho c)^{1/2}$ , of 0.004. This is comparable to values observed for dry, finely divided, uncompacted samples of dust. In calculating the thermal inertia, the effects of the atmosphere were considered in a semiquantitative fashion. While a more precise consideration of heat exchange between it and the surface via radiation and conduction will change the derived value, it would be surprising if the general conclusion were altered.

**3. The dark areas.** The dark areas are probably the most fascinating of the many Martian enigmas, since their appearance and behavior have stimulated many



2. 1956 Aug 29  $\lambda 16^\circ$   
U.T. 22:09 June 2 M.D. R



5. 1941 Nov 10  $\lambda 38^\circ$   
U.T. 6:09 July 30 M.D. R

Fig. 10. The great dust storm of 1956 (Ref. 2)

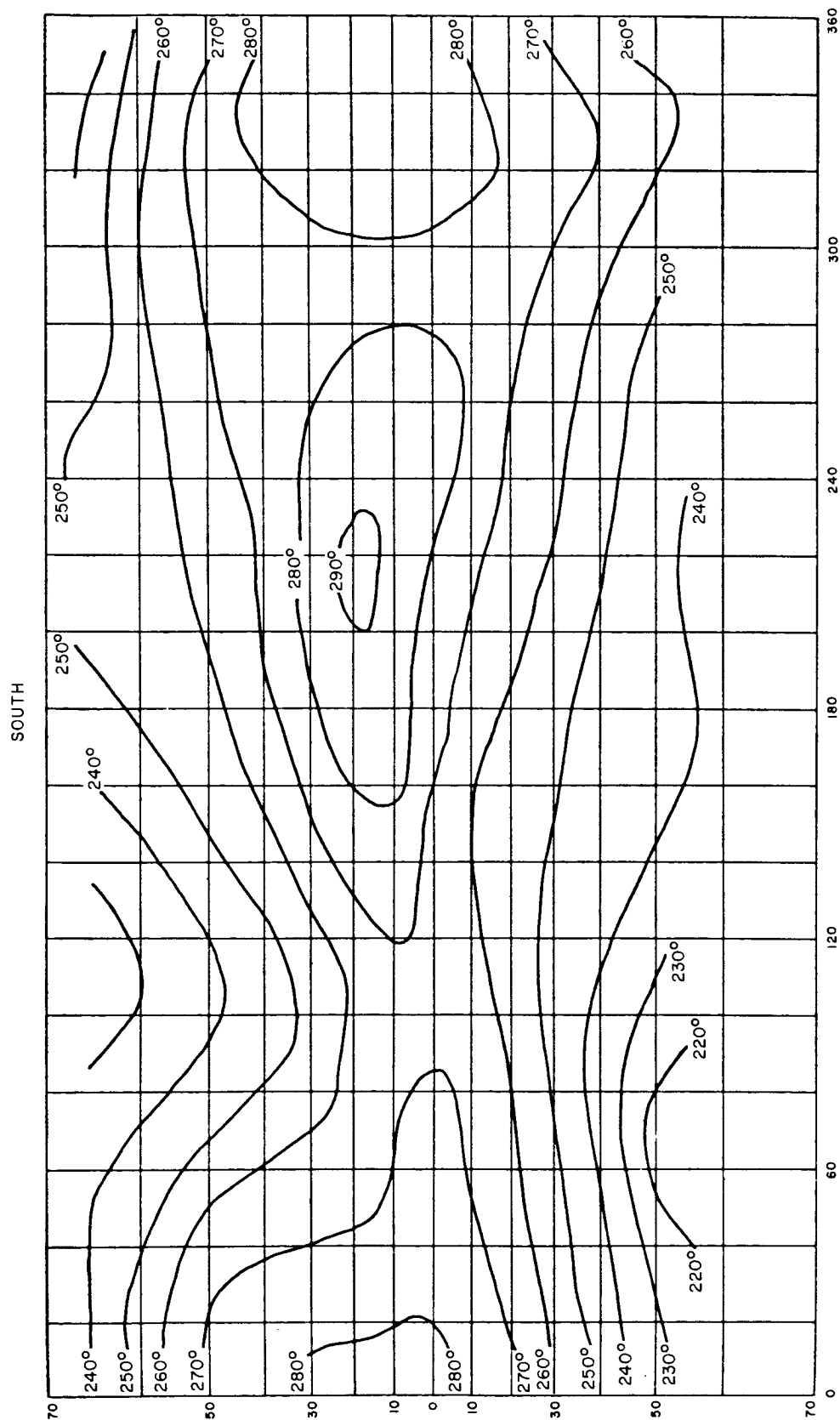


Fig. 11. Average Martian southern hemisphere summer isotherms (Ref. 30). (From *The Astrophysical Journal*, 1956, Vol. 123, p. 159)

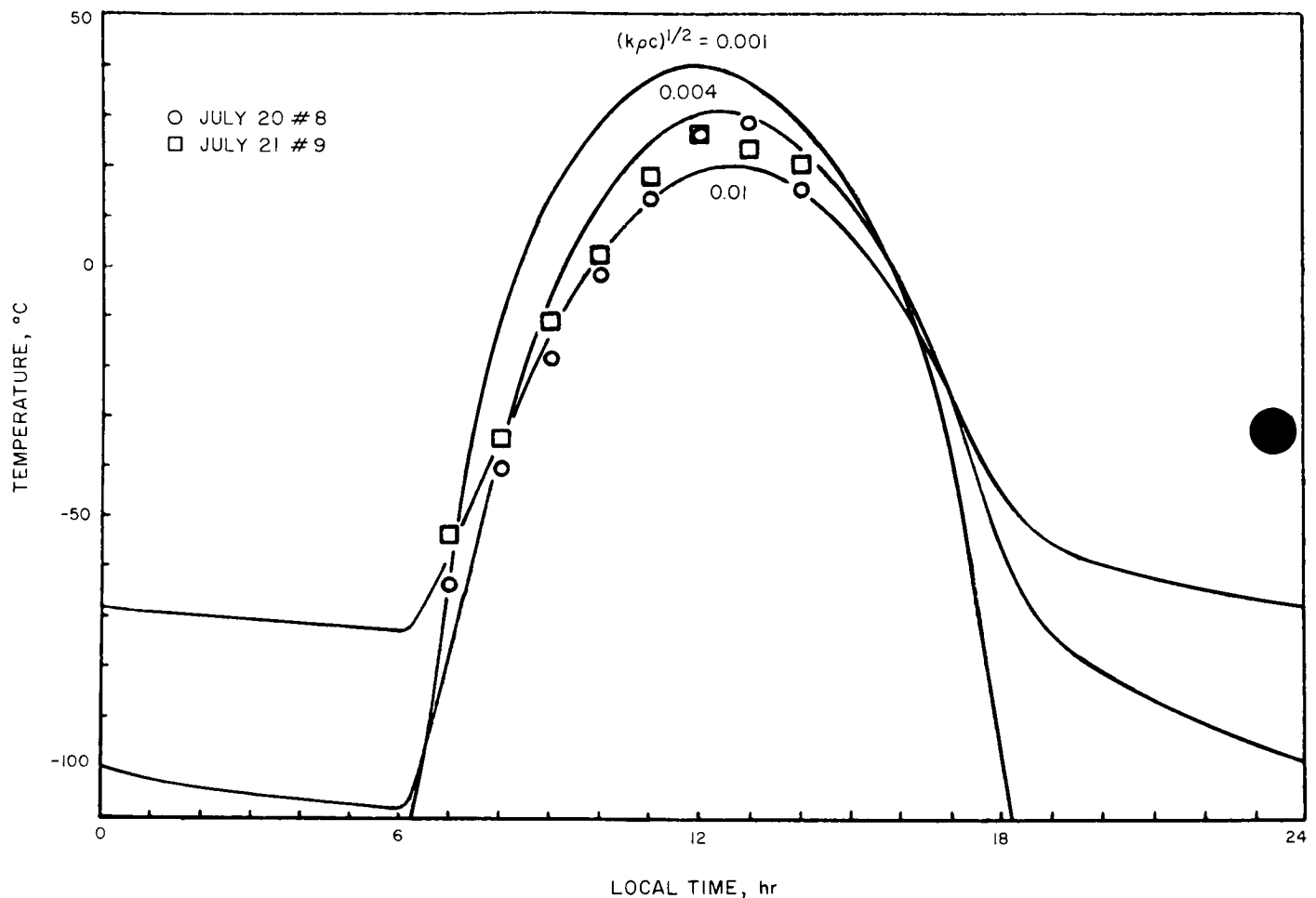


Fig. 12. Theoretical and observed diurnal temperature variation at the equator (Ref. 32). (From *The Astrophysical Journal*, 1960, Vol. 131, p. 466)

scientists to propose there is life on Mars. They consist of three distinct classes—maria, e.g., Syrtis Major; canals; and oases<sup>1</sup>, where several canals may intersect, Fig. 13. When seeing conditions are good, the maria are split up into collections of dark nuclei on a lighter background (Ref. 25), and the canals are resolved into disconnected areas more or less aligned, e.g., cf. Focas (Ref. 33) and Dollfus (Ref. 34). The intricate system of over 400 canals described by Percival Lowell has not withstood the test of time, but a complex system of disconnected aligned dark spots has taken its place, Fig. 14. It should be noted that the connecting lines lie close to, or on, great circles, that several may intersect at an oasis, and that they commonly connect oases with nearby oases and with the “tips” of the extended areas.

<sup>1</sup>This is a convenient designation although nobody today believes there are Martian areas similar to our seas, canals, and oases.

The colors of the dark areas have been debated at considerable length. Visual observers have cited almost the entire spectrum, from red to blue. However, there has been no objective confirmation of many of these, and the only shade recorded spectrographically is the one that is reddish, but less so than the bright areas, Fig. 8. The visually reported colors have been ascribed to bad seeing (Ref. 35) and to a contrast effect with the adjacent, more reddish, bright areas. Until positive evidence to the contrary is produced, I prefer to ignore the reportings of blues and greens, which have been used to form a part of the case for life on Mars.

Polarization studies have been as fruitful in examining the dark areas as the bright areas. Just as for the latter, the polarization vs phase angle has a distinctive appearance, Fig. 15. A provocative seasonal effect that

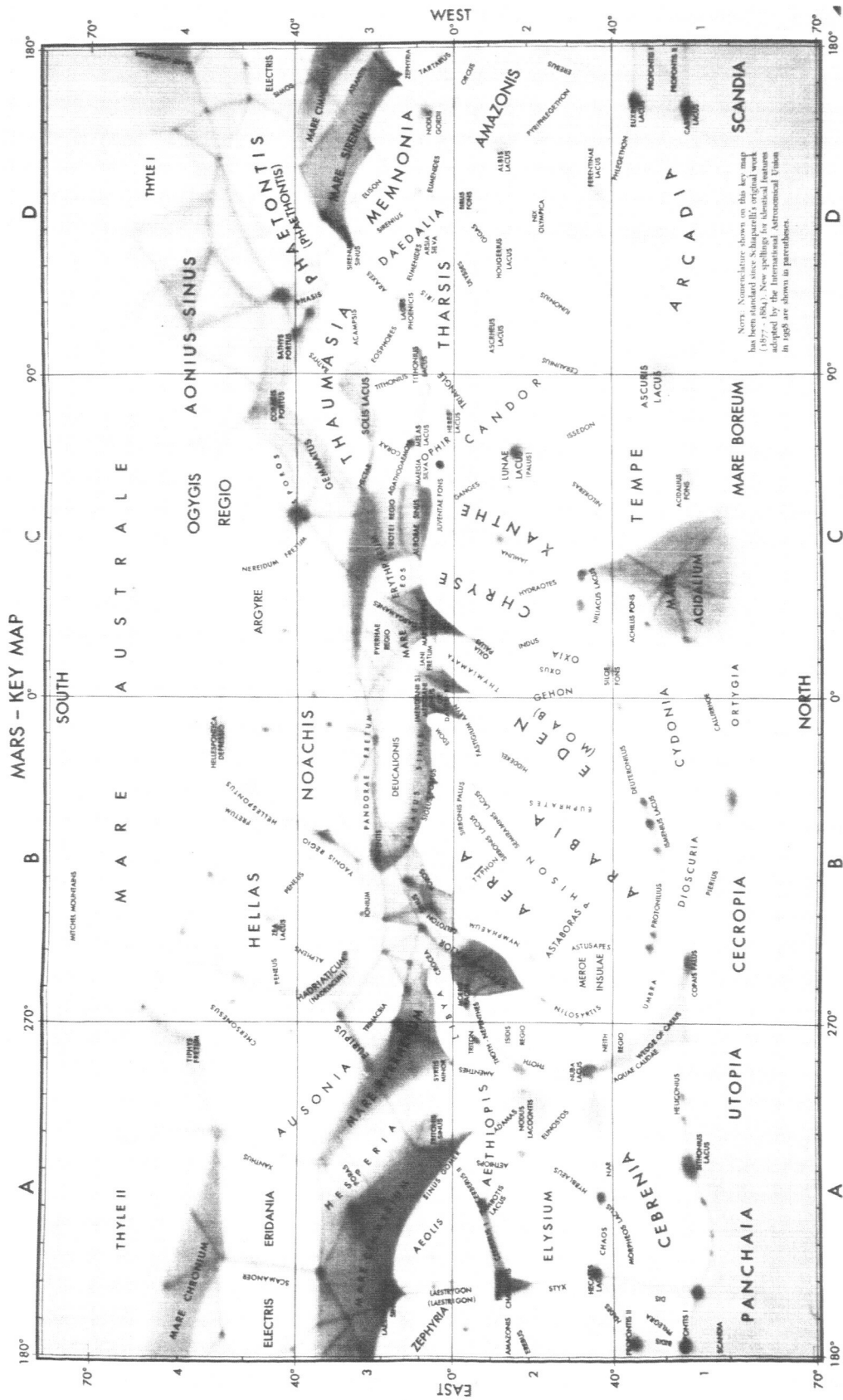
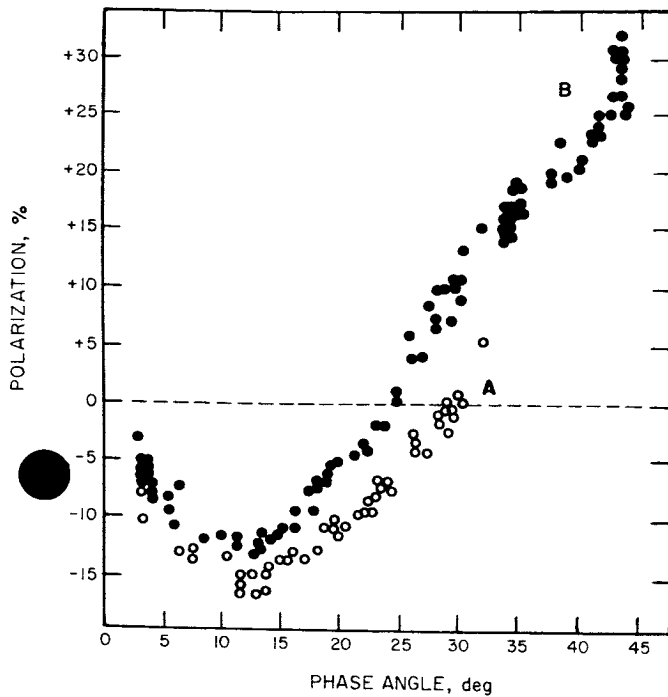


Fig. 13. A drawing of Mars by Slipher (Ref. 2)



Fig. 14. A drawing of Mars in 1958 by Focas (Ref. 33)



**Fig. 15.** The polarization vs phase angle for the dark areas. The filled circles are for equatorial markings, the open circles for markings in the northern hemisphere at Martian spring (Ref. 28).

was discovered will be discussed in the following paragraph on the darkening wave.

As the season in a particular hemisphere changes from winter to spring, the polar cap recedes. As it begins to do so, the dark areas adjacent to the cap become darker. As the season progresses the darkening moves towards the equator and ultimately crosses it. Behind this darkening front is a brightening front, so that there appears to be a wave of darkening moving along the planet, Fig. 16 (Refs. 28, 33). Associated with the decrease in brightness is a change in the polarization, with the negative branch becoming more pronounced and the inversion point shifting to higher angles, Fig. 15.

Not only is there a seasonal change in the appearance of the dark areas, but secular changes also occur, Fig. 17. Two regions where such changes have been particularly marked over the past several decades are Solis Lacus and the Thoth-Nepenthes canal system.

A promising means of studying a surface is to observe its infrared spectrum in the hope of detecting vibrational bands that will be indicative of the composition. This

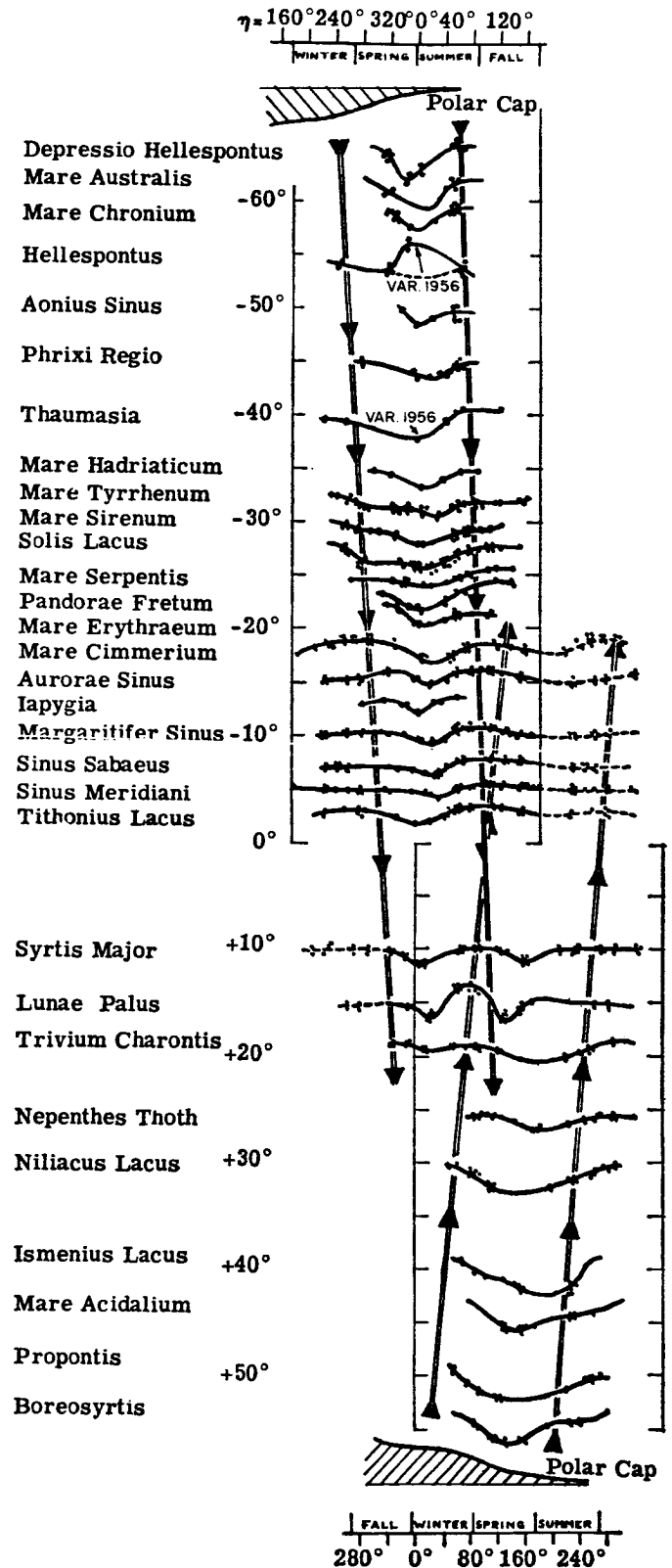
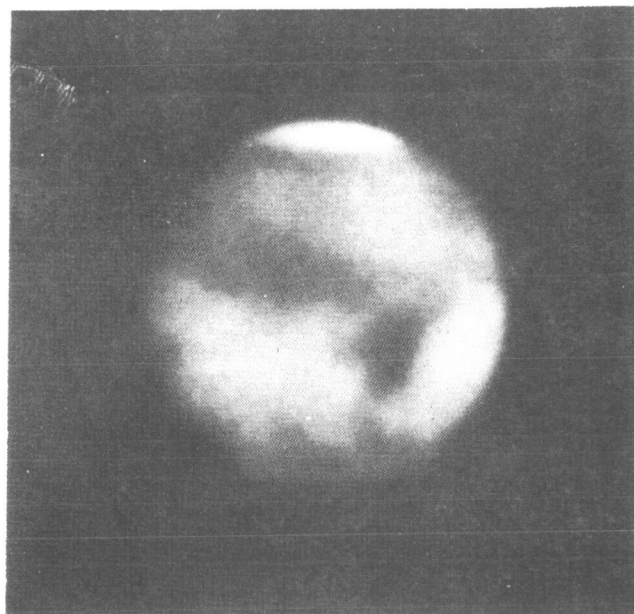
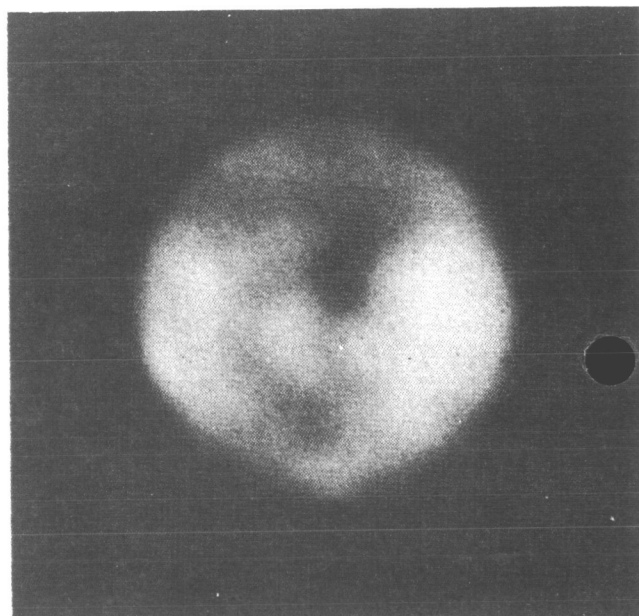


**Fig. 16.** Brightness of the dark areas vs heliocentric longitude. South is at the top, north at the bottom (Ref. 33).

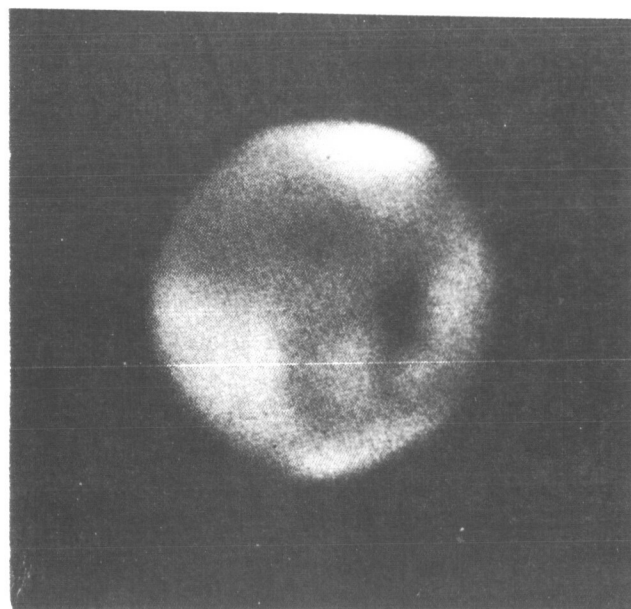




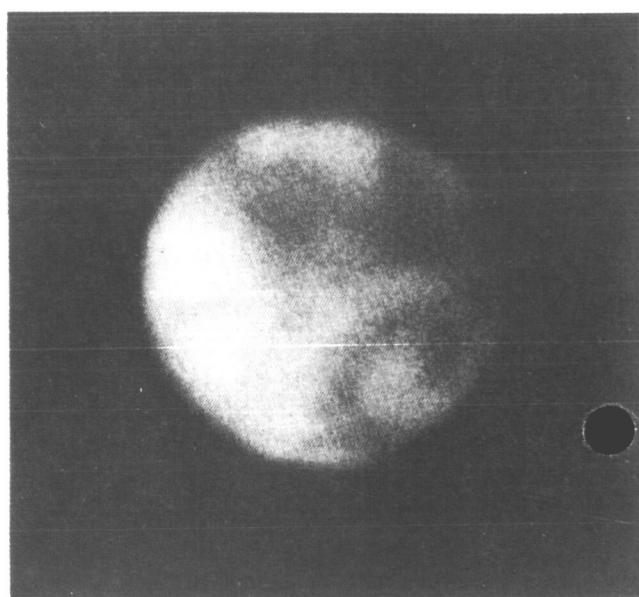
2. 1907 July 3  $\lambda 270^\circ$   
U.T. 4:21 Apr 7 M.D. Y



8. 1920 Apr 23  $\lambda 285^\circ$   
U.T. 8:47 Jan 25 M.D. Y



9. 1922 June 18  $\lambda 260^\circ$   
U.T. 7:25 Mar 16 M.D. Y



12. 1928 Dec 29  $\lambda 245^\circ$   
Sept 28 M. D. Y

Fig. 17. Pronounced secular changes in the Thoth-Nepenthes region (Ref. 2)

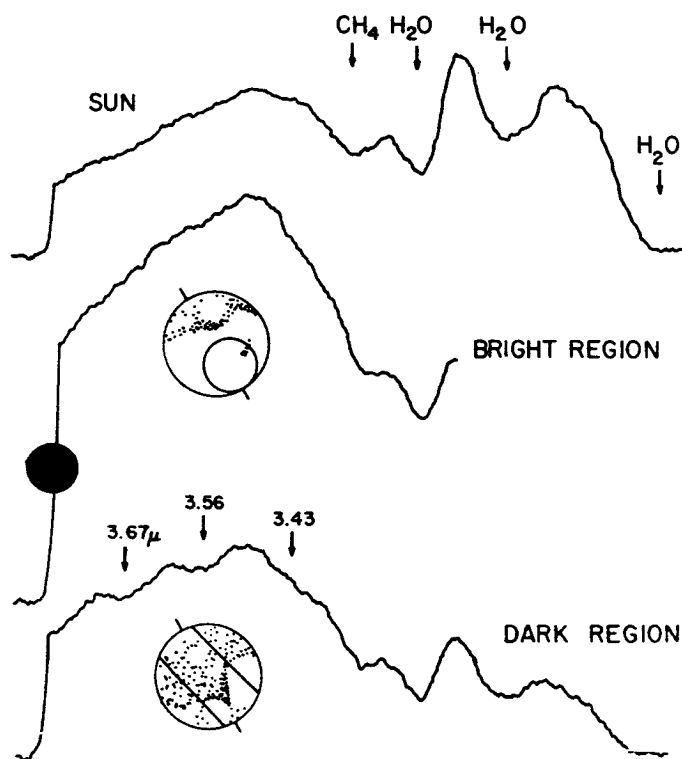


Fig. 18. Spectra of the Sun and Mars recorded at Mt. Palomar in October 1958 (Ref. 36). (From *Science*, 1959, Vol. 130, p. 1235)

approach was taken by Sinton (Ref. 36) when he obtained spectra in the  $3\text{--}4\ \mu$  region, Fig. 18. His initial observations were that minima existed at 3.43, 3.56, and  $3.67\ \mu$ , that they were more pronounced for the dark areas, and that they strongly suggested the presence of organic matter thereon. As noted earlier, Colthup (Ref. 20) believed that one band, that at  $3.67\ \mu$ , may be due to acetaldehyde. However, after a critical re-examination of the data, it has been concluded that the bands at 3.56 and  $3.67\ \mu$  are almost certainly due to HDO in our own atmosphere (Ref. 37), Fig. 19. The band at  $3.43\ \mu$  has not been questioned, but it requires confirmation, especially since it is on the shoulder of a strong telluric  $\text{CH}_4$  band. Moroz (Ref. 38) has also reported a minimum at  $3.43\ \mu$ , together with others at 3.53, 3.59, and  $3.69\ \mu$ . The reported resolution of the features at 3.53 and  $3.59\ \mu$  conflicts with his stated spectral band width of  $0.09\ \mu$ . In view of this discrepancy the confirmation of the  $3.43\ \mu$  feature should be regarded as only tentative. If it is real, it may be due to surface carbonates or organic material (Ref. 39).

Temperatures of the dark areas have been found to be somewhat higher than those of the bright areas. Specifi-

cally, "the maximum temperature at a favorable opposition for a desert area near the equator of the planet appears to be close to  $25^\circ\text{C}$ , and for a dark area it is about  $8^\circ$  hotter" (Ref. 32). This difference is roughly what one would expect owing to the difference in albedos if the thermal inertia of the dark areas is low, comparable in magnitude to that of the bright areas.

**4. Microwave observations.** During the opposition of 1963, Jet Propulsion Laboratory scientists observed Mars with their 12.6-cm radar for a total of 65 hours (Ref. 40). A spectral analysis of the returned signal, Fig. 20, showed the signal to be coming predominantly from a small area near the center of the disk, implying that the surface is, in fact, quite smooth. However, the data were too noisy to justify any attempt to quantify the roughness. A plot of signal vs Martian longitude suggested a higher signal from the Syrtis Major region, but again the noise was too high to enable positive statements to be made.

Passive observations have been carried out by several workers, most recently by Kellermann (Ref. 41). At  $\lambda = 21\text{ cm}$ , Davies (Ref. 42) had derived a temperature of  $1140 \pm 50^\circ\text{K}$ , which presumably would have to arise from radiation belts. This was not confirmed by Kellermann, who has reported the temperatures in Table 7. These agree very well with previous data of Giordmaine, Alsop, Townes, and Mayer, and of Drake. Because of the lack of confirmation of the high temperature, and the absence of a magnetic field and radiation belts as determined by *Mariner IV*, it seems reasonable to reject Davies' result. The data of Kellermann are consistent with a planet whose microwave radiation comes from depths where the temperature is constant, with no diurnal variation. This is equivalent to stating that the microwave temperature is equal to an infrared temperature calculated from the average flux emitted by the entire disk.

**5. *Mariner IV* pictures.** The most exciting event for students of Mars has undoubtedly been the flight of *Mariner IV* and the information it has provided on the

Table 7. Microwave Martian temperature measurements of Kellermann

$\lambda$ , cm	$T$ , $^\circ\text{K}$
6.0	$192 \pm 26$
11.3	$162 \pm 18$
21.3	$190 \pm 41$

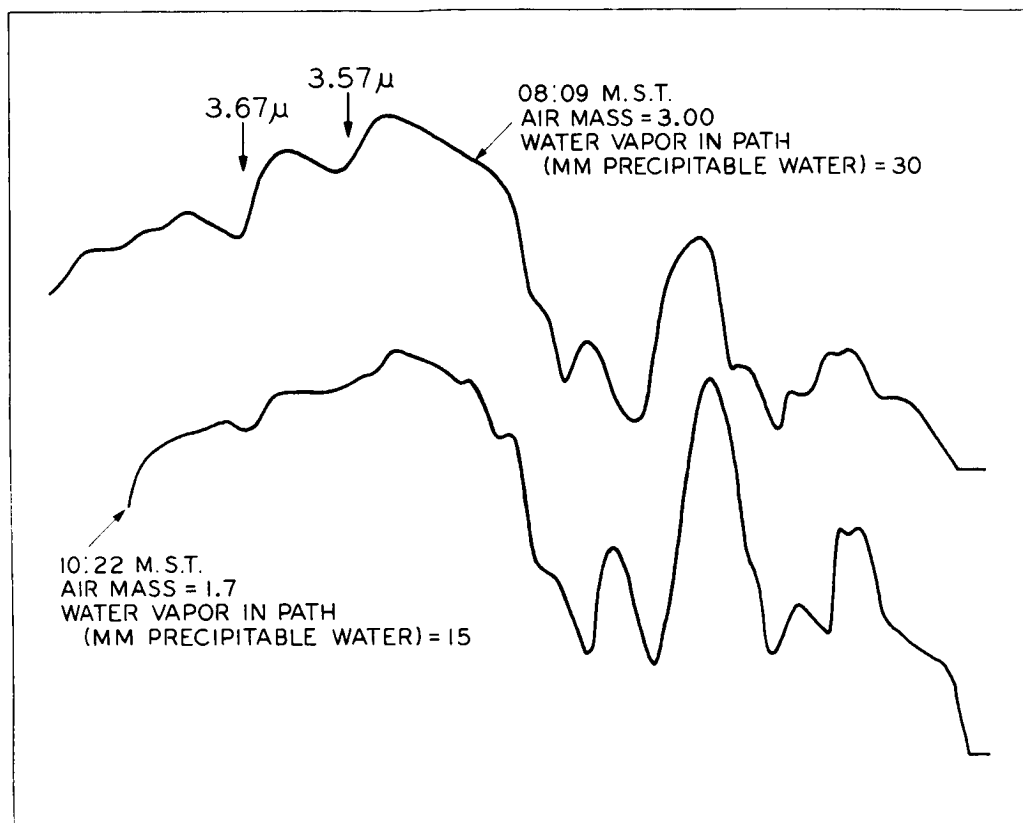


Fig. 19. Spectra of the Sun recorded at Denver on May 12, 1955 (Ref. 37).

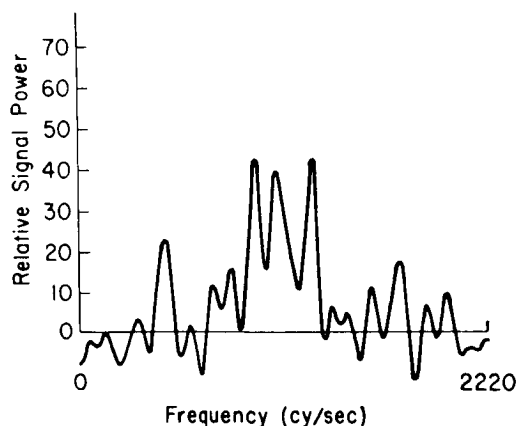


Fig. 20. A spectrogram showing the average 12.6-cm radar echo from Mars obtained over several weeks (Ref. 40).

planet. This will be discussed in detail in a later session; at present, I will restrict myself to a few remarks on the TV experiment (Ref. 43). The outstanding point that it has introduced is the large number of craters (of an apparent impact nature) that dot the surface, Fig. 21.

These are evidently even more numerous than for the average lunar surface, Fig. 22. The high crater density has been interpreted as indicating the Martian surface is very old, perhaps 2-5 billion years. This in turn implies that erosive forces over this period have been slight and that liquid water as surface bodies and as rain has been rare and probably absent. This conclusion, important to exobiologists, must be regarded as tentative for two reasons: (1) only 1% of the surface was photographed, and (2) the proximity of Mars to the asteroid belt may make the frequency of impact higher than on the Moon. But the observation that the crater density on Mars is high is an important one, and must play a significant role in the construction of models depicting surface phenomena.

**6. The radiation environment.** The flux of ultraviolet radiation and charged particles at the surface is an important parameter to consider when discussing the viability of living organisms and also perhaps when examining the mineralogical state of the surface. The  $\text{CO}_2$  in the atmosphere is sufficient to absorb completely the ultraviolet radiation with  $\lambda < 1700\text{--}1750 \text{ \AA}$ , and water

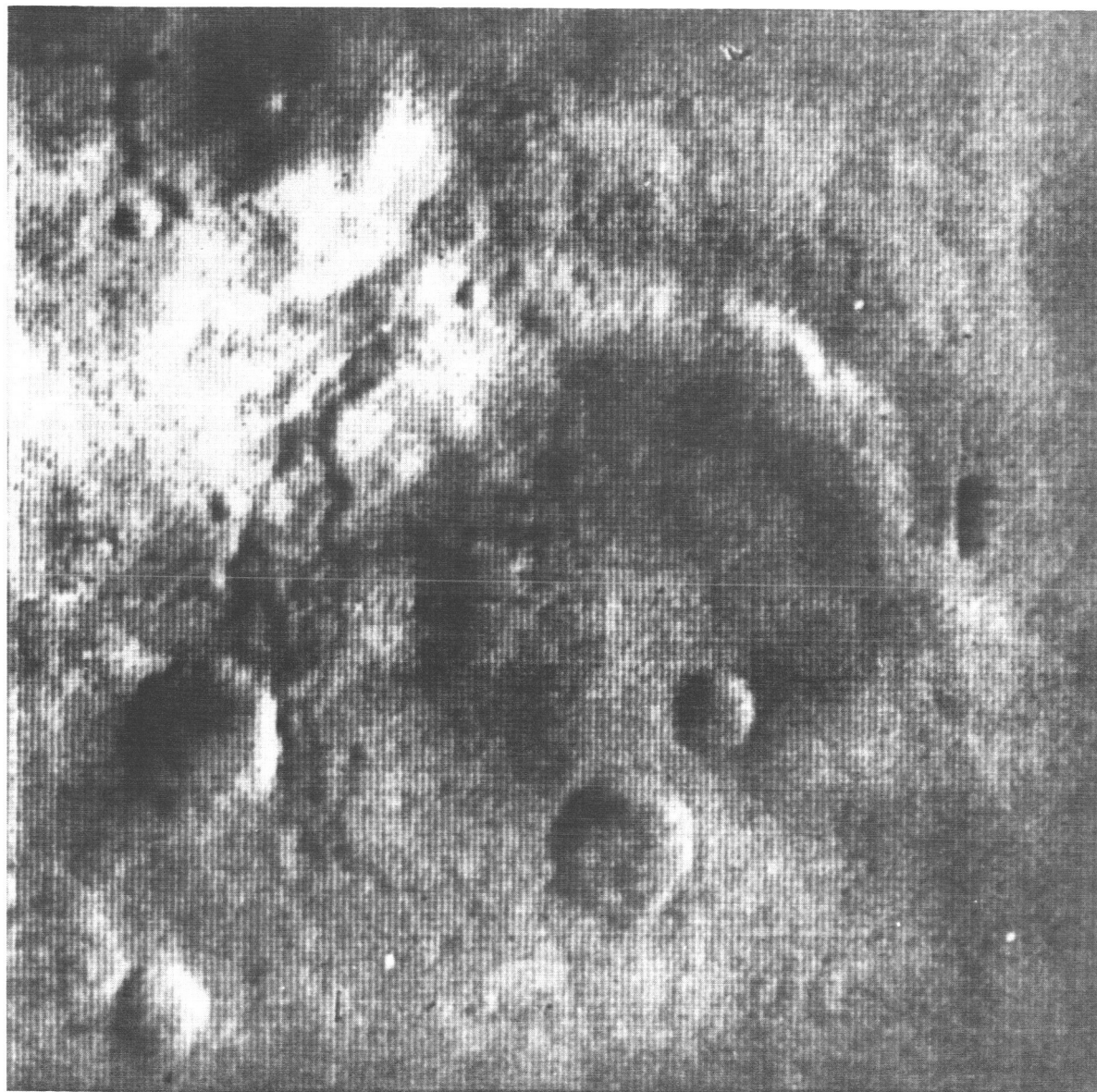


Fig. 21. Frame 11 of the *Mariner IV* TV series (Ref. 43).

vapor when present at a level of  $14 \mu$  precipitable  $H_2O$  will absorb efficiently with dissociation for  $\lambda < 1850 \text{ \AA}$  (Ref. 23). From Evans' ultraviolet spectra (Ref. 15) it appears that there are no significant absorbers at longer wavelengths, and that only Rayleigh scattering is active in reducing the ultraviolet flux at the surface. At  $\lambda = 2000 \text{ \AA}$ , he estimated that for a solar zenith angle of  $60^\circ$  at least 70% of the direct solar radiation will reach the surface. This will increase at longer wavelengths. He notes that the evident ultraviolet fluxes at the surface would be lethal to terrestrial organisms.

Yagoda (Ref. 44) has estimated particle fluxes at the surface, but for a pressure of 85 mb. His results must be extensively revised to take account of the low pressures now accepted.

#### B. Interpretation

In discussing the variety of interpretations put forward for surface phenomena I must of necessity restrict myself to a manageable number. I will then make a critical selection, choosing for examination those that have

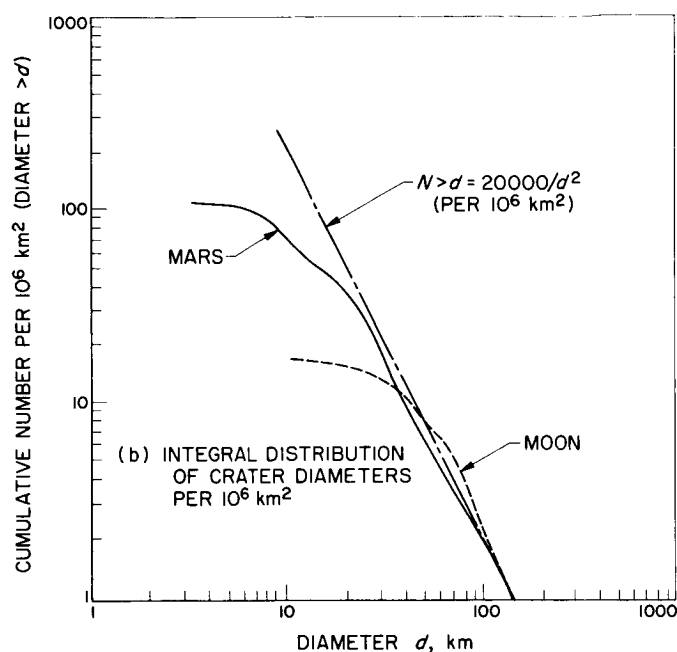


**Fig. 22. A comparison of crater density vs crater diameter for Mars and the Moon (averaged over the maria and terrae) (Ref. 43)**

aroused the greatest controversy or that have the greatest promise. It should be noted that the two categories are not identical.

**1. The composition of the bright areas.** The spectrum, polarization, and thermal inertia of the bright areas and the characteristics of the dust clouds have been used in speculating on the composition. It is generally accepted that the latter three properties testify to finely divided material, with grain sizes ranging from 100 to 1  $\mu$ . It must also be uncompacted, and since bodies of liquid water have probably been absent for periods up into the billions of years, the aeolian erosion must have resulted in large quantities of dust, which, in places, may now form a very deep surface covering.

As for the mineralogical composition, very little can be said with certitude. A considerable number of ob-

servations, both spectral and polarimetric, are in the literature, which also contains some positive conclusions based on these data. However, a general criticism may be laid against almost all of this work, since only rarely was the material studied in the laboratory characterized in any but the most general manner. Investigators have examined the spectral and polarimetric properties of a wide range of minerals, but the state of aggregation has seldom been specified. This is distressing, since both parameters depend critically on the particle size and the presence or absence of a surface coating. Some observations reported have been made on rock surfaces, a surface that must be rare and may be completely absent in the Martian bright areas. Moreover, the mineralogical composition of the samples has never been adequately given. A substance mentioned frequently as the bright material is limonite, but this is one of the most poorly characterized substances in mineralogy. Hovis (Ref. 45), in his spectral study, has given the most complete description of his samples, Table 8. While it is not complete, e.g., the elemental composition is not given, it serves to demonstrate the range of materials that geologists group under the term "limonite." And his spectra reflect this range in their details. I would like to stress this point of sample characterization, which is important not only for its implications on the Martian surface, but also for checking between terrestrial laboratories. Thus Coulson (cited by Cann et al., Ref. 13) attempted to check Dollfus' polarization data on limonite, but failed. This was presumably due to the fact that different samples were examined by the two investigators.

With this preamble let us look at the materials that have been suggested. The reddish color and the cosmic abundance of iron led the early investigators to propose a highly oxidized surface containing iron in the ferric state. Polarization and unpublished spectral measurements of Dollfus led him to conclude that the material was essentially limonite. However, the polarization curve was derived from the observed by subtracting out a component that would be expected for a Rayleigh scattering atmosphere of terrestrial composition and with

**Table 8. Three samples of limonite examined by Hovis**

U.S.N.M. Specimen No.	Locality of origin	Iron oxide minerals	Percent other minerals	Other minerals
109590	Cartersville, Georgia	Goethite	27	More than 90% quartz, minor mica group minerals
109592	Alabama	Goethite	5.3	Quartz
18274	Caracas, Venezuela	Goethite	47	More than 90% quartz

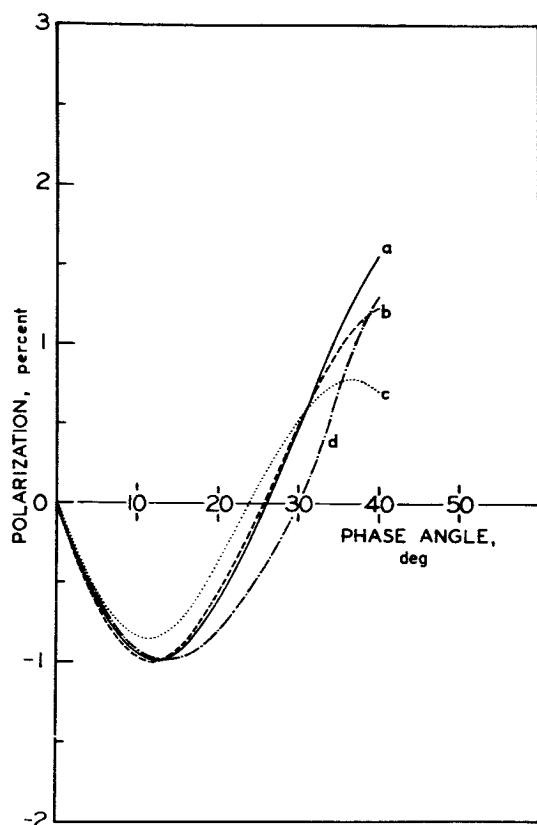


Fig. 23. The polarization vs phase angle for the Martian bright areas. (a), observed; (b), (c), derived for atmospheres containing aerosols of different distributions; (d), pulverized limonite (Ref. 46).

a surface pressure of 90 mb. This is clearly overcorrected in view of our present knowledge of the atmosphere, and moreover, if aerosols are present, the correction can be exactly the opposite (Ref. 46), Fig. 23, and a variety of materials can then fit the reduced curve.

The visible and near-infrared spectrum was used by Kuiper in arriving at an identification of felsitic rhyolite. However, it has been noted that the surface examined was old and may have had a weathered coating of limonite (Ref. 47). The spectrum of limonite, cited so commonly, is similar to those of other ferric oxides in exhibiting a minimum at 8750 Å, Fig. 24. The absence of this minimum, or its weakness if present, in the Martian spectrum argues strongly *against* a covering that is pure ferric oxides and their hydrates, a point recognized by Adamcik and his co-workers (Ref. 48). They prepared a synthetic mixture of goethite ( $\text{Fe}_2\text{O}_3 \cdot \text{H}_2\text{O}$ ), kaolin ( $\text{Al}_2\text{O}_3 \cdot \text{SiO}_2 \cdot 2\text{H}_2\text{O}$ ) and hematite ( $\text{Fe}_2\text{O}_3$ ) in the weight ratio 16 : 100 : 16 and added "a few percent" of a black material (magnetite). The resulting spectrum closely resembled Mars'.

This demonstration relieves one of the necessity of postulating mechanisms for producing a spectrum equivalent to "pure" limonite. One such proposed was a surface covering, or paint, on silicate particles (Refs. 47, 49). Another was a concentration of the fine, soft limonite particles on the surface, resulting from fractionation during settling after dust storms (Ref. 50). My personal

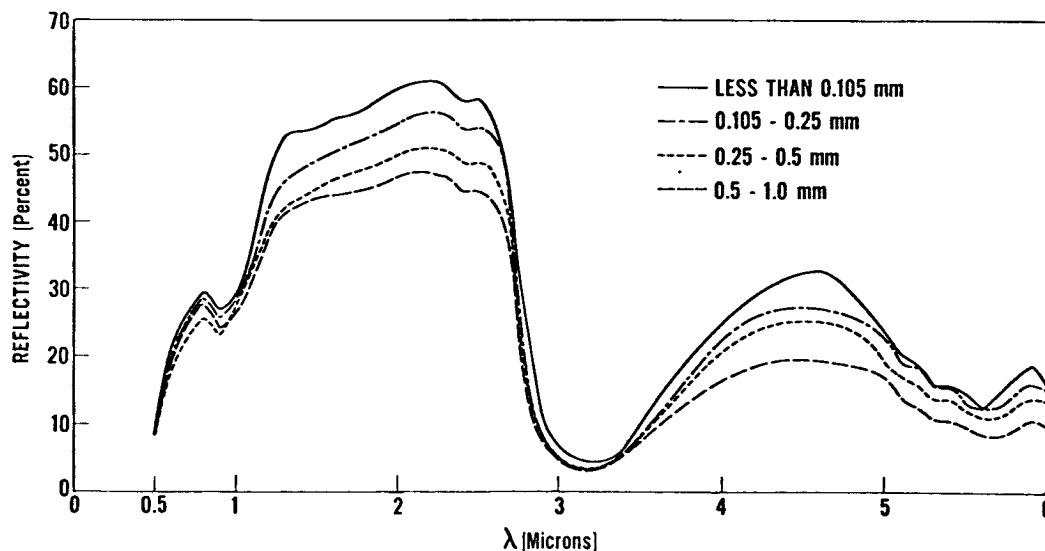


Fig. 24. The laboratory spectrum of pulverized limonite samples (Ref. 45)

opinion now is that the bright areas are oxidized, the color is due to the  $\text{Fe}^{+3}$  ion, and the Fe/Si atom ratio need be little different from the solar value of 1:3.5 (Ref. 51).

**2. The nature of the dark areas.** This is the topic that has generated the greatest heat, owing to its possible association with a Martian biota. In treating it, I will divide it into sections dealing with the biological and nonbiological interpretations. Some of the latter invoke life phenomena, but their main features are nonbiological.

*The biological interpretation.* This theory reached its culmination in the hands of Lowell, who peopled the planet with intelligent beings capable of constructing an intricate system of irrigation canals. As our knowledge has improved and we have become aware of the desiccated state of the surface and atmosphere, the low atmospheric pressure, the lack of oxygen, and the possibly high radiation flux at the surface, an element of sobriety has entered into the deliberations. Still, one should certainly not exclude the possibility of a Martian biota and, accepting this, it is natural to try to explain some of the observed phenomena on this basis.

The darkening wave moving from the poles towards and across the equator is the most intriguing effect to explain. On a life basis it is handled in the following manner. On Earth, organisms have plenty of water, so that temperature is the critical factor in their growth. Accordingly a terrestrial darkening wave exists, but moves from the equator towards the poles as the season progresses from winter to summer. On Mars, however, while the temperatures are certainly not benign, it is the availability of water that is critical. When the polar caps begin to sublime and recede, the water released moves towards the equator and becomes available to organisms present in the soil. They then proceed to proliferate, darkening the surface and changing its color. Then as the relative humidity decreases, owing to the passage of the wave of moisture, the organisms become dormant and the areas brighten. An attempt by Dollfus to duplicate the polarization behavior by terrestrial organisms failed, but then life has manifold forms and one can always conceive of some hypothetical form that has the desired properties. The secular changes in the dark areas are considered to be the expansion of organisms into a previously barren region, or a regression of them from one previously fertile.

I have been skeptical of this model in the past (Ref. 52) and have not altered in this respect. The range of non-

reddish colors, in particular greens and blues, are doubtful and may well be artifacts introduced by our own atmosphere and our psychological processes. The temperatures prevalent in at least some of the dark areas during the darkening process also argue against an associated biological activity. Thus, Depressio Hellespontica, located at 60–65°S latitude, participates prominently in the darkening wave and yet attains a maximum summer temperature of  $-23^{\circ}\text{C}$ , and a temperature at the height of the darkening wave of only  $-28^{\circ}\text{C}$ , Fig. 25. This is a measured brightness temperature and should be raised about  $2\text{--}3^{\circ}$  to allow for an emissivity of ca 0.95. There may be a certain experimental error, and there may be localized areas where the albedo is lower and, as a consequence, the temperature higher. Still, the surface temperature will probably never exceed  $0^{\circ}\text{C}$ , even on the hottest day. This seems extraordinarily low to permit a proliferation of life based on water as solvent. It is true that salts, in particular alkali and alkaline earth halides, if present in large concentrations, can significantly lower the freezing point of water. Therefore an unequivocal rejection of a biological explanation for the darkening of Depressio Hellespontica cannot be made, but I regard it as highly improbable. It is only natural then to extend this conclusion to other areas participating in the darkening wave, and to conclude that the biological interpretation for the wave itself is improbable.

The secular changes, or at least some of them, also are difficult to explain by biological activity. The area Hellas, normally bright, was dark during the 1954 opposition, but in 1956 returned to its normal appearance. Since it covers an area of 290,000 square miles, any organisms that can quickly extend over it sufficiently to change its visual appearance so drastically must be unique.

Finally must be mentioned the ability of the dark areas to regain their original appearance after a dust storm. Öpik (Ref. 53) argued that the only means of accomplishing this was by invoking vegetation that would grow through the dust layer. This is a possibility and is perhaps the most telling argument for interpreting the dark areas as being vegetation-covered.

It should be noted that no terrestrial life forms have been demonstrated to have the requisite hardiness and proliferation to explain the Martian phenomena. Kuiper (Ref. 9) has suggested lichens as the Martian cover because of their ability to live in very hostile environments, and because of the range of colors they may possess. Salisbury (Ref. 54) has criticized this proposal, noting



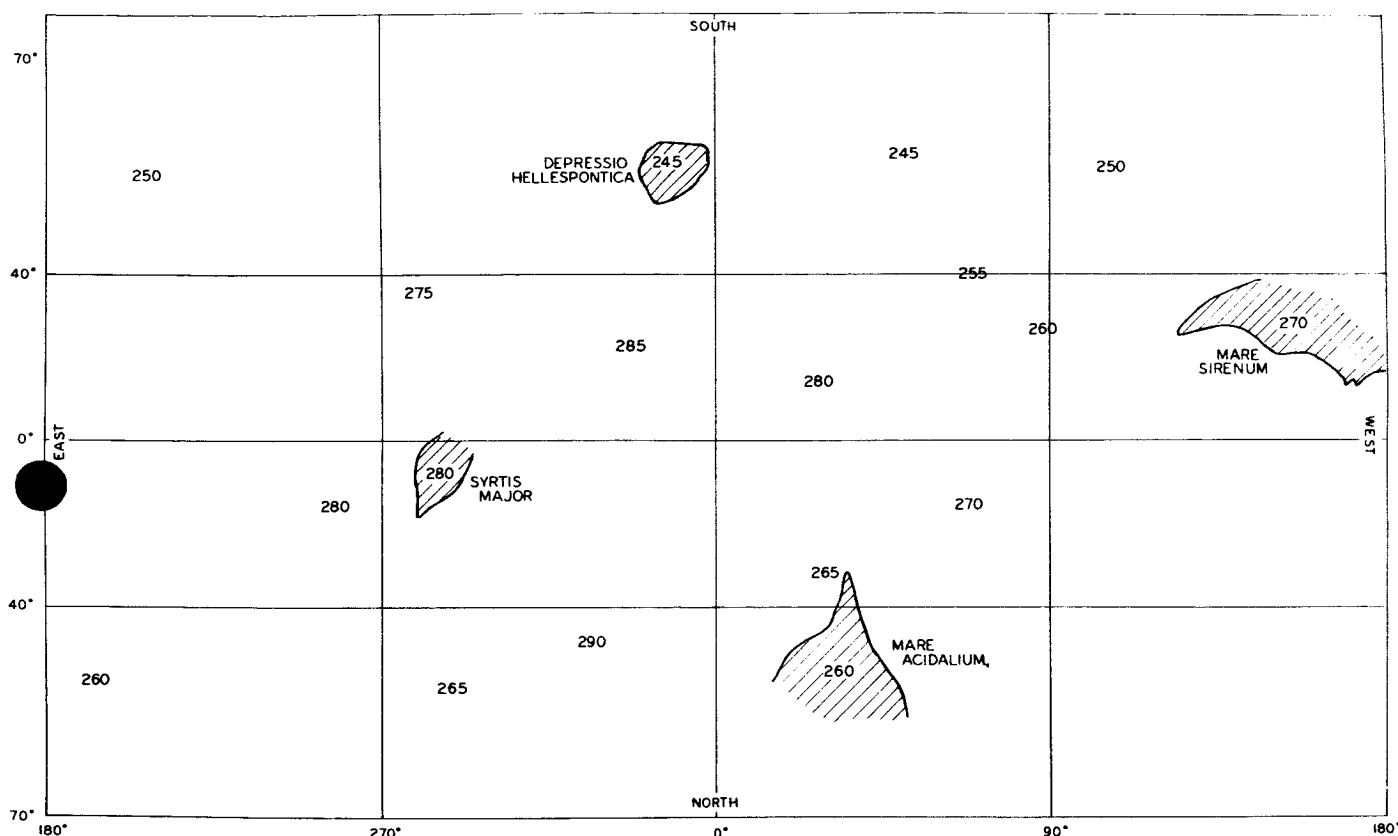


Fig. 25. Observed temperatures at the height of the darkening wave

that the growth rate of lichens is far less than that required. Not only lichens, but also certain strains of bacteria, are hardy, but populating a planetary surface with such organisms to the level required to explain the Martian phenomena seems ludicrous. If a Martian biota is responsible for these visual effects it must have properties quite different from any species with which we are familiar. Of course, this is only to be expected, since any existing Martian life would have to evolve to fit into the developing ecological niches. Since these are so different from any on Earth, the organisms would in all probability be quite unfamiliar.

*The nonbiological interpretations.* In this category I want to single out work by four authors who, in my opinion, have proposed ideas that have considerable merit. They are Tombaugh (Ref. 55), McLaughlin (Refs. 27, 56), Kuiper (Ref. 35), and Smoluchowski (Ref. 57). I will first describe briefly the salient points of their proposals and then extract certain ideas and meld them into a description that has the greatest appeal to me.

Tombaugh suggests that the shrinkage of the planet has produced a "tetrahedral deformation" with the maria

lower than the bright areas, a result that he states is in conformity with the evidence available. The oases are depicted as craters formed by the collision of small asteroids, and the radiating canals are cracks in the crust resulting from the impact. The colors and seasonal behaviors are "undoubtedly due to the growth of vegetation" with the "fractured zones," i.e., the canals, giving "haven to a hardy vegetation in regions of unfavorable environment." The mechanism of this is not spelled out, and it is not clear whether he regards the canals as valleys or as the loci of volcanic activity, either of which could provide the necessary haven. The vegetation part of this hypothesis and the idea that the dark areas are depressed I find difficult to accept. Specifically, I know of no good evidence suggesting the dark areas are depressed. It is believed that Hellas is an elevated plateau, but this need not imply that all of the bright areas are elevated. In view of the widespread dust storms it would seem more natural that the low areas would be covered with this dust and hence would be bright.

In his two papers McLaughlin developed a volcanic model to explain the maria and certain of the canals. The peculiar tendency of the maria to be concentrated near



the equator, to have "triangular" or funnel-shaped estuaries, and to trend in a south-east north-west direction suggested to him that they are the result of volcanic action. If, at the point of the funnels, there exist volcanoes, the expected prevailing trade winds in the southern summer will blow the ash in just the right direction to explain the extended areas. In northern summer the planet is further from the Sun and the counter winds will be much weaker. Rather than produce long dark areas, they blow the ash into the thin streams that we see as canals radiating from the volcanic tips. McLaughlin states that the volcanoes all lie close to a great circle inclined at  $25^\circ$  to the equator and likens this to Earth's circum-Pacific volcano belt. However, when the volcano positions are plotted on a stereographic projection, it is seen that between  $0^\circ$ – $180^\circ$  areographic longitude his statement is valid, but that between  $180^\circ$ – $360^\circ$  they scatter

about the equator, Fig. 26. The canals are attributed to a variety of possible causes, of which ash deposit from active volcanoes is only one. They may be (1) linear chains of small volcanoes along major crustal fractures, (2) major fault zones in which the surface irregularities have trapped drifting volcanic ash, (3) rift valleys related to fault zones, or (4) igneous dikes. The seasonal changes may be due to (1) moistening of the surface, or (2) a new fall of ash. Secular changes can arise from an increase or decrease of volcanic activity. The concept that volcanic activity has played, and maybe still plays, a major role in shaping the surface is intriguing, although some of the details are difficult to accept. Continuously active volcanoes required for the seasonal changes are improbable, and the humidity is too low for any moistening of the soil that is more than transient. Explaining some of the canals as ash deposits from a central volcano at an

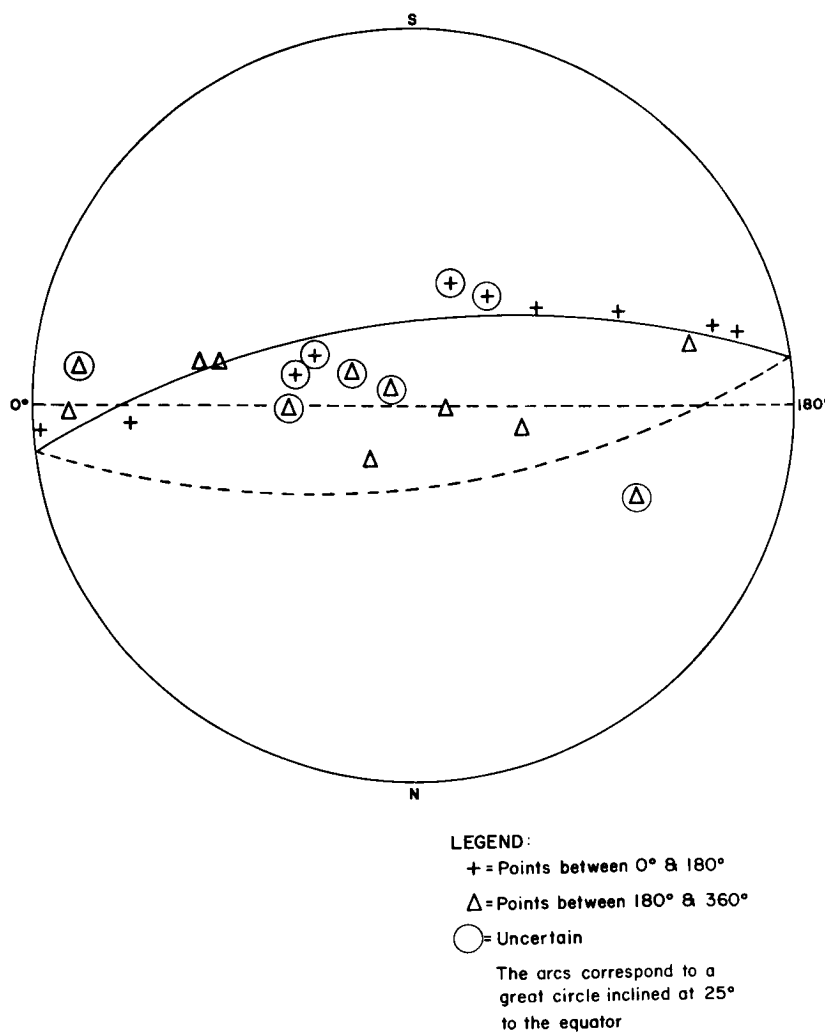


Fig. 26. A stereographic projection of presumed Martian volcanoes

oasis is improbable in view of their narrowness relative to the extended areas and in view of the fact that in general several canals intersect at any one oasis. The attribution of canals to valleys has already been criticized, and associating them with faults seems unlikely because of their tendency to intersect. Not only do they meet at oases, but they also intersect with no apparent influence on one another's path. This behavior has not been reported for faults on Earth, and certainly appears unusual.

A different proposal was advanced by Kuiper (Ref. 35) after making extensive visual observations during the 1956 opposition. He suggests the dark areas are lava flows, and that the dust cover is variable, depending on the seasonal winds. Secular changes are the result of secular changes in the wind pattern. The regenerative power is due to the ability of the wind to blow the dust particles off the lava. He believes that some of the reported green colors are valid observations and includes in his model "a partial cover of some very hardy vegetation." He gives no further details of his model, in particular he makes no proposal regarding the relative elevations of the dark and bright areas, nor of the actual behavior of the presumed vegetation.

The possibly high ultraviolet ( $\lambda > 2000 \text{ \AA}$ ) flux at the surface prompted Smoluchowski (Ref. 57) to suggest that UV-produced color centers may explain some of the Martian phenomena. The high flux may produce color centers whose population is temperature-dependent. In winter the centers would be depopulated, while in summer they would be populated and the material would be darker. Secular changes could be the result of extraordinarily high irradiation due to photons and corpuscular matter from solar flares. No mineralogical systems were advanced as demonstrating these phenomena, and no effort was made to explain the regenerative property of the dark areas. While the hypothesis is interesting it would seem to predict a wave that moves from equator to pole since this is the direction in which the maximum daily temperature increases, and it is this temperature that presumably is most critical in the kinetics. The observed wave appears to be correlated more with the atmospheric transport of water vapor, a factor not considered in Smoluchowski's treatment.

Finally, I would like to extract some ideas from these works, add one or two of my own, and present a picture that seems most reasonable, at least to me. It is essentially an extension of some previous ideas (Refs. 52, 58). First, the dark areas are considered to be elevated, and

the bright areas depressed and dust covered. The observation by Slipher (Ref. 2) of temporary dark areas adjacent to yellow clouds is interpreted simply as areas from which the dust cover has been temporarily removed during the storm. His explanation invoking a wetting of the soil by precipitated water is untenable in view of the dryness of the atmosphere. The maria are probably the deposits of volcanic ash, wind-blown from volcanoes at their vertices. The oases are most likely impact craters and the canals strings of small volcanoes aligned along crustal fractures linking the impact craters with themselves and with the major volcanoes. The possibility that the canals are ejecta thrown out from the primary crater was considered, but was rejected because (1) they would probably require too much material for their formation, and (2) they would not be expected to connect oases and volcanoes to the degree apparent. The darkening wave may be due to (1) small dust particles seasonally transported on and off the dark areas, or to (2) a seasonal darkening of a permanent surface, due perhaps to a reaction with  $\text{H}_2\text{O}$  vapor that is promoted by the high radiation fluxes. The polarization changes may be a result of a change in particle size or of the decrease in brightness. The influence of the latter may be an intrinsic surface effect or a consequence of an increased relative contribution of aerosol scattering (Ref. 46). Secular changes may be ascribed to changes in the wind pattern, to volcanic activity, or to both. The regenerative ability results from the settling of the dust into the lower areas. The dark material is essentially unweathered volcanic ash, the bright material the products of its weathering. Even though liquid water is rare, if present at all, a slow weathering may still occur (Ref. 56) and may in fact be facilitated by the incident energetic radiation.

#### IV. Concluding Remarks and Acknowledgment

This is a highly selective review. It is intended to illustrate recent important advances in our knowledge and to provide a critical appraisal of the current theories on the atmosphere and surface. Encyclopedic coverage has not been attempted, and I sincerely hope that no papers of significance for the present purpose have been omitted.

Much of the appraisal has benefitted from collaboration and discussion with several colleagues, notably W. J. Welch, M. Calvin, T. Belsky, B. T. O'Leary, and R. A. Wells. I am particularly indebted to J. Nicholls for assistance in evaluating the work on the surface phenomena.

This work was supported by NASA Grant NsG 101-61 and NASA Contract NASr 220.

## REFERENCES

1. de Vaucouleurs, G., 1954, *Physics of the Planet Mars*, Faber and Faber, London.
2. Slipher, E. C., 1962, *Mars, The Photographic Story*, Sky Publishing Corp., Cambridge, Mass.
3. Sharpless, B. P., 1945, *Astron. J.*, Vol. 51, p. 185.
4. Shklovsky, I. S., 1959, *Komsomol'skaya Pravda*, May 1 and 31.
5. Redmond, J. C., and Fish, F. F., 1964, *Icarus*, Vol. 3, p. 87; Redmond, J. C., 1964, *J. Geophys. Res.*, Vol. 69, p. 4173.
6. Schilling, G. F., 1964, *J. Geophys. Res.*, Vol. 69, p. 1825; *ibid.*, Vol. 69, p. 4176.
7. Dollfus, A., 1962, *Compt. Rend.*, Vol. 255, p. 2229.
8. MacDonald, G. J. F., 1963, *Space Sci. Rev.*, Vol. 2, p. 473.
9. Kuiper, G. P., 1952, Chapter XII in *The Atmospheres of the Earth and Planets* (2nd ed., G. P. Kuiper, ed.), University of Chicago Press, Chicago.
10. Kaplan, L. D., Münch, G., and Spinrad, H., 1964, *Astrophys. J.*, Vol. 139, p. 1.
11. Campen, C. F., and Stallkamp, J. A., private communication.
12. Chamberlain, J. W., and Hunten, D. M., 1965, *Reviews of Geophysics*, Vol. 3, p. 299.
13. Cann, M. W. P., Davies, W. O., Greenspan, J. A., and Owen, T. C., 1965, Parts I and II, W6096 Final Report, Contract No. NASr-9037, Illinois Institute of Technology Research Institute.
14. Musman, S., 1964, *Planetary Space Sci.*, Vol. 12, p. 799.
15. Evans, D., 1965, *Science*, Vol. 149, p. 969; and personal communication.
16. Spinrad, H., Münch, G., and Kaplan, L. D., 1963, *Astrophys. J.*, Vol. 137, p. 1319.
17. Kiess, C. C., Karrer, S., and Kiess, H. K., 1960, *Publ. Astron. Soc. Pacific*, Vol. 72, p. 256; *ibid.*, 1963, Vol. 75, p. 50.
18. Marshall, J. V., 1964, *Communications of the Lunar and Planetary Laboratory*, Vol. 2, p. 167.
19. O'Leary, B. T., 1965, *Publ. Astron. Soc. Pacific*, Vol. 77, p. 168.
20. Colthup, N. B., 1961, *Science*, Vol. 132, p. 529.
21. Rea, D. G., 1962, *Space Sci. Rev.*, Vol. 1, p. 159.
22. Kuiper, G. P., 1964, *Communications of the Lunar and Planetary Laboratory*, Vol. 2, p. 79.
23. Kellogg, W. W., and Sagan, C., 1961, editors, *The Atmospheres of Mars and Venus*, Publication 944, National Academy of Sciences, National Research Council.
24. Wells, R. A., 1965, *Nature*, Vol. 207, p. 735.

## REFERENCES (Cont'd)

25. Finsen, W. S., 1961, Chapter 17 in *Planets and Satellites*, Vol. III of *The Solar System*, ed. by G. P. Kuiper and B. M. Middlehurst, Univ. of Chicago Press, Chicago.
26. Dollfus, A., 1957, *Compt. Rend.*, Vol. 244, pp. 162, 1458.
27. McLaughlin, D. B., 1954, *Publ. Astron. Soc. Pacific*, Vol. 66, p. 221.
28. Dollfus, A., 1957, *Ann. d'Astrophys.*, Supp. No. 4; 1961, Chapter 9 in *Planets and Satellites*, Vol. III of *The Solar System*, ed. by G. P. Kuiper and B. M. Middlehurst, Univ. of Chicago Press, Chicago.
29. Ryan, J. A., 1964, *J. Geophys. Res.*, Vol. 69, p. 3759.
30. Gifford, F., 1956, *Astrophys. J.*, Vol. 123, p. 154.
31. Pettit, E., 1961, Chapter 10 in *Planets and Satellites*, Vol. III of *The Solar System*, ed. by G. P. Kuiper and B. M. Middlehurst, Univ. of Chicago Press, Chicago.
32. Sinton, W. M., and Strong, J., 1960, *Astrophys. J.*, Vol. 131, p. 459.
33. Focas, J., 1961, *Ann. d'Astrophys.*, Vol. 24, p. 309.
34. Dollfus, A., 1961, Chapter 15 in *Planets and Satellites*, Vol. III of *The Solar System*, ed. by G. P. Kuiper and B. M. Middlehurst, Univ. of Chicago Press, Chicago.
35. Kuiper, G. P., 1957, *Astrophys. J.*, Vol. 125, p. 307.
36. Sinton, W. M., 1957, *Astrophys. J.*, Vol. 126, p. 231; *Science*, 1959, Vol. 130, p. 1234; 1961, *Science*, Vol. 134, p. 529.
37. Rea, D. G., O'Leary, B. T., and Sinton, W. M., 1965, *Science*, Vol. 147, p. 1286.
38. Moroz, V. I., 1964, *Astron. Zh.*, Vol. 41, p. 350.
39. Rea, D. G., Belsky, T., and Calvin, M., 1963, *Science*, Vol. 141, p. 3584.
40. Goldstein, R. M., and Gillmore, W. F., 1963, *Science*, Vol. 141, p. 1171.
41. Kellermann, K. I., 1965, *Nature*, Vol. 206, p. 1034.
42. Davies, R. D., 1964, Thirteenth International Astronomical Union General Assembly, Hamburg.
43. Leighton, R. B., Murray, B. C., Sharp, R. P., Allen, J. D., and Sloan, R. K., 1965, *Science*, Vol. 149, p. 627.
44. Yagoda, H., 1963, Paper presented at the COSPAR meeting, Warsaw.
45. Hovis, W., submitted for publication.
46. Rea, D. G., and O'Leary, B. T., 1965, *Nature*, Vol. 206, p. 1138.
47. Binder, A. B., and Cruikshank, D. P., 1963, *Communications of the Lunar and Planetary Laboratory*, Vol. 2, p. 193.
48. Adamcik, J. A., Draper, A. L., and Gibson, E. K., 1965, *American Geophysical Union Transactions*, Vol. 46, p. 546.
49. Van Tassel, R. A., and Salisbury, J. W., 1964, *Icarus*, Vol. 3, p. 264.
50. Rea, D. G., 1965, *Icarus*, Vol. 4, p. 108.

## REFERENCES (Cont'd)

51. Aller, L. H., 1963, *The Atmospheres of the Sun and Stars*, 2nd ed., The Ronald Press Co., New York.
52. Rea, D. G., 1963, *Nature*, Vol. 200, p. 114.
53. Öpik, E. J., 1962, in *Progress in the Astronautical Sciences*, ed. by S. F. Singer (Interscience Publishers, Inc., New York).
54. Salisbury, F. B., 1962, *Science*, Vol. 136, p. 17.
55. Tombaugh, C. W., 1950, *Astron. J.*, Vol. 55, p. 184.
56. McLaughlin, D. B., 1954, *Publ. Astron. Soc. Pacific*, Vol. 66, p. 161.
57. Smoluchowski, R., 1965, *Science*, Vol. 148, p. 946.
58. Rea, D. G., 1964, *Nature*, Vol. 201, p. 1014.

(Copyright notices: Volume III of *The Solar System*, Copyright 1961 by the University of Chicago; cited volumes of *Science*, Copyright 1963 and 1965, American Association for the Advancement of Science.)

## **JPL RADAR OBSERVATIONS OF MARS\***

*Richard Goldstein*

*Jet Propulsion Laboratory  
Pasadena, California*

Recent radar experiments at JPL's Goldstone Tracking Station have "mapped" the roughness and/or reflectivity of the Martian  $21^{\circ}$  N latitude circle. A very smooth, strongly reflecting region was found, extending  $20$  to  $30^{\circ}$  in longitude about Trivium Charontis. Laocoontis was found to be a similar, but rougher, region. Elysium was a poor radar reflector, as were the dark markings Asraeus Lacus and Albi Lacus. The large "desert" region Amazonis was also a poor reflector. Mars, as a whole, is smoother than Venus (to 12.5-cm radiation). The average reflection coefficient of Mars was measured to be 8.6%.

---

\*Abstract of paper.

N66 31473

## CO<sub>2</sub> BANDS AND THE MARTIAN SURFACE PRESSURE

Donald M. Hunten

Kitt Peak National Observatory  
Tucson, Arizona

The surface atmospheric pressure on Mars is a matter of great current interest, primarily for two reasons connected with the space program. First, as Dr. Rea has just pointed out, the design of a landing vehicle is critically dependent on this figure; second, the beautiful radio-occultation experiment with *Mariner IV* has just given us a precise new source of information. The preliminary result, reported in this week's *Science* by Kliore et al. (1965), is a surface pressure of 4 to 7 mb, with a mean molecular weight of around 40. The ground-based spectroscopic measurements are now suggesting CO<sub>2</sub> partial pressures in the 5- to 13-mb range; the molecular weight of CO<sub>2</sub> is 44. Chamberlain keeps telling me that this looks like a bandwagon effect, and I have to admit that it does look suspicious, because only a few months ago the spectroscopic measurements suggested a total pressure of 20 to 30 mb, only 10% or so being CO<sub>2</sub>. However, I can't help what the measurements say, and what they seem to say to me is that carbon dioxide is the major constituent, perhaps the only important one, with a surface pressure of 5 to 10 mb.<sup>1</sup>

<sup>1</sup>It is only honest to record that several of the later speakers preferred to jump off this bandwagon, although the highest spectroscopic pressure suggested was only 13 mb, 30% CO<sub>2</sub>.

Until about 2 years ago, the accepted value of the pressure was higher yet, around 85 mb, and there was a great deal of reluctance about accepting even the 20 or 30 given about that time by the first spectroscopic measurements. At the request of NASA, Chamberlain and I reviewed the subject, and the published version of our conclusions appeared recently (1965). I would like to be able to say that we foresaw the current situation, but I have to admit that we did not. Just the same, we found that the method at best contained uncertainties of a factor of 3, and at worst could be completely vitiated by violation of certain assumptions. I shall now present a summary of that review, with a few comments added here and there in the light of the current state of knowledge. Dr. Michael Belton and I have been measuring a CO<sub>2</sub> band ourselves at Kitt Peak, and although our reductions are not complete, the preliminary results will be presented for comparison with those of the other speakers.

A brief discussion of pressure units may be in order here. Probably the only gravitational unit still in common use by physicists is the torr, or millimeter of mercury. However, this has such obvious potentialities for confusion that it is quickly abandoned in discussions of other

planets. The absolute unit, the millibar, contains no gravitational fields in its definition. However, it is helpful to recall that the relation between pressure and integrated density does involve the local gravitational acceleration  $g$ :

$$p = g \int \rho \, dz$$

Thus, a given mass of atmosphere exerts only about  $\frac{3}{8}$  the pressure on Mars that it does on Earth.

Aside from the spectroscopic technique, only two ground-based methods have been found to give useful values of the Martian atmospheric pressure. They are the photometric and the polarimetric methods, based on different aspects of the Rayleigh law of molecular scattering. Visible effects of the presence of an atmosphere are described in almost any elementary textbook of astronomy. Surface features are difficult to distinguish, especially near the limb, and are sometimes blotted out by haze or dust; practically no detail can be distinguished in blue and violet light; polar caps appear and disappear. One is left with the feeling that the Martian atmosphere should be not much less dense than the terrestrial; the old pressure of about  $1/12$  atm seemed surprisingly low, if anything, and the new value of  $1/100$  or less surprising indeed.

This qualitative evidence is all very well, but how can one hope to get a quantitative result from it, in the presence of the strong scattered light from the surface? It is first necessary to measure as much as possible about the photometric properties of the surface itself; usually this information is supplemented by measurements on similar terrestrial materials. One then uses either the wavelength variation or the polarization known to be characteristic of Rayleigh scattering to disentangle the wanted component. The difficulty is well illustrated by the recent result of Dollfus that, at the center of the disk, the atmospheric component is only 0.9% of the total. The spectroscopic and space-probe measurements suggest that even this figure is too large by a factor of about 3.

The photometric method depends on photographic or visual measurements, as a function of wavelength, of the brightness of selected spots on the planet as they rotate to different positions on the disk. The best measurements are those of Sytinskaya and de Vaucouleurs. With the aid of the  $\lambda^{-4}$  variation of the Rayleigh law, and some assumptions about the scattering properties of the surface,

the component scattered by the atmosphere was estimated. Some allowance for permanent haze gave a pressure of about 90 mb; the haze component seemed to be about half the total.

A more refined method, applied by Dollfus, is to make use of the characteristic polarization of Rayleigh scattering at different angles. In principle this technique is far more discriminating, but again the problem is to determine the surface polarization accurately enough so that it can be subtracted with assurance. The required measurements are made both on the planet and on analogous terrestrial materials. The atmospheric scattering is assumed to follow the Rayleigh law; any contribution from aerosols must be neglected, and the justification is that only those observations made under unusually clear Martian conditions are used. The original result reported by Dollfus was about 85 mb, but it is interesting to compare a current value given by him at this meeting. A new reduction of the old data, with improved allowance for the light from the surface, reduced the result to 40 mb. Recent measurements over a much wider wavelength range ( $0.4$  to  $1 \mu$ ) at the center of the disk give a still lower value of 25 mb. Dollfus stresses that this is on the unproved assumption that no haze is present when the atmosphere is clearest. If half the scattering is by small particles, smaller than the wavelength so as to imitate Rayleigh scattering, no serious disagreement with the spectroscopic value would remain. In any case, our review suggests that a possible error of a factor of 3 is likely for this method, even under optimum conditions. And there is still the doubt about how accurately the light from the surface has been subtracted.

The spectroscopic method is based on the possibility of observing vibration-rotation bands of  $\text{CO}_2$  having widely different transition probabilities. The first strong band, at  $1.6 \mu$ , was discovered in 1947 by Kuiper; shortly after, the presence of still stronger ones near  $2 \mu$  was demonstrated. These bands, being heavily pressure-broadened, give a value for the product ( $\text{CO}_2$  abundance)  $\times$  (total pressure). The pressure so found corresponds to a mean height in the atmosphere, but it is conventional to refer it to the surface. The  $\text{CO}_2$  abundance can be determined from the weak bands at 8689 and  $10,500 \text{ \AA}$ . With a surface pressure of 85 mb, these bands could be predicted to be far too weak to observe, and the discovery of the 8689  $\text{\AA}$  band by Spinrad was made on a plate exposed for another purpose. Kaplan, Münch, and Spinrad quickly showed that the corresponding pressure was only 10 to 40 mb. The flurry of observations at the 1965 opposition is the direct result of Spinrad's discovery.



These recent results suggest an even larger abundance, and the corresponding pressure is so low that the chief pressure-broadening agent may be the CO<sub>2</sub> itself. The first realistic treatment of the pressure-broadened bands was given in 1955 by Grandjean and Goody, and two years later Goody pointed out that a lower limit to the pressure could be derived in this way. At the time, and until very recently, this was considered an interesting but academic result, but now it shows strong signs of becoming an independent, useful determination. The first explicit suggestion that the pressure could be found from the CO<sub>2</sub> bands is due to Kaplan, but it is implicit in the earlier work just mentioned.

The accepted value of the pressure-abundance product has fallen steadily as the measurements improved. Probably the chief difficulty has been in defining the level of the continuum, since the low sensitivity of the PbS cell does not allow resolution of individual rotational lines. In addition, there is an appreciable terrestrial component, since the high pressure enhances the absorption of the small amount of CO<sub>2</sub>. The interpretation of the observations must also take account of the fact that the broadening by CO<sub>2</sub> itself is slightly greater than that by N<sub>2</sub>. (The factor 2.2 has been used quite a bit recently, but Spinrad has just pointed out to me that the laboratory value is actually 1.2.) For simplicity, I shall quote the results in terms of the Goody limit for a pure CO<sub>2</sub> atmosphere; this does not necessarily imply that no other interpretation is possible or even likely. Measurements of the 2  $\mu$  bands by Kuiper and by Sinton suggest a pressure of about 10 mb, on this interpretation; the early results of Kuiper at 1.6  $\mu$  give about the same value. However, the more recent measurements by Owen and Kuiper of the 1.6  $\mu$  bands suggest about 6.8 mb, and this is undoubtedly more reliable. Since this figure is not far from the one suggested by the weak bands, the atmosphere may indeed be mostly CO<sub>2</sub>.

Instead of giving any kind of impartial review of the weak-band measurements, I am going to give you the details of one particular program, by Dr. Michael Belton and myself at Kitt Peak (Belton and Hunten, 1966). Several other groups have been working on the problem, using data taken at the recent opposition, and you will be hearing from them this afternoon. Although our reductions are not completed, they have gone far enough that I can give you some preliminary answers. We felt that photoelectric scanning would have advantages over the photographic method used by all the other workers. We used the 60-inch solar telescope with its large spectrograph, scanning repeatedly over a range of 8 Å and

accumulating the photoelectron counts in a 400-channel memory device. In fact, we did not get as smooth a continuum as would be expected from counting statistics alone, and we were unable to see the lines of the 8689 Å band at all. But the photomultiplier has another strong point: its spectral sensitivity extends to the considerably stronger band at 10,500 Å, which is very difficult to observe photographically.

Fig. 27 shows our composite spectrum, plotted out by the computer after smoothing by a suitable weighted running mean. The individual scans covered about one-third of the total range; they have been shifted appropriately in wavelength before averaging them together. We are still not satisfied with the method to define the continuum, and the equivalent widths must still be considered preliminary. The uncertainty in the abundance is considerably greater, because many of the lines are nearly saturated. The temperature determination is seriously affected as well, and at present we can give only rough values.

With the 15 or so line intensities available, we have enough data to fit a curve of growth. It is readily shown that all the lines are on the doppler part of the curve, and this part can be constructed with adequate accuracy even if only a rough temperature is known; we used 200° K. The theoretical relative intensities were calculated from the standard formula for an R branch:

$$I(J) = \text{const } (J + 1) \exp \left[ - \frac{Bhc}{kT} J(J + 1) \right]$$

In a detailed analysis, account will have to be taken of the fact that there is a temperature gradient in the atmosphere, and a suitable average taken. Once the curve of growth is fitted to the observed points, the line-of-sight CO<sub>2</sub> abundance can be deduced, and our current estimate is

$$\eta \mathcal{N} = 340 \text{ m-atm}$$

Here  $\mathcal{N}$  is the actual Martian abundance, and  $\eta$  is the path-length multiplying factor. The observations were made with an image-slicer that accepted nearly the whole disk, and the value of  $\eta$  is estimated to be 3.4. Thus, the abundance is  $\mathcal{N} = 100 \text{ m-atm}$ , which corresponds to a surface partial pressure of 7.1 mb. This is actually a bit higher than the maximum value required by the pressure-broadened bands, but of course the possible errors can easily account for the discrepancy.

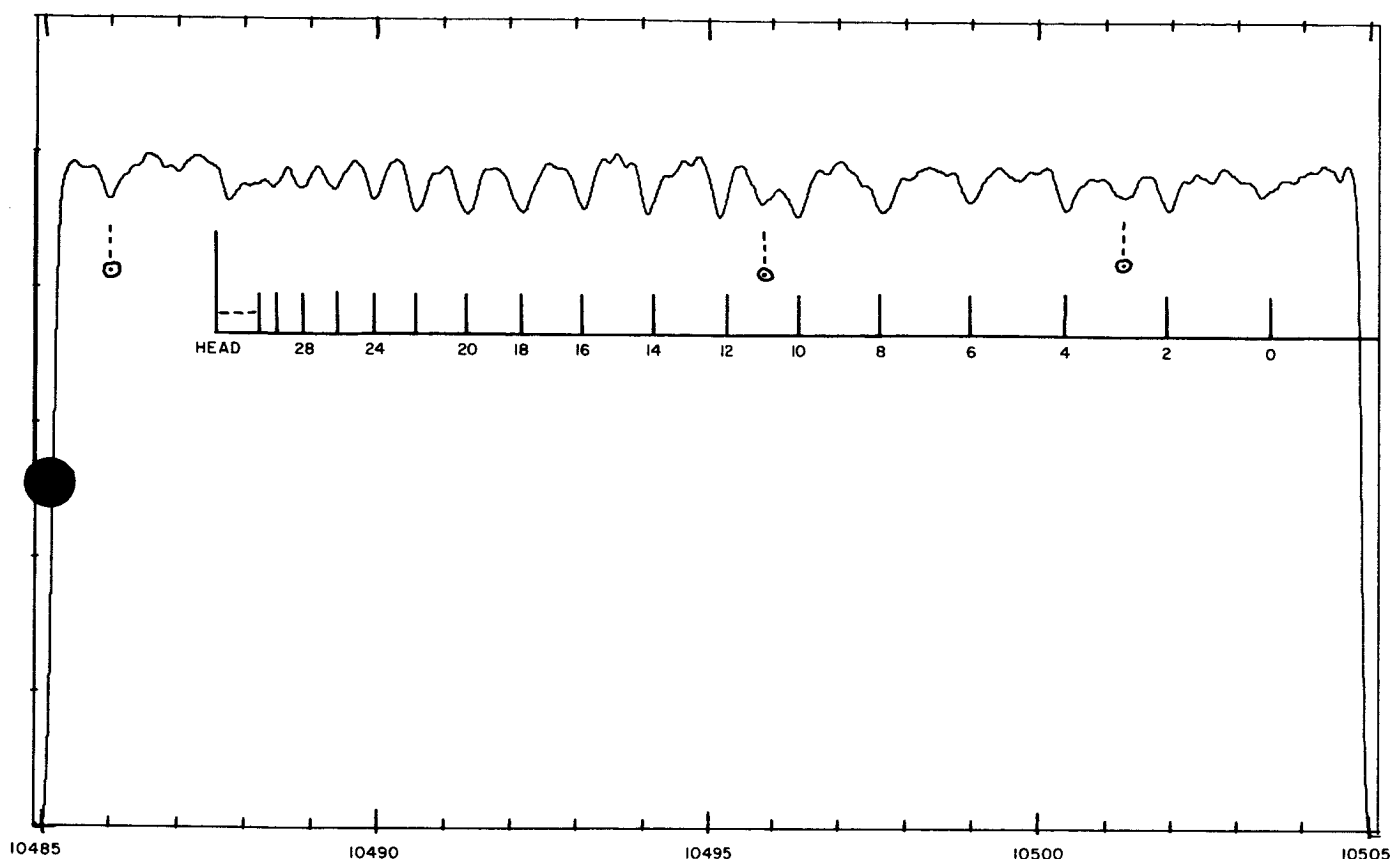


**Fig. 27. Observed spectrum of the R-branch of the  $\nu_1 + 2\nu_2 + 3\nu_3$  band of  $\text{CO}_2$  at  $1.05 \mu$  in Mars. Three weak Fraunhofer lines are marked with  $\odot$  symbols.**

However, the results suggest an atmosphere in which  $\text{CO}_2$  is the major constituent, if not the only important one. It seems likely that the partial pressure of other gases is not over 3 or 4 mb.<sup>2</sup>

My confidence in the picture of a nearly pure  $\text{CO}_2$  atmosphere is greatly strengthened by the *Mariner IV* results. The scale height is so small as to require a mean molecular weight of at least 40 (or else an unacceptably low temperature). The surface pressure for a pure  $\text{CO}_2$  model is 4 to 6 mb, in remarkably good agreement with the lower spectroscopic results; with 50% argon, the range is 5 to 7 mb. As the experimenters point out, their pressure is not necessarily for the average surface, but refers to whatever point on the horizon actually occulted the radio waves.

Finally, let me mention the preliminary value of the rotational temperature indicated by our measurements.

<sup>2</sup>The other measurements, reported in the later papers, all gave a lower  $\text{CO}_2$  abundance, with partial pressures ranging from 4 to 6 mb. The corresponding total pressures were as high as 13 mb.

It is 160 to 180° K, again remarkably closer to the *Mariner* value of 180°. As I have mentioned, we hope to be able to refine this determination considerably.<sup>3</sup>

To sum up: the spectroscopic measurements suggest a surface partial pressure of  $\text{CO}_2$  in the range 4 to 7 mb and a total pressure of 13 to 7 mb. The strong possibility that  $\text{CO}_2$  is the major constituent is reinforced by the *Mariner IV* results suggesting a high molecular weight and a pressure of 4 to 7 mb. The old photometric and polarimetric result of 85 mb is completely discredited, and indeed a new polarimetric value of 25 mb was

<sup>3</sup>Note added October 1965. The final reduction of the 10,500 Å spectra has now given a projected abundance  $\eta\mathcal{N} = 207$  m-atm, probably good to about 20%. An improved estimate of  $\eta$ , allowing for the phase of the planet, gives about 3.0, so that the abundance is  $\mathcal{N} = 69$  m-atm. The corresponding partial pressure is 4 mb. These figures are still consistent with a pure  $\text{CO}_2$  atmosphere, but if taken literally suggest the presence of a few millibars of other gases. The temperature determination is now greatly improved and yields an average value of 194° K; this has yet to be corrected for the temperature gradient in the atmosphere.

given at the meeting. It is still not established whether the discrepancy is due to additional scattering by aerosols

in the atmosphere, or to the inherent difficulty of subtracting all the effects of light from the surface.

## REFERENCES

- Belton, M. J. S., and Hunten, D. M., 1966, "The Abundance and Temperature of CO<sub>2</sub> in the Martian Atmosphere," *Astrophys. J.*, August 1966 (in press).
- Chamberlain, J. W., and Hunten, D. M., 1965, *Reviews of Geophysics*, Vol. 3, p. 299 (gives references to all the earlier papers mentioned in the text).
- Kliore, A., Cain, D. L., Levy, G. S., Eshleman, V. R., Fjeldbo, G., and Drake, F. D., 1965, *Science*, Vol. 149, p. 1243.

# SPECTROSCOPIC OBSERVATIONS OF MARS, 1964-5\*

Hyron Spinrad

University of California  
Berkeley, California

Spinrad, R. Schorn, H. J. Smith, L. P. Giver, and R. Moore have found doppler-shifted Martian water vapor lines on high-resolution coudé spectrograms of Mars taken at McDonald and Lick Observatories during the 1964-5 season. Affiliations of investigators are: Schorn, JPL; Smith, University of Texas; Giver, University of California; and Moore, RAND Corp.

\*Abstract of paper.

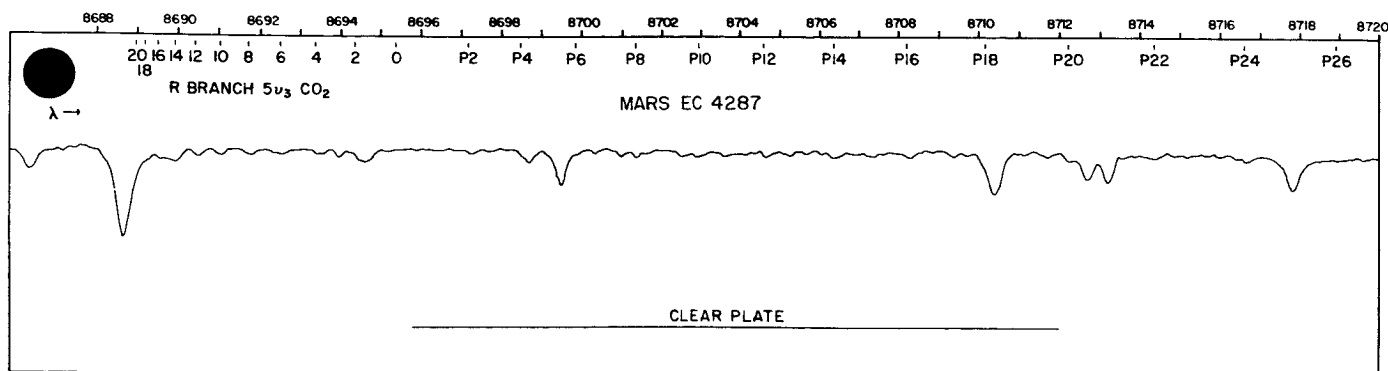


Fig. 28. A portion of the Mars spectrum at the  $5 \nu_3$   $\text{CO}_2$  band. Positions of the weak rotational lines of  $\text{CO}_2$  in the R and P branches are indicated. The original dispersion was 4 Å/mm. Note the clearly visible R12, 10, and 8 lines.

The amount of water vapor on Mars again seems quite small, averaging about  $15 \mu$  precipitable when it is detected. The location of the Mars  $\text{H}_2\text{O}$  apparently varies with Martian season; the weak lines first appeared over the subliming North Polar Cap and then migrated south over the planet.

We have also redetermined the Mars  $\text{CO}_2$  abundance using the  $5 \nu_3 \text{CO}_2$  band at  $\lambda 8700$ . Our preliminary result is  $w_{\text{CO}_2} = 80 \text{ m-atm CO}_2$ , which gives a carbon dioxide partial pressure near 6 mb. Combining this result with recent data of Kuiper and Owen on the saturated  $\text{CO}_2$  band at  $1.6 \mu$ , we find the total Mars surface pressure  $P_s = 8 \pm_4^6 \text{ mb}$ . Carbon dioxide therefore is the major constituent. (See Fig. 28.)

## RECENT OBSERVATIONS OF THE PHOTOGRAPHIC SPECTRUM OF MARS—A PRELIMINARY REPORT

Tobias Owen

*IIT Research Institute  
Chicago, Illinois*

### **I. Introduction**

A series of spectra of Mars at wavelengths ranging from 4000 to 11,000 Å was obtained at the McDonald Observatory in March 1965. The violet region of the spectrum was examined for evidence of NO<sub>2</sub> absorption and N<sub>2</sub><sup>+</sup> emission. The results were negative, supporting Marshall's (1964) conclusion that an upper limit of 8 μ-atm may be placed on the abundance of NO<sub>2</sub> in the Martian atmosphere. The upper limit on N<sub>2</sub><sup>+</sup> has not yet been evaluated, but it is not anticipated that this will be a sensitive test for the presence of N<sub>2</sub>.

The main effort of the spectroscopic program was concentrated on a redetermination of the Martian CO<sub>2</sub> abundance by means of observations of the weak bands at 8689 Å and 1.05 μ. Four plates of the 8689 Å band and three of the 1.05 μ band were obtained. Three of the spectra of the 8689 Å band recorded measurable absorptions for lines in the P branch as well as the R branch. The best of these plates is reproduced in Fig. 29. Only one of the 1.05 μ band spectra included measurable P branch absorptions.

At this writing, the reduction of these plates is not yet complete. However, sufficient data are available to per-

mit a preliminary report on the results. Equivalent widths for all the lines that could be measured have been determined from densitometer tracings. Additional tracings should permit greater precision, since at least two non-overlapping tracings can be obtained from each plate. In addition, direct comparisons will be made with synthetic spectra obtained by using sunlight as a source of illumination for an absorption cell containing CO<sub>2</sub>. The solar lines appearing in the Martian spectra were used to calibrate the tracings; the Liège Atlas of Delbouille and Roland served as the standard for solar equivalent widths. The procedure for converting the measured equivalent widths of the CO<sub>2</sub> lines into the amount of this gas in a vertical column in the Martian atmosphere is outlined in Secs. II and III. Section IV consists of a discussion of the determination of a value for the atmospheric surface pressure based on these data and the measures made by Kuiper and Moroz of the strong band absorption of CO<sub>2</sub> at 1.6 μ and 2.06 μ in the Martian spectrum.

### **II. Method of Reduction**

The method of reduction included determination of the mean atmospheric temperature, correction of line intensities, and determination of air mass.

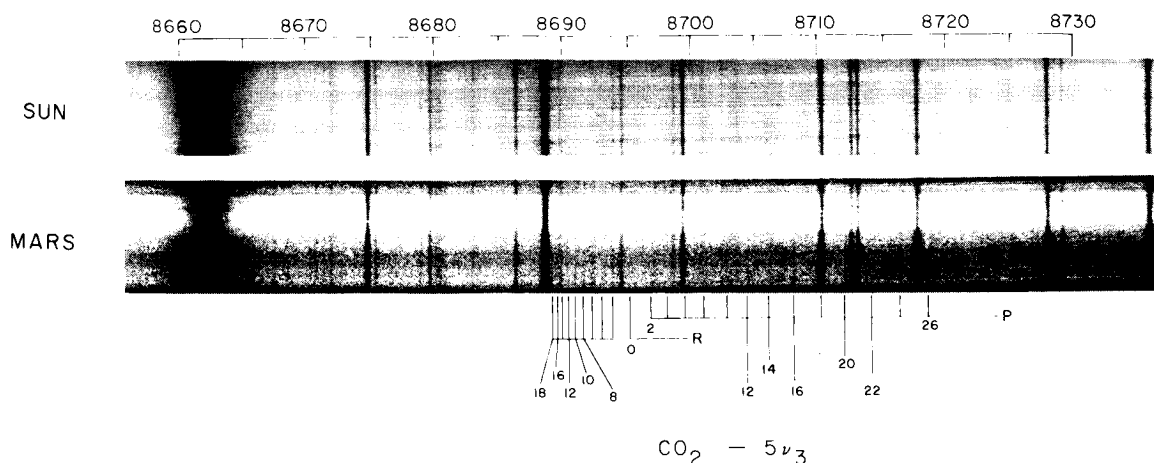


Fig. 29. The  $5 \nu_3$  absorption band of  $\text{CO}_2$  in the spectrum of Mars and the solar spectrum in the same region and at the same resolving power

#### A. Determination of Temperature

The first step is a determination of the mean atmospheric temperature. A series of intensity profiles for the P branch of the 8689 Å band was constructed, corresponding to different temperatures. The relative intensities of the rotational lines measured in the Martian spectra were compared with these profiles and indicated that a value of 200°K provided the best fit. The scatter is quite large, however, leading to an uncertainty on the order of  $\pm 50^\circ\text{K}$ . Additional support for this result may be obtained from an argument based on the assumption of a dry adiabatic lapse rate from the surface, but this method also involves uncertainties (Owen, 1964).

#### B. Correction of Line Intensities

After a value has been chosen for the temperature, the integrated intensities for the  $\text{CO}_2$  lines measured by Rank and his collaborators (1964) (8689 Å) and by the writer ( $1.05 \mu$ ) can be corrected to this temperature. This involves a straightforward application of the Boltzmann distribution; the amount of gas corresponding to a given intensity being specified at NTP. However, a recalculation of the predicted average intensity of the  $J = 8, 10$ , and 12 lines in the R branch of the 8986 Å band has led to a slightly different value from that quoted by Kaplan, Münch, and Spinrad (1964), viz.,  $0.032 \text{ cm}^{-1}/\text{km-atm}$  instead of  $0.030 \text{ cm}^{-1}/\text{km-atm}$ . This calculation was prompted by the apparent disagreement between the band intensity quoted by Kaplan et al. and that published by Rank et al. The intensities determined for the  $1.05 \mu$  band are preliminary, since the available data are not of the highest quality and include only the P branch lines.

#### C. Determination of Air Mass

Because the various plates were scanned in different sections of the spectrum, a uniform air mass could not be used. Values ranging from 2.4 to 4.0 were employed; the uncertainty probably lies in the range of  $\pm 5\text{--}10\%$ .

### III. The Abundance of $\text{CO}_2$

A summary of present results is given below, along with a discussion of the possibility of a systematic error.

#### A. Summary of Present Results

Knowing the intensities, the equivalent widths, and the air mass values, one can solve for the abundance of  $\text{CO}_2$ . The weak line approximation furnishes the necessary relation:

$$w = \frac{W}{\eta S} \quad (1)$$

where  $W$  is the equivalent width,  $\eta$  the effective air mass,  $S$  the line intensity, and  $w$  the amount of  $\text{CO}_2$ . However, the pressure on Mars is so low that it appears there will be some saturation of these lines. This possibility can be examined by means of the theoretical description of the doppler profile as elaborated by Ladenburg (1930). A straightforward comparison of the doppler and pressure-broadened half-widths indicates that at pressures on the order of 10 mb ( $1/2$  the maximum likely surface pressure), the doppler half-width is an order of magnitude greater than the pressure-broadened width. Thus only the doppler correction was made.

Subject to the constraints given above, abundances were calculated for the R branch lines on all the plates and for the P branch lines on the plates that clearly showed them. Weights were assigned to these abundances on the basis of the quality of the plates and the number of tracings made. The previous calibration of the Mount Wilson spectrum obtained by Kaplan et al. was included in this list with a low weight. This work is still in progress and thus the abundances and their relative weights are subject to change.

At this writing, the weighted mean of these results is 56 m-atm; the mean error is  $\pm 11$ . The total probable error was computed as the square root of the sum of the squares of the errors in the equivalent width, air mass, and line intensities. This comes out to be  $\pm 10$  m-atm. Thus, in round numbers, the preliminary value for the CO<sub>2</sub> abundance based on the McDonald plates may be expressed in meter atmospheres as  $55 \pm 10$  (pe) for an assumed mean temperature in the Martian atmosphere of 200°K. Implicit in this determination is the assumption that the lines returning from the R branch band head do not overlap the R8, 10, 12 lines. If overlapping occurs, the value of the abundance must be decreased by a maximum of about 4% (there is obviously no effect on the value obtained from the P branch lines).

To appreciate the effect of the various parameters on this calculation, it should be noted that the use of an atmospheric temperature of 225°K and the average intensity of the R branch lines given by Kaplan et al. for this temperature would lead to an abundance of 63 m-atm.

## B. Systematic Error

Because the absorptions that are measured are so weak, the possibility of a significant systematic error arises. In an attempt to evaluate this, a spectrum of CO<sub>2</sub> obtained in the laboratory with an absorption cell illuminated by sunlight was reduced in an identical manner to the Mars spectra. The same solar lines were used as standards in each case for the calibration of the equivalent widths. The total amount of gas in the absorbing path was 354 m-atm (NTP). From a reduction of the R branch lines, an amount of 320 m-atm was obtained; from the P branch, 326 m-atm. The significance of this result is twofold. First, it suggests that if there is a systematic error, it is on the order of -10% (with only one plate measured thus far, it is obviously premature to assess the reality of such a small deviation compared with the random uncertainty of  $\pm 20$  %). Second, using the maximum air mass employed in reducing the Mars observations

( $\eta = 4$ ), the corresponding values of the CO<sub>2</sub> abundance reduced to a unit column would be 81 m-atm (observed) and 89 m-atm (true). None of the new reductions of the Martian spectra led to values of the CO<sub>2</sub> abundance that were this high, suggesting that a value of 85-90 m-atm must be close to an absolute upper limit.

## IV. Determination of Surface Pressure

In order to obtain a value for the surface pressure of the Martian atmosphere, it is necessary to use observations of the strong bands of CO<sub>2</sub> for which the absorption is a function of pressure. Two sets of such bands have been observed in the Martian spectrum: at 1.6  $\mu$  and 2.06  $\mu$ . In this discussion, we will first consider the treatment of both sets of bands that has been carried out by Moroz (1964). This will be followed by a more detailed treatment of new observations of the 1.6  $\mu$  bands made by Kuiper following the method of Owen and Kuiper (1964).

### A. The Method of Moroz

Moroz observed both the 1.6  $\mu$  and 2.06  $\mu$  bands in the spectrum of Mars. He reduced these observations by means of an Elsasser band model calibrated by means of the telluric CO<sub>2</sub> bands observed in the solar spectrum. From this analysis, he derived the following relation for the surface pressure  $p$  and the CO<sub>2</sub> abundance  $\eta w$ :

$$\eta w p = 175 \quad (2)$$

in which  $p$  is in millibars and  $\eta w$  is in g/cm<sup>2</sup>. Using the value of the CO<sub>2</sub> abundance derived by Kaplan et al. (1964), Moroz found  $p = 15^{+15}_{-5}$  mb. However, in reviewing Moroz' method, we found several minor errors; this finding suggested that a better value for the pressure (with a CO<sub>2</sub> abundance of 45 m-atm) would be  $p = 13$  mb. If the value of the abundance derived in this paper is used in this revised relation, one obtains  $p = 11$  mb. The relative uncertainties are at least as high as for the original value.

An interesting aspect of Moroz' work is that he derived an expression for the volume concentration of CO<sub>2</sub>:

$$\alpha = (40 \pm 10)/p^2 \quad (3)$$

When this relation is corrected in the same manner as that for  $\eta w p$ , one obtains

$$\alpha = (35 \pm 10)/p^2 \quad (4)$$



By setting  $\alpha = 1.0$ , we can establish a useful lower limit on the surface pressure as well as an upper limit on the  $\text{CO}_2$  abundance. These are  $6 \pm 1$  mb and  $80 \pm 15$  m-atm, respectively. In other words, if only the strong line data are used and we assume that the atmosphere is composed entirely of  $\text{CO}_2$ , the strength of the strong band absorptions requires a surface pressure of  $6 \pm 1$  mb and the corresponding amount of  $\text{CO}_2$  is  $80 \pm 15$  m-atm.

## B. The Method of Owen and Kuiper

Owen and Kuiper (1964) based their determination of the Martian surface pressure exclusively on the strong bands at  $1.6 \mu$ . The observations of the  $1.6 \mu$  bands were obtained by Kuiper when the planet was near quadrature, in order to maximize the wavelength shift of the Martian absorptions due to the doppler effect. This is an important point, since  $\text{CO}_2$  in the Earth's atmosphere absorbs strongly at these wavelengths. However, the doppler shift at the time of observation was sufficiently great to separate the Martian and telluric components, permitting the subtraction of the telluric absorption by means of observations of the Moon at a similar air mass. One can therefore obtain a value for the equivalent width of the Martian bands. Dr. Kuiper (private communication) repeated these observations at the last opposition and found a slightly higher value for the equivalent width ( $16.2 \text{ \AA}$  vs  $15.8 \text{ \AA}$ ). We will use the new value in this discussion.

The basic method of analysis is that described by Owen and Kuiper (1964). We confine our attention to Figs. 15, 16, and 17 of that reference. It is only necessary to raise the line corresponding to the Martian equivalent width in these diagrams (in view of the new value of this quantity) to make them suitable for this discussion. Upper and lower limits were estimated from the intercept of the line representing the Martian equivalent width with the laboratory data. These limits are then compared with calculated values for the surface pressure of the appropriate column of gas. In the present case, these numbers are based on the abundance of 56 m-atm presented in Sec. III. One then obtains a revision of Table 4 in Owen and Kuiper (1964) corresponding to the new values for the calculated and empirically derived measures. Making the customary assumption that the pressures deduced from the absorption measurements are equal to one-half the surface pressure (the Curtis-Godson approximation) one finds a best fit for a surface pressure of 13 mb.

If one assumes a simple proportionality between the equivalent widths of the strong  $\text{CO}_2$  absorptions in

the spectrum of Mars and the telluric spectra, one obtains the relation

$$P_M = \frac{\eta_E P_E w_E W_E^{-1/n_E}}{\eta_M w_M W_M^{-1/n_M}} \quad (5)$$

where the subscripts  $E$  and  $M$  refer to the Earth and Mars, respectively, and the other symbols have their usual meanings. Using the new values for  $W_M$  and  $w_M$  and taking the other numerical data from Owen and Kuiper (1964), we find  $P_M = 12$  mb after correcting for the difference in the relative dilution of  $\text{N}_2$  in the two atmospheres.

Finally, a lower limit on the surface pressure may be derived for comparison with that of Moroz on the assumption of a pure  $\text{CO}_2$  atmosphere. This is obtained by finding the amount of gas that would produce a surface pressure on Mars exactly equal to twice the pressure required to match the strength of the Martian  $1.6 \mu$  bands when that same amount of gas is observed in the absorption tube. The result is  $6.5 \pm 1$  mb, and the corresponding amount of  $\text{CO}_2$  is  $85 \pm 15$  mb, in good agreement with Moroz.

## V. Conclusions

It is worthwhile to stress again that the numbers given in this report are preliminary and may change slightly as additional work is carried out on the raw data. At present, the best value for the abundance of  $\text{CO}_2$  in the atmosphere of Mars obtained from the data analyzed in this report appears to be  $55 \pm 10$  m-atm (pe). This result is derived from measurements of the weak  $\text{CO}_2$  bands at  $8689 \text{ \AA}$  and  $1.05 \mu$  in the Martian spectrum. A possible systematic error would increase this value to 60 m-atm.

This value for the  $\text{CO}_2$  abundance may be used to obtain the surface pressure in one of several ways, all of which rely on observations of the strong, pressure-broadened bands at  $1.6 \mu$  and/or  $2.06 \mu$ . The three methods used in this paper lead to an average value of  $12 \pm 12$  mb. Because this is a preliminary report, undue significance should not be attached to the number 12. To avoid this possibility, it is perhaps more appropriate to consider this analysis as suggesting a Martian surface pressure on the order of 10 mb. A more precise value must await further work on the data.

It has been demonstrated by two independent methods that the strong-line data require a lower limit to the surface pressure in the range 5.5–7.0 mb. This limit corre-

sponds to an atmosphere composed entirely of  $\text{CO}_2$ . The corresponding amount of this gas is then 70–95 m-atm. It seems unlikely that the atmosphere is pure  $\text{CO}_2$ , not only because of the observational evidence presented, but because of the contribution that must be made by radiogenic argon, even if the exospheric temperature were sufficiently high that nitrogen could escape.

With the realization that the Martian atmosphere is so tenuous, we must consider the possibility of relatively large contributions from outside sources in addition to outgassing from the crust. The two most logical sources for such a contribution are impacting meteorites and comets. As an example of this effect, let us consider the impact of a large comet, having a mass of  $10^{19}$  g. If all of this material is volatilized, it would contribute 25 % of the presently observed atmospheric mass. This is clearly an extreme assumption, but suggests that an attempt should be made to derive a quantitative estimate of contributions from such sources. Anders (private communication) has suggested that at least the presently observed amount of water on Mars could have been produced in this way.<sup>1</sup>

### Acknowledgments

The writer is grateful to Dr. Harlan Smith for generously providing time at the McDonald Observatory for the Mars observations and to Dr. G. P. Kuiper for permitting the use of unpublished data. This study is being supported by a grant from the IIT Research Institute.

*Note Added in Proof:* The analysis of the McDonald spectra has been completed and has led to results differing somewhat from those quoted in this preliminary report. The systematic error suspected in the determination of the  $\text{CO}_2$  abundance has been confirmed. With revised values of the line intensities and additional measurements of the equivalent widths, the derived value of the  $\text{CO}_2$  abundance has been increased to  $67 \pm 20$  m-atm. The corresponding surface pressure (using the method of Owen and Kuiper, 1964) lies between 8 and 9 mb with a lower limit of 5 mb and an upper limit of 20 mb. The upper limit of 89–95 m-atm for the  $\text{CO}_2$  abundance has been verified. A consideration of the low surface pressure and high  $\text{CO}_2$  content in the context of the formation and history of planetary atmospheres suggests that the present atmosphere of Mars may be similar in composition to the primitive outgassed atmosphere of the Earth, with the exception of the low Martian abundance of water. If this view is correct, it implies that Mars may never have had a more massive atmosphere than it possesses at the present time.

### REFERENCES

- Delbouille, L., and Roland, G., 1963, *Photometric Atlas of the Solar Spectrum from 7498 Å to 12016 Å*, Liège, Belgium.
- Kaplan, L., Münch, G., and Spinrad, H., 1964, *Astrophys. J.*, Vol. 139, p. 1.
- Ladenburg, R., 1930, *Zs. f. Physik*, Vol. 65, p. 200.
- Marshall, J. V., 1964, *Communications of the Lunar and Planetary Laboratory*, Vol. 2, p. 167.
- Moroz, V. I., 1964, *Astron. Zh.*, Vol. 41, p. 350.
- Owen, T. C., 1964, *Communications of the Lunar and Planetary Laboratory*, Vol. 2, p. 133.
- Owen, T. C., and Kuiper, G. P., 1964, *Communications of the Lunar and Planetary Laboratory*, Vol. 2, p. 113.
- Rank, D. H., Fink, U., Foltz, J. V., and Wiggins, T. A., 1964, *Astrophys. J.*, Vol. 140, p. 366.

## A SEARCH FOR LIMONITE NEAR-INFRARED SPECTRAL FEATURES ON MARS\*

Robert L. Younkin

Jet Propulsion Laboratory  
Pasadena, California

Previous authors have found limonite to be the only mineral whose polarization, color, and albedo duplicate those of the bright areas of Mars in the visual spectral region. Recent measurements of spectral reflectance show that, in the near-infrared, limonite exhibits two characteristics, a wide-band absorption with minimum reflectance in the 8200–9500 Å region, and just beyond this absorption, a rise in reflectance.

Spectrophotometric measurements from 0.5 to 1.1  $\mu$  have been made at the Mount Wilson Observatory of the integral intensity of the disk of Mars, and of a bright area and a dark area. Comparison of the intensities of the two areas gives no indication of any difference in limonite content. The integral intensity has been reduced to relative reflectance by means of the energy distribution of  $\alpha$  Lyr, and independently, it has been compared directly with the intensity of the lunar crater Plato. An upper limit of 2% may be placed on the strength of the limonite features in the reflectance of Mars.

---

\*Abstract of paper.

The complete paper will be published in the May 1966 issue of the *Astrophysical Journal*.

## RECENT RADAR OBSERVATIONS OF MARS

R. B. Dyce

Cornell University  
Arecibo Ionospheric Observatory, Puerto Rico

Results at 430 Mc/sec from the Arecibo Ionospheric Observatory confirm the JPL results at 2388 Mc/sec. Pulse widths of 4 ms and 0.5 ms (approximating a continuous-wave observation) were processed incoherently over short periods of time (2.25 min). Significant short-term fluctuations in amplitude with a scale on the order of 1 deg of longitude were customary. This is signified in Fig. 30 by

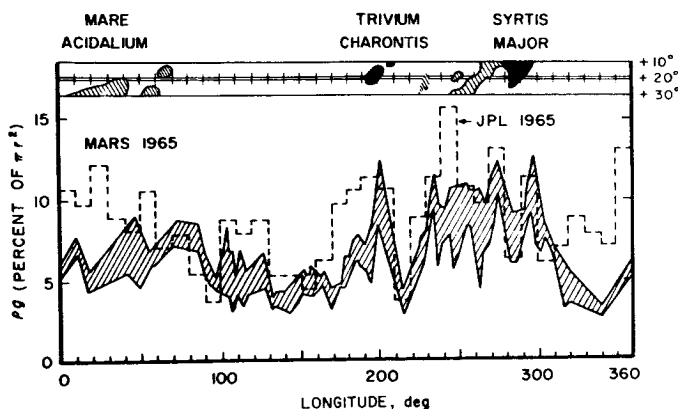


Fig. 30. Radar cross section of Mars as a function of longitude

the shaded region. The cross-section has a mean value similar to that of the Moon but varies between approximately 3 and 12% of the geometrical area. A correlation of echo strength with the position of Trivium Charontis is obvious (see section from optical map at top of figure) but the complexity near Syrtis Major is not so readily related to the observed echo strength.

The 1965 JPL data are shown superimposed as a dotted bar graph. At many longitudes, the two sets of data are in excellent agreement despite a ratio in operating frequencies of 5.5 to 1.

## RADIO AND RADAR EVIDENCE ON THE STRUCTURE AND COMPOSITION OF THE MARTIAN SURFACE\*

*Carl Sagan*

*Harvard University  
and Smithsonian Astrophysical Observatory  
Cambridge, Massachusetts*

*James B. Pollack*

*Smithsonian Astrophysical Observatory  
Cambridge, Massachusetts*

The maximum Martian radar reflectivities of Goldstein and collaborators, as observed at the last two oppositions, are found to be systematically correlated with the Martian dark areas in three respects: the position of maximum reflectivity, the relative reflectivity ranking, and the width of the feature. It is unlikely that effects of roughness play a major role in determining reflectivity differences on the Martian disk, and the observed reflectivities can most probably be correlated with dielectric constants. Derived characteristic dielectric constants for bright areas uncontaminated with dark nuclei are  $\leq 1.8$ ; for a typical bright area, 2.0; for a typical dark area, 2.8; and for a typical dark nucleus of the dark areas, about 4. These dielectric constants are consistent with a wide range of inorganic materials, provided that they are pulverized or in highly porous form to a depth of at least some meters. If a typical Martian bright area is composed principally of limonite, its porosity must be some 78%. The corresponding value for a dark nucleus is 50%. These porosities are typical of naturally occurring terrestrial limonite powders. There is no evidence against the presence of fair amounts of organic materials in the dark nuclei, but pulverized or porous inorganic materials are also probably present.

---

\*Abstract of presentation.

The disk-integrated thermometric temperature of the Martian surface, as deduced from passive microwave observations, appears to be significantly lower than the corresponding infrared surface temperature of the same area and projection of the planet. The radio observations refer to depths at which the thermal wave due to the diurnally varying insolation at the surface is significantly damped. It follows that  $\gamma \gg 1$ , where  $\gamma$  is the ratio of the electromagnetic to the thermal skin depth, and that the microwave temperatures are therefore a measure of temperature averaged over day and night—and to some extent, over the seasons as well. Large values of  $\gamma$  at the wavelengths of observation are expected for limonite and for many other materials. Within the range of observational error, the surface temperatures deduced from microwave observations, the surface temperatures deduced from infrared observations, and the surface temperatures deduced from recent estimates of the bolometric albedo of Mars are in acceptable concordance.

## PRELIMINARY RESULTS OF THE MARINER IV OCCULTATION MEASUREMENT OF THE ATMOSPHERE OF MARS

A. J. Kliore, D. L. Cain, and G. S. Levy

Jet Propulsion Laboratory  
Pasadena, California

V. R. Eshleman and G. Fjeldbo

Stanford University  
Stanford, California

F. D. Drake

Cornell University  
Ithaca, New York

### I. Introduction

This paper is intended as a review of the preliminary results of the radio occultation measurement of the atmosphere of Mars that was carried out as the *Mariner IV* spacecraft passed behind the planet on July 15, 1965. Most of these results are abstracted from previous publications (Ref. 1).

From the very precise data that were acquired in the course of the experiment, preliminary analysis has produced several unexpected results. Among these the following points summarize the findings.

1. The values of density, pressure, scale height, and temperature near the surface of Mars have been found to be lower than expected.

2. Based on the occultation results, as well as terrestrial spectroscopic measurements of CO<sub>2</sub> abundance in the atmosphere of Mars, it is concluded that carbon dioxide must be the primary constituent.

### II. Experiment

The *Mariner IV* Occultation Experiment (Ref. 2) has been carried out by investigators from the Jet Propulsion Laboratory, Stanford University, and Cornell University. Previous knowledge of such atmospheric properties as the surface pressure and density, as well as scale height, has been quite poorly defined. The surface pressure, as deduced from recent spectroscopic observations of weak and strong CO<sub>2</sub> absorption bands, was thought to lie



somewhere between 10 and 40 mb (Refs. 3, 4). The vertical structure of the atmosphere has not previously been accessible to direct Earth-based measurement, and could only be estimated by assuming atmospheric constituents and temperatures.

The results of the *Mariner IV* occultation experiment, when fully analyzed, will provide an improved definition of the surface density and pressure, as well as the vertical structure of the atmosphere and the electron density profile of the ionosphere of Mars. However, even a rather superficial analysis performed in the time since acquisition of the data on July 15 has yielded significant results.

As the spacecraft approached the limb of the planet, the presence of an atmosphere and ionosphere caused the velocity of propagation of the radio signal to deviate from that in free space because of the non-unity index of refraction of the neutral and ionized media. Also, the radial gradient of the effective index of refraction caused the radio beam to be refracted from a straight line path. Both of these effects caused the phase path length of the propagation to differ from what would have been observed in the absence of an atmosphere and ionosphere. Thus, since the geometry, obtained from the estimated trajectory, is known, the measured deviation in phase can be used to estimate the spatial characteristics of the index of refraction (or refractivity) in the atmosphere and ionosphere by a process of integral inversion or by model fitting (Refs. 5-7).

The analysis of doppler tracking data taken before and after planetary encounter yields the trajectory of the spacecraft at the time of occultation with such precision that the range rate of the spacecraft is known to an accuracy of 0.0015 m/sec. Thus any significant deviation of the received doppler data from orbit determination predictions can be expected to be caused by atmospheric and ionospheric phase-path effects.

It must be pointed out that the phase changes due to the atmosphere amount to about 30 cycles (wavelengths), and those due to the ionosphere about 10 cycles. These changes are obtained by subtracting from the total radio frequency phase change of about  $3 \times 10^{11}$  cycles during the time period of the experiment all the predictable phase-shift caused by the motion of the spacecraft, motion of the stations on the Earth, reference phase changes, light-transit time effects, the effects of the Earth's troposphere, and others. Thus it is implied that the total phase change due to all causes other than the

atmosphere and ionosphere of Mars must be known to an accuracy of less than 1 part in  $10^{11}$ .

Before discussing the data obtained in this manner, the geometry of occultation for both entry and exit will be described. At entry into occultation, the spacecraft was at a distance of 25,570 km from the limb of Mars, traveling at a velocity of 2.07 km/sec normal to the Earth-Mars line. The point of tangency on the surface of Mars was at a latitude of  $50.5^\circ$  South and a longitude of  $177^\circ$  East, corresponding to a point between Electris and Mare Chronium. At the time of exit from occultation, the distance from the limb of Mars had increased to 39,150 km, and the point of tangency was located at about  $60^\circ$  North latitude and  $34^\circ$  West longitude, falling within Mare Acidalius.

### III. Data

Doppler and amplitude data were taken both during entry and exit by the NASA/JPL Deep Space Instrumentation Facilities (DSIF) at Goldstone, California, and Tidbinbilla and Woomera in Australia. The Goldstone stations (Echo and Pioneer) took standard tracking data doppler (closed-loop) as well as open-loop records (described elsewhere in this report) of the received signal. The Australian stations took only doppler data. At entry all data were taken while the spacecraft transmitter frequency reference was provided by a frequency standard on the Earth. At exit, a 9-sec portion of the data was received while the spacecraft transmitter frequency reference was provided by an on-board crystal oscillator. In the latter mode, the precision of phase measurements is significantly degraded.

Figure 31 shows the range rate doppler residuals (observed minus predicted phase change in 1 sec) based on data received at the various DSIF stations at entry. The points marked O/L have been obtained from the open-loop records by means of spectral density analysis, and the other points are derived directly from data processed through the JPL orbit determination program. One may observe that the data from the various sources show a high degree of consistency, except for the doppler points at  $02^h31^m11^s.5$ , which are suspect because the time of loss of signal is estimated to be between  $02^h31^m11^s.2$  and  $02^h31^m11^s.6$  GMT.

A different presentation is shown in Fig. 32, which represents the total phase change as a function of time, derived from Station 11 (Goldstone-Pioneer) doppler residuals. The maximum effect of the ionosphere appears

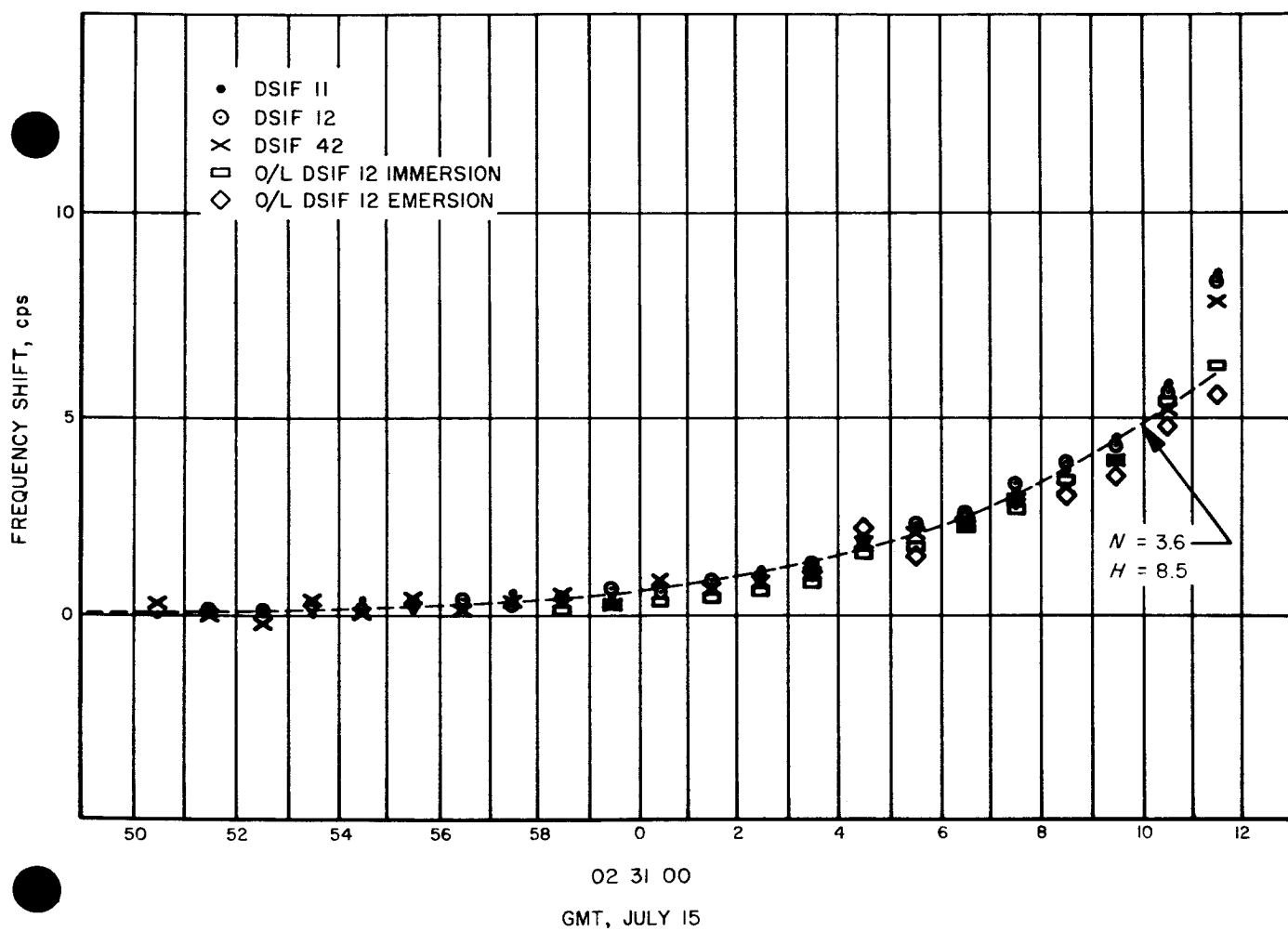


Fig. 31. Range-rate doppler residuals from all DSIF stations

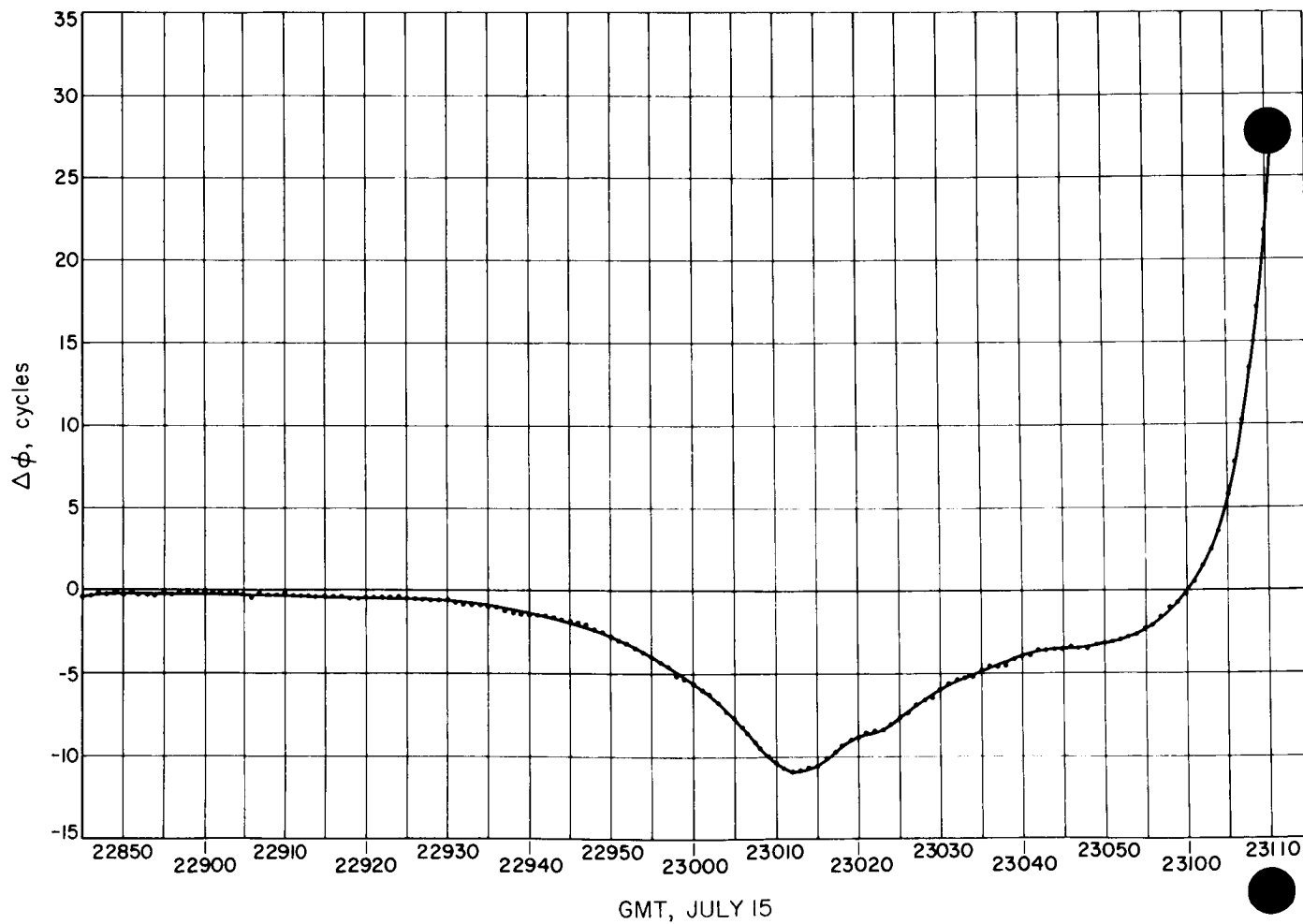


Fig. 32. Phase change at DSIF Station 11

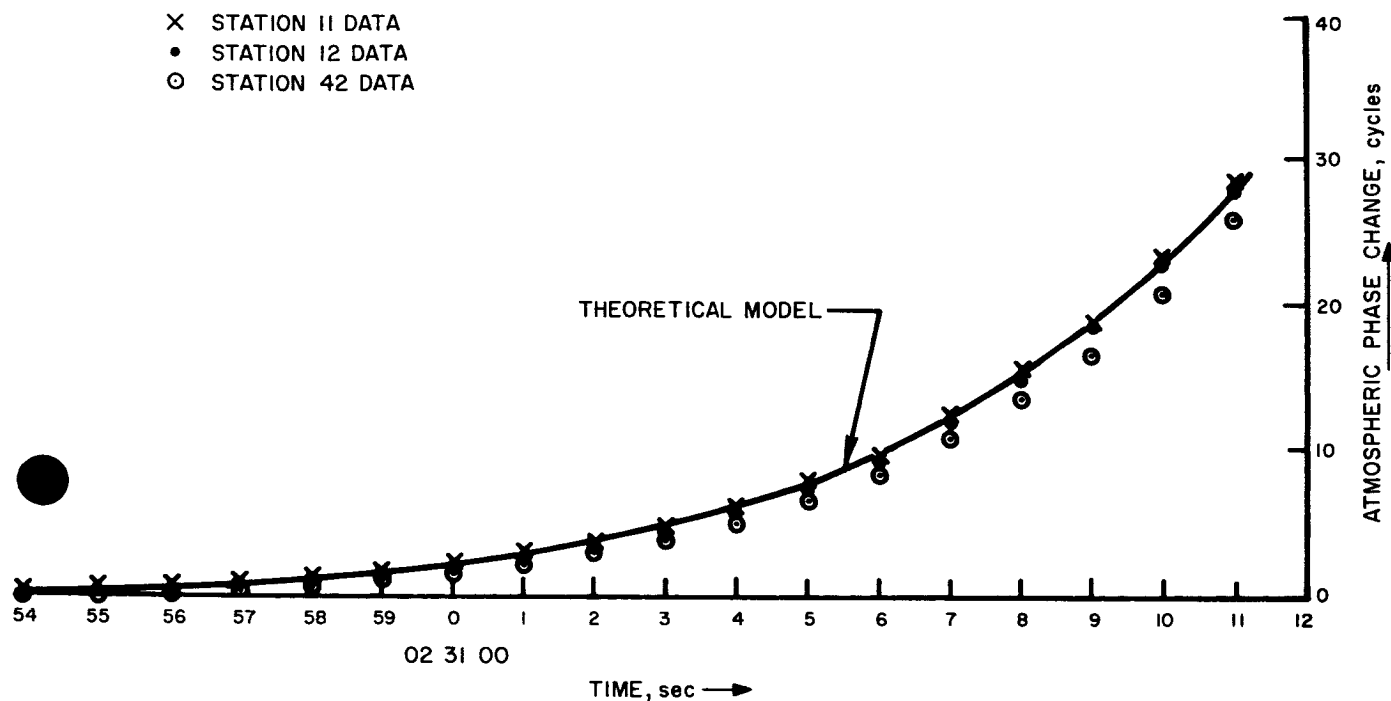


Fig. 33. Phase change due only to atmosphere

at about 02<sup>h</sup>30<sup>m</sup>10<sup>s</sup>, and the final upswing beginning at about 02<sup>h</sup>30<sup>m</sup>50<sup>s</sup> is caused by the neutral atmosphere. It is interesting to note the extreme smoothness of data suggested by the low scatter of the data points.

An expanded portion of the phase change plot is shown in Fig. 33. This graph relates only to the neutral atmosphere, as the estimated effects of the ionosphere have been removed. Signal extinction time is assumed as 02<sup>h</sup>31<sup>m</sup>11<sup>s</sup>2 GMT.

#### IV. Atmosphere

The solid curve in Fig. 33 represents the computed phase change for a theoretical exponential model atmosphere having a surface refractivity of 3.7 N-units and a scale height of 9 km. It is obvious that even with this relatively crude model the fit is excellent. The dotted line in Fig. 31 represents the computed doppler residuals for a similar model atmosphere, having a scale height of 8.5 km and  $N = 3.6$ . As in the case of the phase change, the fit of the data appears to be quite good.

Figure 34, due to G. Fjeldbo of Stanford University, relates maximum phase change, maximum frequency change (doppler), and refractive gain (at the time of extinction of signal of 02<sup>h</sup>31<sup>m</sup>11<sup>s</sup>2) to the surface refractivity

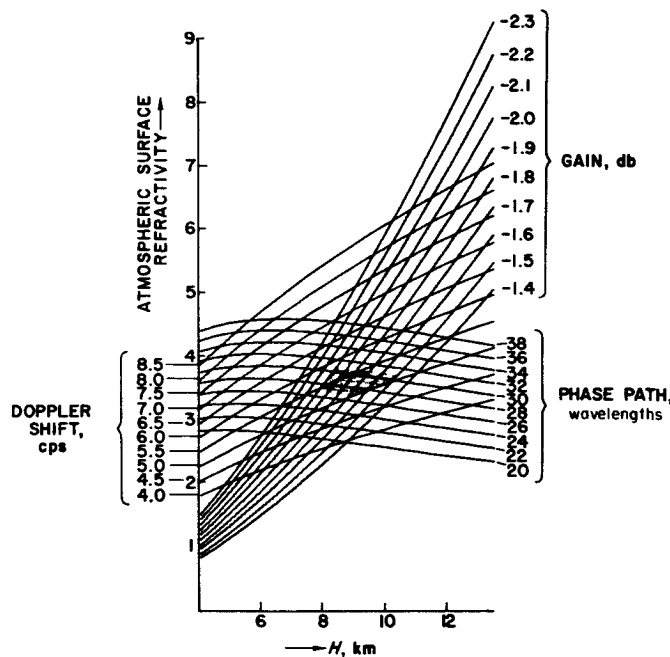


Fig. 34. Maximum changes in doppler shift, phase, and amplitude as functions of surface refractivity and scale height

and scale height of the atmosphere, using an exponential profile of refractivity. Suggested values of  $5.5 \pm 0.5$  cps,  $29 \pm 2$  cycles, and 1.5 to 2.0 db lead to the stippled area

in the figure. This area corresponds to a surface refractivity of  $3.6 \pm 0.2$  N-units and a scale height of  $9 \pm 1$  km. The gain figure is least reliable, but it can be seen that better values to be obtained from detailed analysis of data from all the stations should help considerably in reducing uncertainty.

A cursory study of the amplitude recordings leads us to believe that signal dropout was due to a diffracting edge, establishing the very important fact that the final ray paths grazed a surface feature on Mars. All references to surface conditions in this paper refer to the altitude of this surface feature. We do not know, of course, its altitude relative to the mean surface of Mars, but the geometry of the experiment would make it likely that it was higher than the mean surface. The refractivity would change by approximately 1% for each 90 m of elevation of the limiting surface feature above the mean surface spheroid of Mars.

In essence then, a simple refractivity model of the Martian atmosphere has been established. It now remains to infer density and pressure, thus bringing into focus the question of composition and temperature.

Figure 35 shows the relationship between refractivity and mass density as a function of composition, ranging

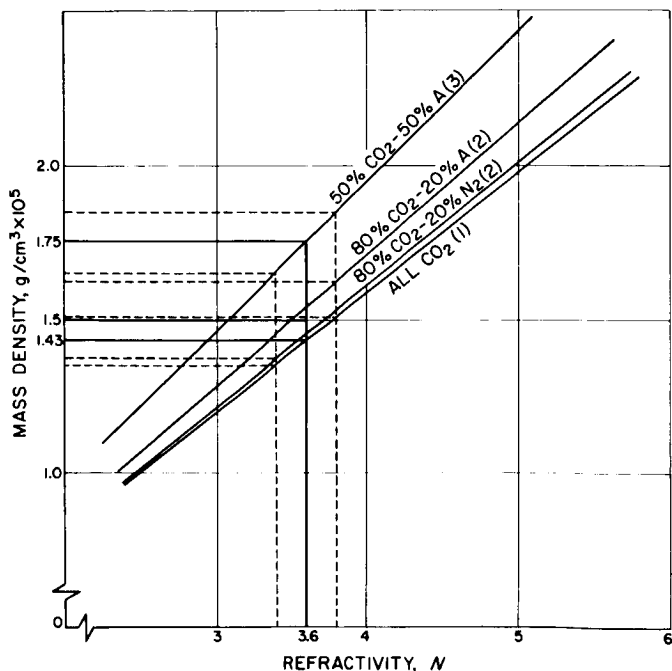


Fig. 35. Mass density vs refractivity for various atmospheric compositions

from pure CO<sub>2</sub> to 50% CO<sub>2</sub> and 50% argon. To be consistent with the value of scale height determined in this analysis and with the estimated surface temperatures existing at the latitude in question, the composition of the atmosphere must be considered to be predominantly CO<sub>2</sub>, with possibly up to 20% argon and small amounts of other gases. This finding is also consistent with the spectroscopically observed CO<sub>2</sub> abundance on Mars.

Two composition models are considered here: (1) pure CO<sub>2</sub> and (2) 80% CO<sub>2</sub> and 20% argon.

For the atmosphere composed of pure CO<sub>2</sub> (model 1) the total number density at the surface corresponding to the measured refractivity values stated above was found to be about  $1.9 \pm 0.1 \times 10^{17}$  molecules/cm<sup>3</sup>. The mass density (see Fig. 35) is then about  $1.43 \pm 0.10 \times 10^{-5}$  g/cm<sup>3</sup>. From the measured value of scale height, the temperature range would have to be about  $180 \pm 20^\circ\text{K}$ , leading to a surface pressure range of 4.1 to 5.7 mb.

For the atmosphere consisting of 80% CO<sub>2</sub> and 20% argon (model 2), the various properties are as follows: number density =  $2.1 \pm 0.10 \times 10^{17}$  molecules/cm<sup>3</sup>; mass density =  $1.55 \pm 0.1 \times 10^{-5}$  g/cm<sup>3</sup>; temperature =  $175 \pm 20^\circ\text{K}$ ; and surface pressure = 4.4 to 6.0 mb.

The number densities derived for these models correspond to from 0.7 to 1.0% of the molecular number density of the Earth's atmosphere at the surface. Since the scale height in the Martian atmosphere is almost equal to that of the Earth, the total number of molecules above a unit area on the surface of Mars is on the order of 1% of that on the Earth.

In addition to the analysis described above, a least-squares fit to the tracking data is being carried out, using a digital computer program due to D. L. Cain, which computes refractive effects in the tracking signal, starting with the orbits of the Earth, Mars, and the spacecraft, and then compares these effects with observations.

Results of a preliminary 5-parameter fit, fitting two atmospheric parameters (surface refractivity and scale height) and three parameters of a single Chapman-layer ionosphere, indicate a surface refractivity of about 3.88 and a scale height of 9.4 km.

The higher value of surface refractivity obtained in this manner could possibly be explained by the circumstance that the exact paths of the up-link and down-link

signals are computed in the program, whereas in the previously described determination these paths were assumed to coincide.

## V. Instrumentation

The results described in previous sections have been derived from frequency, phase, and amplitude measurements at the DSIF receiving stations during the occultation experiment. To better understand these measurements, it will be helpful to have a brief description of the DSIF radio system, including the special modifications for the experiment. The block diagram of the system is illustrated in Fig. 36.

The ground station uses a rubidium standard to drive a frequency synthesizer. Its output is then modulated, multiplied 96 times in frequency, amplified, and transmitted to the spacecraft at 2.1 Gc/sec. When the spacecraft receiver is in lock with the ground-station signal, the down-link frequency is derived from the receiver's voltage-controlled oscillator (VCO), which is phase-locked to the received up-link signal. When no up-link

is received, however, the down-link frequency is derived from a free-running crystal oscillator in the spacecraft. The RF signal is amplified and transmitted from a high-gain spacecraft antenna.

The ground transmitter and receiver system employs an 85-ft parabolic antenna with a Cassegrainian simultaneous-lobing feed. A traveling-wave maser cooled by a closed-cycle helium refrigerator operating at 4.2°K is used for the receiver front end. After amplification by the maser, the signal is split into two separate receiver channels. The first channel consists of a triple-conversion phase-locked receiver. It is operated in the standard DSIF receiver configuration. This receiver's VCO is kept in phase synchronism with the received signal. By a series of frequency multiplications, divisions, and additions, the transmitter exciter frequency is coherently compared with the receiver VCO to obtain the two-way doppler frequency. The receiver automatic gain control (AGC), which is a received-signal power-level tracking servo, is used to determine received power level. Appropriate AGC voltages were recorded on magnetic tape, and the doppler count was digitized. This system yielded

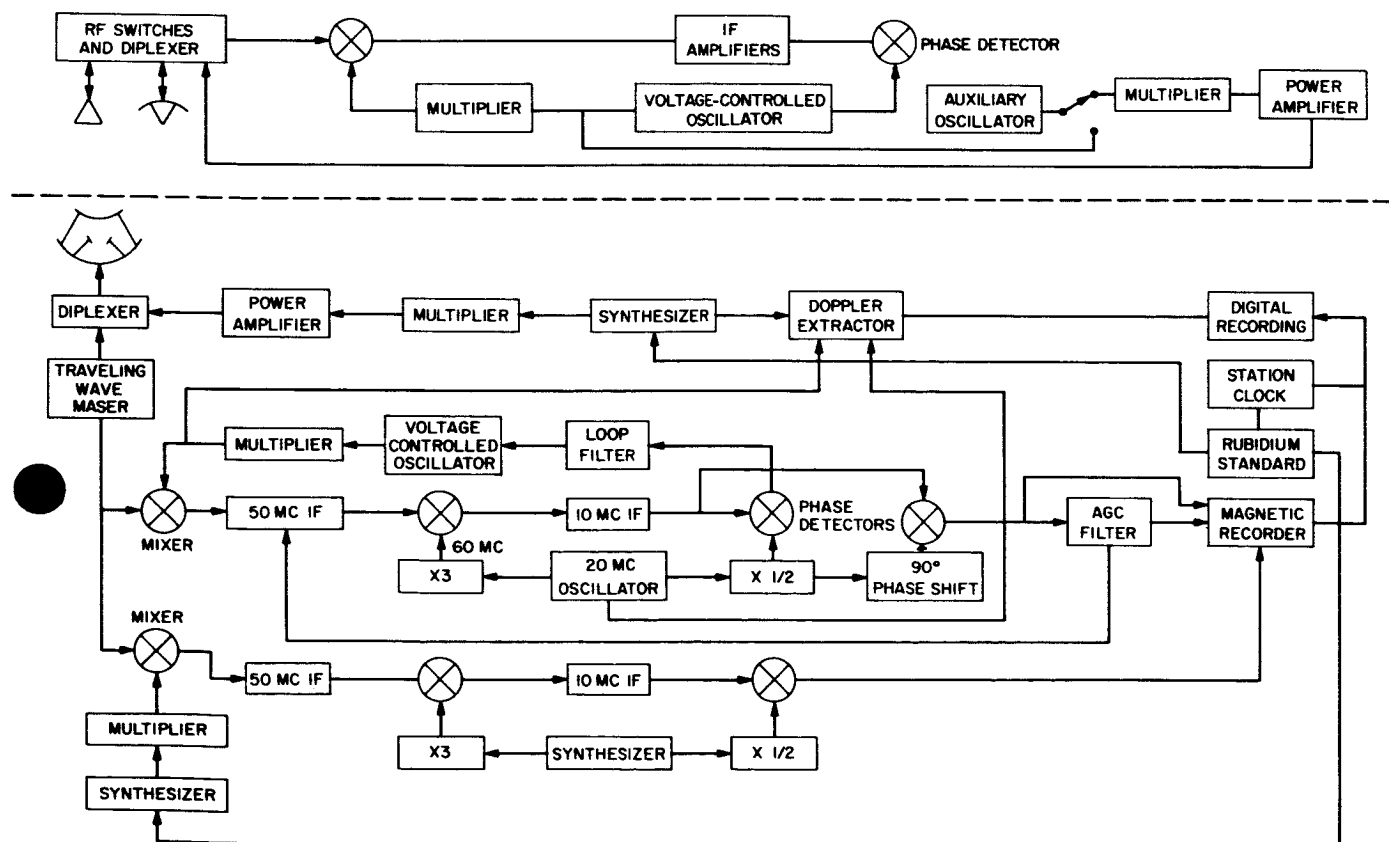


Fig. 36. DSIF instrumentation for the occultation experiment

frequency information in real time. This channel is also used as the sum channel of the pointing system for the simultaneous-lobing antenna.

The second receiver channel, as modified by G. S. Levy, is a manually tuned, constant-gain, triple-conversion superheterodyne operated in a nonstandard configuration. It amplifies and frequency-translates the down-link

signal to the audio-frequency region of the spectrum and then records it on magnetic tape. The local-oscillator (LO) signals for this receiver were derived from the rubidium frequency standard, which drives a pair of synthesizers. The first LO frequency was periodically stepped to keep the signal in the receiver's passband. The second and third LO's were derived from the second synthesizer operating at 19.996 Mc/sec. The output of

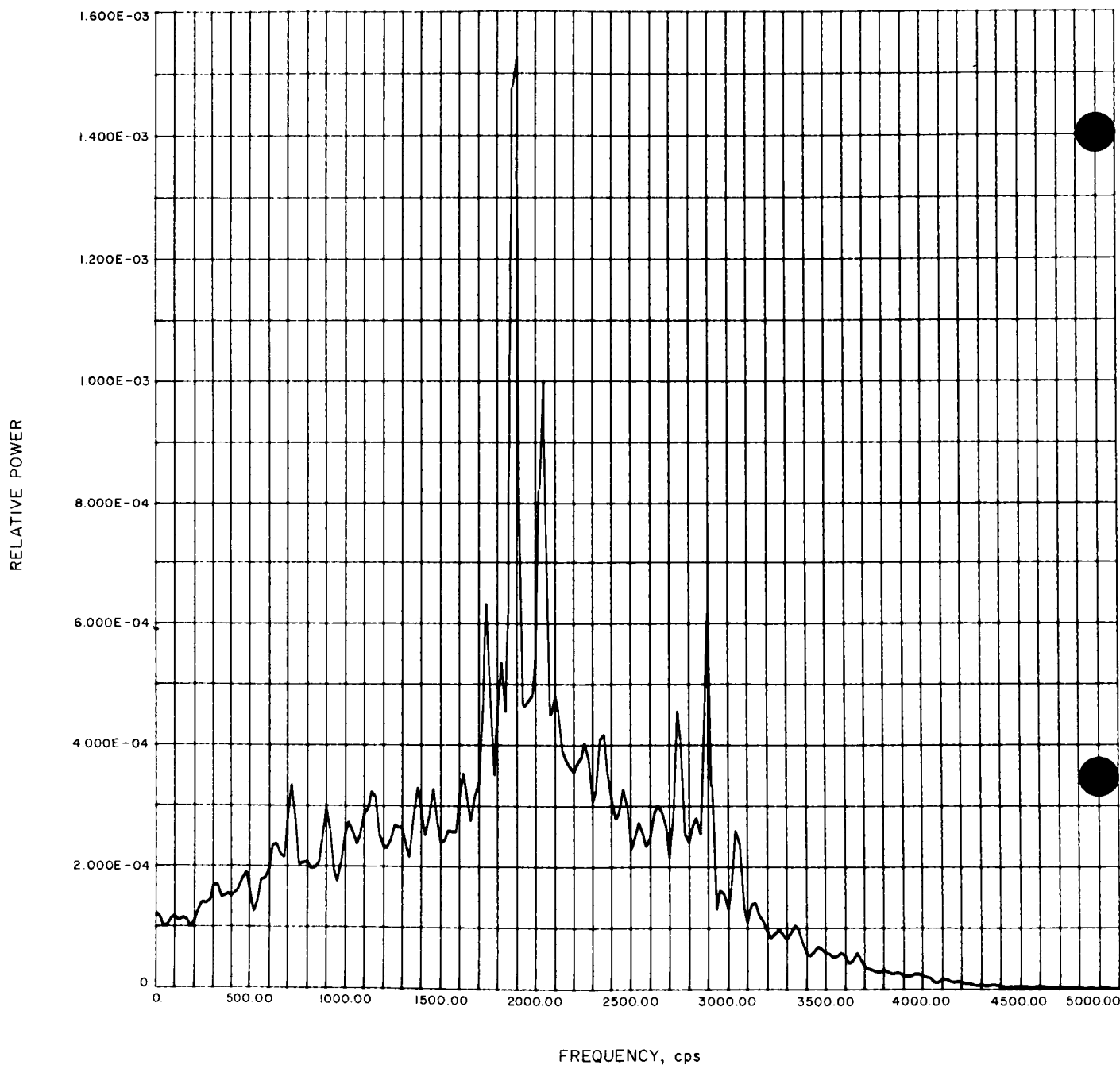


Fig. 37. Power spectrum of signal at the time of switching from one-way to two-way frequency

the third mixer had a passband of 1–3 kc/sec, which was recorded on magnetic tape. Since the LO frequencies were derived from the rubidium standard, the frequency integrity of the doppler was maintained. The analog information on the magnetic tape was digitized after the mission for use in a digital computer.

Figure 37 is a power spectrum of the audio open-loop signal made from the digitized tape on an IBM 7094 computer. The time interval from 03:25:16 to 03:25:17 was chosen. During this second, the one-way frequency, which was first observed as the vehicle reappeared at 03:25:08, was switched off. (This signal component can be seen at 2900 cps.) After the one-way signal decayed, the two-way signal was recorded at an audio frequency of 1900 cps. The phase modulation sidebands at  $\pm 150$  cps can be seen on both signals.

## VI. Conclusions

In conclusion, the results of the preliminary analysis of occultation atmospheric data are summarized in Table 9.

It should be pointed out again that these numbers are the results of less than one month's analysis using relatively crude techniques. As the analysis proceeds, the results will be refined, taking into account additional data as well as more sophisticated theoretical investigations of the physical characteristics of the atmosphere.

## Acknowledgment

The authors wish to thank the *Mariner* Project and Deep Space Net personnel of JPL for their excellent per-

Table 9. Preliminary analysis of occultation data

Property	Value
Surface refractivity, N-units	$3.6 \pm 0.2$
Scale height, km	8–10
Surface number density, mol/cm <sup>3</sup>	
All CO <sub>2</sub>	$1.9 \pm 0.1 \times 10^{17}$
20% argon	$2.1 \pm 0.10 \times 10^{17}$
Surface mass density, g/cm <sup>3</sup>	
All CO <sub>2</sub>	$1.43 \pm 0.1 \times 10^{-5}$
20% argon	$1.55 \pm 0.10 \times 10^{-5}$
Temperature, °K	
All CO <sub>2</sub>	$180 \pm 20$
20% argon	$175 \pm 20$
Surface pressure, mb	
All CO <sub>2</sub>	4.1–5.7
20% argon	4.4–6.0

formance in the preparation for the experiment and the acquisition of data. Special gratitude is due P. K. Eckman and T. W. Hamilton of JPL and B. B. Lusiguan of Stanford University for their many contributions to the success of the experiment.

This paper presents the results of one phase of research carried out at the Jet Propulsion Laboratory, California Institute of Technology, sponsored by the National Aeronautics and Space Administration under Contract No. NAS 7-100, and at Stanford University under National Aeronautics and Space Administration Contracts NSG-377 and NGR 05-020-65.

## REFERENCES

1. Kliore, A. J., Cain, D. L., Levy, G. S., Eshleman, V. R., Fjeldbo, G., and Drake, F. D., 1965, *Science*, Vol. 149, p. 1243.
2. Kliore, A. J., Cain, D. L., Levy, G. S., Eshleman, V. R., Drake, F. D., and Fjeldbo, G., 1965, *Astronautics & Aeronautics*, Vol. 7, p. 72.
3. Kaplan, L. D., Münch, G., and Spinrad, H., 1964, *Astrophys. J.*, Vol. 139.
4. Kuiper, G. P., 1964, *Communications of the Lunar and Planetary Laboratory*, University of Arizona, Vol. 2.



## REFERENCES (Cont'd)

5. Kliore, A., Cain, D. L., and Hamilton, T. W., 1964, *Technical Report No. 32-674*, Jet Propulsion Laboratory, Pasadena, California.
6. Fjeldbo, G., 1964, *Final Report NSF G 21543, SU-SEL-64-025*, Stanford University.
7. Fjeldbo, G., and Eshleman, V. R., 1965, *J. Geophys. Res.*, Vol. 70, p. 13.

## PRELIMINARY RESULTS OF THE MARINER IV RADIO OCCULTATION MEASUREMENTS OF THE UPPER ATMOSPHERE OF MARS\*

G. Fjeldbo and V. R. Eshleman

Stanford University  
Stanford, California

A. J. Kliore, D. L. Cain, and G. S. Levy

Jet Propulsion Laboratory  
Pasadena, California

F. D. Drake

Cornell University  
Ithaca, New York

The radio occultation experiment conducted with the tracking and telemetry system of the *Mariner IV* spacecraft has provided new and precise information on the physical properties of the Martian atmosphere (Ref. 1).

The purpose of this paper is mainly to discuss that part of the occultation data analysis that is related to the upper atmosphere of Mars. This portion of the study is important because:

1. It helps us form a more complete picture of how the Martian atmosphere changes with the altitude (that is, the temperature profile, number density profiles, etc., together with the controlling physical and chemical processes).

2. The precision with which one can determine the refractive index, and therefore the number density, in the lower neutral atmosphere depends on how well one can separate the refractive effects caused by the ionized and the neutral regions of the atmosphere.

When an electromagnetic wave propagates through an ionized medium, its wavelength is longer than it would be in free space. Figure 38 illustrates how this effect caused a decrease in the two-way phase path as *Mariner IV* moved in behind the Martian ionosphere.

---

\*Presented by G. Fjeldbo. The principal investigator for the *Mariner IV* radio occultation experiment was A. J. Kliore.

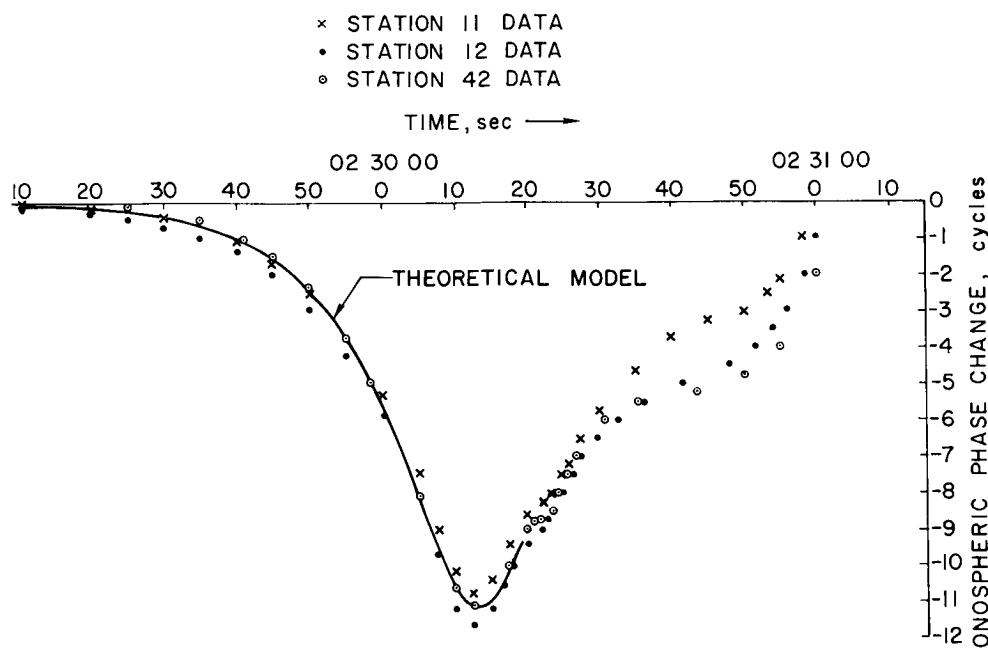


Fig. 38. Ionospheric phase change vs time, during immersion

Data from three different JPL tracking stations are shown in this figure.

It can be seen from Fig. 38 that the main ionospheric layer on Mars caused an 11-cycle phase decrease—or an apparent position change of the spacecraft of about 75 cm in the direction of the Earth ( $\lambda \approx 13.6$  cm). Starting at about 02<sup>h</sup> 30<sup>m</sup> 20<sup>s</sup>, another change of only about 4 cm was observed at each of the tracking stations, and it is believed that this was caused by a minor layer in the lower ionosphere.

From the ionospheric phase path data one can determine the electron density profile of the Martian ionosphere (Ref. 2). The preliminary electron density profile shown in Fig. 39 was computed from the data taken as the propagation paths probed through the ionosphere above the bright area Electris. The solar zenith angle was about 70°, and the Martian local time was early afternoon. Electris is in the southern hemisphere of Mars at latitude 50°, and it was winter there at the time of the measurement.

The peak electron density is seen to be of the order of  $10^5 \text{ cm}^{-3}$  at a height of 120 km. The plasma scale height at the top side is about 24 km. Both the small scale height and the low altitude of the main layer show that the Martian atmosphere is considerably colder than previously anticipated.

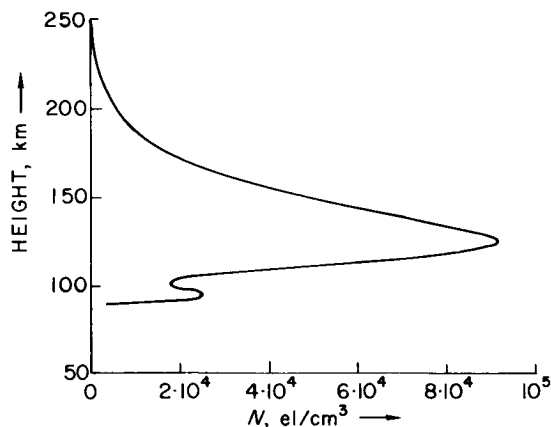


Fig. 39. Electron number density vs altitude above Electris. Martian local time, 1 p.m.

Measurements were also made during occultation exit. In that case the radio energy probed through the nighttime ionosphere above Mare Acidalius in the northern hemisphere of Mars. The signature of the night-side ionosphere appears to be very weak, however, and about all we can say at present is that the measurements suggest that the electron density on the night side was down by at least a factor of 20 from the peak density measured on the day side.

The problem is of course that sensitivity to these low electron densities is not very great at S-band frequencies.

However, this low sensitivity is by no means inherent in the radio occultation method when this technique is seen from a broader point of view. Thus, a somewhat different scheme has been suggested—in which two or more harmonically related frequencies may be used to probe the atmosphere of Mars (Refs. 3 and 4). Choosing the lowest frequency at a few hundred Mc/sec would provide a more sensitive measurement of ionospheric electron densities. In addition, the two-frequency technique has the advantage that one can separate the effects of the electrons and the neutral molecules because of their different dispersive properties.

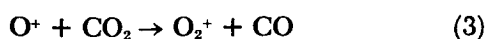
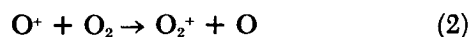
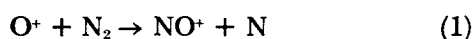
Next, a brief discussion will be given of the temperature and some of the reactions thought to be important in the upper atmosphere of Mars.

Carbon dioxide is apparently the main constituent in the lower atmosphere of Mars (Ref. 1). In addition, there may be some nitrogen and argon. At a higher altitude, CO<sub>2</sub> is dissociated into CO and O by the solar ultraviolet flux shortward of about 1700 Å (Ref. 5).

Atomic oxygen is lighter than CO, N<sub>2</sub>, Ar, and CO<sub>2</sub>; thus the number density of O is not expected to decrease as rapidly with altitude as do the number densities for the other constituents. Hence, above some altitude one might expect atomic oxygen to become the main constituent.

Some of the preliminary models we have made for the Martian atmosphere have O<sup>+</sup> as the main ion at and above the electron density peak. These models have a temperature at the top side of the ionosphere of about 90°K—which corresponds to an electron scale height of 24 km.

Bates has shown that radiative recombination of O<sup>+</sup> with electrons takes place somewhat faster at low than at high temperatures (Ref. 6). In spite of this temperature effect, it does not seem possible to explain the loss rate in the Martian ionosphere on the basis of radiative recombination of O<sup>+</sup>. It is therefore necessary to assume that molecules of minor constituents take part in the loss processes. One can, for instance, consider the following possibilities:



where the molecular ions may lose their charge quite easily through dissociative recombination with electrons.

The two first reactions are relatively well known and are thought to play an important role in the Earth's ionosphere (Refs. 7 and 8). The last reaction, brought to our attention by E. E. Ferguson, should also be considered because the lower atmosphere of Mars contains large amounts of CO<sub>2</sub>.

In models where O<sup>+</sup> is the principal ion and where one of Reactions (1)–(3) is the main loss process, there is a Bradbury-type layer (such as the Earth's F2 layer) at 120 km altitude. The number density of atomic oxygen is of the order of 10<sup>9</sup> cm<sup>-3</sup> at the peak of this layer. If Reaction (1) is assumed to be the main loss process ( $k \approx 10^{-12}$  cm<sup>3</sup>/sec), one finds that there would have to be large amounts of N<sub>2</sub> present in order to account for the loss rate, which is of the order of 10<sup>2</sup> cm<sup>-3</sup> sec<sup>-1</sup>. In fact, a rate coefficient of 10<sup>-12</sup> cm<sup>3</sup>/sec requires that N<sub>2</sub> should have a higher abundance than CO<sub>2</sub> in the lower atmosphere of Mars, at least if it is assumed that the lower atmosphere is mixed. However, CO<sub>2</sub> must be the main constituent in the lower atmosphere in order to explain the occultation data and the spectroscopic measurements (Ref. 1). Therefore, it is tempting to look for other alternatives.

If Reaction (2) is assumed to be responsible for the loss of O<sup>+</sup>, one finds that with  $k \approx 10^{-11}$  cm<sup>3</sup>/sec it would be necessary to have on the order of 20% O<sub>2</sub> at the peak of the main ionospheric layer in order to account for the loss rate. The spectroscopic observations indicate that there is less than 0.1% O<sub>2</sub> in the lower atmosphere of Mars (Ref. 9). However, the O<sub>2</sub> distribution in the Martian atmosphere is complicated by the fact that atomic oxygen, produced by photodissociation of carbon dioxide, associates to form O<sub>2</sub>. Molecular oxygen might, therefore, still be of some importance for the loss of O<sup>+</sup>, at least in the lower portion of the Martian ionosphere.

At present, the most promising model appears to be one in which O<sup>+</sup> mainly loses its charge through Reaction (3). With a reaction rate coefficient of the order of 10<sup>-9</sup> cm<sup>3</sup>/sec (Ref. 10), one finds that it is necessary to have on the order of 10<sup>6</sup> CO<sub>2</sub> molecules/cm<sup>3</sup> at 120 km altitude. This appears to be within reach of what can be supplied through upward diffusion.

Another approach one might take in constructing models for the Martian atmosphere is to assume that a considerable portion of the oxygen formed through the

dissociation of carbon dioxide has been lost. (If this could take place to such an extent that  $\text{CO}^+$  became the principal ion, then the main ionospheric layer would be of a Chapman type. The temperature on the top side, corresponding to a molecular weight of 28, would be about  $150^\circ \text{K}$ . The ion  $\text{CO}^+$  could lose its charge through dissociative recombination with electrons.)

There are two ways that O could conceivably be lost: escape into space or loss of  $\text{O}_2$  through oxidation processes involving the surface crust. The first process is not expected to be important because the temperature is too low (Refs. 11 and 12). The second process would require diffusive and convective transport of oxygen from the dissociation region down to the surface. However, such a transport would probably not have too important an effect on the  $\text{CO/O}$  ratio in the upper atmosphere of Mars, since both constituents probably would be transported downwards at approximately the same rate. Therefore, it appears that we are left with atomic oxygen as the principal constituent in the Martian ionosphere.

One of the main difficulties in identifying the ion loss processes in the Martian ionosphere is the uncertainty in the reaction rate coefficients, particularly with respect to temperature dependence. Thus, further studies of these effects might require revision of the preliminary conclusions in this paper.

The low temperatures obtained from the occultation data appear to be in reasonable agreement with atmospheric models where  $\text{CO}_2$  is the main constituent at ground level. This conclusion is based on calculations utilizing the work of Bates, Chamberlain, and others, which shows that  $\text{CO}_2$ , CO, and O are more effective in radiatively cooling the upper atmosphere than is molecular nitrogen, which was previously believed to be the main constituent (Refs. 12, 13, 14, and 15).

Most of the clouds and hazes in the Martian atmosphere are observed at altitudes below 30 km (Ref. 16). However, there is also some evidence of violet haze layers around 100 km altitude. Urey and Brewer (Ref. 17) have suggested that this might be caused in part by  $\text{CO}^+$ , which absorbs in the ultraviolet and blue. The occultation experiment strengthens this suggestion, since  $\text{CO}^+$  is quite certainly one of the important ions in the upper atmosphere of Mars.

Figure 40 illustrates how the atmospheric mass density varies with altitude. With a Bradbury-type ionospheric layer where the principal ion  $\text{O}^+$  is losing its charge through one of Reactions (1)–(3), we find that the mass density at 120 km altitude should be of the order of  $2 \cdot 10^{-14} \text{ g/cm}^3$ . However, the mass density could be two orders of magnitude higher if the main ionospheric layer were a Chapman layer with  $\text{CO}^+$  as the principal ion.

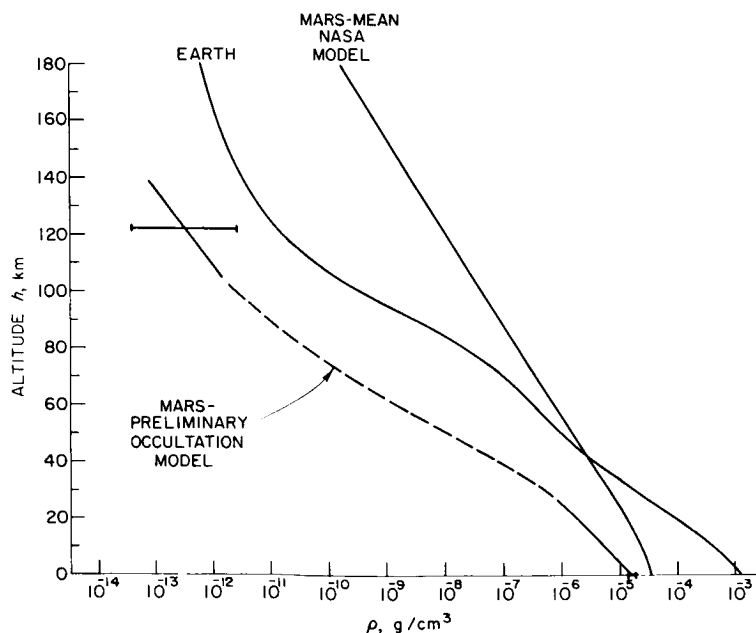


Fig. 40. Atmospheric mass density vs altitude

This difference in interpretation results in the uncertainty indicated by the error bar shown at 120 km altitude.

The most interesting point illustrated in Fig. 40 is that the mass density distribution shown for Mars and for the Earth do not cross each other at higher altitude. Previously the opposite was believed to be true, and the argument was that since the gravity is less on Mars than on the Earth, the scale height has to be larger.

The question of how the mass density varies with altitude in the Martian atmosphere has also some practical implications. If one wants to put a satellite in orbit around Mars, one needs to know how the atmospheric density varies with altitude. Most previous models required an orbit altitude of several thousand kilometers for a satellite with 50 years lifetime, but the occultation results suggest that a few hundred kilometers may be sufficient.

Table 10 summarizes the more striking features of the upper atmosphere of Mars.

### Acknowledgment

The work reported in this paper was sponsored by the National Aeronautics and Space Administration under contracts NGR 05-020-065 and NsG-377, and NAS 7-100.

**Table 10. Summary of preliminary results for the upper atmosphere of Mars**

Property	Value
	<b>Immersion<sup>a</sup></b>
Maximum electron density, el/cm <sup>3</sup>	$9.0 \pm 1.0 \times 10^4$
Altitude of maximum, km	$120 \pm 5$
Electron scale height above maximum, km	$24 \pm 3$
Temperature at the top side, °K	
O principal ion	$90 \pm 12$
CO principal ion	$150 \pm 20$
Preliminary estimate of the atmospheric mass density at 120 km, g/cm <sup>3</sup>	$2 \times 10^{-14}$ to $2 \times 10^{-13}$
	<b>Emersion<sup>b</sup></b>
Maximum electron density, el/cm <sup>3</sup>	$< 5 \times 10^3$
<sup>a</sup> Over Electris at 50° S latitude, 177° E longitude, early afternoon, winter, solar zenith angle 70°.	
<sup>b</sup> Over Mare Acidaliu at 60° N latitude, 36° W longitude, night, summer, solar zenith angle 106°.	

### REFERENCES

1. Kliore, A. J., Cain, D. L., Levy, G. S., Eshleman, V. R., Fjeldbo, G., and Drake, F. D., 1965, *Science*, Vol. 149.
2. Fjeldbo, G., and Eshleman, V. R., 1965, *J. Geophys. Res.*, Vol. 70, pp. 3217-3227.
3. Eshleman, V. R., 1965, Chapter 14 in *Solar System Radio Astronomy*, ed. J. Aarons, Plenum Press, New York, p. 267.
4. Fjeldbo, G., Eshleman, V. R., Garriott, O. K., and Smith, F. L., III, 1965, *J. Geophys. Res.*, Vol. 70, p. 3701.
5. Herzberg, G., 1961, *Molecular Spectra and Molecular Structure: I. Spectra of Diatomic Molecules*, D. Van Nostrand Co., Inc., New York.
6. Nawrocki, P. J., and Papa, R., 1963, *Atmospheric Processes*, Prentice-Hall, Inc., New Jersey.

## REFERENCES (Cont'd)

7. Rishbeth, H., and Garriott, O. K., 1964, *Introduction to the Ionosphere and Geomagnetism*, Tech. Rpt. No. 8, NSG-30-60, SU-SEL-64-111, Stanford Electronics Laboratories, Stanford University, Stanford, California.
8. Nicolet, M., and Swider, W., 1963, *Planetary Space Sci.*, Vol. 11, pp. 1459-1482.
9. Owen, T. C., and Kuiper, G. P., 1964, *Communications of the Lunar and Planetary Laboratory*, No. 32.
10. Fehsenfeld, F. C., Schmetlekoepf, A. L., and Ferguson, E. E., *J. Chem. Phys.*, to be published, private communication.
11. Kuiper, G. P., 1947, Chapter 12 in *The Atmospheres of the Earth and Planets*, ed. G. P. Kuiper, University of Chicago Press, Chicago, Illinois.
12. Chamberlain, J. W., 1962, *Astrophys. J.*, Vol. 136, pp. 582-593.
13. Bates, D. R., 1951, *Proc. Phys. Soc.*, Vol. B64, pp. 805-821.
14. Norton, R. B., 1964, *A Theoretical Study of the Martian and the Cytherean Ionospheres*, NASA Tech. Note TN D-2333, National Aeronautics and Space Administration, Washington, D. C.
15. McElroy, M. B., L'Ecuyer, J., Chamberlain, J. W., 1965, *Astrophys. J.*, Vol. 141, pp. 1523-1535.
16. de Vaucouleurs, G., 1954, *Physics of the Planet Mars*, Faber and Faber, Ltd., London.
17. Urey, H. C., Brewer, A. W., 1957, *Proc. Royal Soc. of London*, Vol. A241, pp. 37-43.

## COMMENTS ON THE MARINER IV PHOTOGRAPHS OF MARS\*

Robert B. Leighton

California Institute of Technology  
Pasadena, California

The 22 photographs of Mars that were sent to the Earth by the *Mariner IV* spacecraft are being processed and studied. An interim account of the processing and of some of the preliminary measurements is given here.

The optical system of the camera was a Cassegrain reflecting telescope with a  $4\frac{1}{2}$ -cm aperture and a 30-cm focal length, operating at an equivalent focal ratio of  $f/8$ , with an exposure time of 0.2 sec. The receptor was a miniaturized all-electrostatic vidicon tube, whose output, the target current, was amplified and digitized into 64 "quantum levels" of intensity. To avoid poor discrimination at low exposures, four gain stages were available and were switched automatically, one step at a time, when needed.

The mechanical and electronic performance of the camera system was almost precisely as designed; the data recording and transmission to Earth were extremely good; and the optical sensitivity seemed quite normal.

\*Dr. Leighton's comments are given here in shortened form.

Processing the photographs is very involved and goes rather slowly. The JPL numerical data processing used on the *Ranger* program is being applied to the *Mariner* photographs. The main attention has been given to geometrical distortions, which are not serious. After rectifying the geometry, we can introduce the calibration data, increase the contrast, look for differences in the intensity of neighboring elements, and enhance the resolution by a spatial filtering program.

Figure 41 shows the first photograph received from Mars, after a certain amount of computer processing. Above the limb of the planet can be seen a "cloud," or possibly a large amount of glare; if it is indeed a cloud, its top level would be about 25 km above the surface of Mars.

Figure 42 (Frame 7) was the first to show unambiguously that large craters exist on Mars; ten or more can be counted. Figure 43 (Frame 11) shows the largest crater (about 120 km) that we have seen, and one of the smallest (6 km). Figure 44 (Frame 14) shows some bright



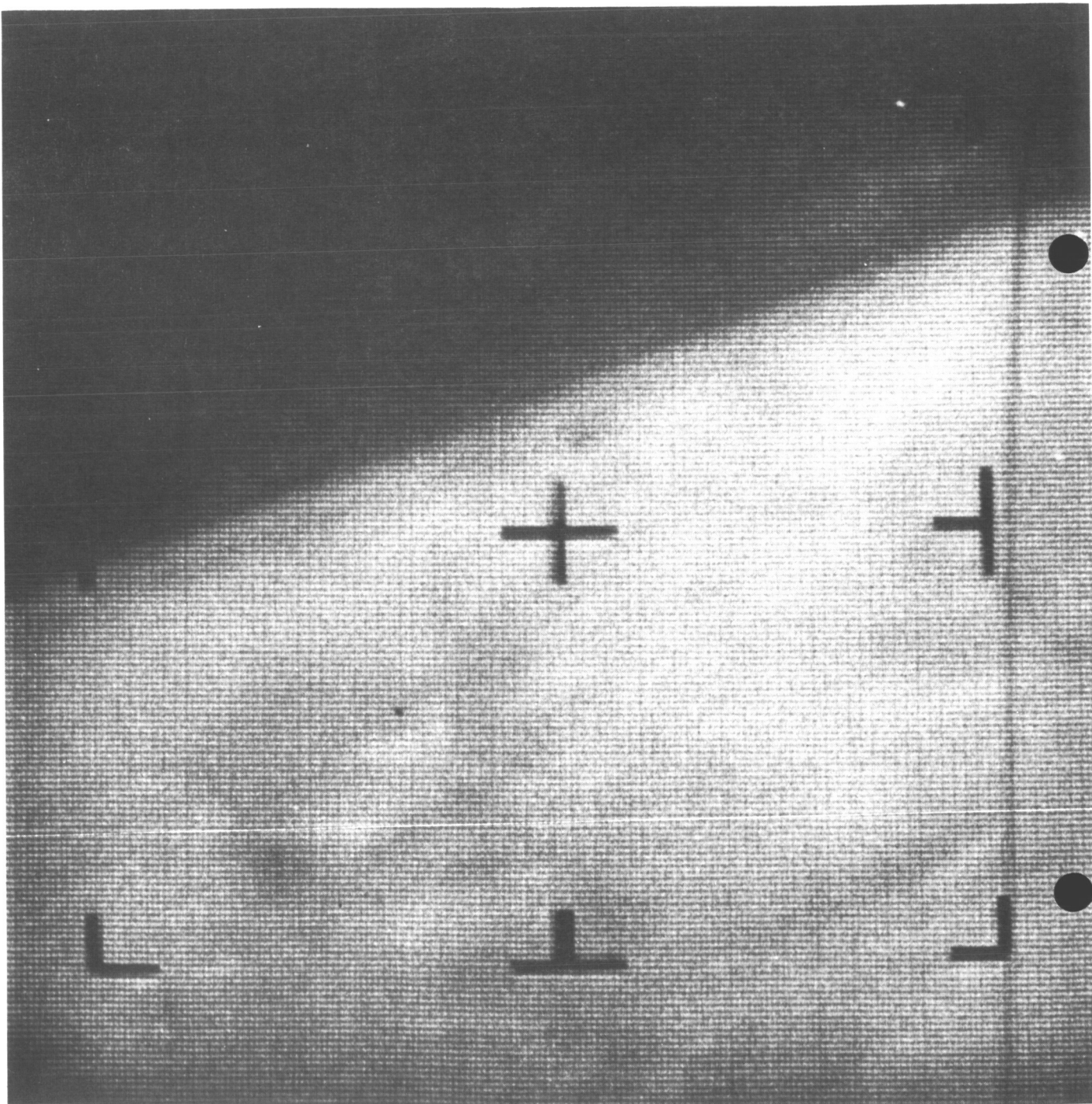


Fig. 41. Frame 1 of the Mariner IV photographs

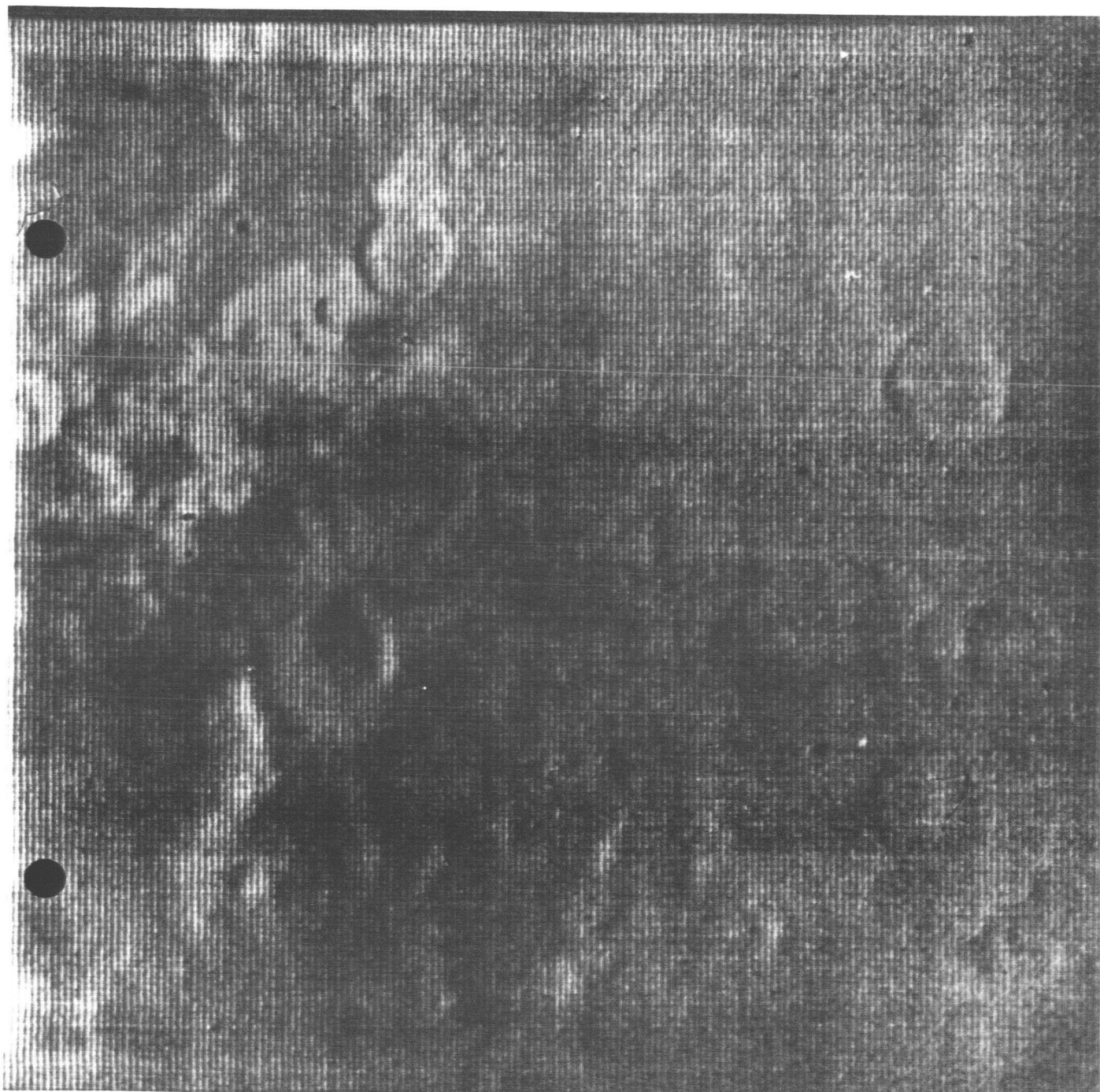


Fig. 42. Frame 7 of the *Mariner IV* photographs

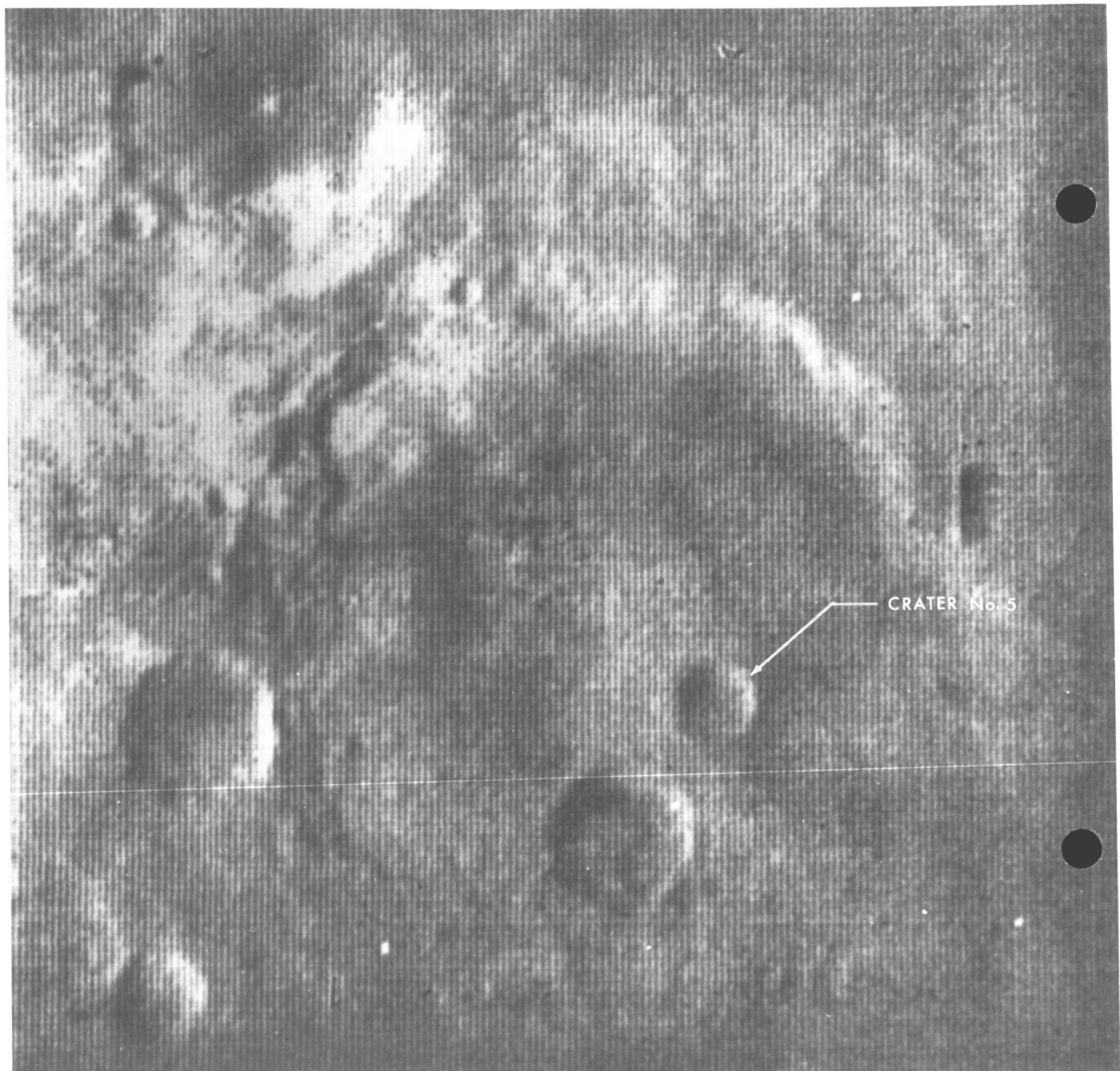


Fig. 43. Frame 11 of the *Mariner IV* photographs



spots near the top and some circular bright areas evidently associated with craters. I believe these are frost on the surface.

Preliminary study of the craters suggests that:

1. Craters are apparently distributed variably over the planet.
2. There is a dearth of small craters (of less than 10 km in diameter).
3. The larger and medium-sized craters have rather flat floors, as compared with similar craters on the Moon.

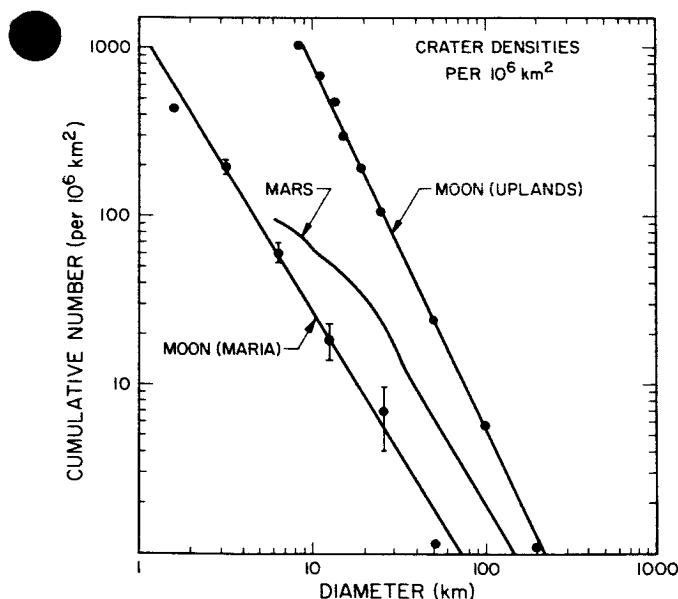


**Fig. 45. Plot of Martian crater distribution compared with lunar uplands and maria**

Concerning crater distribution, Fig. 45 shows a comparison of Mars' craters with those in the lunar maria and uplands, reduced to a unit area of a million square kilometers; the Martian crater count lies almost midway on this logarithmic scale, between the lunar maria and the lunar uplands. At a crater diameter of 20 km, where the linear portion of the Mars crater plot ends, the factor between the lunar maria and Mars is about 3.5, and the lunar uplands are about a factor of 20 at that same crater diameter. Thus the Martian crater density is 3.5 greater than that of the lunar maria, but does not approach the densely packed condition of the lunar uplands.

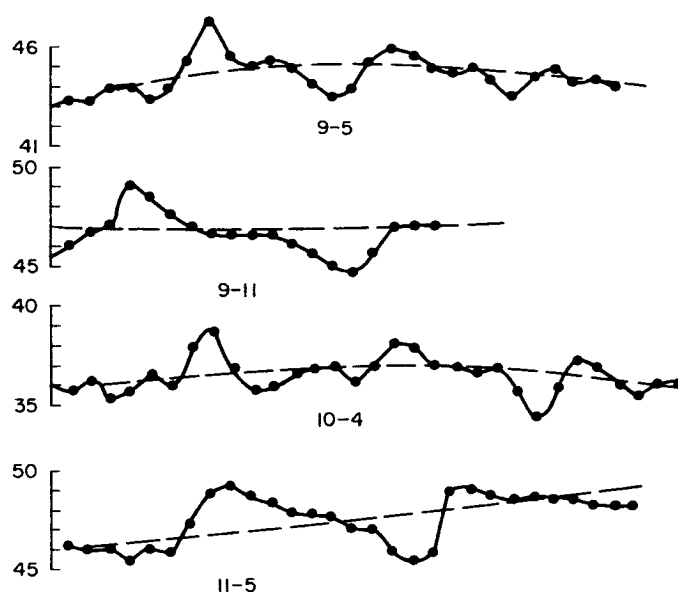


**Fig. 46. Analysis of Martian crater wall slopes and heights**

An analysis of the wall slopes and heights of the craters is shown in Fig. 46. In this analysis, one quantum level of intensity on the photographs corresponds to a slope of from 1.5 to 2.5° throughout the picture sequence. (This relationship neglects the effect of any glare that might have reduced the contrast.) Shown in the figure are plots of actual data numbers from 0 to 64, taken in a traverse across the diameter of several craters. For example, crater No. 5 of Frame 11 shows a crater that has almost classic form; it has little outer wall, is dark on the inside rim, comes down to a small flat region in the middle, and then becomes lighter on the opposite wall.

Why were the craters on Mars so unexpected and why is their appearance on the photographs so important? The world is full of people who had thought there might be craters, but very few had arrived at this conclusion by scientific reasoning and described the analysis in writing. Actually, the total range of opinion on the subject of the Martian surface has been so broad and controversial that it didn't really help much to know that the truth might lie somewhere between the extremes. We think that the *Mariner* pictures have removed certain matters from the realm of fruitless controversy and focused attention on new opportunities and new problems. There is still plenty of room for difference of opinion on many aspects of Mars!

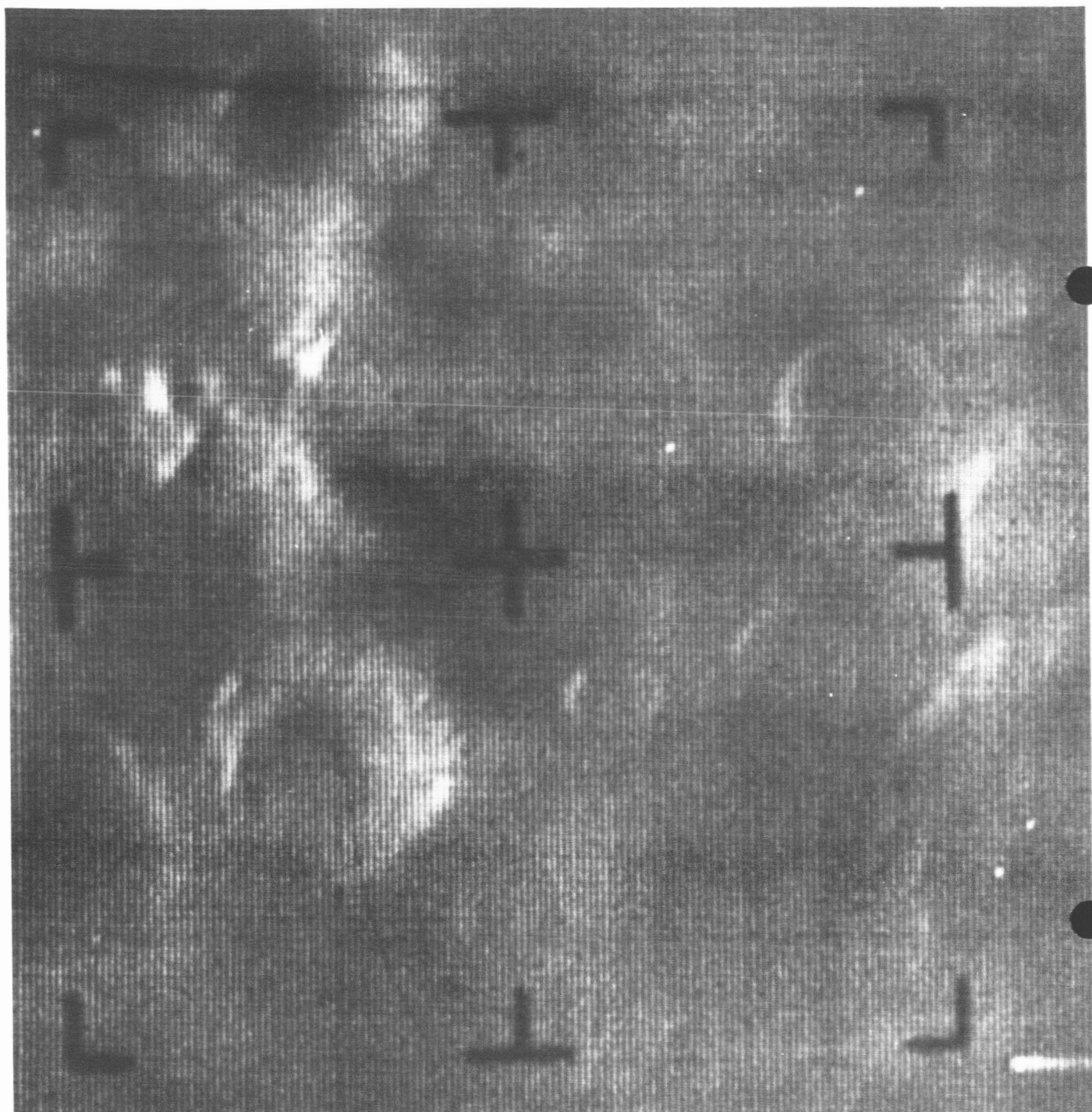


Fig. 44. Frame 14 of the *Mariner IV* photographs

## HIGH-RESOLUTION PLANETARY PHOTOGRAPHY AND THE DETECTION OF LIFE

Carl Sagan

Harvard University  
and Smithsonian Astrophysical Observatory  
Cambridge, Massachusetts

The brilliant success of the *Mariner IV* photographic mission has lent increased interest in the possibility of detection of extraterrestrial life by high-resolution photography from planetary flyby or orbiter spacecraft. The following discussion is primarily a brief summary of the conclusions of two recent studies of this problem (Refs. 1 and 2) to which reference may be made for further details.

For organisms or the artifacts of organisms to be detected from high altitude, they must, under most circumstances, have dimensions greater than the ground resolution of the photographic system; and they also must have a detectable contrast difference with their surroundings. The principal exception is in the case of a rectilinear feature, which, if it has high contrast with its surroundings, may be detected even if its width is significantly below the limiting ground resolution. It must, of course, be at least several resolution elements long. Such rectilinear features are, in principle, of possible significance in the detection of extraterrestrial life, because, as terrestrial experience indicates, the combined factors of geometry and economy lead a technical civilization to construct rectilinear artifacts.

The *Mariner IV* spacecraft was designed to obtain a maximum of 22 photographs of the planet Mars, each of 64 shades of gray and with a ground resolution of a few kilometers. This performance is comparable with that of the *Tiros* and *Nimbus* series of meteorological satellites, where there are 16 to 32 shades of gray and where the ground resolution ranges from about 2 km to about 0.2 km. The best *Tiros* and *Nimbus* photographs of the Earth, therefore, can detect contrast variations only half to a quarter as well as *Mariner IV*; at the same time, the ground resolution may be an order of magnitude better.

A typical *Tiros* photograph of a relatively cloud-free region of the Earth's surface is contained in Fig. 47, a photograph in slightly unusual perspective of the eastern seaboard of the United States. The cross and right-angle markings are fiducial standards. No sign of life on Earth, intelligent or otherwise, is detectable in this picture. Similar conclusions apply to photographs taken of the major populated regions of the Earth. Almost without exception, no sign of the vast highway networks, bridges, dams, contour farming, dikes, breakwaters, and great

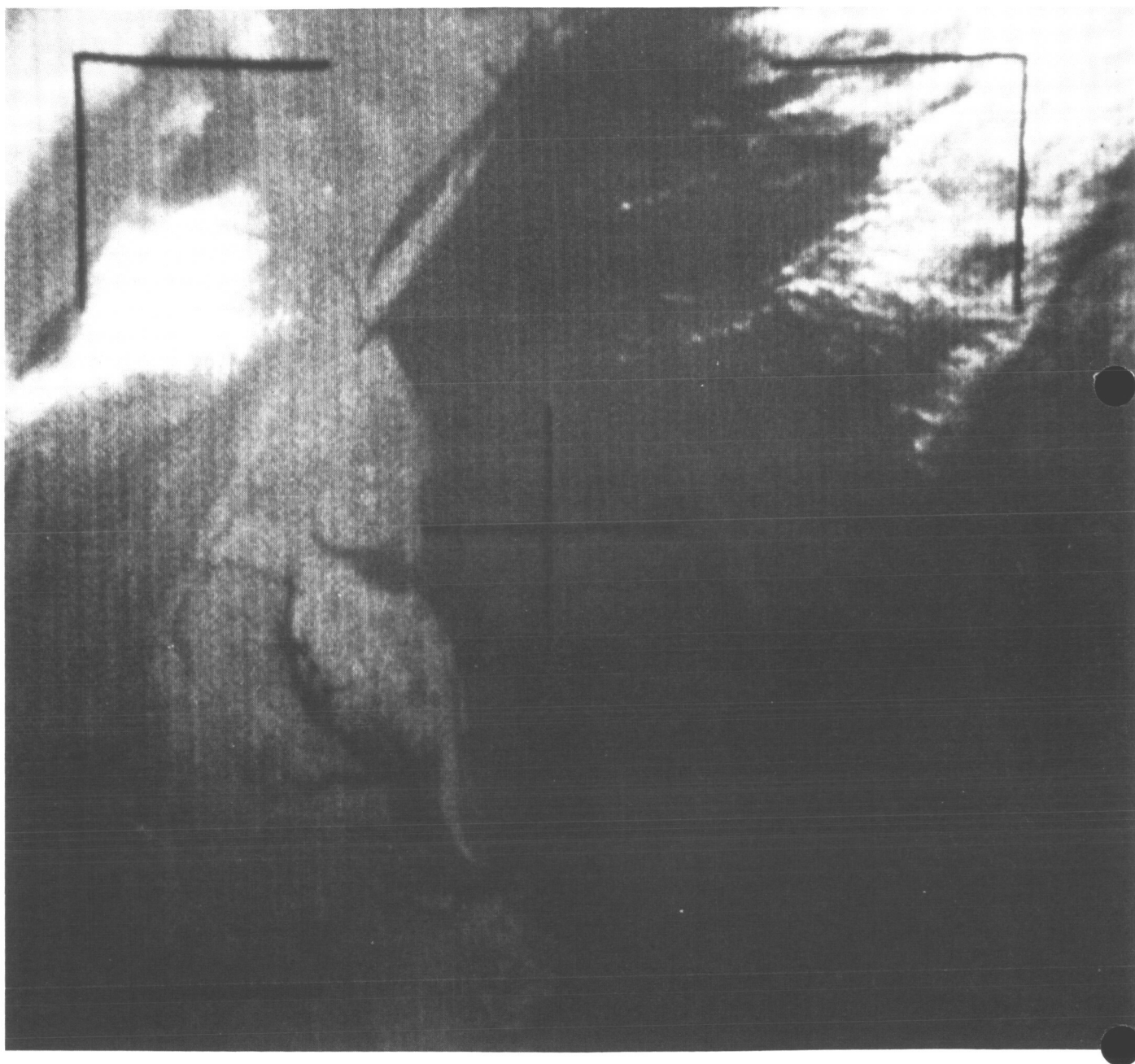


**Fig. 47. A typical *Tiros* photograph of the Earth's surface. The Atlantic Ocean is the dark region in the right half of the picture; the eastern seaboard of the United States is the brighter region towards the left. The very bright features at the left and upper left are clouds. Cape Cod is just off the top of the picture. In this unusual projection, Long Island can be seen stretching upwards and to the right. Chesapeake Bay is towards the lower end of the figure. Courtesy of Goddard Space Flight Center, National Aeronautics and Space Administration.**

walls can be found on the Earth with a ground resolution  $\sim 1$  km. Similarly, seasonal contrast changes in such high-contrast crops as cotton and in deciduous forests are difficult to detect, because of the small absolute con-

trast changes sometimes involved, problems of intercalibration of widely spaced photographs, and the difficulties in properly correcting for changing angles of insolation and view.



Very rarely an apparent rectilinear marking such as that seen in Fig. 48 can be detected. This particular rectilinear feature, about 25 km long, and in some places 1.5 km wide, despite its apparent artificiality, turns out

to be most likely a natural peninsula, and not a breakwater. In Fig. 49, a comparison is made between the feature as it appears in the *Nimbus* photograph and as it is represented in Mercator projection by the U. S. Army

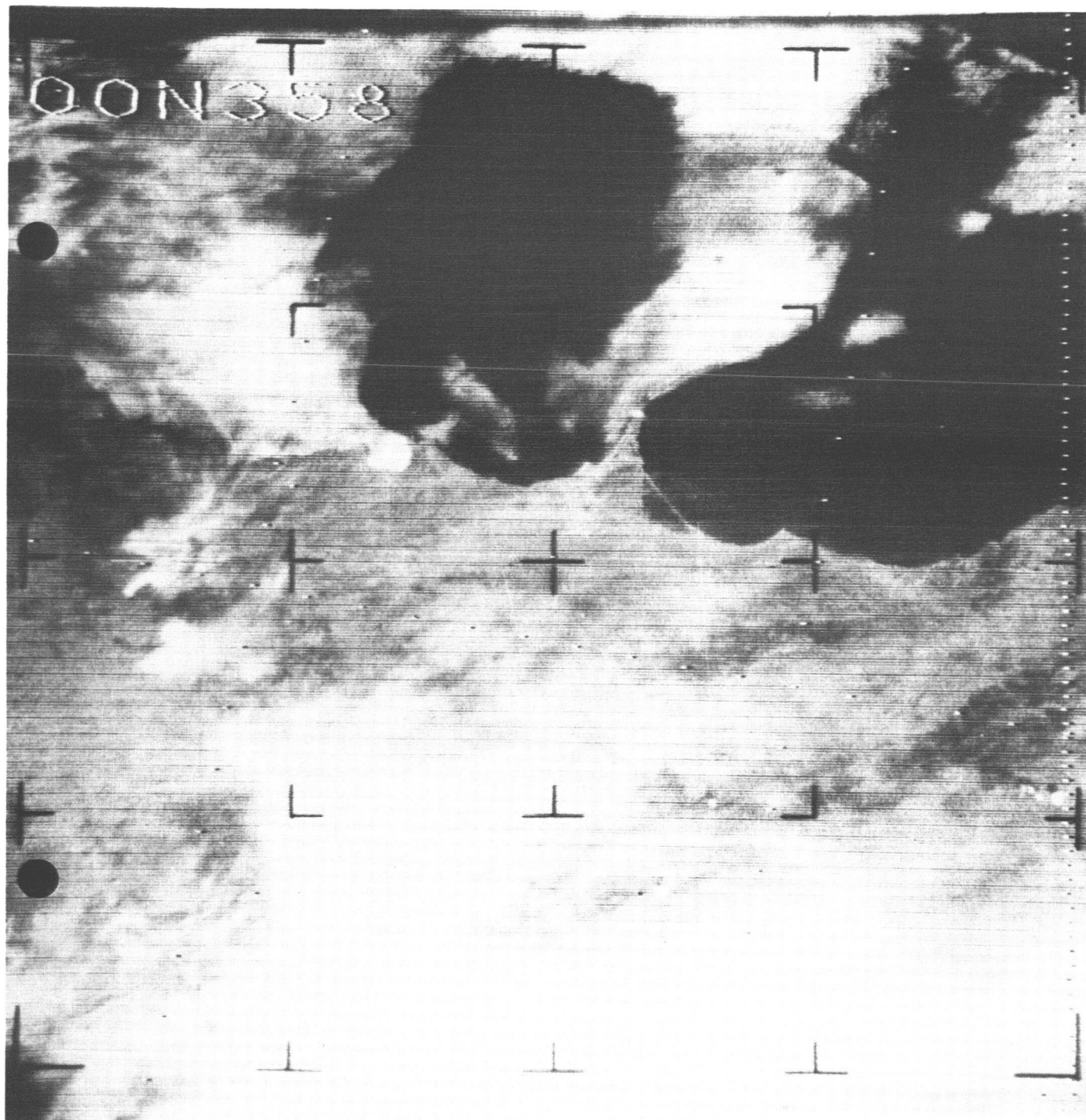
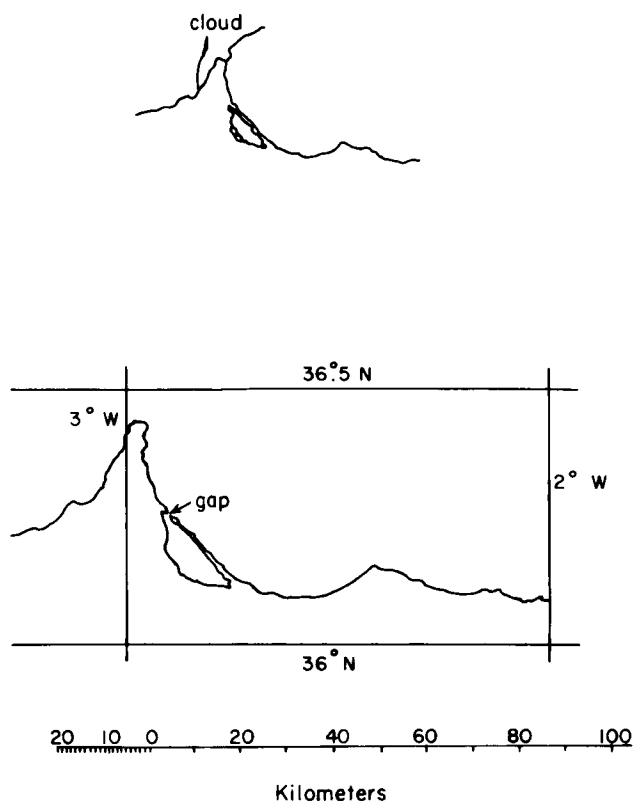


Fig. 48. A *Nimbus I* photograph of the northern coast of Morocco, orbit 295, September 1964. Courtesy of Goddard Space Flight Center, National Aeronautics and Space Administration.





**Fig. 49. Upper: drawing of the appearance of a section of the northern coast of Morocco from the *Nimbus I* photograph of Fig. 48. Lower: Mercator projection cartography of the same region taken from U. S. Army Map Service Maps, Series 1301, Sheets NJ29, NJ30, NI29, NI30 (1955).**

Map Service. The lesson that all apparent rectilinear features are not artifacts of intelligent life is useful to bear in mind in interpreting photographs of other planets.

A successful detection of life on Earth is shown in Fig. 50, which displays a bright orthogonal array on a dark background towards the upper left corner. The width of the rectilinear features is  $\sim 1/2$  km. The photograph is of an area near Cochrane, Ontario, Canada, a lumber region. The grid pattern is the result of a lumbering operation in which parallel swaths were cut through the forest, with wide avenues of trees left standing to insure later reforestation. Then similar cuts were made at right angles. When the logging operation was completed, snows fell, heightening the contrast. But were a similar orthogonal array to found in *Mariner IV* photographs of the Martian surface, we would be hasty in concluding that it was *prima facie* evidence for an advanced technical civilization on that planet. We would

first want to be very sure that the grid was not an artifact of the photographic reduction, or was not a feature that could be attributed to geological causes. There is, for example, a lunar grid system that is attributed to fracture patterns on the surface of the Moon.

Rectilinear features have, of course, been reported on the Martian surface; these are the so-called "canals," whose apparent straightness seemed explicable to Percival Lowell only if they were the artifacts of an indigenous and advanced technical civilization. The classical representation of the canals can be seen in the left-hand portion of Fig. 51, a drawing of single and double rectilinear markings as observed by Schiaparelli. On the right-hand portion of this same figure is seen the identical area of Mars as drawn by Antoniadi (Ref. 3) under conditions of superb seeing. The canals have been resolved into a disconnected sequence of fine mottling, which, when the atmosphere grows slightly less steady, the eye tends to string up in linear order. It is much easier to recall a few straight lines from the moment of superb seeing than it is to remember a more or less disordered array of disconnected detail.

Yet one might still ask how it is that some of this disconnected fine detail seems to be ordered in approximately a linear array. Now that we know, from the *Mariner IV* photographs, that the Martian surface is covered with craters, it is possible to suggest that such ordered spots as those in the right-hand portion of Fig. 51 are actually chains of dark craters. While a more or less straight chain of six or eight craters, each about 100 km in diameter, is not common on the Moon, there are a few examples, most notably the chain Ptolemaeus, Alphonsus, Arzachel, Purbach, Walter, and Stöfler; and vast numbers of smaller crater chains exist. Alternative explanations of the canals have been offered—e.g., Gifford (Ref. 4) has suggested that they may be similar to the seif sand dunes of terrestrial desert regions. This explanation, however, does not explain the high-resolution appearance of the canals (again, cf. the right-hand side of Fig. 51). At any rate, there is no reason to attribute the reported Martian canals to biological activity on that planet.

It appears that several thousand photographs of the Earth, with approximately 0.1-km resolution, are required before any convincing signs of intelligent life on the Earth can be detected (Ref. 1). Had the *Mariner IV* vehicle passed the same distance from the Earth that it did from Mars, and obtained 22 comparable photographs of the Earth, no sign of life on our planet would have

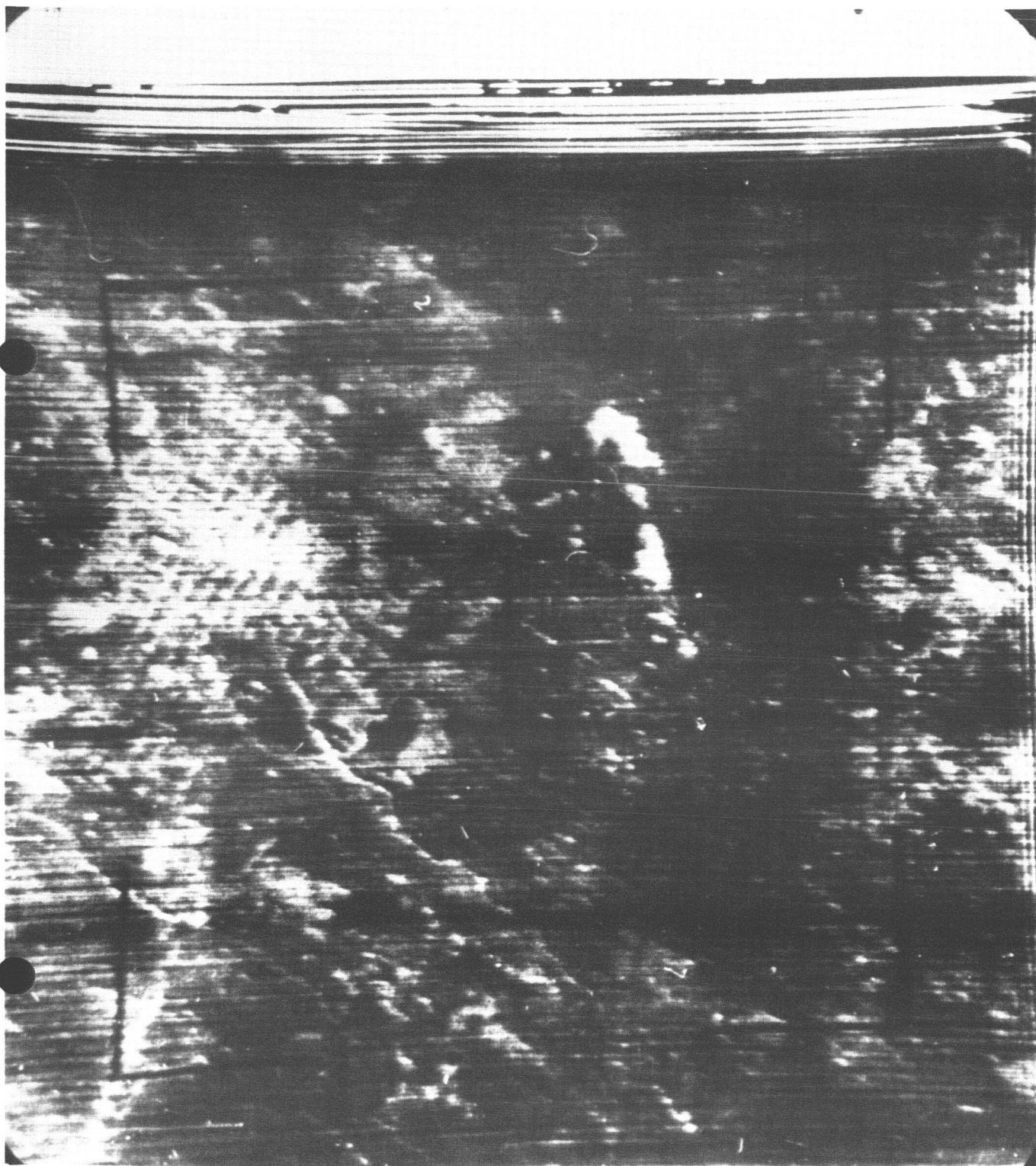
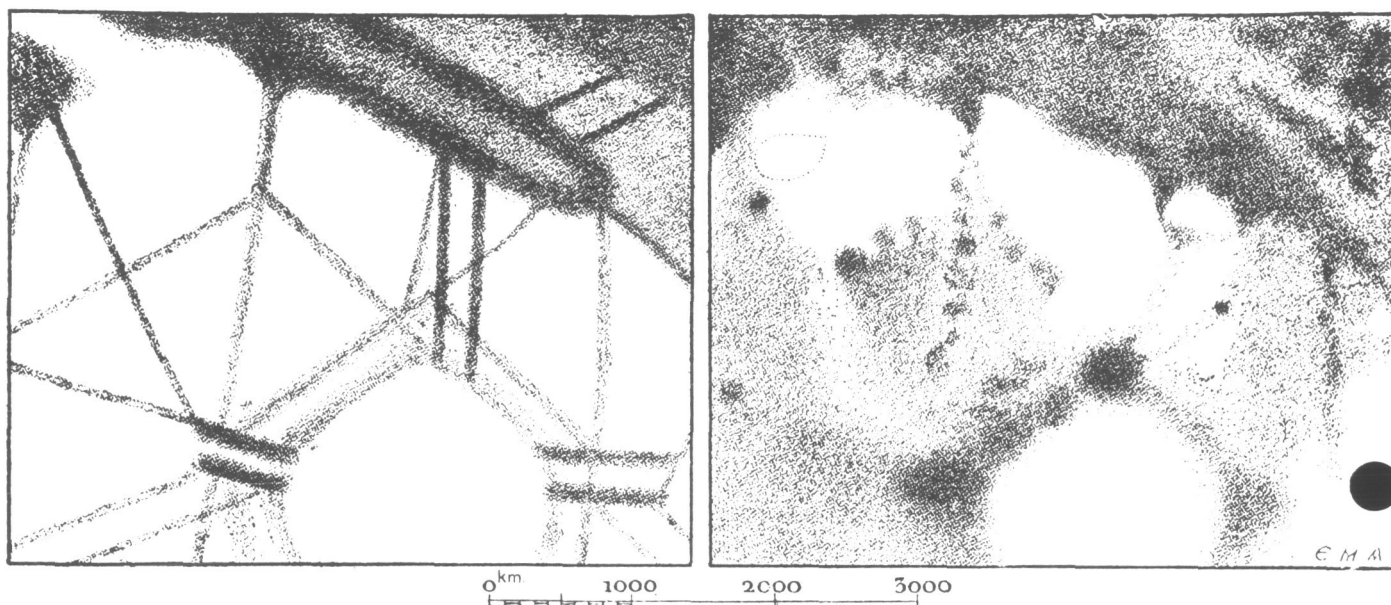


Fig. 50. *Tiros 2* photograph with the narrow-angle camera, of the region of Cochrane, Ontario, Canada, taken on April 4, 1961. Courtesy of Goddard Space Flight Center, National Aeronautics and Space Administration.



**Fig. 51. Comparison of views of the same region of the Martian surface; at left as seen by Schiaparelli; at right, as seen under superior seeing conditions by Antoniadi (1930). (Reproduced from *La Planète Mars*. E. M. Antoniadi, Hermann et C<sup>ie</sup>, 1930.)**

been uncovered. The *Mariner IV* photographic system was designed for geological exploration of Mars; in this it succeeded admirably. The absence of obvious extensive water erosion features suggests that the planet did not have open bodies of liquid water in its immediate past; this was, in any case, expected from the absence of open bodies of liquid water at the present time. The most recent estimate of the age of the oldest features revealed on the *Mariner IV* photographs is  $\sim$  several hundred million years (Ref. 5). Thus, in the early history of the planet, open bodies of water are still possible. Significant quantities of subsurface water are, in any case, likely, and the origin of life on the planet Mars seems as likely now, after the *Mariner IV* mission, as it did before. Thus, as the experimenters themselves have stressed, the *Mariner IV* photographic reconnaissance neither demonstrated nor precluded the possibility of life on Mars.

The existence of military reconnaissance satellites demonstrates that the detection of life on Earth at orbital altitudes is feasible. Figures 52 and 53 are aerial photographs of the planet Earth in the San Francisco-Sacramento region, with a ground resolution some 30 times better than that of the best *Tiros* and *Nimbus* photographs displayed earlier in this discussion. It is easy to calculate that similar ground resolutions are possible from characteristic orbital altitudes. We see that, with this ground resolution, contour farming, urban developments, railways, and airports are all easily dis-

cernible. Even if we had no previous acquaintance with any of these manifestations of intelligent life on Earth, we would have little doubt that these features are of intelligent origin.

Were our resolving power to improve by another factor of 30 it would be possible to detect—especially when the Sun is at large zenith angles—individual large organisms such as trees, horses, or cows. The fact that these organisms tend to be found near others of their kind would enhance the probability of successful interpretation.

Only a few hundred randomly situated photographs of the Earth's surface with a resolution of that of Figs. 52 and 53 would give unambiguous evidence of the existence of intelligent life on our planet. A similar number of photographs with a resolution  $\sim 1$ —especially taken at low sun—would probably give unambiguous evidence of forms of life other than Man. If we are interested in pursuing biological exploration of Mars by flyby or orbital photography, our strategy should be to photograph a small fraction of the planet's surface at the highest possible resolution, rather than to photograph the entire surface at low resolution. With the orbital altitudes and spacecraft payloads now envisioned for the *Voyager* exploration of Mars, ground resolution in the 1- to 10-m range seems quite feasible. Whether or not Mars is a life-bearing planet, high-resolution photography of its surface is of the greatest scientific interest.





Fig. 52. Reproduction, made at the Smithsonian Astrophysical Obs., of a section of a photo montage of the San Francisco—Sacramento, California, area. Prepared by Aero Service, Inc., Philadelphia. Courtesy of Dr. Robert N. Colwell.



Fig. 53. Reproduction, made at the Smithsonian Astrophysical Obs., of a section of a photo montage of the San Francisco—Sacramento, California, area. Prepared by Aero Service, Inc., Philadelphia. Courtesy of Dr. Robert N. Colwell.

## REFERENCES

1. Kilston, S. D., Drummond, R. R., and Sagan, C., 1966, *Icarus*, Vol. 5, pp. 79–98.
2. Sagan, C., et al., 1966, "Remote Reconnaissance of the Earth," *Biology and the Exploration of Mars*, U.S. National Academy of Sciences, Washington, in press.
3. Antoniadi, E. M., 1930, *La Planète Mars*, Librairie Scientifique, Hermann et Cie, Paris.
4. Gifford, F., 1964, *Icarus*, Vol. 3, No. 2, pp. 130–135.
5. Anders, E., and Arnold, J., 1965, *Science*, Vol. 149, No. 3691, pp. 1494–96.

N66 31481

## CONTRIBUTION AU COLLOQUE CALTECH-JPL SUR LA LUNE ET LES PLANETES: MARS

Audouin Dollfus

Observatoire de Paris  
Meudon, France

### ***1. Mesure de la quantité d'eau dans l'atmosphère de la planète Mars***

J'ai décrit dans la séance du présent Colloque consacrée à Vénus, le dispositif qui m'a permis, en 1963, de déceler et de mesurer la vapeur d'eau dans l'atmosphère de la planète Vénus. La même technique a été appliquée pour mesurer la quantité d'eau sur la planète Mars.

Le télescope Cassegrain azimuthal de 50 cm associé au spectrophotomètre à filtre polarisant, d'un type nouveau, a déjà été décrit (1)(2)(3)(4). Cet instrument donne l'intensité de la bande 1,4 microns de la vapeur d'eau dans les atmosphères des planètes par simple comparaison photométrique entre les planètes et les sources de comparaison que représentent le Soleil, la Lune ou certaines étoiles.

Les astres de comparaison donnent la quantité de vapeur d'eau interposée dans l'atmosphère terrestre, à différentes distances zénithales, en différents points du ciel et au cours de la nuit; les mesures relevées sur Vénus et

sur Mars révélèrent des différences significatives attribuables à la vapeur d'eau présente dans leurs propres atmosphères.

J'ai choisi la forte bande spectrale 1,4 microns parce qu'elle correspond au maximum de la réponse photoélectrique des cellules au sulfure de plomb et donne la sensibilité désirée; mais cette bande se sature pour une quantité d'eau voisine de 0,1 gr/cm<sup>2</sup>, et il faut observer à une altitude suffisante pour réduire à une valeur inférieure à cette limite la quantité d'eau restant dans l'atmosphère terrestre.

L'instrument possède un champ de mesure aussi étendu qu'à 25' d'arc; je pouvais l'utiliser à bord de la nacelle d'un ballon libre en pointant le télescope manuellement sans le secours d'aucun dispositif de guidage photoélectrique.

J'ai d'abord essayé un prototype de ce nouvel instrument grâce à une ascension en ballon que j'ai effectuée

dans la nuit du 29 au 30 Mai 1954 jusqu'à l'altitude de 7000 mètres (5). Puis l'appareil fut associé à un habitacle étanche et climatisé pour protéger l'observateur à des altitudes encore plus élevées. A bord de celui-ci, dans la nuit du 22 au 23 Juin 1959, j'ai effectué une nouvelle ascension jusque dans la stratosphère à l'altitude de 14.000 mètres (6). Les observations permirent d'adapter et l'étalonner ce nouveau spectrophotomètre, et de mesurer la teneur en vapeur d'eau de la haute atmosphère terrestre.

Ensuite, j'ai utilisé l'instrument en haute montagne à la Station Scientifique Internationale du Jungfraujoch en Suisse à l'altitude de 3.600 mètres (7)(8). J'ai bénéficié de la nuit de 5 très bonnes nuits d'observation, en Janvier 1963. Le résultat des mesures se trouve sur la figure 54; en abscisse, j'ai reporté la quantité d'eau contenue dans l'atmosphère terrestre le long du trajet optique visant la planète Mars. En ordonnée, on trouve la différence entre les valeurs recueillies sur Mars et pour l'atmosphère terrestre. Les quantités d'eau sont données en grammes par centimètre carrés à la pression atmosphérique ordinaire. Lorsque la bande devient saturée (à droite sur la figure) un léger écart correspondant à  $0,008 \text{ gr/cm}^2$  persiste entre Mars et les astres de comparaison Bételgeuse et la Lune. Ce résidu est attribuable aux répartitions spectrales différentes de la lumière entre ces astres et la planète dans le domaine couvert par le filtre de part et d'autre de la bande saturée.

La dérivée de la courbe d'étalonnage encadrant au mieux les mesures est figurée en trait fin; elle donne un excès de vapeur d'eau sur Mars correspondant à  $0,022 \text{ gr/cm}^2$ .

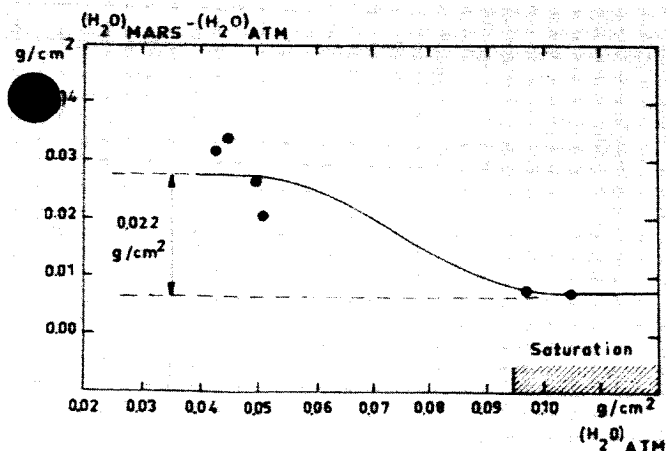


Figure 54

Selon nos mesures polarimétriques et différents résultats spectrophotométriques, le sol martien est très probablement recouvert superficiellement par une poudre fine d'oxyde de fer hydraté, du type limonite, qui contient vraisemblablement une forte proportion de molécules  $\text{H}_2\text{O}$ . Des spectres de laboratoire publiés récemment montrent en particulier la bande 1,4 microns faible, élargie, et légèrement déplacée vers les grandes longueurs d'onde. A travers notre spectrophotomètre à filtre polarisant, ces substances donneraient un faux signal correspondant à  $0,006 \text{ gr/cm}^2$ . Nous avons retranché ce signal à la valeur observée qui devient alors  $0,016 \text{ gr/cm}^2$ .

Cette valeur est donnée par l'étalonnage à la pression atmosphérique terrestre, tandis que, sur Mars, l'atmosphère est au moins 30 fois moins dense. Des courbes d'étalonnage ont été calculées pour différentes pressions, à l'aide des profils de la bande 1,4 microns publiés par ailleurs (9). Ces calculs révèlent que le signal donné par notre spectromètre est presque indépendant de la pression, ce qui avait échappé lors de notre publication préliminaire: en effet, lorsque la pression augmente, les ailes du profil élargi de la bande empiètent sur les domaines de transmission latéraux du filtre qui servent de référence, ce qui compense presque exactement l'augmentation de signal que donne l'accroissement de l'intensité. La correction de pression, très faible, donne finalement  $0,018 \text{ gr/cm}^2$  pour la lumière de l'ensemble du disque de Mars.

L'atmosphère martienne est traversée deux fois par la lumière, et l'observation oblique au bord du disque double le parcours moyen, de sorte que la quantité d'eau totale contenue verticalement dans l'atmosphère martienne vaut  $0,0045 \text{ gr/cm}^2$ , soit 45 microns d'eau précipitable (8).

La même année, par une méthode différente, H. Spinrad, G. Münch et L. D. Kaplan ont décelé à leur tour la vapeur d'eau sur Mars. Leur détermination quantitative, plus faible, donne environ 14 microns (27).

## II. Propriétés photométriques du sol martien

### Courbe photométrique globale des régions claires du sol martien

Pendant l'opposition de 1952, j'avais réalisé 22 comparaisons photométriques entre Mars et  $\alpha$  Virginia,  $\pi$ ,  $\delta$  et  $\beta$  Scorpii en lumière jaune, à l'aide d'un photomètre photoélectrique (10). La sensibilité semblait voisine de 0,05 magnitudes. La magnitude globale de l'astre dépend des configurations sombres du sol qui se déplacent avec



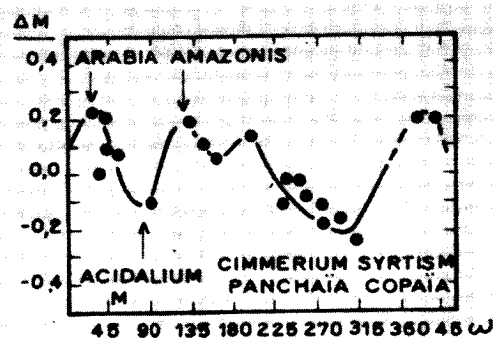


Figure 55

la rotation de l'astre. La figure 55 donne ces variations en fonction de la longitude du méridien central de Mars ainsi que les noms des contrées claires et sombres qui les engendrent. En corrigeant les mesures, grâce à cette courbe, j'ai déterminé la magnitude qu'aurait la planète si, privée de taches sombres, elle montrait un sol orange clair uniforme. La figure 56 donne, dans ce cas, la variation de la magnitude en fonction de l'angle de phase. Cette *courbe photométrique* des régions claires montre une décroissance uniforme de la magnitude entre les phases  $10^\circ$  et  $47^\circ$ , à raison de  $+0,0145 \text{ mag/deg}$ .

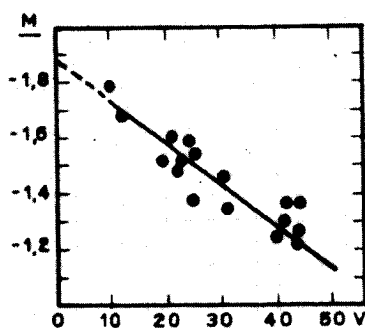


Figure 56

Comparons ce coefficient à ceux donnés par ailleurs pour différents corps célestes pratiquement dépourvus d'atmosphère.

Corps célestes	Coeff. de phase
Mars	$+0,0145 \text{ mag/deg}$
La Lune	$+0,028$
Mercure	$+0,030$
Astéroïdes (moyenne)	$+0,023$

La décroissance d'éclat de Mars est presque deux fois plus faible que celle des autres corps célestes de comparaison. Voici l'explication de cette singularité :

La rapide décroissance de l'éclat de part et d'autre de la phase nulle sur Mercure, la Lune et les Astéroïdes est attribuable aux jeux d'ombres et de lumière dans les cavités du sol, ses structures poreuses ou les enchevêtrements complexes des petits grains de poussière qui recouvre la surface. Ces structures superficielles sont probablement produites sur ces astres par le foisonnement de la roche, ou par l'accumulation pendant une durée très prolongée des impacts par les petits météores. La planète Mars n'est pas exempte d'une telle action, mais l'atmosphère et ses vents déplacent les grains les plus fins : la poussière mobile efface les petites cavités du sol.

### Photométrie absolue des régions claires

En 1950 et 1952, j'ai effectué l'analyse photométrique détaillée du sol martien dans la partie visible du spectre. J'avais mis au point dans ce but le *photomètre polariscopique à franges*, déjà décrit dans d'autres publications (11)(12). Dans cet instrument, la planète apparaît striée par les franges d'interférences serrées, données par un polariscope de Savart. Une plage de comparaison d'éclat uniforme et réglable se superpose à l'image du disque planétaire et donne des franges complémentaires qui s'imbriquent exactement entre celles produites par la planète. Lorsqu'une région du disque planétaire possède la même luminance que la plage de comparaison, les franges se détruisent exactement et disparaissent sur cette portion du disque planétaire. En contrôlant l'éclat de la plage de comparaison, je pouvais de la sorte mesurer successivement, par disparition des franges, la luminance des différentes régions de la surface martienne. J'obtenais ainsi des mesures relatives.

Je mesurais ensuite la luminance moyenne de l'ensemble de la planète. Pour cela, j'ajoutais dans le faisceau une lentille qui remplaçait l'image de l'astre par celle de l'objectif de la lunette uniformément éclairée par la lumière de l'ensemble de la planète. Je réglais la disparition des franges sur cette image de l'objectif et, compte tenu des surfaces respectives de cette image et de Mars au foyer, j'obtenais la luminance moyenne du disque de la planète; je pouvais alors donner la luminance des différentes régions de la surface de Mars en fonction de cette luminance globale du disque.

Enfin, je mesurai à la même époque, la magnitude réelle de Mars, comme décrit ci-dessus; il devenait alors facile de déduire les *luminances absolues*, appelé *B*, des

différents points de la surface martienne, exprimées en *stilb* à la distance moyenne de Mars au Soleil 1,52 UA.

Les rapports de ces valeurs avec celle calculée pour un écran blanc parfaitement diffusant éclairé normalement à la même distance par le Soleil donnent finalement les facteurs de diffusion, appelé  $K$ , des différents points de la surface martienne.

Avec le réfracteur de 60 cm du Pic-du-Midi, à la faveur des nuits de bonnes images, je pouvais mesurer de la sorte des régions martiennes aussi petites que 3" de diamètre apparent. La précision semble de l'ordre de 3 centièmes.

Ces mesures absolues en lumière orangée (0,59 micron) ont été complétées par des déterminations à travers 8 filtres colorés couvrant l'intervalle spectral visible entre 0,65 micron et 0,47 micron.

J'ai encore effectué des séries de mesures en comparant les plages entre elles à l'aide du photomètre à double image décrit en 1952 (13).

La figure 57 donne le facteur de diffusion  $K$  des régions claires, au centre du disque, à l'opposition exacte, en fonction de la longueur d'onde. On remarque la décroissance très rapide vers le bleu.

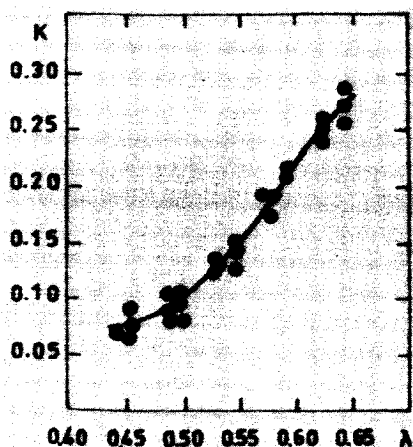


Figure 57

La figure 58 donne la variation du facteur de diffusion, en lumière jaune 0,59 micron, pour les régions claires ayant le Soleil au zénith, en fonction de l'angle de phase. On lit en ordonnée le facteur de diffusion  $K$  ainsi que la brillance  $B$  en stilbs à 1,524 UA.

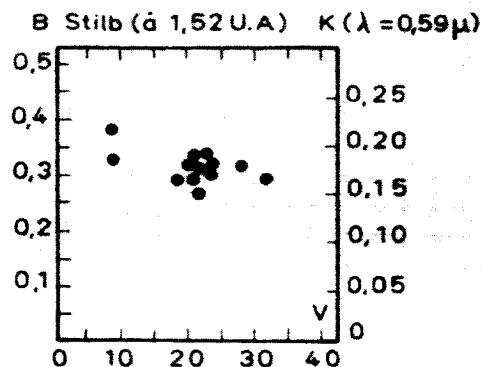


Figure 58

La figure 59 donne la variation du facteur de diffusion des régions claires en fonction de la distance  $\theta$  au centre du disque, pour trois valeurs de l'angle de vision : 10°, 20° et 30°. Les trois courbes sont respectivement décalées verticalement. Les mesures absolues sont figurées par des cercles. Les mesures visuelles non étalonnées ainsi que les mesures sur les clichés, respectivement représentées par des croix et des points, ont été adaptées pour encadrer les mesures absolues.

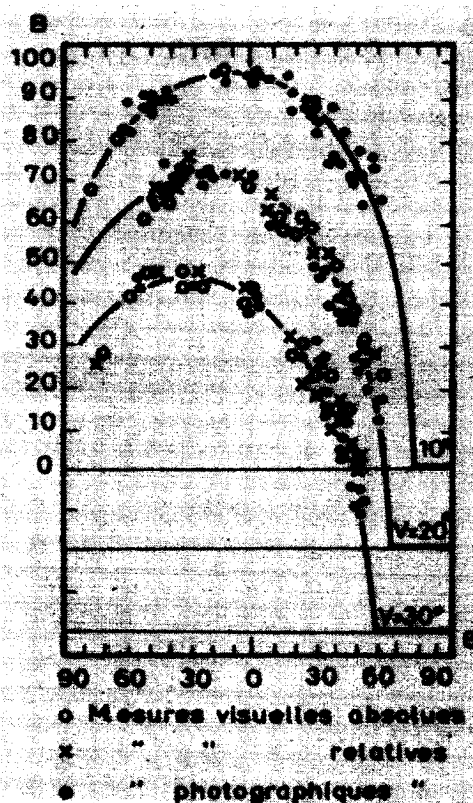


Figure 59

Les courbes de la figure 60 résument les variations de  $B_s$  en fonction de  $\theta$  et  $V$  pour les régions claires du sol

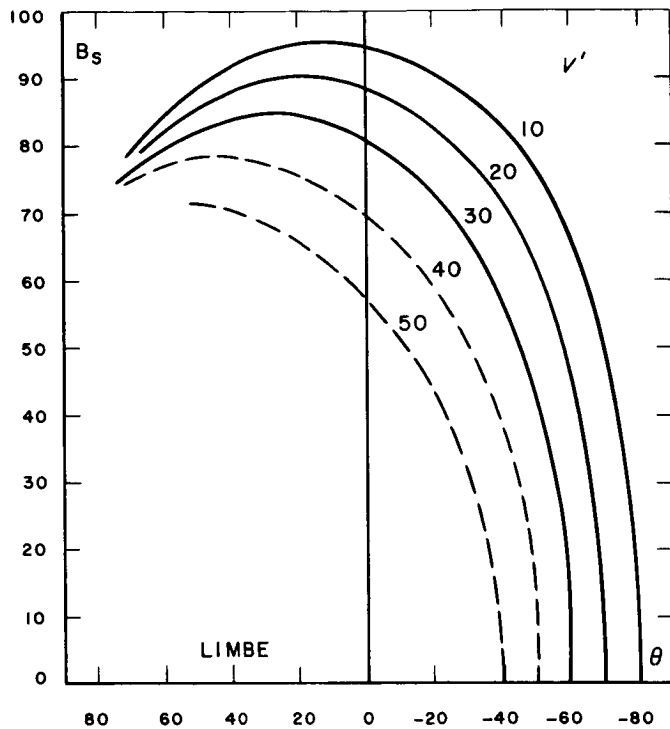


Figure 60

martien et la longueur d'onde  $0,59 \mu$  selon l'analyse de l'ensemble des résultats précédents.

Ces courbes s'écartent de celles que donnerait la loi de Lambert, valable pour une sphère lisse ayant un facteur de diffusion élevé; à  $60^\circ$  du point ayant le Soleil au zénith, l'éclat du sol vaut en effet 0,73 fois l'éclat maximum; cette valeur serait 0,50 pour un diffuseur parfait. Ces courbes s'écartent encore plus de celles observées sur la Lune, dont la grande rugosité de la surface ne donne aucun assombrissement au bord du disque pour la phase nulle; la courbe correspondante pour l'angle de Phase  $V = 0^\circ$  serait une droite horizontale.

Il faut que les formations de la surface de Mars contrairement à celles de la Lune, aient une structure non pas rugueuse, mais seulement modérément vallonnée (14).

#### Interprétation des propriétés photométriques des régions claires

Pour interpréter ces résultats, j'ai établi au laboratoire des courbes photométriques en fonction de  $\theta$  et de  $V$  sur des surfaces poudreuses ayant des facteurs de diffusion progressivement décroissants.

La figure 61 concerne un dépôt lisse de magnésie. Le facteur de diffusion  $K$  vaut par définition 1,0; les grains sont pratiquement transparents et la plus grande partie

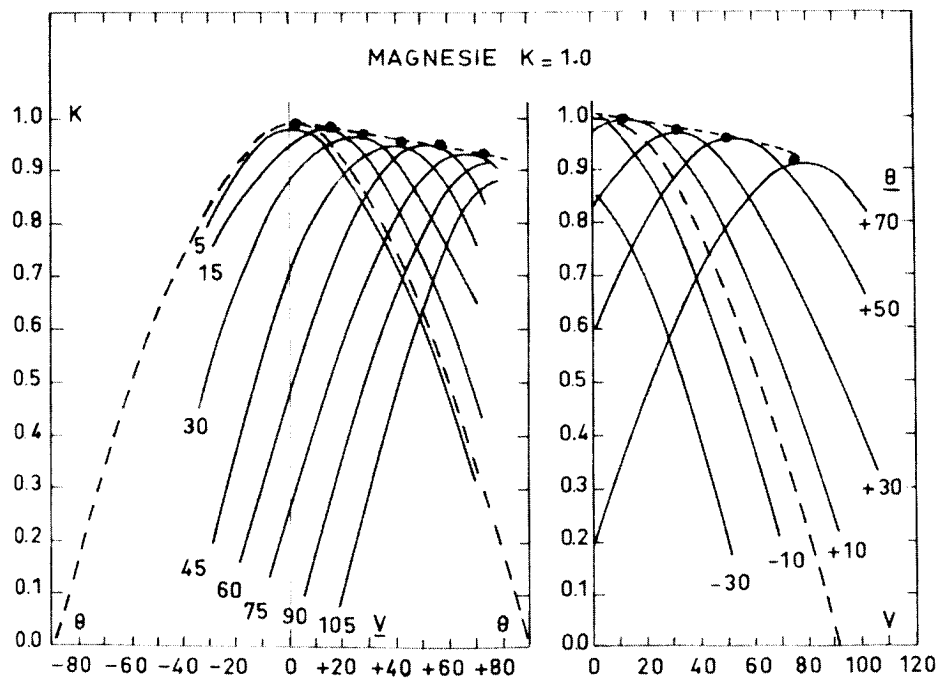


Figure 61

de la lumière pénètre à l'intérieur de la couche; cette lumière ressort ensuite dans toutes les directions; par suite, cet échantillon obéit à peu près à la loi de Lambert, représentée pour  $V = 0^\circ$  sur la figure par la courbe en tirets. On décelé de faibles écarts à cette loi théorique car la courbe en pointillé correspondant au cas de l'éclairement perpendiculaire à la surface n'est pas une droite horizontale.

La figure 62 concerne une cendre volcanique naturelle très claire de l'éruption du Mandoza de 1932, pour laquelle  $K = 0,57$ . La poudre est tamisée en un dépôt aéré

sur une surface plane. La loi de Lambert est encore à peu près respectée pour des angles de vision  $V$  inférieurs à  $90^\circ$ ; mais l'absorption par la matière est plus grande, la lumière directement renvoyée par la surface des grains joue un rôle plus important.

La lumière incidente qui a pénétré entre les interstices des grains superficiels est renvoyée par réflexion ou diffusion sur les grains plus profonds; elle ne trouve aucun obstacle à revenir exactement dans la direction de la source; on observe donc un léger maximum d'éclat sous les angles de vision  $V$  voisins de zéro.

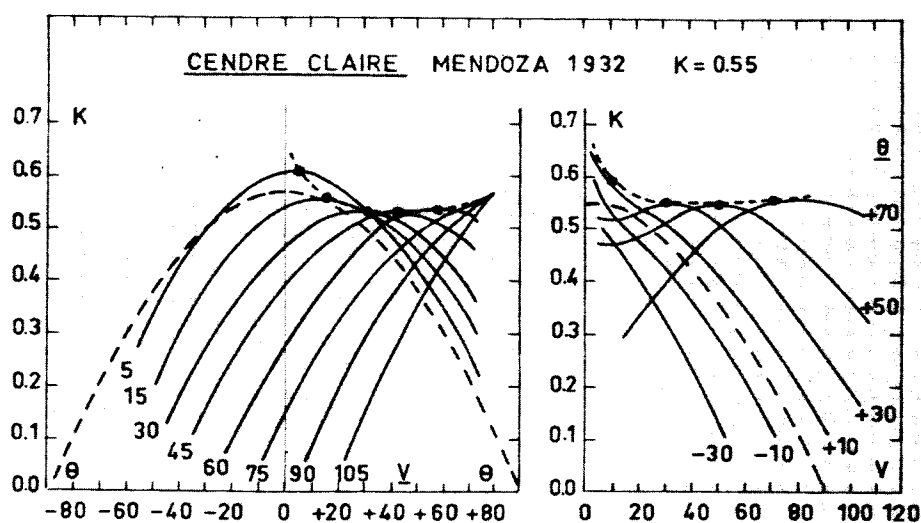


Figure 62

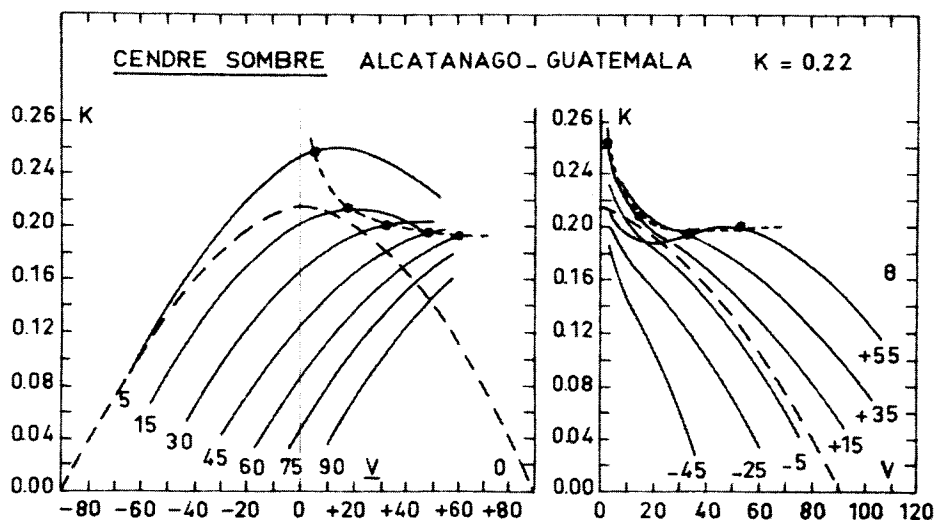


Figure 63

La figure 63 est donnée par une cendre sombre de l'Alcatanago, dont le facteur de diffusion  $K = 0,20$  est comparable à celui des régions claires de la surface de Mars en lumière jaune. La matière très absorbante ne laisse ressortir qu'une très faible partie de la lumière ayant pénétré dans l'intérieur des grains : l'éclat observé provient principalement des réflexions et diffusions simples et multiples par les surfaces mêmes des grains. La loi de Lambert est très mal suivie et ne le serait plus du tout si la surface était onduleuse ou tourmentée. La concentration de lumière dans la direction de la source devient très prononcée, mais cet effet s'atténue lorsque le dépôt poudreux est comprimé au lieu d'être tamisé de haut car les grains sont alors tassés.

Une cendre encore plus sombre, de facteur diffusant  $K = 0,09$  (analogue à la Lune, ou la planète Mars en lumière bleue) donne les courbes de la figure 64. Les grains, complètement opaques, n'agissent plus que par leurs surfaces. Certains cristaux miroitent sur cet échantillon, et déforment les courbes. La loi de Lambert n'est plus aucunement respectée; la forme des courbes dépend beaucoup du vallonement de la surface; la concentration de lumière vers la source caractérise la tassement des grains.

J'ai étudié plus particulièrement un échantillon obtenu en concassant un mélange de limonite et goethite, avec hématisite, reproduisant au mieux les propriétés polarimétriques et photométriques des régions claires de Mars, telles qu'elles ressortent de nos observations. Le dépôt tamisé uniforme donne pour  $\lambda = 0,59 \mu$  les courbes photométriques de la figure 65.

La comparaison avec Mars conduit aux conclusions suivantes :

1. Le facteur de diffusion  $K$  dans la direction de la Terre pour le point éclairé verticalement sur la surface de Mars dépend de l'angle de phase  $V$ . Nos mesures déjà données sur la figure 58, sont reportées sur la figure 66, en même temps que la courbe obtenue sur notre échantillon; l'accord est bon, mais il n'est pas certain que l'accroissement de l'éclat pour la phase nulle soit aussi prononcé sur Mars que sur la couche déposée par tamisage.
2. La courbe de l'assombrissement au bord du disque  $K(\theta)$  pour les petits angles de phase  $V$  caractérise le vallonement de la surface. Pour l'angle  $V = 0^\circ$ , la courbe de Mars est encadrée très exactement, sur la figure 67, par les mesures relevées sur notre échantillon presque lisse et plan. Une surface rugueuse donnerait une droite horizontale. Il est donc à prévoir que, dans l'ensemble, la surface des déserts martiens sera trouvée peu rugueuse et peu vallonnée.
3. La variation spectrale de  $K$ , donnée sur Mars par la figure 57, est comparée à divers mélanges de poudres de limonite, hématisite et goethite (figure 68), broyées et plus ou moins tamisées (j'ai reçu des échantillons de A. Cailleux, C. Sagan, J. Adamcik, etc. . .). Ces oxydes de fer plus ou moins hydratés, dont certains reproduisent exactement la courbe de polarisation de la lumière observée sur Mars, donnent à peu près la variation spectrale de l'éclat, sur les régions claires du sol martien. Des mélanges adroits pourraient donner cette courbe exactement.

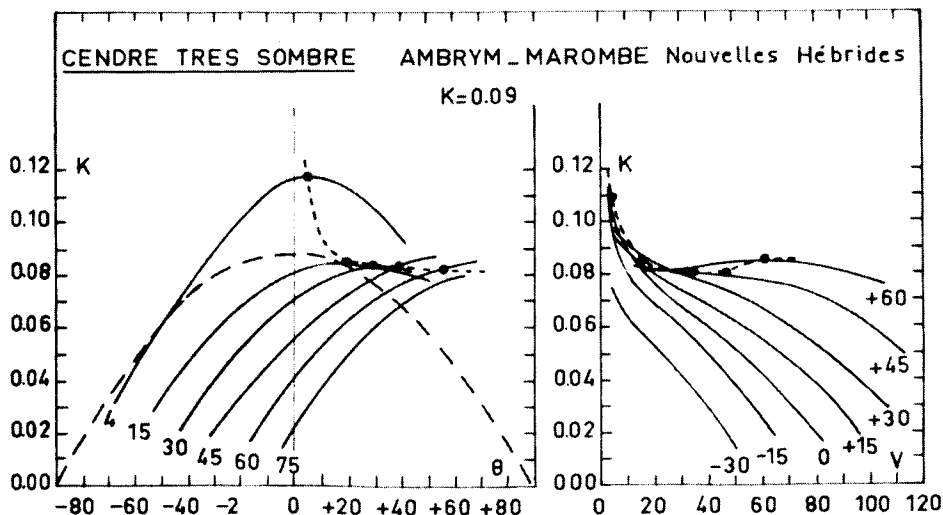


Figure 64

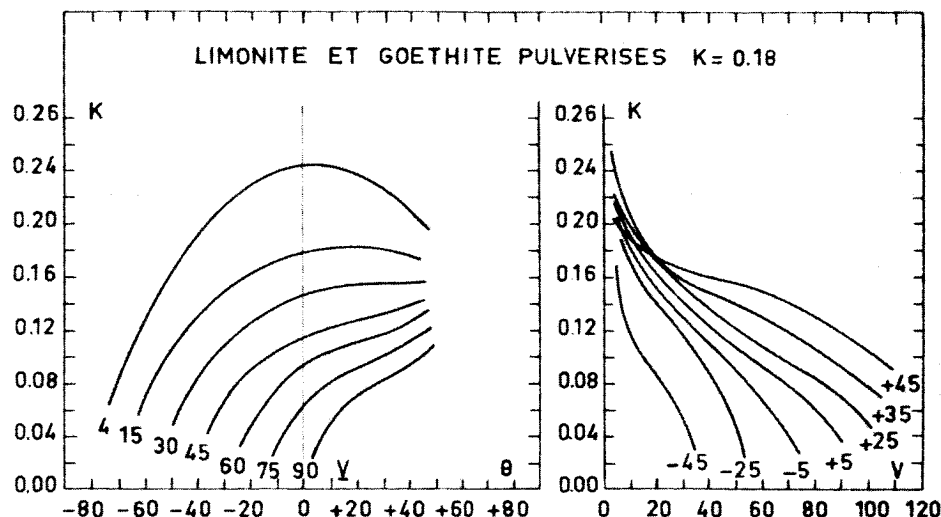


Figure 65

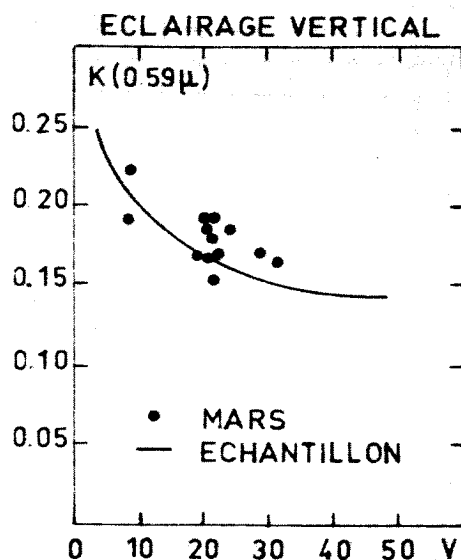


Figure 66

### Photométrie absolue des régions sombres

Les facteurs de diffusion des taches sombres sont plus difficiles à déterminer sous les différents angles d'éclairage et de vision que dans le cas des régions claires; les taches sombres sont moins nombreuses et plus petites; elles demeurent plus sensibles aux effets des voiles atmosphériques (15).

Pour la longueur d'onde 0,6 microns, les contrées sombres appelées "mers" donnent des éclats  $E$  voisins de

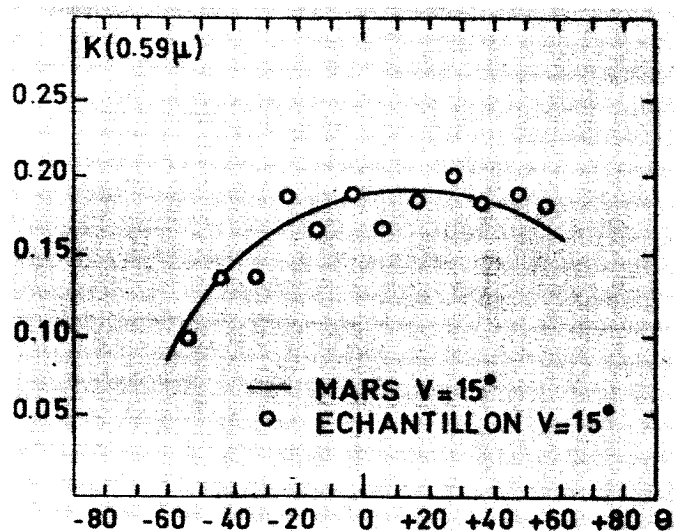


Figure 67

0,7 fois celui de  $E_0$  des régions claires désertiques orangées au centre du disque. Les taches les plus sombres (Syrtis Major) donnent 0,50.

La figure 69 donne, pour Erythraeum Mare, la variation de l'éclat en fonction de l'inclinaison  $\theta$ . En 1950 et 1952 j'ai recueilli des déterminations analogues sur environ 30 régions d'éclats divers (430 mesures). Au cours des oppositions suivantes, de nombreuses mesures comparatives ont été relevées par J. H. Focas, avec le même photomètre à franges, sur des clichés photographiques (12).

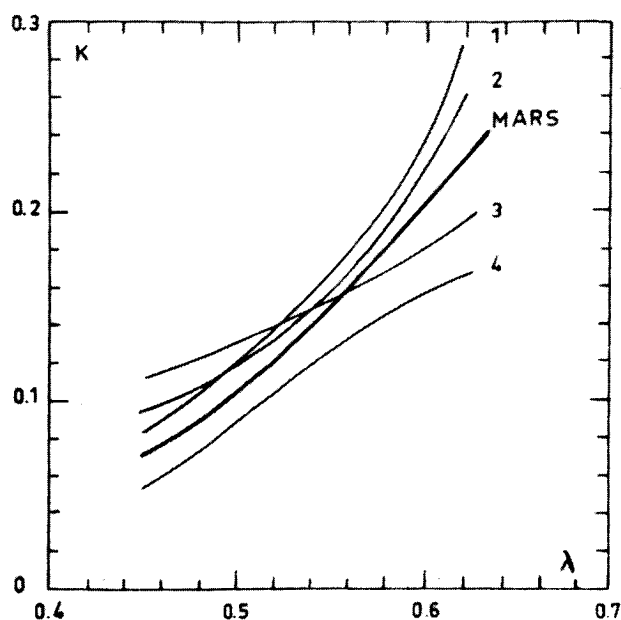


Figure 68

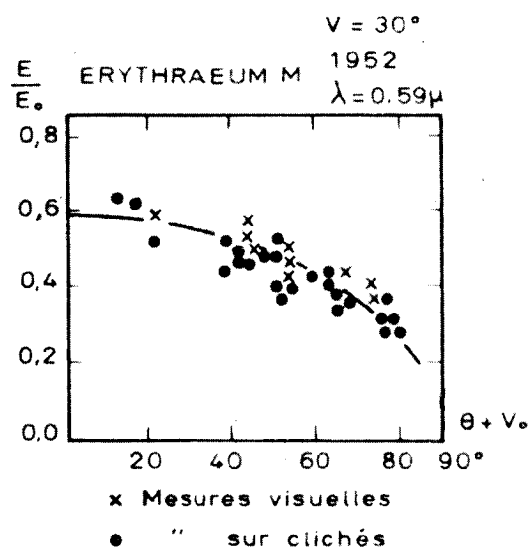


Figure 69

Les variations de l'éclat des taches sombres de Mars en fonction de  $\theta$  et de  $V$  paraissent analogues à celles des régions claires. Les écarts sont souvent dus à des voiles ou brumes dans l'atmosphère et ne paraissent pas significatifs. Il faut conclure que les mers sombres de la surface de Mars ont une structure superficielle comparable à celles des régions claires de couleur ocrée.

TACHE SOMBRE  
 $\frac{E}{E_0} = 0,70$  pour  $\lambda = 0,6 \mu$

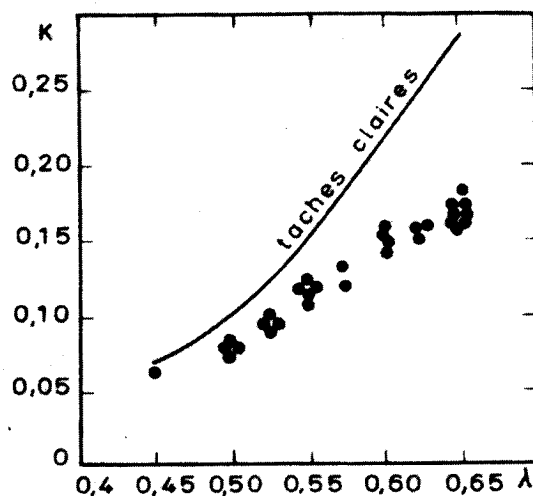


Figure 70

La figure 70 donne le facteur de diffusion  $E$  en fonction de la longueur d'onde pour les contrées sombres de contraste 0,3 dans le jaune. Les taches sombres donnent toujours une décroissance progressive de l'éclat vers les courtes longueurs d'onde. Cette tendance indique une couleur plutôt orangée. Ces régions sont vues cependant bleutées, verdâtres, quelquefois vert vif; il s'agit surtout d'un effet de contraste avec les régions claires voisines dont la couleur orange est encore plus vive. Le Dr. Kuiper avait déjà signalé cette propriété.

Les taches sombres atteignent un facteur de diffusion voisin de celui des régions claires dans le bleu-violet et leur contraste relatif devient inférieur à 10%. Les taches deviennent à peine perceptibles. Il n'est pas nécessaire de supposer l'existence d'une "couche violette" absorbante ou fortement diffusante permanente dans l'atmosphère martienne pour expliquer l'affaiblissement des taches sol. En effet, nous montrerons plus loin que la luminance de l'atmosphère en lumière bleue, lorsqu'il est très pur, ne représente que 7% de la luminance du sol.

Ces propriétés photométriques indiquent que les parties sombres du sol martien pourraient être constituées par un amalgame entre une poudre de petits grains ocrés analogue à celle des régions claires, et une matière sombre additionnelle.

J'ai mesuré au laboratoire, par exemple, une poudre orangée de limonite et goethite saupoudrée avec des particules de carbone. On peut imaginer aussi des blocs

très sombres effleurant de part et d'autre le dépôt poudreux.

### III. Diffusion par l'atmosphère martienne

Le facteur de diffusion de l'atmosphère martienne peut être déterminé grâce à des mesures de polarisation de la lumière. Ce facteur est relié à la pureté et la densité de cette atmosphère.

#### Etude de la polarisation de la lumière de Mars

J'avais entrepris d'étude détaillée de la polarisation de la lumière de Mars sur les différentes régions de sa surface, depuis 1948 (16)(17)(18). Le Dr. J. H. Focas s'est joint à ce grand programme depuis 1954 (12). Les Observatoires du Pic-du-Midi, de Meudon, d'Athènes, de Harvard, ont contribué à cette entreprise, grâce à l'appui de l'Union Astronomique Internationale (19). Toutes ces mesures de proportion de lumière polarisée concernent de petites régions de la surface du disque; elles ont été recueillies à l'aide de polarimètres visuels à franges de Lyot (20).

Nous disposons de 5200 mesures recueillies au cours des neuf dernières oppositions. Depuis 1963, des mesures photoélectriques à travers 8 filtres couvrant un large domaine de longueurs d'onde ont été recueillies à l'Observatoire de Kiev par le Dr. Morozenko qui a bien voulu les communiquer aussi; de même en France, aux Observatoires de Meudon et du Pic-du-Midi, nous avons recueilli des mesures photoélectriques dans l'infra-rouge, en particulier grâce à une importante convention de recherche avec l'U.S. Air Force (21).

La figure 71 donne l'exemple d'une séance de mesures avec le polarimètre visuel de Lyot et le réfracteur de 60 cm. de l'Observatoire du Pic-du-Midi. Les proportions de lumière polarisées  $P$  sont exprimées en millièmes; elles concernent des régions de la surface quelquefois aussi petites que  $1''5$  de diamètre. Les mesures sont accompagnées d'appréciations sur l'état de l'atmosphère martienne, et d'un croquis en lumière bleue complétant ces informations. On lit également la longitude du méridien central  $\omega$ , la latitude du centre du disque  $\phi$ , le diamètre apparent du disque  $d$ , l'angle de phase  $V$  et la longitude héliocentrique  $\eta$ . Pour l'angle de phase  $V = 15^\circ 5'$ , la polarisation au centre du disque sur les régions claires vaut  $-4,2$  millièmes; cette valeur se conserve au bord levant à droite, noté exempt de tout voile atmosphérique décelable. Les taches sombres polarisent plus fortement dans le sens négatif, la calotte polaire

montre une polarisation nulle. Au bord couchant (à gauche), de fortes anomalies de polarisation caractérisent des voiles, décelés par leurs blancheurs le long du contour de l'astre mais qui perturbent la polarisation sur une étendue beaucoup plus vaste en échappant aux observations visuelles. L'une des deux taches blanches, au bord, donne une polarisation nulle, qui n'est pas celle des nuages, mais caractérise un givre analogue à celui de la calotte polaire. Des observations analogues aux précédentes avaient déjà indiqué que cette région, appelée Nix Olympica, doit être un massif montagneux élevé, enveloppé de voiles nuageux, et dont certains sommets couverts de givre peuvent émerger au-dessus de la couche nuageuse.

Les figures 72 et 73 donnent la polarisation de la lumière des régions claires au centre du disque en fonction de l'angle de phase  $V$ , au cours des deux dernières oppositions. Les mesures s'accordent à peu près au millième et ne dépendent ni de l'Observatoire, ni de l'instrument, ni de l'observateur. La courbe au trait donne la polarisation du sol martien telle que nous avons pu la déterminer en l'absence de tout voile atmosphérique apparent. Les écarts caractérisent l'état de pureté de l'atmosphère martienne. Des voiles blancs de cristaux de glace et des voiles jaunes de fines poussières persistent quelquefois dans l'atmosphère; leurs propriétés de polarisation sont étudiées dans d'autres publications (17)(18).

En 1963, figure 72, l'atmosphère martienne était bien dégagée de voiles pendant la période du 1er au 30 Décembre 1962 correspondant à la portion de courbe de A à B. Puis du 1er au 15 Janvier 1963, de B à C sur la figure, de légères brumes souvent invisibles altéraient la limpidité de l'air. De C à D l'angle de vision était trop faible pour donner des résultats significatifs. Entre le 15 Février et le 30 Mars 1963, de D à E, les mesures très dispersées et de valeur trop faibles indiquaient la présence de légers voiles de poussière (voiles jaunes) en complément de quelques nuages de cristaux. Puis, jusqu'au milieu de Mai, de E à F, les voiles jaunes se sont résorbés mais quelques brumes de cristaux localisées, notées par des anomalies au bord du disque, dispersaient encore les mesures.

De Décembre 1964, à la fin de Mars 1964, de G jusqu'à I sur la figure 73, la polarisation de la lumière caractérise le sol à travers une atmosphère particulièrement pure. La dernière période, de I à J, donne des écarts de polarisation produits par des voiles fréquents.



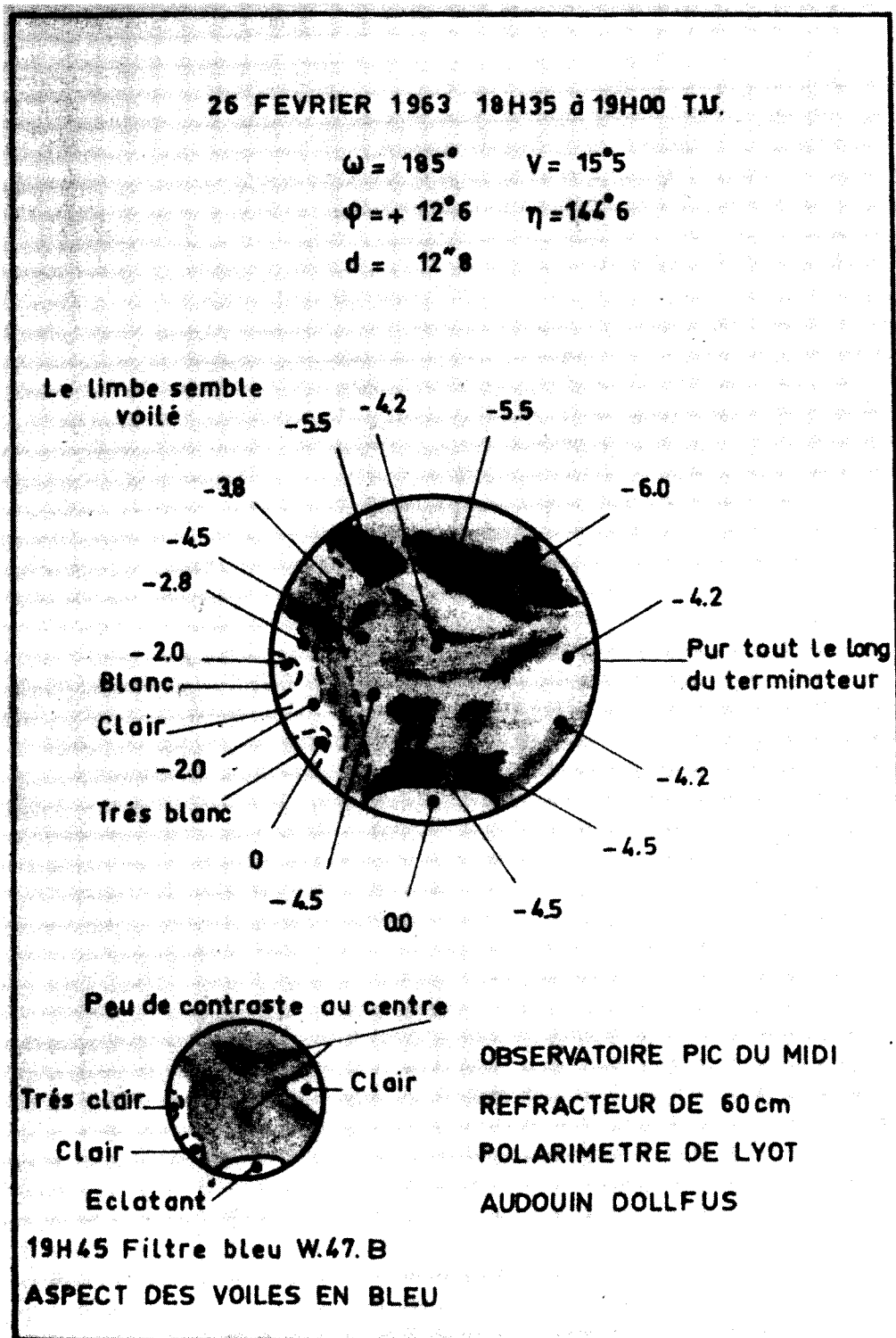


Figure 71

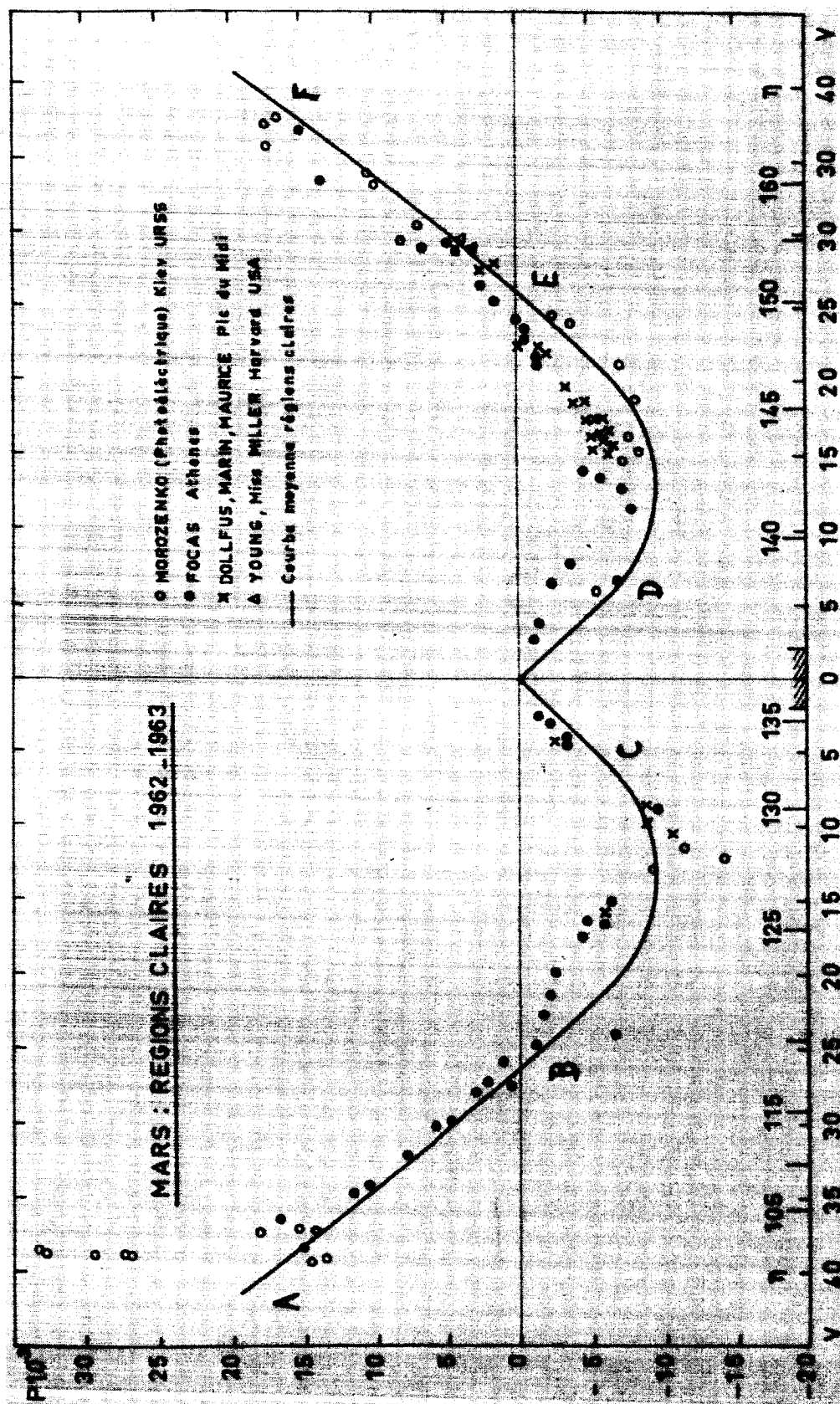


Figure 72

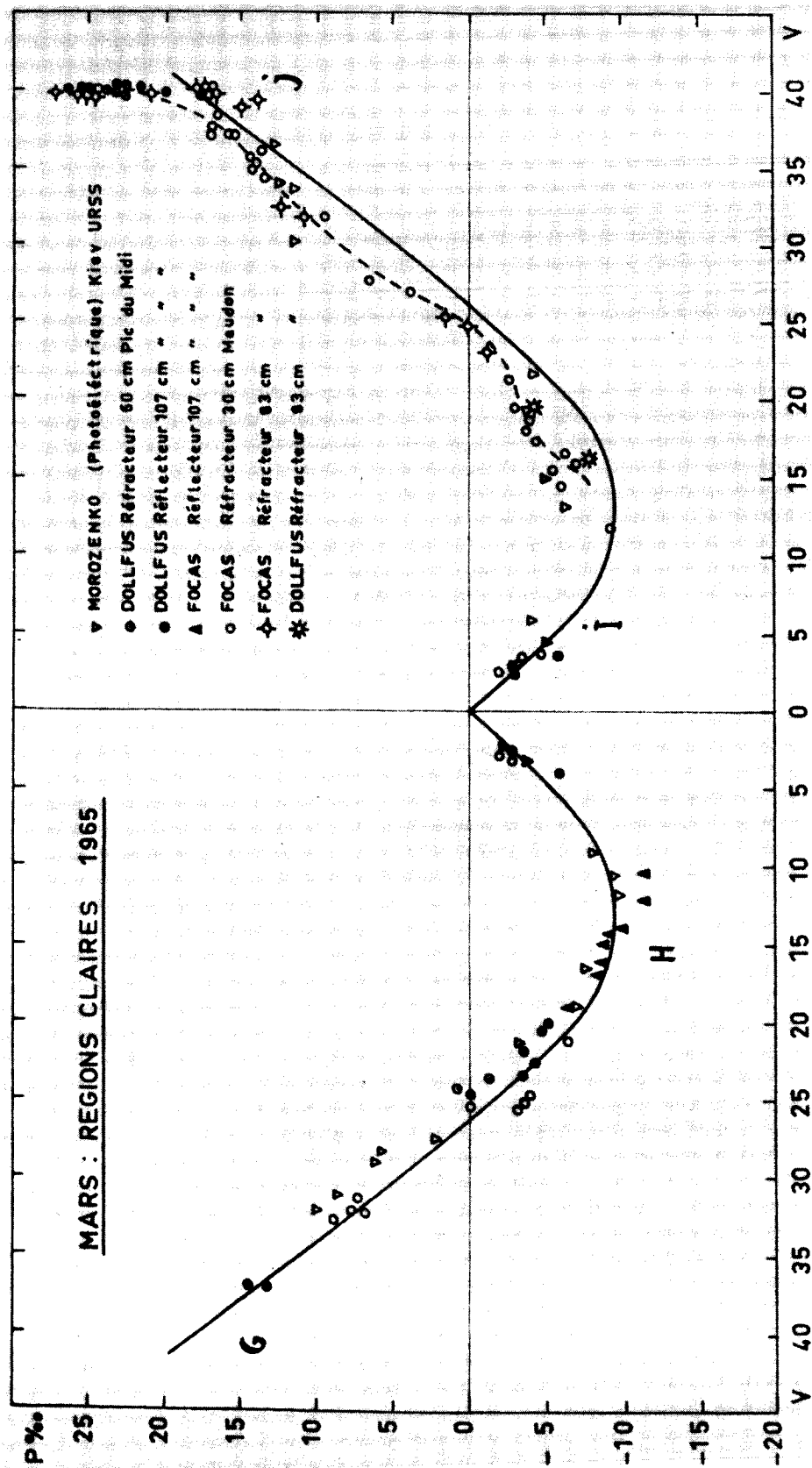


Figure 73

La figure 74 donne les courbes de polarisation pour les régions claires au centre du disque, à travers 7 filtres couvrant le spectre de 0,50 micron jusqu'à 1,05 microns. On a évité, sur ces courbes, les mesures nettement altérées par des aérosols.

#### Pouvoir diffusant de l'atmosphère martienne à 0,61 micron

J'avais donné en 1951 une estimation préliminaire de la quantité de lumière diffusée par l'atmosphère de Mars, d'après les mesures de polarisation (22)(16). La luminance de l'atmosphère martienne sous toute son épaisseur au centre du disque à la phase nulle fut estimée à 0,023  $\text{stilb}$  à la distance 1 UA du Soleil pour  $\lambda = 0,61$  micron, se qui donne un facteur de diffusion de 0,0017  $\text{stilb/phot.}$  Si l'atmosphère était complètement dépourvue d'aérosols, la pression au sol nécessaire pour donner cet éclat serait de 80 à 90 millibars. Cependant, cette première détermination ne reposait que sur quatorze séquences polarimétriques recueillies de 1948 à 1951; elles furent combinées avec les seules mesures photométriques alors disponibles; nous ne pouvions connaître en détail à cette époque les propriétés de pollution de l'atmosphère martienne.

Récemment, M. W. P. Cann (23) révisa cette valeur en utilisant les mêmes mesures polarimétriques et les combinant avec les déterminations photométriques plus précises décrites ci-dessus. Cette amélioration donna 0,013  $\text{stilb}$  à 1 UA, correspondant pour un air pur à une pression au sol de 50 mb.

Je viens de déterminer une nouvelle valeur beaucoup plus précise (24). J'ai examiné pour cela les 5200 mesures polarimétriques disponibles. J'ai sélectionné comme indiqué ci-dessus les périodes pendant lesquelles l'atmosphère martienne semblait particulièrement dépourvue d'aérosols; l'analyse des observations visuelles, des clichés photographiques et de la répartition détaillée de la lumière polarisée au bord du disque m'a permis en outre une nouvelle sélection pour éliminer les brumes locales ou pollutions atmosphériques temporaires. J'ai finalement retenu 45 nuits d'observation seulement, caractérisées par une limpidité particulière de l'atmosphère martienne. Ces séquences donnent la proportion de lumière polarisée  $P(\theta)$ , sur les régions claires et uniformes du sol martien, à différentes distances  $\theta$  du centre du disque, dans la direction perpendiculaire à la ligne des cornes.

On forme ensuite les différences  $P(\theta) - P(0^\circ)$  entre les mesures près des bords et au centre du disque, que l'on

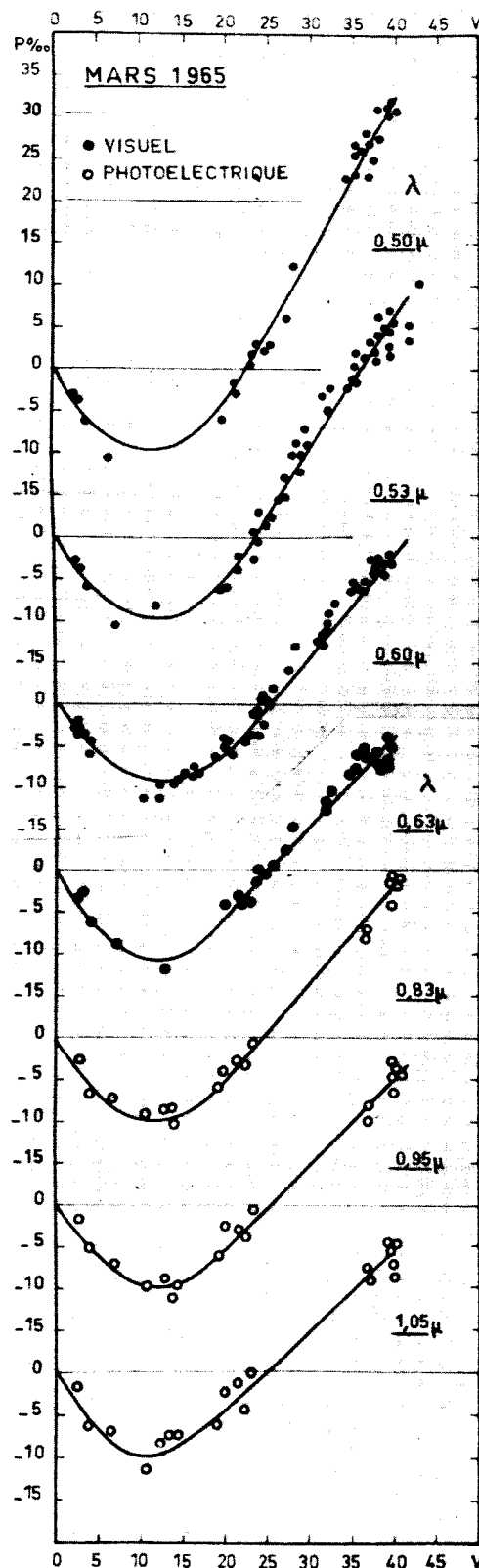


Figure 74

obtient ainsi pour différentes valeurs de l'angle de phase  $V$ .

Soit  $B_a(V, \theta)$  la luminance de l'atmosphère martienne observée sous toute son épaisseur, à la distance  $\theta$  du centre du disque, sous la phase  $V$ . Soit  $B_s(V, \theta)$  la luminance des régions claires du sol martien, donnée par les mesures photométriques reportées dans les figures 58 et 60. Soit  $P_s(\theta)$  la différence des polarisations données par le sol au centre du disque et sous l'inclinaison  $\theta$ ; cette quantité  $P_s(\theta)$  est donnée par des mesures sur des échantillons donnant les mêmes propriétés polarisantes que le sol martien; les valeurs, faibles, sont reportées sur la courbe du haut de la figure 75.

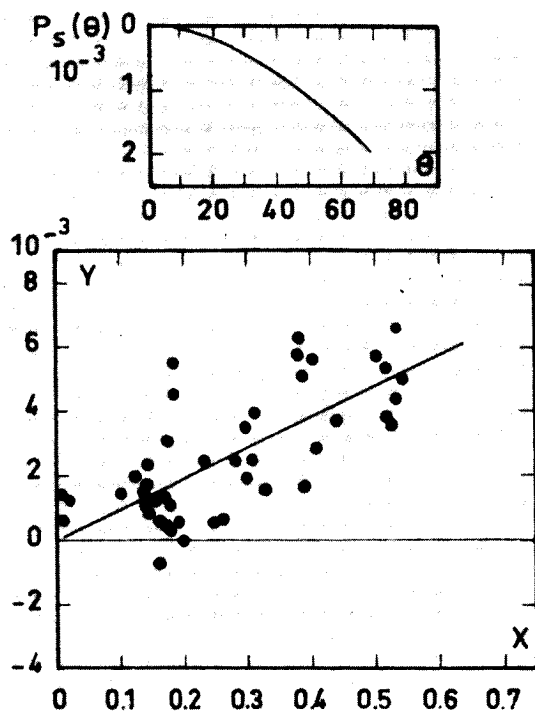


Figure 75

Supposons que, en raison de leur choix, les mesures concernent les régions où l'atmosphère martienne n'est composée que de molécules et éventuellement d'aérosols de diamètres plus petits que la longueur d'onde donnant une diffusion analogue à celle des molécules; un calcul développé par ailleurs (16)(24) donne :

$$P(\theta) - P(0) - P_s(\theta)$$

$$= \frac{B_a(0,0)}{B_s(0,0)} \frac{\sin^2 V}{2} \left[ \frac{B_s(0,0)}{B_s(V,\theta)} \frac{1}{\cos \theta} \frac{B_s(0,0)}{B_s(V,0)} \right]$$

de la forme  $Y = (B_a/B_s) X$ . Sur le graphique  $X,Y$  de la figure 75, les 45 déterminations polarimétriques définissent une droite dont la pente donne la brillance  $B_a$  de l'atmosphère martienne, rapportée à celle  $B_s$  des régions claires du sol, à l'opposition exacte, au centre du disque et pour  $\lambda = 0,61$  micron, soit  $B_a/B_s = 10,0 \cdot 10^{-3}$ .

Les mesures photométriques reportées plus haut donnent  $B_a = 0,35$  stilb à 1,52 UA du Soleil. L'éclairement donné par le Soleil à 1 UA vaut 13,5 phot. Par suite, le pouvoir diffusant global d'une colonne verticale d'air au centre du disque, à la phase nulle, en lumière orangée 0,61 micron, vaut, dans les meilleures conditions de pureté atmosphérique martienne observable:

$$K_a(0,61 \mu) = 10,0 \cdot 10^{-3} \times 0,35 \times (1,52)^2 \times 1/13,5$$

$$\text{soit } K_a(0,61 \mu) = 6,0 \cdot 10^{-4} \text{ stilb/phot.}$$

#### Pouvoir diffusant de l'atmosphère martienne à 0,47 micron

Le Dr. Focas et moi-même avons mis à profit la dernière opposition de Mars, de Décembre 1964 à Juillet 1965 pour étudier la variation spectrale de la polarisation de la lumière de la planète (25). Huit filtres colorés découpaient le spectre de 0,47 à 1,05 microns (figures 74 et 76). A la fin de Juin 1965, l'angle de phase atteignait la valeur maximum  $V = 39^\circ 9'$ ; la figure 76 donne les mesures de polarisation relevées à cette époque sur les régions claires au centre du disque. Entre le 15 Juin et le 10 Juillet, des écarts forts et toujours positifs traduisaient la présence de faibles voiles de cristaux de glace; ces voiles apparurent quelquefois comme de légères blancheurs et plus souvent comme une simple augmentation de la polarisation de la lumière lorsque ces régions étaient vues aux bords levants et couchants. L'atmosphère martienne semblait au contraire dépourvue de brumes de poussières qui donneraient des écarts de signe négatif.

Nous avons sélectionné celles des mesures relevées entre l'angle de phase  $39^\circ 6'$  et la valeur maximum  $39^\circ 9'$  qui ne semblaient pas altérées par les voiles. Ces données sont reportées en fonction de l'inverse de la longueur d'onde sur la figure 77. La courbe donne la variation spectrale de la polarisation pour l'angle de phase  $V = 39^\circ 8'$  lorsque l'atmosphère martienne paraît pure.

Des échantillons de limonite et goethite pulvérisés reproduisent la polarisation de la lumière observée pour le sol martien et donnent la variation spectrale définie

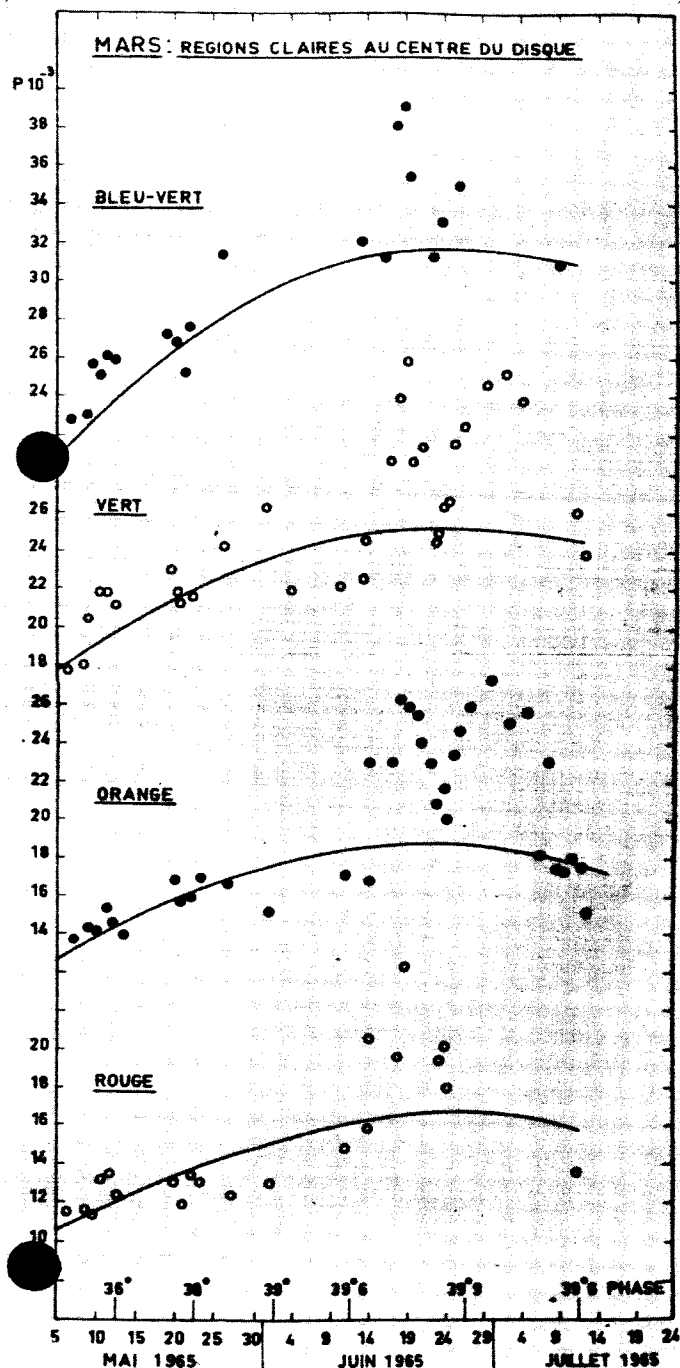


Figure 76

par des cercles sur la figure 77. Dans l'infra-rouge, les polarisations relevées sur Mars et l'échantillon s'accordent. Vers le bleu, les courbes divergent; l'écart est attribuable à l'atmosphère martienne, dont l'éclat augmente rapidement vers les courtes longueurs d'onde. La différence atteint  $\Delta P = 23$  millièmes pour  $\lambda = 0,47$  micron. Soit  $B_a(\lambda, V)$  et  $B_s(\lambda, V)$  les luminances de l'atmosphère

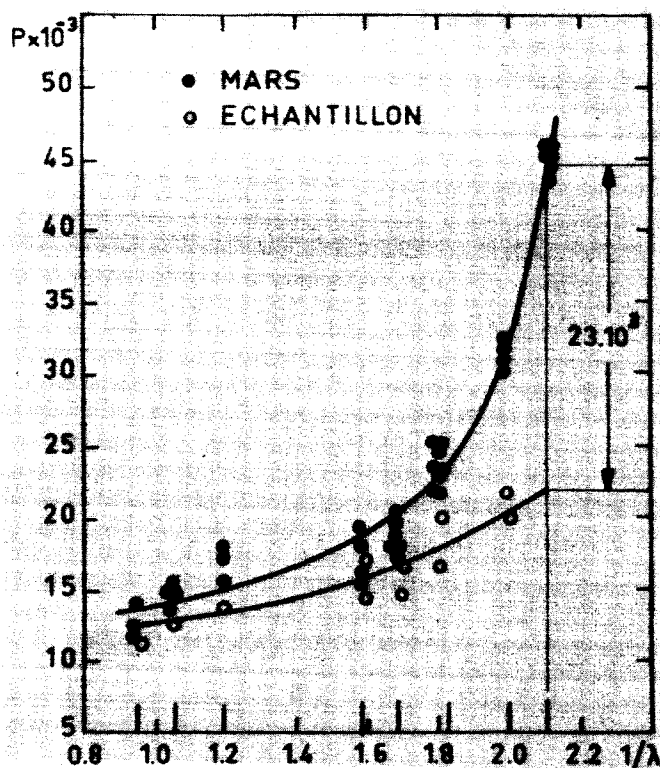


Figure 77

et du sol au centre du disque. Si l'atmosphère diffuse comme un gaz de molécules ou de très petites particules, un calcul déjà exposé (16)(25) donne:

$$P = \frac{B_a(\lambda, 0^\circ) \sin^2 V}{B_s(\lambda, V) \cdot 2}$$

soit :

$$\frac{B_a(0,47 \mu, 0^\circ)}{B_s(0,47 \mu, 39^\circ 8')} \frac{2 \cdot \Delta P}{0,410} = 0,110$$

La luminance  $B_s$  du sol dans le bleu au centre du disque, sous la phase  $39^\circ 8'$ , n'est encore donnée par aucune mesure directe. Nous pouvons en extrapoler l'ordre de grandeur à partir des mesures photométriques reportées ci-dessus, soit 0,050 fois la luminance d'un diffuseur parfait, correspondant à 0,08 stilb à 1,52 UA. La luminance de l'atmosphère pour toute son épaisseur, au centre du disque à la phase nulle, pour  $\lambda = 0,47$  micron, vaut donc à peu près  $0,11 \times 0,08 = 8,8 \cdot 10^{-3}$  stilb à 1,52 UA, et donne un coefficient de diffusion de l'ordre de:

$$K_a(0,47 \mu) = 15 \cdot 10^{-4} \text{ stilb/phot}$$

### Pollution résiduelle de l'atmosphère martienne

Les valeurs trouvées pour le coefficient de diffusion de l'atmosphère martienne dans ses régions pures ont été pour le rouge :  $K_a(0,61 \mu) = 6,0 \cdot 10^{-4}$  stilb/phot, et pour le bleu :

$$K_a(0,47 \mu) = 15 \cdot 10^{-4} \text{ stilb/phot}$$

Si l'atmosphère martienne dépourvue d'aérosols décelables diffuse comme les molécules d'un gaz pur,  $K_a$  devrait varier comme  $\lambda^{-4}$  et donner :

$$\frac{K_a(0,47 \mu)}{K_a(0,61 \mu)} = \left( \frac{0,61}{0,47} \right)^4 = 2,8$$

La valeur observée  $15/6 = 2,5$  en est très proche. Il faut donc que l'atmosphère martienne, dans les régions où elle est vue très pure, ne contienne plus qu'une quantité faible d'aérosols résiduels diffusant la lumière d'une façon différente des molécules, en particulier des particules ayant un diamètre supérieur à la longueur d'onde.

Des particules de beaucoup plus petit diamètre que la longueur d'onde accroissent le pouvoir diffusant de l'air mais polarisent à peu près comme des molécules et pourraient échapper à notre analyse. Supposons l'atmosphère martienne dépourvue d'une telle pollution résiduelle et constituée, par exemple, d'azote pur dont le pouvoir diffusant vaut, dans les conditions normales de pression et températures sous l'épaisseur  $h$  cm :  $K_{N_2} = 2 R h$ , avec  $R$  = constante de Rayleigh =  $4,3 \cdot 10^{-9}$  pour  $\lambda = 0,61$  microns. Le pouvoir diffusant observé  $K_a(0,61 \mu) = 6,0 \cdot 10^{-4}$  stilb/phot donne alors l'épaisseur de l'atmosphère réduite aux conditions normales,  $h = 7,10^4$  cm, et la pression atmosphérique au sol, soit environ 30 millibars.

Les nouvelles déterminations de la pression atmosphérique par spectroscopie (26)(27)(28) ou par la sonde spatiale Mariner IV (29) donnent des valeurs plus faibles comprises entre 9 et 20 millibars. Si de telles valeurs sont exactes, il faut alors que l'atmosphère martienne con-

tienne en permanence une faible quantité d'aérosols très petits, polarisant la lumière comme les molécules mais accroissant le pouvoir diffusant de l'air. Selon la valeur réelle de la pression au sol, la contribution de ces aérosols à la diffusion totale de l'atmosphère serait comprise entre 0,5 et 2 fois la diffusion par le gaz lui-même.

### Transparence de l'atmosphère martienne dans le bleu

Les taches sombres du sol martien disparaissent presque dans le bleu et le violet; on a souvent invoqué pour cela la forte absorption que donnerait une hypothétique "couche violette" permanente dans l'atmosphère martienne.

Cependant, les valeurs établies ci-dessus donnent en lumière bleue :  $B_a(V=0^\circ) = 0,110 B_s(V=39^\circ 8)$ , et d'autre part :  $B_s(V=39^\circ 8) = 0,05/0,08 B_s(V=0^\circ)$ . La luminance  $B_a$  de l'atmosphère vaut donc, pour un angle de phase nul,  $0,11 \times 0,05/0,08 = 0,07$  fois seulement la brillance du sol. Certes, la luminance de l'atmosphère est déterminée ci-dessus à partir de sa quantité de lumière polarisée  $B_a \cdot P_a$  et une pollution résiduelle par de très petits aérosols pourrait donner une polarisation  $P_a$  trop faible, et par suite un éclat  $B_a$  de l'atmosphère légèrement supérieur. Mais, même dans ce cas, le voile atmosphérique dans le bleu reste beaucoup trop faible pour voiler appréciablement le sol.

Les taches sombres du sol deviennent très faible dans le bleu, non pas en raison d'une "couche violette" mais parce que leur facteur de diffusion devient voisin de celui des régions claires sur le fond desquelles elles se détachent.

Le contraste réel des taches est si faible que de très légers voiles atmosphériques additionnels suffisent alors à les effacer complètement, tel par exemple les "nuées bleues" que l'on observe presque en permanence aux bords levants et couchants, et très souvent dans les régions du disque (30), ainsi que les plus rares "voiles jaunes" constitués de poussières volantes (18).

### REFERENCES

1. C. R. Acad. Sci. Paris 1963, 256 3009.
2. "L'Astronomie" Décembre 1959, p. 468.

## REFERENCES (Cont'd)

3. "The Origin and Evolution of Atmospheres and Oceans," chap. 12, p. 257. Pub. Branczario et Cameron, John Wiley and Son, Inc. 1964.
4. Detection of Water Vapor in the Atmospheres of Venus and Mars, Proc. 1964 AFCRL "Scientific Balloon Symposium," USAF-OAR le 409.
5. C. R. Acad. Sci. Paris 1954, 239 954.
6. C. R. Acad. Sci. Paris 1959, 249 2602.
7. C. R. Acad. Sci. Paris 1963, 256 3009.
8. C. R. Acad. Sci. Paris 1965, 261 1603.
9. J. N. Howard, L. Burch, D. Williams: Geoph. Rs. Paper N° 40 1955, AFCRL TR-55-231.
10. C. R. Acad. Sci. Paris 1957, 244 162.
11. C. R. Acad. Sci. Paris 1956, 243 1833.
12. J. H. Focas: Ann. Astroph. 1961, 24 309.
13. C. R. Acad. Sci. Paris 1956, 243 2023.
14. P.A.S.P. 1958, 70 56.
15. C. R. Acad. Sci. Paris 1957, 244 1458.
16. "Etude des planètes par la polarisation de leur lumière", Thèse, Paris 1955 et Supplément Annales d'Astrophysique. Traduction en anglais, NASA TT.F-188.
17. "Polarization studies of planets," chap. 9 "The Solar System" Tome III. G. P. Kuiper éditeur. Univ. of Chicago Press.
18. Ann. Astroph. 1965, 28 722.
19. Commission 16 de l'U.A.I. "Etude physique des planètes et satellites."
20. B. Lyot : "Recherches sur la polarisation de la lumière des planètes et de quelques substances terrestres", Thèse, Paris 1929 et Ann. Observat. Meudon 1929.
21. USAF Contract A.F. 61(052)—508.
22. C. R. Acad. Sci. 1951, 232 1066.
23. M. W. P. Cann : IIT RI Report W. 0696, 1965, Chicago.
24. C. R. Acad. Sci. 1966.
25. C. R. Acad. Sci. 1966, sous presse.
26. T. C. Owen, J. P. Kuiper : Communic. Lunar Planet. Lab. Univ. Arizona—N° 32, 1964.
27. L. D. Kaplan, G. Münch, I. Spinrad : Astroph. Jl. 1964, 139, 1.
28. V. Moroz : Astron. Zhur. 1964, 41, 350.
29. A. Kliore : Voir ce présent volume.
30. L'Astronomie Mars 1963, p. 85.



## SUMMARY REMARKS ON MARS

Guido Münch

Mount Wilson and Palomar Observatories  
Carnegie Institution of Washington  
California Institute of Technology

The highlights of the Mars sessions of our Conference were undoubtedly the results obtained from the *Mariner IV* spacecraft. There would be hardly any point in attempting to summarize these results, and what I propose to do instead is to place or mention some of the *Mariner IV* results in the context of our present knowledge of the Martian atmosphere, as derived from telescopic observations from the Earth and as discussed by various investigators during the sessions.

The problem of determining the pressure in the Martian atmosphere has played a central role in our discussions. In addition to its purely scientific value, it has recently acquired great practical interest in relation to the *Voyager* program. Plans for the soft-landing of an instrumented capsule on the surface of Mars have been considered since the beginning of the Space Age, say, 1960. At that time it was generally accepted, on the basis of photometric and polarimetric observations, that the pressure of the Martian atmosphere at ground level was slightly less than one tenth that of the Earth. A study of the CO<sub>2</sub> absorption features in the spectrum of Mars, carried out at the Mount Wilson Observatory and JPL in 1963, led to estimates that the pressure of the Martian atmosphere at ground level was instead one fortieth that

on Earth, with an uncertainty of about 60%. This determination, based on the comparison of very weak, unsaturated CO<sub>2</sub> absorption lines with strong, pressure-broadened bands of the same substance, is more straightforward and reliable than estimates based on photometric procedures. For the practical purpose of designing an entry capsule and a lander, however, the uncertainty affecting the determination has severe consequences in weight penalties and in the variety of modes that have to be considered. It was thus imperative to obtain a more precise value, and, at the most recent opposition of the planet, observations of the weak CO<sub>2</sub> absorption lines in its spectrum were carried out at the Kitt Peak, Lick, McDonald, and Mount Wilson Observatories. The values obtained by the various groups of investigators for the net CO<sub>2</sub> content along the vertical of Mars atmosphere range from 50 to 100 m-atm. The resulting values of the pressure depend on the measures of the strong infrared bands, which do not seem to have kept pace with those of the weak lines. If the measurements of Kuiper for the 1.57  $\mu$  CO<sub>2</sub> band are used, values for the pressure between 7 and 14 mb are obtained. It might appear that the percent uncertainty in the value of the pressure has not been reduced by the recent observations, but when we recall the difficulty involved in measuring the weak

lines, the various determinations should be considered in essential agreement.

On the average, the spectroscopic values for the pressure would appear somewhat high when compared with the values of 5 to 6.7 mb obtained from the preliminary analysis of the occultation experiment of *Mariner IV*. It should, however, be taken into account that the results of the occultation experiment are also affected by uncertainties arising from: (1) The use of a constant scale height in the reduction of the data; (2) The Fresnel diffraction of the radio beacon by the planet's limb; (3) Uncertainty in the local height of the Mars terrain where the occultation took place, and (4) The possibility that a significant degree of ionization exists down to the ground. An atmospheric temperature of 230°K at ground level, instead of the 180°K assumed, would increase the nominal value of the surface pressure by about 25%. An increase of equal magnitude would be produced by an elevation of 5000 ft. The eventuality that the level of ionization at the ground is high enough to make the refractivity measures unreliable indicators of the total pressure appears unlikely, but it cannot be ruled out *a priori*. The upper limit of the Martian magnetic field set by the *Mariner IV* magnetometer indicates that cosmic rays and energetic solar particles will reach the ground. It can be shown that a solar cosmic ray event accompanying a flare of importance 3+ would produce sufficient ionization at ground level to change, by a factor of two, the pressure that would be derived from an occultation experiment carried out within a week after the flare. While the solar activity during the days preceding the occultation of *Mariner IV* was insufficient to introduce uncertainty in the results of the experiment, we have no information about the degree of radioactivity of ground exposed for geological times to cosmic and solar high-energy particles. Under these conditions, and pending a complete error analysis of the spectroscopic observations as well as a thorough discussion of the *Mariner IV* occultation experiment, it would appear that the best estimate for the pressure at the base of the Martian atmosphere is 8 to 10 mb.

New and interesting results have been reported at this Conference on the water vapor of the Martian atmosphere. According to recent observations made by Spinrad, water vapor is not always detectable in the spectrum of Mars, but only sometimes at certain locations on the planet, in a manner indicating that the small water vapor content varies, depending on local meteorological conditions. Such a result should be expected from the small amount of solid or liquid water available on the surface of the planet and the low prevailing temperatures.

Of particular importance for the study of the solid crust of the planet have been the advances reported on radar methods. So far the study of the surface of Mars has been made on the basis of polarimetric and colorimetric observations. Indeed, interesting results of this nature were presented at this Conference by Dollfus and Younkin. But the radar experiments carried out at Goldstone and Arecibo have shown that it is possible to obtain information about the reflectivity or dielectric constant of the surface materials. The conspicuously high reflectivity of the Trivium Charontis, an area long known to be a "cloud producer," is particularly intriguing. Considering the weakness of the target return signals, the radar results should be regarded as a remarkable achievement. Undoubtedly this kind of work will produce increasingly important results, as the power of the transmitters and the antennas becomes larger, the signal-to-noise ratios thereby increasing also.

This short summary of the Mars discussions should perhaps be finished by expressing an opinion shared by all the astronomers who actively studied Mars during the last opposition: that the scientific interest in the planet has increased because of the recent ground studies and the results from *Mariner IV*. At the next opposition, more experiments will undoubtedly be carried out, with higher accuracy and novel design. We hope that they will serve as a basis for the forthcoming exploration of the planet to be done by *Voyager*.